

"THE CHEMICAL CHARACTERISTICS OF VICTORIAN BROWN COAL"

G. J. Perry, D. J. Allardice and L. T. Kiss*

Victorian Brown Coal Council, 151 Flinders Street, Melbourne, 3000 Australia,
*State Electricity Commission of Victoria, Herman Research Laboratory, Howard Street, Richmond, 3121 Australia.

1. INTRODUCTION

Extensive deposits of soft brown coal exist in Tertiary age sediments in a number of areas in Victoria and the largest single deposit occurs in the Latrobe Valley, about 150 kilometers east of Melbourne. In this region the coal seams often exceed 150 metres in thickness, with an overburden to coal ratio usually better than 1:2 making the coal ideally suited for large-scale open-cut mining.

A recent study (1) has estimated the State's brown coal resources to be almost 200,000 million tonnes with approximately 52,000 million tonnes defined as usable reserves. About 85% of this coal is located in the Latrobe Valley.

Since 1920 Latrobe Valley brown coal has been developed for power generation. The State Electricity Commission of Victoria (SECV) wins coal from two major open cuts at Yallourn and Morwell and operates coal fired power stations which presently consume approximately 35 million tonnes per annum. In addition to power generation, small quantities of brown coal are used for briquette manufacture and char production.

Brown coal accounts for about 95% of Victoria's non-renewable energy reserves and it is now recognized that with suitable up-grading, primarily drying, it has the potential to become the basis of the supply of energy in a variety of forms. Currently various studies for major conversion projects proposed by Australian, Japanese and German interests are being undertaken with the co-operation of the Victorian Brown Coal Council, the most advanced project being a 50 tonne per day hydrogenation pilot plant currently under construction at Morwell funded by New Energy Development Organization (NEDO) of Japan.

The chemical characteristics of Latrobe Valley brown coals have been extensively studied over the last twenty-five years, primarily in relation to the effect of coal quality on combustion for power generation. More recently a research project was initiated with the objective of determining the characteristics and suitability of the State's brown coal resources for uses other than power generation, primarily conversion to liquid fuels.

This paper outlines the chemical characteristics of Victorian brown coal and discusses the variability of the coal both between fields and within a seam. The importance of chemical properties in relation to coal quality and the implications for utilization are also briefly addressed.

2. PROPERTIES OF VICTORIAN BROWN COAL

The development and adaptation of modern analytical techniques for analysis of Victorian brown coal was pioneered jointly in the 1960's by the Commonwealth Scientific and Industrial Research Organization and the State Electricity Commission of Victoria. As a result the total coal analysis time was halved and the determination of the ash forming constituents directly on the coal took one sixth of the time of conventional ash analysis. More importantly brown coal analysis was put onto a rational basis taking its unique properties into account; and providing more pertinent information concerning the genesis, occurrence and use of Victorian brown coal.

Moisture

One of the most important chemical measurements made on brown coal is the bed moisture content which is also a good measure of physical rank; the greater the degree of compaction of the coal and its degree of coalification, the lower is the moisture content. To obtain meaningful results the sampling and sample preparation have to be carried out quickly to avoid moisture loss. The choice of the method of determination is important as thermal decomposition of functional groups can result in loss of CO₂ as well as H₂O. The preferred methods therefore involve direct measurement of the water released either by azeotropic distillation or adsorption from an inert carrier gas rather than by weight loss of the coal.

It is important to realize that the bed moisture content of soft brown coals is significantly higher than the equilibrium moisture holding capacity, a parameter which is used to characterize higher rank coals. This is illustrated in Table 1 for a range of Victorian brown coals.

In terms of moisture the economic value of high rank coals is best indicated by the moisture holding capacity because it reflects the condition of the coal for utilization. In the case of Victorian brown coal the bed moisture content is the critical value, since the coal is used directly from the open cut.

Mineral and Inorganic Content

Ash content has been traditionally used to assess the magnitude of combustion residue and to derive the so called "coal substance" by difference which allows meaningful comparisons of different coals. In this context the ash is used as an approximation of the mineral matter content. The tacit assumption made, of course, is that the ash is derived solely from coal minerals, and this is certainly not the case for Victorian brown coal where the bulk of the ash forming material occurs as inherent inorganic matter in the form of exchangeable cations, associated with oxygen containing functional groups. This is also the case with many other low rank coals.

Using a combination of X-Ray fluorescence (XRF) on coal pellets and Atomic absorption (AA) techniques on acid extracts, direct chemical analyses of the ash forming elements in Victorian brown coal has been performed. Arising from this, a method of expression of results has been developed (2) which is based on classifying the mineral matter in brown coal into mineral and inorganic matter fractions and expressing each in a way which reflects their occurrence in the coal.

The Inorganics are a group of exchangeable cations and water soluble salts, analysed by AA on dilute acid extracts from the coal and expressed in terms of chemical analysis on a coal basis as -

$$\text{Inorganics} = \text{Na} + \text{Ca} + \text{Mg} + \text{Fe} + (\text{Al}) + (\text{Si}) + \text{NaCl}$$

where Fe refers to the non-pyritic iron and (Al) and (Si) to the acid soluble aluminium and silicon respectively. This expression is complicated by the fact that some iron and aluminium can be present as acid soluble hydroxides, but these are not usually significant.

The group named Minerals, which occurs as discrete particles principally of quartz, kaolinite and pyrite/marcasite is expressed in terms of chemical analysis as -

$$\text{Minerals} = \text{SiO}_2 + \text{Al}_2\text{O}_3 + \text{TiO}_2 + \text{K}_2\text{O} + \text{FeS}_2$$

This expression ignores the water of constitution of clays which is usually of negligible magnitude for Victorian brown coals.

The total weight of Minerals and Inorganics expressed on a dry coal basis gives the best estimate corresponding to "mineral matter" in high rank coal technology. In the case of Latrobe Valley coals the Inorganics are far more important than Minerals both in quantity and from a utilization point of view.

From a knowledge of the chemical constitution of the mineral matter it is possible to calculate and predict the composition of the ash or inorganic residue remaining after most technological processes. Table 2 illustrates the comparison between mineral matter content and ash content and the successful calculation of ash content from mineral matter data for a number of typical Victorian brown coals. Table 3 illustrates the futility of predicting the quantities of ash produced in modern, pulverized fuel fired power stations from the empirical ash test results. It illustrates for Morwell and Yallourn coals the quantities of ash produced in a boiler as opposed to the ash test; and it compares the laboratory ash composition with the precipitator ash actually produced. The mineral matter composition is also given as a guide. Both the laboratory and precipitator ash compositions can be calculated from the composition of the mineral matter by allowing for the difference in the degree of sulphation of the Inorganics. By extending this approach it should also be possible to calculate the composition of the inorganic residue obtained in hydrogenation processes.

It should also be noted that oxygen can only be estimated by difference if the mineral matter is known; using the ash value will yield misleading results.

Oxygen Functional Groups

Oxygen is one of the major elements present in the organic substance of Victorian brown coal. For Latrobe Valley brown coals oxygen generally comprises over 25% on a dry mineral and inorganic free (dmif) basis and about half of this oxygen can be accounted for in the acidic functional groups -phenolic hydroxyl, free carboxylic acid and carboxylate. The 40-50% of the oxygen not accounted for as acidic oxygen is primarily contained in carbonyl groups, ether linkages and heterocyclic ring structures.

3. VARIATION OF CHEMICAL PROPERTIES WITHIN A SEAM

The variation of chemical properties in a brown coal seam is attributable to the influence of two independent variables, namely coal rank and coal type. Rank variations are due to the burial history of the coal, that is the time, temperature and pressure it has undergone since its deposition. However, type (or lithotype) variations also significantly influence brown coal properties. Lithotypes arise from variations in the prevailing botanical communities, in the depth and nature of the swamp water and in the conditions of decay and decomposition of plant material. In Victorian brown coal these lithotypes are macroscopically recognizable bands or layers within a coal seam which become readily apparent on partially dried and weathered faces of open cuts. The basic factors on which lithotypes are classified are colour and texture in air dried coal, with degree of gelification, weathering pattern and physical properties used as supplementary characteristics which varies from pale to dark brown. In the case of Latrobe Valley coals, the colour of the air dried coal as measured by its diffuse reflectance and expressed as a Colour Index gives a numerical value related to lithotype.

The variation in rank with depth in the Morwell Open Cut is illustrated by the yearly weighted averages for each operating level. The gradation in rank is clearly illustrated in Figure 1 by the increase in carbon content, and the associated increase in gross dry specific energy; the volatile matter also decreases slightly with depth. These samples were not selected on a lithotype basis and the gradual changes in these coal properties are presumed to arise primarily from the increase in rank with depth.

The variation of coal properties with lithotype has been examined within continuous sequences of samples taken from five Latrobe Valley coal fields (3). The results indicate that the coal properties related to the organic coal substance, eg: volatile matter, hydrogen, carbon, oxygen and specific energy vary with lithotype layers in the coal seam. The dependence of carbon and hydrogen on lithotype (as measured by colour index) is illustrated in Figure 2 for a typical bore. All the major constituents of the organic coal substance are lithotype dependent and their variation within a seam is a direct consequence of the changes in depositional environment which occurred during formation of the seam.

The occurrence of organic sulphur and organic nitrogen is independent of lithotype although the concentration of nitrogen is influenced by the presence of wood in the coal.

Generally speaking, the concentration of minerals in the coal is highest near the overburden and the interseam sediment layers. Because of the discrete nature of the minerals their sporadic distribution in a seam cannot be accurately assessed from a single traverse of sampling through the seam.

The concentration of inorganics, particularly sodium, magnesium, calcium and non-pyritic iron show no relationship to lithotype (Figure 2) although some depth related concentration gradients are apparent. Sodium and magnesium often show a concentration increase near the top of a bore whilst the aluminium concentration tends to increase near the bottom. This is believed to be due to diffusion of aluminium into the coal from the clay containing sediments below the coal seam. On the other hand calcium in the Morwell open cut has the highest concentration near the middle of the profile.

The lack of correlation between these inorganic species and lithotype indicates that the inorganics are probably post-depositional in origin. This is consistent with their diffusion through the water of the coal giving rise to concentration gradients.

4. VARIATION IN CHEMICAL PROPERTIES BETWEEN COALFIELDS

In addition to the variation of chemical properties within coal seams, significant variation also occurs between different coalfields in Victoria. An extensive research programme in which this variation was investigated has been conducted by the State Electricity Commission of Victoria on behalf of the Victorian Brown Coal Council.

In this Brown Coal Evaluation Programme a sampling philosophy was adopted that would highlight the natural variability of the coal and indicate the range of coal qualities which may be encountered during mining and utilization of the deposits.

The programme commenced in the Latrobe Valley coalfields by sampling open-cut faces and 220 mm diameter bore cores and was later extended to include major coal deposits in Victoria. Lithotype logs were prepared using quarter core sections laid out to dry, and selected lithotype samples from each core were analysed for a variety of chemical, physical and petrographic characteristics and utilization parameters; 144 parameters in all. To date, a total of 219 coal samples have been analysed from three open cut faces and twenty 220 mm diameter bore cores, representing 11 coalfields throughout Victoria. Coal samples from a further six bores are presently being characterized.

The data generated from these analyses and tests was evaluated by statistical methods and correlation coefficients have been determined between all pairs of variables. Analysis of this data has revealed significant differences in the chemical properties of the coal from different fields and enables the selection of coal with specific properties for particular applications. Table 4 illustrates

some of these differences by showing the range of values determined for selected coal properties from 219 samples (11 coalfields). Typical values from the two open cut mines currently operating in the Latrobe Valley are shown for comparison. These differences in chemical properties between the different coalfields are generally more significant than lateral variations within a particular field (ie: between different bores within a field) and they are primarily related to rank.

5. EFFECT OF CHEMICAL PROPERTIES ON UTILIZATION

As a result of the Brown Coal Evaluation Programme, the understanding of the variability of Victorian brown coals and its implications for utilization have improved substantially. It has become apparent that certain chemical properties can have important consequences for utilization of the coal for power generation, liquefaction and other applications.

A number of examples will be briefly described -

Carbonate Formation During Hydrogenation

The formation of carbonate minerals during hydrogenation of low rank coals can cause serious operational difficulties in the reactor systems. A good correlation has been found between the calcium content of a number of Victorian brown coals and the carbonate formed during hydrogenation. However, the results indicated that cations other than calcium were involved in the formation of carbonate.

XRD analysis has revealed the presence of several different types of carbonate minerals in residues from a number of coals. Minerals identified included vaterite and calcite (two polymorphs of CaCO_3) dolomite ($\text{CaMg}[\text{CO}_3]_2$) and in the residue from a high sulphur (2.26% db) coal anhydrite, (CaSO_4) was identified. The types of mineral deposits formed depend not only on the coal but also on the reaction conditions. Our data indicates that whilst vaterite forms at low temperatures (380°C) as the temperature increases the vaterite becomes progressively converted to calcite, the more stable form. After further increases in temperature, particularly at long reaction times, dolomite begins to form.

The reaction to form anhydrite, in the case of the high sulphur coal, must compete for calcium with the formation of calcium carbonate, and this may have a beneficial effect.

Clearly the types of inorganic precipitates which form during hydrogenation of Victorian brown coal are dependent on the nature of the exchangeable cations and to some extent the available coal sulphur.

Sodium and Boiler Fouling

The concentration of sodium in coal is regarded as the most significant factor in the formation of troublesome ash deposits during combustion. Although Victorian brown coals are generally low in ash forming constituents, coals with a high proportion of sodium can form ashes which contain of large amounts of low melting point, sodium sulphate compounds. These are formed during combustion from the inorganic sodium and organic sulphur in the coal.

The sodium sulphate condenses on the surface of boiler tubes and together with fly-ash particles forms sticky deposits, which can consolidate on heating and lead to extremely dense hard-to-remove deposits. The presence of high sodium sulphate content ash thus requires special consideration during the design and operation of boilers.

Aluminium and Precipitator Ash

In some Victorian brown coals significant quantities of acid soluble aluminium are found. This is believed to be present as aluminium hydroxide which is dispersed throughout the water phase of the coal. During combustion of this coal the refractory aluminium oxide formed takes the shape of the relics of the plant material present in the coal, thus forming an extremely low density ash (approximately 100 kg/m³). Whilst the collection of these particles by electrostatic precipitation is possible, the problem of reentrainment on rapping has necessitated the use of larger sized units than would otherwise be required. It is therefore important to determine the acid soluble aluminium fraction in the coal to determine if precipitation of fly ash is likely to be a problem.

6. ACKNOWLEDGEMENTS

The authors wish to acknowledge the support of the State Electricity Commission of Victoria (SECV), the Victorian Brown Coal Council (VBCC), and the companies in the VBCC Industrial Participants Group. The associated drilling, logging and sampling activities were managed by the SECV's Geological and Exploration Division, and the analytical work was performed by the staff at the Herman Research Laboratory.

7. REFERENCES

1. Victorian Brown Coal Resource Development Study, Kinhill Pty Ltd. 9 Volumes. December 1982.
2. Kiss LT and King TN. Fuel 56, 340 (1977).
3. King TN, George AM, Hibbert WD and Kiss LT. Variation of Coal Properties with Lithotype Pt 2. SECV Report No. SO/83/55 (1983).

TABLE 1. **BED MOISTURE AND MOISTURE HOLDING CAPACITY FOR SELECTED VICTORIAN COALS**

<u>Coal Field</u> <u>(Selected Values)</u>	<u>Bed Moisture (As Received)</u>		<u>Moisture Holding Capacity</u>
	<u>Kg/Kg Dry</u> <u>Coal</u>	<u>Weight</u> <u>Percent</u>	<u>% (Equilibrium Moisture)*</u>
Yallourn-Maryvale	1.82	64.2	38.4
Morwell-Narracan	1.54	60.5	38.2
Loy Yang	1.63	61.9	42.1
Flynn	1.76	63.5	41.2
Yallourn North Ext	.98	49.5	41.2
Coolungoolun	1.19	54.4	35.0
Gormandale	1.27	56.0	39.0
Gelliondale	1.83	64.6	35.3
Stradbroke	1.41	58.4	37.1
Anglesea	.87	46.6	32.9
Bacchus Marsh	1.53	60.4	31.2

* Determined at 97% humidity and 30°C

TABLE 2.

**COMPARISON OF ASH CONTENT AND MINERAL MATTER FOR
SELECTED VICTORIAN BROWN COALS**

Coal Field (Selected Values)	% Ash, Coal Dry Basis		% Mineral Matter, Coal Dry Basis
	Determined	Calculated	
Yallourn-Maryvale	2.3	2.4	1.7
Morwell-Narracan	2.4	2.6	1.5
Loy Yang	1.0	1.1	0.8
Flynn	1.4	1.5	0.1
Yallourn North Ext	4.3	4.5	3.0
Coolungoolun	2.3	2.4	2.2
Gormandale	1.6	1.6	1.3
Gelliondale	5.8	5.8	3.4
Stradbroke	3.9	3.6	2.0
Anglesea	3.9	3.4	2.2
Bacchus Marsh	7.4	7.4	3.5

TABLE 3.

COAL-ASH CHEMISTRY : MORWELL OPEN CUT

Coal % Dry Basis		Laboratory		Ash%	Boiler Precipitator
Minerals					
FeS ₂	0.13	-	-	-	-
SiO ₂	0.19	SiO ₂	6.2		8.0
Al ₂ O ₃	0.04	Al ₂ O ₃	1.3		1.7
Inorganics					
Fe	0.32	Fe ₂ O ₃	17.6		22.7
Ca	0.70	CaO	32.0		41.2
Mg	0.24	MgO	13.1		16.8
Na	0.08	Na ₂ O	3.6		4.6
Cl	0.04	-	-		-
Organic S	0.25	SO ₃	26.1		5.0
Total Ash			3.1		2.6

TABLE 4.

**VARIATION IN SELECTED CHEMICAL PROPERTIES BETWEEN
VICTORIAN BROWN COALFIELDS**

Property	Yallourn Open Cut	Morwell Open Cut	Range of Values (219 Samples)	
Moisture (wt %)	66.4	60.2	43.7	- 71.0
Net wet specific energy (MJ Kg ⁻¹)	6.87	8.95	5.24	- 13.87
Ash (wt %)	1.3	3.5	0.5	- 12.8
Minerals and Inorganics				
(wt %, db)	1.3	2.7	0.3	- 12.8
Volatile Matter (wt%, dmif)	52.1	49.2	43.3	- 67.8
H/C Atomic Ratio	0.86	0.86	0.77	- 1.16
Oxygen (wt%, dmif)	26.2	24.2	17.4	- 30.0
Nitrogen (wt%, dmif)	0.52	0.62	0.36	- 0.85
Sulphur (wt%, dmif)	0.27	0.34	0.14	- 5.36
SiO ₂ (wt% db)	0.38	0.14	0.01	- 7.6
Calcium (wt% db)	0.04	0.74	0.01	- 2.07
Magnesium (wt% db)	0.18	0.23	0.02	- 0.85
Sodium (wt% db)	0.06	0.13	0.02	- 0.47
Iron - total (wt% db)	0.18	0.19	0.01	- 1.80
Phenolic - OH (meq/g)	3.72	3.70	1.91	- 4.44
-COOH (meq/g)	2.21	1.90	0.90	- 2.94
-COO ⁻ (meq/g)	0.49	0.59	0.03	- 1.66
dmif - dry, mineral and inorganic-free basis		db - dry basis		

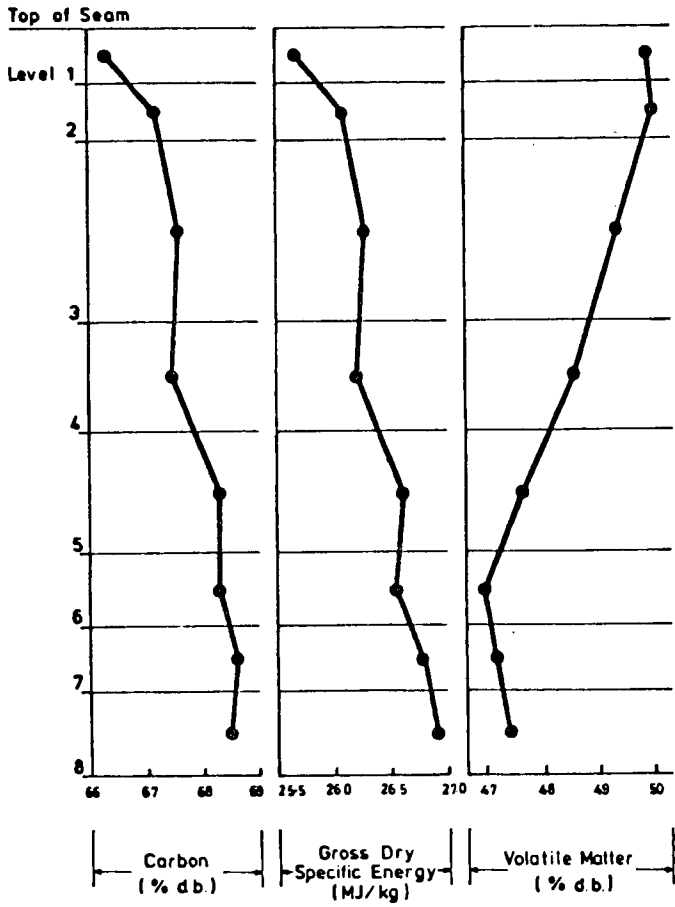


Fig. 1. Variation in selected coal properties with depth in the Morwell Open Cut.

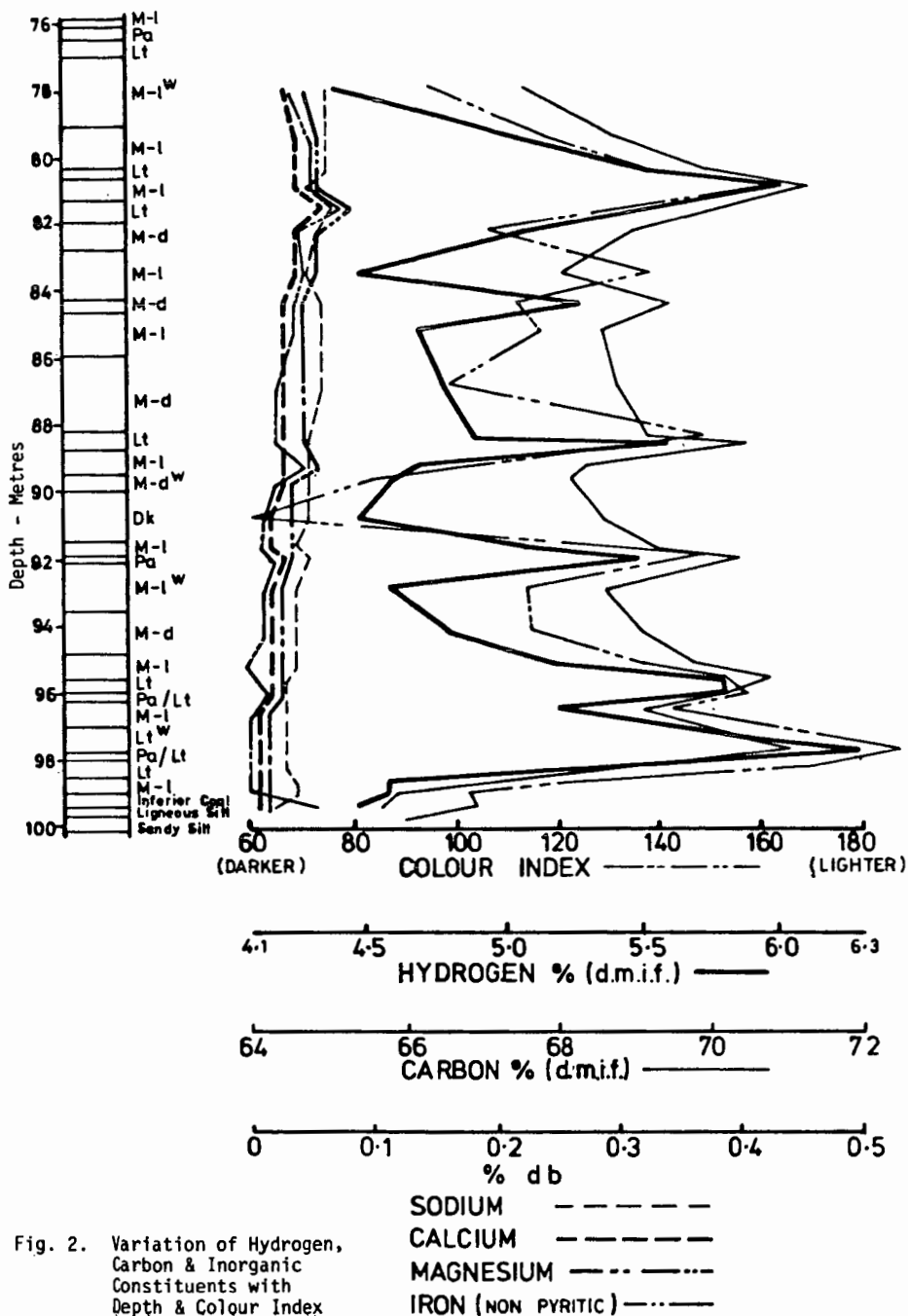


Fig. 2. Variation of Hydrogen, Carbon & Inorganic Constituents with Depth & Colour Index

Correlations between petrographical properties,
chemical structure and technological behaviour
of Rhenish brown coal

E. A. Wolfrum

Rheinische Braunkohlenwerke AG
Stüttgenweg 2
5000 Köln 41

Federal Republic of Germany

1. Introduction

The Brown coal reserves in the Federal Republic of Germany amount to approx. 56 billion metric tons, 55 billion metric tons of which are in the Rhenish brown coal district located west of Cologne (Fig. 1). About 35 billion metric tons of that reserve are considered to be technologically and economically mineable today what, in terms of energetics, equals the overall oil reserves of Iran (1).

Rhenish brown coal is mined in five opencast mines (Fig. 2) with an average depth of about 280 m. Modern mining equipment having a daily capacity of some 240,000 m³ of brown coal and high-speed belt conveyor systems are used. About 119 million metric tons of brown coal were mined in 1981.

84.5 % of that output was used for power generation, 7.9 % for briquette production in 4 briquetting plants of the Rheinische Braunkohlenwerke and 4.2 % for powdered brown coal production in two grinding mills. A low portion, viz. 0.3 % was used in a Salem-Lurgi rotary hearth furnace to produce about 96,000 metric tons of fine coke in 1981. 2.7 % of the brown coal output was used for other purposes, inter alia in test plants for processes, like gasification and hydrogenation (Fig. 3).

Longt-term mining plans ensure that this source of energy will be available in sufficient quantities well beyond the turn of the millennium.

This calls for opening up the deep-seated seam horizons as it is being done for the first time with depths of 240 to 450 m at the Hambach mine which is now developed. Today's technology allows opencast mines with a maximum depth of 600 m to be operated.

Mining in greater depths leads to a change of the geotectonic conditions and hence a natural change in the brown coal quality characteristics.

This has varying and graduated effects on the individual refining processes (2).

The petrographical and chemical investigations presented in the following were carried out in order to describe the behaviour of the coal types characteristics of the Rhenish brown coal area during refining processes.

As an introduction, a short survey of the geological conditions of the Rhenish brown coal deposit is given.

2. Geological conditions in the Rhenish brown coal district

In geological terms, the deposit is part of the Lower Rhine Basin extending over about 2,500 km² which was formed by a subsidence in the Early Tertiary. Brown coal itself was formed about 15 to 20 million years ago in the Miocene; during millions of years it was repeatedly flooded with sea or river water and covered with sands, clays and gravels.

The geological profile from NE to SW across the southern part of the Lower Rhine Basin (Fig. 4) shows that the brown coal seams sank down to ever growing depths towards the southwest and then rose again from their deepest point below the Erft river towards the west. Tectonic events caused faults and fractures of several hundred meters.

Accounting these geological conditions, the opencast mines - following the seam - have to operate in ever growing depths.

Therefore selective mining for refining purposes is getting more and more expensive.

3. Structure and composition of Rhenish brown coal

Rhenish brown coal consists of a variety of lithotypes which are discernible in the coal seam already by brightness variations (Fig. 5).

Recent pollen analytical investigations proved that the bright and dark layers result mainly from changing conversion and decomposition conditions. The bog facies has only a limited influence.

The gradation from dark to bright layers reflects the degree of brown coal destruction (3.4).

Figures 6 to 8 show three different types of coal, viz. a bright unstratified coal, a medium-dark stratified coal and a dark heavily stratified coal. The high degree of decomposition of the lithotype represented in Figure 6 indicates an aerobic formation while the high-texture fibrous coal (Fig. 8) is an indicator of an anaerobic formation.

The discovered textures are above all gymnosperms represented by highly resistant coniferous woods which account for a quantity overproportionate to their share of the mainly angiospermous vegetation which formed brown coal.

Only a model can establish the complex, heterogeneous structure of brown coal.

Figure 9 shows a model that inter connects the various structural components, namely lignin, humic acid and

aromatic structural elements. High content of functional groups causes high reactivity. Figure 10 shows how oxygen-containing functional groups are distributed in the Rhenish brown coal.

3.1 Macropetrographical characterization

Based on macropetrographical criterias 15 brown coal lithotypes were selected for the investigations described in the following; they represent more than 90 % of the main seam.

Figure 11 shows these 15 brown coal lithotypes arranged according to stratification an texture.

The coal can be subdivided into 3 groups depending on the mode of stratification: unstratified, slightly stratified and heavily stratified.

The brightness tends to abate from unstratified to heavily stratified coals.

3.2 Micropetrographical characterization

Micropetrography evaluates the coal components ascertainable by microscopy. Figure 12 shows an extract of the results obtained from the combination analysis of the 15 brown coal lithotypes.*

Obviously the investigated brown coal lithotypes differ in micropetrographic respect.

*We thank H.W. Hagemann, PhD., member of the faculty of geology, geochemistry and oil and coal deposits of the Aachen technical university for having carried out the investigations.

Based on the qualitative assignment of the individual coal components, rhenish brown coal can be divided into four groups having similar petrographical properties which, correspond with the macropetrographical features (principle of classification: stratification and texture). This classification into 4 groups differs only negligibly from the macropetrographical division into three main groups.

The classification into four main groups results in the correlations shown in the following Figures. Figure 13 shows the liptinite content as a function of the group classifications 1 to 4. With rising group number, corresponding to stronger stratification and texture, the liptinite content declines. Figure 14 which shows the huminite as a function of the group numbers indicates that the huminite content rises with increasing stratification and texture.

These two correlations stand for a variety of functions of technological relevance between brown coal maceral groups.

3.3 Chemical and physical composition

Subsequent to the petrographical coal analysis, both a chemical and a chemo-physical investigation were carried out. Figure 15 shows the chemical and physical properties of the investigated brown coal lithotypes.

Rhenish brown coal has an average ash content of about 4 % (wf), a volatile matter of about 52 % (waf) and a lower heating value of 11.000 Btu/lb of coal (waf). The final analysis of the coal under waf conditions shows the following average composition:

69 % carbon, 5 % hydrogen, 1 % nitrogen and approx. 25 % oxygen; the sulphur content amounts to about 0.35 % (waf) about 50 to 70 % of which is bound to the ash during the combustion process since approx. half of the mineral components of Rhenish brown coal consist of basic alkali and alkaline earth compounds - primarily those of calcium.

The following investigations were aimed at revealing correlations between the chemical and chemo-physical coal data and the petrographical analysis that may help assess the coal quality prior to its use as a feedstock in various refining processes.

4. Correlations between petrographical structure, chemical composition and refining behaviour of Rhenish brown coal

The correlations between the chemical brown coal data, petrographical parameters and the refining behaviour are described in the following complex regression calculations therefore were carried out. Statistic calculation methods were applied as an objective criterion to prove such correlations.

To nearly all brown coal refining processes is applicable that

- the quality of the desired refinement products
- the refining cost
- the quality of the raw material

have a direct correlation. Hence, it is indispensable for any refining operation to know and assess the composition of the raw material and its behaviour during the refining process.

The usability of the results obtained from the raw material characterization in everyday practice depends on

- the spacing of drillings usable for quality assessment
- the level of geological knowledge of the coal forming conditions
- a representative sampling in the opencast mine, taking into account the cutting geometry of the excavator (position of the excavator cuts to the deposit), the fast mining advance and the high mass flow involved.

4.1 Correlations between chemical and petrographical parameters

4.1.1 Heating value

Figure 16 shows that the heating value declines with increasing coal stratification. A comparison of the heating value of coal and its hydrogen content in Figure 17 indicates that according to expectation the heating value of the coal rises parallel to an increase in its hydrogen content. This again is due to the portion of hydrogen-rich minerals, such as liptinite, declining in the said order - a correlation clearly evident in Figure 18. The heating value of the coal obviously rises in proportion to its liptinite share. The oxygen-rich lignitic coal components, such as huminite, have the opposite effect on the heating value: Figure 19 shows that the heating value of the coal is down sharply with an increase in the portion of this maceral group.

4.1.2 Volatile content

The individual coal constituents contribute different shares to the volatile matter of the coals (5). With increased stratification, the volatile matter decreases, caused by the respective distribution of the various maceral groups. Figure 20 gives an example how the content of volatile matters and that of the hydrogen-rich liptinite maceral correlate. It is obvious that this constituent contributes a lot to the volatile matters.

4.1.3 Hydrogen content

Figure 21 shows that also the hydrogen content is closely corresponding to the petrographical brown coal properties. Figure 22 shows the correlation between the hydrogen content and the Lipto-Humodetrite and/or the Humo-Telinite content of the investigated lithotypes. A higher amount of Lipto-Humodetrite leads to an increased hydrogen content. The content of the Humo-Telinite maceral, however, has a totally different effect: This component has a high portion of oxygen-rich molecular groups what causes the hydrogen content of the brown coal to drop.

4.2 Correlations between coal quality and refining behaviour

4.2.1 Briquetting and coking

There are many investigations and publications available on the briquetting behaviour of brown coals, both from the GDR and the Rhenish area (6 to 9).

In order to establish statistically usable data on the briquetting behaviour of Rhenish brown coals, the 15 brown coal lithotypes were briquetted under identical conditions with a laboratory press (water content, grain size distribution and mould pressure).

For assessing the briquettability of these coals, a number of briquetting parameters were correlated with the petrographical properties of the brown coal types. A statistic evaluation of these briquetting parameters and the micropetrographical composition of the coals reveal only a minimal degree of interdependence. Figure 23 clearly shows that the Humo-Telinite content stands for the height and volume expansion of the briquettes.

The briquetting expenditure is related to the Telo-Humocollite content. The definition factor (r^2) varies between 0.58 and 0.67; and is comparatively low. All the other correlations between the briquetting parameters (e.g. diametrical expansion) and the petrographical coal composition turned out to be rather insignificant so that they need not to be taken into consideration.

These investigations on correlations established between the raw material properties and briquettability of Rhenish brown coal led to the following results:

1. A macro- and micropetrographical analysis with a view to technological problems involved in the briquetting process allows at the most to judge the briquettability of Rhenish brown coal on the basis of trend data.
2. A correlation analysis of the chemo-physical parameters of Rhenish brown coal and its briquettability gives only trend data as well.

Therefore generally an anticipated quality assessment of the briquettes is restricted to the following points:

1. Macropetrographical assessment of the coal seam and evaluation of the briquettability on the basis of values gained by experience.
2. Laboratory production of briquettes and determination of their pressure resistance.
3. Determination of the ash content as an essential factor for the assessment of brown coal briquettability. Ash contents exceeding 3 to 4 % result both in a reduction of the resistance to pressure and a high wear of the molds of the briquetting presses, and are not suited to be processed into briquettes. Gelled coals, unsuitable for briquetting purpose as well, are used as steam coal.

Coking

Numerous publications (10 to 12) have been made above all in the GDR on the required quality properties of brown coal and their influence on the quality characteristics of formed coke. Since the Rheinische Braunkohlenwerke AG does not consider formed coke production at present, raw material quality and coking behaviour are of interest only for the production of fine coke using the rotary hearth furnace principle (13, 14) (Fig. 24).

This technology is dependent only to a low extent on the specific raw material composition. The petrographical factors of the feedstock have an impact above all on grain size and grain size distribution. It is not the final coke strength that is crucial for this process but the grain spectrum caused by grain decomposition.

Correlations so far unknown may lie in the petrographical composition of brown coal (in connection with the mineral composition) and the reactivity of fine coke to oxygen. Therefore, an anticipated quality assessment of feed coals corresponds to that used for briquetting coal.

4.2.2 Gasification

Two gasification processes under development, namely gasification using oxygen (HTW) and hydrogasification; (HKV), helped to study the gasification behaviour of various brown coal lithotypes (15).

The reactivity of the residual char is the speed-controlling factor for brown coal hydrogasification (16). Laboratory-scale investigations on the gasification behaviour of various types of brown coal coke showed that the mode of pretreatment has a greater influence on the gasification process than the raw material properties. To give an example, helium flushing of the coke under gasification temperature has a very favourable effect on gasification.

With one exception only, gasification rates close to 100 % were achieved.

Differences in gasification speeds are due to the heterogeneous pore structure and the inhomogeneous iron distribution in the coal matrix.

Irregularly localized iron groupings contained in cokes of the lithotypes 1 and 8 show a varying reactivity behaviour.

Cokes of the lithotypes 4, 5, 9, 11, 13 and 15 with similar gasification behaviours have a comparatively homogeneous distribution of all ash components (Fig. 25). No correlation was established between the maceral composition and the reactivity behaviour of the cokes (17).

As it was the case with the mentioned hydrogasification process, the results obtained with HTW gasification did not show any statistically significant correlations between the petrographical composition of the lithotypes and their gasification behaviour.

4.2.3 Liquefaction

To determine potential raw material impacts on brown coal hydroliquefaction, the 15 lithotypes were converted into liquid products using various techniques (18).

1. moderate indirect hydrogenation with tetralin as a hydrogen-transferring solvent
2. direct hydrogenation with hydrogen and different catalysts similar to operational conditions.

- Indirect hydrogenation with tetralin

Indirect hydrogenation using tetralin at a reaction temperature of 410 °C, a pressure of 400 bar and an overall reaction time of 2 h produced carbon conversion rates from 50 to 79 (%wt) and liquid product yields from 43 to 69 (%wt). Of the multitude of correlations established between the results of the hydrogenation tests and the micropetrographical composition of the coal types only a few examples are given.

Figure 26 shows the product yields of indirect brown coal hydrogenation with tetralin as a function of stratification and texture (lithotype number). It is obvious that with increasing stratification and texture, i.e. with rising lithotype number, the liquid product yield drops and the portion of hydrogenation residue increases. Regarding the fine structure of the coal the following correlations turn out:

Figure 27 represents the carbon conversion rate as a function of the liptinite and huminite maceral portions. It can be seen that an increase in the hydrogen-rich liptinite constituent improves carbon conversion while the oxygen-rich huminite reduces the carbon conversion rate. These trends also apply to the yield of liquid products. It should be pointed out again that it is only possible to give trend data. Quantitative assignments are impossible since the statistical certainty is insufficient.

- Direct hydrogenation with molecular hydrogen and catalyst

The influence of the raw material was expected to weaken using hydrogen and a catalyst under the conditions similar to those in the real hydroliquefaction process. An increase in the carbon conversion rate up to a maximum of 96 (%wt) shows that both brown coals with high or low carbon-to-hydrogen ratios achieve high product yields. Plain impacts of the raw material on the liquefaction results are no longer observed.

Resuming it can be said that the hydrogenation degree from indirect to direct hydrogenation rises parallel to an increase in carbon conversion. The result is that nearly all brown coal types mineable in the Rhenish area can be converted into liquid products with high yields. Hydrogenation process engineering, i.e. the optimization of the reaction conditions (temperature, pressure, residence time, catalyst type), is considered with priority over the raw material properties.

The investigations showed that in general practice no importance is attributed to a micropetrographical assessment of the coal types as a criterion for selecting specific brown coals from the Rhenish area. Tar content and/or low-temperature carbonization product yield and paraffin content suffice as parameters to assess the hydrogenatability of Rhenish brown coals. For exploratory drilling programmes, these parameters are determined separately. In general, brown coals from various areas that meet the quality parameters given in Figure 28 have satisfactory hydrogenation properties.

5. Summary

For the purpose of an assesement with a view to refining, the petrographical, chemical and physical properties of lithotypes of Rhenish brown coal were established and compared with one another.

The investigated coal typs cover more than 90 % of the coal types proved in the Rhenish deposit. A correlation of the results shows a describable, sometimes multidimension al dependancy.

A comparison of raw material properties and the results of the technical experiments quickly reveals the limits set to such an approach.

Out of all the refining processes subjected to investigation briquetting places the highest requirements on the raw material properties. The major part of the established parameters leads only to qualitative indications of the briquetting properties of the coals. Parameters of greater significance can hardly be utilized in practice. What remains in the experience gained by coal technologists, is the determination of the classical coal properties and indications from laboratory briquetting.

For the gasification process no usable quantitative relations were established between the petrographical coal properties and the gasification behaviour. It is possible without any material problems to convert nearly all the Rhenish coal types into gaseous hydrocarbons or synthesis gas.

This statement applies without any restriction to coal liquefaction as well. Apart from a few comparatively rare coal types, all brown coals from the Rhenish area can be converted into liquid hydrocarbons with high product yields. Hence, hydrogenation process engineering, i.e. the optimization of the reaction conditions, has priority over the raw material properties.

Under the given conditions of the Rhenish brown coal deposit, an opencast mining operation, a high output and the large feed quantities required for future refining plants brown coal petrography is one out of many tesserae for quality assessment.

The development of appropriate modes of determining the quality characteristics of raw brown coal is a task indispensable for the future.

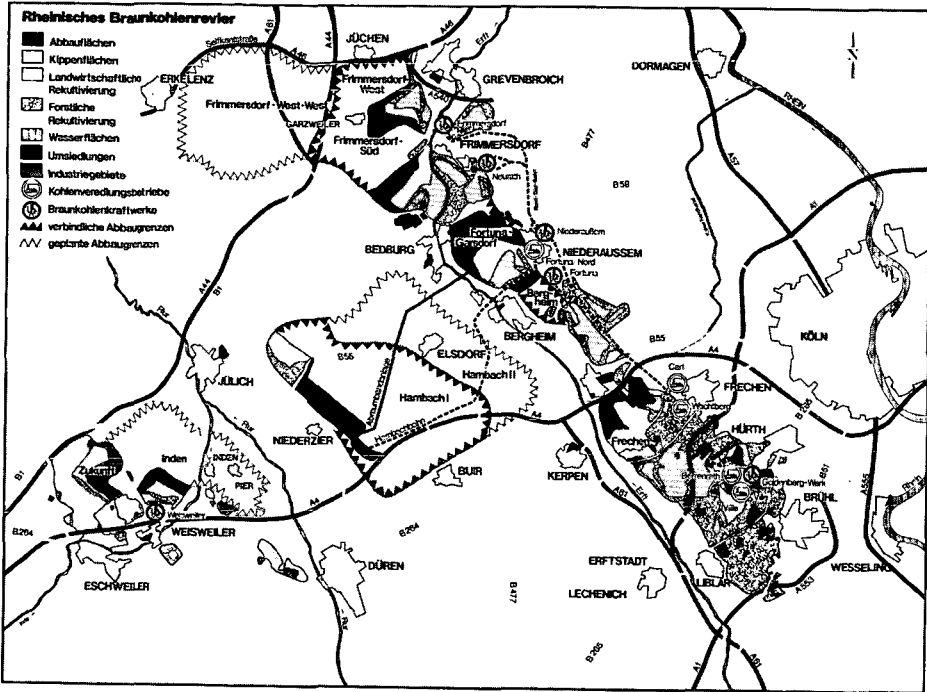
6) References

- 1) P. Speich:
"Technische und wirtschaftliche Gesichtspunkte der Braunkohlenveredlung"
Brennstoff-Wärme-Kraft 32 (1980) Nr. 8, 307-312
- 2) E. Wolfrum, J. Wawrzinek:
"Beziehungen zwischen petrographischen und chemischen Eigenschaften Rheinischer Braunkohle"
Braunkohle Heft 11/81, 381-386
- 3) G. von der Brelie, M. Wolf:
"Zur Petrographie und Palynologie heller und dunkler Schichten im rheinischen Hauptbraunkohlenflöz"
- Fortschr. Geol. Rheinld. u. Westf. (1981) 29; 95-163
- 4) H. W. Hagemann, A. Hollerbach
"Relationship between the macropetrographic and organic geochemical composition of lignites"
- Advances in organic Geochemistry 1979,
A. G. Douglas, J. R. Maxwell (Editors)
Pergamon Press Oxford, New York, Frankfurt
- 5) R. Kurtz, E. Wolfrum, W. Assmann:
"Die Verkokungseigenschaften chemischer Stoffgruppen in einigen Braunkohlentypen des rheinischen Reviers"
Comm. Eur. Communities, Rep EUR 1977
EUR 6075, Round Table Meet. Chem. Phys. Valorization Coal,
125-150
- 6) E. Sontag, M. Süss:
"Beispiel petrologischer Untersuchungen zur Klärung rohstoffabhängiger verfahrenstechnischer Probleme der Braunkohlenveredlung"
Bergbautechnik 19 (1969) 5. 255-260:7. 376-381

- 7) R. Kurtz:
"Zusammenhang zwischen mikropetrographischem Aufbau der Weichbraunkohlen und ihrer Brikettierbarkeit"
Dissertation, RWTH Aachen, Fakultät für Bergbau und Hüttenwesen (1970)
- 8) E. Rammler:
"Zur Kenntnis der Brikettierbarkeit von Braunkohle"
Freiberger Forschungshefte A99 (1958), 81-104
- 9) H. Jakob:
"Neuere Ergebnisse der angewandten Braunkohlenpetrologie"
Berg- und Hüttenmännische Monatshefte 105, Heft 2 (1960), 21-29.
- 10) E. Rammler, G. Bilkenroth:
"Zur technischen Entwicklung der Braunkohlenkokerei"
Freiberger Forschungshefte A 184 (1961) 85 - 113
- 11) E. Rammler, W. Fischer, G. Hänseroth:
"Schrumpfverhalten von Braunkohlen Feinstkornbriketts bei der Verkokung bis 1000 °C"
Freiberger Forschungshefte A453 (1968), 121-145
- 12) W. März:
"Untersuchungen zum Verlauf der Verkokung von Braunkohlenbriketts, insbesondere bei der Spülgasverkokung"
Freiberger Forschungshefte A375 (1966), 79-99
- 13) R. Kurtz:
"Koksherstellung aus Braunkohle"
Braunkohle Heft 11, Nov. 1975, 352-356.
- 14) E. Scherrer:
"Herstellung von Braunkohlenkoks im Salem-Lurgi-Herdofen"
Braunkohle Heft 7, Juli 1981, 242-246.

- 15) H. Teggers, K.A. Theis, L. Schrader:
"Synthesegase und synthetisches Erdgas aus Braunkohle"
Erdöl und Kohle-Erdgas ver. mit Brennstoff-Chemie Bd.35,
Heft 4, April 1982, 178-184
- 16) L. Schrader, H. Teggers, K.A. Theis:
"Hydrierende Vergasung von Kohle"
Chem.-Ing.-Tech. 52 (1980) Nr. 10, 794-802
- 17) M. Ghodsi, J.P. Lempereur, E. Wolfrum:
"Etude cinétique de l'hydrogénation directe des cokes de
différents lithotypes de lignite"
Vortrag gehalten auf der Internationalen Kohlenwissen-
schaftlichen Tagung, Düsseldorf 07. - 09.09.81
- 18) E. Wolfrum, J. Wawrzinek, W. Dolkemeyer:
"Einfluß der Rohstoffeigenschaften auf die Verflüssigung
Rheinischer Braunkohlen"
Vortrag gehalten auf der Internationalen Kohlenwissen-
schaftlichen Tagung, Düsseldorf 07.-09.09.81

Fig. 1 Rhenish Brown Coal District



Rhenish brown coal district

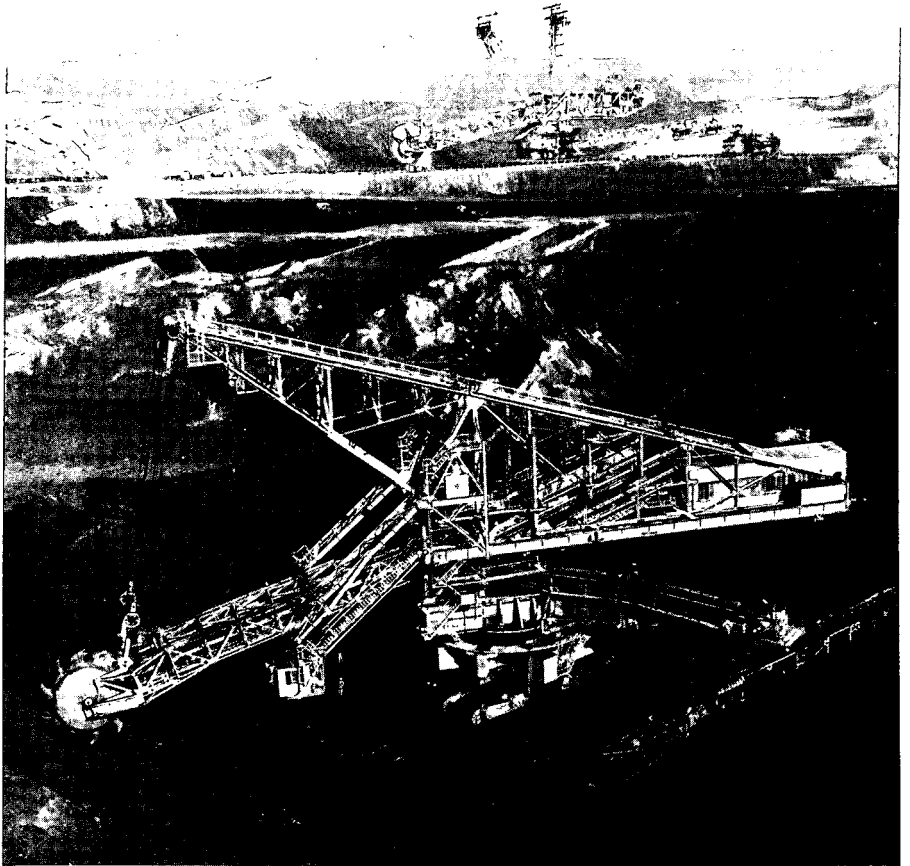
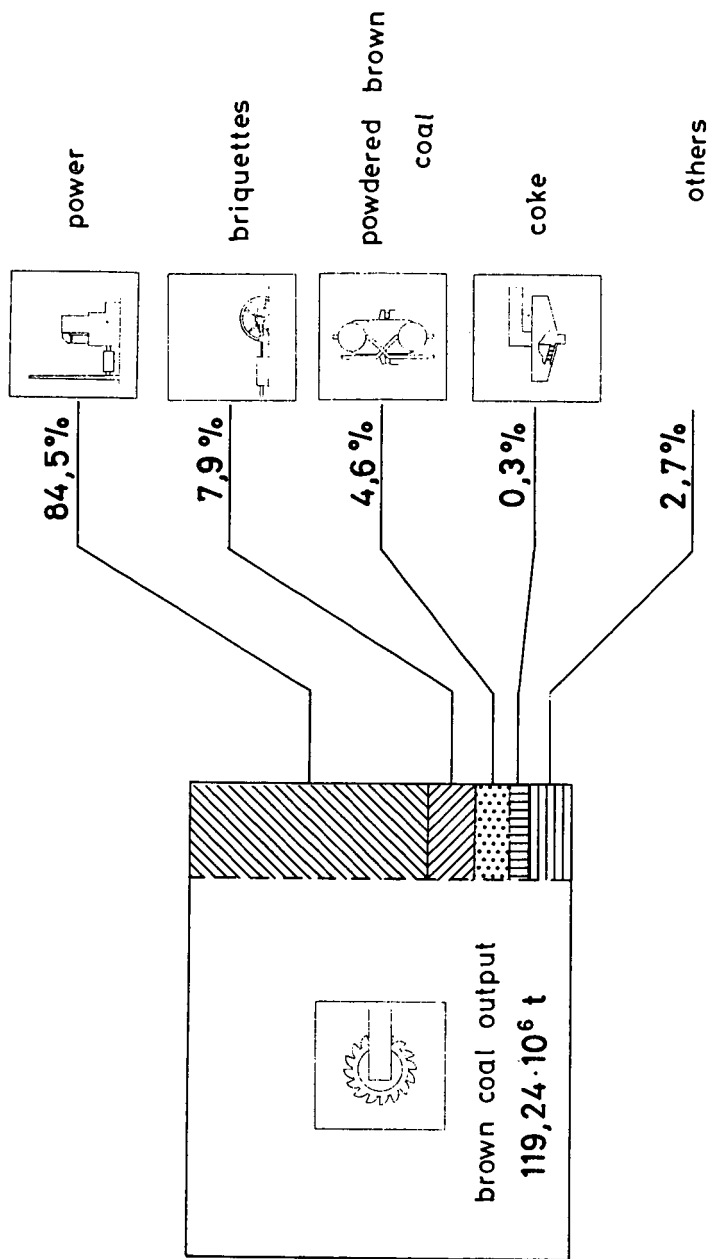


Fig.2 Excavator

Fig. 3



raw brown coal output and use
Rheinbraun 1981

RHEINBRAUN

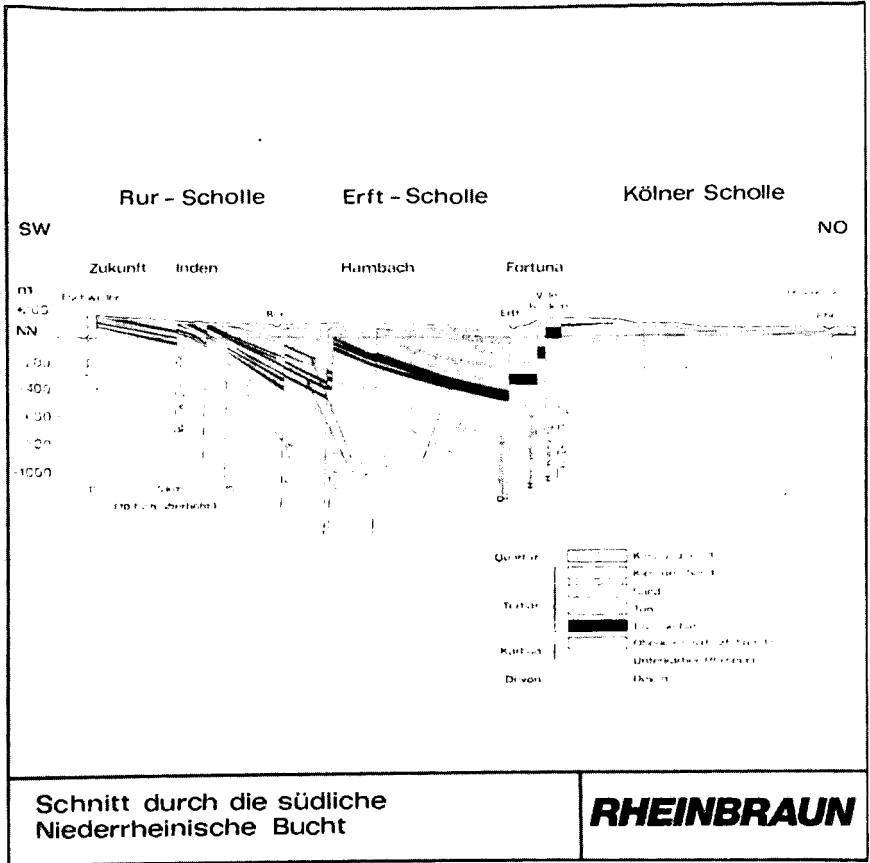


Fig.4 Geological profile

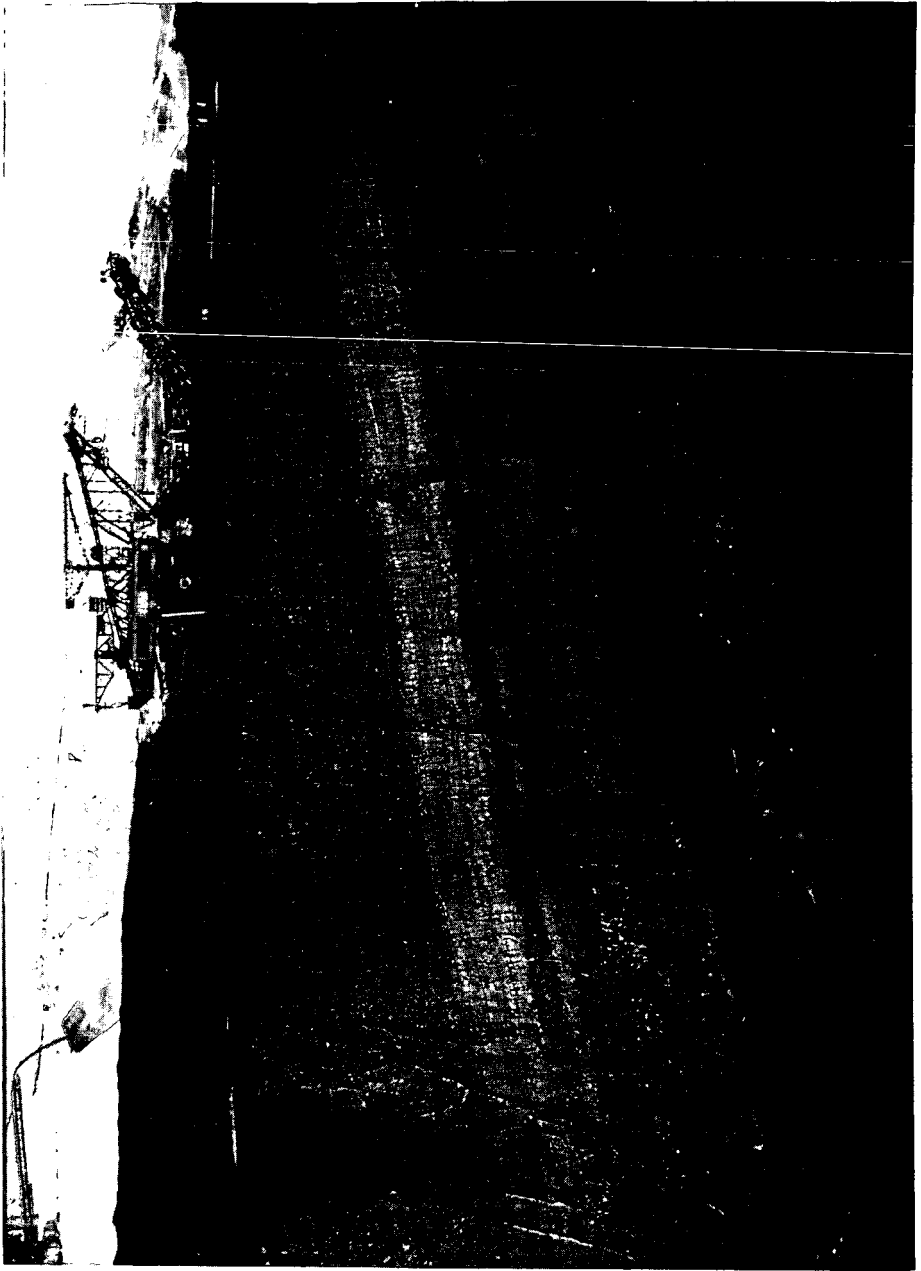


Fig.5 Brown coal seam

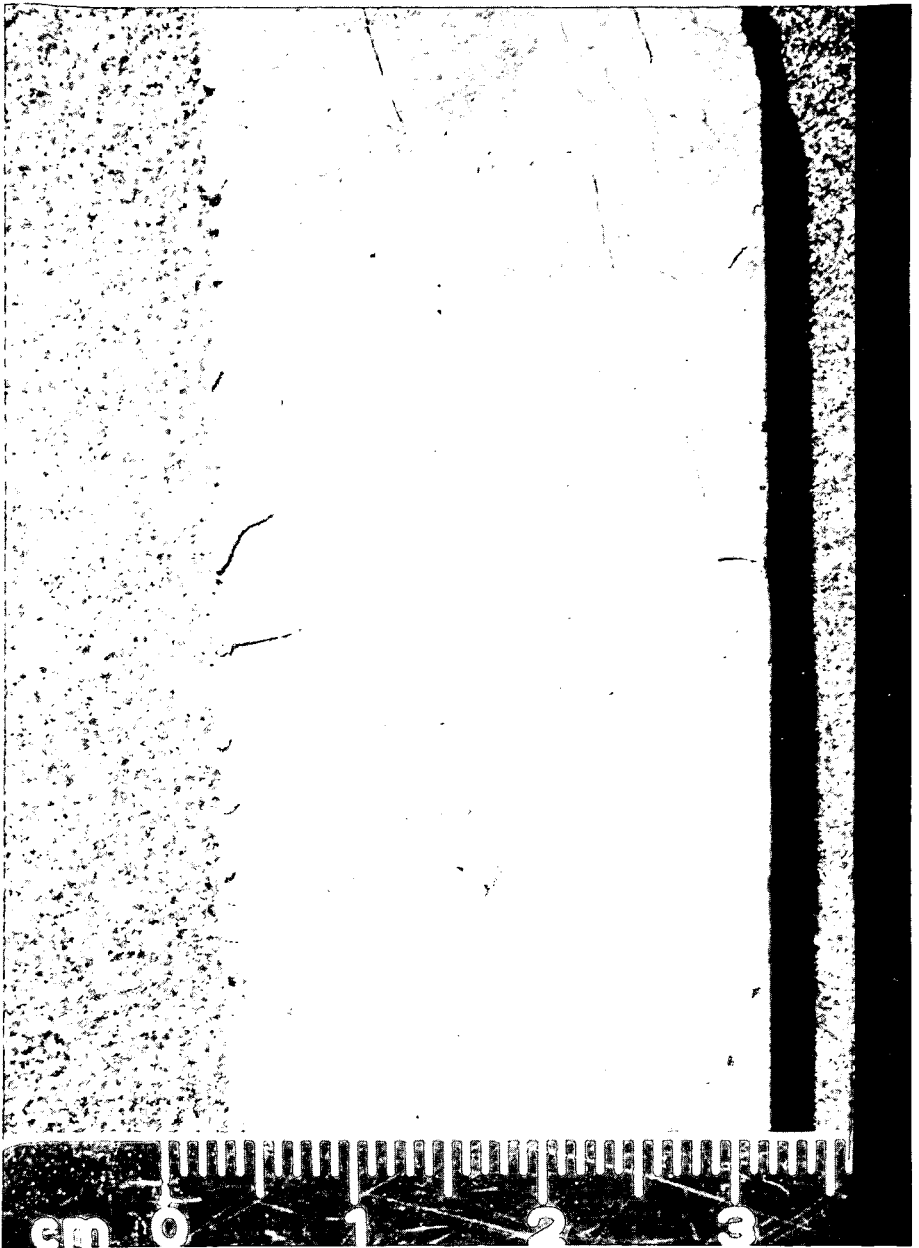


Fig. 6 Lithotype 1

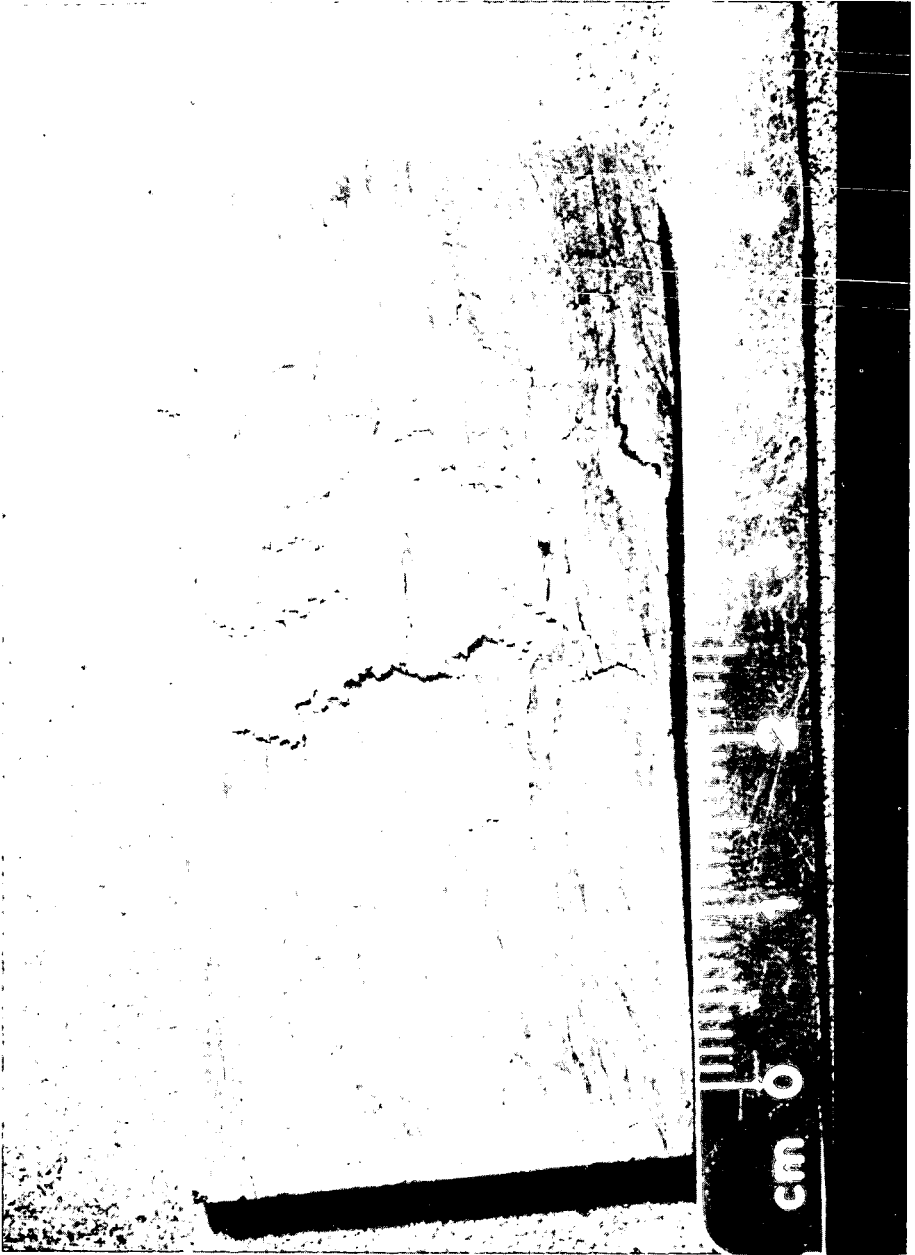


Fig. 7 Lithotype 9

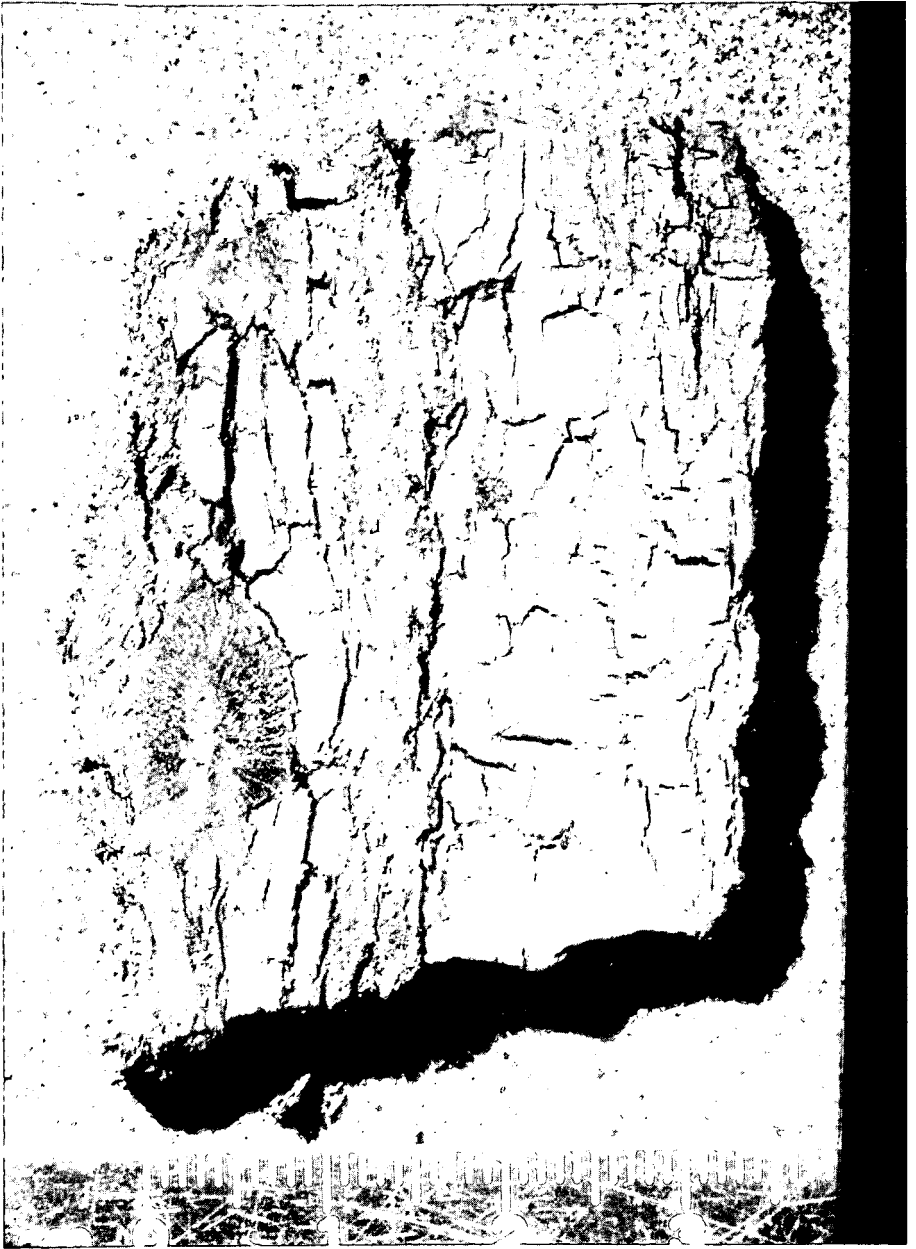
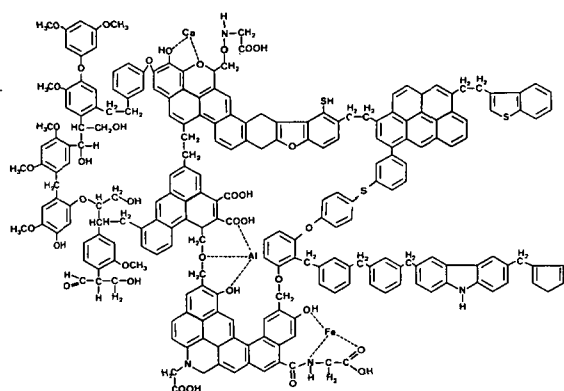


Fig. 8

Lithotyp 15

Fig. 9



lignin

humic acids

structural aromatic elements

Schematic composition of the brown coal structure

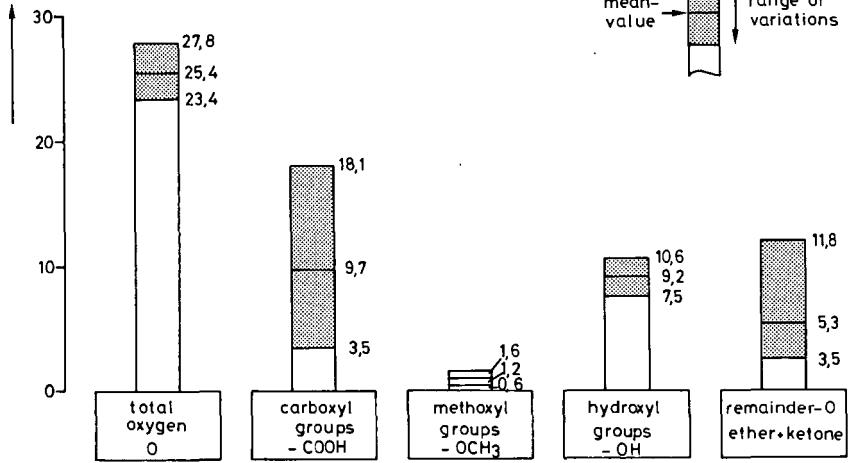
element	Rhenish brown coal (mat)
C	68,7
H	5,05
O	25,0
N	1,0
S (avg)	0,25

typical composition

elementary analysis

Fig. 10

oxygen(% wt)
reference: maf coal



Distribution of the oxygen-containing functional groups in Rhenish brown coal

RHEINBRAUN

Fig. 11

percentage of a seam section	sample no.	structure matrix / texture	brightness and colour	gelification rate accessory intercalations
4,2 %	1	unstratified coal	bright	xylite-and mineral-free, matrix
3,9 %	2	unstratified coal	dark	granular gelification nests, xylite
5,5 %	3	unstratified coal	medium-bright	xylite-containing
15,0 %	4	unstratified coal	medium-bright	slightly textured and xylite
12,8 %	5	unstratified coal	medium-dark	slightly textured, xylite, surface gel
7,8 %	6	unstratified coal	medium-bright	slightly textured, xylite-free
5,8 %	7	unstratified coal	dark	slightly textured, xylite, gel, fusite
18,5 %	8	slightly stratified coal	medium-bright	textured, xylite and resinous substance
9,2 %	9	slightly stratified coal	medium-dark	textured, xylite and bright texture
3,0 %	10	slightly stratified coal	dark	xylite and gelled, textured
5,7 %	11	slightly stratified coal	dark	textured, xylite and fusite nests
1,9 %	12	heavily stratified coal	medium-bright	sub. heavily textured, bright texture, resinous
2,5 %	13	heavily stratified coal	dark	heavily textured, xylite and fusite nests
2,2 %	14	heavily stratified coal	dark	heavily textured, xylite, gelled
2,0 %	15	fibrous coal	dark (black)	heavily textured, fusite texture

Macropetrographical classification of 15 brown coal lithotypes from the Rhenish area

RHEINBRAUN

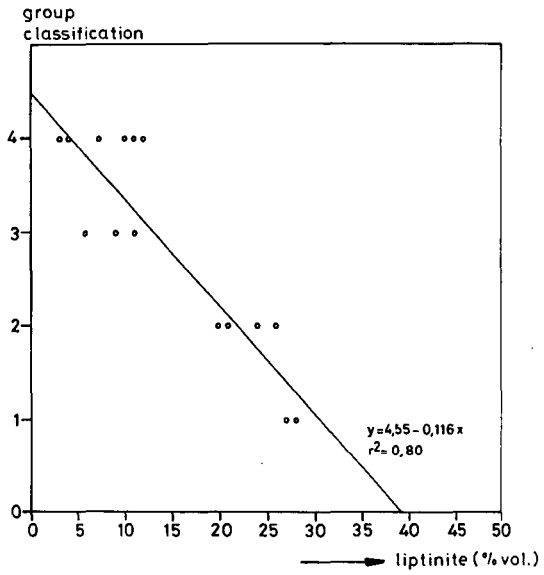
Fig. 12

maceral, maceral subgroup, lithotype	group no.	1	2	3	4
	lith. no.	1,2	7,3,4,6	5,10,8	14,15,11 13,9,12
Liptinite	% vol.	26 - 28	20 - 26	6 - 11	3 - 12
Humo-Detrinite	% vol.	56 - 59	54 - 58	31 - 43	12 - 31
Humo-Telinite	% vol.	3 - 5	10 - 17	26 - 33	34 - 50
Humo-Collinite	% vol.	6 - 7	3 - 8	19 - 26	17 - 31
Huminite	% vol.	67 - 69	72 - 79	87 - 92	80 - 90
Inertinite	% vol.	5	1 - 3	1 - 4	2 - 17
Lipto-Humodetrinite	% vol.	79 - 80	56 - 67	3 - 17	-
Telo-Humodetrinite	% vol.	3	21 - 30	8 - 15	10 - 30
Telo-Humocollite	% vol.	-	-	9 - 15	3 - 17
Detro-Humocollite	% vol.	-	-	3 - 7	3
Gelo-Humotellite	% vol.	3	3	10 - 12	10 - 39

Micropetrographical classification of 15 lithotypes into 4 groups

RHEINBRAUN

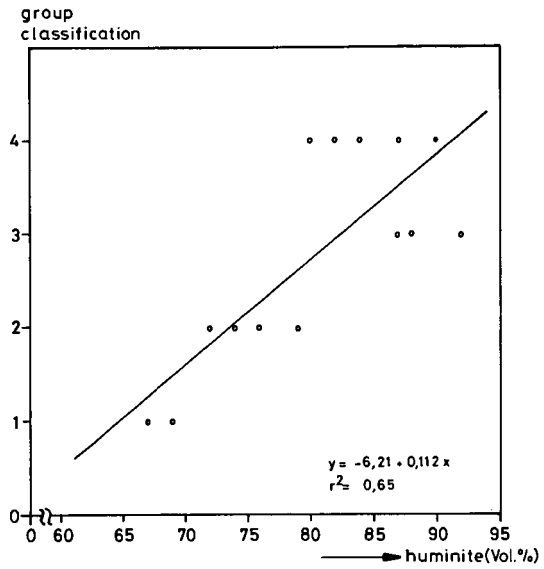
Fig. 13



Liptinite content as a function of micropetrographical classification

RHEINBRAUN

Fig. 14



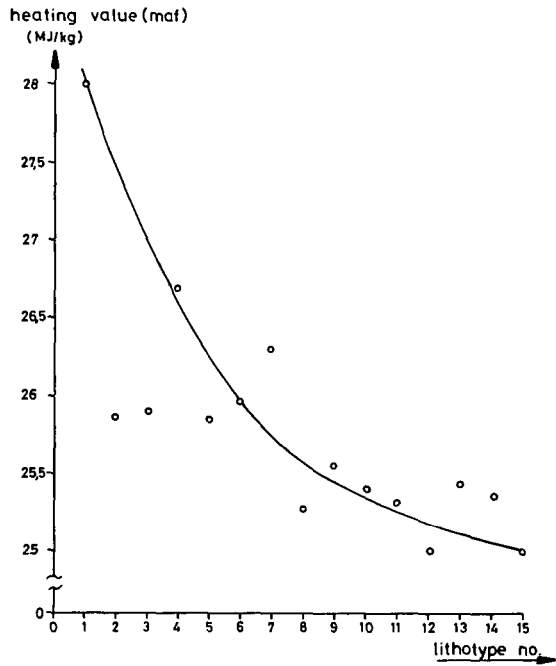
Huminite content as a function of
micropetrographical classification

RHEINBRAUN

Fig. 15

Lithotype no.			1	2	3	4	5	6	7	8	9	10	11	12	13	14	15
Short analysis																	
- brown coal (raw)	an	% wt	52,2	50,4	50,1	55,6	52,0	55,6	54,0	50,0	53,4	55,1	54,0	50,7	50,8	58,8	49,0
- ash content	ar	% wt	6,03	3,44	2,78	3,86	3,80	4,42	3,80	4,27	3,04	3,52	3,73	2,73	3,56	3,38	3,92
- volatiles	maf	% wt	59,69	55,25	55,11	54,70	52,42	52,09	51,91	52,98	49,65	49,79	49,36	53,72	51,74	51,77	49,79
- C-fix	maf	% wt	40,32	44,75	44,89	48,30	47,58	47,2	48,00	47,02	50,35	50,24	51,64	46,28	48,26	48,23	51,21
- heating value	maf	kJ/kg	27,99	25,87	25,89	26,69	25,85	25,97	26,30	25,27	25,55	25,43	25,31	24,96	25,43	25,36	24,98
Elementary analysis																	
- carbon	maf	% wt	86,6	87,5	87,8	88,0	88,2	89,3	89,6	89,7	89,5	89,4	89,9	87,4	88,3	87,4	89,0
- hydrogen	maf	% wt	5,89	5,60	5,24	5,59	5,19	5,21	5,25	4,71	5,10	4,92	4,96	4,91	4,79	4,88	4,91
Extraction analysis																	
- bitumen content	maf	% wt	12,87	12,25	10,86	12,04	8,78	7,43	8,86	7,28	7,10	6,40	9,18	7,20	9,65	5,11	7,31
- paraffin content	maf	% wt	10,19	9,46	9,00	10,00	4,83	5,53	7,48	6,00	5,77	3,93	6,90	5,90	8,20	4,19	3,18
* as received																	
Chemical-physical characterization of the brown coal lithotypes subjected to investigation											RHEINBRAUN						

Fig. 16

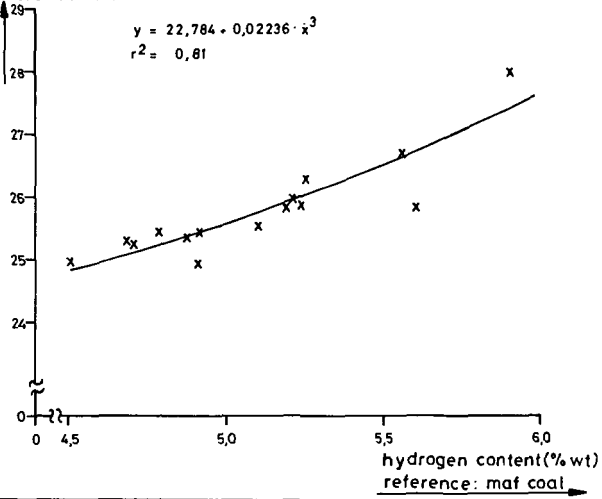


Heating value of the brown coal lithotypes
as a function of macropetrographical
classification

RHEINBRAUN

Fig. 17

heating value (MJ/kg)
reference: maf coal

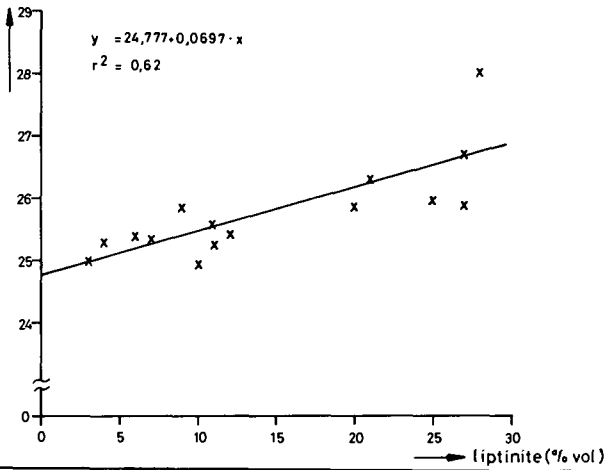


Correlation between the heating values and hydrogen contents of the 15 lithotypes investigated

RHEINBRAUN

Fig. 18

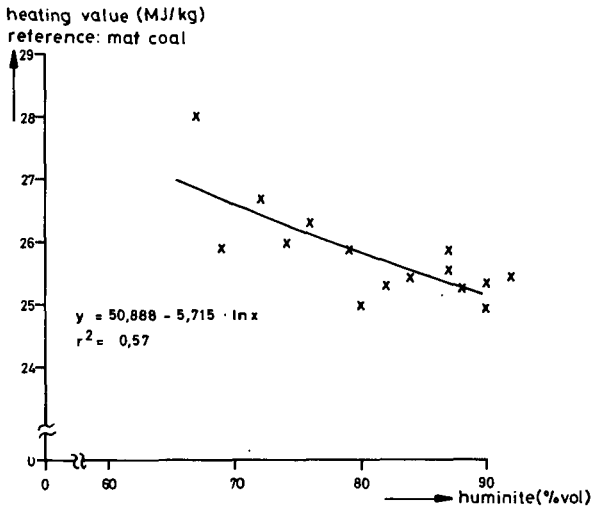
heating value
reference: mat coal



Heating value as a function of the liptinite content of the 15 lithotypes investigated

RHEINBRAUN

Fig. 19



Correlation between heating values and
huminite contents of the 15 lithotypes
investigated

RHEINBRAUN

Fig. 20

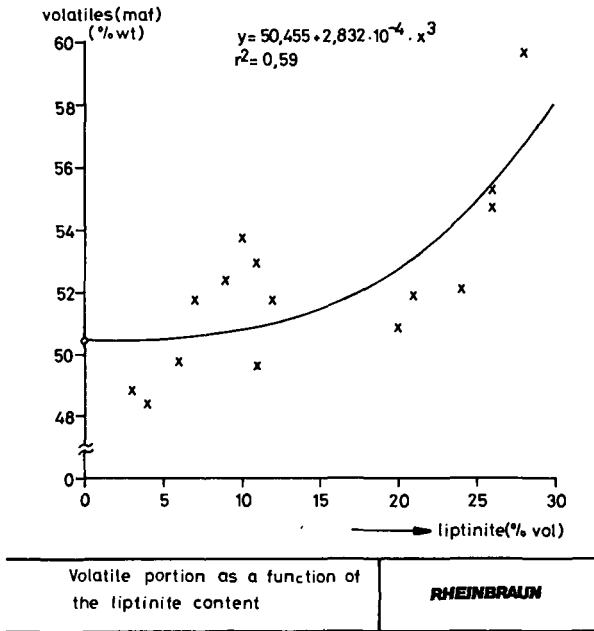
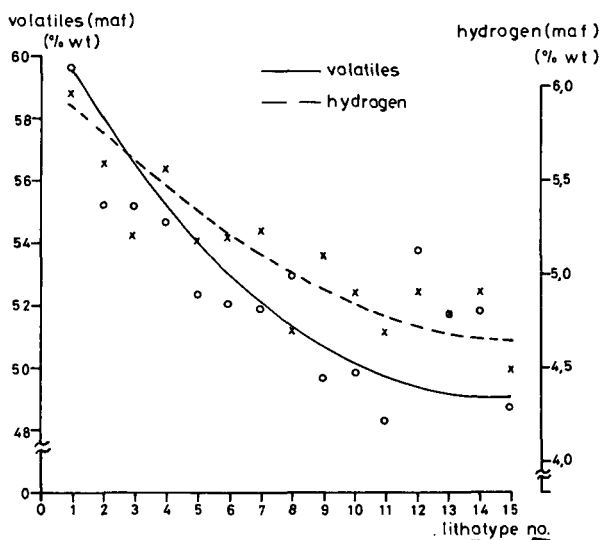


Fig. 21

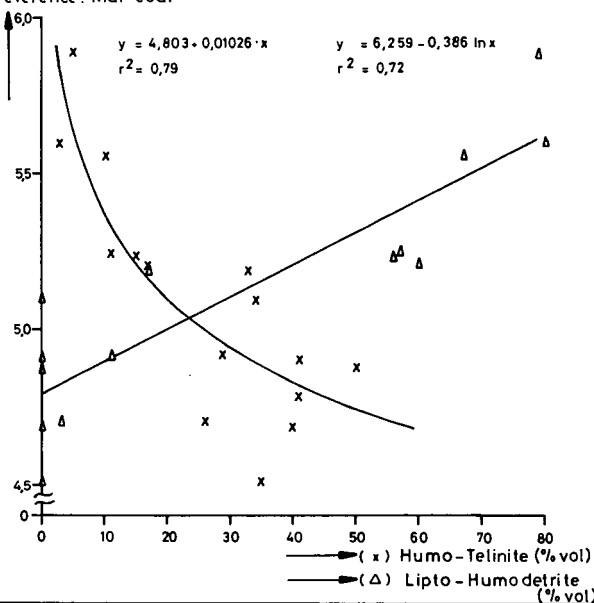


Correlation between volatile matters, hydrogen contents of the lithotypes and the macro-petrographical classification

RHEINBRAUN

Fig. 22

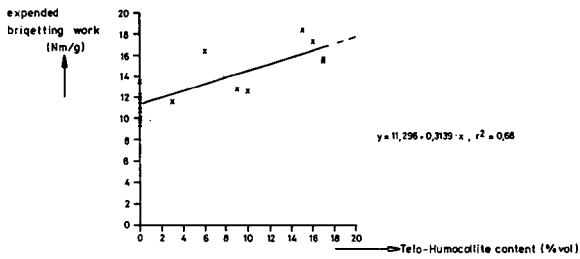
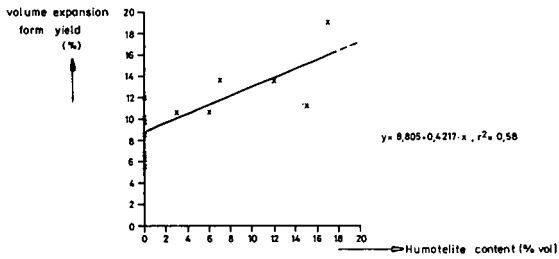
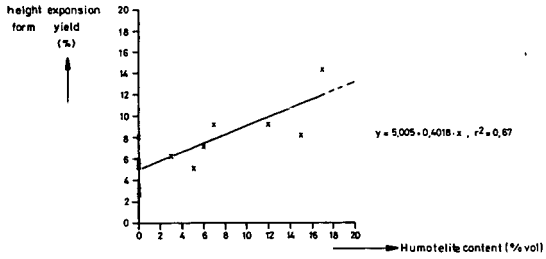
hydrogen content (% wt)
reference: maf coal



Correlation between hydrogen and Humo-Telinite
and Lipto-Humodetrinite portions

RHEINBRAUN

Fig. 23



Correlation between the contents of various microlithotypes and for subgroups and various briquetting results

RHEINBRAUN

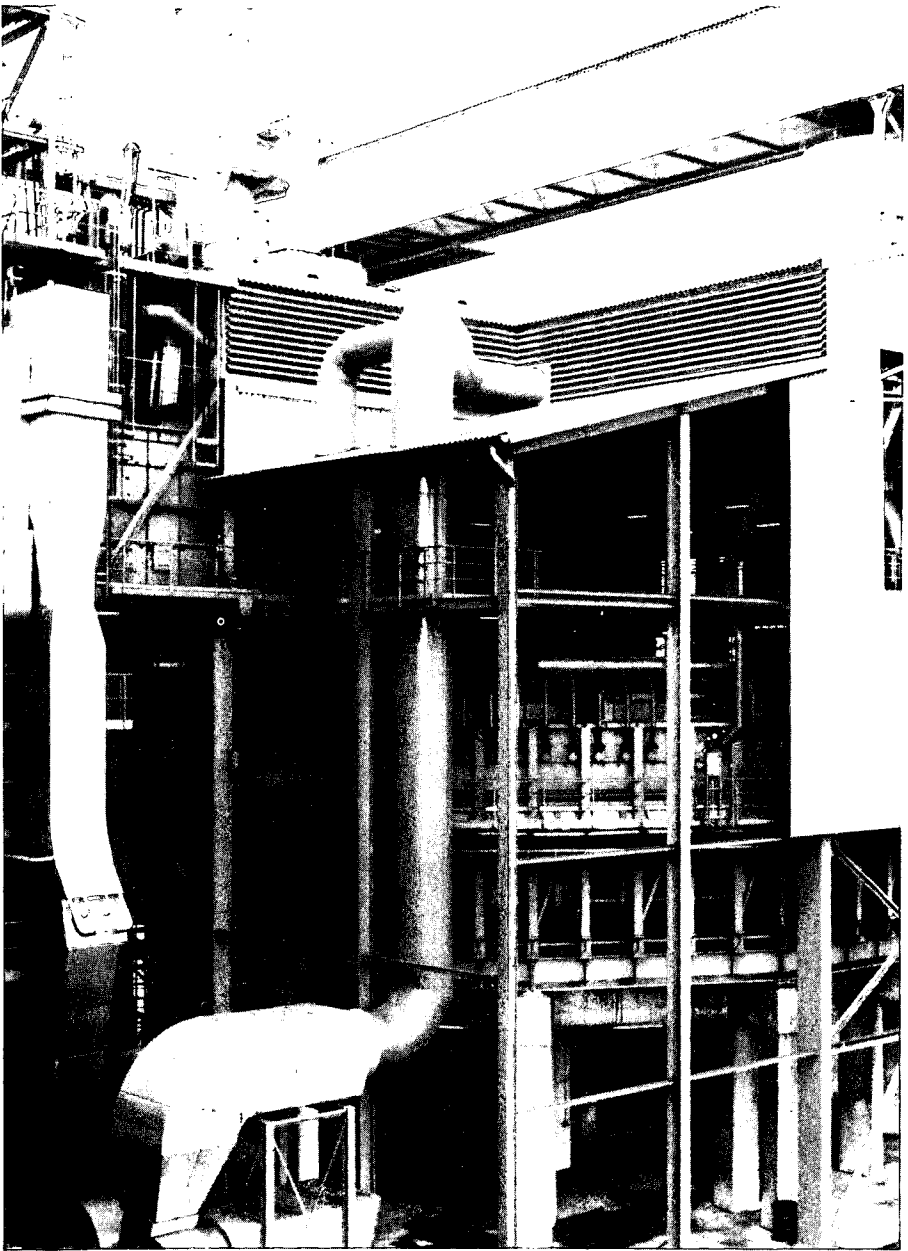
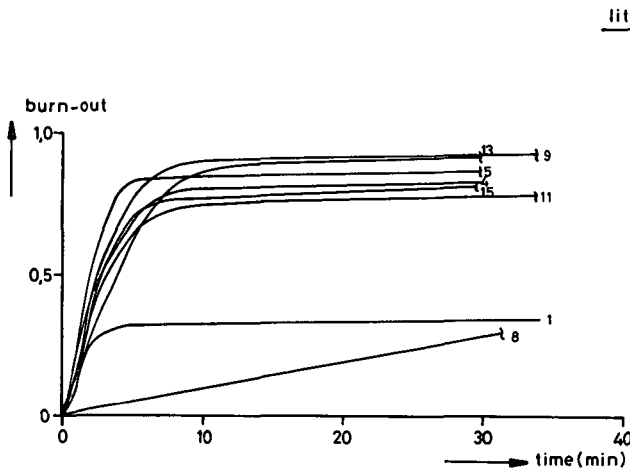


Fig. 24 rotary hearth furnace

Fig. 25

40 atm H₂ bei 900°C

Vorbehandlung: 1/2 h im Heliumstrom von 1 atm bei 900°C

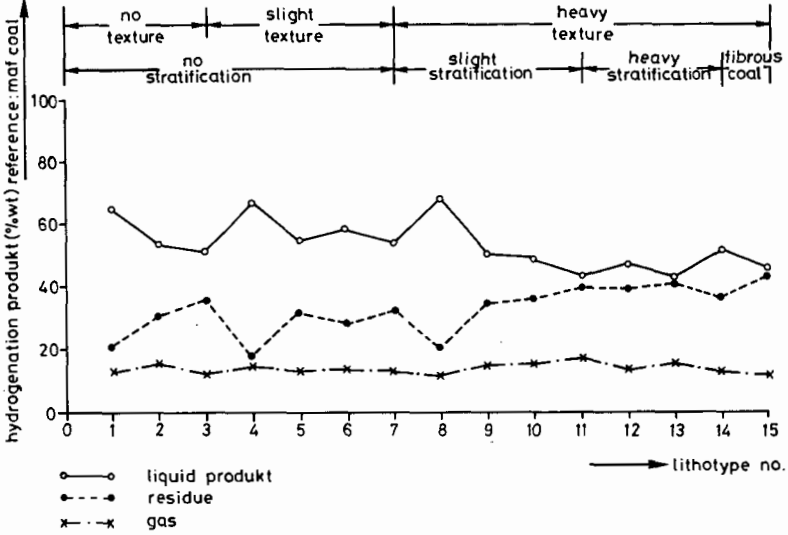


lith. no.	burn-out	time (min.)
9	93,3	72
13	92,5	80
5	88,3	120
4	82,1	30
15	82,4	46
11	87	240
1	34,1	34
8	100	390

Conversion as a function of time with hydrogasification
of brown coal cokes

RHEINBRAUN

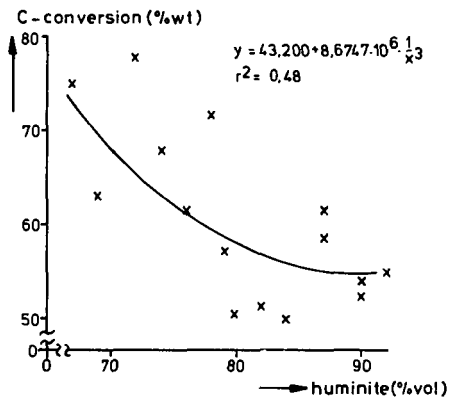
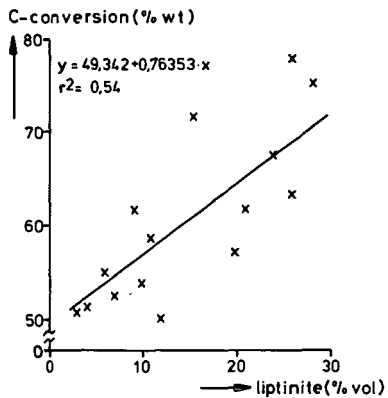
Fig. 25



Produkt yields achieved through indirect hydrogenation with tetralin as a function of stratification and texture (lith. no.)

RHEINBRAUN

Fig. 27



Carbon conversion achieved through indirect hydrogenation with tetralin as a function of the liptinite and huminite contents

RHEINBRAUN

Fig. 28

1. Petrographical properties

Liptinite content	>20 % vol
Lipto - Humodetrinite content	>50 % vol
Humo - Detrinite content	>50 % vol
Inertinite content	< 3 % vol
Gelo - Humotelite content	< 6 % vol
Reflectance value	> 7 % vol

2. Chemical properties

Tar content	> 11 % wt (mf)
Paraffin content	> 7 % wt (maf)
Hydrogen content	> 5,3% wt (mf)
C/H ratio	< 1,1
Volatiles	> 53 % wt (maf)
Carbonization water	< 8,7% wt (mf)

Under the conditions stated above, the 5th and 6th seam of the Fortuna - Garsdorf mine contain approx. 78 %wt of good hydrogenation coals

Petrographical and chemical properties of good hydrogenation coals	RHEINBRAUN
---	-------------------

SOME ASPECTS OF THE STRUCTURE AND REACTIONS OF NORTHERN GREAT PLAINS LIGNITES

W.R. Kube¹, H.H. Schobert², S.A. Benson², and F.R. Karner²

¹Department of Chemical Engineering,
University of North Dakota, Grand Forks, North Dakota

²Grand Forks Energy Technology Center, USDOE, Grand Forks, North Dakota

The lignites of the Northern Great Plains are in the Fort Union Region, which contains the largest reserves of lignite of any coal basin in the world. The Fort Union Region encompasses areas of North Dakota, South Dakota, Montana, and Saskatchewan. The identified resources of lignite in this region amount to 422 Gt (465 billion short tons), of which 24 Gt (26 billion short tons) constitute the demonstrated reserve base (1).

Until about 1970, the utilization of lignite was limited, accounting for no more than 1-2% of the total annual U.S. coal production. In recent years the production of low-rank coals has increased dramatically, so that by 1980 production represented about 24% of the total national coal production. It has been estimated that in another ten years, low-rank coals could amount to half the total coal production (1).

It has long been recognized that lignites possess unusual properties which can have profound effects on utilization. Such properties include high moisture content, high quantities of oxygen functional groups in the carbon structure, an alkaline ash, and inorganic cations attached to carboxylic acid groups. The rapid expansion of lignite utilization in recent years has brought with it an increasing realization of the importance of developing a better understanding of the organic and inorganic structures in lignite and of how those structural features influence lignite reactivity or processing behavior. Here we present results from some current studies in progress in our laboratories on lignite structure and reactivity.

Comparison of Northern Great Plains Lignites with Bituminous Coals

The predominant position of bituminous coal in the total U.S. coal production has resulted, not unreasonably, in the properties of bituminous coals being more extensively studied and thus better known to the general coal research community than those of lignites.

The average proximate and ultimate analyses of Fort Union lignites are summarized in Table 1, together with average values for a Pittsburgh seam bituminous coal. The data in Table 1 were taken from references (2) and (3) for lignite and bituminous coal, respectively. The important points to note are the much higher moisture content, higher oxygen, and lower heating value of the lignite.

Usually, lignitic ash contains a much higher proportion of alkali and alkaline earth elements, and consequently lower proportions of acidic oxides such as silica and alumina, than does ash from bituminous coals. These differences are illustrated by the data in Table 2, as taken from reference (1). The data on spruce bark ash are taken from reference (4) and show the similarity of lignitic and woody ashes. Of interest are the contrasts between the lignite and bituminous averages first with regard to silica and alumina and, second, to lime, magnesium, and sodium oxide.

TABLE 1
 AVERAGE ANALYSES OF NORTHERN GREAT PLAINS LIGNITE
 AND BITUMINOUS COAL SAMPLES, AS-RECEIVED BASIS

	<u>Northern Great Plains Lignite</u>	<u>Pittsburgh Seam Bituminous</u>
<u>Proximate, %</u>		
Moisture	37.2	2.3
Volatile Matter	26.3	36.5
Fixed Carbon	30.3	56.0
Ash	6.2	5.2
<u>Ultimate, %</u>		
Hydrogen	4.9	5.5
Carbon	71.9	78.4
Nitrogen	1.1	1.6
Oxygen	21.0	8.5
Sulfur	1.1	0.8
<u>Heating Value, MJ/kg</u>	15.9	32.6

TABLE 2
 AVERAGE ASH COMPOSITIONS OF NORTHERN GREAT PLAINS LIGNITES
 AND BITUMINOUS COALS, SO₃ - FREE BASIS

	<u>Spruce Bank</u>	<u>Lignite</u>	<u>Bituminous</u>
<u>Acidic Components:</u>			
SiO ₂	32.0	24.9	48.1
Al ₂ O ₃	11.0	14.0	24.9
Fe ₂ O ₃	6.4	11.5	14.9
TiO ₂	0.8	0.5	1.1
P ₂ O ₅	-	0.4	0.0
<u>Basic Components:</u>			
CaO	25.3	31.1	6.6
MgO	4.1	8.7	1.7
Na ₂ O	8.0	8.2	1.2
K ₂ O	2.4	0.5	1.5

Organic Structural Relationships

Lignite is an early stage in the coalification process and thus could be expected to retain some characteristics of wood. This relationship is illustrated by the electron micrographs shown as Figures 1 and 2. Pieces of plant debris, presumably twigs or rootlets, can be seen in Figure 1. Remains of the cellular structure are visible in Figure 2; the close similarity to the structure of softwood may be seen by comparing reference (5) for example.

On the molecular level, the distinguishing features of the organic structure of lignite are the lower aromaticity (or fraction of total carbon in aromatic structures), compared to bituminous coals; aromatic clusters containing only one or two rings; and the prevalence of oxygen-containing functional groups. A proposed structural representation, modified slightly from the original version (6), is given in Figure 3. We do not claim that this represents the structure of Northern Great Plains lignite, but rather use it as an illustration of major structural features.

The aromaticity has been studied by pressure differential scanning calorimetry (PDSC). The details of the experimental technique and of the methods for calculating aromaticity from a PDSC thermogram have been published elsewhere (7). Briefly, the PDSC experiment provides for controlled combustion of a 1-1.5 mg sample of -100 mesh coal in a 3.5 MPa atmosphere of oxygen. The sample is heated at 20°C/min in the range 150° to 600°C. The instrument response is a thermogram plotting heat flux, Δq , versus temperature, the integrated value thus being the heat of combustion. For most coals, and many organic compounds and polymers, the thermogram in this region consists of two peaks, which, from comparison to the behavior of model compounds, arise primarily from combustion of the aliphatic and aromatic portions of the sample. The aromaticity may be deduced from a comparison of peak heights.

The aromaticity for several samples of Northern Great Plains lignites, as measured on run-of-mine material, lies in the range of 0.61 to 0.66. For comparison, a sample of Australian brown coal available to us was found to have aromaticity of 0.56; a sample of Minnesota peat had an aromaticity of 0.50. Samples of vitrinite concentrates from the Northern Great Plains lignites were more aromatic, with values in the range of 0.72 to 0.74.

The temperature at which the maximum of the aromatic peak occurs has been shown to be a function of the extent of ring condensation (7), the maximum shifting to higher temperatures with increasing condensation. In support of the studies on coal structure, we have measured the PDSC behavior of over 30 organic compounds (most of which have been suggested as coal models or have been identified in the products of coal processing) and about 50 polymers. The maxima of the aromatic peaks in the thermograms of Northern Great Plains lignites generally fall into the same temperature range (375°-400°C) as those for compounds or polymers having benzene or naphthalene rings. One example is given in Figure 4, in which the PDSC thermograms of Gascoyne (N.D.) lignite and poly(4-methoxystyrene) are compared. We conclude that the aromatic ring systems therefore are mostly one- or two-ring systems.

Much less is known about the hydroaromatic structures or aliphatic bridges between ring systems. A methylene bridge is often suggested as a typical aliphatic bridging group, and was originally shown in the proposed structural representation (6). However, considerations based on thermochemical kinetics predict a half-life of 10^6 years for bond cleavage of diphenylmethane in tetralin at 400°C (8). Exhaustive analyses of the products from liquefaction of Northern Great Plains lignite at 400°C and higher in the presence of tetralin, (see (9) for example) have never identified diphenylmethane or related compounds. Absence of diphenylmethane constitutes strong circumstantial evidence for the relative unimportance of methylene linkages between aromatic clusters.

Oxygen is distributed among carboxylate, phenol, and ether functional groups. The carboxylate concentration has been measured by reaction of demineralized coal with calcium acetate following the procedure of van Krevelen and co-workers (10). A study of the carboxylate concentrations is still in progress; preliminary data for the Northern Great Plains lignites indicate carboxylate concentrations ranging from 1.75 to 1.93 meq/g on a dry basis. Concentrations of phenolic or ether functional groups have not yet been measured. Electron spectroscopy for chemical analysis (ESCA) provides a means for discriminating between carbon atoms incorporated in C=O and C-O structures by a Gaussian-Lorentzian decomposition of the carbon 1s spectrum (11). Figure 5 provides a comparison of the decomposed carbon 1s spectra of Beulah (N.D.) lignite and polyethylene terephthalate. At present, the ESCA data cannot be resolved into phenolic and etheric carbons. However, it can be shown that the ratio of carbon in carboxylate groups to that in (phenol plus ether) groups is about 0.62 (11). The presence of methoxy groups has been qualitatively confirmed; as-yet unpublished work by E.S. Olson and J.W. Diehl demonstrates the production of methanol from sodium periodate oxidation of Beulah lignite.

Little consideration has yet been given to the three-dimensional structure. A preliminary examination of lithotypes of Beulah lignite has been conducted by laser Raman spectroscopy (11). The lithotype having a higher concentration of carboxylic acid groups has a weaker band at 1600 cm^{-1} . If this band is assigned as a graphite mode (12), results suggest that the relatively bulky carboxylate groups, with their associated counterions, may disrupt, or preclude, three-dimensional ordering.

Distribution of Inorganic Constituents

In lignites the inorganic constituents are incorporated not only as discrete mineral phases, but also as relatively mobile ions, presumably associated with the carboxylic acid functional groups. The distribution of inorganic constituents has been studied principally by the chemical fractionation procedure developed by Miller and Given (13).

Extraction of the coal with 1M ammonium acetate removes those elements present on ion exchange sites, which are presumed to be carboxylic acid functional groups. Sodium and magnesium are incorporated almost exclusively as ion-exchangeable cations. For a suite of Northern Great Plains lignites tested, 84 to 100% of the sodium originally in the coal and 88 to 90% of the magnesium are removed by ammonium acetate extraction. Figure 6 is an electron micrograph showing an electron backscatter image due to the presence of sodium intimately associated with the organic material. Calcium is largely present in cationic form, 48 to 76% being extracted. Some potassium is also extracted in this step, in amounts ranging from 20 to 57%.

Further treatment with 1M hydrochloric acid then removes elements present as acid-soluble minerals or possibly as acid-decomposable coordination compounds. This acid extraction removes essentially all of the calcium and magnesium not removed by ammonium acetate. This finding is suggestive of the presence of calcite or dolomite minerals, which are known to be present in Northern Great Plains lignites (14). The hydrochloric acid extraction behavior of other major metallic elements is quite variable, which suggests significant differences in the mineralogy of the samples. Of those elements not extracted at all by ammonium acetate, some iron, aluminum, and titanium are removed by hydrochloric acid.

The portions of elements which are not removed by either reagent are considered to be incorporated in acid-insoluble minerals, particularly clays, pyrite, and quartz. This group includes all of the silicon, the remaining sodium and potassium, and the residual iron, aluminum and titanium. The acid-insoluble minerals are present as discrete phases. Frequently the mineral particles are quite small (see Figure 7, for example) and very highly dispersed through the carbonaceous material, to such

an extent that only about 15-30% of the discrete mineral matter is separable in a traditional float/sink experiment.

Effects of Structure on Reactivity

The small aromatic clusters, the high concentration of organic oxygen functional groups, and the presence of inorganic species as ion-exchangeable cations are unique features of low-rank coals. Each of these features should influence the reactivity of low-rank coals, thereby giving low-rank coals distinctly different reactions when compared to bituminous coals. The reactivity indeed has unique features. As yet, however, little has been done in a deliberate way to develop an understanding of the connections between structure and reactivity.

The carboxylic functional group is thermally labile and is driven off by heating to 450°C (15). Although the volatile matter content of lignite is higher than that of bituminous coals, much of the material released from lignite is carbon dioxide rather than hydrocarbon gases or tars. Thus only about 17% of the calorific yield occurs in volatile products from Northern Great Plains lignites at 500°C, compared with 30% for some bituminous coals (16). Since this thermal decomposition removes much of the oxygen from the coal, in a liquefaction reaction the removal of oxygen would require no net consumption of external hydrogen.

Oxygen functional groups can promote β -bond scission (8), which may be an important process in the degradation of the coal structure. The role of ether, carboxyl, and other groups in wood pyrolysis and combustion has been discussed (17); it seems reasonable to assume that analogous reactions would occur in low-rank coals. Other possible roles for oxygen functional groups include ether cleavage, cleavage of aliphatic bridges linked to aromatic rings bearing a phenolic group, and the enhancement of the ability of free radicals to form adducts with potential solvent or reactant molecules. The relationship of organic structure to reactivity should be a fertile field for research.

Sodium is the best-studied of the inorganic constituents of Northern Great Plains lignite. The combustion of the sodium carboxylates generates sodium-containing vapor species which can then be deposited on boiler tubes. The relationship of the sodium content of the coal to the formation of ash deposits on boiler tubes is well known. While the ash deposition problem can be severe and expensive for commercial installations (18), the mobility of cationic sodium holds out the promise for sodium removal or reduction by ion-exchange processes (19). The possible role of the ion-exchangeable sodium in the catalysis of liquefaction reactions has been studied by Given (20).

Acknowledgements

We thank Edwin Olson and John Diehl for the data on periodate oxidations, and George Montgomery for the ESCA spectrum. Thanks are due to several participants in Associated Western Universities' research participation programs, particularly David Kleesattel for separation of the lithotypes of Beulah lignite and for providing Figure 2, Kathleen Groon for the PDSC thermograms, and Paul Holm for chemical fractionation and carboxylate functional group data.

Literature Cited

1. Low-Rank Coal Study Volume 1 Executive Summary. U.S. Department of Energy Report DOE/FC/10066-T1 (Vol. 1), 1980.
2. Low-Rank Coal Study Volume 2 Resource Characterization. U.S. Department of Energy Report DOE/FC/10066-T1 (Vol. 2), 1980, p.40.
3. Banmeister, T. Standard Handbook for Mechanical Engineers, McGraw-Hill Book Co. Inc., New York, 1967, p. 7-4.
4. Tillman, D.A., Rossi, A.J., and Kitto, W.D. Wood Combustion, Academic Press, New York, 1981, p.42.
5. Went, F.W. The Plants, Time-Life Books, New York, 1963, p. 51.
6. Sondreal, E.A., Willson, W.G., Stenberg, V.I. Fuel, 1982, 61 925-38.
7. Benson, S.A., Schobert, H.H. In Technology and Use of Lignite, U.S. Department of Energy Report GFETC/1C-82/1, 1982, pp. 442-70.
8. Stein, S.E. In New Approaches in Coal Chemistry, American Chemical Society, Washington, 1981, p. 104.
9. Farnum, S.A., Farnum, B.W. Analytical Chemistry, 1982, 54 979-85.
10. Blom, L., Edelhausen, L., van Krevelen, D.W. Fuel, 1957, 36 135-53.
11. Schobert, H.H., Montgomery, G.G., Mitchell, M.J., Benson, S.A. Proc. 9th Int. Conf. Coal Sci. (In press, 1983).
12. Zerda, T.W., John, A., Chmura, K. Fuel, 1981, 60 375-8.
13. Miller, R.N., Given, P.H. In Ash Deposits and Corrosion Due to Impurities in Combustion Gases, Hemisphere Publishing Corp., Washington, 1977, pp. 39-50.
14. Schobert, H.H., Benson, S.A., Jones, M.L., Karner, F.R. Proc. 8th Int. Conf. Coal Sci., 1981, pp. 10-15.
15. Suuberg, E.M., Peter, W.A., Howard, J.B. Ind. Eng. Chem. Process Des. Devel. 1978, 17 37-46.
16. Goodman, J.B., Gomez, M., Parry, V.F., Landers, W.S. U.S. Bureau of Mines Bulletin 530, 1954.
17. Tillman, D.A., Rossi, A.J., Kitto, W.D. Wood Combustion, Academic Press, New York, 1981, Chapter 4.
18. Honea, F.I., Montgomery, G.G., Jones, M.L. In Technology and Use Of Lignite, U.S. Department of Energy Report GFETC/1C-82/1, 1982, pp. 504-45.
19. Paulson, L.E., Baria, D.N., Kube, W.R. In Technology and Use of Lignite, U.S. Department of Energy Report GFETC/1C-82/1, 1982, pp. 756-74.
20. Given, P.H., Cronauer, D.C., Spackman, W., Levell, H.L., Davis, A. and Biswas, B. Fuel 1975, 54 34-9.

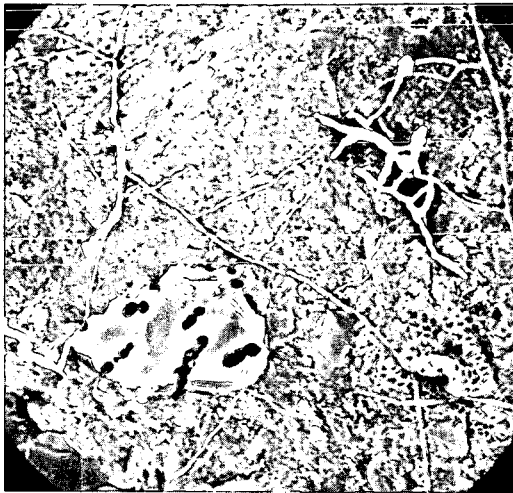


FIGURE 1. Electron micrograph of ion-etched Beulah lignite, showing rootlets or other plant debris. 7800x.



FIGURE 2. Electron micrograph of woody lithotype of Beulah lignite showing cellular structure. 390x. Compare softwood structure in reference (5).

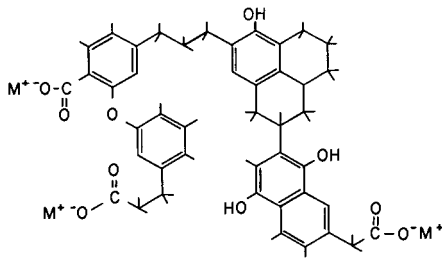


FIGURE 3. Proposed representation of structural features of lignite. Adapted with minor modification from reference (6).

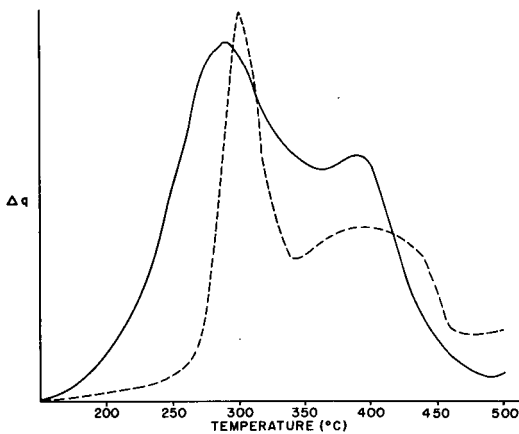


FIGURE 4. PDSC thermograms of Gascoyne lignite (solid line) and poly(4-methoxystyrene) (dashed line). Plot is of heat flux in arbitrary units versus temperature, $^{\circ}C$.

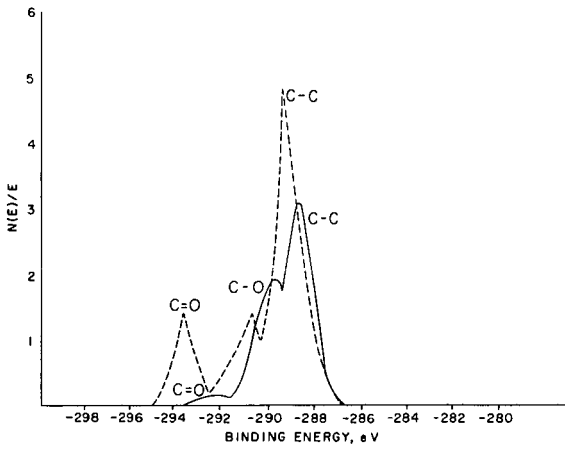


FIGURE 5. Decomposed ESCA carbon 1s spectra of Beulah lignite (solid line) and polyethylene terephthalate (dashed line). Plot is of number of electrons per energy in arbitrary units versus binding energy in electron volts. The lignite spectrum has been corrected for sample charging (11).



FIGURE 6. Electron micrograph of Beulah lignite showing organic region enriched in sodium (circular structure in lower center of view).

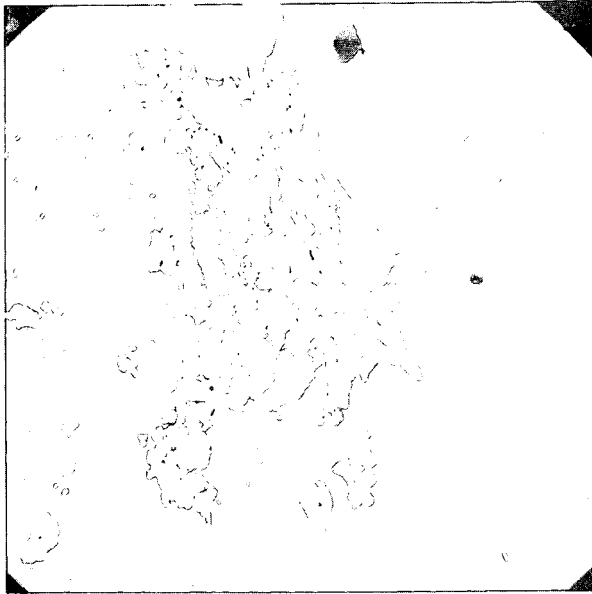


FIGURE 7. Electron micrograph of pyrite particles intergrown in carbonaceous structure of Beulah lignite, suggesting difficulty of removal by float/sink. 200x.

STRUCTURE AND REACTIVITY OF TEXAS LIGNITE

C. V. Philip, R. G. Anthony and Zhi-Dong Cui
Kinetic, Catalysis and Reaction Engineering Laboratory
Texas A&M University
College Station, Texas 77843

INTRODUCTION

The conversion of low rank coals such as lignites into gaseous and liquid fuels and chemical feed stocks received considerable attention in the last decade.¹⁻³ Data for liquefaction and gasification of various lignites have been reported.^{1,3-16} Although extensive analytical data are available on lignite conversion product, their use to monitor chemical reactions involved in any liquefaction or gasification process is limited due to the enormous amount of time and effort required for the complete characterization of Lignite conversion products.¹⁷⁻²¹ In the case of most of the reports on liquefaction experiments, the data are usually limited to total conversion, amount of certain fractions as oils, asphaltenes, preasphaltenes, tetrahydrofuran solubles, and certain physical characteristics.¹⁷ This study involves one lignite sample from a Texas mine and its conversion products from mini reactor experiments using varying liquefaction conditions. The gaseous products are analyzed by gas chromatography (GC)¹⁴ and the THF solubles are characterized by gel permeation chromatography (GPC)⁸⁻¹⁵ and high resolution gas chromatography (HRGC).

EXPERIMENTAL

Lignite samples were collected fresh from the mine near Carlos, Texas and stored under distilled water prior to use. The Lignite was ground to less than 20 mesh size and stored in a closed jar which was kept in the refrigerator. The lignite liquefaction experiments were conducted in four 6.3 ml mini reactors which were heated in a fluidized sand bath. The reactors were fabricated using 'Autoclave' fittings. Each reactor was the same, but only one reactor was fitted with a pressure transducer. The absence of pressure gauges on the other three reactors allowed the minimization of the dead volume outside the sand bath. In most cases 1.5 gm lignite, 1ml solvent (decalin or tetralin) and a gas (nitrogen or hydrogen or 1:1 CO/H₂ mixture at 1000 psi) were charges to the reactor. The reactions were quenched by dipping the reactors in cold water. The gases from the reactors were analyzed using an automated multi-column gas chromatograph equipped with sample injection and column switching valves.⁴ The contents of the reactors were extracted with tetrahydrofuran (THF) by using an ultrasonic bath. The THF extract (about 15 ml) was filtered through a 1 micron micro-pore filter (Millipore) and separated into fractions by using a gel permeation chromatograph (GPC).¹⁵

The GPC fractions were obtained with a Waters Associate Model ALC/GPC 202 liquid chromatograph equipped with a refractometer (Model R401). A Valvco valve injector was used to load about 100 μ l samples into the column. A 5 micron size 100 \AA PL gel column (7.5 mm ID, 600 mm long) was used. Reagent grade THF, which was refluxed and distilled with sodium wire in a nitrogen atmosphere, was used as the GPC carrier solvent. A flow rate of 1 ml per

minute was used. THF was stored under dry nitrogen, and all separations were conducted in a nitrogen atmosphere to prevent the formation of peroxides.

Straight chain alkanes from Applied Science, aromatics from Fisher Scientific Company and polystyrene standards from Waters Associate were used without purification for the linear molecular size calibration of the GPC. Since the solubility of the larger alkanes in THF is very low, approximately 0.2-1 mg of each standard was dissolved in 100 μ l of THF for the molecular size calibrations. The fractions of the lignite derived liquid separated by GPC were analyzed by a gas chromatographic system (VISTA 44, Varian Associates) equipped with a 15 M long and 32 mm ID bonded phase fused silica capillary column and flame ionization detector.

RESULTS AND DISCUSSIONS

The lignite samples from Carlos, Texas have heating values of 4000 to 6000 BTU/lb on an as received basis or about 12000 BTU/lb on dry mineral matter free (dmmf) basis. The samples may contain as much as 40% moisture which escapes from lignite even while stored in the refrigerator (water condenses on the walls of the container). The oxygen content varied from 20 to 30 % and has about 1 to 1.5 % sulfur on a dmmf basis. As much as 50% of the oxygen may exist as carboxylic groups which may produce carbon dioxide at the liquefaction conditions.⁵ The substantial amount of hydrogen sulfide that was usually liberated, decreased rapidly as a function of sample ageing and storage conditions. The lignite seams are soaked with water under hydrostatic pressure in a virtually anaerobic condition. Immediately after mining, the lignite samples continuously loose moisture and are oxidized by air. There is no ideal way the lignite samples can be stored to preserve its on seam characteristics.

The lignite liquefaction conditions are listed in Table 1. The composition of gaseous products are listed in Table 2. The data in Table 2 illustrate that the composition of gaseous products are unaffected by reaction conditions such as reactor pressure, feed gas or the solvent system (whether hydrogen donating or not). Higher temperatures favor the production of hydrocarbons. Apparently the fragile species produced by the pyrolytic cleavages of bonds in the coal structure are converted to stabler species which form the components of lignite derives gases without consuming hydrogen from the gaseous phase or from the hydrogen donor solvents. The species which require hydrogen for stabilization are abstracting hydrogen from carbon atoms in the vicinity. It is quite possible that the bond breaking and hydrogen abstraction are simultaneous and hydrogen from the donor solvent or the gaseous phase may not reach the reaction site in time to hydrogenate the fragile species.

To illustrate the gaseous hydrocarbon production from lignite, experiments were conducted using butylatedhydroxytoluene (BHT), a widely used antioxidant and food preservative, as a model compound (see Table 1 & 2). BHT decomposed to products including isobutylene and isobutane in an approximate 1:1 molar ratio in the absence of hydrogen from hydrogen donor solvent or gaseous phase. Addition of tetralin favored the production of isobutane over isobutylene. It appears that coal lignite can give some hydrogen to the isobutane formation but tetralin can readily reach the reaction vicinity in time for the hydrogen transfer reaction.

The elution pattern of the GPC using 5 micron 100 Å PL gel column is illustrated in Figure 1 where the GPC separation of a standard mixture containing straight chain alkanes and aromatics is shown. The polystyrene standard (mol. wt. 2350 and chain length 57 Å) gave a broad peak at 11 ml retention volume. The peak position is marked in the figure rather than using polystyrene standard in the mixture in order to save the $nC_{44}H_{80}$ peak from the enveloping effect of the broad polystyrene peak. The retention volume of several aliphatic phenolic, heterocyclic, amine and aromatic compounds in THF and toluene have been reported elsewhere.⁹ It is clear that aromatic compounds, as expected from their valence bond structures, have smaller linear molecular sizes compared to n-alkanes of similar molecular weight.¹⁵ It is expected that most of the condensed ring aromatics such as naphthalene, anthracene and even big ones like coronene (seven fused rings with molecular weight of 300.4) are smaller than n-hexane and hence have retention volumes larger than that of n-hexane. The polystyrene standard with a 57 Å appears to be larger than expected from the alkane standard. The large number of phenyl groups on the main polyethylene chain (57 Å) make the molecule into a large cylindrical structure with large steric hinderance for penetrating the pores of the gel. The two terminal phenyl groups also contribute to an increased chain length. The polystyrene peak (57 Å) is very close to the total exclusion limit of the 100 Å PL gel column.

The THF solubles of lignite liquefaction products were separated by GPC on the basis of effective linear molecule sizes in solution.¹⁵ Although GPC can be used for molecular weight or molecular volume separation of homologous series such as polymers, such separations of complex mixtures like coal liquid is not feasible. The only molecular parameter which has the least variation from a calculated value is effective linear molecular size in solution. Lignite derived liquids are separated on the basis of effective molecular length which is expressed in carbon numbers of straight chain alkanes. The GPC fraction with species larger than $nC_{44}H_{80}$ is in fraction 1 which is composed of nonvolatile species. Fraction 2 has molecular sizes in the range of nC_{14} to nC_{44} and composed of volatile species mostly alkanes and nonvolatile species generally known as asphaltenes. Fraction 3 is composed of alkylated phenols such as cresols, alkyl indanols and alkyl naphthols as well as, some small amount of nonvolatiles namely low molecular weight asphaltenes. Fraction 4 is composed of species with molecular size less than that of $n-C_7H_{16}$. This fraction may not contain any straight chain alkanes as they are very volatile. It is composed of aromatic species such as alkylated benzenes, alkylated indans and naphthalene and even large species such as pyrenes and coronenes. The solvent system used for liquefaction (tetralin and decalin) separate from the bulk of the lignite derived products as the last peak (peak at 20.5 ml). Although the column is overloaded with respect to the solvent system, the efficiency of separation of the lignite derived products are unaffected. The volatile species of all fractions can be identified by GC-MS¹⁵ and nonvolatiles by the IR and NMR spectroscopy.^{12,13,17}

The effect of hydrogen donor solvent and feed gases such as hydrogen and CO/H_2 mixture on lignite dissolution at 700°F is shown in Figure 2. Decalin dissolves less coal compared to tetralin. CO/H_2 as feed gas gave less liquid products which contained more larger molecular size species. When decalin with nitrogen (not shown in Figure 2) was used for liquefaction of lignite the

species appearing at total size exclusion limit of 100 Å gel column were totally absent. Figure 3 shows GCs of fraction 2s of two lignite derived liquids to illustrate the role of the hydrogen donor solvent on alkane production. If the alkanes are formed by breaking of alkyl chains from other groups, they are expected to contain more olefinic species in the absence of hydrogen donor solvents such as tetralin. Since the species in figure 4 a and b are very similar, the role hydrogen or hydrogen donor solvent plays in the production of alkanes are limited. Simple pyrolysis can liberate them from the coal matrix. The alkane may be existing as free while trapped inside the pores or their precursors are either carboxylic acids or species which decompose during heating to produce alkanes easily.

Figure 4 illustrates the effect of reaction time on liquefaction. Figures 5 and 6 show the liquefaction of lignite at 750°F and 800°F using different feed gases. Hydrogen tends to give more phenols and aromatics compared to nitrogen. CO/H₂ tends to produce higher molecular size species at the expense of phenols and aromatics. A qualitative estimation of the solvent systems can be obtained estimating the width of the solvent peak, and the area of the rest of the GPC may give the dissolved product from lignite. The use of CO/H₂ did not increase the total liquefaction yield while it has decreased the total yield of liquid products. The experiments using CO/H₂ gave liquid product which are difficult to filter through micro pore filters compare to the products obtained from experiments using either nitrogen or hydrogen as the feed gas. It could be assumed that CO/H₂ will give a product which contained more large size asphaltenes.

Based on our data on lignite liquefaction products and various coal liquids and their distillates, we proposed a structure for coal as shown in figure 7. The major structural constituents of coal are derived from three sources namely cellulose, lignin and other plant components dispersed in the plant tissues. The first two are polymers. The coalification process which is mostly a deoxygenation process, might not create a sufficiently large number of tertiary bonds needed for binding various constituents of coal together to a strong three dimensional structure. The coals including lignite may have loose structures. The cellulose derived structures may have large pores in which species such as large alkanes could be trapped. Although low temperature (less than 300°F) extractions can extract some soluble components of coal, the alkanes are not liberated, except as small amount of carboxylic acids. The low temperature oxidation studies do not detect large alkanes. The higher temperatures (above 650°F) can either break the pore structures or the alkanes can distill out of the pores.

ACKNOWLEDGEMENTS

The financial support of The Texas Engineering Experiment Station, The Texas A&M University Center for Energy and Mineral Resources, is very much appreciated. The lignite was supplied by TMPA, Carlos, Texas.

REFERENCES

1. Sondreal, E. A., Wilson, W. G. and Sternberg, V. I. Fuel 1982 61, 925.
2. Proceedings of Low-Rank Coal Technology Development Workshop, San Antonio, Texas June 17-18, 1981.
3. Proceedings of the Basic Coal Science Workshop Houston, Texas, Dec. 8-9, 1981.
4. Philip, C. V., Bullin, J. A. and Anthony, R. G., J. Chromatogr. Sci. 1979, 17, 523.
5. Philip, C. V., and Anthony, R. G., Fuel Processing Technology, 1980.
6. Philip, C. V., and Anthony, R. G., Proceedings Coal Technology - 78, 2, 710.
7. Philip, C. V., and Anthony, R. G., Preprints ACS Org. Coat & Polym. Div. 20 August (1980).
8. Zingaro, R. A., Philip, C. V., Anthony, R. G., and Vindiola, A., Fuel Processing Technology (1981) 4, 169.
9. Philip, C. V. and Anthony, R. G., Am. Chem. Soc. Div. Fuel Chem. Preprints 1979, 24(3), 204.
10. Philip, C. V., Zingaro, R. A. and Anthony, R. G., Am. Chem. Soc. Fuel Chem. Preprints 1980, 25(1), 47.
11. Philip, C. V., Zingaro, R. A. and Anthony, R. G., "Upgrading of Coal Liquids" (Ed. R. F. Sullivan) Am. Chem. Soc. Symp. Ser., 1981, 156, 239.
12. Philip, C. V. and Anthony, R. G., Am. Chem. Soc. Div. Fuel Chem. Preprints 1977, 22(5) 31.
13. Philip, C. V. and Anthony, R. G., "Organic Chemistry of Coal," Am. Chem. Soc. 1978, p. 258.
14. Philip, C. V. and Anthony R. G., Fuel 1982, 61, 351.
15. Philip, C. V. and Anthony, R. G., Fuel 1982, 61 357.
16. Farnum, S. A., Olson, E. S., Farnum, B. W., Wilson, W. G., Am. Chem. Soc. Div. Fuel Chem. Preprints 1980 25 245.
17. Aczel, T., Williams, R. B., Pancirov, R. J. and Karchmer, J. H., "Chemical Properties of Synthoil Products and Feeds", Report prepared for US Energy Research and Development Administration, FE8007, 1976.
18. Baltisberger, R. J., Klabunde, K. J., Sternberg, V. I., Woolsey, N. F., Saito, K. and Sukalski, W., Am. Chem. Soc. Div. Fuel Chem. Preprints 1977, 22(5), 84.
19. White, C. M., Sulz, J. L. and Sharkey, Jr. A. C., Nature 1970, 268, 620.
20. Pugmire, R. J., Grant, D. M., Zilm, K. W., Anderson, L. L., Oblad, A. G. and Wood, R. E. Fuel 1978, 57(4).
21. Seshadri, K. S., Albangh, E. W. and Bacha, J. D., Fuel 1982, 61, 336.

Table 1. Lignite Liquefaction Conditions

Run No.	Coal g.	Solvent l ml	Feed Gas	Initial Pressure (psi)	Temp °F	Time min.	Comments
1	1.5	tetralin	N ₂	1000	700	30	+ BHT 0.2 g
2	1.5	tetralin	N ₂	1000	700	120	+ BHT 0.2 g
3	1.5	tetralin	N ₂	1000	700	120	
4	1.5	decalin	N ₂	1000	700	120	+ BHT 0.2 g
11	1.5	tetralin	CO+H ₂ (1:1)	1000	700	120	
12	1.5	tetralin	N ₂	1000	700	120	
13	1.5	decalin	N ₂	1000	700	120	
14	1.5 (old)	tetralin	N ₂	1000	700	120	
21	1.5	tetralin	N ₂	1000	700	120	
22	1.5	tetralin	no	0	700	120	+ BHT 1 g
23	1.5	no	no	0	700	120	
24	1.5 (old)	tetralin	N ₂	1000	700	120	
31	1.5	tetralin	H ₂	1000	700	120	
32	1.5	tetralin	CO+H ₂ (1:1)	1000	700	120	
33	1.5	decalin	H ₂	1000	700	120	
34	1.5	decalin	CO+H ₂	1000	700	120	
41	1.5	tetralin	N ₂	1000	700	15	
42	1.5	tetralin	N ₂	1000	700	120	
43	1.5	tetralin	N ₂	1000	700	360	
51	1.5	tetralin	N ₂	1000	850	30	
52	1.5	tetralin	H ₂	1000	850	30	
53	1.5	tetralin	CO+H ₂ (1:1)	1000	850	30	
61	1.5	tetralin	N ₂	1000	800	30	
62	1.5	tetralin	H ₂	1000	800	30	
63	1.5	tetralin	CO+H ₂ (1:1)	1000	800	30	
71	1.5	tetralin	N ₂	1000	750	30	
72	1.5	tetralin	H ₂	1000	750	30	
73	1.5	tetralin	CO+H ₂	1000	750	30	

TABLE II Composition of Product Gas %

Run No.	H ₂	CO ₂	CO	H ₂ S	CH ₄	C ₂	C ₂ ^F	C ₃	C ₃ ^F	n-C ₄	i-C ₄	i-C ₄ ^F
1	13.0	11.2	26.1	-	8.4	1.3	1.9	0.8	0.15	0.07	12.6	24.1
2	2.1	61.5	3.6	-	9.2	2.8	2.8	1.8	0.23	0.19	11.9	5.9
3	0.9	80.0	0.9	-	11.8	3.7	7.3	1.2	0.13	0.17	0.1	0.03
4	0.3	61.9	2.1	-	8.6	2.0	1.5	1.0	0.10	0.07	8.7	13.2
11	3.2	60.4	2.5	22.4	6.8	2.6	0.2	1.0	0.12	0.14	0.1	0.01
12	3.7	70.5	2.8	10.5	7.9	2.6	0.3	1.0	0.14	0.15	0.1	0.1
13	0.5	75.9	3.8	7.8	8.4	2.2	0.6	0.6	0.10	0.06	0.04	0.02
14	2.3	78.2	2.9	1.1	9.7	3.4	1.2	1.1	0.10	0.13	0.1	0
21	1.1	80.7	1.5	-	9.5	2.6	0.3	1.5	0.15	0.16	1.8	0.8
22	5.2	51.2	3.4	-	28.1	3.6	0.04	3.2	0.01	0.06	3.9	0.9
23	-	76.5	3.6	-	11.4	3.9	0.2	2.0	0.31	0.41	0.2	0.1
24	0.8	83.7	1.6	-	8.3	3.1	0.3	1.2	0.18	0.17	0.1	0.03
31	0.7	71.3	2.7	13.1	7.3	2.6	0.7	0.9	0.12	0.18	0.2	0.2
32	0.7	70.1	1.9	12.7	5.3	1.8	0.4	0.6	0.10	0.09	0.1	0.1
33	0.7	75.5	2.1	11.3	7.3	1.9	0.1	0.7	0.12	0.07	0.1	0.03
34	0.8	63.0	2.4	-	19.1	4.2	1.1	2.2	1.64	0.90	1.3	1.1
41	-	80.8	2.1	11.5	3.9	0.8	0.3	0.2	0.09	0.03	0.03	0.03
42	1.0	74.3	1.5	10.2	7.5	3.2	0.8	1.1	0.13	0.15	0.1	0.02
43	5.6	41.2	1.3	37.1	9.2	3.7	0.1	1.4	0.11	-	0.1	0.01
51	8.8	44.7	4.7	8.8	21.0	5.5	0.4	2.2	0.26	0.44	0.2	-
52	8.1	46.6	5.3	7.6	23.2	6.6	0.4	1.7	0.23	0.17	0.1	0.02
53	9.9	47.5	5.4	9.9	19.0	5.5	0.1	1.8	0.24	0.29	0.2	-
61	1.7	65.8	6.0	9.4	11.1	4.3	1.2	0.1	0.23	0.21	0.1	0.03
62	1.6	65.8	6.0	8.8	11.8	3.9	0.6	1.0	0.16	0.11	0.1	0.02
63	1.6	66.1	5.9	10.4	11.5	3.2	0.1	0.9	0.14	0.09	0.1	0.02
71	0.7	78.4	3.7	4.9	8.3	2.4	0.4	0.7	0.14	0.11	0.1	0.03
72	0.7	76.9	2.4	6.6	9.2	2.9	0.1	0.8	0.14	0.10	0.1	0.02
73	0.7	75.2	2.9	8.7	8.0	2.8	0.5	0.8	0.16	0.10	0.1	0.02

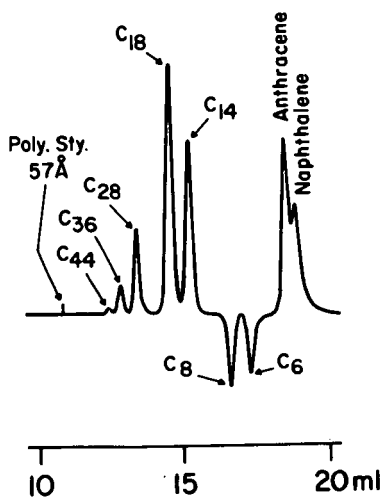


Figure 1. GPC of calibration mixture

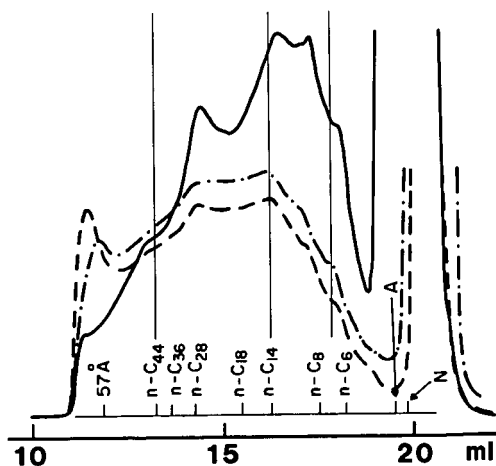


Figure 2. GPC of THF solubles of lignite from reactions at 700F in — decalin and H_2 (33), --- tetralin and H_2 (31) -.- tetralin and CO/H_2 (32)

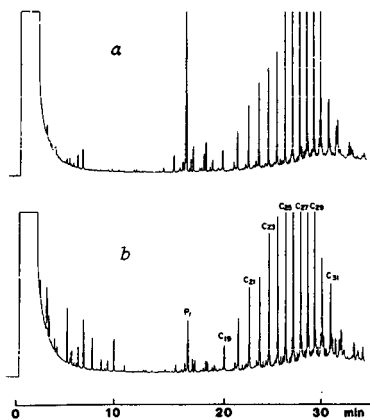


Figure 3. GC of alkane fractions from THF solubles of lignite a. tetralin and H_2 (21) b. Decalin and N_2 (13)

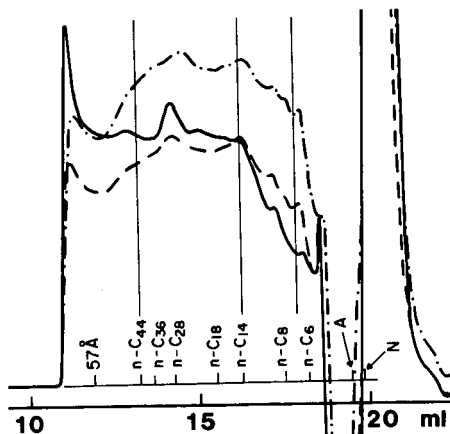


Figure 4. Effect of reaction time on THF solubles of lignite in tetralin and H_2 at 700F. — 15 min. (41), --- 120 min. (42), -.- 360 min. (43)

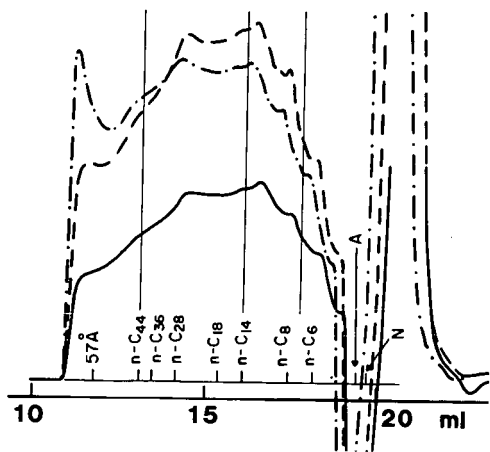


Figure 5. Effect of feed gas on lignite liquefaction in tetralin at 750 F — N_2 (71), --- H_2 (72), -.- CO/H_2 (73)

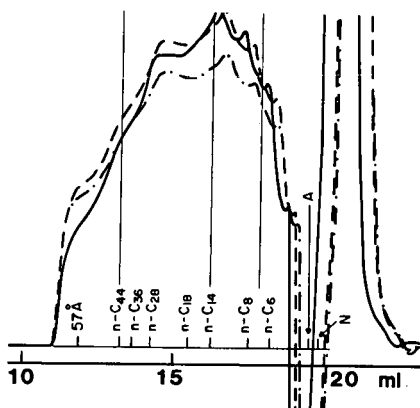


Figure 6. Effect of feed gas on lignite liquefaction in tetralin at 800 F. — N_2 (61), --- H_2 (62), -.- CO/H_2 (63)

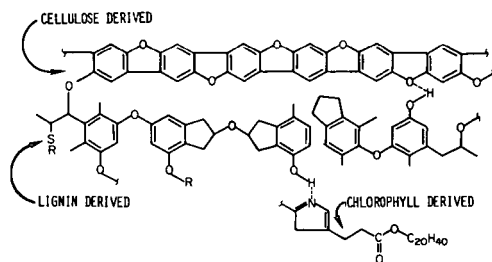


Figure 7. A structural model of coal

SOME SMALL-ANGLE X-RAY SCATTERING TECHNIQUES FOR
STUDYING THE SUBMICROSCOPIC STRUCTURE OF COALS AND COAL-DERIVED LIQUIDS

Paul W. Schmidt, Chul Y. Kwak, and Mohanan Kalliat

Physics Department, University of Missouri, Columbia, MO 65211

Small-angle x-ray scattering is often useful for investigating submicroscopic structures--that is, structures with dimensions between about 20 and 2000 Å (1). This technique has been employed in several studies of the porosity and other submicroscopic structure of coals (2--7).

In this review, we will summarize the results we obtained in Reference (7), and we will discuss briefly some of our more recent scattering studies of coal porosity (8). We also will illustrate how scattering techniques can provide useful information about the properties of coal-derived liquids aged under oxygen for periods up to 8 weeks (9).

First, however, we will review some of the methods and techniques which we employed in our interpretation of the small-angle x-ray scattering data from coals. Figure 1 is a schematic drawing of a small-angle x-ray scattering system. X-rays from the tube T are formed into a beam by slits and fall on the sample S. A small fraction of the x-rays striking the sample are re-emitted, without change of wavelength, in directions different from that of the incoming beam. The intensity of these re-emitted x-rays, which are called the scattered rays, and their dependence on the direction in which they are emitted depend on the structure of the sample. In a scattering experiment, the intensity of the x-rays scattered in different directions is measured, and from an analysis of these data, an attempt is made to obtain information about the structure of the sample producing the scattering. Figure 1 shows a ray scattered at an angle θ with respect to the incoming beam. The scattered radiation is recorded by the detector C.

While no universal prescription can be given for analyzing the scattering pattern from an arbitrary sample, we will review some general principles useful for interpretation of scattering measurements. For a sample which has a structure characterized by a dimension a , most information obtainable from scattering measurements will be found at scattering angles θ in an interval for which

$$0.1 < ha < 10, \quad (1)$$

where $h = (4\pi/\lambda) \sin(\theta/2)$; and λ is the x-ray wavelength. For angles no greater than about 7 degrees, $\sin \theta/2$ can be approximated by $\theta/2$, and so for small scattering angles, h can be considered proportional to θ . According to (1), for a structure with dimension a , the scattering is determined by the product ha , so that there is an inverse relationship between the size of the structure and the h values at which the scattered intensity from this structure is appreciable. Since the x-ray wavelengths are normally of the order of 1 or 2 Å and thus are of the same magnitude as the interatomic spacing in solids and liquids, Inequality (1) states that the x-ray scattering from structures with dimensions between about 20 and 2000 Å will be observed at scattering angles no greater than a few degrees. Small-angle x-ray scattering thus can be used to study these submicroscopic structures.

X-rays are scattered by electrons, and the small-angle scattering will be appreciable when the sample contains regions in which fluctuations or variations in electron density extend over distances of 20 to 2000 Å. At small angles, the scattering process is unable to resolve structures smaller than about 10 Å, and so in the analysis of the scattering data, the atomic-scale structure can be

neglected. For many scattering studies, it is therefore convenient to consider the sample to be composed of two phases, with constant but different electron densities.

If this two-phase approximation holds and the two phases always are separated by a sharp, discontinuous boundary, when the minimum characteristic dimension a_m of the structure satisfies the condition $ha_m > 3.5$, the scattered intensity $I(h)$ can be approximated by (7)

$$I(h) = \frac{2\pi\rho^2(S/M)}{h^4} \frac{M}{A} I_e A, \quad (2)$$

where ρ is the difference of the electron densities of the two phases, I_e is the intensity scattered by a single electron; S is the total surface area separating the two phases in the sample; M is the mass of the sample; and A is the cross-sectional area of the sample perpendicular to the incident beam. In the outer part of the small-angle scattering curve--that is, when $ha > 3.5$, the scattered intensity is proportional to h^{-4} and thus to the inverse^m fourth power of the scattering angle. Moreover, when $I(h)$ has this angular dependence, the magnitude of the scattered intensity is proportional to the specific surface S/M , which is the surface area per unit sample mass separating the two phases.

As we explain in Reference (7), the quantities $I_e A$ and M/A can be evaluated from the x-ray data, and so Equation (2) can be employed to calculate the specific surface S/M from the scattering data for samples with submicroscopic porosity.

We have made use of this technique to determine the specific surfaces of a number of PSOC coals. As our x-ray studies showed (7) that the almost all of the small-angle x-ray scattering was due to pores and that the scattering from the mineral matter in the coal was almost negligible, we have interpreted the small-angle x-ray scattering from coals as being due to submicroscopic pores, which are filled with air and for scattering purposes thus are essentially empty.

Our scattering studies show (7) that the rank of the coal is the main factor which determines the form of the angular dependence of the scattered intensity. The scattering curves for the coals which we studied can be grouped in four classes, as Figure 2 illustrates. Since both axes of Figure 2 are logarithmic, the curves in Figure 2 are straight lines with slopes -4 when Equation (2) describes the scattering. An angular dependence of this form is obtained for all types of coals at the smallest angles at which data could be recorded--that is, for scattering angles smaller than about 0.005 radian. For Pennsylvania Buck Mountain anthracite coal (PSOC 81, triangles), this inverse-fourth power continues to scattering angles as large as about 0.015 radian, and then the intensity decreases less rapidly with increasing scattering angle. Of all coals shown in Fig. 2, the scattering in the outer part of the plot is most intense for the anthracites. We interpret (8) this result as being due to the presence of a relatively large number of micropores, with average dimensions smaller than about 30 Å. As we have obtained similar curves for other anthracites, we have concluded that in these high-rank coals, there is a large fraction of micropores and an appreciable number of macropores, which have dimensions of 1000 Å or more. In a low-rank coal like Washington Queen #4 (PSOC 95, circles), there also are macropores, but since in the outer part of Fig 1 the intensity is lower than for the anthracite, we conclude that the anthracites have a larger fraction of micropores. Lignites gave scattering curves similar to the curve for PSOC 95. In the scattering curves for low volatile bituminous coals like Pennsylvania E. Kittanning coal (PSOC 127, plus signs), there is a maximum near 0.080 radians. This maximum has been ascribed (10) to interactions between the fundamental scattering units in these coals, which are planar aggregates of aromatic rings. In the fourth type of curve in Fig. 2, which we obtained for Illinois No. 6 coal (PSOC 22, squares) and for many other but not all low and medium-rank bituminous

coals, there is a shoulder on the scattering curve at intermediate scattering angles. On both sides of the shoulder or inflection, the intensity is proportional to the inverse fourth power of θ . (The shoulder on the curve in Fig. 3 occurs at such small angles that in this curve the inner region where the intensity is proportional to the inverse fourth power of θ is barely visible.) As we explain in Reference 7, we consider this shoulder to be the result of the fact that in these coals, there is a relatively high fraction of transitional pores, with average dimensions of the order of 50 to 200 Å. We calculated a specific surface from each part of the scattering curve which was proportional to the inverse fourth power of θ . These two surfaces are the specific surfaces of the macropores and the transitional pores. We have found that the presence of an inflection in the scattering curve is an indication that the coal has a relatively large number of transitional pores.

At the time we wrote the manuscript for Reference (7), we were unable to relate this high fraction of transitional pores to any other property of the coals. We have now found (8) that there are inflections only in coals with fixed carbon contents in the interval from about 72% through 83% per cent (dry, mineral-matter free). These results are summarized in Figure 3, which is a preliminary plot of the sum of the specific surfaces of the macropores and transitional pores as a function of carbon content.

The ability to distinguish between the specific surfaces associated with the macropores and the transitional pores is, we feel, a unique property of small-angle x-ray scattering.

By making some reasonable assumptions, we have also been able to estimate the specific surfaces and dimensions of the micropores in many coals (8).

The value of the specific surface obtained in studies of porous materials often depends on the techniques used for the measurement. For example, Gan, Nandi, and Walker (11), in their adsorption studies of a number of PSOC coals, obtained much larger specific surfaces by carbon dioxide adsorption at room temperature than by low-temperature adsorption of nitrogen. As we mentioned in Reference (7), the difference may be the result of the fact that carbon dioxide at room temperature can penetrate smaller pores than can be entered by nitrogen molecules at low temperature (12). As can be seen by comparison of the magnitudes of the specific surfaces in Figure 3 with the nitrogen specific surfaces in Figure 1 of Reference (11), the x-ray specific surfaces are much nearer to those measured by low temperature nitrogen adsorption than by room temperature carbon dioxide adsorption. As the micropores are too small to satisfy the conditions necessary to give a scattered intensity proportional to the inverse fourth power of the scattering angle, the "x-ray specific surface" includes only contributions from the macropores and transitional pores and does not take account of the specific surface of the micropores.

With reasonable assumptions, the dimensions and the specific surface of the micropores in anthracites and, at times, other coals can be estimated from the small-angle scattering data.

We have recently completed a small-angle x-ray scattering study of some coal-derived liquids prepared from West Virginia Ireland Mine coal in the U. S. Department of Energy Pittsburgh Energy Technology Center 400 lb/day Bruceton Liquefaction Unit and aged under oxygen for different lengths of time (9). To analyze the scattering data, we used the radius of gyration approximation, according to which, for independently-scattering, randomly-oriented particles (Ref. 1, pp. 24-28),

$$I(h) = I(0) e^{-\langle h^2 R^2 \rangle / 3}, \quad (3)$$

where $I(0)$ is the zero-angle scattered intensity, and R , the radius of gyration, is a characteristic dimension of the particle. According to Equation (3), which approximates the scattering when hR is not large with respect to 1, a plot of the logarithm of the scattered intensity as a function of the square of the scattering angle should be a straight line, from the slope of which the radius of gyration can be calculated. In Fig. 4, the radius of gyration plots, which are at least approximately linear, show that the radii of gyration of the coal-derived liquids, and thus the average size of the particles, at first grows slowly, but after the sample is aged for more than 4 weeks, there is a sharp rise in the radius of gyration. This increase in the radius of gyration is accompanied by a large increase in the viscosity. The scattering data thus relate the rise of the viscosity to the presence of relatively large, agglomerated colloidal particles in the coal-derived liquids.

By use of helium density and chemical composition measurements of the coal-derived liquids, we were able to show that in the early stages of aging--that is, before appreciable agglomeration took place, the number of colloidal particles remained essentially constant, and that the main effect of aging was to cause the colloidal particles already present to grow larger, rather than to produce new particles. We also have been able to make a rough estimate of the fractions of the volume occupied by the small and large colloidal particles.

Acknowledgements

We wish to express our sincere gratitude to S. R. Koirttyohann for assistance with the preparation of the ash samples used in our tests of the contribution of the mineral matter to the scattering from the PSOC coals, to Robert G. Jenkins for measuring the specific surface of PSOC Coal 105, to Dennis H. Finseth for preparing the samples of the coal-derived liquids, to L. B. Thomas, C. Leon Krueger, and Clifford R. Holmes for their help in the design and construction of the sample cell, to Charles D. Crowder and Chul Y. Kwak for assistance during the measurements of the scattering from the coal-derived liquids, to Richard G. Lett for obtaining the helium density and chemical composition of the coal-derived liquids, and to S. S. Pollack, D. W. Houseknecht, B. E. Cutter, R. G. Jenkins, D. E. Briggs, and P. L. Walker, Jr. for advice and assistance. This work was supported by contracts from the U. S. Department of Energy.

References

1. Guinier, A.; Fournet, G.; Walker, C. B.; Yudowitch, K. L.; "Small-Angle Scattering X-Rays"; Wiley: New York, 1955.
2. Durif, S. *J. Chim. Physique* 1963, **60**, 816-24.
3. Krüger, C.; Mues, G. *Brennstoff-Chemie* 1961, **42**, 77-84.
4. Spitzer, Z.; Ulický, L. *Fuel* 1978, **11**, 621-625.
5. Lin, J. S.; Hendricks, R. W.; Harris, L. A.; Yust, C. S. *J. Appl. Cryst.* 1978, **11**, 621-625.
6. Gonzales, J.; Torriani, I. L.; Luengo, C. A. *J. Appl. Cryst.* 1982, **15**, 251-254.
7. Kalliat, M.; Kwak, C. Y.; Schmidt, P. W., in "New Approaches To Coal Chemistry"; B. D. Blaustein, B. C. Bockrath, and S. Friedman, eds., ACS Symposium Series No. 169, pub. 1981, Amer. Chem. Soc., Washington, 1981; pp. 3-22.
8. Kwak, C. Y.; Kalliat, M.; Schmidt, P. W. Research to be published. 1984.
9. M. Kalliat, Schmidt, P. W.; Finseth, D. H. Research to be published. 1984.
10. Hirsch, P. B. *Proc. Roy. Soc. (London)* 1954, **226A**, 143-169.
11. Gan H.; Nandi, S. P.; Walker, P. L., Jr. *Fuel* 1972, **51**, 272-277.
12. Gregg, S. J.; Sing, K. S. W. "Adsorption, Surface Area, and Porosity"; Academic Press: London and New York, 1967, pp. 211-217.

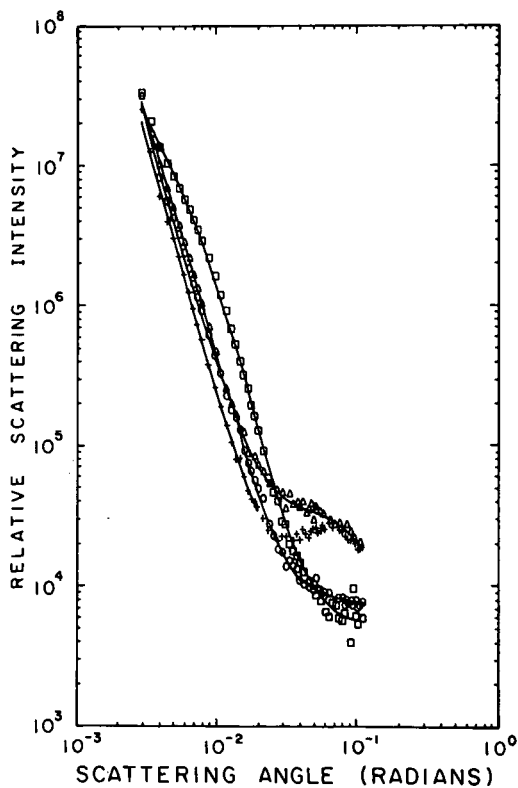
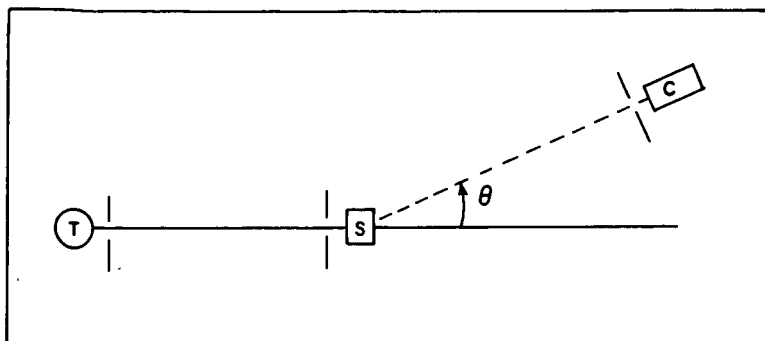


Fig. 1. (above) Schematic diagram of a small-angle x-ray scattering system. (Reproduced from Reference 7 by permission of the American Chemical Society.)

Figure 2. (left) Typical scattering curves for the coal samples. Curves 1--4 show the data for PSOC coals 95 (circles), 127 (plus signs), 81 (triangles) and 22 (squares). (This plot is reproduced from Reference 7 by permission of the American Chemical Society.)

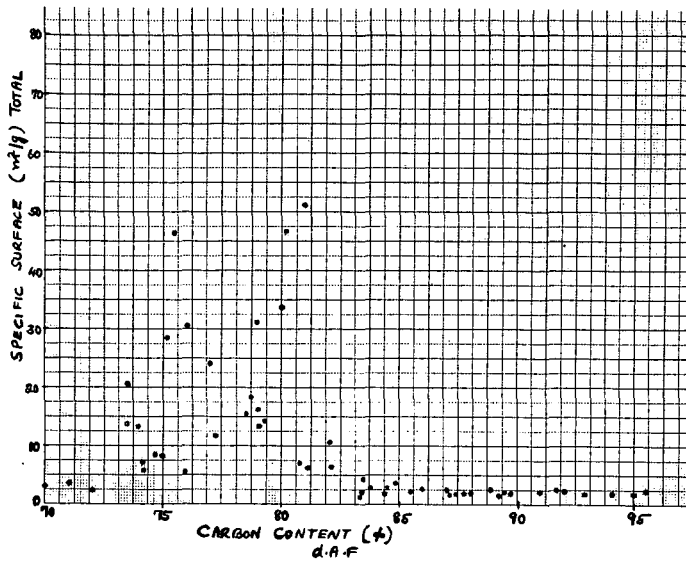


Figure 3. The combined x-ray specific surfaces of the macropores and transitional pores for coals of different carbon content (dry, ash-free).

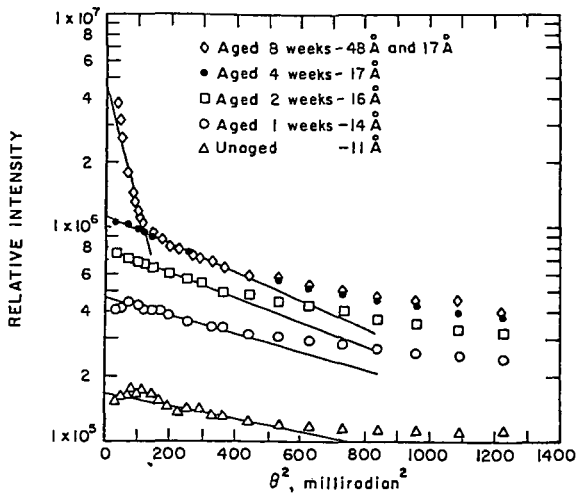


Figure 4. Radius of gyration plots for the coal-derived liquids.

DETERMINATION OF THE MICROSTRUCTURE OF WET AND DRY BROWN COAL
BY MEANS OF X-RAY SMALL ANGLE SCATTERING

M. SETEK, I.K. SNOOK AND H.K. WAGENFELD

DEPARTMENT OF APPLIED PHYSICS
ROYAL MELBOURNE INSTITUTE OF TECHNOLOGY
124 LATROBE STREET, MELBOURNE, VICTORIA
AUSTRALIA 3000.

That brown coal is a highly porous substance and that a knowledge of this pore structure is vital to the efficient and diverse use of brown coal is obvious.

However, what is not so obvious is how to characterize and measure the pore structure of such a heterogeneous material as Victorian brown coal. Even defining what we mean by structure is difficult for such a complex material as coal which contains such diverse constituents as water, carbon, minerals, plant matter, pollen, etc. and whose composition may even vary within a seam. In practice, then, it seems that a Physicist must abandon his usual, precise but simplistic ideas of structure obtained from the study of objects with very regular structures such as crystals and give a description only in terms of such gross parameters as total pore volume, V, total surface area, S, and the distribution of some characteristic dimension, D, of the pores.

There appear to be currently two methods for the determination of the above mentioned parameter.

- 1) Gas Adsorption (GA) - where the total volume of a gas taken up by the coal is measured and V and S are obtained from this by the use of a model of the adsorption process.
- 2) Small Angle X-ray Scattering (SAXS) - where the intensity of radiation scattered by the coal is interpreted in terms of the pore structure which causes this scattering.

Both methods are to some extent dependent on models which are used in order to interpret the observed data. No known method can give a very detailed description of the microstructure at this stage. Indeed by the very nature of brown coal such a detailed description is not even, in principle, possible.

However, we will attempt to show that the SAXS method has very many advantages over other methods and we will also show what we have done to date using SAXS.

OUTLINE OF THE TECHNIQUE

Basically x-rays are scattered (just as is light) when a system contains regions which are inhomogeneous over some distance scale, d. These inhomogeneities cause scattering of intensity, I, through various angles, θ . The scattering curve, i.e. intensity as a function of θ or more precisely as a function of

$$h = \frac{2\pi}{\lambda} \sin \frac{\theta}{2}$$

(λ , the X-ray wavelength), contains information about the characteristic dimensions of the inhomogeneities (simplistically h is the reciprocal of d). However, when a wide range of characteristic distances are present the scattering

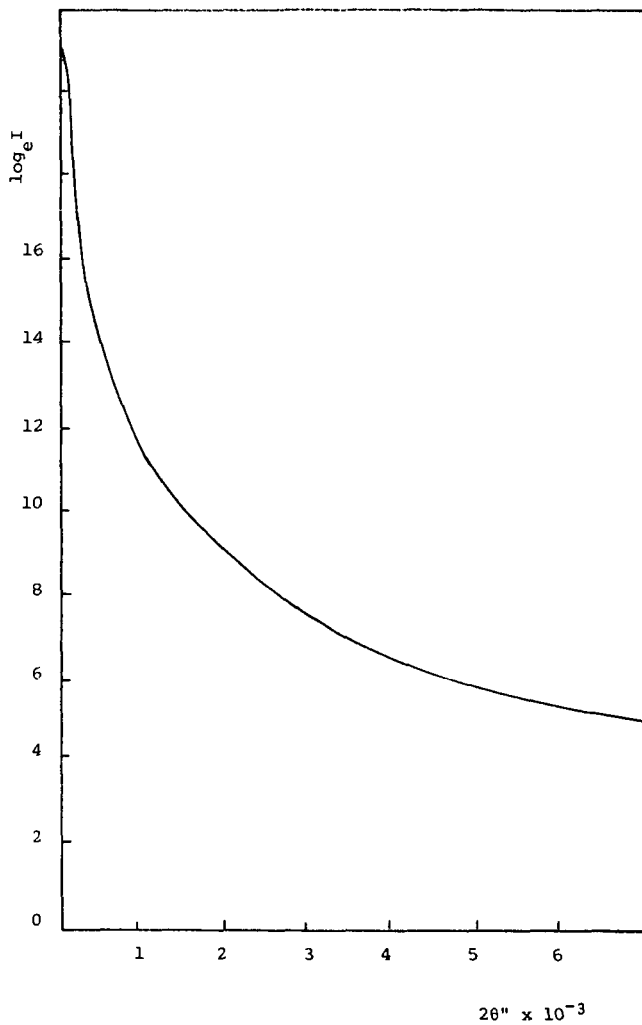


Fig. 1 Scattering curve of air dried coal (light lithotype).

curve is a superposition (convolution) of the effects of all these characteristic distances.

Thus, the scattering curve must be deconvoluted to obtain the information about the spacial distribution of inhomogeneities in the material, e.g. the pore structure in coal.

No known method can do this unambiguously, however, we believe realistic information may be readily and conveniently obtained by this method, e.g. total pore volume.

Furthermore, this method has several advantages over other available methods:

- 1) the sample can be wet or dry;
- 2) one can follow various stages of processes involving known coal or even, potentially, follow the material as it goes through these processes e.g. drying;
- 3) slurries may be studied.

DATA ANALYSIS AND RESULTS

Once the scattering curve has been obtained and stored in some convenient form it must be analysed (deconvoluted) to give details of the pore structure.

Technique to extract the micropore volume and the surface area from the scattering curves has been developed some years ago [1].

All scattering diagrams from brown coals (wet or dry) showed continuous strongly concave curves (Figure 1). This characteristic is assumed to be due to the presence of dilute system of micropores polydisperse in size but approximately identical in shape. From these curves several average pore length parameters can be obtained such as the mean radius of gyration, R_g , calculated by assuming a Maxwellian pore size distribution. Such parameters, although precise do not exactly define the form of the pores, however, can be used to calculate further physical quantities such as the micropore surface area. This quantity was obtained from the combined knowledge of the number of pores in the sample, the micropore volume (both quantities obtained by absolute intensity measurements), the mean radius of gyration, pore shape, and the pore size distribution. The micropore volume is computed directly from the scattering diagram in absolute units. Results are given in Table 1 together with data obtained by means of gas adsorption [2].

For the determination of the surface area we assumed two different shapes for the pores. In (1) we assumed a cylindrical shape and in (2) a disc shape.

Our method of interpretation of the scattering data shows only a partial success as can be seen when the results from the SAXS technique are compared to the results of the GA technique. Theoretically, this method seems to have several major faults:

- 1a) Assumption, that the pore size distribution is a single mode distribution. Pore size distribution may be more complicated, that is, it may follow a bimodal or even many modal type of distribution function. Indeed this can vary from sample to sample.

- 1b) Estimation of intensity scattered at zero angle. This point is not reachable experimentally and hence must be estimated, usually by some form of extrapolation. This is a very important quantity since it is directly proportional to the number of micropores within the irradiated volume.
- 1c) Assumption, that the shape of the micropores is identical. This is only an approximation that significantly simplifies the theoretical equations. It is quite possible that the micropores are not only polydispersed in size but also in shape.

TABLE 1 Comparison of microstructure parameters determined by gas adsorption (GA) and small angle X-ray scattering methods.

LITHOTYPE		MICROPORE VOLUME ml/g		SURFACE AREA m ² /g			RAD. OF GYR. nm
		GA	SAXS	GA	SAXS		
					(1)	(2)	
DARK	WET	-	0.100	-	30	210	158
	DRY	0.079	0.095	298	90	1100	83
LIGHT	WET		0.110	-	40	390	136
	DRY	0.058	0.060	216	70	830	72

REFERENCES

- [1] Kratky, O., 1940, Zs. El. Chem., 46, 550.
 Porod, G., 1951, Koll. Zs., 124, 83.
 Guinier, A., and Fournet, G., John Wiley & Sons, 1955, Chapter 2, New York.
- [2] Wagenfeld, H.K., Setek, M., Kiss, L. and Stacy, W.O. (1981), Determination of porosity and pore size distribution of brown coal. Proceedings of International Conference on Coal Science, Dusseldorf.

Chemical Variation as a Function of Lithotype and Depth in Victorian Brown Coal

R. B. Johns, A. L. Chaffee and T. V. Verheyen

Department of Organic Chemistry, University of Melbourne, Parkville, Victoria, Australia, 3052.

Introduction

Victorian brown coal occurs in randomly sequenced stratified layers, known as lithotypes, which are distinguishable by their air-dried colour, maceral composition and many physical and chemical properties. The five major lithotypes can be related to generalized paleoenvironments of deposition and are known to influence many coal utilization parameters (1-3). Across the thick coal intervals which occur (up to 300 m) there is a small increase in coal rank observable via parameters such as % carbon and % volatiles (1). The purpose of this paper is to contrast the variation in the organic chemical nature of the coal occurring as a function of depth for a series of (nearly) identical lithotypes with that occurring as a function of lithotype. We have employed techniques giving both precise molecular level information (e.g., the distribution of extractable lipid classes) and average structural characterization of the whole coal (e.g., parameters derived from IR, solid state ^{13}C -NMR, etc.). All of these techniques have been able to provide much deeper insights into the varying nature of the coal than the conventional elemental and functional group type analyses which have been carried out extensively in the past.

Materials and Methods

Coal samples were taken from a single bore core (LY 1276) from the Flynn field in the Loy Yang region of the Latrobe Valley, Victoria, Australia. The core consists of > 100 m of continuous coal, but penetrates two coal seams, viz. Morwell 1A and Morwell 1B. These seams range from late Oligocene to Miocene in age. It is estimated that deposition of the 100 m of coal would have taken approximately 1 million years. Samples were chosen by visual examination of the air-dried colour of the coal. Lithotype classifications on this basis are usually, but not always correct; it was therefore found necessary to modify some of the initial classifications after a consideration of all the available petrographic and chemical data. This correction has not been incorporated in previous publications from our group (4). Further details relating to these samples, methods of fractionation and experimental techniques can be found elsewhere (5-6).

Characterization of Whole Coals

Before considering the results of other more sophisticated analyses it is useful to demonstrate the divergent chemical nature of the coal lithotypes by a more classical approach. When elemental analytical data are expressed in bond equivalence form it can be seen (Figure 1) that there is some inherent spread in the plotted points for the suite of light lithotype samples. The different lithotypes are, however, readily distinguishable due to the much greater variance in their analytical figures. The distinguishing features are especially exhibited at the extremes of the lithotype classification as an increase in the number of bonds associated with carbon at the expense of hydrogen for the dark lithotype and visa versa for the pale lithotype. For the light samples the bond equivalent data are most consistent for carbon, with the mean values for hydrogen and oxygen exhibiting higher proportional standard deviations. The bond equivalence data implies that the difference between the lithotypes resides in the type of chemical structure(s) that the elements form.

There are only a few solid-state techniques capable of providing structural information on "whole" coals. The CP-MAS ^{13}C -NMR spectra of Victorian brown coals exhibit significant fine structure including phenolic and carboxylic resonance envelopes which are consistent with their low aromaticity and rank. The proportion of aromatic carbon atoms, $f(a)$, in the coal can be determined from the spectra and the variation in this parameter across the sample suite is illustrated in Figure 2. While there is some spread in the $f(a)$ values amongst the light samples ($\bar{x} = 0.52$, $\sigma = 0.03$) there is no obvious trend with depth. The variation as a function of lithotype transcends the inherent spread in the light samples and there is an obvious increase in aromaticity for the progression from paler to darker lithotypes. Only the medium-light sample cannot be adequately distinguished within the sample suite by this technique. In addition to their higher aromaticities the spectra of the medium-dark and dark lithotypes exhibit prominent phenolic and methoxyl carbon absorptions similar to the spectra of degraded lignins. Hence the variation in $f(a)$ as a function of lithotype is considered to be predominantly the result of variation in the original organic input and in the relative preservation of various biopolymeric materials within the corresponding depositional paleoenvironments. Although aromaticity is known to correlate with coal rank over a wider regime, there is no suggestion of a regular increase in $f(a)$ over the depth interval examined. The small variation in $f(a)$ for the several light samples is probably a reflection of minor changes in the depositional paleoenvironments.

Absorption mode IR spectroscopy provides greater sensitivity for the observation of specific functional groups. The variation in the absorption coefficients K_{2920} (aliphatic C-H stretch) and K_{1710} (carbonyl, carboxyl stretch) across the suite of samples is illustrated in Figure 3. It is again obvious that the variation as a function of lithotype exceeds the spread inherent in the set of light samples. The proportional spread for the light samples is significantly more intense for K_{2920} ($\bar{x} = 14.1 \text{ cm mg}^{-1}$, $\sigma = 2.9$) than for K_{1710} ($\bar{x} = 36.2$, $\sigma = 2.2$), but in neither case is there any definitive trend with depth. A strong negative correlation ($r = -0.95$) exists between K_{1710} and $f(a)$ for all samples examined. The correlation between $f(a)$ and K_{2920} is significantly lower ($r = -0.84$) as would be expected from the higher proportional spread in the K_{2920} values. The structural implications of these relationships are not entirely clear, but the IR data provide a further clear indication of the effect of the depositional paleoenvironment upon the coal structure(s) which are ultimately preserved.

Rock-Eval analysis is a form of temperature programmed pyrolysis often applied to petroleum source rocks in which the level of evolved carbon dioxide and hydrocarbon-like material are quantitatively measured via oxygen (OI) and hydrogen (HI) indices. The temperature at which the maximum amount of volatile material is evolved (T_{max}) is also recorded, and this can be related to the rank of the organic substrate. The average T_{max} values for the samples under consideration was observed to be 397°C ($\sigma = 2.6$), a value which corresponds to a vitrinite reflectance of ~ 0.30 . No significant regular variation in T_{max} was observed with either depth or lithotype and this method, also, does not provide any indication of the slight increase in rank over the 100 m coal interval. A plot of HI versus OI (Figure 4), however, provides a further method for distinguishing the lithotypes. Although there is a significant spread in the HI values for the light samples, the OI data enable better discrimination between the different lithotypes. This observation supports the NMR and IR data in suggesting that lithotype is a coal property especially influenced by the nature and concentration of oxygen containing species. HI is a measure of the hydrocarbon production potential and correlates strongly ($r = +0.94$) with the percentage of extractable material (see later); it is a parameter which has substantial significance for coal-to-oil conversion. It can be seen that the lighter lithotypes and especially the pale sample provide greater potential in this respect.

Characterization of Coal Fractions

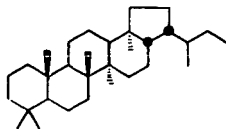
The variation in the weight percentage of total solvent extractable (TSE) material (extraction with chloroform/methanol/toluene) and solvent extractable humic acid (SEHA) for the coal samples is illustrated in Figure 5. There is a substantial reduction in the weight % of these fractions in the progression from paler to darker lithotypes. It can also be seen that the variation with lithotype is significantly more extreme than the variation within the suite of light lithotypes. Within the latter suite there is a notably large difference in the weight percentages between the two adjacent samples from 59 m and 78 m depth in the core. The jump across this interval can be related to the Morwell 1A/Morwell 1B seam boundary which occurs at the 73 m depth. Taking into account this aberration the data are consistent with an increase in extractable material as a function of depth (for samples within a particular lithotype classification and seam). The increase across the interval from 78 to 119 m depth is quite marked by comparison with the increase in extractable material which accompanies increasing rank within the subbituminous rank regime (7). There have been, however, no previous systematic studies giving any indication of what to expect within this lower rank interval. A more intense study of rank dependent phenomena within this interval could significantly enhance our understanding of coal forming processes.

The distributions of extractable n-alkanes from the different lithotypes are illustrated in Figure 6. All the distributions exhibit a marked predominance of odd carbon chain length homologues and in this respect all are similar to the distribution of n-alkanes which occur in living higher plant waxes. In other respects, however, the distributions differ markedly. For example, the dark lithotype exhibits a primary maximum at C₂₉ and a secondary one at C₂₅. The medium dark and pale lithotypes exhibit only primary maxima at C₃₁ and C₂₉, respectively. By contrast, all the light samples exhibit primary maxima at C₂₉ and secondary maxima at C₃₇. These C₃₇ maxima appear to be a distinctive feature of the light samples and have almost certainly resulted from the input of some fairly specific taxon which was viable only in association with the paleoenvironment of deposition for this lithotype. The distribution can be further characterized by Carbon Preference Indices (CPIs), a parameter which is effectively the ratio of the abundance of odd relative to even carbon chain lengths. It can be seen (Figure 7) that there is considerable spread in the CPI values for the light samples and that only the CPI value for the dark lithotype lies significantly outside this margin. There is no apparent changes in the distribution of n-alkanes as a function of depth and it would appear that the distributions remain substantially representative of those contributed by the higher plant progenitors of the coal.

A consideration of the extractable n-fatty acid distributions gives a complementary characterization of the sample suite. The distributions are again a reflection of those observed in the higher plant precursors to the coal. The distributional differences between lithotypes and the similarities within a single lithotype classification are less obvious than in the case of the n-alkanes, but a statistical approach involving the determination of covariance between sample pairs was able to effectively differentiate the divergent nature of the distributional variations as a function of depth and lithotype (5). CPI values for the n-fatty acid distributions are plotted in Figure 8 (CPI, in this case, is effectively the ratio of even relative to odd chain lengths). Again there is a considerable difference in the values for the various lithotypes, but the spread of values within the light sample suite is relatively small. Within this spread, however, it is possible to discern a general reduction in the CPI values with depth. There is again a discontinuity across the seam boundary. There is a corresponding general reduction in the level of extractable n-fatty acids over this depth interval and the consistent variation in these two parameters is believed to indicate that progressive diagenetic removal and alteration of the fatty acids is occurring with depth within this coal sequence. The discontinuity across the seam

boundary is an indication of the complex combination of paleobotanical, geochemical and microbiological factors which control the diagenetic progression.

Many coals contain extended chain (> 31 carbon atoms) hopanes and related compounds which appear to be diagenetically derived from the lipids of certain procaryotic organisms. Biologically produced hopanoids exclusively possess 17 β H,



17 β H, 21 β H-homohopane

21 β H stereochemistry. The thermodynamically more stable 17 α H, 21 β H stereochemistry has usually been explained to form in the geosphere via diagenetic acid catalyzed and temperature dependant isomerization from the biological diastereomers. Hence the diastereomeric ratio, 17 α H, 21 β H/17 β H, 21 β H has been observed to rise in simulated maturation studies and with increasing depth of burial in sedimentary sequences. The present data exhibit a reversal of this trend; that is, there is a reduction in this ratio with depth for the series of light samples (Figure 9). Although there must be some mechanism to account for the formation of the abiological 17 α H, 21 β H-diastereomers in the first place, the data suggest that 17 β H, 21 β H-diastereomers are being progressively produced with depth in the coal seam. On the basis of present understanding this could only occur by microbiologically mediated processes. The temperatures reached within the coal seam are obviously insufficient to force the isomerization towards its thermodynamic equilibrium. There is also a significant difference in the diastereomeric ratios determined by lithotype. This marked difference is probably substantially determined during the early stages of coal deposition where it may be significantly influenced by the pH of the surrounding swamp water or the coal surface acidity. The significant difference in the diastereomeric ratios (Figure 10) as a function of lithotype is consistent with the preceding explanation; that is, the dark lithotypes can be generally associated with higher acidities (and hence pH) which would favour the formation of the abiological isomer, as observed.

The polycyclic aromatic hydrocarbons (PAHs) in brown coal consist predominantly of pentacyclic angularly condensed hydroaromatic moieties. These compounds appear to be derived from C₃₀ triterpenoid precursors which occur as natural products in angiosperm waxes. It can be seen (Figure 10) that there is a marked variation in the concentration of PAHs as a function of both lithotype and depth. The variation as a function of lithotype is consistent with our views on the generalized paleo-environments of deposition, i.e., the lighter lithotypes are deposited in relatively anaerobic environments more conducive to the preservation of the originally deposited organic material, while the darker lithotypes are deposited in relatively aerobic environments in which much of the less resistant organic material is removed by oxidation or substantially altered microbiologically. The increasing concentration in PAH concentration with depth for the series of light samples suggests that the formation of PAHs is also occurring within the coal seam. It seems most likely that this transformation, too, is microbiologically mediated.

Conclusions

The organic chemical nature of Victorian brown coal has been shown to vary as a function of both depth and lithotype. In the latter case the structural differences occur predominantly as a result of the differing nature of the depositional paleoenvironments and are readily distinguishable by both gross and molecular level parameters. The differences with depth are considerably more subtle and were observed only by specific molecular techniques; e.g., the level of PAHs, the diastereomeric ratio of hopanoids and the CPIs of the n-fatty acid distributions. Since the observed structural differences at the molecular level involve only a small proportion of the total coal substrate (parts per thousand level) it is hardly surprising that they are not manifested at the gross structural level. Although mild increases in temperature certainly occur across the sampled coal interval, the specific nature of the chemical changes observed with depth suggests that microbiological processes rather than geochemical (temperature dependent) processes are chiefly responsible. It may be that the warmer conditions deeper in the seam favour the viability of anaerobic microorganisms which can modify the coal substrate in the required manner, or more probably that the closer proximity of the deeper samples to underground aquifers (and potential sources of oxygen and inorganic nutrients) favour the viability of aerobic microorganisms.

Acknowledgements

The authors acknowledge the Victorian Brown Coal Council and the State Electricity Commission of Victoria for the provision of coal samples. Mr S. Bombaci is thanked for technical assistance.

References

- (1) Allardice D. J., George A. M., Häusser D., Neubert K. H. and Smith G. C., State Electricity Commission of Victoria, Research and Development Department, Report No. 342 (1977).
- (2) Blackburn D. T., presented at "Cainozoic Evolution of Continental South-Eastern Australia" conference, Canberra, Nov. 1980.
- (3) George A. M., State Electricity Commission of Victoria, Petrographic Report No. 17 (1975).
- (4) Johns R. B., Verheyen T. V. and Chaffee A. L., "Proceedings of the International Conference on Coal Science, Düsseldorf, 1981", Verlag Glückauf, Essen, pp. 863-868 (1981).
- (5) Chaffee A. L., "The Organic Geochemistry of Australian Coals", Ph.D. dissertation, University of Melbourne (1981).
- (6) Verheyen T. V., "Structural Characterization of Selected Australian Coals", Ph.D. dissertation, University of Melbourne (1982).
- (7) Radke M., Schaefer R. G., Leythausen D. and Teichmüller M., Geochim. Cosmochim. Acta, 44, 1787-1800 (1980).

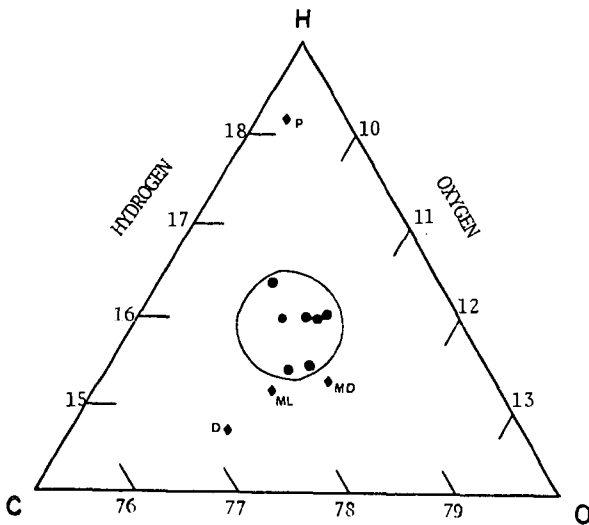


Figure 1 Ternary % bond equivalence diagram for whole coal samples.
 ● - Light lithotype samples; ◆ - other lithotypes as labelled:
 P - pale, ML - medium light, MD - medium dark, D - dark.

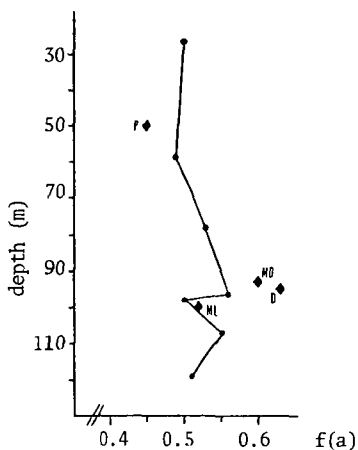


Figure 2 Aromaticity versus depth. Data for the light lithotype samples are joined to illustrate the spread of values.

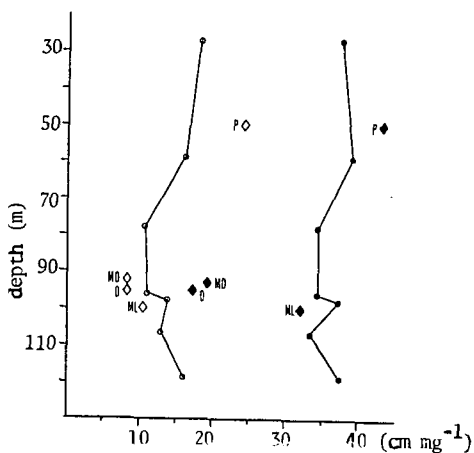


Figure 3 Infrared absorption coefficients versus depth. Closed symbols refer to K_{1710} ; open symbols refer to K_{2920} .

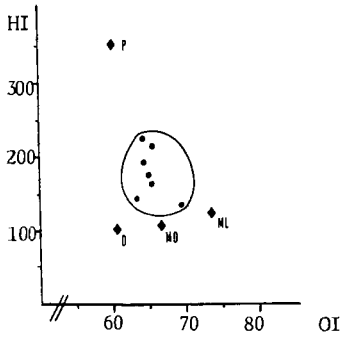


Figure 4 Hydrogen index (HI, mg HC/g TOC) versus oxygen index (OI, mg CO₂/g TOC) from Rock-Eval analysis.

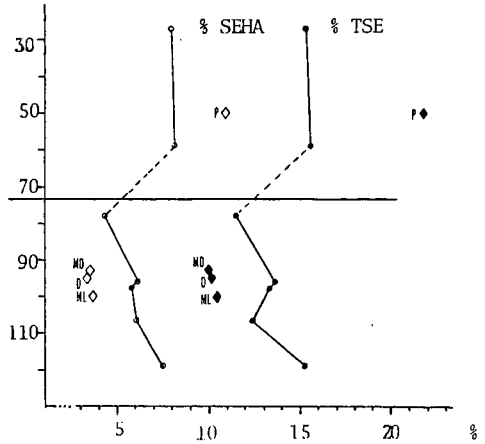


Figure 5 Weight % TSE (closed symbols) and SEHA (open symbols) versus depth. The horizontal line at 73 m represents the Morwell 1A/Morwell 1B seam boundary.

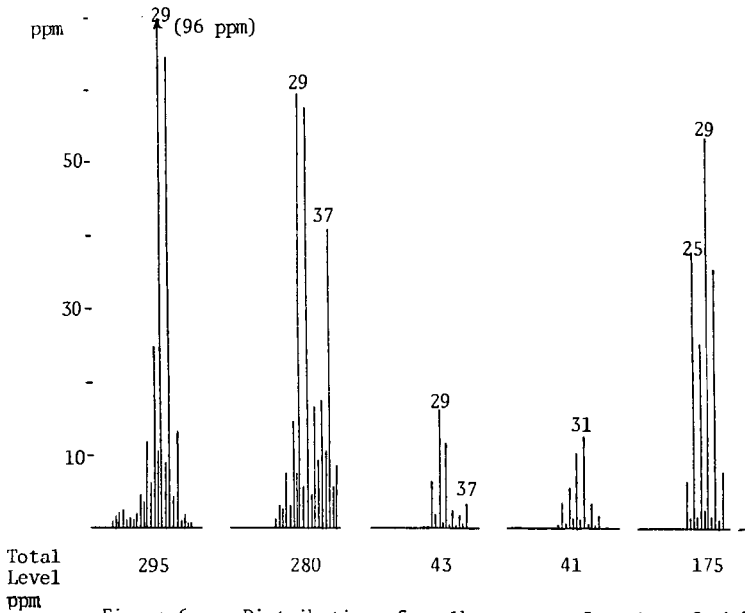


Figure 6 Distribution of n-alkanes as a function of lithotype.

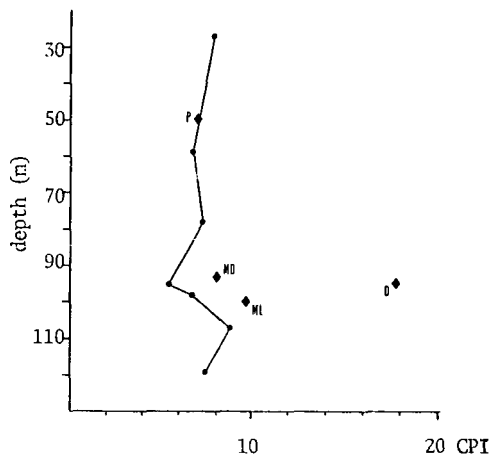


Figure 7 Carbon Preference Indices of n-alkanes versus depth.

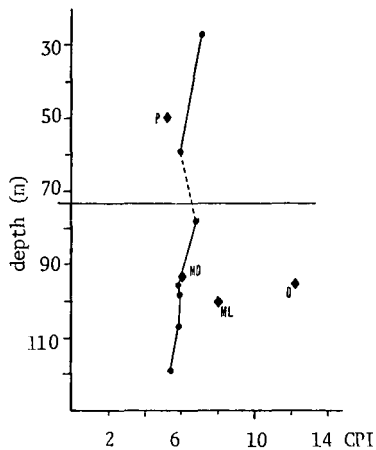


Figure 8 Carbon Preference Indices of n-fatty acids versus depth.

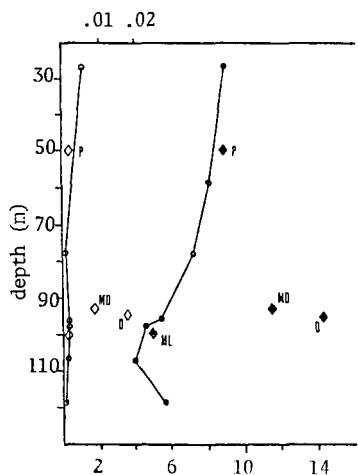


Figure 9 Ratio of diastereomers, $17H,21H/17H,21H$, for homohopane (closed symbols, bottom axis) and biohomohopanoic acid (open symbols, top axis).

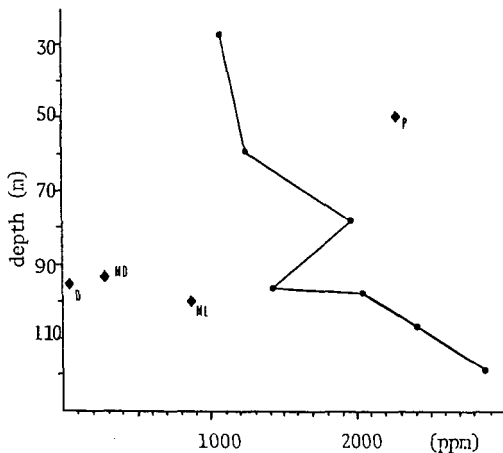


Figure 10 Level of extractable polycyclic aromatic hydrocarbons versus depth.

COMPARISON OF HYDROCARBON EXTRACTS FROM SEVEN COALS BY CAPILLARY GC AND GC/MS

Sylvia A. Farnum, Ronald C. Timpe*, David J. Miller, and Bruce Farnum

U.S. Department of Energy
Grand Forks Energy Technology Center
Box 8213, University Station
Grand Forks, North Dakota 58202

Coals have been shown to contain paraffinic hydrocarbons whose structures arise directly from biological precursors. The types of hydrocarbons usually considered in this group of biological markers include n-alkanes, acyclic isoprenoids, steranes and terpanes. The amounts of these materials that can be extracted from coal are small but even the characterization of these small amounts of alkanes can be very important in determining the origin and maturity of coals. A detailed understanding of the origin of coals and of the diagenesis and maturation of coals may someday be deduced by drawing upon the large body of available information on the relationships of biological markers to the geologic history of rocks, sediments, oil shales and petroleum. The subject has been reviewed (1,2). Some biological markers have also been detected in coal liquefaction products (3,4).

Seven coals were selected for analysis in this study. These seven coals have also been utilized for various liquefaction studies at the Grand Forks Energy Technology Center (GFETC). Their proximate and ultimate analyses are shown in Table 1.

The finely pulverized (-100 mesh) coals were sequentially extracted with chloroform (Soxhlet, 6 hr) and the ternary azeotrope chloroform: acetone: methanol, 47:30:23 (Soxhlet, 14 hr). Each extract was separated into a hexane-soluble and a hexane-insoluble portion. This report deals with the analysis of the hydrocarbons in the hexane-soluble portion (CHX) of the chloroform extract. This fraction contained the hydrocarbons of interest as biological markers. Extraction under these mild conditions gave the extraction yields shown in Table 2.

Capillary GC comparison of retention times with authentic standards and GC/MS were used to characterize the acyclic alkanes present in the CHX extracts. The extracts of Beulah 3 North Dakota lignite (B3), Wyodak Wyoming subbituminous coal (WY01), Highvale Alberta subbituminous coal (ALB1) and Powhatan Ohio bituminous coal (POW1) all contained homologous series of n-alkanes, Table 3. The low-rank coal CHX extracts for the limited members of the series present all gave Carbon Preference Indices, CPI's, (1), greater than one. The alkane distributions and the CPI values are shown in Figure 1. The observed n-alkane distributions were in agreement with the observation by Rigby et al. that increasing maturity of the coal was attended by a shift in maximum concentration to shorter chain length alkanes in extracts (5).

As has been previously reported, high temperature high pressure coal liquefaction as well as coal maturation lowers the odd/even carbon preference values to near 1.0 (3). This effect was also noted when the analyses of processed liquid products from the GFETC continuous processing liquefaction unit were compared with the CHX coal fractions extracted under mild conditions. CPI values of 1.0 were obtained for the processed liquids from B3 and WY01 low-rank coals compared with values of 1.8 for the fractions extracted under mild conditions. These coal extracts should contain alkanes that were present in the coal, whereas, the heat-altered, processed products also contain alkanes formed from cracking of waxes, other alkanes, and other aliphatic portions of the coal. In the case of the higher rank bituminous coal, POW1,

*Associated Western Universities, Inc., Summer Faculty Research Participant
present address -- Mayville State College, Department of Chemistry, Mayville,
North Dakota 58275

TABLE 1
ANALYSIS OF COALS

	Beulah 3	Morwell	Big Brown 1	Big Brown 2	Wyodak	Highvale	Powhatan
	(ND) B3	(Australia) MOC	BB1 (TX)	BB2 (TX)	(Wyoming) WY01	(Alberta) ALB1	(Ohio) POW1
<u>Proximate Analysis</u>							
<u>As received:</u>							
Moisture	28.84	10.19	27.55	28.87	30.99	17.79	4.00
Volatile Matter	28.99	43.00	32.10	38.27	30.43	39.83	39.47
Fixed Carbon	30.76	43.63	30.72	19.53	32.96	32.01	46.71
Ash	11.70	3.19	9.63	13.33	5.62	10.37	9.81
<u>Ultimate Analysis</u>							
<u>Moisture-free:</u>							
Ash	16.44	3.55	13.29	18.74	8.15	12.61	10.22
<u>Moisture and ash-free</u>							
<u>(maf):</u>							
Carbon	69.49	70.64	73.15	74.00	73.74	74.41	79.01
Hydrogen	4.43	5.01	5.22	6.09	5.38	4.92	5.43
Nitrogen	0.99	0.46	1.40	1.22	1.22	0.95	1.29
Sulfur	2.81	0.33	1.30	1.21	0.53	0.20	3.92
Oxygen (by difference)	22.26	23.56	18.93	17.48	19.12	19.52	10.35

the CPI was the same, 0.9 both before and after processing indicating maturation of the coal.

TABLE 2

SEQUENTIAL EXTRACTION OF COALS WITH CHCl_3 (SOXHLET), CHCl_3 :
ACETONE: METHANOL, 47:30:23, AZEOTROPE (SOXHLET) AND SEPARATION OF HEXANE
SOLUBLES (% MAF COAL, DUPLICATES WERE AVERAGED)

	Total CHCl_3 Soluble (Soxhlet)	Hexane Soluble Portion of CHCl_3 Extract	Total Azeotrope Soluble (Soxhlet)	Hexane Soluble Portion of Azeotrope Extract
B3	2.8	1.0	1.6	0.13
MOC ⁺	0.82	0.58	1.7	0.59
BB1	4.2	1.7	2.2	0.16
BB2	3.7	1.7	2.4	0.19
WY01	3.2	2.9	5.0	0.21
ALB1	0.58	0.35	1.8	0.28
POW1	0.70	0.51	5.8	1.1

⁺Values given from single extraction only.

The CHX extracts from B3 and POW1 were the only extracts of the seven that contained pristane. The bituminous coal, POW1, extract had more pristane than the B3 extract, Table 3. Phytane was not detected in any of the extracts, although both pristane and phytane were found in all of the coal liquefaction products from B3, BB1, WY01, and POW1. The ratio of pristane to phytane was about 5:1. It has been reported that the pristane content of the saturated hydrocarbon fraction from subbituminous coals of more than 76% C begins to increase (1). The increase in phytane concentration corresponds roughly to 83-85% C.

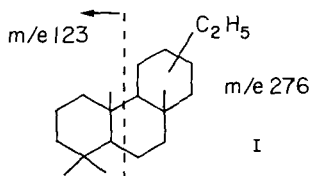
Some of the cyclic hydrocarbons found in the CHX coal extracts are shown in Table 4. They were tentatively identified by capillary GC/MS except for the naphthalenes, for which authentic standards were available. Selected ion scans were used to detect sesquiterpenes (m/e 206, 191), sesquiterpanes (m/e 208), alkanes (m/e 141), alkyl benzenes (m/e 191, 163), steranes (m/e 217), and tricyclic terpenoids (m/e 191, 163) as well as the m/e values for the parent ion of specific compounds. Figure 2 shows the results of one of these selected ion scans, m/e 206, from the CHX extract of WY01 along with a portion of the total ion chromatogram. The peaks shown in the m/e 206 trace between scan numbers 240 and 300 correspond to the sesquiterpenes listed in Table 4. All of these compounds showed M-15 peaks of various intensities (m/e 191), relatively intense M-29 peaks (m/e 177) and m/e 121 peaks. One compound, c, had a prominent even mass peak at 178. Six had more prominent M-43 (m/e 163) peaks than the others. The fragmentation patterns shown by these $\text{C}_{15}\text{H}_{26}$ sesquiterpenes resemble those reported by Richardson (6) for a series of $\text{C}_{15}\text{H}_{28}$ bicyclics identified in a crude oil. The sesquiterpene distribution for the CHX extracts of B3 and WY01 were distinctive and similar. The distribution for ALB1 gave smaller concentrations of sesquiterpenes, Table 4, but the mass spectra were identical for comparable ALB1, WY01, and B3 sesquiterpenes with the same GC retention times. POW1, MOC, BB1, and BB2 CHX extracts did not contain these compounds. No sesquiterpanes with (m/e 208) were detected in any of the CHX extracts. Gallegos (7) found a number of sesquiterpenes (m/e 206, 191) in pyrolysis products of six coals including Wyodak subbituminous coal and Noonan North Dakota lignite. Gallegos also detected cadalene (m/e 198, 183). Cadalene was present in the ALB1 extract and was probably a small component in the B3 extract. It was not found in the extracts of the other coals.

TABLE 3

ACYCLIC HYDROCARBONS FOUND IN EXTRACTS OF COALS AND THEIR
DISTILLABLE LIQUEFACTION PRODUCTS
(Capillary GC, Area Percent, FID)

	<u>Retention Time, min.</u>	<u>B3 Coal Extract</u>	<u>WY01 Coal Extract</u>	<u>ALB1 Coal Extract</u>	<u>POW1 Coal Extract</u>
<u>Isoprenoids:</u>					
pristane (2,6,10,14,tetramethyl- pentadecane)	168.9	0.15			1.35
<u>n-alkanes:</u>					
C-14					
C-15	125.8	0.82			
C-16					
C-17					
C-18					
C-19	194.1	0.74			0.49
C-20	205.0	0.99			0.41
C-21	215.6	1.38			0.26
C-22	223.9	1.22	1.04		0.46
C-23	232.7	0.69	0.73	1.38	0.31
C-24	241.2	0.67	0.33	0.43	0.46
C-25	249.2	1.89	0.82	1.85	0.34
C-26	256.9	1.55	0.57	0.37	0.29
C-27	264.5	2.92	0.99	0.92	0.33
C-28	271.6	0.42	0.31	0.31	0.25
C-29	278.5	0.76	0.98	0.77	0.25
C-30	285.1	0.57	0.52	0.2	0.25
C-31	290.2	0.29	0.56	0.59	0.10
C-32	296.1				0.02
C-33	300.1				0.03
C-34	304.3				0.001
C-35	308.7			0.19	0.03
C-36	312.0			0.09	0.004
C-37	316.6				0.01
C-38	320.4				0.006
C-39	324.0				0.008

Another compound which gave identical mass spectra in two of the extracts, WY01 and ALB1, appears to be one of the tricyclic alkanes, $m/e = 276$. An intense peak at m/e 247 corresponds to M-29. The mass spectrum was an excellent match with that presented by Philip, et al. (8) for which structure I was proposed. An intense peak at m/e 123 was noted and is probably due to the fragmentation shown.



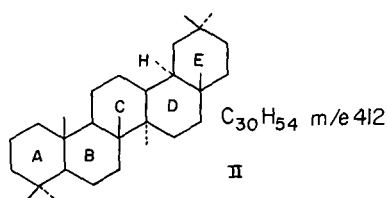
At a slightly longer retention time the component m/e 234 appears to be another tricyclic alkane, $C_{17}H_{30}$. Several similar tricyclic alkanes were reported by Jones et al. (4).

The spectrum of m/e 252, identical in WY01 and ALB1 extracts, corresponds to $C_{18}H_{36}$ but is not dodecylcyclohexane (9). There is a prominent M-15 peak at m/e 237 and relatively intense peaks at m/e 111 and 195. The peak at 111 could be assigned as a dimethyl-cyclohexyl fragment.

The compounds detected in the mass range 398-454 in B3, BB1, BB2, and POW extracts appear to be pentacyclic triterpanes since all have prominent m/e 149, 177, 191, and 205 peaks (10). When selected ion chromatograms are compared, WY01 extract shows no m/e 191 peaks for GC retention times in the pentacyclic triterpane region. The BB coal extracts, B3, ALB1 and POW1 all have numerous small peaks that are probably triterpenoids. Some of these gave appreciable GC FID responses and good mass spectra.

The spectrum of m/e 398 is identical for ALB1 and POW1 extracts. The compound is not adiantane since the m/e 191 is greater than 177, not of similar intensities (11). $C_{27} - C_{31}$ triterpanes, especially adiantane, C_{29} , have been found in bituminous coal extracts (12).

The pentacyclic component at m/e 412 resembles the spectrum of oleanane (II) or gammacerane. It is also similar to that of lupane (11,13) but lacks the M-43 (369) fragment indicative of any isopropyl sidechain. Therefore, ring E is probably 6-membered, not 5-membered as in lupane or the hopanes. Although the mass spectrum is a slightly better match to gammacerane, the short retention time probably rules out gammacerane but not oleanane.



The two different $C_{31}H_{54}$ pentacycles (m/e 426), one observed in BB2 extract and one in POW1 extract had no M-29, M-43 or M-57 fragments. The m/e 205 was small

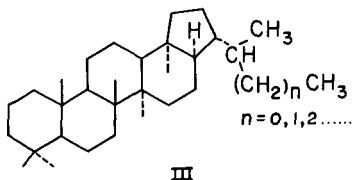
ruling out structures like lupan-3-one (14). Other differences also eliminate friedelan-3-one and oleanan-3-one type of structure (14).

The m/e 440 pentacyclic representative found in BB1 and BB2 had an M-29 peak (411) and a prominent peak at 369. It could therefore be a homohopane. None of pentacyclic structures found in any of the extracts could correspond to the unaltered less stable $17\beta H$, $21\beta H$ hopane series because m/e 191 is much larger than the secondary fragment in all cases. The structure could be a $17\alpha H$, $21\beta H$ hopane which is common in geologically altered sediments of all kinds (III).

TABLE 4
OTHER HYDROCARBONS FOUND IN EXTRACTS OF COAL CAPILLARY
GC AND GC/MS, AREA %, FID

	Retention Time, Min.	m/e, Parent Ion	Capillary GC, Area %				POMI			
			B3	MOC	BB1	BB2		WY01	ALB1	
Miscellaneous:										
naphthalene	47.9			0.32				0.18	0.12	1.2
2-methylnaphthalene	72.0			0.29				0.19	0.38	2.7
1-methylnaphthalene	75.6			0.04				0.09	0.13	2.0
C ₂ -naphthalene	95.3									0.68
cadalene	160.4	198	0.31							1.3
Alicyclic terpenoids:										
C ₁₅ H ₂₆ sesquiterpene	100.7	206						2.8		
"	104.8	206						1.0		
"	106.8	206	1.9					13.2	0.70	
"	108.9	206	1.12					3.3		
"	111.2	206	0.24					8.3	0.17	
"	113.0	206						4.6	0.27	
"	114.9	206	2.3					1.5	1.9	
"	116.2	206	0.10					0.96	0.17	
C ₂₀ H ₃₆ tricyclic alkane	230.3	276						0.96	0.46	
"	233.4	252							0.50	
C ₁₇ H ₃₀ tricyclic alkene	236.4	234	1.2					1.0	0.50	0.10
"	272.5	Not Shown					0.66			
C ₂₉ H ₅₀	284.6	398							0.27	0.13
C ₃₀ H ₅₂	285.2	412								0.13
C ₃₁ H ₅₄	287.0	426					3.3			
C ₃₁ H ₅₄	295.8	426								0.03
C ₃₂ H ₅₆	312.0	440					3.0	1.1		
C ₃₃ H ₅₈	321.7	454	0.07				1.7	3.5		

The m/e 454 pentacyclic triterpene (BB1, BB2 extracts) is also unidentified.



A number of hydrocarbon fractions from liquefaction products produced at GFETC from the coals studied here were investigated using selected ion scans of the capillary GC/MS analyses. None of the hydrocarbon biological markers other than the acyclic alkanes already discussed were detected. There were no sesquiterpenes, sesquiterpanes, steranes, triterpanes or other cyclic terpenoids found.

CHX extracts of the seven coals were profiled using capillary GC. The best results were obtained using a J. & W. DB5 60 N fused silica capillary column with H₂ carrier and flame ionization detector. Temperature programming from 50° to 125°C at 0.5°C/min, from 125° to 250°C at 1.0°C/min and from 250° to 350°C at 1.5°C/min, then an isothermal plateau at 350°C was used.

There were some striking similarities and differences between profiles for the coal CHX extracts. The profiles for CHX extracts of MOC, BB1 and BB2 were very similar. They show no detectable alkanes and very few peaks until 230 min when the maximum temperature was reached. Between 230 min. and 320 min. a large group of peaks form a dense envelope.

The capillary GC profiles for B3 and WY01 extracts are also strikingly similar, with nearly every major GC peak having a counterpart in each chromatogram. ALB1 extract shows some similarity to the WY01 trace but differs, the POW1 extract profile is also different. All of the GC profiles for B3, WY01, ALB1 and POW1 CHX extracts have continuous baseline resolved peak distributions from about 50 to 350 minutes with various recognizable patterns. From duplicate extractions of the same coal and by comparing BB1 and BB2 extracts, it may be seen that the profiling of the hydrocarbon extracts is reproducible and may be used to identify and group coals.

Each of the CHX extracts also contained some oxygen compounds. The elemental analyses showed 5-6% oxygen present. Although the characterization of these compounds is not complete, it may be noted that all of the extracts contained some 60-70 carbon nonvolatile waxes (long chain fatty acid esters). The presence of these esters was demonstrated by methanol/BF₃ transesterification followed by capillary GC and 200 MHz ¹H NMR analyses.

SUMMARY

The chloroform extraction of seven coals yielded extracts that gave unique capillary GC profiles. Several groups of hydrocarbon biological markers were detected in the coal extracts by mass spectrometry using selected ion scans. n-Alkanes, pristane, sesquiterpenes, several tricyclic alkanes and pentacyclic triterpanes with molecular weights from 398 to 454 were detected. The coal extract profiles fell into four groups: 1) BB1, BB2 (Texas lignites) and MOC (Australian lignite); 2) B3 (North Dakota lignite) and WY01 (Wyoming, subbituminous); 3) ALB1 (Alberta, Canadian subbituminous), and 4) POW1 (Ohio, bituminous). Profiles were characteristic and reproducible for each coal.

ACKNOWLEDGEMENTS

The authors would like to thank Art Ruud for the extensive coal analyses he and his group carried out. Thanks also to John Diehl for running the capillary GC profiles of the seven coal extracts.

REFERENCES

1. Bartle, K.D., Jones, D.W., Pakdel, H. "Analytical Methods for Coal and Coal Products," Academic Press, New York, San Francisco, London, 1978; Part II, 209-262.
2. Bartle, K.D., Jones, D.W., Pakdel, H. "Coal and Coal Products: Analytical Characterization Techniques," American Chem. Society Symp. Ser., American Chemical Society, Washington, D.C., Volume 205, 1982, 27-45.
3. White, C.M., Shultz, J.L., Sharkey, A.G., Jr. Nature, 1977, 268, 620-622.
4. Jones, D.W., Pakdel, H., and Bartle, K.D. Fuel, 1982, 61, 44-52.
5. Rigby, D., Batts, B.D., and Smith, J.W. Org. Geochem., 1981, 3, 29-36.
6. Richardson, J.S. and Miller, D.E. Anal. Chem., 1982, 54, 765-768.
7. Gallegos, E.J. J. Chromatog. Sci., 1981, 19, 156-160.
8. Philip, R.P., Gilbert, T.D., and Friedrich, J. Geochim Cosmochim Acta, 1981, 45, 1173-1180.
9. Rubinstein, I. and Strausz, O.P. Geochim. Cosmochim Acta, 1979, 1387-1392.
10. Kimble, B.J., Maxwell, J.R., Philip, R.P., Eglinton, G., Albrecht, P., Ensminger, A., Arpino, P., and Ourisson, G. Geochim. Cosmochim. Acta, 1974, 38, 1165-1181.
11. Henderson, W., Wollrab, V., Eglinton, G. Advan. Org. Geochem., Proc. Int. Meet., 4th, 1968, (1969), 181-207.
12. Allan, J., BJORORY, M., Douglas, A.G. Advan. Org. Geochem., Proc. Inst. Meet., 7th, 1975, (1977), 633-654.
13. Ekweozor, C.M., Okogun, J.I., Ekong, D.E.U., and Maxwell, J.R. Chem. Geol. 1979, 27, 11-28.
14. Budzikiewicz, H., Wilson, J.M., Djerassi, C.D. J. Am. Chem. Soc., 1963, 85, 3688-3699.
15. Ensminger, A., Van Dorsselaer, A., Spyckerelle, Ch., Albrecht, P., Ourisson, G. Adv. Org. Geochem., Proc. Int. Meet., 6th, 1974, (1976), 245-260.

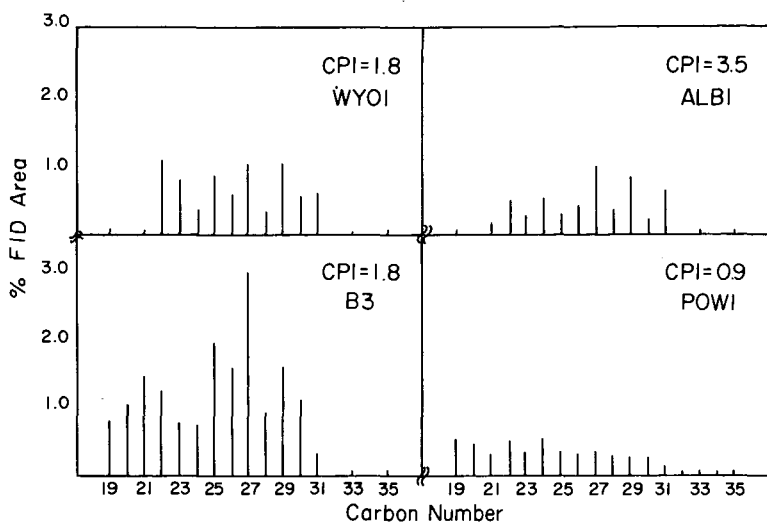


FIGURE 1. Alkane distribution in coal extracts.

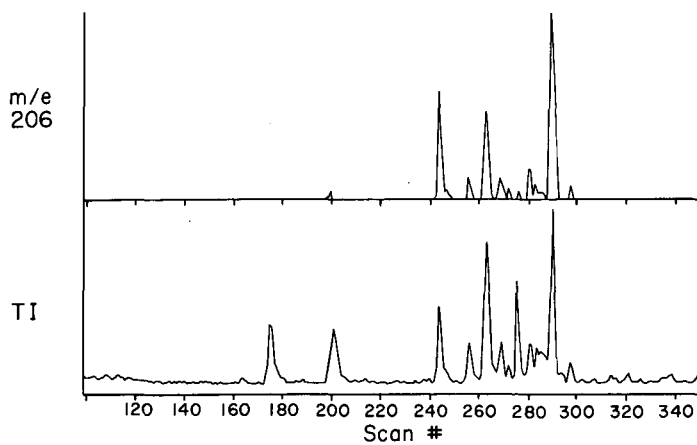


FIGURE 2. m/e 206 selected ion scan for sesquiterpenes and total ion current chromatogram, WY01 CHX extract.

THE ORGANIC CONSTITUTION OF WILCOX LIGNITE

N. Maliya, R.A. Zingaro, R.D. Macfarlane and J.H. Zoeller, Jr.

Department of Chemistry, Texas A&M University,
College Station, Texas 77843

The distribution of functional groups in low rank coals has been the subject of a body of investigations [summarized by Meyers (1982) and Spiro and Kosky (1982)] oriented towards a description of the kinetics and mechanism of thermal conversion processes. Use of the new technique of Californium-252 Plasma Desorption Mass Spectrometry (CFPDMS) as a probe to the structural features of coal have been described by Lytle, Tingey and Macfarlane (1982). The interpretation of CFPDMS spectra has necessitated a functional group characterization of the coal substrate by conventional spectroscopic and chemical techniques. CFPDMS requires the use of organic soluble fractions, and we have utilized DMSO extracts as they seem quite representative of the organic functionalities present. Dry Wilcox Lignite (WL) and some of its solubility fractions have been so characterized, including its DMSO solubles (SD), DMSO insolubles (ID), humic acids (HA), a sample demineralized (DM) by the method of Bishop and Ward (1958), the DMSO extract of this (SDM), and the insoluble residue (IDM). The coal sample used was obtained from a drill core near Rockdale, Texas.

Extraction of WL with DMSO for 24 hours at room temperature gives a 20% yield of extract. Humic acids were obtained by aqueous NaOH extraction and precipitation with HCl. Removal of residual DMSO in the solubles and insolubles can be accomplished by HI treatment with subsequent removal of dimethyl sulfide and HI, but at the cost of some iodine incorporation, ether cleavage, and mineral matter loss.

Acidic Group Titration

Titration for carboxylic acid content, (COOH), were carried out on WL, SD, DM, and SDM according to the methods of Schafer (1970a, 1970b); total acidity was determined on SDM and IDM. The results are reported on a daf basis in Table 1. An enrichment in (COOH) in the DMSO extracts of Wilcox lignite and the demineralized lignite amounts to 0.16 and 0.4 meq(COOH)/g respectively. Carboxylate bound cation content (COOM) is estimated from

$$\text{meq(COOM)/g} = (\text{COOH})_{\text{Demineralized}} - (\text{COOH})_{\text{Dry}}$$

Thus the bound cation content of WL and SD is some 1.5 and 1.8 meq(COOM)/g respectively. From the total acidity data, the concentration of hydroxyl and pyrrole hydrogen (OH, > NH) is estimated from

$$(\text{OH}, > \text{NH}) = \text{total acidity} - (\text{COOH})$$

For the demineralized samples, DM and SDM, this amounts to 4.9 and 5.0 meq(OH, > NH)/g.

Nuclear Magnetic Resonance

Solid state C 13 NMRCPMS spectra for selected solubility fractions were obtained by the NMR Center at Colorado State University. Aromaticities derived from the spectra shown in Figure 1 for WL, ID, SD, and HA are 0.53, 0.55, 0.52, and 0.72. The higher aromaticity of HA is due to both the enhanced height of the 123 ppm absorption due to the truly aromatic carbons, and to the profusion of carboxylates and aromatic oxygen functions in the skirt downfield of 150 ppm.

Proton NMR of SD in d_6 -DMSO exhibits the proton populations shown in Table 2. The chemical shift of hydrogen attached to, or alpha to, oxygen atoms is not at all clear. What is apparent is that the high oxygen content

of this fraction gives rise to peaks in the 3.0-4.0 ppm region of the proton NMR spectrum.

Oxygen bound carbon also accounts for absorption in the downfield flanks of both aromatic and aliphatic peaks in the carbon 13 NMR spectra. Use of shift reagents (Shue and Yen (1983)) is under study in identifying the functionalities involved.

FOURIER TRANSFORM INFRARED SPECTROSCOPY (FTIR)

FTIR spectra of WL, ID, SD and HA were obtained on a Digilab 20C spectrometer in KBr discs. Although grossly similar in appearance, the spectra reveal some notable differences. Aliphatic absorptions at 2825 and 2920 cm^{-1} appear in all the spectra, but the 2825 cm^{-1} peak is much more intense in WL and ID. SD exhibits a prominent band at 2970 cm^{-1} , absent in the others. The carbonyl absorption at 1700 cm^{-1} appears as a shoulder in WL and ID, but is nearly as intense as the coal band (1600 cm^{-1}) in SD and HA. SD shows a pair of intense bands at 1260 and 1010 cm^{-1} , tentatively assigned to the asymmetric and symmetric aryl alkyl ether C-O-C stretch. Both bands are small in HA. In WL and ID, the 1260 cm^{-1} absorption is small, and the 1010 cm^{-1} absorption is masked by the kaolinite doublet at 1010 and 1035 cm^{-1} . Of the aromatic out of plane bending modes, only the 860 cm^{-1} band (isolated hydrogen) is present in all the fractions. The diminutive aromatic C-H stretching band (3000-3100 cm^{-1}) in all the fractions, and the low population of aromatic protons (15.3%) seen in the ^1H -NMR spectrum of SD, suggests that the aromatic moieties are sparse and highly substituted. An unidentified absorption at 800 cm^{-1} appears in all the spectra, but is quite intense in SD.

Pertrifluoroacetic Acid Oxidation (PTFA)

The PTFA reaction described by Deno (1979) has been reinvestigated by Hessley et al (1982) in the analysis of Wyodak coal. In our laboratory, that procedure has led to low and variable product yields when applied to Wilcox lignite. Using a chloroform cosolvent during the oxidation moderates the degradation of aliphatic reaction products. This modification was developed by Lawrence Shadle at Pennsylvania State University. Wilcox lignite yields one hundred methyl esters, as detected by GC/MS, of which fifty comprise over 90% of the product. Fragmentation patterns indicate that the majority of the products are methyl esters of branched and naphthenic hydrocarbons in the molecular weight range of 200 to 400. Methyl laurate is prominent among the straight chain esters present. Aromatic esters and oxirane carboxylates have not been detected among the products. Proton NMR of the crude acids of WL, SD, ID and HA discloses the presence of variable amounts of C₂ to C₅ mono- and dicarboxylic acids. No aromatic absorptions are seen in these spectra, with the notable exception of a 7.3 ppm absorption from SD.

Californium Plasma Desorption Mass Spectrometry (CFPDMS)

In the CFPDMS experiment described by Macfarlane and Torgerson (1976), a fission fragment of Cf-252 impinges on a thin film of substrate, forming high molecular weight ions whose mass is measured by a TOF mass spectrometer. Collision results in a localized hot spot for one picosecond, reaching temperatures of some 10^4 °K. Extracts of Wilcox lignite typically show positive and negative ions in clusters in the mass range of m/z 400 to 800. Isolated clusters of peaks are seen at low signal intensity up to m/z 2000. Although identification of these peaks is only tentative at this time, one of the

fragments does behave as a carboxylate functionality. In the positive ion spectrum of SD, peaks at m/z 646, 668 and 684 occur in a ratio of 8:5:1. The negative ion spectrum exhibits a peak at m/z 644. By analogy with the behavior of known carboxylic acids and their salts, these peaks correspond to structures RCOOHH^+ , RCOOHNa^+ , RCOOHK^+ and RCOO^- respectively. The positive ion peaks at m/z 645 and 668 are also seen in the spectrum of HA.

Functional Description of Wilcox Lignite

On the basis of the ultimate analysis of Wilcox lignite, the organic constitution can be formulated as $\text{C}_{100}\text{H}_{76}\text{O}_{21}\text{NS}$. The titration data indicates 0.6 (COOH)/g., 1.6 meq(COOM)/g., and 4.9 meq.(OH, > NH)/g. In the C_{100} formulation, this corresponds to one carboxylic acid, three carboxylate salts, six hydroxyls and one pyrrole. The remaining seven oxygen atoms are semiarbitrarily distributed among two aryl alkyl ethers, three quinone carbonyls and one ester. By this accounting, eight of the carbons in the C_{100} formulation appear in the downfield skirt of the aromatic C-13 NMR absorption. From this we project forty eight aromatic carbons (not bound to oxygen) and forty three aliphatic carbons. Hydrogen atoms not bound to heteroatoms are assigned according to their integrated populations in the NMR spectrum of SD. Table 3 compiles this distribution within the C_{100} formulation.

Acknowledgements

Support for this project was provided by the Gas Research Institute and the Center for Energy and Mineral Resources. Carbon 13 NMR spectra were obtained by Dr. Bruce Hawkins at the NMR Center at Colorado State University. We thank Lawrence Shadle of the Pennsylvania State University for suggesting his modified procedure for the pertrifluoroacetic acid oxidation.

References

- Bishop, M. and Ward, D.L. (1958) "The Direct Determination of Mineral Matter in Coal": *Fuel* 37, 191.
- Deno, N.C., Griegger, B.A., Jones, A.D., Rakitsky, W.G. and Stroud, S.G. (1979) "Coal Structure and Coal Liquefaction"; Final Report to Electric Power Research Institute from Pennsylvania State University, AF-960, RP-779-16.
- Hessily, R.K., Benjamin, B.M. and Larsen, J.W. (1982) "Deno Oxidation. Isolation of High Molecular Weight Aliphatic Material from Coals and Further Model Compound Studies"; *Fuel* 61, 1085.
- Lytle, J.M. Tingey, G.L. and Macfarlane, R.D. (1982) "Californium-252 Plasma Desorption Mass Spectrometry of Solid Coal": *Anal. Chem.* 54, 1881.
- Macfarlane, R.D. and Torgerson, D.F. (1976) "²⁵²Californium Plasma Desorption Time of Flight Mass Spectrometry": *Int. J. of Mass Spec. and Ion Physics*.
- Meyers, R.A. (1982) "Coal Structure": Academic Press, New York.
- Schafer, H.N.S. (1970a) "Carboxyl Groups and Ion Exchange in Low Rank Coals": *Fuel* 49, 197.
- Schafer, H.N.S. (1970b) "Determination of Total Acidity of Low Rank Coals": *Fuel* 49, 271.
- Spiro, C.L. and Kosky, P.G. (1982) "Space Filling Models for Coal. 2. Extension to Coals of Various Ranks": *Fuel* 61, 1080.
- Shue, F.F. and Yen, T.F. (1983) "Application of Lanthanide NMR Shift Reagents for Functional Group Studies of Shale Bitumen Asphaltenes" *Fuel* 62, 127.

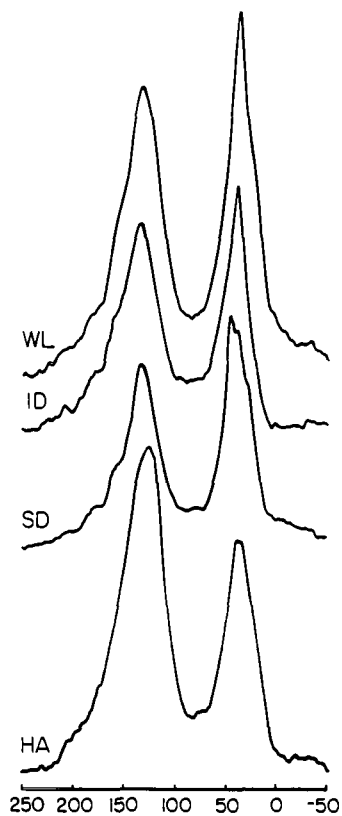


Figure 1. ^{13}C NMR CP/MAS Spectra of Wilcox Lignite (WL), its DMSO Insolubles (ID), DMSO Solubles (SD) and Humic Acids (HA). Scale is in ppm.

Table 1. Acidic Group Concentration of Wilcox Lignite Fractions
(meq/g., daf)

Sample	(COOH)	Total Acidity
Wilcox Lignite, (WL)	.55	---
DMSO Solubles of WL, (SD)	.71	---
Demineralized WL, (DM)	2.1	7.0
DMSO Solubles of DM, (SDM)	2.5	7.5

Table 2. Proton Population (Area %) in Wilcox Lignite DMSO Solubles,
by H-NMR

Proton Type	δ (ppm)	%
H(AR)	4.5-9.0	15.3
H(α 2)	3.3-4.5	14.2
H(α 1)	2.0-3.3	24.0
H(N)	1.5-2.0	12.0
H(β)	1.0-1.5	20.8
H(γ)	0.5-1.0	13.7

Table 3. Accounting of Functional Groups and Atoms in the $C_{100}H_{76}O_{21}NSM_3$ Formulation of Wilcox Lignite Organic Matter. M = Na, Ca, etc.

Group	Population in the C_{100} Formulation	Atoms Present in Specified Groups					
		C	H	O	N	S	M
-COOH	1	1	1	2			
-COOX	3	3		6			3
-OH	6		6	6			
>N-H	1		1		1		
R-O-Ar	2			2			
>C=O	3	3		3			
RCOOR	1	1		2			
Aromatic C	49	49					
Aliphatic C	43	43					
H(AR)	10.4		10				
H(α_2)	9.9		10				
H(α_1)	16.3		16				
H(N)	8.2		8				
H(β)	14.1		14				
H(γ)	9.3		10				
Thiophene(?)							

Table 4. Analyses* of Wilcox Lignite and its Solubility Fractions
 (% Dry Basis).

Sample	C	H	O	N	S	Halogen	Ash
WL	62.75	4.45	19.38	1.28	1.32	0.83	14.16
SD	68.38	5.17	18.22	1.41	1.80	1.04	2.98
ID	64.89	4.67	17.92	1.28	1.50	1.06	8.09
HA	66.83	4.02	23.17	1.41	2.54	0.88	1.26
DM	70.49	5.01	19.57	1.48	1.97	0.78	0.23

*Huffman Laboratories, Inc.

ANALYSIS OF THE INORGANIC CONSTITUENTS IN LOW-RANK COALS

G. P. Huffman and F. E. Huggins

U.S. Steel Corporation, Research Laboratory
125 Jamison Lane, Monroeville, PA 15146

Introduction

In recent years, numerous modern analytical techniques have been applied to the analysis of the inorganic constituents in coal. At the U.S. Steel Research Laboratory, Mossbauer spectroscopy and computer-controlled scanning electron microscopy have been emphasized(1-5). With the advent of very intense synchrotron radiation sources, the technique of extended X-ray absorption fine structure (EXAFS) spectroscopy has been applied in many areas of materials science, and several very recent articles on EXAFS studies of the inorganic constituents of coal have appeared(6-8). For the most part, previously published work has reported investigations of bituminous coals by these three techniques. In the current article, we present some examples of the analysis of the inorganic constituents of lower-rank coals, principally lignites, by these methods. Although the suite of low-rank coals investigated is rather limited, some distinct differences between the inorganic phase distributions in these coals and those in bituminous coals are apparent.

Experimental

Mossbauer spectroscopy is a spectroscopy based on the resonant emission and absorption of low-energy nuclear gamma rays. The ^{57}Fe nucleus exhibits the best Mossbauer properties of all isotopes for which the Mossbauer effect has been observed, and ^{57}Fe Mossbauer spectroscopy is perhaps the best method available for quantitative analysis of the iron-bearing phases in complex, multiphase samples. As discussed in recent review articles(2,9,10) every iron-bearing compound exhibits a characteristic Mossbauer absorption spectrum, and the percentage of the total iron contained in each phase can be determined from absorption peak areas. Detailed descriptions of the Mossbauer spectrometer and data analysis programs used in this laboratory, and discussion of the physical basis of the Mossbauer technique are given elsewhere(10).

The computer-controlled scanning electron microscope (CCSEM) developed in this laboratory consists of an SEM interfaced by minicomputer to a beam-control unit and an energy dispersive X-ray analysis system. Detailed descriptions of this instrument and its use in the determination of coal mineralogy and other applications are given elsewhere(3,11). Briefly, the beam is stepped across the sample in a coarse grid pattern, with typically 300×300 grid points covering the field of view. At each point, the backscattered electron intensity is sampled, and the minicomputer decides whether or not the beam is on a particle. Once a particle is identified, the grid density is increased to 2048×2048 and the area of the particle is measured. The beam-control unit then places the electron beam back

at the center of the particle and an energy dispersive X-ray spectrum is collected. Each particle is then placed into one of up to 30 categories (minerals, compounds, etc.) on the basis of the chemistry indicated by its X-ray emission spectrum, and approximate weight percentages of all categories are calculated. CCSEM is capable of measuring the size and chemical composition of up to 1000 particles per hour for many kinds of particulate samples.

EXAFS spectroscopy examines the oscillatory fine structure above the absorption edge in the X-ray absorption spectrum of a particular element. These oscillations arise from interference between the outgoing photoelectron wave and scattered waves produced by interaction of the photoelectrons with neighboring atoms. As discussed elsewhere (12,13), Fourier transform techniques can be used to extract from these oscillations information about the bond distances, coordination numbers, and types of ligands surrounding the absorbing element. Additional information about the valence or electronic state of the absorbing ion and the ligand symmetry can be obtained from examining the X-ray absorption near-edge spectra, or XANES, in the energy region very close to the absorption edge (within approximately $\pm 20-30$ eV). Such XANES spectra frequently provide characteristic fingerprints for different types of ligand bonding to an absorbing ion (6,7,14,15).

The X-ray absorption spectra of calcium-containing coals and reference compounds discussed in this paper were recorded at the Stanford Synchrotron Radiation Laboratory (SSRL) during a dedicated run of the Stanford Positron-Electron Acceleration Ring at an electron energy of 3.0 GeV. The calcium K-edge occurs at 4038 eV and data were collected from 3800 to 5000 eV, using a double Si (111) monochromator and a fluorescence detector similar to that of Stearn and Heald (16). A more detailed discussion of this work will appear elsewhere (17).

The samples examined were predominantly lignites from the Pust seam in Montana. However, data for two North Dakota lignites, for slagging and fouling deposits produced by those lignites, and for several subbituminous coals are also included.

Results and Discussion

Mossbauer spectroscopy results for all samples investigated are summarized in Table I. The percentages of the total sample iron contained in each of the iron-bearing minerals identified are given in columns 1 to 4, and the weight percentage of pyritic sulfur, determined from the pyrite absorption peak areas as discussed elsewhere (1), are given in column 5. It is seen that pyrite and minerals (iron sulfates and iron oxyhydroxide) that are probably derived from pyrite by weathering are the only iron-bearing species in these low-rank coals. Notably absent are contributions from iron-bearing clays and siderite which are common constituents of bituminous coals (1,2). Pyrite and iron oxyhydroxide are difficult to separate with room temperature Mossbauer spectroscopy (18). For example, in Figure 1 are shown the room temperature and 77 K spectra obtained from the Pust seam, C, lignite, which had been stored for several years prior to measurement. Although it is quite difficult to determine the relative amounts of pyrite and oxyhydroxide from the room temperature Mossbauer spectrum, the spectral contributions of the two phases are

readily resolved at 77 K.

CCSEM results for the approximate weight percentages of all inorganic phases are given in Table II. Perhaps the most interesting aspect of the CCSEM results for these low-rank coals as compared with similar data for bituminous coals is the abundance of Ca-rich phases. In most cases, these phases are not calcite, but are Ca-enriched macerals in which the Ca is uniformly dispersed throughout the coal, as illustrated by the SEM micrograph in Figure 2. The Ca-enriched macerals appear gray in this inverted backscattered electron image. An energy dispersive X-ray spectrum obtained from an individual maceral is shown on the right. As discussed below, EXAFS data indicate that this calcium is dispersed as salts of carboxylic acids.

The backscattered electron intensity of the Ca-enriched macerals is significantly smaller than that of calcite, and CCSEM can make a distinction, albeit somewhat imprecisely, between Ca-enriched macerals and calcite or other Ca-rich minerals on this basis. However, the CCSEM programs have not been properly calibrated to deal with the case of macerals enriched in an inorganic component such as Ca at this point. Consequently, the percentages indicated in Table II for the Ca-rich category are only a qualitative indication of the relative amounts of this species in the various low-rank coals examined. On the basis of the backscattered electron intensity, it appears that calcium is dispersed throughout the macerals of the lignites that have been examined, and is present partially in dispersed form and partially as calcite in the subbituminous coals. In fresh bituminous coals, calcium is present almost exclusively as calcite(3-5).

For comparison with Tables I and II, Table III gives the range and typical values of the mineral distributions observed in bituminous coals by the CCSEM and Mossbauer techniques, derived from studies of perhaps a hundred different bituminous coal samples in this laboratory. Some obvious differences in mineralogy are apparent. In addition to the difference in calcium dispersion and abundance already noted, it is seen that certain minerals common in bituminous coals, such as Fe-bearing clays (illite and chlorite) and siderite, are virtually absent in the low-rank samples of Tables I and II. Conversely, minerals such as barite (BaSO_4), apatite ($\text{Ca}_5(\text{PO}_4)_3\text{OH}$), and other Ca, Sr phosphates, are rather uncommon in bituminous coals.

EXAFS and XANES data for a Ca-rich sample of the Pust seam, A, lignite can be briefly summarized by reference to Figures 3 and 4. Figure 3 shows the XANES of the lignite, Ca acetate, and a fresh bituminous coal from the Pittsburgh seam rich in calcite. The strong similarity between the lignite and calcium acetate spectra is apparent. Similarly, a close similarity is also observed for the XANES of the fresh bituminous coal and that of a calcite standard. Examination of the XANES of several other standard compounds (CaO , $\text{Ca}(\text{OH})_2$, and $\text{CaSO}_4 \cdot 2\text{H}_2\text{O}$) showed that none of these phases were present in detectable amounts in either coal. The strong similarity of the XANES of calcium acetate and that of the lignite is direct evidence that the calcium in this coal is associated with carboxyl groups in the macerals and is not contained in very fine ($<0.1 \mu\text{m}$) mineral matter.

Mathematical analysis of the EXAFS associated with the nearest-neighbor oxygen shell surrounding the Ca ions in the lignite was

accomplished using programs developed by Sandstrom(13). Briefly, the results indicate that the Ca is coordinated by six oxygens, possibly contributed in part by water molecules, at an average nearest neighbor distance of 2.39 Å. Additionally, the EXAFS data indicate that structural order at distances further from the Ca ions than the first coordination shell is essentially absent in the lignite, implying that the Ca sites are more or less randomly distributed throughout the macerals. This point is well illustrated by phase-shift subtracted Fourier transforms of the EXAFS data, which, as discussed elsewhere (12,13), should bear a reasonably close relationship to the radial distribution functions appropriate for the local environment of the Ca ions. In Figure 4, the magnitude of the phase-shift subtracted Fourier transform, $|F(r)|$, is shown for the lignite sample, calcium acetate, and a calcite-rich bituminous coal from the Pittsburgh seam. It is seen that the $|F(r)|$ curves for calcium acetate and the calcite-rich bituminous coal exhibit maxima corresponding not only to the nearest-neighbor oxygen shell, but also at the approximate locations of more distant calcium neighbor shells. The $|F(r)|$ curve of the lignite exhibits a clear maximum only at the oxygen nearest-neighbor shell distance. It is possible, however, that the small shoulder that appears on the high side of the oxygen shell peak in the lignite $|F(r)|$ curve (at approximately 3.5 Å) could correspond to the initial stages of Ca ion clustering.

Finally, it is noted that XANES and EXAFS spectra obtained from a severely weathered bituminous coal were nearly identical to those obtained from the lignite sample. This indicates that in the weathered coal calcium is also present in a dispersed form in which it is bonded to carboxyl groups in the macerals. A more detailed report of the Ca EXAFS investigation of lignite, fresh and weathered bituminous coal, and Ca reference compounds will appear elsewhere(17).

Analysis of Fouling and Slagging Deposits. It was observed that one of the two North Dakota lignites listed in Tables I and II produced heavy fouling deposits during combustion in a large utility furnace, while little or no difficulty was experienced in firing the other. As seen in Tables I and II, the inorganic phase distributions of these two coals are rather similar. Additionally, CCSEM and Mossbauer analysis of boiler-wall slag deposits produced by both coals gave rather similar results. A typical Mossbauer spectrum obtained from a boiler wall deposit (wall temperature $\approx 1250^\circ\text{C}$) is shown in Figure 5, and a summary of the approximate phase distributions of the wall slag deposits produced by both coals is given in the inset. From the observed phases, it appears that the $\text{CaO-SiO}_2\text{-Fe}_2\text{O}_3$ phase diagram plays a key role in determining the slagging behavior of these coals. CCSEM analyses of fouling deposits produced by the two lignites are given in Table IV. It is seen that the only significant difference between the light and heavy deposits is the presence of an alkali sulfate mixture, containing Na, K, and Ca sulfates, in the latter. It is well known that alkali sulfates can react strongly with metal surfaces to produce alkali-iron sulfate mixtures that are partially molten over the temperature range from approximately 700 to 1100°C , causing severe fouling and corrosion problems(19).

Conclusions

In this paper, we have presented some examples of the usefulness of three techniques, Mossbauer spectroscopy, CCSEM, and EXAFS in the analysis of low-rank coals and combustion products of low-rank coals. Points of interest regarding the inorganic constituents of these coals include the high abundance of calcium bonded to carboxyl groups and dispersed throughout the macerals, the low abundance of illite, siderite, and calcite, and the presence of significant amounts of accessory minerals such as barite, apatite, and other phosphates. Areas that merit further investigation by these techniques include the analysis of fouling and slagging deposits, and structural studies of inorganic elements such as calcium that are dispersed through and bonded to the coal macerals.

Acknowledgments

The EXAFS experiments discussed in this paper were conducted in collaboration with F.W. Lytle and R.B. Gregor of the Boeing Company at the Stanford Synchrotron Radiation Laboratory, which is supported by the National Science Foundation and the Department of Energy.

References

1. Huffman, G.P., Huggins, F.E., Fuel, 1978, 57, 592-604.
2. Huggins, F.E., Huffman, G.P., Anal. Methods for Coal and Coal Products, Clarence Karr, Jr., Ed.; Academic: New York, 1979, Vol. 3, 371-423.
3. Huggins, F.E., Kosmack, D.A., Huffman, G.P., Lee, R.J., SEM/1980/I, 531-540, SEM Inc., AMF O'Hare (Chicago), IL (1980).
4. Huffman, G.P., Huggins, F.E., Lee, R.J., Proc. Int. Conference on Coal Science, Dusseldorf, 1981, 835-840, Verlag Glückauf GmbH, Essen, Germany (1981).
5. Huggins, F.E., Huffman, G.P., Lee, R.J., Coal and Coal Products: Analytical Characterization Techniques, E.L. Fuller, Jr., Ed.; ACS Symposium Series No. 205, 1982, 239-258, Amer. Chem. Soc., Washington, D.C.
6. Maylotte, D.H., Wong, J., St. Peters, R.L., Lytle, F.W., Gregor, R.B., Science, 1981, 214, 554.
7. Sandstrom, D.R., Filby, R.H., Lytle, F.W., Gregor, R.B., Fuel, 1982, 61, 195.
8. Hussain, Z., Barton, J.J., Umbach, E., Shirley, D.A., SSRL Activity Report, May 1981, A. Bienenstock and H. Winick, Eds.; p. VII-102.
9. Huffman, G.P., Huggins, F.E., Mossbauer Spectroscopy and Its Chemical Applications, J.G. Stevens and G.K. Shenoy, Eds.; Advances in Chemistry Series No. 194, 1981, 265-301, Amer. Chem. Soc., Washington, D.C.
10. Huffman, G.P., Huggins, F.E., Physics in the Steel Industry, F.C. Schwerer, Ed.; AIP Conf. Proc. No. 84, Amer. Inst. Physics, 1982, 149-201.

11. Lee, R.J., Kelly, J.F., SEM/1980/I, 303-310, SEM Inc., AMF O'Hare (Chicago), IL, (1980).
12. Lee, P.A., Citrin, P.H., Eisenberger, P., Kincaid, B.M., Rev. Mod. Phys., 1981, 53, 769.
13. Sandstrom, D.R., Proc. Workshop on EXAFS Analysis of Disordered Systems, Parma, Italy, 1981, to be published in Nuovo Cimento B.
14. Kutzler, F.W., Natoli, C.R., Misemer, D.K., Doniack, S., Hodgson, K.O., J. Chem. Phys., 1980, 73, 3274-88.
15. Bair, R.A., Goddard, W.A., Phys. Rev. B, 1980, 22, 2767-76.
16. Stearn, E.A., Heald, S., Rev. Sci. Instrum., 1979, 50, 1579.
17. Huggins, F.E., Huffman, G.P., Lytle, F.W., Gregor, R.B., "An EXAFS Investigation of Calcium in Coal," to be published in Proc. Int. Conference on Coal Science, Pittsburgh, 1983.
18. Huggins, F.E., Huffman, G.P., Kosmack, D.A., Lowenhaupt, D.E., Int. J. Coal Geology, 1980, 1, 75-81.
19. Reid, W.T., Chemistry of Coal Utilization, 1983, M.A. Elliot, Ed.; Suppl. Vol., Chapt. 21, 1389-1445, John Wiley & Sons, Inc.

TABLE I

Mossbauer Results For Low-Rank Coals

Sample	Percent of Total Iron Contained in				Wt.% of Pyritic Sulfur
	Pyrite	Jarosite	Ferrous Sulfate	Iron Oxy-hydroxide	
Pust seam, A-3	100	-	-	-	0.30
Pust seam, A-4	92	7	1	-	2.26
Pust seam, A-6	91	9	-	-	0.15
Pust seam, A-7	>100+	-	-	-	<0.03+
Pust seam, B-3	100	-	-	-	0.06
Pust seam, B-5	100	-	-	-	0.05
Pust seam, B-7	100	-	-	-	0.09
Pust seam, C	43	26	-	31	0.29
N.Dakota lignite, heavy fouling	91	6	2	-	0.50
N.Dakota lignite, light fouling	95	5	-	-	0.38
Rosebud subbituminous	65	16	19	-	0.15
Colstrip subbituminous	81	19	-	-	0.27

+Very weak spectrum; sample contained only 0.07% iron.

TABLE II

CCSEM Results for Low-Rank Coals (approximate weight percentages)

Sample	Mixed		Fe		Barite	Apatite	Other Phases					
	Quartz	Kaolinite	Silicates	Illite			Pyrite	Sulfates	Fe-rich	Ca-rich+		
Pust seam, A-3	7	45	8	-	1	-	6	26	1	-	Montmorillonite	1
Pust seam, A-4	12	20	3	-	26	4	7	15	7	2	Rutile	1
Pust seam, A-6	7	27	-	-	1	-	-	51	5	3	Fe-Ca-S	3
Pust seam, A-7	7	35	3	-	1	-	-	49	3	-	-	-
Pust seam, B-3	10	43	13	1	1	-	-	22	3	3	Montmorillonite	4
Pust Seam, B-5	14	38	3	-	1	-	-	38	5	-	Rutile	1
Pust seam, B-7	16	38	2	-	5	-	-	27	5	-	Ca-Fe-S	1
Pust seam, C	9	29	5	1	4	5	14	13	4	-	Ca-Fe	6
											Ca-Sr-Al-P*	4
N. Dakota lightite, heavy fouling	24	13	20	3	19	1	1	14++	-	-	Jarosite	2
N. Dakota lignite, light fouling	28	16	13	2	10	-	2	23++	-	-	Montmorillonite	1
Rosebud, subbituminous	23	36	6	2	6	2	3	8	1	1	Ca-Sr-Al-P*	6
Eveleth, subbituminous	18	23	22	12	4	-	3	7	-	1	Rutile	1
Colstrip, subbituminous	22	25	6	3	8	-	3	29	-	-	Gypsum	4
Absaloka subbituminous	56	22	8	-	3	-	-	5	-	-	Rutile	3

*As discussed in the text, percentages given for the Ca-rich category are not quantitative.

*Minerals denoted by Ca-Sr-Al-P are probably crandallite (Ca,Sr)Al₃(PO₄)₂(OH)₅H₂O.**Macerals enriched in Ca and S, with Ca/S ratios \approx 1 to 6/1; some gypsum is probable.

TABLE III

Mineralogy of Bituminous Coals

CCSEM Analysis, Wt. % of Mineral Matter			Mossbauer Analysis, % of Total Sample Iron		
Mineral	Range	Typical	Mineral	Range	Typical
Quartz	5-44	18	Pyrite	25-100	62
Kaolinite	9-60	32	Ferrous Clay	0-56	18
Illite	2-29	14	Siderite/Ankerite	0-58	9
Chlorite	0-15	2	Ferrous Sulfate	0-18	3
Mixed Silicates	0-31	17	Jarosite	0-21	4
Pyrite	1-27	8	Wt. % Pyritic Sulfur*	0.08-	0.35
Calcite/Dolomite	0-14	3		1.51	
Siderite/Ankerite	0-11	2			
Other	0-12	4			

*Determined by method of Ref. 1.

TABLE IV

CCSEM Results For Fouling Deposits, 800-1000°C

Species	Heavy (wt%)	Light (wt%)
Al, Si-rich	5	5
Quartz	3	8
Hematite	2	3
Ca-rich	10	7
Mg-Ca	3	5
Ca Ferrite	2	<1
Ca-Si-Fe Glass	21	22
Ca-Si + Glass	40	40
Alkali Sulfate	2	0
CaSO ₄ + Alkali Sulfate	4	6 CaSO ₄ only
Other	8	4

Alkali Sulfate - Na/Ca/K = 1.0/0.5/0.1

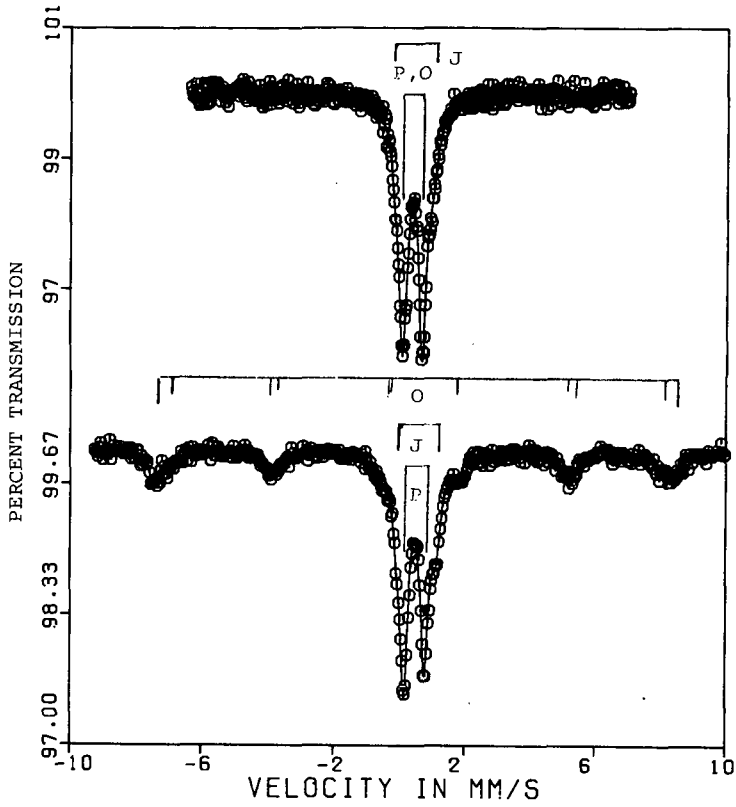


Fig. 1 Mössbauer spectra of the Pust seam, C, lignite. Pyrite (P), jarosite (J), and iron oxyhydroxide (O) are indicated.

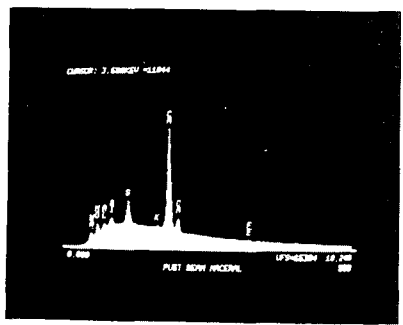


Fig. 2 **BACK-SCATTERED ELECTRON IMAGE** **ENERGY-DISPERSIVE X-RAY SPECTRUM**

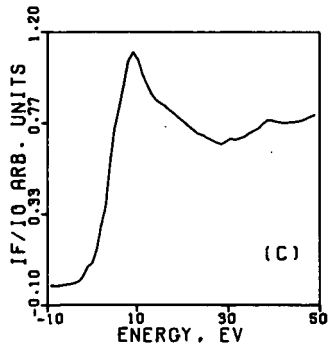
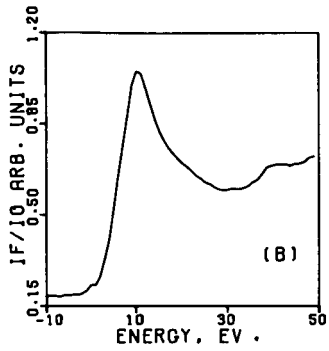
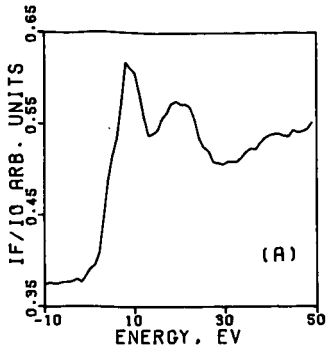


Fig. 3 XANES of: (A) calcite-rich bituminous coal; (B) the Pust seam lignite; (C) calcium acetate.

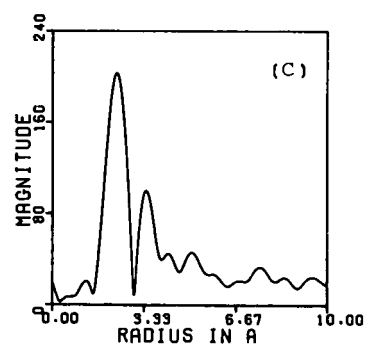
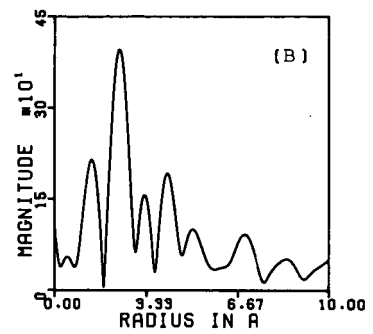
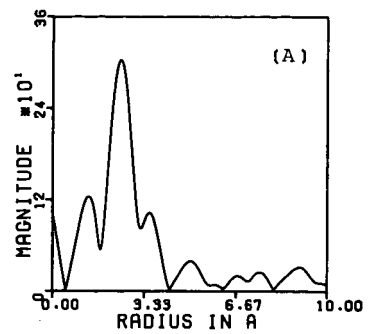


Fig. 4 Magnitudes of the phase-shift subtracted Fourier transform of: (A) the Pust seam lignite; (B) calcite-rich bituminous coal; (C) calcium acetate.

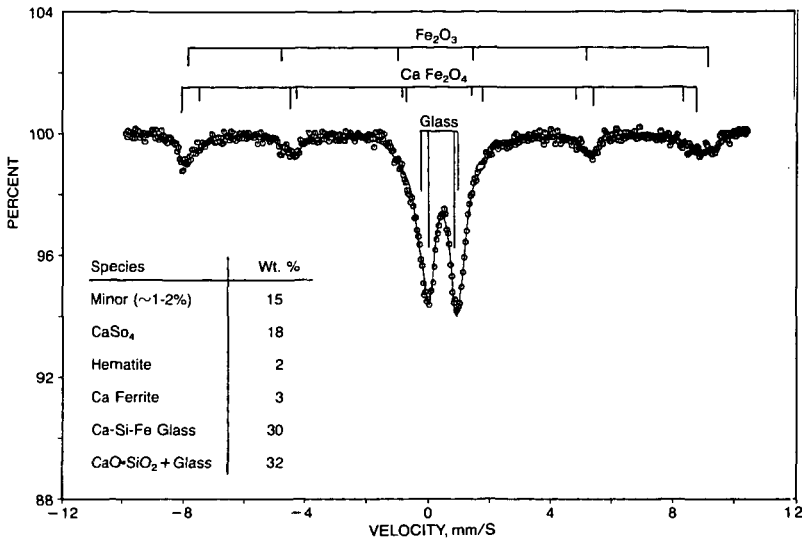


Fig. 5 Mossbauer spectrum of boiler-wall slag deposit. The approximate phase distribution determined from CCSEM and Mossbauer results is shown in the inset.

GEOCHEMICAL VARIATION OF INORGANIC CONSTITUENTS IN A NORTH DAKOTA LIGNITE

Frank R. Karner, Steven A. Benson, Harold H. Schobert, and Robin G. Roaldson

U.S. Department of Energy
Grand Forks Energy Technology Center
Box 8213, University Station
Grand Forks, North Dakota 58202

INTRODUCTION

This paper summarizes information on the distribution of major and trace elements in a stratigraphic sequence of sedimentary materials in a major lignite producing portion of the Fort Union region of the Northern Great Plains. Previous study of the geochemical variation in these sediments is summarized in the literature (1,2). Major patterns of elemental variations in lignite are related to factors affecting accumulation of both organic and inorganic components during deposition and aqueous precipitation, dissolution, and ion-exchange processes after deposition. Variations in overburden and underclay are dependent upon specific clay mineral variation and relative abundances of quartz- and feldspar-rich silt fractions versus clay mineral-rich fractions of the sediment, as well as upon local variation in carbonates and other elements.

GEOLOGIC RELATIONSHIPS

The Center mine, Oliver County, North Dakota is in the Fort Union Coal Region, which is one of the largest reserves of lignite in the world. The Fort Union Coal Region lies within the North Great Plains Coal Province and encompasses portions of north-central United States and south-central Canada, including both the subbituminous coals of the northern Powder River Basin and the lignites of the Williston Basin (2), a broad structural and sedimentary intracratonic basin that extends over an area of about 40,000 km². Over 4600 m of sedimentary rocks overlie the Williston Basin in its deepest portions of McKenzie County, North Dakota.

Important lignite beds of the Fort Union Region occur within Ludlow, Slope, Bullion Creek, and Sentinel Butte Formations of the Paleocene Fort Union Group.

The Sentinel Butte Formation has been described as a "lignite-bearing, nonmarine, Paleocene unit whose outcrops are somber gray and brown" (3). Rock types include sandstone, siltstone, claystone, lignite, and limestone. The lignite beds typically vary from less than 1 meter to 3-5 meters in thickness (4). The Oliver-Mercer County district is located in eastern Mercer and northeastern Oliver Counties with the principal bed, the Hagel bed, ranging in thickness from 3 to 4 meters at the Center Mine (4).

The sampling program (5) was designed to obtain stratigraphically controlled specimens for a study of the character, distribution, and origin of the inorganic constituents in lignite. The objectives of the field sampling were to obtain:

1. Incremental samples of underclay, lignite, and overburden at each mine.
2. Duplicate vertical sections and lateral samples to test variation.
3. Samples of specific beds, lenses, fault zones, mineral concentrations, or other areas of unusual aspect.

Lignite, lignite overburden, and underclay were collected from a vertical section on the high walls at the Center mine. Figure 1 illustrates the stratigraphic sections and sample locations. Choice of sections to be sampled was based on accessibility to areas in the mines due to mining activity.

To minimize contamination, material from slope wash and mining activity was first removed from each section. In order to obtain samples of underclay it was necessary to dig down at the base of the lowest lignite, since in surface mining the underclay is normally left undisturbed. Once the section to be sampled was exposed it was measured and marked at 30 cm intervals (through the lignite, starting at the base) and then at additive increments of 1 m through the extent of the overburden in the mine cut.

Samples were collected (Table 1) over a 10 cm by 50 cm area at the bottom of each marked interval of the measured section. Samples were collected at all contacts between lithologic units when the contact was found and at points of interest (for example: iron sulfide-coated joints, clay partings, sand lenses, concretions). All samples were stored in plastic bags inside cardboard cartons.

TABLE 1
SAMPLE DESCRIPTIONS AND LOCATION, CENTER MINE

<u>Sample #</u>	<u>Height, meters*</u>	<u>Description</u>
1-1-D	-0.05	Underclay, gray
1-2-D	0.05	Black lignite, very hard
1-3-D	0.40	Black lignite, very hard
1-4-D	0.70	Black lignite, very hard
1-5-D	1.00	Black lignite, very hard
1-6-D	1.25	Black lignite, very hard
1-7-D	1.50	Black lignite, very hard
1-8-D	1.70	Black lignite, very hard
1-9-D	1.90	Black lignite, very hard
1-10-D	2.10	Black lignite, very hard
1-11-D	2.45	Black-brown lignite, soft and fractured, top of seam
1-12-D	2.55	Dark gray organic rich silt
1-13-D	3.65	Gray sand, fine-grained, fossilized
1-14-D	4.15	Gray sand with a clay matrix
1-15-D	4.50	Concretion zone
1-16-D	4.75	Brown lignite, very soft, silty
1-17-D	4.85	Gray-green clay
1-18-D	5.15	Brown lignite, very soft, silty
1-19-D	5.45	Brown lignite, top of seam
1-20-D	5.60	Gray silty clay
1-21-D	5.75	Brown lignite with silty interbedded layers
1-22-D	5.85	Gray siltstone
1-23-D	6.45	Gray siltstone, 1-2 mm laminae

*Height from base of major lignite seam.

GEOLOGICAL CHARACTERISTICS

The Center mine lignite is a black to brownish black coal that slacks rapidly on exposure to the atmosphere and typically contains dark carbonaceous clay or grey clay partings (4). The underclay is a grey-green clay with lignite fragments. The overburden is grey fine-grained sediment primarily consisting of clayey silts and silty clays with minor concretionary zones and sands. Logan (6) has described the overburden sequence as the Kinneman Creek interval and has interpreted it to be of lacustrine origin. Generally the early Cenozoic sediments in this region are believed to have been deposited in a coastal complex of stream channel and flood plain, swamp, lake, and delta environment.

INORGANIC CONSTITUENTS

Inorganic constituents in the Sentinel Butte sediments are present as 1) detrital mineral grains and volcanic glass fragments, 2) components of organic debris, 3) authigenic mineral grains and cement, and 4) ions adsorbed by clay and other minerals and organic material (7,8,9,10).

A summary of minerals observed in the Sentinel Butte Formation is given in Table 2 (9). Major original detrital constituents include montmorillonite, quartz, plagioclase, alkali feldspar, biotite, chlorite, volcanic glass and rock fragments. Major minerals formed during deposition and diagenesis by conversion of original detrital constituents consist of montmorillonite, chlorite, and kaolinite. Pyrite, gypsum, hematite, siderite, and calcite (?) formed in post-depositional reducing and oxidizing reactions related to changing conditions of deposition, burial, and groundwater movements.

TABLE 2

INORGANIC CONSTITUENTS IN THE SENTINEL BUTTE FORMATION

<u>Constituent</u>	<u>Overburden</u>	<u>Lignite</u>	<u>Underclay</u>
Alkali feldspars	XX	X	X
Augite		X	
Barite		X	
Biotite	X		
Calcite/Dolomite	XX	X	
Siderite	XX		
Chlorite	XX	X	X
Gypsum		XXX	
Hematite		XX	
Hornblende	X		
Illite	XX	X	X
Kaolinite	XX	XXX	XXX
Magnetite	X		
Montmorillonite	XXX	X	XXX
Muscovite	X		
Plagioclase	XXX	X	X
Pyrite		XX	
Quartz	XXX	XXX	XXX
Volcanic Glass	X		
Rock fragments	XX		

XXX = Abundant

XX = Common

X = Minor

GEOCHEMICAL VARIATION IN OVERBURDEN AND UNDERCLAY

Previous work (7,8) and our current work seeks to relate chemical variations to variations in the original mineral content of the sediments and to variations due to post-depositional mineral reactions.

Overburden sediments are typically silty clays with about 80 pct clay and 20 pct silt. Other sediments include clayey silts and fine sands with varying organic content and calcareous cement. Sideritic concretion zones are present. Clay-rich sediments are enriched in some elements particularly Al, Mg, and Ti. Carbonate-rich sediments are enriched in Ca and Fe (concretionary zones). Sodium shows a tendency to increase downward to a high in organic-rich silty clay, above the lignite. Specific beds, including the underclay, are markedly enriched in potassium, possibly related to high mica content.

EXPERIMENTAL

Samples of coal, overburden, and underclay were dried and analyzed by neutron activation (NAA) and x-ray fluorescence analysis (XRF). NAA analysis was performed by the Nuclear Engineering Department, North Carolina State University. The system description and detection limits for coal and coal fly ash are summarized by Weaver (11). XRF was done at GFETC with an energy dispersive x-ray system. Mineralogy of the overburden and underclay was determined by x-ray diffraction (XRD). The crystalline phases present in the coal were determined by XRD of the low-temperature ash of the coal.

RESULTS AND DISCUSSION

Mineralogy of the Stratigraphic Sequence - X-ray diffraction was used to determine the major minerals present in the overburden, underclay, and of the low-temperature ash of the coal. The results are summarized in Figure 2, which illustrates the distribution of minerals throughout the sequence. The most distinct variation in the overburden is the concretion zone, which is a very compact, cemented zone rich in siderite and dolomite. The remaining fractions of the overburden are consistent with varying amounts of quartz, kaolinite, muscovite, and plagioclase.

The bulk mineralogy of the coal also represented in Figure 6 reveals the presence of quartz, calcite, bassonite, kaolinite, and pyrite in varying amounts. Bassonite is possibly a product of organic sulfur fixation with organically bound calcium (12). Pyrite appears to increase with depth in the seam.

Variations of Elements in the Stratigraphic Sequence - The results of the neutron activation and x-ray fluorescence analysis for the stratigraphic sequence are listed in Table 3. Descriptions of the samples are listed in Table 1.

Variation Within Major Coal Seam - The distribution of elements throughout the section sampled in the coal seam can be summarized by four general trends: 1) concentration of elements in the margins; 2) concentration in the lower part of the seam; 3) even distribution; 4) without a clear pattern. These trends can be best examined by plotting or charting them with location in the seam.

The elements which were concentrated at or near the margins of the coal seam included Al, Ti, Fe, Cl, Sc, Cr, Co, Ni, Zn, As, Ru, Ag, Cs, Ba, La, Ce, Sm, and U. An example of a typical distribution is a graph of Zn shown in Figure 3, which illustrates the distribution of zinc throughout the entire stratigraphic sequence.

The elements which are concentrated at the margins of the lignite seam are most likely associated with the detrital constituents, such as finely divided clay min-

TABLE 3
ELEMENTAL ANALYSIS FOR SELECTED MAJOR AND MINOR ELEMENTS, PARTS PER MILLION
(Dry Basis)

ID	Height* ft.	No.	Mg.	Al	K	Ca	Ti	Fe	Cl	Sc	V	Cr	Mn	Co	Ni	Zn	As
1-1-D	Underclay	9534	26788	9605	4052	26761	411	15	137	99	144	5	59	42	4		
1-2-D	Lignite	1736	10200	2153	6247	9377	132	6	219	49	39	2	34	25	16		
1-3-D	Lignite	1607	5586	806	5984	6685	55	2	25	6	49	2	21	14	20		
1-4-D	Lignite	1677	2595	1000	7658	2909	44	1	4	2	69	1	16	10	6		
1-5-D	Lignite	1375	3313	615	6888	2326	59	1	22	5	47	1	12	6	6		
1-6-D	Lignite	1861	2949	1000	6820	1745	55	1	4	1	68	0	13	8	5		
1-7-D	Lignite	2209	6051	1000	6994	2182	67	1	16	5	76	1	16	12	8		
1-8-D	Lignite	827	1970	1000	4689	6128	36	0	1	1	24	1	13	6	31		
1-9-D	Lignite	1979	10813	1104	6330	17133	74	3	47	10	61	4	28	19	15		
1-10-D	Lignite	9219	100370	1000	8691	4070	51	7	101	68	100	3	33	34	7		
1-11-D	Lignite	1848	6620	1000	7935	4070	51	7	12	5	56	1	33	25	21		
1-12-D	Overburden	10564	79761	25718	10564	29506	336	13	138	80	257	11	47	44	8		
1-13-D	Overburden	5331	71239	1000	16988	34822	407	11	116	72	287	11	36	36	3		
1-14-D	Overburden	4.15	4461	95029	1000	21466	508	15	170	94	175	15	55	54	3		
1-15-D	Overburden	4.50	1422	3673	96920	233070	116	29	138	21	128	1	190	108	2		
1-16-D	Lignite	4.75	750	1762	5813	28510	113	15	185	34	66	10	46	40	28		
1-17-D	Overburden	4.85	5767	10951	96097	30072	428	14	165	93	187	16	49	45	8		
1-18-D	Lignite	5.15	718	1652	2512	3552	43	4	6	4	79	1	25	20	17		
1-19-D	Lignite	5.45	609	2208	7230	6391	125	3	24	10	108	4	24	18	27		
1-20-D	Overburden	5.60	4485	82608	1000	12364	3869	145	3724	63	3	75	424	14	47		
1-21-D	Lignite	5.75	3510	50912	21576	7039	2133	314	11	158	92	262	13	64	37		
1-22-D	Overburden	5.85	4900	10756	87974	8418	3429	499	14	151	106	387	19	96	46		
1-23-D	Overburden	6.45	7708	9368	64715	18107	3081	30374	395	13	106	119	436	15	50		

*Height from base of major coal seam.

TABLE 3
(continued)

ID	Se	Br	Ru	Ag	Cd	Sb	Cs	Ba	La	Ce	Sm	Eu	Yb	Th	U
1-1-D	Underclay	2	160	2.48	3	2	5	1132	27	53	3	1	1	10	4
1-2-D	Lignite	2	16	1.42	5	19	4	370	9	18	2	1	1	4	5
1-3-D	Lignite	1	5	0.83	9	5	1	185	3	9	2	0	0	1	6
1-4-D	Lignite	1	3	0.60	5	1	0	64	3	5	1	0	0	0	0
1-5-D	Lignite	2	3	0.71	5	2	0	39	3	4	0	0	0	1	1
1-6-D	Lignite	0	3	0.49	5	0	0	45	2	3	0	0	0	0	0
1-7-D	Lignite	1	3	0.67	4	1	0	66	4	6	1	0	0	1	2
1-8-D	Lignite	0	3	0.46	1	1	0	496	1	4	0	0	0	1	0
1-9-D	Lignite	1	5	1.12	9	5	1	114	4	8	2	0	1	2	5
1-10-D	Lignite	2	119	2.05	5	1	6	745	26	50	2	1	1	11	4
1-11-D	Lignite	1	6	1.64	7	4	0	266	5	9	2	0	1	3	4
1-12-D	Overburden	2	147	2.57	5	2	4	661	35	58	4	1	2	10	4
1-13-D	Overburden	2	107	2.19	5	1	3	673	31	60	3	1	2	11	2
1-14-D	Overburden	2	144	3.11	5	2	5	781	32	63	4	1	2	11	3
1-15-D	Overburden	9	3	46	20	0	0	595	23	6	3	1	3	3	3
1-16-D	Lignite	2	9	2.33	18	15	6	179	5	1	3	0	1	2	9
1-17-D	Overburden	2	138	2.00	5	2	1	761	32	56	3	1	2	10	3
1-18-D	Lignite	1	3	4	0	5	1	161	3	6	1	0	1	1	1
1-19-D	Lignite	1	3	1.09	4	4	1	95	2	4	1	0	0	2	3
1-20-D	Overburden	2	1	122	2.74	5	1	640	29	57	3	1	2	10	2
1-21-D	Lignite	4	3	66	2.21	8	4	559	10	36	3	1	2	8	5
1-22-D	Overburden	2	131	2.75	2	2	4	911	26	49	3	1	1	9	2
1-23-D	Overburden	1	2	90	2.30	5	2	691	29	55	3	1	2	9	2

*Height from base of major coal seam.

erals. The possible associations of trace and minor elements with clays are summarized by Finkelman (13). The elements which have possible affinities to clay and other sedimentary environments in relation to coal seams include Al, Sc, Ti, Cl, Cr, La, Mg, and Fe. A second group of elements, including Fe, Co, Ni, Zn, As, and Ag, may associate in the margins with pyrite or other sulfides. Uranium can be associated with the organic part of the coal but can be associated with a diverse suite of uranium minerals (13). Other elements, such as Ru, Ce, Sm, have not been extensively studied but appear to have an association with detrital minerals.

The elements which have an even distribution include Cd, Mn, Mg, Na, and Ca. As an example, Figure 4 represents the distribution of Ca within the stratigraphic sequence. The majority of these elements are organically bound or associated with authigenic minerals. The elements which are considered to be organically bound include Ca, Na, Mg, and Mn (14). This association would be as the counter ion with the carboxylic acid functional groups of the carbonaceous structure. Calcium, Mg, and Mn may also exist as carbonates which form in the coal during coalification. Calcite (CaCO_3), for example, was identified in the low-temperature ash of the coal. Cadmium in other coals has been found associated with sulfides (13). Its inclusion in this group may rather indicate an organic association, at least in this lignite. The calcium and cadmium ions have similar ionic potentials (~ 2) and may therefore behave similarly toward carboxylic groups.

Elements which showed a tendency to concentrate toward the base of the lignite seam are V, K, and Sb. Figure 5 represents this trend by a graph of the distribution of Sb. The increased concentration of K toward the base of the seam is very subtle. Vanadium and Sb increase sharply at the base of the seam. Vanadium has strong organic tendencies (13). Sb has strong chalcophile tendencies (15) so it is possible that Sb is associated with the sulfides.

The elements which reveal no clear pattern of distribution include Se, Br, Cs, Eu, and Yb. Bromine is an example, as illustrated in Figure 6. The probable reason is that low concentrations of these elements are near the detection limits of the analysis and thus may have greater experimental error.

Although the concentrations of rare earth elements are quite low, there is nevertheless a reasonable agreement with the rare earth abundance pattern in sedimentary rocks. This pattern can be seen in Table 4, which compares average concentrations in the main seam of lignite (samples 1-2-D through 1-11-D), after rejection of outliers, with the sedimentary rock pattern. For convenience in comparing the data, both sets of data have been calculated as ratios. The sedimentary rock data is from reference 16. Note that this comparison is only of the patterns of abundance, and not of the magnitudes. In the case of europium, the comparison is certainly influenced by working near the detection limit in the lignite samples.

TABLE 4
PATTERNS OF ABUNDANCE OF RARE EARTHS
IN LIGNITE AND SEDIMENTARY ROCKS

<u>Element</u>	<u>Lignite Ratio, La/x</u>	<u>Sedimentary Rock Ratio, La/X</u>
La	1.0	1.0
Ce	0.91	0.63
Sm	3.1	3.1
Eu	10	19
Yb	9.1	9.4

Reasonable qualitative agreement exists among the elemental variations observed here, the ionic potential of the elements, and the chemical fractionation behavior. Chemical fractionation determines the amount of each element present as ion-exchangeable cations, as acid-soluble minerals or coordination complexes, and as insoluble minerals. Our application of this procedure to other lignites has been discussed previously (17). In general, those elements which would be predicted to form insoluble hydrolysates on the basis of their ionic potential (that is, $3 < Z/r < 12$) are found concentrated near the margins of the seam and, in chemical fractionation, mainly occur as acid-insoluble minerals. Examples of elements in this category are Al, Ti, Cr, and Ni. On the other hand, elements of $Z/r < 3$ would likely exist as hydrated cations; these elements generally show even distribution through the seam and are removed by ion-exchange with ammonium acetate in chemical fractionation. Examples are Ca, Mg, and Na.

Variation Within the Overburden - The distribution of elements in the overburden is consistent in the clay-silt-sand regions with the exception of the concretion zone. This zone is extremely high in iron due to the siderite. The other elements which are concentrated in the concretion zone include Ag, Ni, Fe, Sc, Yb, Cd, Se, and Zn. The elements which are depleted are Co, Ce, Cs, As, Cr, Ru, Cl, and Na. The small coal seam directly above the concretion zone has high concentrations of As, V, Sb, and U. Figure 7 represents uranium distribution throughout the stratigraphic section, note that the highest concentration of uranium anywhere in the section is in the lignite seam directly above the concretion zone.

Many of the minor metallic elements have concentrations lying within 20% of the average values for shales. This comparison is illustrated by the data in Table 5, which compares the average concentrations in the underclay and overburden samples, after statistical rejection of outliers, with tabulated values from the literature (18). The most notable exception is manganese.

TABLE 5
COMPARISON OF AVERAGE MINOR ELEMENT CONCENTRATIONS FOR
OVERBURDEN/UNDERCLAY SAMPLES WITH AVERAGE CONCENTRATIONS FOR SHALES
CONCENTRATIONS IN PPM

Element	Overburden/Underclay	Shales	Element	Overburden/Underclay	Shales
Ba	760	600	Sc	15	15
Ce	56	70	Th	10	12
Co	13	20	Ti	3650	4600
Cr	92	100	U	2.8	3.5
Mn	269	850	V	139	130
Ni	72	80	Zn	51	90

The variation of potassium in the overburden and underclay is extreme, ranging from 1000 to 30,000 ppm. The reasons for this variability are not clearly understood, but may be due to the minerals in the overburden and underclay, some of which would be potassium-containing clays and others not. Figure 8 represents the distribution of potassium within the stratigraphic sequence.

INTERPRETATION OF PATTERNS OF ELEMENT DISTRIBUTION

The observed patterns of element distribution in the lignite seam may be explained by both changes in depositional conditions during accumulation and subsequent chemical changes during diagenesis and post-diagenetic processes. Depositional factors involving addition of greater fractions of detrital clay and silt at the beginning and end of peat deposition would increase Si, Al, Mg, Ca, Na, K, and possibly other elements in the margins of the lignite. Other possible depositional factors include changing of Eh or pH, influx of ash, or changing botanical factors at the beginning and end of peat deposition. Post-depositional factors related to the flow of meteoric water (i.e., water derived from the atmosphere) through the lignite laterally might selectively concentrate elements in the margins of the seam or at its center. Vertical flow might concentrate elements at either the upper or lower margin, depending on flow direction and on the nature of the adjoining sediments. Other post-depositional factors might be related to the changing geochemistry of the lignite-forming environment, such as Eh and pH changes, botanical changes due to breakdown of plant material, and geological factors such as depth of burial, temperature, compaction, or changes in groundwater chemistry. The existence of several types of patterns suggests that several processes have been operative during the geological history of this sequence.

Future work will include a very detailed sampling of several vertical sections of a mine to describe groundwater influences on the formation of authigenic minerals and on the distribution of organically associated elements.

ACKNOWLEDGEMENTS

The authors would like to thank Diane K. Rindt for the x-ray diffraction work and Arthur L. Severson for x-ray fluorescence analysis. Mr. Roaldson acknowledges support from Associated Western Universities, Inc. as a part of their summer undergraduate research participation program.

REFERENCES CITED

1. Sondreal, E.A., W.R. Kube, and J.L. Elder. Analysis of the Northern Great Plains Province Lignites and Their Ash: A Study of Variability. U.S. Bureau of Mines Report RI 7158 (1968).
2. Energy Resources Co. Inc., Walnut Creek, CA 94596. Low-rank Coal Study, National Need for Resource Development-Resource Characterization. DOE/FC/10066-TI (Vol. 2) Nov. 1980.
3. Jacob, A.F. Geology of the upper part of the Fort Union Group (Paleocene), Williston Basin, with reference to uranium: North Dakota Geol. Survey Report of Investigation No. 58, 1976, 49 p.
4. Groenewold, G.H., L.A. Hemish, J.A. Cherry, B.W. Rehm, G.N. Meyer, and L.M. Winczewski. Geology and geohydrology of the Knife River Basin and adjacent areas of west-central North Dakota: North Dakota Geol. Survey Report of Investigation No. 64, 1979, 402 p.
5. Karner, F.R., S.F. White, D.W. Brekke, and H.H. Schobert. Geologic Sampling of Lignite Mines in Mercer and Oliver Counties, North Dakota. DOE/FC/FE-1, 1983, (in preparation).
6. Logan, Katherine J. The Geology and Environment of Deposition of the Kinneman Creek Interval Sentinel Butte Formation (Paleocene), North Dakota. Unpublished Masters Thesis, University of North Dakota (1981).
7. Karner, F.R., W. Beckering, D.K. Rindt, and H.H. Schobert. Inorganic Constituents in Lignite: Overview and Some Effects on Coal Utilizations. Geological Society of America Abstracts with Programs 11 454 (1979).
8. Karner, F.R., G. Winbourn, S.F. White, and A.K. Gatheridge. Sodium and calcium in overburden, lignite and underclay at the Beulah and Baukol-Noonan Mines, Mercer and Oliver Counties, North Dakota [abs.]: North Dakota Academy of Science Proceedings, vol. 33, pt. 1, 1979, p. 70.
9. Schobert, H.H., S.A. Benson, M.L. Jones, and F.R. Karner. Studies in the Characterization of United States Low-rank Coals. Proceedings, International Conference on Coal Science, Dusseldorf, Sept. 1981, p. 10-15.
10. Karner, F.R., S.A. Benson, H.H. Schobert, R.G. Roaldson, and Cirtchlow. Organic and Inorganic Components of Lignite: A Scanning Electron Microscope and Microprobe Study. Geological Society of America Programs with Abstracts, (Abstract), v. 14, 1982.
11. Weaver, J.N. in Analytical Methods for Coal and Coal Products, Vol. I, p. 377-401, Karr, C., Jr. (Ed.), Academic Press, Inc., New York (1978).
12. Miller, R.N. and P.H. Given. A geochemical study of the inorganic constituents in some low-rank coal. U.S. DOE report FE-2494-TR-1 (1979).
13. Finkelman, R.B. Modes of Occurrence of Trace Elements in Coal. University of Maryland. Ph.D. dissertation (1980), 301 p.
14. Holm, P.L. Distribution of Inorganics in Selected Low-rank Coals. GFETC IR-5, 1982.

15. Goldschmidt, V.M. Geochemistry, Oxford Press, 1954, 730 p.
16. Henderson, P. Inorganic Geochemistry, Pergamon Press, New York, 1982, p. 27.
17. Benson, S.A. and P.L. Holm. Comparison of Inorganics in the Three Low-Rank Coals. ACS Division of Fuel Chemistry Preprints, 28 (2), 234 (1983).
18. Krauskopf, K.B. Introduction to Geochemistry, McGraw-Hill Book Co., New York, 1979, p. 482.

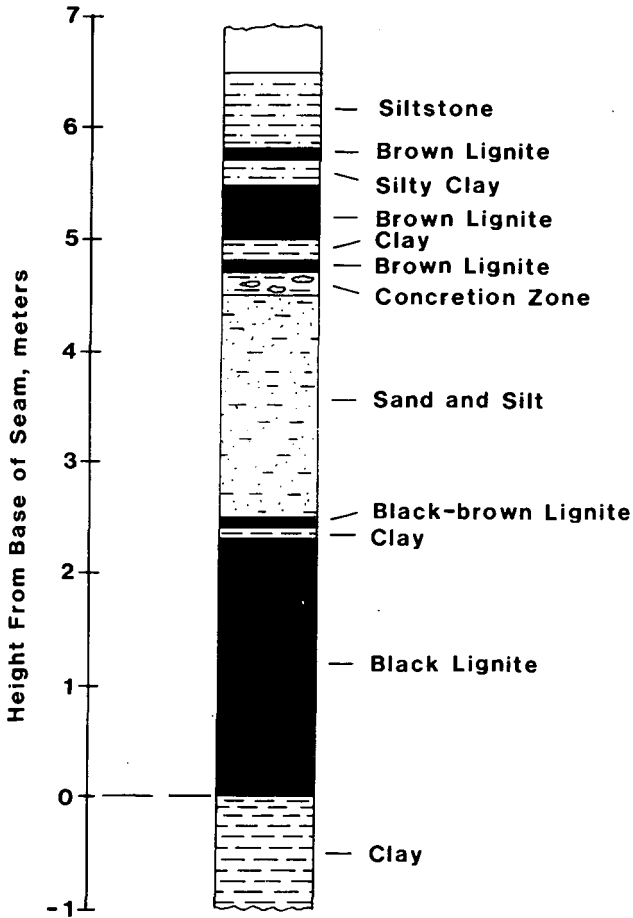
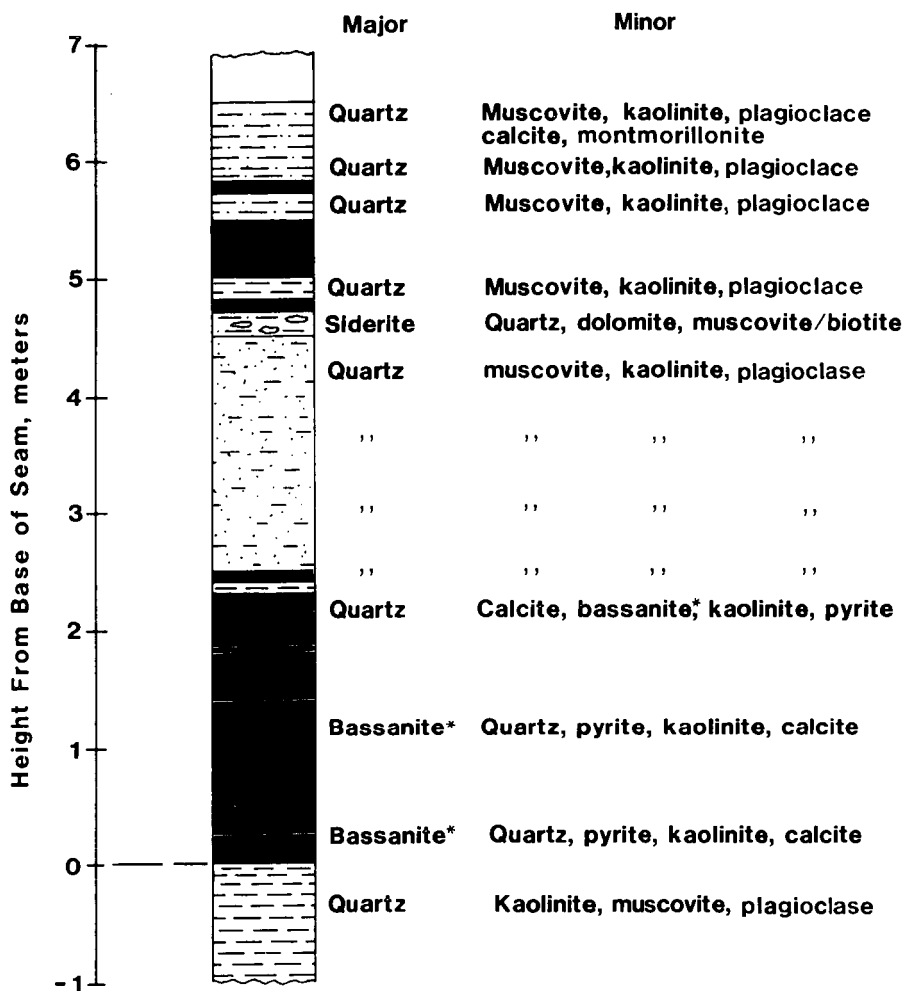


FIGURE 1. Description of stratigraphic sequence.

X-ray diffraction mineral identification⁺



⁺Abundance listed in decreasing order

*Bassanite may be a product of the Low-temperature ashing procedure

FIGURE 2. Mineralogy of the stratigraphic sequence.

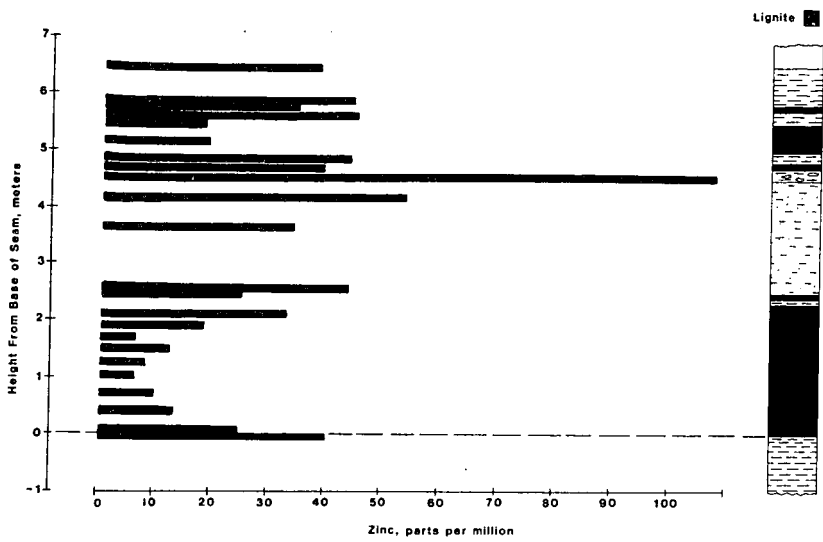


FIGURE 3. Zinc distribution in the stratigraphic sequence.

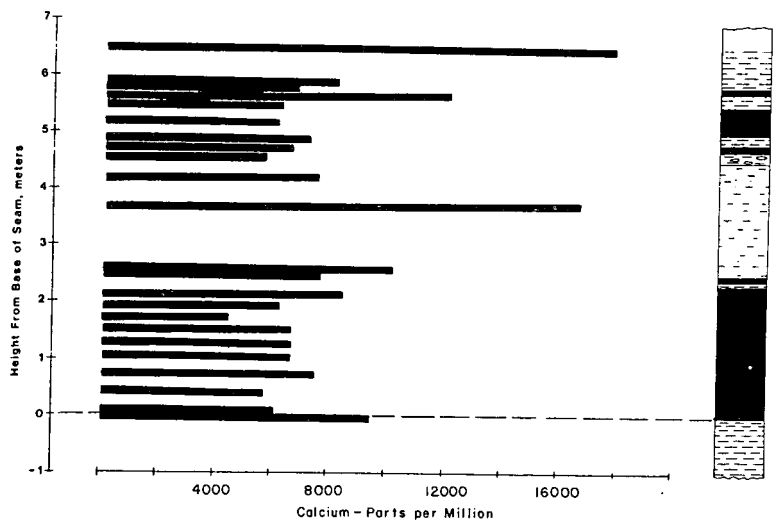


FIGURE 4. Calcium distribution in the stratigraphic sequence.

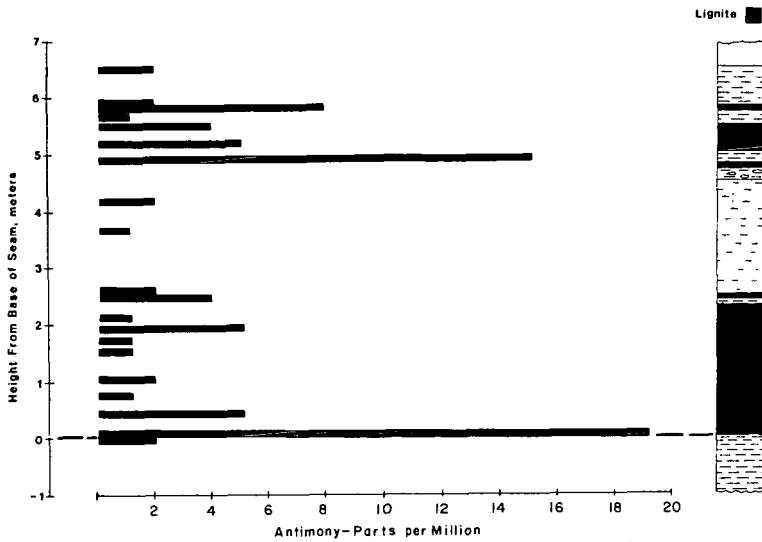


FIGURE 5. Antimony distribution in the stratigraphic sequence.

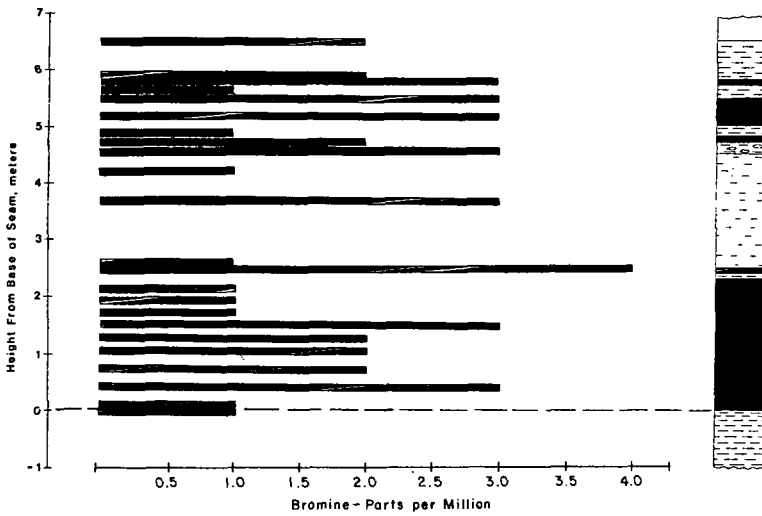


FIGURE 6. Bromine distribution in stratigraphic sequence.

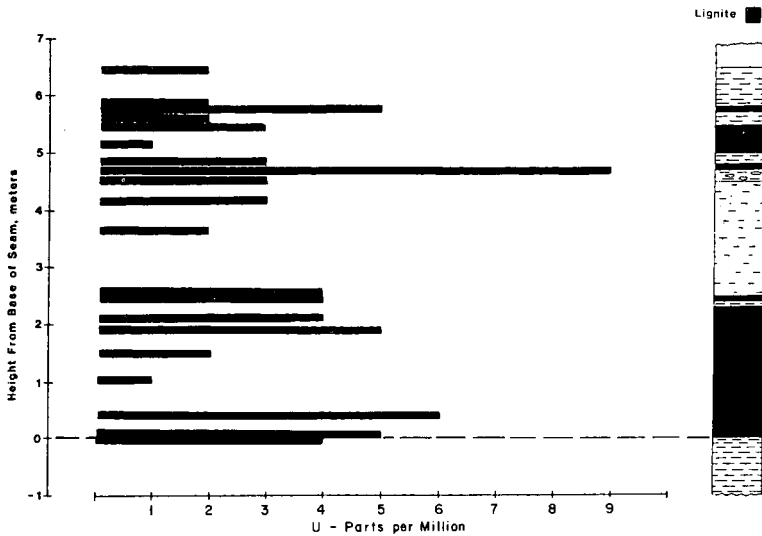


FIGURE 7. Uranium distribution in the stratigraphic sequence.

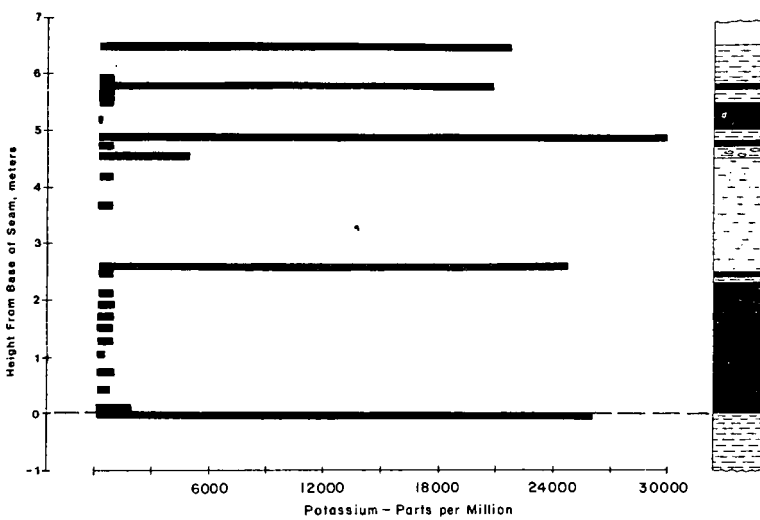


FIGURE 8. Potassium distribution in the stratigraphic sequence.

ROLE OF EXCHANGEABLE CATIONS ON THE RAPID PYROLYSIS OF LIGNITES

Mark E. Morgan* and Robert G. Jenkins

Department of Materials Science and Engineering
The Pennsylvania State University
University Park, PA 16802

INTRODUCTION

Recently, research concerned with utilization of the vast reserves of American lignites has expanded greatly. Studies have shown that lignites react quite differently than coals of higher rank when subjected to utilization and conversion schemes. The behavior of lignites is believed to be greatly influenced by the inorganic constituents present. The most significant feature of the inorganic constituents of lignites is the large concentration of exchangeable metal-cations. These cations are mainly alkali and alkaline earth metals associated with the carboxyl groups present in lignites. This research is concerned with the effect of exchangeable cations on rapid pyrolysis of a lignite.

EXPERIMENTAL

Pyrolysis was carried out in a dilute-phase entrained-flow reactor. The system is a modified version (1) of that utilized by Scaroni et al. (2). The system allows pyrolysis to be studied under high heating and cooling rates ($10^4 - 10^5$ K/s). Under these conditions, examination of pyrolysis over residence times from 0.03 to 0.30 s and at temperatures up to 1300 K is possible. Pyrolysis occurs in a dilute stream in order to reduce the role of secondary reactions resulting from contact between the pyrolysis products.

A Montana lignite (Fort Union Seam) was utilized in this study. Details of the organic and inorganic analyses of this coal can be found elsewhere (3). In this study, three types of samples were utilized: raw lignite, acid-washed lignite and cation-loaded lignite. In the acid-washed lignite the carboxylate cations are in the hydrogen (acid) form. In the acid washing procedure, 50 g of raw lignite were mixed with 900 ml of 0.1 N HCl for 16-24 h, filtered, mixed with a new batch of HCl for an additional 4 h, filtered, and washed repeatedly. It was then refluxed in 1000 ml of boiling distilled water for 1 h to remove excess HCl (3,4).

Cation loading was always performed on the acid-washed samples because it facilitates the determination of the extent of cation loading and eliminates complexities caused by the presence of more than one cation. The conditions utilized for ion exchange can be seen in Table 1. Further details can be found elsewhere (5). Also shown in Table 1 are the results of the cation loading. As can be seen, there are four different loadings of calcium. Calcium was chosen as the cation to be studied most, because it is the predominant cation in American lignites (3).

A number of gauges of the effects of pyrolysis were utilized, the most informative is weight loss. Because of experimental conditions, weight loss was determined by using ash as a tracer. This technique has been used previously by a number of workers (2,6,7).

In addition, the decomposition of the carboxyl groups was studied by measuring the carboxylate concentrations in the chars after pyrolysis. The technique to determine the carboxyl group content is outlined in detail elsewhere (3), and is based on the work of Schafer (8). There are three basic steps involved: acid washing, exchange with barium acetate and determination of the extent of exchange.

*Current address: Atlantic Research Corporation, Alexandria, VA, 22314.

TABLE 1

ION EXCHANGE CONDITIONS AND RESULTS

Sample	Exchange Media	Starting pH	g coal/l	Stir Period	m moles/g DICF Coal
Ca1	1 M Ca Acetate	8.0	55	24 h	0.84
Ca2	.25 M Ca Acetate + .25 M CaCl	6.0	100	24 h	0.75
Ca3	.25 M Ca Acetate	5.5	160	24 h	0.49
Ca4	1 M Ca Acetate	8.0	55	24 h + 24 h + 24 h + 24 h	1.11
Na	1 M Na Acetate	8.0	55	24 h	0.94
Mg	1 M Mg Acetate	8.0	55	24 h	0.71
Raw	-----	---	---	-----	0.94

RESULTS AND DISCUSSION

Total Weight Loss -- In Figure 1, the weight loss versus time behavior for the raw, acid-washed and Ca1-form samples are displayed. As can be seen, the presence of metal-cations dramatically affects the weight loss behavior in the entrained flow reactor. All three samples undergo a period of rapid weight loss followed by a region of slow weight loss. In the case of the raw and Ca1-form samples, weight loss lasts for about 0.15 s until a value of about 30 wt% (Dry Inorganic Content Free-DICF) is achieved. For the acid-washed sample, the rapid weight loss is completed in 0.05 s and the final weight loss value is 50 wt% (DICF). It is very interesting to note the similarity between the behavior of the raw and Ca1 samples. This similarity indicates the reversibility of the ion exchange treatments in terms of coal pyrolysis behavior. This strongly suggests that the difference in pyrolysis behavior between the metal cation and hydrogen-form samples is mainly due to the presence of cations, and not to the chemical treatments to which the coals were subjected.

While Ca1 contains about the same amount of exchangeable cations as the raw coal, it is possible to load various amounts of calcium onto the acid-washed lignite. Figure 2 displays the results of a study on the effects of varying the quantity of exchanged calcium. In this figure, the weight loss at maximum residence time in the entrained flow reactor at 1173 K is plotted for samples (270x400 mesh) with five levels of calcium ranging from 0 to 4.7 wt% (DICF). As can be seen, as the calcium content of the coal is increased there is a gradual and significant decrease in the maximum weight loss. This behavior is similar to that observed by Tyler and Schafer (9).

Other exchangeable cations are found in lignites, thus, a study was made into the effects of sodium and magnesium on pyrolysis. Results of this study are summarized in Table 2 which lists weight loss values at maximum residence time for a number of different cation loaded samples pyrolyzed at 1173 K. Firstly, it can be seen that the presence of metal cations always results in a decrease in weight loss. This result is important in itself in that it reemphasizes the importance of cations in lignite pyrolysis. Secondly, information can be gained about the relative activity of the various cations studied. If one compares the two divalent cations (calcium and magnesium), it can be seen that the elements have a similar effect on a per mole basis. The samples Ca2 and Mg have almost the same number of moles of cations, and both samples lose approximately the same weight. If one tries to assess the relative activity of sodium, it can be seen that, in general, the sodium-form coal undergoes a relatively large weight loss during pyrolysis.

TABLE 2

EFFECT OF CATIONS ON MAXIMUM WEIGHT LOSS IN ENTRAINED FLOW REACTOR
1173 K, DICF BASIS

<u>Sample</u>	<u>Weight Loss</u>
Raw	30.8
Ca1	28.7
Ca2	34.9
Mg	33.4
Na	38.7
Acid Washed	49.4

The monovalent nature of sodium makes a comparison of the concentrations difficult. It contains the highest molar concentration of cations, but they cover the least number of carboxyl groups.

Extended Residence Time Studies -- It was just pointed out that coals undergo rapid weight loss followed by what appears to be a region of little weight loss in the entrained flow reactor. However, although samples reach this region of constant weight loss, no samples undergo complete pyrolysis in the residence times available. Rather, this "plateau" region of weight loss is a regime of relatively slow decomposition. While it takes as little as 0.05 to 0.15 s to reach this leveling off point, it can take on the order of minutes to complete pyrolysis.

In order to determine the total pyrolysis yield, another technique was used. Basically, the approach involves capturing the pyrolyzing coal particles in a crucible at the maximum residence distance in the reactor. The captured samples are then held in the reactor for 10 min to complete pyrolysis. It is thought that this technique gives a reasonable estimation of the total pyrolysis yield possible in an entrained flow reactor.

The results of this study can be seen in Table 3 in which weight loss values for extended residence time runs are listed. If one compares the weight loss of

TABLE 3

EXTENDED RESIDENCE TIME RUNS IN THE ENTRAINED FLOW REACTOR
1173 K, DICF BASIS

<u>Sample</u>	<u>Weight Loss</u>	<u>A.S.T.M. Volatile Matter Content</u>
Raw	54.0	43.7
Acid Washed	63.3	43.2
Ca1	46.1	43.0

these samples, it can be seen, once again, that the presence of metal-cations greatly reduces the amount of volatile material evolved. It is interesting to compare these results with those gained by the ASTM volatile matter test. The ASTM volatile matter contents display no effect of cation-loading. It will be recalled that this test is performed in a fixed bed (crucible) which is felt to increase the amount of secondary char-forming reactions. Thus, when secondary char-forming reactions are increased, there is little difference in the weight loss values for pyrolysis. However, decreasing the likelihood of these reactions leads to large differences in total weight loss.

Kinetics of Total Weight Loss -- The method chosen is a simple first order Arrhenius treatment in which a single overall activation energy is utilized. The technique has been applied to the kinetics of the initial weight loss, and therefore, the weight loss values were compared to the maximum weight loss in the entrained flow reactor. Values of the apparent activation energy and preexponential factor found in this study are displayed in Table 4. It is clear that there is a similarity in the behavior of the raw and calcium-form coals. The acid-washed coal exhibits the largest activation energy, almost three times larger than that found for the raw lignite and 50% greater than that of the calcium form. Again, it is obvious that the absence of metal-cations can have a profound effect on pyrolysis kinetics and mechanisms.

TABLE 4
KINETIC PARAMETERS FOR TOTAL WEIGHT LOSS

Sample	Activation-Energy (kJ/mole)	Preexponential Factor (s ⁻¹)
Raw	58	8 x 10 ³
Acid Washed	147	2 x 10 ³
Cal	99	5 x 10 ⁵

Effect of Exchangeable Cations on Tar Release -- Table 5 lists the results of a study in which the quantity of tar, collected on a filter, in the outlet gas

TABLE 5
TARS RELEASED IN ENTRAINED FLOW REACTOR

Residence Time (s)	mg Tar/g Coal Fed	
	Raw Coal	Acid Washed Coal
0.042	3	10
0.078	9	30
0.112	3	48

stream, was measured for the raw and acid washed samples at 1173 K at three residence times. At each residence time the amount of tar released by the acid-washed coal was significantly greater than those released by the raw coals. This trend is in the same direction as the weight loss data. That is, increases in total weight loss when metal cations are removed are also accompanied by increases in tar yield.

Tar samples (1173 K, 0.078 s) were analyzed by Fourier Transform Infrared Spectroscopy, spectra were created by use of KBr pellets in the manner described by Painter et al. (10). Spectra from the raw and acid-washed coal tars were recorded as well as the "difference spectrum" from the two samples.

The spectra of these tars from the raw and acid-washed coals were similar in many ways. The same general major features were present, such as methyl, phenol and carboxyl groups. However, there is a significant difference between the two spectra in the intensities of the carbon-hydrogen aliphatic bond stretching absorbances at about 2800 - 3000 cm⁻¹. Integration of this band for the two samples leads to the conclusion that tars from the raw coal contain three times the quantity of aliphatic hydrogen as do the tars from the acid-washed coal.

Effect of Exchangeable Cations on Carboxyl Group Decomposition -- Decomposition of the carboxyl groups was followed by measuring the quantity of carboxyl

groups in the parent coal and in the resulting chars. It should be pointed out that data on the decomposition of carboxyl groups enables one to study the behavior of a single species during pyrolysis, thus yielding information that cannot be extracted from overall weight loss data. Also, it should be noted that since there are about 3.1 meq/g DICF of carboxyl groups on this lignite, the decomposition of this species can account for a weight loss of up to 14% of the lignite.

Results from this study can be seen in Figure 3 in which the quantities of carboxyl groups remaining on the raw lignite as a function of residence time at 1173 are shown. The loss of the carboxyl groups is very similar to the total weight-loss behavior presented in Figure 1. That is, there is a very rapid loss of carboxyl groups followed by a region of slow decomposition. It is interesting to note that both the raw and Cal-form samples appear to complete decarboxylation at about 2.6 meq/g DICF while the acid-washed sample releases all of the 3.1 meq/g DICF present.

Although previous researchers have studied the effects of cations on the pyrolysis of carboxyl groups, most of the work has been concerned with weight loss as a function of temperature and/or the evolution of oxides of carbon. Little work has been concerned with direct determination of the kinetics of decarboxylation. Table 6 lists the results of a first-order kinetic analysis of decarboxylation of the raw and acid washed forms of the lignite. The activation energies for decarboxylation are somewhat different for the two samples studied, that found for the raw lignite is about 20% greater than that calculated for the acid-washed coal. However, the values are quite similar when compared to the spread of activation energies found for the overall weight loss data (Table 4).

CONCLUSIONS

It must be concluded that the presence of metal cations in lignites dramatically affects pyrolysis behavior under rapid heating conditions. The presence/absence of metal cations are important in terms of the rate of evolution total weight loss and nature of the pyrolysis products. It is suggested that these data have significant importance in gasification and combustion of lignites.

ACKNOWLEDGEMENTS

This study was supported by USDOE under Contract No. DE-AC01-79ET14882.

REFERENCES

1. Maloney, D. J., Ph.D. Thesis, The Pennsylvania State University, 1983.
2. Scaroni, A. W., Walker, P. L., Jr. and Essenhigh, R. H., Fuel, 1981, (60), 71.
3. Morgan, M. E., M.S. Thesis, The Pennsylvania State University, 1980.
4. De, G. S., Tumuluri, S., Lahari, K. C., Fuel, 1971, (50), 272.
5. Morgan, M. E., Ph.D. Thesis, The Pennsylvania State University, 1983.
6. Anthony, D. B. and Howard, J. B., AIChE Journal, 1976, (22), 625.
7. Badzioch, S. and Hawksley, P. G. W., Ind. Eng. Chem. Process Des. Dev., 1970, (9), 521.
8. Schafer, H. N. S., Fuel, 1970, (49), 197.

9. Tyler, R. J. and Schafer, H. N. S., Fuel, 1980, (59), 487.
10. Painter, P. C., Kuehn, D. W., Snyder, R. W. and Davis, A., Fuel, 1982, (61), 691.

TABLE 6
KINETIC PARAMETERS FOR DECARBOXYLATION

Sample	Activation Energy (kJ/mole)	Preexponential Factor (s ⁻¹)
Raw	106	4×10^5
Acid Washed	80	8×10^4

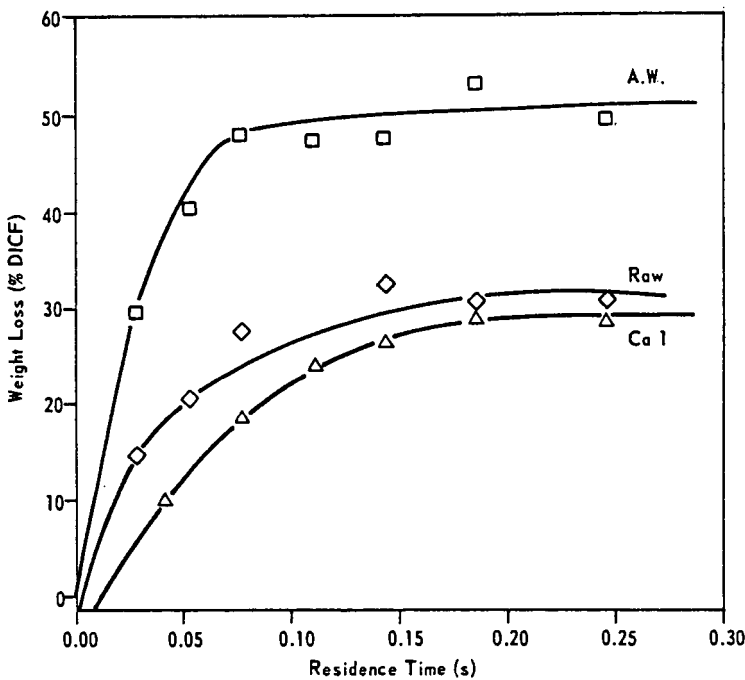


Figure 1. WEIGHT LOSS IN ENTRAINED FLOW REACTOR
270 x 400 mesh Lignite at 1173 K

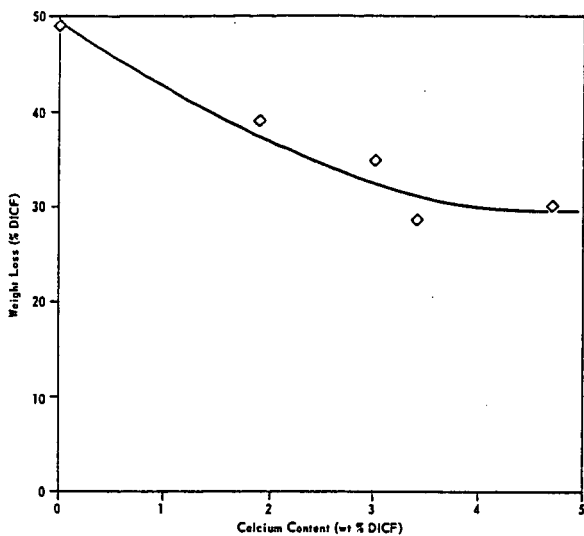


Figure 2. WEIGHT LOSS IN ENTRAINED FLOW REACTOR
Effect of Ca Loading at 1173K

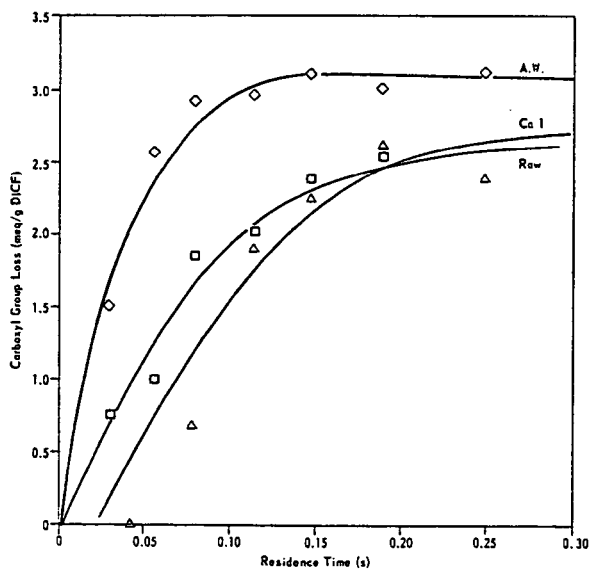


Figure 3. DECOMPOSITION OF CARBOXYL GROUPS (1173 K)

INVESTIGATION OF LOW-RANK COAL HYDROLYSIS

C. S. Wen and T. P. Kobylinski

Gulf Research & Development Company, P. O. Drawer 2038, Pittsburgh, PA 15230

INTRODUCTION

Recently, increased attention is being directed toward the pyrolysis route of processing coal to produce liquid and gaseous fuels, in particular when coupled with the use of char by-product for power generation.(1) In view of the increased interest in coal pyrolysis, a better understanding of the thermal response of coals as they are heated under various conditions is needed.

Conventional liquefaction processes developed for Eastern bituminous coals might not be the best choice for Western low-rank coals because of the substantial property and structural differences between them. In general, low-rank coals are more susceptible to reaction with H_2 , CO , or H_2S .

Coal hydrolysis is defined as pyrolysis under hydrogen pressure and involves the thermal decomposition of coal macerals followed by evolution and cracking of volatiles in the hydrogen. It is generally agreed that the presence of hydrogen during the pyrolysis increases overall coal conversion.(2,3)

In the present study we investigated pyrolysis of various ranks of coals under different gaseous environments. Low-rank coals such as Wyoming subbituminous coal and North Dakota lignite were pyrolyzed and their results were compared with Kentucky and Illinois bituminous coals.

EXPERIMENTAL

The coals used in this study included Wyoming subbituminous coal, North Dakota lignite, Kentucky bituminous coal, and Illinois No. 6 bituminous coal. Proximate and ultimate analyses of the coals studied are given in Table I.

All pyrolysis experiments were carried out in the thermogravimetric apparatus (TGA) having a pressure capacity of up to 1000 psi. A schematic of the experimental unit is shown in Figure 1. It consists of the DuPont 1090 Thermal Analyzer and the micro-balance reactor. The latter was enclosed inside a pressure vessel with a controlled temperature programmer and a computer data storage system. The pressure vessel was custom manufactured by Autoclave Engineers. A similar set-up was used previously by others.(4) A chromel-alumel thermocouple was set in close proximity to the sample inside a reactor. The reactor was made of a quartz tube which was surrounded by a tubular furnace. In a typical coal pyrolysis run, the coal sample (20-30 mg) was placed in a platinum boat which was suspended from the quartz beam of the TGA balance. The coal particle size used was 100-200 mesh. Samples were heated to desired temperatures at linear heating rates or heated isothermally under various gaseous environments.

FT-infrared was also used to monitor the degree of pyrolysis for various samples at different temperatures. The KBr (potassium bromide) pellet of sample was prepared for FTIR analysis.

RESULTS AND DISCUSSION

Typical thermograms of Wyoming coal under hydrogen pressure are given in Figure 2. The TGA and the weight loss rate thermograms show a major weight loss at temperatures ranging from 350-600°C. A secondary hydrolysis peak occurs above 600°C most likely due to the gas releases from the further decomposition of coal.

Figure 3 shows a comparison of derivative thermograms for four different rank coals. The differences of devolatilization rate are not large at temperatures up to 500°C, however, above 500°C, the secondary hydroxyprolysis peak of low-rank coal becomes dominant.

The influence of heating rate on coal hydroxyprolysis was studied over a range of 5-100°C/min. As shown in Figure 4, the two peaks were observed, the first of which we call the primary volatilization, and the second, characteristic of local hydroxyprolysis. The primary peak increased rapidly with the increase of the heating rate. The second characteristic peak becomes relatively dominant at lower heating rates. It seems that the hydroxyprolysis peak is favored by slow heating rates, indicating a heat transfer limitation within the secondary hydroxyprolysis region. In contrast, coal pyrolyzed under an inert nitrogen atmosphere results in an increase of weight loss rate with increasing heating rates, but the shape of the curves remains the same (Figure 5).

The effect of hydrogen on coal pyrolysis can further be illustrated by Figure 6, where we compared derivative thermograms of Wyoming coal pyrolyzed at 200 psig of N₂ and 200 psig of H₂ at the same heating rates (20°C/min). The secondary hydroxyprolysis peak observed at 580°C in the H₂ run was absent in the N₂ atmosphere.

FTIR spectra of the original coal and char from pyrolyzing Wyoming coal under H₂ pressure at various temperatures are shown in Figure 7 (only wave numbers between 1700 and 400 cm⁻¹ were shown here for comparison). The strongest absorption band located at 1600 cm⁻¹ begins to decrease in intensity at 470°C. This band has been assigned to aromatic ring C-C vibration associated with phenolic/phenoxy groups.(5) Similarly, the aromatic-oxygen vibration band near 1260 cm⁻¹ shows an equivalent decrease. The absorption bands between 720 to 870 cm⁻¹ (which arise from the out-of-plane aromatic CH vibrations) increase markedly at 470°C, indicating a growth in size of aromatic clusters in the reacted coal. At 650°C, most organic absorption bands were diminished except for a broad band ranging from 1000-1090 cm⁻¹ due to clay mineral absorption.(7) An increase in the structureless background absorption is observed, suggesting a growth of graphitization in the residue coal.

The kinetics of coal pyrolysis are complicated because of the numerous components or species which are simultaneously pyrolyzed and decomposed. For measuring kinetic parameters, we treated data following the procedure of Coats and Redfern (8) and Mickelson and Einhorn.(9) The kinetic parameters for four different coals heated under H₂ pressure are presented in Table II. A reaction order equal 2.3 to 2.9 was observed for the primary hydroxyprolysis peaks. A high reaction order was obtained for the secondary reaction peak under hydrogen pressure. The kinetic parameters for four different coals heated under N₂ atmosphere compared with data presented in the literature are listed in Table III.

Kinetic parameters for n (reaction order) and E (activation energy) in the literature show significant variation for different techniques and coal (Table III). By considering the complexity of coal thermal degradation, many authors have contended that a simple, first-order reaction is inadequate. Wisser et al. (10) found that n=2 gave the best fit to their data, while Skylar et al. (11) observed that values of n above 2 were required to fit nonisothermal devolatilization data for different coals. The kinetic parameters obtained in this study also show a non-integer reaction order. The thermal decomposition of coals are complex because of the numerous components or species which are simultaneously decomposed and recondensed.

Figure 8 demonstrates the influence of CO on devolatilization for different ranks of coal. For the higher rank coals (i.e., Kentucky and Illinois bituminous coals), pyrolysis in the presence of CO plus H₂ or H₂ alone follows the

same path. However, lignite showed a marked increase of pyrolysis rate in the run where CO was added. A higher content of reactive oxygenated bonds (i.e., carboxyl or ether linkages) in low-rank coals could be the reason for the high reactivity in the presence of CO. The kinetic parameters determined for coal pyrolyzed in syngas (CO/H₂ mixture) are listed in Table IV. As shown in the table, a high reaction order was obtained for the H₂ and CO/H₂ runs, particularly for the low-rank coals which showed a secondary reaction occurring at temperatures above 500°C.

CONCLUSIONS

Laboratory microscale studies have demonstrated that the coal pyrolysis in a hydrogen atmosphere gave higher degree of devolatilization in low-rank coals than pyrolysis in an inert atmosphere. In hydrogen atmosphere two distinct steps in coal devolatilization were observed as shown by the double peak of the devolatilization rate. Only one step was observed under nitrogen atmosphere. In a comparison of kinetic parameters, a high reaction order and a low activation energy were also obtained in the coal hydrolypyrolysis. Application of data and observations from this study could lead to a better understanding of chemical and physical changes during the coal hydrolypyrolysis and seek alternative coal conversion routes.

REFERENCES

1. H. W. Parker, "Liquid Synfuels Via Pyrolysis of Coal in Association with Electric Power Generation," Energy Progress, 2(1), 4, 1982.
2. R. J. Belt and L. A. Bissett, "Assessment of Flash Pyrolysis and Hydro-pyrolysis," DOE Report METC/RI-79/2, 1978.
3. P. Arendt and K. H. Van Heek, Fuel, 6099, 779, 1981.
4. J. G. Speight, "Assessment of Structures in Coal by Spectroscopic Techniques," in Analytical Methods for Coal and Coal Products, (Ed. by C. Karr, Jr.), Vol II, Chapter 22, pp 75-101, Academic Press, New York, 1978.
5. V. T. Ciuryla, R. F. Weimer, D. A. Bivans, and S. A. Motika, Fuel, 58(10), 748, 1979.
6. P. C. Painter and M. M. Coleman, "The Application of Fourier Transform Infrared Spectroscopy to the Characterization of Coal and Its Derived Products," DIGILAB FTS/IR Notes No. 31, January 1980.
7. A. W. Coats and J. P. Redfern, "Kinetic Parameters from Thermogravimetric Data," Nature, 201, 68, 1964.
8. R. W. Mickelson and I. N. Einhorn, Thermochim. Acta, 1, 147, 1970.
9. W. H. Wisler, Fuel, 47, 475, 1968.
10. W. H. Wisler, G. R. Hill, and N. J. Kertamus, I&EC Process Design and Develop., 6(1), 133, 1967.
11. M. G. Skylar, V. I. Shustikov, and I. V. Virozub, Intern. Chem. Eng., 9, 595, 1969.

Table I

COAL ANALYSIS

	Wyoming		North Dakota Lignite		Kentucky		Illinois	
	Subbituminous Coal		As		Bituminous Coal		Bituminous Coal	
	Received	Dry Basis	Received	Dry Basis	Received	Dry Basis	Received	Dry Basis
Proximate Analysis, wt%								
Moisture	6.1	--	21.2	--	3.0	--	3.9	--
Volatile	39.9	42.5	35.3	44.7	39.8	41.0	38.1	39.6
Fixed Carbon	45.6	48.6	35.9	45.6	48.6	50.1	46.8	48.7
Ash	8.4	8.9	7.6	9.7	8.6	8.9	11.2	11.7
Ultimate Analysis, wt%								
Moisture	6.1	--	21.2	--	3.0	--	3.9	--
Carbon	64.6	68.8	50.5	64.1	70.3	72.5	67.5	70.3
Hydrogen	4.3	4.6	3.5	4.4	4.8	5.0	4.5	4.7
Nitrogen	0.9	1.0	1.1	1.4	1.2	1.2	1.3	1.4
Sulfur	0.5	0.5	0.5	0.6	3.0	3.1	3.4	3.5
Ash	8.4	8.9	7.6	9.7	8.6	8.9	11.2	11.7
Oxygen (diff.)	15.1	16.1	15.6	19.7	9.1	9.4	8.2	8.4

Table II

KINETIC PARAMETERS OF COAL HYDROLYSIS^a

<u>Coal</u>	<u>Reaction Order</u>		<u>Activation Energy (kcal/mole)</u>		<u>Frequency Factor (min⁻¹)</u>	
	<u>1st Peak</u>	<u>2nd Peak</u>	<u>1st Peak</u>	<u>2nd Peak</u>	<u>1st Peak</u>	<u>2nd Peak</u>
Wyoming	2.5	3.4	18.9	64.5	1.6×10^5	1.3×10^{15}
North Dakota Lignite	2.9	4.7	23.9	70.4	4.2×10^7	1.2×10^{18}
Kentucky	2.3	--	23.4	--	3.1×10^6	--
Illinois	2.4	--	29.2	--	1.9×10^8	--

^a Samples were heated at 50°C/min under 500 psig H₂.

^b Hydrolysis characteristic peak occurred in low-rank coals.

Table III

A COMPARISON OF KINETIC PARAMETERS IN COAL PYROLYSIS

<u>Investigators</u>	<u>Coal</u>	<u>Reaction Order</u>	<u>Activation Energy (kcal/mole)</u>	<u>Frequency Factor (min⁻¹)</u>	<u>Reference</u>
Wiser et al.	Utah Bituminous	2	15.0	2.9×10^3	(9)
Stone et al.	Pittsburgh Seam Bituminous	1 ^a	27.3	3.2×10^8	(11)
Ciuryla et al.	Pittsburgh Seam Bituminous	1 ^a	39.5	1.7×10^{11}	(5)
	North Dakota Lignite	1 ^a	53.6	1.7×10^{15}	(5)
	Illinois Bituminous	1 ^a	52.3	1.7×10^{15}	(5)
Skylar et al.	Soviet Coal	2.3	10.0	1.3×10^5	(10)
	Soviet Gas Coal	2.1	14.6	5.1×10^6	(10)
This work ^b	Wyoming Subbituminous	2.1	25.1	6.1×10^5	
	North Dakota Lignite	2.2	23.2	1.2×10^6	
	Kentucky Bituminous	1.9	26.9	4.2×10^8	
	Illinois Bituminous	1.8	30.9	4.8×10^8	

^a Based on a series of first-order reactions.

^b Samples were heated at 50°C/min under 50 cc/min ambient N₂ flow.

Table IV

KINETIC PARAMETERS OF COAL PYROLYSIS UNDER SYNGAS^a

Coal	Reaction Order		Activation Energy (kcal/mole)		Frequency Factor (min ⁻¹)	
	1st Peak	2nd Peak	1st Peak	2nd Peak	1st Peak	2nd Peak
	Wyoming Coal	2.8	3.6	23.1	57.5	1.1x10 ⁷
North Dakota Lignite	2.6	2.8	20.8	32.6	2.6x10 ⁶	1.8x10 ¹²
Kentucky Coal	2.3	--	22.9	--	2.3x10 ⁶	--
Illinois Coal	2.3	--	25.4	--	3.5x10 ⁷	--

^a Samples were heated at 50°C/min under 500 psig H₂ /CO (3/1 mole ratio).

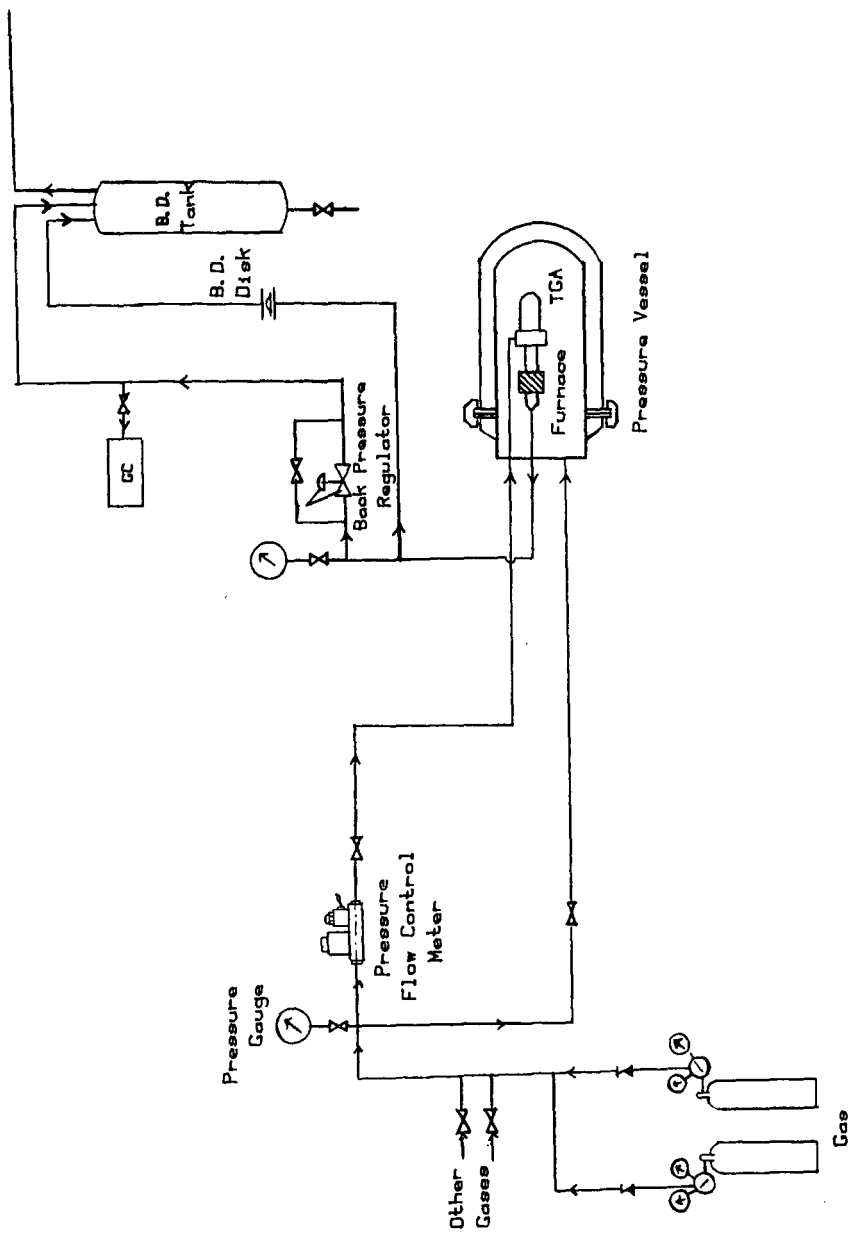


Fig. 1 Schematic Set-up of the Pressure Pyrolysis Apparatus.

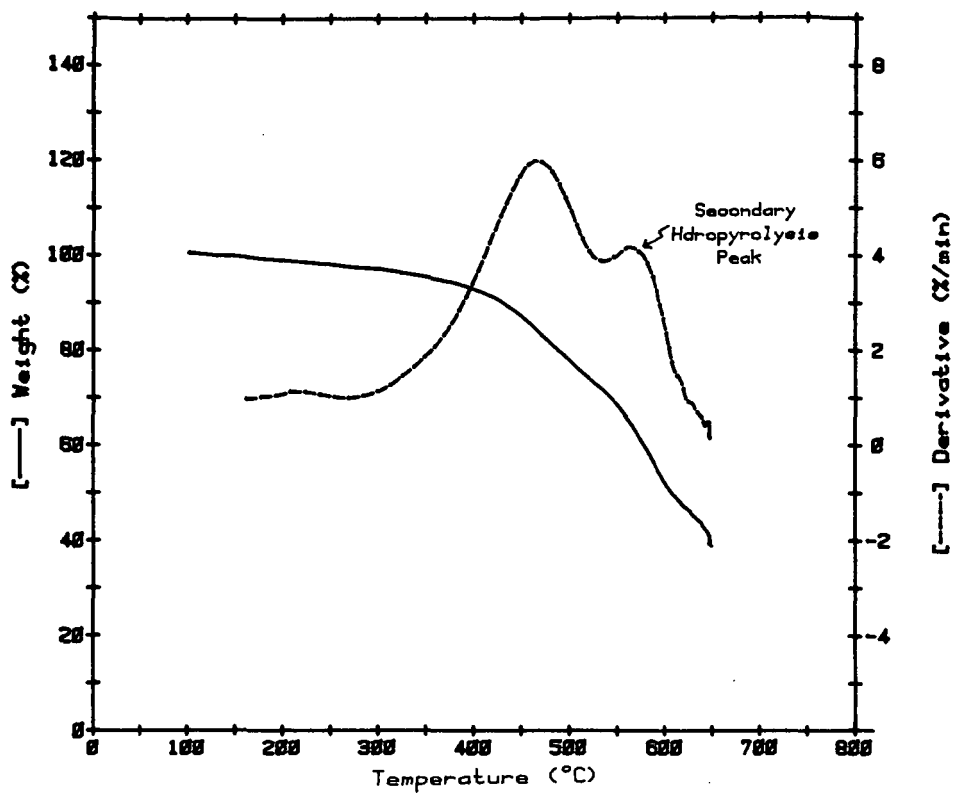


Fig. 2 Typical Pressure TGA Thermograms of Wyoming Coal Heated at 50°C/min and 500 psig H₂.

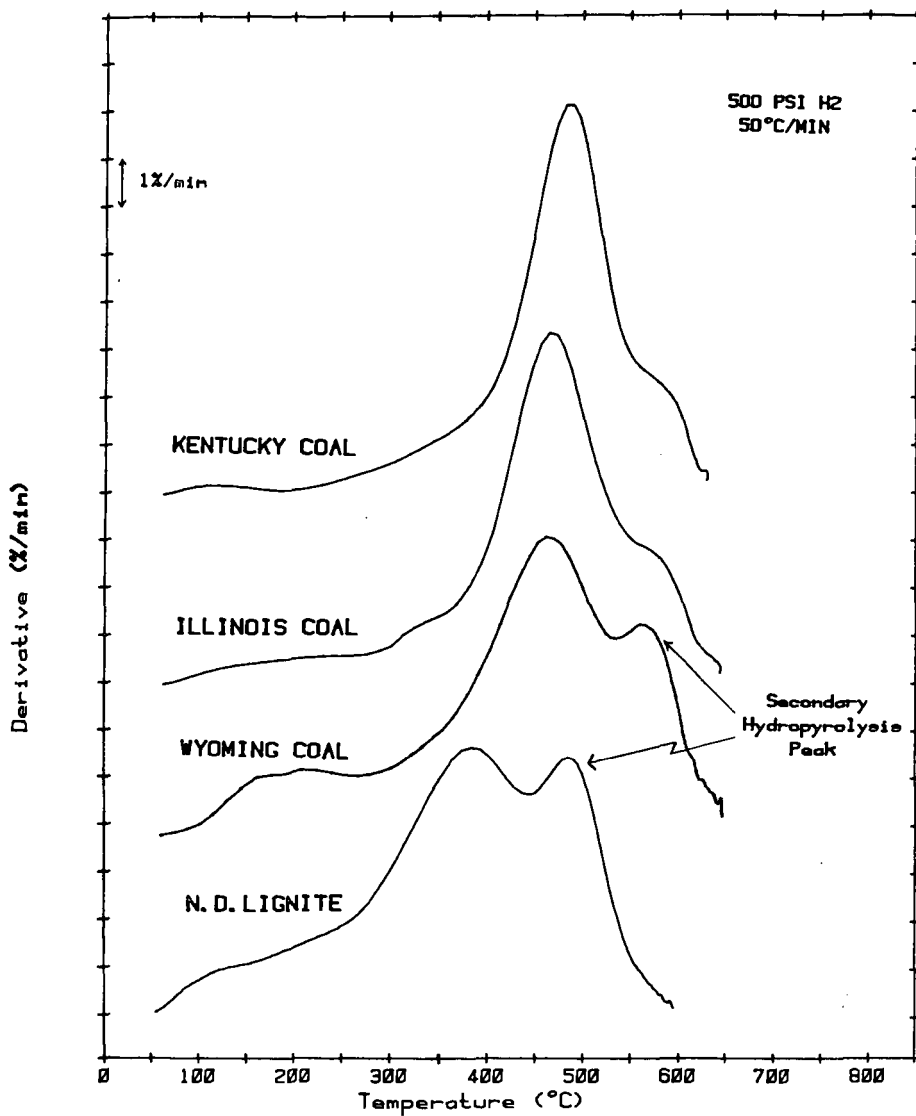


Fig. 3 A Comparison of Hydrolysis Derivative Thermograms for Various Coals at 50 °C/min and 500 psig H₂.

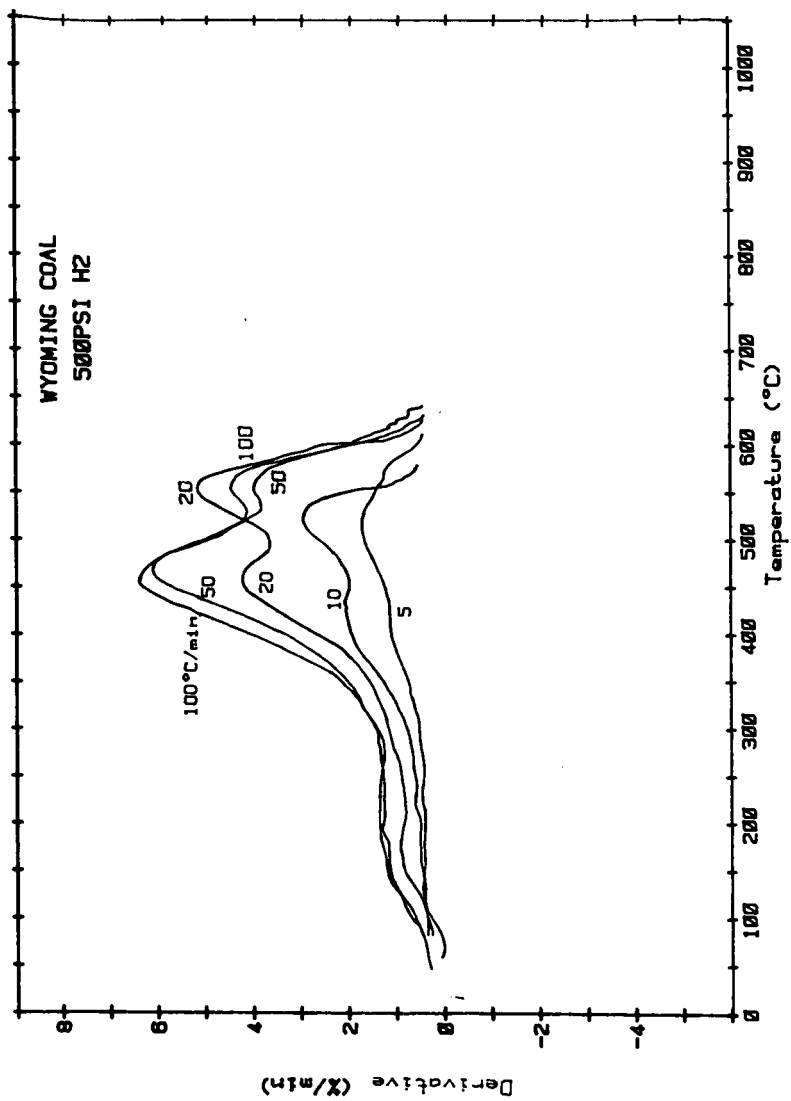


Fig. 4 The Effect of Heating Rate on Devolatilization Rate of Wyoming Coal Hydrolysis.

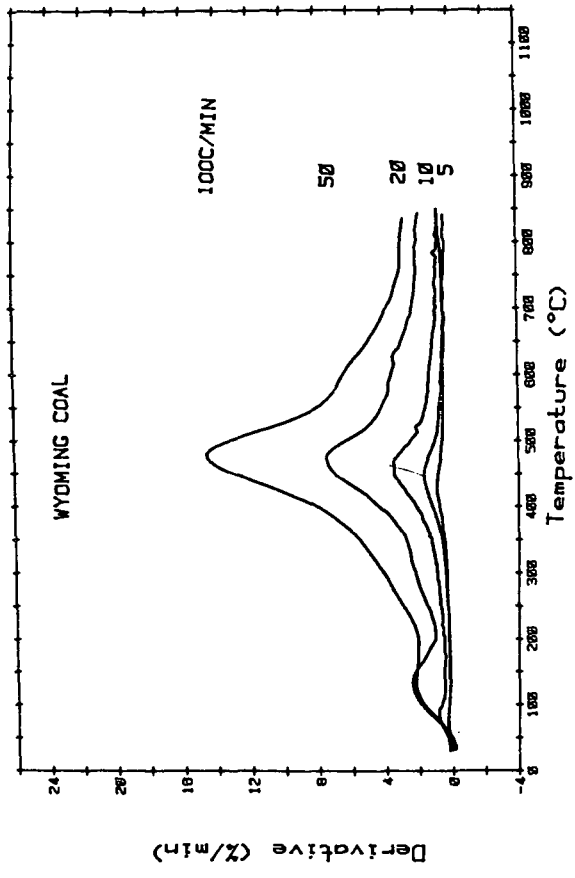


Fig. 5 Derivative Thermograms of Coal Pyrolysis at Different Heating Rates Under 1atm N₂.

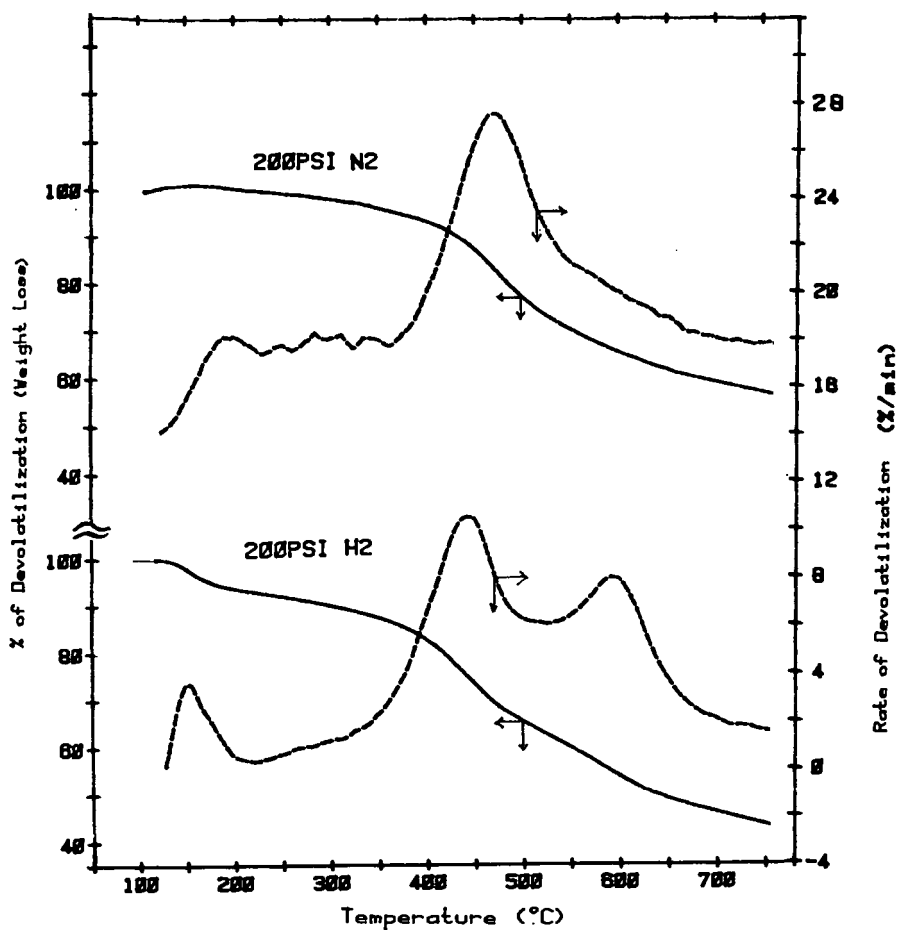


Fig. 6 A Comparison of Thermograms between Wyoming Coal Pyrolyzed in 200 psig N₂ and 200 psig H₂ at 20°C/min.

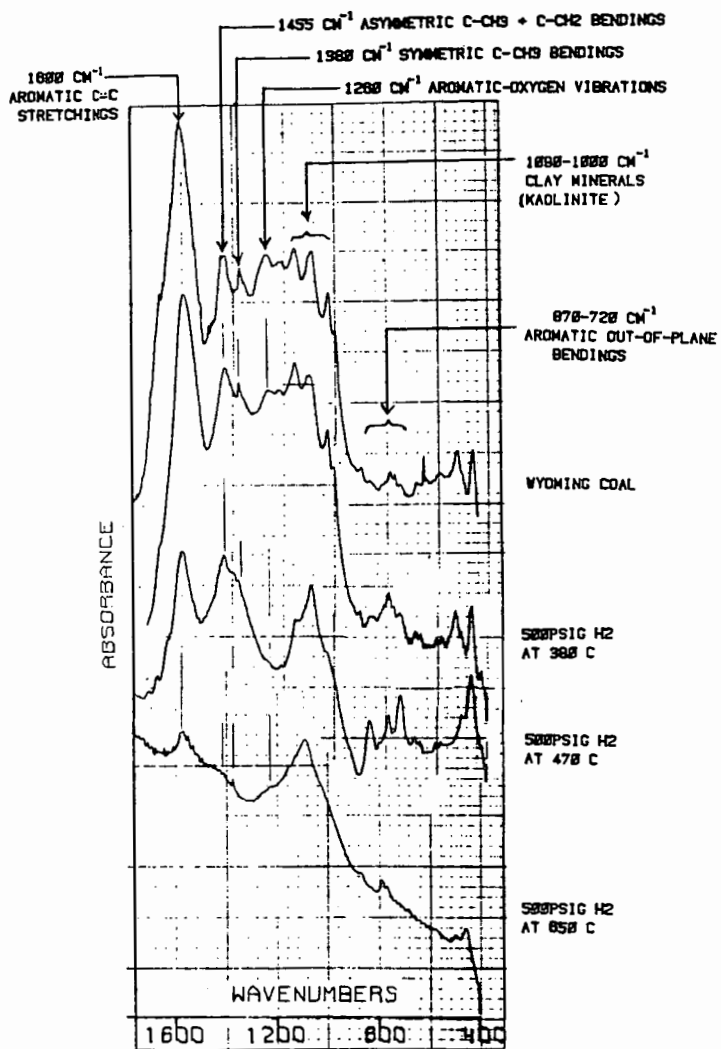


Fig. 7 FT-IR Monitor of Wyoming Coal Pyrolysis under 500 psig H₂ at Various Temperatures.

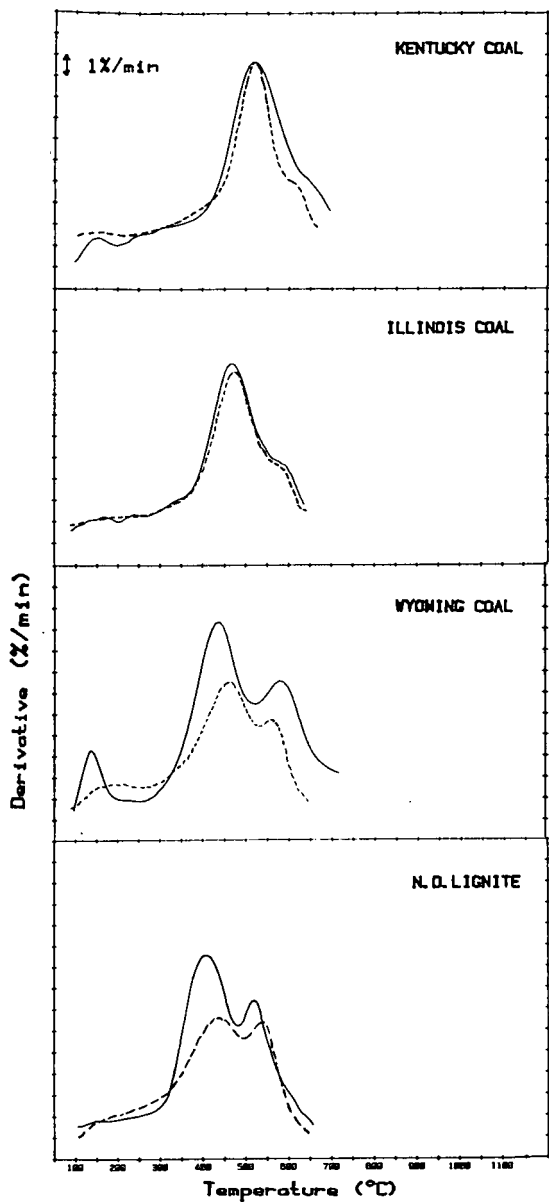


Fig. 8 The Influence of CO on Coal Devolatilization, where —; 500 psig CO/H₂ and ---; 500 psig H₂.

COMBUSTION REACTIVITY OF LOW RANK COAL CHARs

B.C. YOUNG

CSIRO Division of Fossil Fuels, PO Box 136, North Ryde, NSW 2113, Australia

Introduction

For many years the CSIRO has been involved in studies on the combustion kinetics of coal chars and related materials. Early work included studies on a char produced from a Victorian brown coal (1). More recently, the combustion kinetics of chars produced during the flash pyrolysis of sub-bituminous coals have been determined (2,3).

In this paper data are given for the combustion reactivities of four flash pyrolysis chars. Their reactivities are compared with the results for chars produced from low and high rank coals, and petroleum coke. Reactivity is expressed as the rate of combustion of carbon per unit external surface area of the particle, with due correction being made for the effect of the mass transfer of oxygen to the particle.

Experiment and Theory

Details of the method of producing the flash pyrolysis chars are available elsewhere (4), as is information on the procedure for measuring their combustion rates (2,3,5). In brief, pulverized Millmerran and Wandoan coals (Queensland, Australia) were flash pyrolysed at various temperatures between 500 and 800°C. The resulting chars were screened to yield a size fraction having a median mass size around 80 μm. The properties of the chars are presented in Table 1.

TABLE 1 Properties of the CharS

	Millmerran					Wandoan
Pyrolysis temperature, °C	540	585	610	780	800	550
Median mass size, μm	85	76	90	70	88	76
Size below which 90% of material lies, μm	100	95	118	92	98	96
Size below which 10% of material lies, μm	66	52	61	47	74	49
Particle density, g/cm ³	0.88	0.80	0.78	0.99	0.78	1.05
Chemical analysis, % w/w (as received)						
Moisture	2.7	2.2	3.3	2.5	4.7	2.9
Ash	28.0	30.4	35.6	60.1	38.2	22.1
Elemental composition						
C	56.6	55.3	50.7	31.3	50.3	60.3
H	3.8	2.8	2.7	1.1	1.3	3.3
N + S + O	8.9	9.3	7.7	5.0	5.5	11.4

Rate measurements were carried out, using an entrainment reactor, on flowing suspensions of particles in preheated oxygen-nitrogen. From progressive changes in gas composition and gas and wall temperatures along the reactor, the rate of carbon burned per unit external area of particle (ρ) was calculated.

From ρ , the chemical rate coefficient, R_c , was evaluated (6):

$$\rho = R_c [p_g (1 - \chi)]^n \quad \text{g/cm}^2\text{s} \quad (1)$$

where p_g is the partial pressure of oxygen in the bulk gas, n is the order of reaction in relation to p_g , and λ is the ratio of ρ to the maximum possible (i.e. mass transfer limited) burning rate calculated from known physical properties (6,7).

R_c , as will be shown, is strongly dependent on particle temperature, T_p . This temperature is calculated from a heat balance over the burning particle (6).

Results and Discussion

Combustion rate data for Millmerran and Wandoan chars are shown in Arrhenius form in Fig. 1. Data for Millmerran chars produced at 585 and 610°C were combined into a single set, as were the data for the chars produced at 780 and 800°C. Rate data for other chars (derived from low and high rank coals) and also for petroleum coke are also included in Fig. 1. To permit the comparison of results for different materials exhibiting different values of n , the rate data were calculated from the relation:

$$\rho_c = R_c p_g^n \quad \text{g/cm}^2\text{s} \quad (2)$$

where p_g is taken as 1 atm. Values of the Arrhenius parameters, A (pre-exponential factor) and E (activation energy), together with the magnitude of n for each material referred to in Fig. 1 are listed in Table 2.

TABLE 2 Kinetic Data for the Combustion of Chars and Coke

Material	A g/(cm ² s (atm O ₂) ⁿ)	E kcal/mol	n	Reference
Millmerran char (540°C)	15.6	17.5	0.5	2
Millmerran char (585 and 610°C)	22.3	18.8	0.5	3
Millmerran char (780 and 800°C)	73.3	21.7	0.5	3
Wandoan char (550°C)	39.1	18.3	0.5	3
Yallourn brown coal char	9.3	16.2	0.5	1
New Zealand bituminous coal char	8	16.0	1.0	7
Anthracites and semi-anthracites	20.4	19.0	1.0	8
Petroleum coke	7.0	19.7	0.5	5

The data exhibit several notable features:

- (1) The combustion rates of all the materials show a strong dependence on temperature, the values of the activation energies ranging from 16.0 to 21.7 kcal/mol.
- (2) The activation energy increases and the reactivity of Millmerran chars decreases with increasing pyrolysis temperature.
- (3) The most reactive char is that produced from Wandoan coal at 550°C. This material is about twice as reactive as chars produced from other low rank coals (Millmerran and Yallourn) and high rank coals (New Zealand bituminous, anthracites and semi-anthracites), and about ten times as reactive as petroleum coke.
- (4) The low rank coal chars and petroleum coke show an order of reaction of 0.5. Earlier determinations on chars from high rank coals indicate a value of unity. However, a reanalysis (5) of an earlier set of data (9) showed, in the case considered, little to choose between n equal to 0.5 or 1.0.

The values of the activation energy for the Millmerran and Wandoan chars (~ 20 kcal/mol), together with those of the other materials listed in Table 2, imply reactions under circumstances where pore diffusion as well as chemical reaction exercises strong rate control, i.e. regime II (10) conditions apply. Confirmatory evidence that these materials are indeed burning under regime II conditions is provided by the steady decrease in particle size and slight reduction in the particle density of the particles as they burn away (6). This behaviour is illustrated in Fig. 2 by the data on the lowest temperature chars produced from Millmerran and Wandoan coal. Also shown are some theoretical curves indicating the changes in particle size and density to be expected for combustion at constant particle density or at constant particle size (6).

Conclusions

It has been shown that the reactivities to oxygen of chars produced from Millmerran sub-bituminous coal decrease with increasing pyrolysis temperature but are similar in magnitude to the reactivities of chars derived from a brown and a bituminous coal and to the reactivities of anthracites and semi-anthracites. However, Wandoan char, also of sub-bituminous origin, exhibits about twice the reactivity of Millmerran char and about ten times the reactivity of petroleum coke. On the basis of observed activation energy values, particle size and particle density behaviour it is concluded that the combustion rates of Millmerran and Wandoan chars are controlled by the combined effects of pore diffusion and chemical reaction.

Acknowledgements

The author is grateful to R.J. Hamor for carrying out the experimental measurements and to I.W. Smith for valuable discussions.

References

1. Hamor, R.J., Smith, I.W. and Tyler, R.J. *Combustion and Flame*, 21, 153-162 (1973).
2. Young, B.C. *Proceedings of the International Coal Science Conference*, Disseldorf: Verlag Glückauf, Essen, pp. 260-265, 1981.
3. Hamor, R.J. and Young, B.C. *Proceedings of the International Science Conference*, Pittsburgh, in press (1983).
4. Edwards, J.H., Smith, I.W. and Tyler, R.J. *Fuel*, 59, 681-686 (1980).
5. Young, B.C. and Smith, I.W. *Eighteenth Symposium (International) on Combustion*, The Combustion Institute, Pittsburgh, pp. 1249-1255 (1981).
6. Smith, I.W. *Nineteenth Symposium (International) on Combustion*, The Combustion Institute, Pittsburgh, in press (1983).
7. Smith, I.W. *Combustion and Flame*, 17, 303-314 (1971).
8. Smith, I.W. *Combustion and Flame*, 17, 421-428 (1971).
9. Field, M.A. *Combustion and Flame*, 13, 237-252 (1969).
10. Mulcahy, M.F.R. and Smith, I.W. *Review of Pure and Applied Chemistry*, 19, 81-108 (1969).

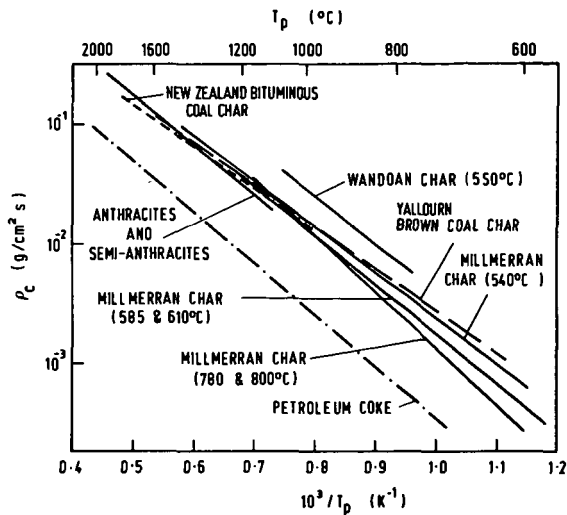


Figure 1 Combustion rate data for chars and coke

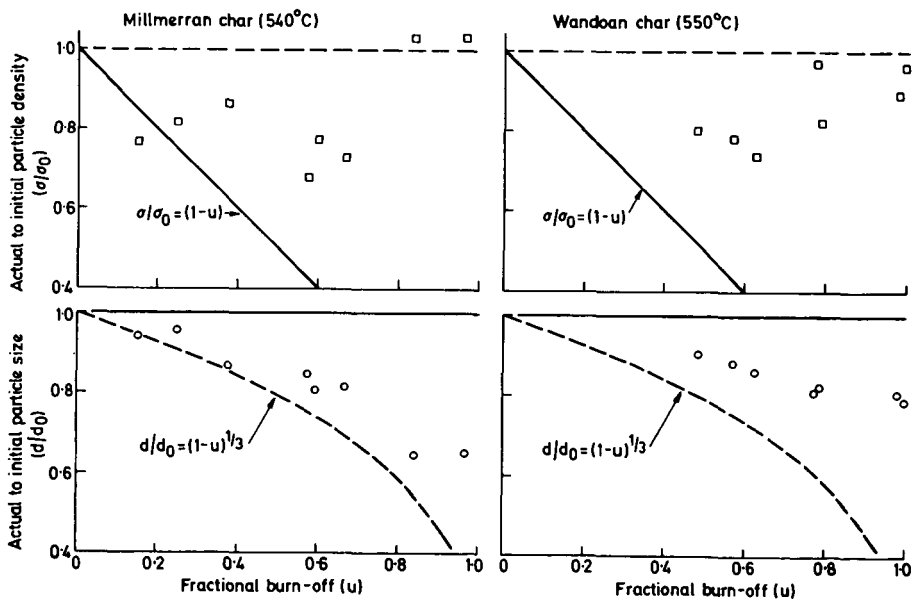


Figure 2 Burning behaviour of Millmerran and Wandooan chars (--- theoretical lines for particles burning with constant density, — theoretical lines for particles burning with constant size)

THE EFFECTS OF CATIONS ON PULVERIZED COAL COMBUSTION

Bruce A. Morgan and Alan W. Scaroni

Fuels and Combustion Laboratory
The Pennsylvania State University
University Park, PA 16802

INTRODUCTION

Although coal has been burned for centuries, many fundamental aspects of the process remain poorly understood. Conflicting theories appear in the voluminous combustion literature. There is, however, general agreement that coal combustion occurs in two stages: pyrolysis or devolatilization of the coal followed by heterogeneous combustion of the char (1-3). In most practical combustors, the latter acts as the rate determining step for the overall process. For more efficient coal combustion, therefore, it is essential to understand the parameters which most affect the rate of heterogeneous char combustion.

Char combustion rate depends primarily on the reactivity of the carbonaceous material to oxygen. This reactivity is controlled by several parameters such as gas diffusion rates to and from the reactive surface and catalysis of combustion by inorganic species present in the char. This research concentrates on the effect of various inorganic species on the rate of pulverized lignite combustion.

Jenkins et al. (4) have shown that the reactivity of coal chars is rank related. Chars from low rank coals such as lignites were found to be more reactive than chars produced from high rank bituminous coals. This has been attributed to the presence of inorganic constituents, in particular ion exchangeable cations, in low rank coals and their chars (5-7).

Walker (7) and McKee (8) have shown that alkali and alkaline-earth metals are catalysts for the carbon-oxygen reaction. Furthermore, the predominant ion exchangeable cations on American lignites are alkali (Na, K) and alkaline-earth (Ca, Mg, Ba) metals (9). Therefore, it is possible that highly dispersed cations on low rank coal chars catalyze the heterogeneous combustion step.

Reactivity data have been generated previously under isothermal conditions in the absence of particle ignition (5-7). The present work reports on lignite combustion under nonisothermal conditions. It was directed primarily towards understanding the effects of cations (K, Ca, Na) on the initial stages of pulverized coal combustion.

EXPERIMENTAL

Sample Preparation. The ion exchangeable cations located on the carboxyl groups of a Texas lignite (PSOC-623) were removed by acid washing with 0.04 M HCl. Alkali (Na, K) and alkaline-earth (Ca) metals were back exchanged on the acid-washed coal using 1 M metal acetate solutions. Details of the procedure are outlined elsewhere (10). The quantity of exchanged cations was determined by atomic absorption spectroscopy.

Combustion Experiments. Raw and modified lignite (mean weight particle size 62 μm) were combusted in an entrained-flow reactor at an initial furnace (gas and wall) temperature of 973 K. The reactor configuration and operating principle have been well documented (10-12). Weight loss rate data were obtained using an ash tracer technique.

RESULTS AND DISCUSSION

Sample Characteristics. Proximate analyses of the raw and modified Texas lignite are shown in Table 1. Acid washing with HCl reduced the total ash yield

TABLE 1

PROXIMATE ANALYSES OF TEXAS LIGNITE (PSOC 623)

	<u>Ash, wt% (Dry)</u>	<u>VM, wt% (Dry)</u>	<u>Moisture, wt%</u>
Raw	15.9	44.7	10.8
Ca Loaded	14.0	46.5	8.0
Na Loaded	13.0	43.4	12.3
K Loaded	15.0	43.9	12.4
Acid-Washed	10.7	46.1	7.7

of the coal by 33 wt%. Subsequent addition of the cations increased the ash yields by between 18% (Na) and 29% (K), based on the raw lignite. The quantity of each cations back exchanged, wt% dry basis, is shown in Table 2. The acid washing was

TABLE 2

CATION LOADINGS ON THE LIGNITE*

<u>Cation</u>	<u>wt% (Dry)</u>	<u>milliequivalents/g of coal (Dry)</u>
Ca	3.8	1.2
Na	2.6	1.0
K	5.0	1.1

* The acid-washed sample had less than 0.1 wt% (dry) cations on the coal.

an efficient procedure since less than 0.1 wt% (dry basis) of the cations remained on the acid washed coal.

Weight Loss Rate Data. Figure 1 illustrates weight loss rate data (wt%, daf) in air for raw and exchanged lignites. Residence times were determined using the model formulated by Morgan (10). Essentially, the model accounts for slip velocity between particles and flowing gas.

In the initial 0.1 s, the acid-washed lignite had the greatest rate of weight loss. The initial step in the combustion process accounting for weight loss is pyrolysis. Figure 2 illustrates the effect of cations on the rate of pyrolysis. These data were obtained in N₂ at a furnace temperature of 973 K. During pyrolysis, the acid-washed lignite had a greater rate of weight loss and a greater total weight loss in the residence time of the reactor. It is suggested that cations catalyze secondary char forming reactions of the primary volatiles, particularly the tars (10). These cracking and/or polymerization reactions on the surface of particles reduced the initial rate of weight loss (when tar evolution was predominant) and the total yield of volatiles due to surface carbon deposition.

As shown in Figure 1, when heterogeneous combustion predominated (residence times >0.1 s) the modified coals lost weight more rapidly than the acid-washed lignites. Alkali and alkaline-earth metals are known to be excellent catalysts for the carbon-oxygen reaction (7,8). Hence, it is suggested that cations exchanged on the coal catalyzed the heterogeneous combustion of the char.

The Na and K loaded lignites underwent greater total weight loss (by about 20 wt%) than the calcium loaded lignite in the total residence time of the furnace. Isothermal reactivity data have shown that K and Na are better catalysts than Ca for the carbon-oxygen reaction (5,7). However, the low weight loss by the Ca loaded coal may be the result of a combination of two factors: catalysis of secondary reactions and catalysis of the carbon-oxygen reaction.

SUMMARY

The effect of cations on the combustion behavior of pulverized lignite can be divided into three main areas: the rate of weight loss due to pyrolysis, the total weight loss due to pyrolysis and the rate of heterogeneous char combustion. The presence of cations (Na, K, Ca) reduced the rate of pyrolysis and the total weight loss due to pyrolysis but increased the char combustion rate.

REFERENCES

1. Field, M. A., Gill, D. W., Morgan, B. B., Hawksley, P. G. W., Combustion of Pulverized Coal, The British Coal Utilization Research Association, Leatherhead, 1967.
2. Smith, I. W., Combustion and Flame, 17, 303, 1971.
3. Field, M. A., Combustion and Flame, 14, 237, 1970.
4. Jenkins, R. G., Nandi, S. P., and Walker, P. L., Jr., Fuel, 52, 288, 1973.
5. Hippo, E. J. and Walker, P. L., Jr., Fuel, 54, 245, 1975.
6. Radovic, L., Ph.D. Thesis, The Pennsylvania State University, 1982.
7. Walker, P. L., Jr., Fuel, 62, 140, 1983.
8. McKee, D. W., Fuel, 62, 170, 1983.
9. Morgan M. E., Jenkins, R. G., and Walker, P. L., Jr., Fuel, 60, 189, 1981.
10. Morgan, M. E., Ph.D. Thesis, The Pennsylvania State University, 1983.
11. Scaroni, A. W., Walker, P. L., Jr., and Essenhigh, R. H., Fuel, 60, 71, 1981.
12. Maloney, D. J., Ph.D. Thesis, The Pennsylvania State University, 1983.

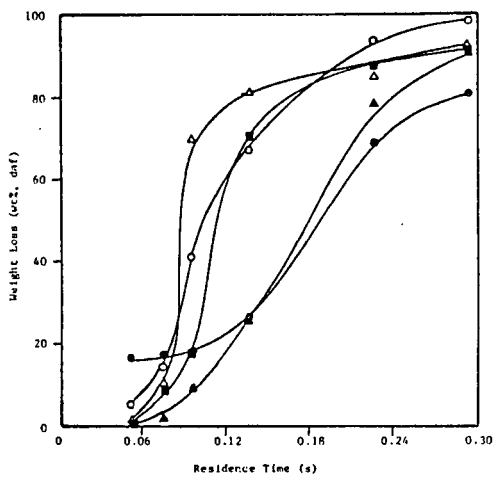


Figure 1. Effect of Cations on Combustion at a Furnace Temperature of 973 K. ■ Na; ○ K; ● Ca; ▲ Acid-washed; ▲ Raw.

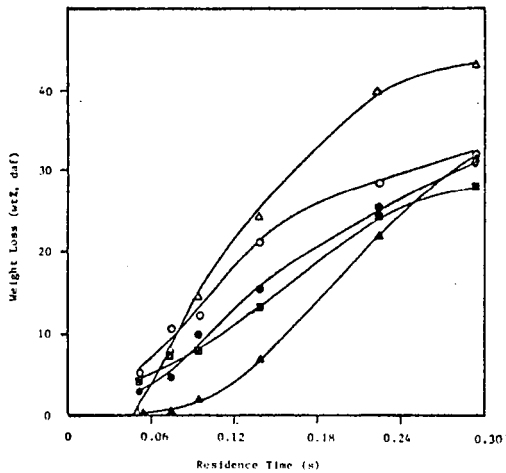


Figure 2. Effect of Cations on Pyrolysis in Nitrogen at 973 K. ■ Na; ○ K; ● Ca; ▲ Acid-washed; ▲ Raw.

CATALYSIS OF LIGNITE CHAR GASIFICATION BY EXCHANGEABLE CALCIUM AND MAGNESIUM

T. D. Hengel and P. L. Walker, Jr.

Department of Materials Science and Engineering
The Pennsylvania State University, University Park, PA 16802

INTRODUCTION

The high intrinsic reactivity of chars derived from lignite coals is primarily due to the presence of well dispersed metal oxide particles, which are formed when carboxyl groups on the lignite surface, having been exchanged with various cations from the local groundwater, decompose as the lignite is heated to gasification temperatures. Roughly half of the carboxyl groups on American lignites have undergone exchange, with Ca and Mg predominantly, and to lesser extents with other alkali and alkaline-earth cations (1). These cations have been shown to be good catalysts for lignite char gasification in air, CO₂ and steam (2).

It is noted, however, that lignite char reactivity decreases rapidly as final heat treatment temperature increases (3,4) or as soak time at temperature increases (4). Radovic and co-workers (5) have shown that the majority of this decrease can be correlated with a decrease in CaO dispersion in the case of Ca loaded demineralized (Dem) lignite chars.

Exchangeable cations play an important role in the behavior of lignite coals in coal conversion processes. It is, therefore, important that a fundamental understanding be attained, first of the possible interaction of exchangeable cations in lignites with each other, and, second, of the possible effects on the subsequent catalytic activity of the cations for lignite char gasification. The aim of this study was to develop such an understanding using the two most abundant cations in American lignites: Ca and Mg. The objective of this work was to study the effect which adding Mg, which is a poor gasification catalyst, to Ca, which is a good gasification catalyst, has on the catalytic behavior of Ca for lignite char gasification. That is, will the presence of Mg in some way affect the sintering of Ca and, hence, affect the catalytic activity of Ca?

EXPERIMENTAL

A Montana lignite (6) was subjected to essentially complete demineralization with HCl and HF in order to remove essentially all the inorganic constituents (exchangeable cations and mineral matter) present (1). The Dem lignite was then ion-exchanged with Ca or Mg using solutions of their acetate salts. Seven levels of Ca and three levels of Mg were obtained using loading solutions of varying concentrations. A sample of Dem lignite was also co-exchanged with Ca and Mg in order to study the effect of their interaction on subsequent char reactivity. Chars were prepared by slowly heating (10 K/min) the treated lignites in a box furnace equipped with an air tight retort under N₂ to final temperatures of 973 or 1273 K and held (soaked) for 1 h. Char reactivities were determined by isothermic thermogravimetric analysis (TGA) in 0.1 MPa air, 0.1 MPa CO₂ and 3.1 kPa steam (saturated N₂). The maximum slope (R_{max}) of the TGA recorder plot was used as a measure of gasification reactivity (normalized to initial weight of char, daf basis). From a series of preliminary runs (7) reaction conditions were selected in order to eliminate heat and mass transfer limitations. Therefore, reported reactivities are believed to be intrinsic, chemically controlled rates.

Selected chars were examined by x-ray diffraction (XRD) to identify Ca and Mg containing species present in the chars. Average crystallite diameters of selected species were determined using the line broadening concept and the Scherer equation (8).

RESULTS AND DISCUSSION

Figures 1 and 2 show the reactivity results in 0.1 MPa air for the 973 and 1273 K chars, respectively. As seen previously, Ca is a good catalyst for char gasification in air, while Mg is a poor char gasification catalyst (2). For Ca loaded chars at both heat treatment temperatures, it is seen that two distinct regions of reactivity behavior are present. For loadings up to ~4 wt% Ca, the reactivity increases linearly with increasing Ca content. For loadings greater than ~4 wt% Ca, however, reactivity remains essentially constant with increasing Ca content. This is contrary to the behavior seen by Hippo et al. (9), who reported a linear increase in reactivity with increasing Ca content up to 12.9 wt% in 0.1 MPa steam for a Texas lignite. Since mass transport limitations are believed to be absent, the plateau is not due to diffusional effects. This suggests that the plateau is the result of a catalyst "saturation effect," that is, adding of catalyst beyond a certain amount does not further increase the observed rate. For the relatively small range of Mg contents a similar saturation effect appears to be operating. Examination of the cation exchanged 1273 K chars by XRD revealed that CaO and MgO were the major species present in the Dem+Ca and Dem+Mg chars, respectively.

Reactivity results for the 1273 K chars reached in 0.1 MPa CO₂ and 3.1 kPa steam at 1053 K are shown in Figures 3 and 4, respectively. The same trends evident for the 1273 K chars reacted in 0.1 MPa air are also seen in these reactant gases. Two regions of reactivity behavior are present in both cases. Calcium is seen to be a good char gasification catalyst, while Mg has very little catalytic effect.

The purpose of this work was to study the effect that adding Mg to Ca has on the subsequent catalytic behavior of Ca for lignite char gasification. To study this effect, the chars of the co-exchanged Dem lignite were used. It was reasoned that the co-exchanged chars should have a Ca content which was in the region where reactivity increased with metal content, as to avoid the saturation region. Also, the char should contain more Mg than Ca on a molar basis, since an effect is more likely to be observed under these conditions. Metal contents of the co-exchanged chars are presented in Table 1.

TABLE 1
METAL CONTENTS IN THE CO-EXCHANGED CHARS (DRY BASIS)

Char	Calcium		Magnesium	
	mmol/g	wt%	mmol/g	wt%
973 K	0.54	2.2	0.91	2.2
1273 K	0.56	2.2	0.94	2.3

To determine if there was any effect, reactivity data of the mono-exchanged chars were used to calculate an expected reactivity. Calculation of these expected reactivities was straight forward, which assumed that the catalytic activities of Ca and Mg were simply additive. From the metal contents in Table 1, the contributions of Ca and Mg to the calculated reactivities could be determined from Figures 1-4 by reading the reactivity value corresponding to that amount of Ca or Mg directly from the appropriate figure. The reactivity of the Dem-char is subtracted once because it is included in both the Ca and Mg contributions, while it is included only once in the co-exchanged char. This step is not necessary when the rate of the uncatalyzed (Dem) reaction is low; but is necessary when the uncatalyzed rate is high, as is the case in CO₂ (Figure 3). For consistency, the Dem reactivity

was always subtracted once. The calculated reactivity is the sum of the Ca and Mg contributions, with the rate of the Dem reactivity subtracted once. By comparing the calculated reactivity with that actually observed for the co-exchanged chars, one will be able to tell if indeed there is an effect. The calculated and observed reactivities are given in Table 2 for the various gases.

TABLE 2
CALCULATED AND OBSERVED REACTIVITIES OF THE CO-EXCHANGED CHARS

Char	Reactivity Contributions (mg/mg h)			Reactivities (mg/mg h)	
	Ca	Mg	Dem	Calculated	Observed
			Air		
973 K	0.31	0.09	0.01	0.39	0.42
1273 K	0.34	0.22	0.03	0.53	0.60
			CO ₂		
1273 K	0.60	0.34	0.32	0.62	0.64
			Steam		
1273 K	0.30	0.10	0.05	0.35	0.31

It is quite clear from Table 2 that the addition of Mg to Ca does not have a significant effect on the subsequent activity of Ca. The observed reactivities are, within experimental error, the same as the calculated reactivities. This shows that the catalytic effects of Ca and Mg are additive and they do not interact in a significant way to either increase or decrease their combined catalytic effects. This is perhaps due to the fact that MgO is not significantly soluble in CaO below 1900 K (10). The presence of MgO does not reduce the sintering of CaO. This is supported by examination of the 1273 K co-exchanged char by XRD. The average crystallite diameter of the CaO was calculated to be 30 nm. This is the same value obtained for a 1273 K Dem+Ca char that has a similar Ca content (1.4 wt%).

CONCLUSIONS

The addition of Mg to Ca does not have a significant effect on the subsequent activity of Ca for lignite char gasification under the slow heating conditions used in this study. Their catalytic effects were found to be additive, indicating that they did not interact in any significant way. This was supported by XRD results which showed that the sintering of CaO was not reduced by the presence of MgO.

REFERENCES

1. Morgan, M. E., Jenkins, R. G. and Walker, P. L., Jr., Fuel 60, 189 (1981).
2. Walker, P. L., Jr., Matsumoto, S., Hanzawa, T., Miura, T. and Ismail, J. M. K., Fuel 62, 140 (1983).
3. Jenkins, R. G., Nandi, S. P. and Walker, P. L., Jr., Fuel 52, 288 (1973).
4. Radovic, L., "Importance of Catalysis and Carbon Active Sites in Lignite Char Gasification," Ph.D. Thesis, The Pennsylvania State University, 1982.
5. Radovic, L., Walker, P. L., Jr. and Jenkins, R. G., J. Catalysis, in press.

6. Penn State/DOE Coal Data Base, PSOC 833, Coal Research Section, The Pennsylvania State University.
7. Hengel, T., "Catalysis of Lignite Char Gasification by Exchangeable Cations: Calcium and Magnesium," M.S. Thesis, The Pennsylvania State University, 1983.
8. Klug, H. P. and Alexander, L. E., "X-ray Diffraction Procedures," 2nd Edition, Wiley, NY, 1974.
9. Hippo, E. J., Jenkins, R. G. and Walker, P. L., Jr., Fuel 58, 338 (1979).
10. Doman, R. C., Barr, J. B., McNally, R. N. and Alper, A. M., J. Amer. Cer. Soc. 46, 313 (1963).

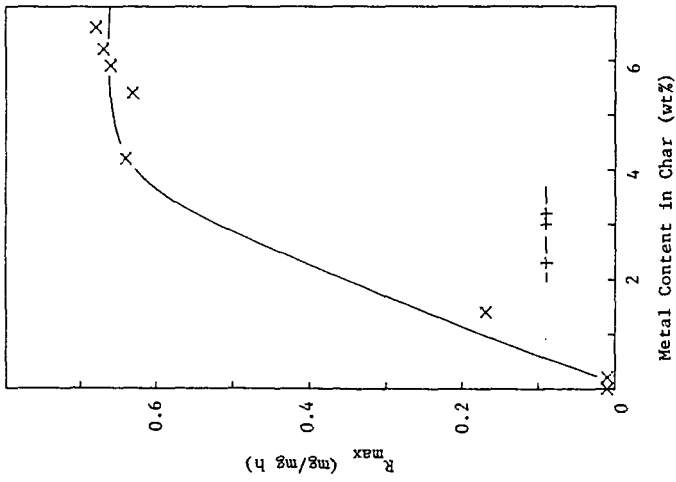


Figure 1
 Reactivities of the 973 K Chars
 in 0.1 MPa Air at 603 K.
 x Demt-Ca, + DemtHg

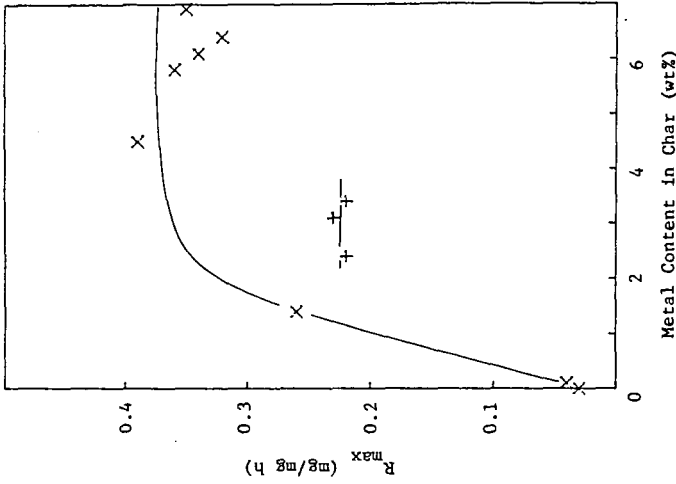


Figure 2
 Reactivities of the 1273 K Chars
 in 0.1 MPa Air at 603 K.
 x Demt-Ca, + DemtHg

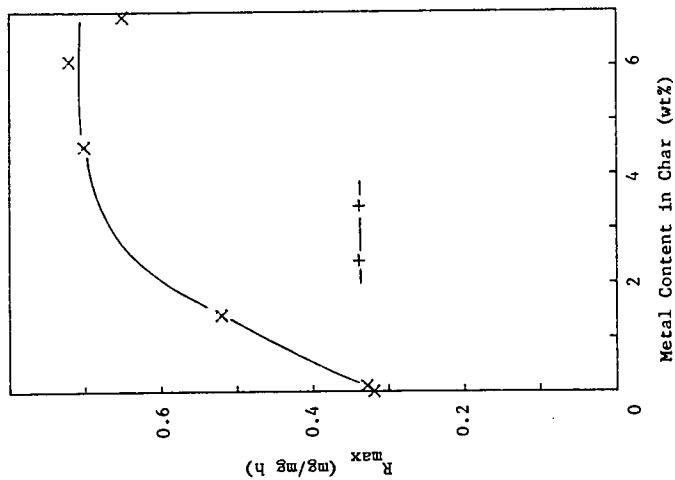


Figure 3

Reactivities of the 1273 K Chars
in 0.1 MPa CO₂ at 1053 K.
x Demt+Ca, + DemtMg

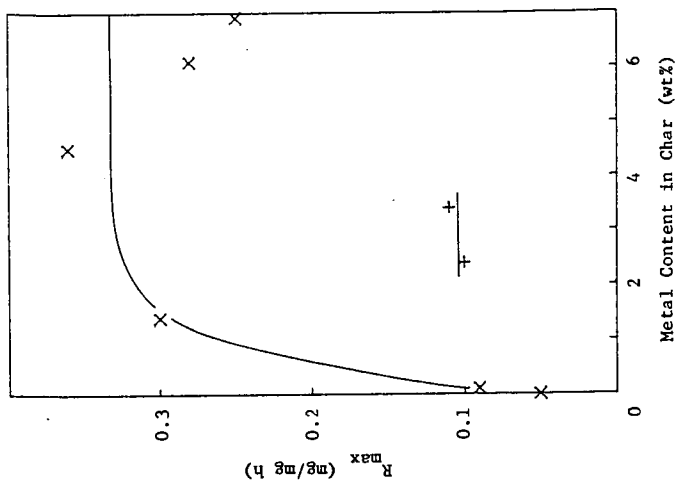


Figure 4

Reactivities of the 1273 K Chars
in 3.1 kPa Steam at 1053 K.
x Demt+Ca, + DemtMg

Measurement and Prediction of Low-Rank Coal Slag Viscosity

Robert C. Streeter,¹ Erle K. Diehl,² and Harold H. Schobert³

Bituminous Coal Research, Inc., Monroeville, PA 15146
and

Grand Forks Energy Technology Center, Grand Forks, ND 58202

INTRODUCTION

Since 1980, Bituminous Coal Research, Inc., (BCR) has been conducting measurements on the viscosity of western U. S. low-rank coal slags under a contract with the Grand Forks Energy Technology Center (GFETC), U. S. Department of Energy. This work has been motivated by the realization that 1) very few data exist in the literature on the viscosity of low-rank-coal slags; 2) published correlations relating slag viscosity to coal ash composition were derived from work with bituminous-coal slags, and attempts to apply them to data from low-rank coal slags generally have been unsuccessful; and, 3) from a practical standpoint, data on slag rheology are of considerable interest in support of the operation of a slagging fixed-bed lignite gasifier at GFETC. As a matter of related interest, BCR's slag viscometer was originally put into operation in 1976 to obtain data on the slagging properties of coals intended for use in the BI-GAS coal gasification pilot plant at Homer City, Pennsylvania; the BI-GAS process incorporates an entrained-bed, slagging gasifier.

Although the data obtained in these studies have been valuable in interpreting the slagging phenomena observed in the Grand Forks gasifier tests, a more fundamental objective of the current work is to develop correlations that can be used to predict a priori the viscosity behavior of low-rank-coal slags from a knowledge of the ash or slag composition.

EXPERIMENTAL

The slag-viscosity apparatus was assembled for BCR by Theta Industries, Inc. It includes a Lindberg furnace with global heating elements of silicon carbide, rated for operation at temperatures up to 2732 F (1500 C). The rotating bob viscometer is a Haake RV-2 Rotovisco unit with a DMK 50/500 dual measuring head, which allows adjustment of torque by a factor of 10 (i.e., ranges of 0 to 50 and 0 to 500g-cm).* The torque on the viscometer bob twists a spiral spring inside the measuring head; the angular displacement of the spring is proportional to shear stress, and is converted to an electrical signal that is plotted on an X-Y recorder as a function of the rotational speed of the bob (shear rate). A microprocessor has been incorporated into the original system to provide automatic temperature programming at the rate of about 1°F/min, and stepwise bob rotation from 0 to 64 rpm in increments of 4 rpm.

To simulate conditions existing in the slagging coal gasifier, all tests are carried out in a reducing atmosphere consisting of 20 percent hydrogen and

¹ Supervising Scientist, Bituminous Coal Research, Inc.

² Manager, Applied Research, Bituminous Coal Research, Inc.

³ Project Manager, Coal Science, Grand Forks Energy Technology Center

* Reference to a company or product name does not imply endorsement of the product to the exclusion of others that may be suitable.

80 percent nitrogen. The gas mixture is injected into the furnace at a flow rate of 500 cc/min through an alumina tube that extends to within 1 inch of the top of the sample crucible.

Although a platinum/rhodium bob was employed initially, some problems were encountered with attack on the bob by molten iron in the slag. In all of the tests discussed herein, the bob was fabricated from 1/2-inch molybdenum bar stock; the bob is approximately 1-inch long with a 30°-angle taper machined on both ends. The top of the bob terminates in a 5/8-inch long, 1/4-inch-diameter shaft which is drilled and tapped to accommodate a 1/8-inch-diameter x 16.5-inch long molybdenum stem. The bob stem is covered by a tubular alumina sleeve to minimize erosion during a test. As originally designed, the viscometer incorporated a universal joint in the measuring head shaft and a Jacobs-type chuck to hold the bob stem. However, this arrangement allowed too much lateral motion of the bob in the slag, and the bob is now attached to the measuring head by a rigid shaft containing three set screws to hold the stem. During a viscosity test, the bob is immersed until the slag just covers its top; the position of the bob can be determined accurately using a depth gauge attached to the measuring head.

In the earlier tests, the slag was melted in crucibles of vitreous carbon, 1-1/4-in. I.D. x 1-3/8-in. high (Atomegic Chemetals Co.). The carbon sample crucible was contained in a larger alumina guard crucible (1-7/8-in. I.D. x 6-in. high) and the annular space between the two crucibles was packed with 60-mesh alundum. The use of carbon crucibles was somewhat influenced by the observation that slag from the gasifier frequently contained particles of devolatilized coal (char), which might be involved in reactions with the molten slag. It soon became evident that iron oxides in the slag were being reduced by reaction with the carbon crucible, as small pools of molten iron invariably settled from the slag during the carbon-crucible tests. With certain coal ashes containing comparatively high amounts of Fe_2O_3 , destruction of the carbon crucible was so severe that the portion in contact with the slag virtually disappeared during the viscosity test. Consequently, the carbon crucibles were eventually replaced with high-purity alumina crucibles (McDaniel Refractory Co.) of the same dimensions.

Since the alumina crucibles were put into use, metallic iron has only rarely been observed in the slag; if formed at all, the iron usually tends to cling to the top of the bob at the gas/liquid interface. On the other hand, varying degrees of attack on the alumina crucible by the slag have been observed. Generally, dissolution of Al_2O_3 by the slag has been slight, but in a few cases noticeable thinning of the crucible walls has occurred. In addition, with the low-form alumina crucibles, there was a tendency for the slag to overflow the sample crucible and seep into the alundum packing. In a few cases, the slag managed to seep beneath the sample crucible, whereupon subsequent outgassing of the slag actually raised and tilted the sample crucible. To alleviate this problem, high-form (3-in. high) sample crucibles have been employed since September, 1982.

Since measured viscosities will vary depending on the dimensions of and the materials employed for the sample crucible and the rotating bob, measured values are related to absolute viscosities by means of an instrument factor. In these studies, the instrument factor was determined by tests with NBS glass viscosity standards whose viscosities are precisely defined and similar to those of the slags over the temperature range of interest. The instrument factor is related to viscosity by the equation:

$$\text{Viscosity} = \text{Instrument factor} \times \text{torque reading} \div \text{bob speed (rpm)}$$

In preparation for a slag-viscosity test, the coal is pulverized to minus-60 mesh and ashed in B&W K-3000 insulating firebrick dishes for 3 hours at 1850 F (1010 C) in a large muffle furnace. This higher-than-normal ashing temperature was chosen after preliminary work showed that sufficient volatiles remained in the ash prepared

at the standard "ASTM temperature" of 1382 F (750 C)* to cause severe frothing and foaming during the ash melting process. This difficulty is still experienced to some extent during melting of the high-temperature ash and is believed due to decomposition of residual sulfates and volatilization of alkali-metal oxides in the ash. The coal ash is sieved again at 60 mesh to remove any foreign particles of firebrick, then compressed into pellets 5/8-inch in diameter weighing about 5 grams each. The ash pellets are dropped, one or two at a time, into the previously heated sample crucible through a long quartz tube; a typical coal-ash charge in the high-form alumina crucibles is about 60 to 70 grams.

Viscosity measurements are normally commenced at the highest temperature at which an on-scale reading can be obtained with a bob speed of 64 rpm. The temperature is then decreased slowly (under microprocessor control) and viscosity measurements are taken at approximately half-hour intervals. This "cooling cycle" is continued until the upper limit of the measuring head is approached (typically about 3000 poises**), then the slag is gradually reheated to observe changes in viscosity during a "heating cycle."

Following each test, samples of the solidified slag and high-temperature ash are submitted to GFETC for compositional analyses by X-ray fluorescence and X-ray diffraction techniques. A Kevex Model 0700 energy dispersive X-ray spectrometer is employed for X-ray fluorescence analysis. Samples are ground to minus 60-mesh and pressed into a pellet using either cellulose or lithium tetraborate as a binder. The instrument is calibrated using mixtures of reagent-grade oxides, blended to approximate the relative amounts present in the slag. X-ray diffraction measurements are conducted on minus 325-mesh samples using a Philips 3600 automated X-ray diffractometer. Compound identification is accomplished with the aid of a computer-based index file.

The selection of low-rank coals for these studies was based to some extent on those which had actually been tested or were candidate feedstocks for the GFETC lignite gasifier; in addition, an effort was made to choose samples that would represent a wide range of ash compositions and diverse geographical locations. The coals selected for these viscosity studies are listed in Table 1.‡

RESULTS AND DISCUSSION

Viscosity can be defined as the resistance to flow offered by a fluid and is customarily expressed as the ratio of shear stress to shear rate. The most commonly encountered regime of viscous flow is termed "Newtonian" flow, in which shear stress is a linear function of shear rate (i.e., viscosity is constant at any given shear rate). For Newtonian substances, the dependence of viscosity (η) on

* ASTM Method D 3174-73, "Ash in the Analysis Sample of Coal and Coke."

**Throughout this paper, viscosities are given in the more familiar units of poises; the accepted SI unit for viscosity is the Pascal-second, and the conversion is poises x 0.1 = Pa·sec.

‡ In view of the considerable within-seam or within-mine variability of low rank coals, it should be understood that these coal samples are not necessarily representative of the total production of a particular mine.

temperature (T) is exponential, such that a plot of $\log \eta$ vs. T yields a straight line.* Three other regimes of non-Newtonian behavior are less commonly encountered:

1. Pseudoplastic - viscosity decreases with increasing shear rates.
2. Plastic - viscosity decreases with increasing shear rates following the appearance of an initial yield stress.

TABLE 1. SAMPLES SELECTED FOR LOW-RANK COAL VISCOSITY STUDIES

Sample	Rank	Location (State)
1. Indian Head.	Lignite	North Dakota
2. Gascoyne	Lignite	North Dakota
3. Baukol-Noonan	Lignite	North Dakota
4. Beulah	Lignite	North Dakota
5. Colstrip	Sub-bituminous	Montana
6. Decker	Sub-bituminous	Montana
7. Sarpy Creek	Sub-bituminous	Montana
8. Naughton	Sub-bituminous	Montana
9. Big Horn	Sub-bituminous	Wyoming
10. Kemmerer	Sub-bituminous	Wyoming
11. Black Butte	Sub-bituminous	Wyoming
12. Emery	Bituminous (low rank)	Colorado
13. Rockdale	Lignite	Texas
14. Martin Lake	Lignite	Texas
15. Big Brown	Lignite	Texas
16. Atlantic Richfield	Lignite	Texas
17. Burns & McDonnell	Lignite	Alabama

3. Thixotropic - viscosity decreases with increasing shear rates and with the duration of the applied shear stress.

In each of these cases, the viscosity varies with shear rate and/or with the period of shear, and the ratio of shear stress to shear rate is customarily designated as "apparent viscosity."

Plots of $\log \eta$ vs. T ($^{\circ}$ F) for three representative low-rank coal slags are shown in Figure 1. Curve A for the Black Butte sample illustrates the behavior of a

* From purely physico-chemical considerations, $\log \eta$ is proportional to $1/T$ where T is in $^{\circ}$ K. In practice, however, it is often more convenient to plot $\log \eta$ directly vs. temperature in $^{\circ}$ C, or (as in these studies where engineering conventions were employed in the design and operation of the coal gasifier) in $^{\circ}$ F.

glassy, siliceous-type slag that exhibits Newtonian properties over a wide temperature range. In addition, the viscosity behavior is reversible in that viscosities measured during reheating of the slag (solid circles) are essentially the same as those determined during the cooling cycle. The type of behavior represented by Curves B and C is more commonly observed for low-rank coal slags; $\log \eta$ is a linear function of temperature down to some point, designated as the temperature of critical viscosity, T_{cv} (as shown for Curve B). Below T_{cv} , the viscosity can increase quite abruptly (Curve B), or the increase may be somewhat more gradual (Curve C). Moreover, a "hysteresis" effect appears in the viscosity/temperature curve as the slag is reheated. This phenomenon is supposedly related to the slow redissolution of crystals, formed on cooling the slag below T_{cv} . (1) In theory, the viscosity of the slag on reheating should eventually return to the linear portion of the curve representing the fully liquid condition. However, as shown by Figure 1, this is not necessarily achieved experimentally, and the extent of the deviation is believed to be due to small compositional changes occurring in the melt during the viscosity determination (to be discussed later). Curve C in Figure 1 includes data points for two separate viscosity tests with Baukol-Noonan, approximately 6 months apart. As shown, the repeatability for the cooling curve is quite good; on the other hand, there is a marked difference in the two curves obtained on reheating the slags, and subsequent analytical data showed subtle differences in the compositions of the slags from the two tests.

The straight-line portion of the viscosity/temperature curve is traditionally designated as the "Newtonian" region of slag behavior, while the area below T_{cv} , where solid species are crystallizing from the melt, is designated as the "plastic" region. Strictly speaking, a slag can retain Newtonian properties below T_{cv} , and transition to a non-Newtonian state can be detected only by a change in the shape of the shear-stress vs. shear-rate curve. As a matter of fact, most of the slags included in this study actually did show pseudoplastic or thixotropic behavior at the higher viscosities.

Of the 17 coals listed in Table 1, 13 were tested in carbon crucibles and the remaining four were tested using alumina crucibles. In addition, the carbon-crucible test with Baukol-Noonan was repeated, and six of the coals from the carbon-crucible tests (Big Horn, Decker, Emery, Colstrip, Rockdale, and Burns & McDonnell) were also selected for alumina-crucible tests. Thus, a total of 24 slag-viscosity tests provided the data discussed in this paper.

The compositions of the slags from these viscosity tests are listed in Table 2 (compositional data are normalized to 100 percent). Also included are several other parameters that traditionally have been employed to characterize coal-ash slags. It should be emphasized that, unless otherwise noted, all calculations discussed herein were based on slag composition data (as opposed to ash composition data). This was done primarily for two reasons:

1) As previously noted, reactions with the sample crucible tended to result in depletion of Fe_2O_3 (carbon-crucible tests) and/or enrichment in Al_2O_3 (alumina-crucible tests), so that in some cases the composition of the slag was significantly different from that of the original coal ash. This effect can be seen by comparing the slag composition data in Table 2 for the carbon- and alumina-crucible tests with Colstrip, Decker, Big Horn, Emery, Rockdale, and Burns & McDonnell.

2) Results of an independent study, comparing high-temperature ash and slag compositions for 18 of the 24 viscosity tests, showed that from 80 to 100 percent of the SO_3 and usually all of the P_2O_5 (if present in the ash) were volatilized during melting of the ash. Admittedly, P_2O_5 is a minor constituent, and losses of SO_3 could be compensated for by normalizing the analytical data to a sulfur-free basis. On the other hand, in 11 out of 15 instances (73 percent) where Na_2O was present in the high-temperature ash, it was volatilized in amounts ranging from 10 to 50 percent of the amount available in the ash. Since the Na_2O content of some ashes

TABLE 2. ANALYSIS OF LOW-RANK-COAL SLAGS PRODUCED IN SLAG VISCOSITY TESTS

Carbon Crucible Tests:	Slag Composition, Weight Percent											Base/Acid Ratio		Lignite Factor (3)
	SiO ₂	Al ₂ O ₃	Fe ₂ O ₃	TiO ₂	P ₂ O ₅	CaO	MgO	Na ₂ O	K ₂ O	SO ₃	(1)	(2)	SiO ₂ /Al ₂ O ₃ Ratio	
Sample	42.4	14.8	3.1	1.4	0.0	25.7	8.2	3.7	0.1	0.2	0.70	53.4	2.86	10.9
Gascoyne	42.4	14.8	3.1	1.4	0.0	25.7	8.2	3.7	0.1	0.2	0.70	53.4	2.86	10.9
BaukoI-Noonan 1	41.4	19.2	1.0	2.3	0.0	21.8	4.3	7.7	0.6	1.2	0.56	60.4	2.16	26.1
BaukoI-Noonan 2	39.3	19.7	4.5	1.7	0.0	18.3	4.4	9.9	0.6	1.1	0.62	59.1	1.99	5.0
CoIstrip	45.0	23.9	2.1	1.8	0.0	20.6	5.9	0.1	0.1	0.4	0.41	61.1	1.88	12.6
Decker	38.4	20.0	6.5	2.1	0.0	18.7	4.2	8.6	0.3	0.9	0.63	56.6	1.92	3.5
Sarpy Creek	44.2	27.4	1.9	1.1	0.0	18.3	4.0	1.2	1.2	0.3	0.37	64.6	1.61	11.7
Naughton	63.5	17.8	5.5	0.8	0.2	6.7	3.6	0.0	1.6	0.1	0.21	80.1	3.57	1.9
Big Horn	27.1	28.6	11.4	1.5	0.7	16.3	6.9	5.0	0.5	1.8	0.70	43.9	0.95	2.0
Kemmerer	59.6	13.3	0.9	0.9	0.0	15.5	7.7	0.8	0.6	0.1	0.35	71.2	4.48	25.8
Black Butte	53.9	18.3	6.0	1.3	0.0	11.7	4.2	4.0	0.3	0.0	0.36	71.1	2.94	2.6
Emery	40.2	21.4	9.1	1.1	0.1	16.9	5.5	2.9	0.2	2.0	0.55	56.1	1.88	2.5
Rockdale	42.9	24.0	2.4	2.0	0.0	23.8	3.9	0.0	0.5	0.3	0.44	58.8	1.79	11.5
Atlantic Richfield	40.6	15.8	2.7	2.0	0.1	29.4	6.7	2.0	0.3	0.2	0.70	51.1	2.57	13.4
Burns&McDonnell	47.0	26.1	12.7	0.8	0.0	6.6	3.7	0.0	2.2	0.5	0.34	67.1	1.80	0.8

TABLE 2. ANALYSIS OF LOW-RANK-COAL SLAGS PRODUCED IN SLAG VISCOSITY TESTS (Continued)

Alumina Crucible Tests:	Slag Composition, Weight Percent										Base/Acid Ratio (1)	Silica Ratio (2)	SiO ₂ /Al ₂ O ₃ Ratio	Lignite Factor (3)
	Sample													
	SiO ₂	Al ₂ O ₃	Fe ₂ O ₃	TiO ₂	P ₂ O ₅	CaO	MgO	Na ₂ O	K ₂ O	SO ₃				
Indian Head	20.0	36.7	12.5	0.6	0.0	17.0	7.1	5.4	0.1	0.0	0.73	35.3	0.54	1.9
Beulah (high sodium)	24.2	33.6	14.0	0.9	0.0	14.4	4.3	8.1	0.2	0.3	0.70	42.5	0.72	1.3
Colstrip	38.0	28.1	11.2	1.5	0.0	17.1	3.9	0.0	0.1	0.0	0.48	54.1	1.35	1.9
Decker	36.1	23.0	8.8	2.1	0.0	18.2	3.8	7.5	0.2	0.0	0.63	54.0	1.57	2.5
Big Horn	30.2	24.7	13.6	1.8	0.8	18.1	5.5	4.5	0.5	0.1	0.74	44.8	1.22	1.7
Emery	44.2	24.7	7.4	1.4	0.0	15.1	4.1	2.6	0.2	0.0	0.42	62.4	1.79	2.6
Rockdale	38.5	27.5	8.9	1.7	0.0	20.0	2.7	0.0	0.4	0.0	0.47	54.9	1.40	2.6
Martin Lake	39.0	22.4	11.6	1.1	0.0	22.4	2.5	0.0	1.0	0.1	0.60	51.6	1.74	2.1
Big Brown	(analytical data for slag not yet available)													
Burns&McDonnell	45.7	23.1	18.9	0.8	0.0	6.0	2.8	0.0	2.0	0.2	0.43	62.3	1.98	0.5

(1) Base/Acid Ratio = $(\text{Fe}_2\text{O}_3 + \text{CaO} + \text{MgO} + \text{Na}_2\text{O} + \text{K}_2\text{O}) / (\text{SiO}_2 + \text{Al}_2\text{O}_3 + \text{TiO}_2)$ (Ref. 2)

(2) Silica Ratio = $100 \text{ SiO}_2 / (\text{SiO}_2 + \text{Fe}_2\text{O}_3 + \text{CaO} + \text{MgO})$ where "Fe₂O₃" = $(\text{Fe}_2\text{O}_3 + 1.11 \text{ FeO} + 1.43 \text{ Fe})$ (Ref. 3)

(3) Lignite Factor = $(\text{CaO} + \text{MgO}) / \text{Fe}_2\text{O}_3$ (Ref. 2). Theoretically, $\frac{1}{2}(\text{CaO} + \text{MgO} + \text{Fe}_2\text{O}_3)$ must be greater than 20% and the lignite factor must be greater than 1.0 for the ash (slag) to be considered a low-rank-coal type; the Burns&McDonnell sample is an obvious exception to this rule.

ranged up to 10 percent, it is probable that volatilization of this constituent would have an effect on the slag viscosity.

The data in Table 2 illustrate the wide variability in concentrations of low-rank-coal slag constituents. This variability is reflected further by Table 3, where the ranges in slag compositions encountered during these studies (Table 2) are compared with the ash composition of an "average" bituminous coal (SO₃-free basis).(4) Especially noteworthy are the higher concentrations of alkaline-earth and alkali metal oxides in the low-rank coal slags.

The experimental viscosity data from these studies are summarized in Table 4. The two viscosity values shown for each sample, corresponding to specific melt temperatures, are sufficient to approximate the linear ("Newtonian") portion of the log η vs. T curve obtained during the cooling cycle. In addition, values for T_c (when observable) and ash fusibility (reducing atmosphere) for the high-temperature ash (HTA) are included for comparison.

Slag Viscosity/Composition Correlations

Several attempts have been made in the past to define the linear portion of the viscosity/temperature curve based on the composition of the coal ash. In the mid-1960's, workers at the British Coal Utilization Research Association (BCURA) developed two such correlations based on work with British (bituminous) coals, now generally referred to as the Watt-Fereday(5) and "S²ⁿ(3) correlations.* The Watt-Fereday correlation is based on results of 276 determinations of slag viscosity using 113 different ash compositions prepared by blending British coal ashes. Unfortunately, attempts to apply this correlation to low-rank coal slags, using either ash- or slag-composition data, have been generally unsuccessful. This is illustrated by Figure 2, in which the viscosity/temperature cooling curves for two Texas lignites, Big Brown and Martin Lake, are plotted. The corresponding Watt-Fereday correlation lines are based on the (750 C ASTM) ash-composition data. As indicated by Figure 2, the ash compositions and ash fusion temperatures of these two coals are very similar. However, the viscosity predicted by the Watt-Fereday correlation for Big Brown was higher than that observed experimentally, while for Martin Lake the Watt-Fereday equation under-predicted the actual viscosity.

Among the possible reasons why these predictive equations fail for low-rank coals are the following:

1. Ash constituents may fall outside the range of those in most bituminous coals (Table 3).
2. The BCURA predictive equations are based on ash analyses. As discussed earlier, significant losses of certain elements may occur as the ash from low-rank coals is heated to the melting point.
3. Sulfur retention is more prevalent in low-rank coal ashes, due to the generally higher calcium contents. Some of the slags from these viscosity studies retained up to 2 percent SO₃ (Table 2), even after being heated above 2600 F (1427 C).
4. In lignites, some 30 to 50 percent of the ash-forming constituents can consist of cations attached to the organic matter in ion-exchangeable form on carboxyl groups or as chelate complexes, rather than being present as distinct mineralogical species.(6)

* Details of the viscosity/composition correlations are presented in Appendix 1.

TABLE 3. COMPARISON OF "AVERAGE" BITUMINOUS COAL
ASH COMPOSITION WITH LOW-RANK-COAL SLAG COMPOSITIONS

Constituent	Range in Low-Rank-Coal Slags from Viscosity Studies, Wt. Percent*	"Average" Bituminous Coal Ash (SO ₃ -free), Wt. Percent
SiO ₂	20.0 - 63.5	48.1
Al ₂ O ₃	13.3 - 36.7	24.9
Fe ₂ O ₃	0.9 - 18.9	14.9
TiO ₂	0.6 - 2.3	1.1
CaO	6.0 - 29.4	6.6
MgO	2.5 - 8.2	1.7
Na ₂ O	0.0 - 9.9	1.2
K ₂ O	0.1 - 2.0	1.5

* From data in Table 2.

TABLE 4. EXPERIMENTAL DATA FROM LOW-RANK-COAL SLAG VISCOSITY STUDIES

Carbon Crucible Tests: Sample	Temperature Range of Viscosity Measurements (Melt Temp., °F)	η, Poises	Measured Viscosity at Indicated Temperature T, °F	T _{cv} , °F (Approx.)	HTA Fusion Temperatures, °F	
					Initial Deformation 2000	Softening (Spherical) 2080
Gascoyne	2510 - 2145	25 102	2458 2237	2180	2000	2120
Baukol-Noonan 1	2480 - 2090	41 482	2480 2133	2125	2000	2040
Baukol-Noonan 2	2340 - 2100	93 548	2343 2128	2125	2000	2040
Colstrip	2560 - 2320	39 102	2557 2463	2450	2100	2180
Decker	2350 - 2110	50 289	2346 2147	2145	2020	2060
Sarpy Creek	2700 - 2460	56 220	2697 2491	2490	2000	2080
Naughton	2730 - 2550	979 3375	2731 2553	none	2100	2200
Big Horn	2490 - 2225	93 325	2407 2272	2270	2060	2100
Kemmerer	2640 - 2340	88 589	2637 2413	2375*	2100	2160
Black Butte	2690 - 2290	140 3375	2688 2294	none	2080	2120
Emery	2620 - 2270	98 422	2548 2354	2325*	2060	2120
Rockdale	2680 - 2440	26 105	2681 2481	2475	2080	2160
Atlantic Richfield	2400 - 2125	27 172	2396 2183	2175	2040	2100
Burns & McDonnell	2690 - 2370	94 272	2690 2535	2500*	2000	2080

TABLE 4. EXPERIMENTAL DATA FROM LOW-RANK-COAL SLAG VISCOSITY STUDIES (Continued)

Alumina Crucible Tests: Sample	Temperature Range of Viscosity Measurements (Melt Temp., °F)	Measured Viscosity at Indicated Temperature η , poises	T, °F	T _{cv} , °F (Approx.)	HTA Fusion Temperatures, °F	
					Initial Deformation	Softening (Spherical) Fluid
Indian Head	2650 - 2350	48 82	2594 2508	2500*	2100	2200
Beulah (high sodium)	2640 - 2270	38 340	2597 2380	2330*	2060	2140
Coilstrip	2650 - 2360	18 34	2653 2520	2470*	2100	2180
Decker	2290 - 2090	69 237	2286 2146	2145	2020	2060
Big Horn	2390 - 2110	90 289	2331 2177	2175	2060	2100
Emery	2560 - 2280	53 114	2564 2441	2420	2060	2120
Rockdale	2620 - 2440	25 36	2617 2553	2525	2080	2160
Martin Lake	2680 - 2260	43 635	2679 2322	2320	2100	2140
Big Brown	2530 - 2300	24 59	2530 2385	2350	2080	2120
Burns & McDonnell	2700 - 2150	40 242	2698 2402	2300*	2000	2080

*T_{cv} not well defined.

The Watt-Fereday equation is approximately a linear equation of the form

$$\log \eta = m \cdot f(T) + c \quad (1)$$

where m is normally positive and c is negative. Revised values for the slope (m') and intercept (c') can be calculated based on the experimental data for the low-rank coals to obtain a good fit to the Watt-Fereday equation. However, for 20 of 23 tests (87 percent) the value of m' was larger than that predicted by the conventional Watt-Fereday equation; similarly, absolute values of c' were also larger for 16 of 23 tests (70 percent). Since the intercept is negative, these two effects should tend to offset each other, resulting in little change in the value of $\log \eta$. In reality, the net result tended to be a larger value for $\log \eta$, such that observed viscosities were higher than predicted viscosities in 18 of the 23 tests (78 percent). Thus, these studies indicate that the viscosities of low-rank coal slags are generally higher than those of slags derived from bituminous coals.

Attempts were made to correlate the experimental values of m' and c' with slag composition data (Table 2) using multiple linear regression analysis. These attempts were generally unsuccessful, although for the carbon-crucible tests, the correlation of m' with Na_2O content was significant at the 99.5 percent confidence level, and for the alumina-crucible tests, Na_2O was ranked second in correlations for both m' and c' (even though not statistically significant). These findings suggest that the role of Na_2O in low-rank-coal slags may be more important than previously realized.

Other combinations of variables, including those listed in Table 2, were employed in efforts to derive empirical correlations with slag viscosity, but again without much success. In addition, the BCURA S^2 correlation(3) and a modified form of the Watt-Fereday correlation developed at the National Bureau of Standards(7) were tested. Of the 23 viscosity tests for which slag composition data are available, the NBS correlation gave a good fit to the experimental data in only two cases, while the S^2 correlation applied in only one case. Generally, the NBS and S^2 calculations gave higher viscosities than those predicted from the conventional Watt-Fereday treatment; the S^2 values were larger for 22 (96 percent) of the 23 tests, and the NBS values were larger for 19 (83 percent) of the tests. On the other hand, all three correlations had a tendency to underestimate the slag viscosity, as observed viscosities were greater than those estimated by any of the three predictive methods in 14 (61 percent) of the tests. Consequently, we conclude that the BCURA methods (or the NBS modification thereof) are generally unsatisfactory for estimating the viscosities of low-rank coal slags.

More recently, two correlations have appeared in the literature that were developed in France in studies with metallurgical (steel making) slags: the IRSID correlation, published by Riboud et al.,(8) and the Urbain correlation.(9) These two correlations are conceptually more appealing because:

• Unlike the BCURA correlations, which are based on the Arrhenius form of the viscosity equation

$$\eta = A \exp(\bar{E}/RT), \quad (2)$$

the IRSID and Urbain correlations are based on the Frenkel relation

$$\eta = AT \exp(B/T) \quad (3)$$

which, according to the authors, is the preferred form.

• All slag constituents are included, rather than just the five major oxides.

• Slag constituents are expressed as mole fractions instead of weight percentages.

• The Urbain correlation is based on the $\text{SiO}_2\text{-Al}_2\text{O}_3\text{-CaO}$ pseudo ternary phase diagram, and these three constituents usually predominate in low-rank coal slags.

However, there is a slight complication in that these correlations assume the oxidation state of iron in the slag is known. Since this information is not currently available for the low-rank-coal slags, and because all tests were in a reducing atmosphere, for computational purposes it was tentatively assumed that all iron was in the form of FeO .*

On this basis, the IRSID correlation gave a reasonably good fit to the experimental data (within 20 percent) for three of the 23 viscosity tests. Unlike the BCURA correlations, which tended to give consistently low results, the error in the IRSID correlation tended to be random; predicted viscosities were too high in 11 cases and too low in nine cases.

The Urbain correlation was acceptable for six tests, too high in seven instances, and too low in 10 instances. Furthermore, even though the Urbain correlation was unsatisfactory for 17 tests, compared with the IRSID correlation, the predicted viscosities were closer to the actual values in 10 instances. Of all the correlations tested (including the BCURA correlations), the Urbain correlation was judged to give the closest agreement to the actual viscosities in seven of the 23 tests; among the remaining 16 tests, the Urbain correlation was judged second-best for nine.

Since the Urbain method appeared to give a fair-to-good correlation for nearly two-thirds of the viscosity tests, efforts were directed toward modifying this procedure with the goal of optimizing the fit to the experimental data. The logarithmic form of the Urbain equation is

$$\ln \eta = \ln A + \ln T + 10^3 B/T \quad (T \text{ in } ^\circ\text{K}) \quad (4)$$

where B is a parameter defined by the composition of the slag and A is a function of B. The equation can be "forced" to fit the experimental data by adding a fourth term

$$\ln \eta = \ln A + \ln T + 10^3 B/T + \Delta \quad (5)$$

where Δ is the difference (either positive or negative) between the actual and computed (by equation 4) values of $\ln \eta$. Since $\ln \eta$ is a linear function of temperature above T_{CV} , Δ will also be a linear function of temperature:

$$\Delta = mT (^\circ\text{K}) + b \quad (6)$$

Thus, for each slag, values for m and b can be derived from the experimental viscosity data which uniquely define the linear portion of the viscosity/temperature curve by means of equation 5. The process then becomes one of correlating the variables m and b with some particular property of the slag.

It was found that, to a first approximation, b could be correlated with m by means of the expression

$$b = -1.6870(10^3 m) + 0.2343 \quad (7)$$

* Some very limited data from Mössbauer spectroscopy analysis indicate the presence of ferrous silicate phases in the slags. In cases where metallic iron was formed as a separate phase, it was normally removed before the slag sample was subjected to X-ray analysis.

with a correlation coefficient $R = -0.988$ for all 23 viscosity tests. The process was then reduced to finding a correlation for the variable m . Unfortunately, however, although a number of such correlations were attempted based on individual slag constituents and combinations thereof, no single correlation was found that satisfied the data from all the viscosity tests.

As a further refinement, the slags were subdivided into three groups based on the magnitude of the parameter B in the Urbain equation (equation 4). The magnitude of this parameter is related to the location of the slag composition in the $\text{SiO}_2\text{-Al}_2\text{O}_3\text{-CaO}$ ternary phase diagram, and it is proportional to the silica content of the slag. Thus, with certain borderline cases, the three subgroups correspond roughly to "high-silica," "intermediate-silica," and "low-silica" slags.

The "high-silica" group included the five tests with Naughton, Burns & McDonnell, Black Butte, and Kemmerer ($B > 28$), and a fair correlation ($R = -0.971$) was found for m of the form

$$10^3 m = -1.7264F + 8.4404 \quad (8)$$

where $F = \text{SiO}_2 / (\text{CaO} + \text{MgO} + \text{Na}_2\text{O} + \text{K}_2\text{O})$ and slag components are in mole fractions. With this correlation, calculated viscosities were within 10 percent (very good) of actual viscosities for one test, within 30 percent (acceptable) for two other tests, and within 60 percent (marginally acceptable) for the 4th of five tests. Similarly, for the "intermediate-silica" slags (Colstrip, Rockdale, Emery, Sarpy Creek, and Martin Lake; $B = 24$ to 28), an expression similar to equation 8 was found. In this case, however, the correlating variable (F) appeared to be the product of the Urbain parameter B times the sum of the mole fractions of Al_2O_3 and FeO . For the eight viscosity tests in this group, the modified correlation was very good for two, acceptable for two others, and marginally acceptable for two more. For the "low-silica" slags (Gascoyne, Baukol-Noonan, Indian Head, Big Horn, Decker, Atlantic Richfield, and Beulah; $B < 24$), the correlating variable chosen was $\text{CaO} / (\text{CaO} + \text{MgO} + \text{Na}_2\text{O} + \text{K}_2\text{O})$ (mole fractions), although the correlation was less satisfactory, being very good for two tests, acceptable for two others, and marginally acceptable for two more, out of 10 tests. The equations developed for the modified Urbain correlations are summarized below, and viscosities calculated using the various correlations are compared with measured viscosities in Table 5.

High-Silica Slags:

$$b = -1.7137(10^3 m) + 0.0509 \quad (R = -0.990 \text{ for } 5 \text{ of } 5 \text{ data points})$$

$$10^3 m = -1.7264F + 8.4404 \quad (R = -0.971 \text{ for } 5 \text{ of } 5 \text{ data points})$$

where $F = \text{SiO}_2 / (\text{CaO} + \text{MgO} + \text{Na}_2\text{O} + \text{K}_2\text{O})$, mole fractions.

Intermediate-Silica Slags:

$$b = -2.0356(10^3 m) + 1.1094 \quad (R = -0.998 \text{ for } 7 \text{ of } 8 \text{ data points})$$

$$10^3 m = -1.3101F' + 9.9279 \quad (R = -0.982 \text{ for } 5 \text{ of } 8 \text{ data points})$$

where $F' = B(\text{eqn. 4}) \times (\text{Al}_2\text{O}_3 + \text{FeO})$

TABLE 5. OBSERVED AND CALCULATED VISCOSITIES FOR LOW-RANK-COAL SLAGS

Sample	Temp., °F	Observed Viscosity, poises	Viscosity, Modified		Conventional		Calculated		From Predictive		Correlations	
			Urban	Urban	Urban	Urban	IRSID	Watt- Fereday	Watt- Fereday	NBS-Modified	BCJRA	
Gascoyne	2458	25	25	33	31	20	44	44				
	2237	102	105	93	103	80	157	157				
Baukol-Noonan 1	2480	41	40	48	56	54	101	101				
	2133	482	524	296	500	822	1523	1523				
Baukol-Noonan 2	2343	93	273	83	91	119	197	197				
	2128	548	2276	269	371	738	1220	1220				
Colstrip	2557	39	117	80	133	37	67	67				
	2463	102	233	128	242	64	118	118				
Decker	2346	50	158	78	94	84	134	134				
	2147	289	911	228	346	414	651	651				
Sarpy Creek	2697	56	45	60	83	27	43	43				
	2491	220	177	169	318	86	144	144				
Naughton	2731	979	611	667	264	262	180	180				
	2553	3375	2018	2110	777	817	587	587				
Big Horn	2407	93	130	44	67	10	22	22				
	2272	325	477	85	172	22	48	48				
Kemmerer	2637	88	118	121	98	116	149	149				
	2413	589	753	415	341	514	649	649				
Black Butte	2688	140	94	109	90	94	91	91				
	2294	3375	2385	1059	1023	1494	1544	1544				
Emery	2548	98	44	42	61	24	37	37				
	2354	422	157	107	201	74	113	113				
Rockdale	2681	26	41	38	55	16	29	29				
	2481	105	165	97	185	44	82	82				
Atlantic Richfield	2396	27	12	42	47	20	46	46				
	2183	172	28	120	163	82	165	165				
Burns & McDonnell	2690	94	105	119	160	54	47	47				
	2535	272	304	272	448	129	118	118				

TABLE 5. OBSERVED AND CALCULATED VISCOSITIES FOR LOW-RANK-COAL SLAGS (Continued)

Alumina Crucible Tests: Sample	Temp., °F	Observed Viscosity, poises	Viscosity (poises) Calculated from Predictive Correlations		IRSID	Watt- Fereday		NBS-Modified BCURA	
			Modified Urban	Conventional Urban		Fereday	Watt-Fereday	S2	S2
Indian Head	2594	48	24	21	19	2	5	4	4
	2508	82	52	30	34	3	7	6	6
Beulah (high sodium)	2597	38	31	24	24	5	8	7	7
	2380	340	249	65	103	13	25	24	24
Colstrip	2653	18	16	43	70	12	18	15	15
	2520	34	30	80	166	23	35	32	32
Decker	2286	69	214	124	180	91	145	143	143
	2146	237	690	273	488	283	451	399	399
Big Horn	2331	90	101	67	91	17	31	41	41
	2177	289	344	150	268	48	81	124	124
Emery	2564	53	66	96	138	51	68	68	68
	2441	114	145	183	309	107	146	142	142
Rockdale	2617	25	24	50	87	16	24	20	20
	2553	36	34	68	131	21	33	29	29
Martin Lake	2679	43	16	27	31	9	13	10	10
	2322	635	135	148	274	54	77	87	87
Burns & McDonnell	2698	40	73	82	97	38	28	32	32
	2402	242	491	401	670	202	156	178	178

Low-Silica Slags:

$$b = -1.8244(10^3m) + 0.9416 \quad (R = -0.999 \text{ for } 6 \text{ of } 10 \text{ data points})$$

$$10^3m = -55.3649F'' + 37.9186 \quad (R = -0.970 \text{ for } 7 \text{ of } 10 \text{ data points})$$

where $F'' = \text{CaO}/(\text{CaO} + \text{MgO} + \text{Na}_2\text{O} + \text{K}_2\text{O})$, mole fractions.

The nature of the "F" terms in the modified Urbain correlations is of interest. Urbain categorizes the constituents of silicate melts as "glass formers" (SiO_2 , P_2O_5), "modifiers" (CaO , MgO , Na_2O , K_2O) and "amphoterics" (Al_2O_3 , Fe_2O_3) which can act either as glass formers or modifiers. The correlating term for high-silica slags is the ratio of SiO_2 to modifiers, suggesting that, for these slags, the silica content of the slag is the dominating factor. On the other hand, for low-silica slags the correlating term is the ratio of CaO to modifiers, which implies that the amount of the CaO relative to total modifiers in the slag is a critical factor. For intermediate-silica slags, the correlating term involves the "amphoterics," suggesting that the role of these constituents becomes more important when the nature of the slag cannot be well defined by its silica content.

SUMMARY AND FUTURE WORK

Data from 23 low-rank coal slag viscosity determinations have been employed in attempts to correlate the linear portion of the log viscosity vs. temperature curve with five published empirical correlations for silicate slags. Of these five correlations, one developed by Urbain for metallurgical slags appeared to give a reasonable fit to the experimental data for nearly two-thirds of the viscosity tests. When the slags were subdivided into three groups, based on a parameter of the Urbain equation that is roughly proportional to silica content, it was possible to derive modified forms of the Urbain equation that gave acceptable correlations (within 30 percent) for 11 of the viscosity tests. Of the remaining 12 tests, the modified correlations were marginally acceptable (within 60 percent) in five cases.

Efforts are still being made to refine these empirical correlations and, in particular, to understand the reasons why certain slags fail to fit the correlations. The ultimate objective is to interpret slag rheological behavior in terms of specific phases present in the slag, to the extent that such phases can be identified and quantified.

ACKNOWLEDGMENTS

This work was conducted with the sponsorship of the U. S. Department of Energy under Contract No. DE-AC18-80FC10159. The authors wish to acknowledge the valuable assistance of S. Benson, D. Rindt, and A. Severson (GFETC) in obtaining the analytical data, and of L. Delaney, T. Kuhlman, and C. Matone (BCR) in conducting the slag viscosity measurements. Thanks are also due to J. Waldron of Commonwealth Edison for providing the Black Butte coal sample, and to Dr. K. Mills of the British National Physical Laboratory for furnishing information on the IRSID and Urbain correlations.

REFERENCES

1. Watt, J. D. and F. Fereday, "The flow properties of slags formed from the ashes of British coals: Part 2. The crystallizing behaviour of the slags," J. Inst. Fuel 42, 131-4 (1969).
2. Barrick, S. M. and G. F. Moore, "Empirical correlation of coal ash viscosity with ash chemical composition," ASME Paper No. 76-Wa/Fu-3 (1976).

3. Hoy, H. R., A. G. Roberts, and D. M. Wilkins, "Behavior of mineral matter in slagging gasification processes," Publication 672, Instn. Gas Engrs., Nov. 1964. 24 pp.
4. Diehl, E. K., "Viscosity of low-rank coal slags," Proc. Low Rank Coal Technology Development Workshop, San Antonio, TX, June 1981. pp. 5-29 to 5-32.
5. Watt, J. D. and F. Fereday, "The flow properties of slags formed from the ashes of British coals: Part 1. Viscosity of homogeneous liquid slags in relation to slag composition," J. Inst. Fuel 42, 99-103 (1969).
6. Given, P. H., D. Weldon and N. Suhr, "Investigation of the distribution of minerals in coals by normative analysis," The Pennsylvania State University; U. S. DOE Report FE-2494-TR-2, Jan. 1980.
7. Frederikse, H. P. R., T. Negas, and S. J. Schneider, "Development, testing, and evaluation of MHD materials," Contract No. E(49-18)-1230, NBS Quarterly Reports, Nos. 1, 2, 3, 4 (1974) and 5 (1975).
8. Riboud, P. V., Y. Roux, L.-D. Lucas, and H. Gaye, "Improvement of continuous casting powders," Fachberichte Hüttenpraxis Metallweiterverarbeitung 19 (10), 859-66 (1981).
9. Urbain, G., F. Cambier, M. Deletter, and M. R. Anseau, "Viscosity of silicate melts," Trans. J. Br. Ceram. Soc. 80, 139-41 (1981).

Appendix 1. Slag Viscosity/Composition Correlations

A. Watt-Fereday Correlation

$$\log \eta = [10^7/m/(t - 150)^2] + c$$

where η = viscosity in poises

t = temperature, °C

$$m = 0.00835 \text{ SiO}_2 + 0.00601 \text{ Al}_2\text{O}_3 - 0.109$$

$$c = 0.0415 \text{ SiO}_2 + 0.0192 \text{ Al}_2\text{O}_3 + 0.0276 \text{ eq. Fe}_2\text{O}_3 \\ + 0.0160 \text{ CaO} - 3.92$$

$$\text{eq. Fe}_2\text{O}_3 = \text{Fe}_2\text{O}_3 + 1.11 \text{ FeO} + 1.43 \text{ Fe}$$

where slag components are expressed in weight percentages

and, on a weight basis,

$$\sum \text{SiO}_2 + \text{Al}_2\text{O}_3 + \text{Fe}_2\text{O}_3 + \text{CaO} + \text{MgO} = 100\%$$

B. NBS-Modified Watt-Fereday Correlation

The equation for $\log \eta$ and units are identical to those above, except that

$$m = 0.0104291 \text{ SiO}_2 + 0.0100297 \text{ Al}_2\text{O}_3 - 0.296285$$

$$\text{and } c = -0.0154148 \text{ SiO}_2 - 0.0388047 \text{ Al}_2\text{O}_3 - 0.016167 \text{ Fe}_2\text{O}_3$$

$$-0.0089096 \text{ CaO} - 0.012932 \text{ MgO} + 1.04678$$

C. BCURA S² Correlation

$$\log \eta = 4.468 (S/100)^2 + 1.265 (10^4/T) - 7.44$$

where η = viscosity in poises

T = temperature, °K

and S = silica ratio = $100 \text{ SiO}_2 / (\text{SiO}_2 + \text{eq. Fe}_2\text{O}_3 + \text{CaO} + \text{MgO})$

(slag components expressed in weight percentages)

D. IRSID Correlation

$$\eta = AT \exp(B/T)$$

$$\text{or } \ln \eta = \ln A + \ln T + B/T$$

where η = viscosity in Pa*s (multiply by 10 to convert to poises)

T = temperature, °K

$$\ln A = -19.81 + 1.73 (\text{CaO} + \text{MnO} + \text{MgO} + \text{FeO}) + 5.82 \text{CaF}_2 \\ + 7.02 (\text{Na}_2\text{O} + \text{K}_2\text{O}) - 35.76 \text{Al}_2\text{O}_3$$

$$\text{and } B = 31,140 - 23,896 (\text{CaO} + \text{MnO} + \text{MgO} + \text{FeO}) - 46,356 \text{CaF}_2 \\ - 39,519 (\text{Na}_2\text{O} + \text{K}_2\text{O}) + 68,833 \text{Al}_2\text{O}_3$$

Slag components are expressed as mole fractions; for coal ash slags, CaF_2 and MnO can be considered as zero.

E. Urbain Correlation

$$\eta = AT \exp(10^3 B/T)$$

$$\text{or } \ln \eta = \ln A + \ln T + 10^3 B/T$$

where η = viscosity in poises

T = temperature, °K

$$\ln A = -(0.2693 B + 11.6725)$$

$$\text{and } B = B_0 + B_1 N + B_2 N^2 + B_3 N^3$$

where N = mole fraction of SiO_2

$$\text{and } B_0 = 13.8 + 39.9355 \alpha - 44.049 \alpha^2$$

$$B_1 = 30.481 - 117.1505 \alpha + 129.9978 \alpha^2$$

$$B_2 = -40.9429 + 234.0486 \alpha - 300.04 \alpha^2$$

$$B_3 = 60.7619 - 153.9276 \alpha + 211.1616 \alpha^2$$

where $\alpha = \text{CaO}/(\text{CaO} + \text{Al}_2\text{O}_3)$

Slag components are expressed as mole fractions. When other minor slag components (modifiers) are present, these are included by redefining α :

$$\alpha' = M/(M + \text{Al}_2\text{O}_3)$$

where M represents the modifiers as a single mole fraction and is defined as $M = \sum M_i L_i$, where M_i 's are the individual mole fractions and L_i is the number of oxygen atoms in the molecule. Thus, for the slags considered in these studies containing CaO , MgO , Na_2O , K_2O , FeO , TiO_2 , and (occasionally) SO_3 ,

$$M = \text{CaO} + \text{MgO} + \text{Na}_2\text{O} + \text{K}_2\text{O} + \text{FeO} + 2 \text{TiO}_2 + 3 \text{SO}_3$$

(again, all components expressed as mole fractions).

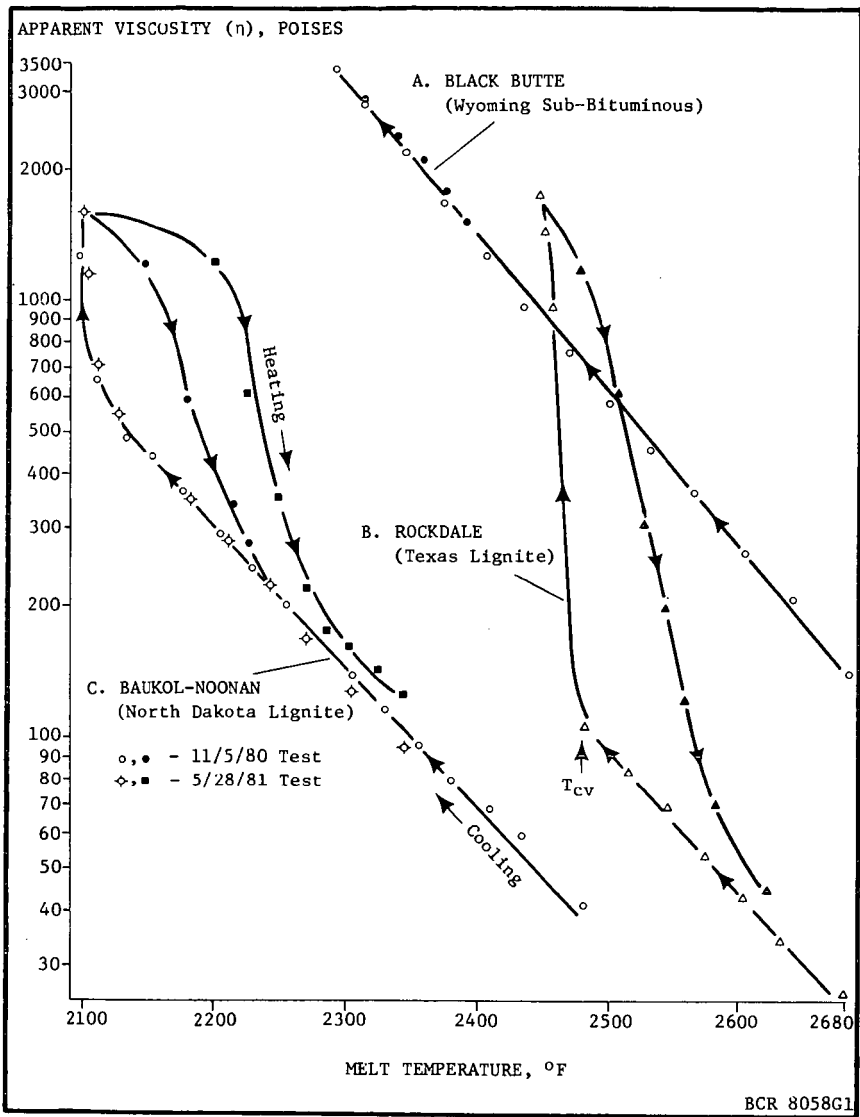


Figure 1. Representative Slag Viscosity Curves for Three Western U.S. Low-Rank Coals

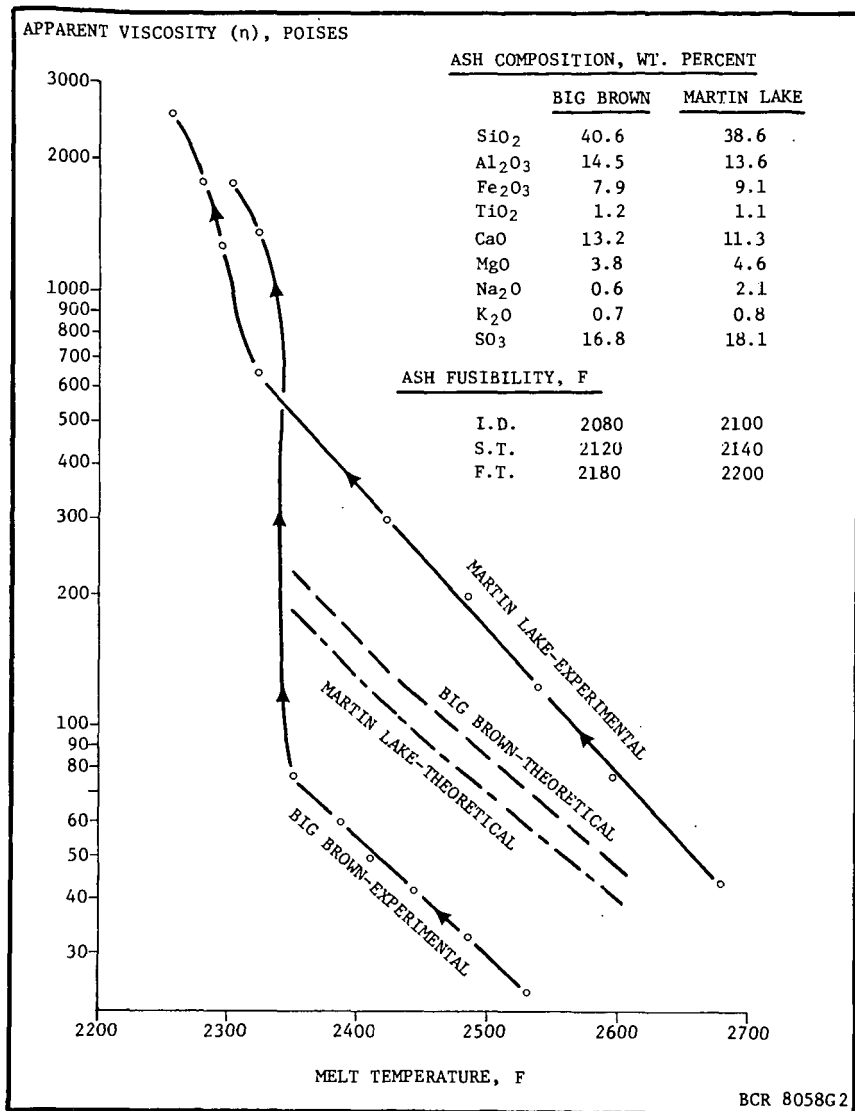


Figure 2. Comparison of Predicted (Watt-Fereday) and Actual Slag Viscosity Curves for Two Texas Lignites

MECHANISTIC STUDIES ON THE HYDROLIQUEFACTION OF VICTORIAN
BROWN COAL AND OF COAL DERIVED PRODUCTS

F.P. Larkins*, W.R. Jackson, P.A. Herten, P.J. Cassidy,
M. Marshall and D. Rash

Department of Chemistry, Monash University, Clayton, Victoria,
Australia 3168.

Introduction

The overall aim of our recent studies has been to obtain a more complete understanding of the mechanisms for the principal reactions which occur during the catalysed hydroliquefaction of low rank, high oxygen containing (ca. 25 wt% db) coals. The results of 70 ml batch autoclave studies with and without added catalysts on Victorian brown coal, on a number of different coal derived products and on related model ether compounds are discussed herein. More complete details of various aspects of this work may be found elsewhere (1-6). On the basis of these investigations a mechanism is proposed for the hydroliquefaction process which emphasises the role of catalysts in inhibiting repolymerisation reactions, the significance of interconvertibility of coal derived products and the importance of hydrogen donation from molecular hydrogen and the vehicle tetralin.

Experimental

Coals: Two samples of dried (105°C, under N₂) Victorian brown coals from the Morwell seam were used in these experiments viz., Drum 66 (1976 100t bulk sample) and Drum 289 (1979 100t bulk sample). The chemical characteristics of the coals on a weight per cent dmmf basis are as follows: Drum 66, C 69.3, H 5.0, O (by diff.) 24.5, N 0.6, S 0.6. Acidic O 9.7 mol kg⁻¹ dmmf coal non-acidic O 5.6 mol kg⁻¹ dmmf coal. Drum 289, C 69.2, H 4.8, O (by diff.) 25.2, N 0.52, S 0.25. Acidic O 9.6 mol kg⁻¹ dmmf coal, non-acidic O 5.3 mol kg⁻¹ dmmf coal. The elemental composition is therefore similar to that of a North Dakota lignite.

The coals (< 250 μm) were hydrogenated in a 70 ml rocking autoclave using a 1:1 slurry of tetralin: coal at initial hydrogen pressures of 1-10 mPa for 1 hour at a reaction temperature of 385°C. In related studies temperatures in the range 345 - 460°C were used at 6 mPa pressure. Both iron and tin-based catalyst systems were examined.

For the work reported herein the catalysts were incorporated by the ion exchange technique (1). In other studies we have shown that impregnation using soluble metal salts is as effective in achieving a comparable level of catalytic activity.

The products from these hydrogenations were separated into gases (analysed by g.c.), water (analysed by azeotropic distillation), insolubles (CH₂Cl₂ insolubles), asphaltene (CH₂Cl₂ soluble/X₄ insoluble), oils (CH₂Cl₂ soluble/X₄ soluble). Hydrogen transferred from the donor solvent was determined by g.l.c. analysis of the ratio of tetralin to naphthalene in the total hydrocarbon liquid product.

Coal derived materials: These products were obtained from our 1 kg h⁻¹ continuous reactor unit (7) as oils (X₄ soluble) asphaltenes (tetralin soluble/X₄ insoluble) asphaltols (tetralin insolubles/tetrahydrofuran (THF) solubles) and THF insoluble materials for subsequent reactivity studies. Methylene chloride was not used in

* Now at Department of Chemistry, the University of Tasmania, Hobart, Tasmania, Australia 7001.

the separation because of concern for its potential catalyst deactivation role in the subsequent series of experiments to be undertaken. Experimental continuous reactor conditions were a 3:1 slurry of tetralin:coal to which an iron (278 ± 30 mmol kg^{-1} dc from $\text{FeSO}_4 \cdot 7\text{H}_2\text{O}$) and tin (20 mmol kg^{-1} dc from $\text{SnCl}_2 \cdot 2\text{H}_2\text{O}$) catalyst had been added. The reaction temperature was 400°C with a developed pressure of 10 MPa and a residence time from 15 to 40 minutes.

Samples of each of the coal derived materials were reacted separately in the presence of several catalysts in a 70 ml batch autoclave using a 1:1 slurry of tetralin:material at 425°C with an initial hydrogen pressure of 6 mPa for 1 h at reaction temperature. The products from these reactions were separated into oils, asphaltenes, asphaltols and THF insolubles.

Model ether systems: A series of ethers have been examined to assist in the elucidation of the role of the iron and tin catalyst systems investigated. Hydrogenation conditions were 1-2 g ether, initial hydrogen pressure 6 mPa, reaction time 1 h with catalyst loadings similar to those used for coal hydroliquefaction studies. Full details are outlined elsewhere (2,5).

Results

Reactions with coal

Total conversion yields for the temperature range $345\text{--}460^\circ\text{C}$ at 6 mPa hydrogen are summarized in figure 1. Absolute conversions are lower than for work with 1 l autoclaves and the continuous reactor unit because of different reactor temperature profiles and residence time; however, the qualitative conclusions are consistent. The effect of increasing the reaction temperature was to increase the total conversion of all reactions irrespective of the catalyst system.

The iron-tin catalyst system was the most temperature sensitive of the four coal-catalyst systems studied. Unlike the iron and tin treated coals which were only sensitive to temperature in the range $365\text{--}405^\circ\text{C}$, the iron-tin treated coal was also sensitive to temperature in the range $385^\circ\text{--}425^\circ\text{C}$ where the conversion rapidly increased from 66% to 85% (daf coal). Thus the iron-tin system was most efficient at the higher reaction temperatures up to 425°C while the iron and tin treated coals were most effective up to 405°C (see Table 1, reference 2).

The initial hydrogen pressure dependent conversion results in the range 1-10 mPa are given in figure 2 for studies at 385°C . The tin catalysed reactions show most pressure dependence, consistent with previous findings that tin facilitates molecular hydrogen transfer during hydrogenation (4). For the untreated coal and for other catalyst systems there is only a small pressure dependence of product yields beyond 4 mPa.

A detailed study of the chemical constitution of the products revealed that their composition is influenced by temperature but not by pressure or the nature of the catalyst. With increased reaction temperature there was a decrease in total and acidic oxygen concentrations in the asphaltenes and a corresponding increase in both aromatic content and C/H ratio. This observation is consistent with the loss of aliphatic side chains from the polycondensed ring systems

Reactions with coal derived products

Hydrogenation studies were undertaken on the parent iron-tin treated coal (Drum 289) as well as the THF insolubles, asphaltol, asphaltene and oil derived from a continuous reactor run as previously discussed. Studies with no additional catalyst added (case A) and with the addition of a sulphided nickel molybdate catalyst supported on alumina (case B) were performed. The results are presented in table 1. The Ni/Mo catalyst in case B did not increase the conversion of the coal or the THF insolubles beyond that for case A because sufficient amounts of

iron and tin materials were already associated with these reactants to catalyse the reaction. The iron-tin treated coal has of course a much greater reactivity than untreated coal as shown in table 1. It is noteworthy that once isolated the THF insolubles showed a similar reactivity (~ 75 wt% daf) to the coal (~ 80 wt% daf).

The results in table 1 show that for reactions at 425°C significant conversion of the asphaltols and the asphaltenes produced at 400°C to other products was possible. In particular for the asphaltol $> 95\%$ interconversion occurred, while for the asphaltene the interconversion was $> 65\%$. A complete range of products was formed from high oil yields to repolymerised THF insoluble material. This reactivity underlines the inherent instability of these intermediate products. The addition of a sulphided Ni/Mo catalyst led to $\sim 50\%$ improvement in oil yields, however addition of the traditional first stage catalysts iron, tin or the iron-tin mixture did not significantly improve the conversion of asphaltene or asphaltol to oil as compared to the reactions without additive (results not presented here). Tin, and to a lesser extent, iron were successful in reducing the amount of repolymerisation of asphaltols to THF insolubles.

Hydrogenation of the oil fraction resulted in the formation of a small amount of the higher molecular weight products (< 4 wt%), but the recovered oil contained a higher proportion of lower boiling point material.

Reactions with model ether compounds

The reactions of a series of lignin related model ether compounds with iron II acetate and tin metal have been investigated (2,5). The models selected contain phenoxy groups ($\text{PhO}-(\text{CH}_2)_n\text{Ph}$ $n = 1,2,3$), benzyl groups ($\text{PhCH}_2\text{-OCH}_2\text{Ph}$) and alkoxy groups ($\text{PhCH}_2\text{CH}_2\text{-OCH}_2\text{CH}_2\text{Ph}$). Conversion results for the reactions of 2-phenylethyl phenyl ether ($\text{PhO-CH}_2\text{CH}_2\text{Ph}$) and dibenzyl ether ($\text{PhCH}_2\text{OCH}_2\text{Ph}$) are shown in figures 3 and 4 respectively. For the phenylethyl phenyl ether the extent of conversion is significantly reduced in the presence of both metal additives with iron being more effective than tin in suppressing the decomposition. For example at 325°C there was only 13% conversion in the presence of an iron based additive compared with 33% with tin and 43% without additive. In contrast, addition of an iron-based catalyst to a reaction of dibenzyl ether (figure 4) was found to promote the conversion while the tin-based catalyst suppressed it relative to no additive being present. At 300°C the conversion was 96% with iron, 12% with tin and 19% without additive. The thermal decomposition of these ethers is believed to be via a radical chain mechanism. (9) It is postulated that while iron catalysts may facilitate carbon-oxygen bond cleavage, as evidenced by the increased reactivity of benzyl and aliphatic ethers, when phenoxy radicals are produced they are strongly adsorbed on the catalyst surface. They are not therefore readily available to propagate the radical chain reactions. This effect is restricted to the phenoxy radical and not observed for a species such as $\text{PhCH}_2\text{CH}_2\text{O}$ in the reaction of $\text{PhCH}_2\text{CH}_2\text{OCH}_2\text{CH}_2\text{Ph}$ because the resonance stabilisation energy associated with the PhO would result in it having a longer half-life and hence time to diffuse to the catalyst surface without being stabilized by hydrogen. The iron catalyst does not show the same affinity for the benzylic radical even though it is also a long-lived species.

The tin additive is present in the liquid state under the conditions of the present experiments. It has a smaller inhibiting effect than iron on the reactivity of the phenoxy and benzyl ethers. Two explanations are plausible. Hydrogen dissolved in the tin may react with the benzyl and phenoxy radicals which are the chain propagators and remove them from the system. The rate of bond cleavage is therefore lowered. Alternatively, tin may promote radical recombination reactions. By either route the tin would be acting to inhibit propagation reactions.

Mechanistic considerations

Many reaction schemes have been proposed to interpret the results of hydro-liquefaction experiments following the pioneering work of Weller et al. in 1951 (8). Factors to be taken into account when considering the complex liquefaction process include

1. Coal-solvent interactions leading to swelling and dissolution of the coal. (10,11)
2. The radical production resulting from thermal degradation of coal molecules. (12,13)
3. Capping of radicals by molecular hydrogen and by hydrogen abstraction from the solvent inhibiting polymerisation of intermediate radical species.
4. Thermal instability of coal derived materials leading to interconvertibility between products including retrograd reactions and the establishment of steady state conditions. The principle of reversibility is of importance in these processes.
5. The role of the catalyst at various stages of the process. Principally in coal dissolution reactions, in stabilisation of reactive radical intermediates against polymerisation, in promotion of bond cleavage reactions and in facilitating the transfer of hydrogen to coal derived materials. It is most unlikely that any single catalyst will have significant activity in all of these steps.

On the basis of our present knowledge of the role of iron- and tin-based catalysts and of the role of the sulphided nickel molybdate catalyst the mechanism shown in figure 5 is proposed to summarize the essential steps in the hydroliquefaction of low rank coals.

At temperatures $> 360^{\circ}\text{C}$ brown coal is rapidly dissolved in the vehicle without significant chemical reaction forming coal (reaction 1) which corresponds to the pyridine soluble material observed by Neavel. (10) At increasing reaction time coal¹ is thermally converted into reactive radical intermediates (reaction 2) which in the absence of a suitable hydrogen donor, either molecular hydrogen or the vehicle, rapidly repolymerises (reactions 3,4,5). In the presence of a good hydrogen donor, hydrogen abstraction reactions (reactions 6,7) compete with polymerisation reactions leading to the formation of oils and asphaltenes. The important concept of reversibility is included in this scheme by the two way arrows between the radical pool and the respective products. It is possible therefore for polymerised material to re-react (reactions 2,8,9) and form lower molecular weight oils and asphaltenes. Thus the system reaches a dynamic equilibrium after a period of time which is primarily dependent on the reaction temperature, the concentration of available hydrogen, and the metal catalyst.

At temperatures greater than 400°C , the asphaltenes rapidly degrade (reaction 10) and can either repolymerise or in the presence of hydrogen, form oil. At higher temperatures ($> 425^{\circ}\text{C}$) thermal cracking of oils, asphaltenes and repolymerised products leads to increasing yields of hydrocarbon gases (reaction 12).

In the presence of a high pressure of hydrogen, tin metal facilitates the stabilisation of radicals formed by initial coal depolymerisation leading to the formation of asphaltols and asphaltenes (reactions 5 and 6). The stronger pressure dependence of the tin catalysed reactions compared with other systems investigated here may be linked to the fact that the amount of hydrogen dissolved in liquid tin is also pressure dependent.

In the absence of tin less asphaltene is produced which manifests itself as increased yields of THF insolubles and asphaltols. At this time the activity of iron is not completely certain as no effects have been observed on the reactions of the coal derived products. However the proven ability of iron to both catalyse the reactions of some ethers while suppressing propagation reactions of phenoxy radicals suggest that its major activity is probably restricted to the first minutes of reaction (reactions 1,2) and to the slow catalytic degradation of polymerised material. The iron-tin synergism can be interpreted as a co-operative action between the catalytic and radical stabilisation activities of iron with the hydrogen utilisation and radical stabilisation activities of tin which allows the radical intermediates to be stabilised as oil and asphaltene.

The conversion of asphaltene to oil is not catalysed by either iron or tin but it is facilitated by increased reaction temperature and the availability of a good H-donor solvent. The resulting oil formed at high temperatures ($> 400^{\circ}\text{C}$) contains much less oxygen (especially acidic oxygen) and the conversion probably is the result of the loss of polar phenolic groups as well as cleavage of carbon-carbon bonds joining aromatic clusters together. Vernon (14) has shown that dibenzyl thermally decomposes above 400°C .

Formation of hydrocarbon gases principally results from thermal cracking although tin catalyses the formation of methane at temperatures $> 425^{\circ}\text{C}$. Weller (15) has also shown that tin II chloride catalyses the formation of methane in the reaction of 1-methylnaphthalene with hydrogen.

The action of sulphided Ni/Mo catalyst was to dramatically increase the yield of oil from the reactions of asphaltol and asphaltenes. It is believed that the mechanism of the Ni/Mo catalyst involves a more conventional dissociative adsorption of both hydrogen and reactant molecule to the catalyst surface followed by hydrogenolysis and hydrogenation reactions. The mechanistic pathway thus differs from both iron and tin and is shown in figure 5 by reactions 13 and 14.

Acknowledgements

Financial support for this work was provided by the Victorian Brown Coal Council and the Australian Government Department of National Development and Energy under the National Energy, Research, Development and Demonstration Program. The view expressed herein are entirely those of the authors.

REFERENCES

1. Marshall, M., Jackson, W.R., Larkins, F.P., Hatswell, M.R., and Rash, D. Fuel 61, 121 (1982).
2. Cassidy, P.J., Hertan, P.A., Jackson, W.R., Larkins, F.P., and Rash, D. Fuel 61, 939 (1982).
3. Hatswell, M.R., Jackson, W.R., Larkins, F.P., Marshall, M., Rash, D., and Rogers, D.E. Fuel 62 (in press) (1983).
4. Cochran, S.J., Hatswell, M., Jackson, W.R., and Larkins, F.P. Fuel 61, 831 (1982).
5. Cassidy, P.J., Jackson, W.R., and Larkins, F.P. submitted to Fuel (1983).
6. Hertan, P.A., Jackson, W.R.; and Larkins, F.P. submitted to Fuel (1983).
7. Agnew, J.B., Hoad, W.G., Prasad, G.N., Rash, D. and Rogers, D.E., submitted to Fuel (1983); Agnew, J.B., Jackson, W.R., Larkins, F.P., Rash, D., Rogers, D.E., Thewlis, P., and White, R. submitted to Fuel (1983).

8. Weller, S., Clark, E.L., and Pelipetz, M.G., *Ind. Eng. Chem.* 42, 334 (1950).
9. Schlosberg, R.H., Ashe, T.R., Paricioie, R.J., and Donaldson, M., *Fuel* 60, 155 (1981).
10. Neavel, R.C., *Coal Science* 1, 1 (1982).
11. Whitehurst, D.D. and Mitchell, T.O., *Am. Chem. Soc. (Div. Fuel Chem.) Preprints* 26(2), 173 (1981).
12. Curran, G.P., Struck, R.T. and Goun, F., *Ind. Eng. Chem. Proc. Des. Dev.* 6, 166 (1967).
13. Grandey, D.W., and Petrakis, *Fuel* 58, 239 (1979).
14. Vernon, L.W., *Fuel* 59, 102 (1980).
15. Weller, S., personal communication.

Table 1: Product distribution from the catalysed and uncatalysed reactions of Victorian Morwell coal and coal derived reactants.

Reactant	P R O D U C T D I S T R I B U T I O N						
	(wt. % reactant)						
	Oil	Asphaltene	Asphaltol	THF Insoluble	H ₂ O	CO/CO ₂	Hydrocarbon Gases
Untreated coal A	26	7	1 ^c	36 ^c	9	13.0	8.0
Iron-tin treated coal ^a A	42	14	1	17	9	12.6	6.6
Iron-tin treated coal B	40	10	2	20	13	12.5	7.1
THF ^a insolubles A	39	13	2	25	11	5.7	6.0
insolubles B	39	14	3	26	12	5.0	6.3
Asphaltol ^a A	44	28	5	13	4	2.2	5.5
Asphaltol ^a B	63	19	3	5	6	1.5	6.0
Asphaltene ^a A	37	41	7	6	3	1.4	5.3
Asphaltene ^a B	67	22	1	3	5	0.5	4.5
Oil ^b A	96	4	tr.	1	0	0.1	1.2
Oil ^b B	97	tr.	1	3	0	0.1	1.0

A No catalyst added. B Sulphided Ni/Mo catalyst (10% by weight reactant)

^a Reactions at 425°C for 1 h using 3 g reactant and 3 g tetralin with initial hydrogen pressure of 6 mPa.

^b Reactions as for a except 1 g oil and 5 g tetralin.

^c Estimated values (asphaltol + THF insoluble = 37).

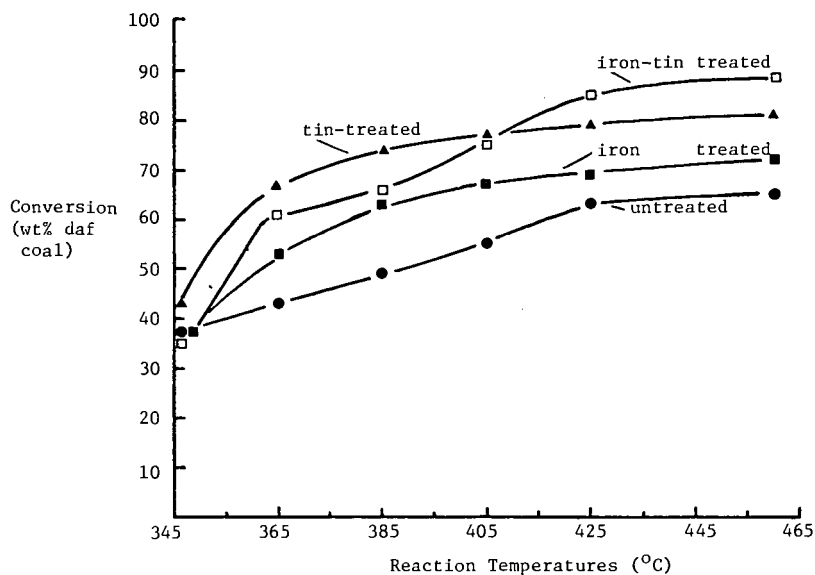


Figure 1: Total conversion versus reaction temperature. Reaction conditions: 6 mPa initial H₂ pressure, 1 h at temperature 1:1 tetralin to coal ratio.

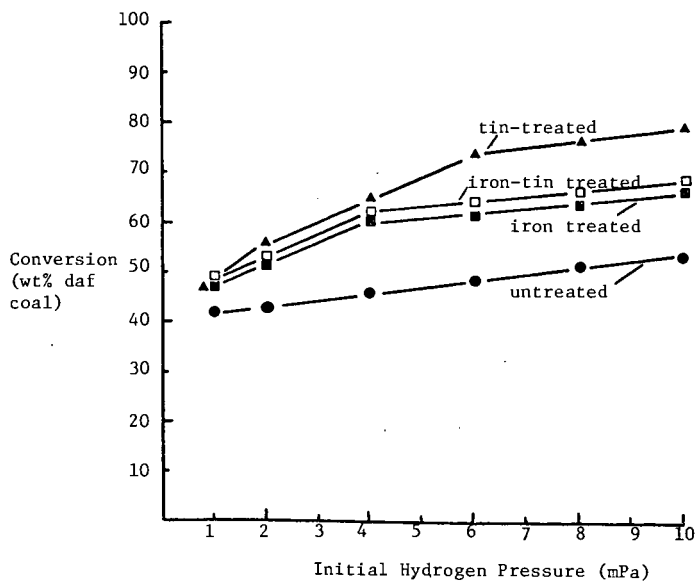


Figure 2: Total conversion versus initial hydrogen pressure. Reaction conditions: 385°C, 1 h at temperature, 1:1 tetralin to coal ratio.

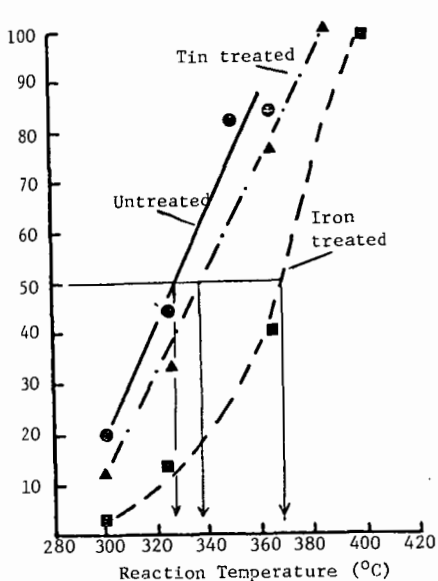


Figure 3: The conversion of 2-phenylethyl phenyl ether versus reaction temperature. Reaction conditions 6 mPa initial H₂ pressure, 1 h at temperature.

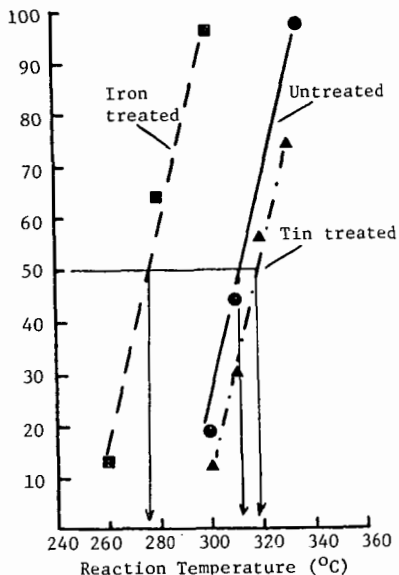


Figure 4: The conversion of dibenzyl ether versus reaction temperature. Reaction conditions 6 mPa initial H₂ pressure, 1 h at temperature.

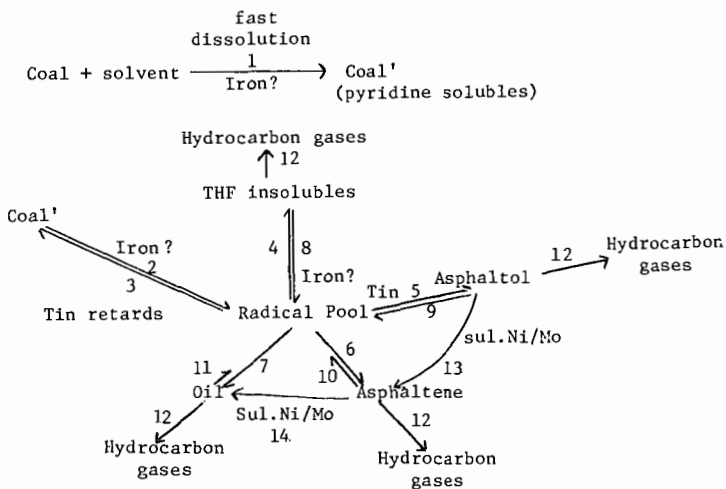


Figure 5: The proposed reaction mechanism of the catalytic hydroliquefaction of Victorian brown coal.

Note: The length of the arrows in reactions 8,9,10,11 indicate the relative reactivities of the respective fractions.

SUPERCritical GAS EXTRACTION OF OIL SHALE

L. E. Compton

Jet Propulsion Laboratory
California Institute of Technology
4800 Oak Grove Drive
Mail Stop: 125/159
Pasadena, California 91109

INTRODUCTION

Green River oil shale in the western United States is considered by many as second only to coal as the largest potential source of fuel in the energy future of the United States. In addition, because of its high indigenous hydrogen content, it is considered superior to coal as a potential feedstock for conversion into liquid fuels. The organic matter in oil shale is conventionally separated by retorting from the inorganics with which it is associated. Temperatures sufficient to crack the organics are used, and a very-high-nitrogen, unstable "petroleum" is produced. It is forecasted by some strategic planners that such oil shale syncrude could enter into the domestic market during the next decade and result in reduction in the nation's dependency on overseas fuel supplies. However, retorting has not yet proven capable of producing a fuel that is truly cost competitive, and present decreases in the price of crude petroleum have reduced at least the short term commercial potential of all synfuels.

Oil shale retorting centers around heating the material, which is typically 85% rock, to about 480°C (900°F) or higher in a low oxygen environment (1). The kerogen and bitumen in the rock are decomposed into oil, gas, and a residual char which remains within the rock. Under favorable circumstances (laboratory analysis by modified Fischer assay) 70 wt% of the organic matter is converted to oil upon heating to 500°C, and the remainder is converted to about 15% gas and 15% char (1,2). These yields change when oil shale is processed in prototype commercial retorts. Oil yield is reduced from 10% to 30% below modified Fischer assay yields, depending on the process (1,3), and char and gas yields are correspondingly increased.

The energy content of the organic matter not converted to oil exceeds net process heat requirements for oil shale retorting. The excess depends on the organic content of the shale and the process design, but for well developed processes using a medium grade of shale (roughly 11 to 15 wt% organic matter) the excess can be 100% greater than heat requirements. For instance, the TOSCO II process is based on discarding 100% of the char produced from 11% organic matter shale (1). The excess can be double or triple this amount when richer material is processed.

The energy contained in the char and gas by-products typically cannot be used efficiently. The gas produced is often greatly diluted with nitrogen and carbon dioxide (1), and the heat content and its efficiency of usage are greatly reduced. In addition, the energy generated by combustion of the residual char in the rock is considerably less than might be anticipated, because of high temperature endothermic mineral carbonate decompositions (4) which occur when the char is burned. In short, the fuels are in dilute forms and the energy contents have low thermodynamic availability. This severely reduces or eliminates their commercial value. Areas in which western oil shale would be developed contain little or no nearby industrial base which could use such fuel, and the gas and char would require prohibitively costly transport. This, combined with very low value, causes char and gas in excess of process fuel requirements to be waste disposal problems, rather than salable byproducts.

The above characteristics of retorting are drawbacks, since energy in salable form is the only product. Requirements for heating rock to high temperature, excessive conversion of organic matter to char and gas, and the low value of the diluted energy content of these by-products combine to reduce the net salable energy to 1/3 to 1/2 below that contained in the raw oil shale. This is a technical problem contributing to an uncertain future for present schemes, and new technology could be useful.

Supercritical gas (SCG) extraction has the potential to make the energy in oil shale available in more concentrated form, because of the high solvent extraction ability of supercritical gases. SCG extraction has been the subject of a number of papers and reviews (5-8), and extensive study has been made of applications to coal (7-12). In the case of coal, simultaneous pyrolysis and extraction of pyrolysis products is effected at temperatures of around 350°C to 450°C. Extract yields in excess of 50% of the organic matter in coal and well in excess of volatile matter contents have been reported (12) when chemically inert SCG solvents are used. The SCG extraction ability is due to near-liquid-density solvent power combined with gas phase mass transfer and penetration properties which inhibit coking reactions that produce char and gas (8). An outstanding characteristic of the extracts is the high molecular weight (11), a property not characteristic of matter which is simply volatilized from coal. These results suggest that SCG extraction might be successfully applied to oil shale. In spite of the drawbacks associated with conventional oil shale retorting and the high SCG coal extraction results, description or discussion of SCG oil shale extraction is apparently absent from the literature, with the exception of a recent patent (13).

EXPERIMENTAL

Experimentation was performed with an apparatus similar to that described elsewhere (10). The apparatus is a 300 cc stainless steel reactor with attendant gauging and controls. The oil shale, 8 grams of material with particle diameters ranging between 50 and 188 microns, was enclosed in a fine mesh stainless steel basket located near the top of the reactor and under a fluid circulating stirrer. This location eliminated any contact between liquid solvent and the oil shale. Experimentation was performed by placing liquid solvent (approximately 150 grams) in the reactor bottom, inserting the extraction basket at the top of the reactor, and then heating reactor and contents to the chosen experimental temperature. The reactor was maintained at constant temperature for four hours and subsequently allowed to cool. Heat-up and cool-down times were both approximately 1 hour. Selected extracts were separated from the condensed SCG by vacuum distillation at 10 torr with a nitrogen flow assist. Raw and extracted shale were analyzed for carbon, hydrogen, and Kjeldahl nitrogen, and results were compared with analyses of raw shale (Table 1) to derive values of the extraction efficiency of organic matter and the H/C ratios of the extracts. It was assumed in these calculations that elemental constituents of oil shale organic matter other than C, H and Kjeldahl N [i.e., oxygen and sulfur at a total of about 6 wt% (1)] were extracted with the same efficiency as the total efficiency in extracting C, H plus N. Extract molecular weights were determined by gel permeation liquid chromatography using detection by differential refractometry and with methylene chloride as solvent. Separate refractive indices of the bulk extracts were determined by dissolving the bitumens in carbon tetrachloride and extrapolating results to zero solvent content or by direct determination for the oil.

RESULTS

This work shows that up to 92% of the organic matter in oil shale can be extracted using a supercritical gas. Results (Figure 1 and Table 1) show for toluene an essentially linear temperature dependence for the percent of total

organic matter extracted (extraction efficiency) in the range 330° to 393°C. A blank experiment at 385°C using pure nitrogen at 0.21MPa shows the difference between extraction with a dense gaseous solvent and a simple volatilization without solvent effects. Toluene extracts at all temperatures except 450°C are bitumens with molecular weights ranging up to about two thousand. At 450°C the toluene extract is a shale oil with an average molecular weight of about 300. The H/C atom ratio of these extracts averages 1.65.

TABLE 1
Extraction Conditions and Results*

<u>Solvent</u>	<u>Temperature (°C)</u>	<u>Pressure (MPa)**</u>	<u>SCG Density (gm/cc)</u>	<u>TOM† Removed (wt%)</u>
Toluenett	330	6.9	0.53	33.8
	340	7.2	0.53	40.5
	357	8.3	0.53	54.7
	385	13.8	0.53	80.1
	393	15.2	0.53	87.5
	450	22.4	0.53	92.5
Pyridinett	363	7.6	0.55	63.3
Nitrogen	385	0.21	0.0013	16.9

* Material Extracted: 12.9 wt% organic matter raw oil shale (21 gallon/ton) produced at Anvil Points, Colorado. Organic carbon and hydrogen contents: 10.3 and 1.53 wt%. Kjeldahl nitrogen content: 0.27 wt%.

** 0.101 MPa/Atm

† Total organic matter

†† Critical parameters: toluene - 319°C, 4.11 MPa; pyridine - 347°C, 5.63 MPa

DISCUSSION

The results demonstrate the powerful solvent properties of supercritical gases and provide incentive for further investigation of SCG oil shale extraction. Residual organic matter after extracting at 450°C is one-half that left by modified Fischer assay, and it is probably one-quarter or less of that which would be generated during prototype commercial retorting. In addition, the data shows organic matter removal occurring below 450°C can be greater than that found with prototype retorting. Certain process advantages associated with the results could occur, namely those associated with near quantitative removal of organic matter and with the presumably lower gas generation associated with lower temperatures and reduced char formation.

The results are not optimized. Questions regarding temperature, solvent power, solute-solvent ratio, pressure, particle size, and the kinetics associated with reactions in the non-gaseous and SCG phases are open. A question of immediate interest involves the temperature dependence of the data in the 330° to 393°C range. Several descriptions of the kinetics describing oil shale decomposition in inert atmospheres without solvent effects have been published (2,14,15). The work indicates oil shale organic matter can be characterized as two materials, kerogen and bitumen, the latter being benzene soluble. Thermal decomposition of the materials can be described by a kinetic mechanism involving two consecutive first order reactions:

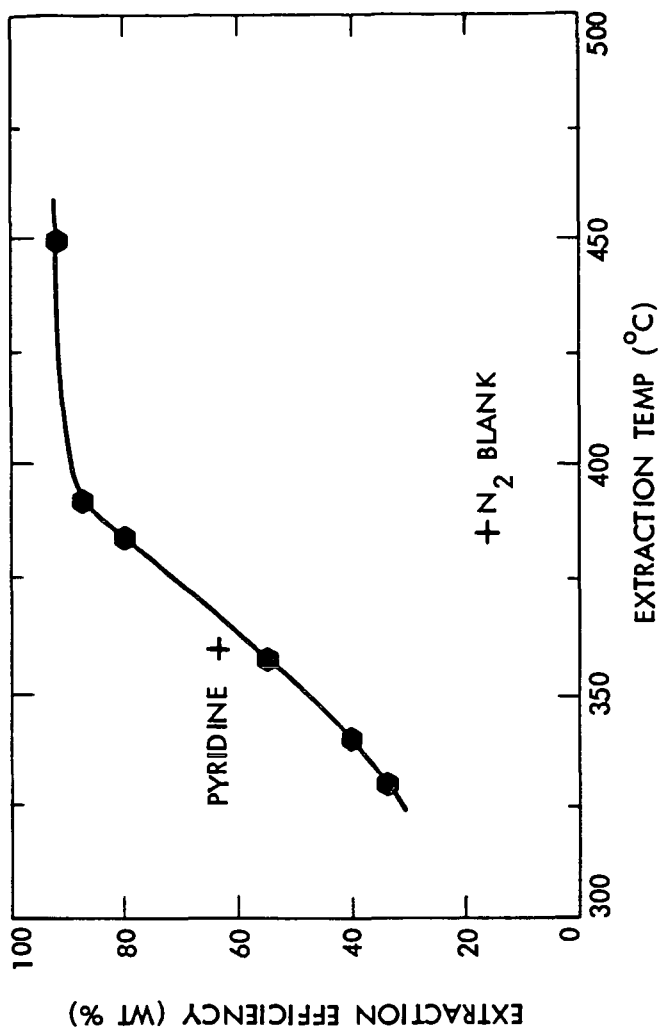


Figure 1. Extraction Efficiency vs. Temperature for Toluene, Compared with Single Temperature Results for Pyridine and Low Density Nitrogen.



The temperature dependence of both rate constants is available for the 400°C to 525°C range (15). Extrapolation of the very linear $\ln k$ versus $1/T$ (°K) dependence of k_1 into the 330° to 393°C range of interest should yield reasonably accurate k_1 values unless a change in the pyrolysis mechanism occurs over the range of the extrapolation. At 350°, k_1 then equals $3 \times 10^{-3} \text{ sec}^{-1}$, and the corresponding first order half life of kerogen during conversion to bitumen would be 230 sec. Extraction times in this work were approximately 10^4 sec at constant temperature, and the observed temperature dependent extraction yield is not predictable if the indicated kinetics are applicable to these SCG experiments. A temperature dependent SCG extraction mechanism could be present.

Solvent theory is useful in examining this possibility. The theory of SCG extraction is currently approached by treating the dense gas either as a highly compressed gas or as an expanded liquid. The subject has been reviewed recently (5), and it is clear that some success has occurred in predicting single-component solubilities in supercritical gases. However, application has not been made to highly complex hydrocarbon mixtures, such as oil and coal extracts. A useful alternative has been to extend the concept of solubility parameter, which is regularly used in understanding liquid solutions, to supercritical gases.

The solubility parameter concept, developed by Hildebrand (17) and Scatchard (18), is based on the concept of cohesive energy density and the well-tested precept that a correlation exists between cohesive energy density and the mutual solubility of substances. The solubility parameter is defined as:

$$\delta = (E/V)^{1/2} \quad 3)$$

where δ is in $(\text{cal/cm}^3)^{1/2}$, E is the energy required to convert one mole of a given substance from the state of interest to an infinitely expanded gas, the cohesive energy, and V is the molar volume of the substance in the state of interest. It has been shown that the free energy of mixing is minimized and complete miscibility occurs for non-polar liquids when the δ of both solvent and solute are equal. Limited solubility occurs when δ values diverge sufficiently. The concept has also been extended to solids and polar liquids. In addition, the theoretical evaluation of solubilities based on solubility parameters is developing (19).

The Van der Waals constant "a" from the equation of state for gases has been used to estimate solubility parameters for liquids (17), and the success has led to the derivation of the following relation for estimating δ values for supercritical gases (20):

$$\delta_g \cong \delta_l (d_g/d_l) \quad 4)$$

where δ_g and δ_l are the solubility parameters of the gas and the room temperature liquid, and d_g and d_l are the densities of the gas and the room temperature liquid. The equation indicates the solubility parameter of a SCG varies directly with density, and there is no provision for temperature. This is a direct result of the use of the Van der Waals equation in the derivation.

The solubility parameter of materials for which values of the cohesive energy and/or molar volume are unavailable, such as oil shale bitumen, can be estimated by using correlations between δ and the refractive index (21). The following estimation is used:

$$\delta = \left[C \left(\frac{n^2 - 1}{n^2 + 2} \right) \right]^{0.5} \quad 5)$$

where n is the refractive index and C is a constant representative of the chemical compound type. C ranges from a low of approximately 230 for branched aliphatic polymers to a high of 353 for aliphatic ester polymers. The average value of C over a broad range of compounds, including but not limited to polymers, is about 308. If it is assumed that the bitumen produced in this experimentation has about the same atomic makeup as oil shale kerogen, namely $C_{200}H_{300}S_{N_5}O_{11}$ (22), then the material should contain a broad range of chemical functional groups, including large contributions from unsaturated and heteroatomic groups. This assumption is consistent with results from analyses of shale oil which show a rough distribution amounting to 11 wt% saturated hydrocarbons, 18% olefins, 10% aromatics, 36% nitrogen compounds, 6% sulfur compounds, and 19% oxygen compounds (23). The value of C used with Equation 5 for the oil shale bitumen is accordingly chosen as the broad range value of 308. The room temperature values for the refractive index of the bitumen and the oil extracted in this work are 1.62 and 1.59, and Equation 5 yields an average room temperature solubility parameter estimate for the compounds comprising the bitumen of 10.4. A somewhat higher value can be derived from a correlation based on the Lorentz-Lorenz function (21). The value of 10.4 has been temperature corrected with the following relationship derived for polymeric materials (24):

$$\delta_2 = \delta_1 \left[\frac{d_2}{d_1} \right]^{1.13} \quad 6)$$

where δ_1 and δ_2 are the solubility parameters at the reference temperature and the temperature of interest and d_1 and d_2 are the respective densities. Basing the density change of the bitumen between room and experimentation temperatures on the volumetric expansion coefficient for petroleum at 100°C, namely $10^{-3}/^\circ\text{C}$, yields estimates of the solubility parameter of the bitumen ranging from 7.7 at 330°C to 7.3 at 393°C.

A comparison between the estimated solubility parameters of the bitumen and supercritical gas solvents can now be made to determine if a temperature dependent extraction could be expected. For SCG toluene at the 0.53 gm/cc density used, the estimated solubility parameter based on Equation 4 is 5.5, compared to the 7.3 to 7.7 estimated for the bitumen. In normal practice these δ values should be sufficiently different to allow prediction of a temperature-dependent, limited solubility for the bitumen in supercritical toluene. A higher δ SCG might be needed to eliminate temperature dependent extraction effects and increase the overall extraction efficiency at temperatures below 400°C.

Extraction with pyridine at 363°C was performed to test this possibility, and a comparison of results between extraction with toluene and pyridine is included in Figure 1 and Table 1. Extraction efficiency is increased by about 1/6 with pyridine, which has an Equation 4 δ of 6.0 under experimental conditions. This single result needs confirmation. However, both organic carbon and organic hydrogen extraction increase by the same amount with pyridine, and it is concluded that

experimentation with yet a higher solubility parameter SCG might result in additionally enhanced extraction at temperatures below 400°C. Results above 400°C might also be improved, but there is little practical incentive, because of the high extraction efficiency already found.

REFERENCES

1. Baughman, G. L. (Ed.), Synthetic Fuels Data Handbook, 2nd Ed., Cameron Engineers, Denver, 1978.
2. Hubbard, A. B. and Robinson, W. E., Bureau of Mines Report of Investigations 4744, 1950.
3. Brantley, F. E., et al., Ind. and Eng. Chem. **44**, 2641 (1952).
4. Campbell, J. H., LLL Report UCRL-52089, Part 2, March 13, 1978.
5. Williams, D. F., Chem. Eng. Sci. **36**, 1769 (1981).
6. Bott, T. R., Chem. and Ind., p. 228 (15 Mar., 1980).
7. Gangoli, N. and Thodos, G., Ind. Eng. Chem. Prod. Res. Dev. **16**, 208 (1977).
8. Paul, P. F. M. and Wise, W. S., The Principles of Gas Extraction, Mills and Boon, London, 1971.
9. Maddocks, R. R., et al., Chem. Eng. Prog. p. 49 (June 1979).
10. Blessing, J. E. and Ross, D. R., ACS Symposium Series 71, Organic Chemistry of Coal, p. 15, 1978.
11. Bartle, K. D., et al., Fuel **58**, 413 (1979).
12. Kershaw, J. R. and Jezko, J., Sep. Sci. and Tech. **17**, 151 (1982).
13. Williams, D. F., U.S. Patent 4,108,760, 1978.
14. Allred, V. D., Chem. Eng. Prog. **62**, 55 (1966).
15. Braun, R. L. and Rothman, A. J., Fuel **54**, 129 (1975).
16. Mackay, M. E. and Paulaitis, M. E., Ind. Eng. Chem. Fund. **18**, 149 (1979).
17. Hildebrand, J. H. and Scott, R. L., The Solubility of Nonelectrolytes, 3rd Ed., Reinhold, New York, 1950.
18. Scatchard, G., Chem. Rev. **8**, 321 (1931).
19. Srebrenik, S. and Cohen, S., J. Phys. Chem. **80**, 996 (1976).
20. Giddings, J. D., et al., J. Chromat. Sci. **7**, 276 (1969).
21. Lawson, D. D. and Ingham, J. D., Nature **223**, 615 (1969).
22. Weitkamp, A. W., and Gutberlet, L. C., Ind. Eng. Chem. Proc. Des. Dev. **9**, 386 (1970).
23. Cady, W. E. and Seelig, H. S., Ind. and Eng. Chem. **44**, 2636 (1952).
24. Fedors, R. F., Polymer Sci. and Eng. **14**, 472 (1974).

ACKNOWLEDGMENT

The research described in this paper was carried out by the Jet Propulsion Laboratory, California Institute of Technology, under contract with the National Aeronautics and Space Administration.

SOLVENT EFFECTS IN SUPERCRITICAL EXTRACTION OF COAL

Nicholas P. Vasilakos, Joseph M. Dobbs, and Anthony S. Parisi

Department of Chemical Engineering, University of Texas
Austin, Texas 78712

INTRODUCTION

Supercritical gas extraction is particularly suitable for the recovery of the liquids formed when coal is heated to above 400°C. These liquids are normally too involatile to distill at this temperature. If the temperature is increased, they polymerize to form heavier and larger molecular species and evolve as gases and liquids. Only a relatively small amount of the coal distills as tar from the decomposing material. Supercritical gas extraction affords a means of recovering these liquids as they are formed while avoiding the undesirable decomposition reactions (1). Supercritical fluids have a density of about 30% of that of a normal fluid, which is high enough to provide for good solvent capability, but also low enough for high diffusivity and rapid mass transfer throughout the complex coal matrix.

The use of supercritical fluids for the recovery of hydrocarbons and related compounds from coal was pioneered by the National Coal Board (NCB) in Britain. Over a number of years, NCB has investigated the direct extraction of coals using light aromatic solvents (mostly toluene) under supercritical conditions. In a recent NCB report, Whitehead (2) summarized the experimental data on supercritical extraction of coal, obtained both on bench-scale units and on a 5 kg/h continuous pilot plant operated in Britain by the Coal Research Establishment. According to these data, the residence time of coal under supercritical conditions was the variable which most influenced the extract yield. The influence of pressure and temperature on the yield was also substantial, and an extract yield of 35% by weight of the dry, ash-free coal could be obtained using toluene at 420°C and 27.5 MPa pressure. It was also determined that it was not essential for the extracting fluid to be above its critical temperature to be effective. For a given operating pressure, the advantages of operating in a supercritical state were associated with the lower density and viscosity of the fluid compared with a subcritical fluid.

In another coal-related effort in the United States, Kerr-McGee Corporation has developed a new solid-liquid separation technique utilizing the unique solvent capabilities of supercritical fluids (3). The process, called Critical Solvent Deashing (CSD), is used to separate mineral matter and unreacted coal from coal liquids. A two-stage CSD pilot plant (integrated into an SRC process unit) has been operated for the last four years at Wilsonville, Alabama.

Despite the strong industrial interest and the extensive research activity in the field of supercritical extraction, much remains to be learned in the application of supercritical fluids to coal processing. An important feature of supercritical coal extraction that has received little attention in the literature concerns the specific characteristics (physical and/or chemical) of the supercritical solvent and solvent mixtures that can affect the yield and the quality of the coal extracts. Paul and Wise (4) in their excellent monograph on gas extraction used the semiquantitative approach of Rowlinson and Richardson (5) to show the strong dependence of supercritical solubility on the cross-virial coefficient B_{12} of the solvent-substrate gas phase. They also discussed empirical correlations for calculating these coefficients in relatively simple cases of nonpolar molecules. The existing B_{12} correlations, however, are most likely to prove completely unsatisfactory for polar solvents, or for solvents that are chemically (as well as physically) involved in the mechanism of coal extraction. Polar or hydrogen bonding solvents, for example, may exert a stronger dissociating or depolymerizing action on coal during the thermal fragmentation stage than nonpolar solvents, thus increasing the yield of extractable coal material.

The present paper discusses some results from the first phase of our experimental investigation into solvent and chemical-reaction effects in supercritical coal extraction. The second phase currently under way is concerned with the combination of supercritical extraction and specific chemical treatment of the coal (such as

catalytic depolymerization, alkylation, hydrogen-donor activity, etc.) to increase the yield of coal extracts and decrease the severity of the extraction conditions.

EXPERIMENTAL

All supercritical extraction experiments were carried out in batch mode, in a 1000 cm³ (free volume: 910 cm³), 316SS AE MagneDrive autoclave equipped with a digital temperature controller/indicator and a digital pressure transducer/indicator in the 0-10,000 psi range (Autoclave Engineers, Model DPS-0201). An Illinois No. 6 bituminous coal, 100x200 mesh size, was used throughout this investigation. Its proximate and ultimate analyses are included in Table 5. The coal was dried under vacuum at 110°C for 24 hours before every run.

In each run a certain amount of solvent, corresponding to the desired supercritical density, was first measured into the autoclave. Then a fine-mesh basket containing 20 grams of the dried and sized coal was suspended at the top of the autoclave, so that no actual contact between the liquid solvent and the coal sample was possible. We took this precaution to eliminate any ambiguity in the results, where a significant fraction of the coal would be soluble under supercritical conditions but insoluble when the system was brought back to ambient conditions, thus precipitating on the extracted coal and causing the extraction yields (which are based on the weight loss of the raw coal) to appear low (6). In our system any material dissolved under supercritical conditions is carried through and recovered outside the basket after the experiment, whether or not this material is still soluble.

After sealing and purging, the reactor was heated for about 1.5 hr to reach extraction temperature (400°C). Following 2 hrs of extraction, the system was cooled to room temperature (2 hrs). Yield was defined as the weight loss of the vacuum dried (24 hrs, 110°C), char-containing basket expressed as a percentage of the raw, dry-coal weight.

The results on weight-percent extraction reported in this paper were reproducible within ±0.5 wt% (absolute). Solvent recoveries after extraction ranged between 96 and 100%. Decreasing the particle size and the amount of coal sample (for a given solvent density), and increasing the extraction time had no effect on extraction yields. Therefore, the reported results reflect a condition of equilibrium extraction with no mass transfer or solvent-saturation limitations.

The extracted coal samples, as well as the supercritical extracts, were analyzed for elemental composition, heating value, and pyridine solubility.

RESULTS AND DISCUSSION

1. Non-polar Solvent Effects

To determine the effect of the physical parameters of the supercritical solvent on coal extraction, coal samples were extracted with a homologous series of n-paraffins (from pentane to dodecane), at 400°C and at a constant solvent density of 2.75 moles/liter. Results on weight-percent extraction and final extraction pressure (which is generated by the supercritical solvent itself) are given in Table 1. The critical parameters of the paraffinic solvents are listed in Table 2.

The results indicate that extraction yield increases with increasing molecular weight of the solvent, dodecane being the best supercritical solvent under the given experimental conditions. On the other hand, extraction pressure displays an interesting behavior, decreasing with increasing molecular weight of the solvent (at constant temperature and molar density), then passing through a minimum (for nonane), and finally increasing with increasing molecular weight.

Based on their experimental results on high-pressure gas chromatography, Giddings et. al. (7) suggested that the solvent power of a supercritical medium is directly related to its solubility parameter, δ . Using the van der Waals equation, they developed the following correlation:

$$\delta \left(\frac{\text{Cal}}{\text{cm}^3} \right)^{1/2} = 1.25 P_c^{1/2} \frac{\rho}{\rho_\ell} \quad 1)$$

where P_c is the critical pressure of the solvent in atmospheres,

ρ_r is its reduced density $\Delta \frac{\rho}{\rho_{\text{critical}}}$, and

ρ_λ is the reduced density of liquids, taken to be about 2.66.

It is important to note here that the above correlation is likely to prove satisfactory for non-polar solvents, but its value in predicting solvent capabilities when special solvent effects are present (polar clustering, hydrogen bonding, etc.) is very much in doubt. Blessing and Ross (6), based on a limited number of supercritical extraction experiments on coal and lignite, concluded that the extraction yield is an almost linear, universal (for a given coal) function of the solubility parameter of the solvent as calculated by the Giddings correlation, and that regardless of their structural differences, all compounds largely perform in accordance with their solvent capabilities. This is a rather arbitrary statement, taking into account the fact that only one polar solvent (methanol) was included in their plot of coal extraction versus solubility parameter of the solvent.

Using Giddings' correlation, solubility-parameter values for the homologous series of n-paraffins were calculated at the experimental solvent density of 2.75 moles/liter. The results are given in the last column of Table 2. Weight-percent extraction is plotted against solvent solubility parameter in Figure 1. As can be seen from the figure, the plot is highly linear (correlation coefficient 0.987), yielding the following correlation:

$$(\text{wt\% extraction}) = 3.05\delta + 11.2 \quad 2)$$

Table 4 includes the results on supercritical coal extraction at 400°C and three different solvent densities, for another nonpolar hydrocarbon solvent, namely toluene. Solubility-parameter values calculated from Giddings' correlation are given in the last column of Table 4. Linear regression on the toluene runs yields the following correlation (correlation coefficient 0.986):

$$(\text{wt\% extraction}) = 3.96\delta + 10.9 \quad 3)$$

A measure of the accuracy of the experimental results is the predicted value for the extraction yield at the limit $\delta \rightarrow 0$ (vacuum pyrolysis of coal), which should be the same for all solvents. Equations 2 (n-paraffins) and 3 (toluene) predict extraction limits very close to each other (11.2 and 10.9 weight percent respectively). However, contrary to the conclusion of Blessing and Ross, the extraction yield depends also on the solvent functionality. By comparing equations 2 and 3 it can be seen that toluene is a better solvent in supercritical coal extraction than straight-chain aliphatic hydrocarbons, for the same value of the Giddings solubility parameter. As we will show later the effect of functionality is even stronger for polar solvents.

It has also been suggested (Fong, et.al, (8)) that extraction yields may be affected by molecular size, and that the longest dimension of each solvent molecule should be considered when comparing the coal extraction efficiencies of various supercritical solvents. The implication here is that penetration of the micropore structure of the coal can be achieved more easily by the smaller molecules. Our results on the homologous series of n-paraffins, where dodecane, the longest molecule, proved to be the most effective extraction solvent, certainly do not support this suggestion. Mass transfer limitations do not appear to be significant in supercritical coal extraction, at least under the given experimental conditions.

The behavior of the extraction pressure at constant temperature and molar density in the homologous series of n-paraffins is worth further consideration from the standpoint of optimizing the extraction conditions. Our results, for example, indicate that n-nonane is a superior solvent than n-pentane in supercritical coal extraction, not only in terms of the higher extraction yield, but also in terms of the considerably lower extraction pressure.

The Redlich-Kwong equation of state

$$P = \frac{RT}{\hat{V}-b} - \frac{a}{T^{1/2}\hat{V}(\hat{V}+b)} \quad 4)$$

where

$$\hat{V} = \text{molar volume} = \frac{1}{\rho} \quad (\rho = \text{molar density})$$

$$a = \frac{0.4278R^2T_c^{2.5}}{P_c}, \text{ and}$$

$$b = \frac{0.0867RT_c}{P_c},$$

was used to examine the extraction-pressure trends in the homologous series of n-paraffins, under the given experimental conditions: $T = 400^\circ\text{C}$ and $\rho = 2.75$ moles/liter or $\hat{V} = \frac{1}{\rho} = 363.6 \text{ cm}^3/\text{mole}$. Critical parameters for the n-paraffins, as well as calculated values for a and b, and estimated (eq. 4) values for the extraction pressure are given in Table 2. These data show that, despite the considerable differences between estimated and observed values of the extraction pressure, especially for the higher paraffins, the Redlich-Kwong equation is able to predict the pressure minimum at almost the same solubility-parameter value as the experimental one. The structure of the Redlich-Kwong equation, and the strong dependence of the pressure on the $(\hat{V}-b)^{-1}$ term in particular, suggests a very interesting path for optimizing extraction conditions. In Table 3 we list estimated extraction pressures and solubility-parameter values for the homologous series of n-paraffins, in supercritical coal extraction at 400°C and two other molar densities. As can be seen from the table, by decreasing the molar density, the pressure minimum shifts towards the heavier hydrocarbons, which still possess the higher solubility-parameter values. Thus, by proper selection of the experimental solvent density (1.8 moles/liter in our case), dodecane becomes an excellent supercritical solvent for coal, both in terms of the highest extraction yield in the hydrocarbon series, and also in terms of the lowest generated extraction pressure.

The same solvent density considerations can, of course, be applied to any other homologous series of nonpolar compounds (e.g. aromatic hydrocarbons).

2. Polar Effects in Supercritical Coal Extraction

We are currently conducting an extensive experimental investigation on the effect of increased solvent polarity on coal extraction yields. A wide range of supercritical solvents is being studied, including simple inorganic molecules (CO_2 , H_2O , NH_3 , BF_3 , etc.), and polar hydrocarbons, particularly alcohols. Table 4 gives the results of some preliminary supercritical extraction experiments at 400°C with simple polar compounds, such as methanol, acetone and water.

Methanol gives a slightly lower extraction yield (20.6% versus 21.3%) than estimated from the Giddings correlation and equation 2. From a practical standpoint, however, methanol is far inferior a supercritical solvent than aliphatic hydrocarbons, because it gives lower extraction yields at much higher extraction pressures (20.6% at 3610 psig compared with 21.2% at 1290 psig for n-nonane).

The predictive value of equation 2 when coupled with the Giddings correlation breaks down completely for a polar solvent such as acetone, which shows anomalously low coal extraction yields at 400°C . These low yields can only in part be attributed to acetone decomposition that was experimentally observed at 400°C .

Water, on the other hand, displays large positive deviations from the estimated extraction values. For example, at 400°C and a supercritical density of 8.25 moles/liter the coal extraction yield is 34.0 wt% compared with 20.9wt%, which is the value calculated from equations 1 and 2. The results in Table 4 seem to indicate that water is an even better supercritical solvent than toluene for coal extraction, affecting high extraction yields at moderately high pressures (34wt% at $T_r=1.04$ and $P_r=1.12$). A very interesting feature of the supercritical water runs is that the extract-containing aqueous phase, when brought back to ambient conditions is an almost clear, strongly smelling solution with a minimal amount of precipitate, and in any case it is completely different from the black coal solutions obtained in supercritical toluene runs. Whether this is a result of supercritical water extracting selectively a different portion of the coal material (e.g. more of the polar, phenolic fraction) than toluene, or it is mainly a result of high-pressure reforming reactions of coal organics with supercritical water than can yield products completely different from simple supercritical extracts (9), is not clear at this point.

We are currently investigating the mechanism of supercritical water/coal interactions using model-compound systems, under similar reaction conditions ($T=400^{\circ}\text{C}$; $P_r=1.1$). We are also in the process of characterizing the toluene, methanol and water supercritical coal extracts by GPC and other analytical techniques, that will enable us to determine the differences in structure and functionality of these extracts.

3. Synergistic Effects of Solvent Mixtures

Possible non-ideal effects arising from polar/nonpolar solvent combinations were studied in supercritical extraction of coal at 400°C and constant total molar density for a series of toluene/methanol and toluene/acetone mixtures. Extraction yields and generated pressures are depicted in Figures 3 and 4.

Figure 3 for the toluene/methanol mixtures reveals a very interesting feature of the extraction curve, which passes through a maximum at a composition of approximately 70 mole% toluene and then descends slowly to the pure toluene value. This extraction maximum, which is higher than the extraction yield of either solvent alone (synergistic effect), is of even greater importance, because it is attained at a pressure much lower than the pressure generated in pure toluene extraction under similar conditions (3700 psig as compared with 5140 psig). Fong et. al. (8) observed a similar maximum-extraction effect in supercritical extraction of coal with toluene/methanol mixtures at 360°C and at a constant pressure of 2000 psig, but their results are of limited practical value, because of the constant-pressure condition that was employed (rather than constant solvent density).

Toluene/acetone mixtures, on the other hand, display almost linear dependence of both the extraction yield and the extraction pressure on molar composition. No synergistic effect is present under the given experimental conditions, so that pure toluene becomes a far superior supercritical solvent than pure acetone or any toluene/acetone mixture, effecting much higher coal extraction at a considerably lower extraction pressure.

4. Physical and Chemical Changes in Coal Structure during Supercritical Extraction

Table 5 gives proximate and ultimate analyses and heat content values for selected coal samples that were extracted with pure supercritical solvents under a variety of experimental conditions. The analysis of the raw coal that was used in all these experimental runs is also included.

The data show a drastic (more than 60% in most cases) reduction in the volatiles content and a consequent increase in the fixed-carbon content of the coal after supercritical extraction. The reduction in volatiles is accompanied by a significant increase in the C/H atomic ratio of the treated coal, thus indicating a progressive extraction of hydrogen-rich fractions from the coal matrix. It is interesting to note, however, that even at high extraction levels, the extracted coal retains most of its fuel value, as indicated by a moderate C/H ratio and a high heat-content value. For example, coal extracted with supercritical toluene at 400°C and at a solvent density of 6.75 moles/liter retains 94.7% of the specific heating value of the raw coal, despite a 36% extraction loss and a corresponding 61.7% loss of volatiles.

The data indicate, once again, that supercritical water may be one of the most promising solvents in supercritical coal extraction, affecting higher extraction yields at much lower heat-content and H/C losses (for the extracted coal) than hydrocarbon solvents (for example, compare the results of the pure toluene and the water runs).

A very interesting selective desulfurization effect is observed in supercritical extraction of coal with methanol-based solvents, and to a lesser extent with acetone and water. Ideally, if there is no special affinity of the supercritical solvent towards sulfur (or other heteroatom), the extraction of sulfur fractions from the coal matrix should be non-selective, so that the sulfur content of the extracted coal, as well as that of the extract, is in every case the same with the sulfur content of the raw coal. Our data show that, although this is true for nitrogen, sulfur undergoes strong selective extraction in the presence of methanol-based solvents.

Supercritical extraction of coal with pure methanol results in a 31.8% level of selective sulfur reduction, while the other two oxygenated solvents, acetone and water, also display significant ($\approx 23\%$) desulfurizing action on extracted coal samples. Chemical participation of the methanol in the coal-pyrolysis stage, that enhances selectively the fragmentation of sulfur clusters in the coal molecule and their subsequent extraction in the supercritical phase is proposed to be the main cause of this effect.

Finally, surface areas of extracted coal samples were measured by nitrogen adsorption at -196°C to determine the effect of possible changes occurring in the physical structure of the coal during supercritical extraction. The results are given in Table 6. A sharp decrease in the available surface area of the coal is observed in all the extracted samples, and this decrease, at least for the paraffinic series, is progressively more pronounced at higher extraction levels. Methanol-extracted coal, on the other hand, shows a higher surface-area reduction than hexane-extracted coal, despite the lower extraction level. The surface-area-reduction effect may be attributed to a shift in the pore-size distribution of the coal caused by the extractive action of the supercritical solvent. The removal of coal material from the solid matrix may result in the progressive opening of larger pore spaces, thus shifting the pore-size distribution towards the macropore range, generally associated with low specific surface areas. Swelling phenomena in the coal matrix caused by strong H-bonding solvents, such as methanol, can contribute further to the closing of smaller pores and, thus, to additional collapse of the microporous network. Fong et. al. (8) proposed a different explanation based on the retention of extract in the pores. At the end of an extraction cycle, the removal of the volatile supercritical solvent from the pores could result in partial condensation of the coal extract and, thus, in extensive pore blockage.

Concluding this section we would like to report some results on the pyridine solubility of raw and extracted coal samples. The pyridine solubilities of dried samples were determined by stirring 0.5 grams in 50 cm^3 pyridine for 2 hrs at room temperature, then filtering and evaporating the solvent, and drying the solid residue under vacuum at 110°C for 24 hrs. Results for the raw coal and for the pure toluene and pure methanol runs are given below:

Supercritical Solvent	Extraction Conditions	Weight Percent Extraction	Pyridine Solubility of Extracted Coal (%)
R A W C O A L			11.2
Toluene	400°C , 6.75 $\frac{\text{moles}}{\text{liter}}$	36.0	0.8
Methanol	400°C , 6.75 $\frac{\text{moles}}{\text{liter}}$	20.6	2.4

The pyridine solubility of coal decreases sharply after supercritical extraction, indicating that most of the coal material that is soluble in pyridine at room temperature dissolves in the supercritical solvent during the high temperature extraction.

It is also important to report here that part of the supercritical extract recovered in the toluene phase after cooling the reactor's contents to room temperature, is in the form of a precipitate, fully soluble in pyridine, and amounting to approximately 8 wt% on the basis of raw dry coal. Therefore, contrary to the claim of Blessing and Ross, a significant part of the coal material which is soluble in the solvent under supercritical conditions, becomes insoluble when the solvent is brought back to ambient conditions.

SUMMARY

The specific physical and chemical characteristics of supercritical solvents and solvent mixtures that can affect the yield and the properties of coal extracts were experimentally investigated. Strong non-ideal interactions, such as polar forces and hydrogen bonding, as well as synergistic interactions in multicomponent solvent mixtures, were shown to produce large deviations from the simple, density-driven supercritical solubility. These interactions can be manipulated to optimize supercritical coal extraction by reducing the severity of the extraction conditions (pressure in particular). Physical and chemical changes occurring in the coal structure during supercritical solvent extraction were also examined.

ACKNOWLEDGEMENTS

This work was supported by the United States Department of Energy under Grant No. DE-FG22-81PC40801 and by the Center for Energy Studies, Austin, Texas. The support of the two agencies is gratefully acknowledged.

REFERENCES

1. Gangoli, N. and Thodos, G., *Ind. Eng. Chem., Prod. Res. Dev.*, 16, 208 (1977).
2. Whitehead, J. C., "Development of a Process for the Supercritical Gas Extraction of Coal", paper presented at the 88th AIChE National Meeting, Philadelphia, June 1980.
3. Adams, R. M., Knebel, A. H. and Rhodes, D. E., *Chem. Engr. Progr.*, 75, 44 (1979).
4. Paul, P. F. M. and Wise, W. S., "The Principles of Gas Extraction", Mills and Boon Ltd., London (1971).
5. Rowlinson, J.S. and Richardson, M. J., *Adv. Chem. Phys.*, 2, 85 (1959).
6. Blessing, J. E. and Ross, D. S., "Supercritical Solvents in the Dissolution of Coal and Lignite", in "Organic Chemistry of Coal", Larsen, J. W. (ed.), ACS Symposium Series No. 71, Washington, D.C., 1978, pp. 171-185.
7. Ciddings, J. C., et. al., *Science*, 162, 67 (1968).
8. Fong, W. S., et. al., "Experimental Observations on a Systematic Approach to Supercritical Extraction of Coal", paper presented at the 89th AIChE National Meeting, New Orleans, Louisiana, November 1981.
9. Modell, M., Reid, R. C. and Amin, S. I., U.S. Patent No. 4113446, 1978.

Table 1. Supercritical extraction of coal with a homologous series of n-paraffins at 400°C and at a (constant) solvent density of 2.75 moles/liter.

Solvent	Weight Percent Extraction	Extraction Pressure (psig)
Pentane	18.43	2032
Hexane	19.26	1635
Heptane	19.70	1441
Octane	20.70	1393
Nonane	21.17	1290
Decane	22.75	1380
Undecane	23.16	1562
Dodecane	23.56	1768

Table 2. Physical solvent parameters for the homologous series of n-paraffins from pentane to dodecane.

Solvent	Critical Temperature (°C)	Critical Pressure (atm)	Critical Density (g/cm ³)	a (x10 ⁹) ¹ (cm ⁶ .atm. ³ .°K ^{1/2}) mole ²	b ¹ (cm ³ /mole)	Extraction Pressure (psig) ²	Solubility Parameter (cal ^{1/2} /cm ^{3/2}) ³
Pentane	196.6	33.3	0.237	0.4137	100.36	1680.2	2.27
Hexane	234.2	29.9	0.233	0.5586	120.72	1531	2.61
Heptane	267.1	27	0.232	0.7238	142.35	1425.9	2.90
Octane	296	24.8	0.232	0.8977	163.27	1383.3	3.17
Nonane	321	22.5	0.231	1.1017	187.87	1492.5	3.42
Decane	344.4	20.8	0.231	1.3125	211.22	1755.3	3.65
Undecane	365.2	19.2	0.230	1.5446	236.53	2363.6	3.85
Dodecane	386	17.9	0.230	1.7951	261.98	3502.1	4.05

¹ Constants of the Redlich-Kwong equation of state

² Calculated from the Redlich-Kwong equation at the supercritical extraction conditions: 400°C, 2.75 moles/liter

³ Calculated from Giddings' correlation at the supercritical extraction conditions: $\rho = 2.75$ moles/liter

Table 3. Extraction pressures calculated from the Redlich-Kwong equation of state at 400°C and two different solvent densities.

Solvent	$\rho = 2$ moles/liter		$\rho = 3$ moles/liter	
	Extraction Pressure(psig)	Solubility Parameter ¹	Extraction Pressure(psig)	Solubility Parameter ¹
Pentane	1236.2	1.65	1849.3	2.48
Hexane	1106.3	1.90	1713.3	2.85
Heptane	978.8	2.11	1650.7	3.16
Octane	863.1	2.31	1687.4	3.46
Nonane	771.8	2.49	1974.5	3.73
Decane	705.9	2.65	2538.0	3.98
Undecane	690.8	2.80	3757.3	4.2
Dodecane	727.1	2.95	6239.7	4.42

¹ Calculated from Gidding's correlation

Table 4. Supercritical extraction of coal
with various solvents at 400°C.

Solvent	Weight Percent Extraction	Extraction Pressure ¹ (psig)	Solvent Density ¹ (moles/liter)	Solubility Parameter ²
Toluene	36.0	5140	6.75	6.46
"	27.6	1440	4.0	3.83
"	20.3	1260	2.75	2.63
Acetone	4.0	2180	4.0	2.69
"	7.3	3480 ³	5.5	3.70
Methanol	20.6	3610	6.75	3.31
Water	34.0	3580	8.25	3.17
"	29.5	3070	7.08	2.72

¹ Experimental value

² Calculated from Giddings' correlation

³ Significant decomposition of acetone was observed

TABLE 5. Proximate and ultimate analyses of coal samples extracted with supercritical solvents at 400 °C

Solvent	Pentane	Octane	Dodecane	Toluene	Toluene	Methanol	Acetone	Water
Supercritical Density (moles/liter)	2.75	2.75	2.75	4.0	6.75	6.75	4.0	7.08
Weight Percent Extraction	18.43	20.70	23.56	27.6	36.0	20.6	4.0	29.5
<u>Proximate Analysis¹ (%)</u>								
Volatiles	42.3	21.9	25.4	21.6	25.3	24.6	23.1	18.1
Fixed Carbon	43.6	59.4	55.4	58.0	53.4	57.5	60.4	64.0
Ash	14.1	18.7	19.2	20.4	21.3	17.9	16.5	17.9
<u>Ultimate Analysis¹ (%)</u>								
Carbon	62.9	62.2	67.8	61.8	63.6	56.9	53.2	55.6
Hydrogen	4.7	3.5	3.7	3.1	3.1	3.6	3.7	3.2
Nitrogen	1.1	1.1	1.2	1.1	1.1	1.1	0.8	1.0
Sulfur	4.4	4.1	4.2	4.1	3.9	3.0	3.4	3.4
Oxygen (by difference)	26.9	29.1	23.1	29.9	28.3	35.4	38.9	36.8
Heating Value (Btu/lb)	11415	11560	11510	10980	10805	11690	12280	11510
C/H ratio	1.11	1.48	1.53	1.66	1.71	1.32	1.20	1.45
‡ Sulfur reduction	0	6.8	4.5	6.8	11.4	31.8	22.7	22.7

¹On a dry basis

Table 6. Nitrogen-surface areas of coal samples extracted with various supercritical solvents at 400°C.

Solvent	Raw Coal	Hexane	Decane	Undecane	Dodecane	Methanol
Supercritical density ($\frac{\text{moles}}{\text{liter}}$)	-	2.75	2.75	2.75	2.75	6.75
Weight percent extraction	0	19.3	22.8	23.2	23.6	20.6
N ₂ surface area (m ² /g)	38.4	12.7	3.0	2.5	2.4	1.6
Surface-area reduction (%)	0	66.9	92.2	93.5	93.8	95.8

HOMOLOGOUS SERIES OF N-PARAFFINS

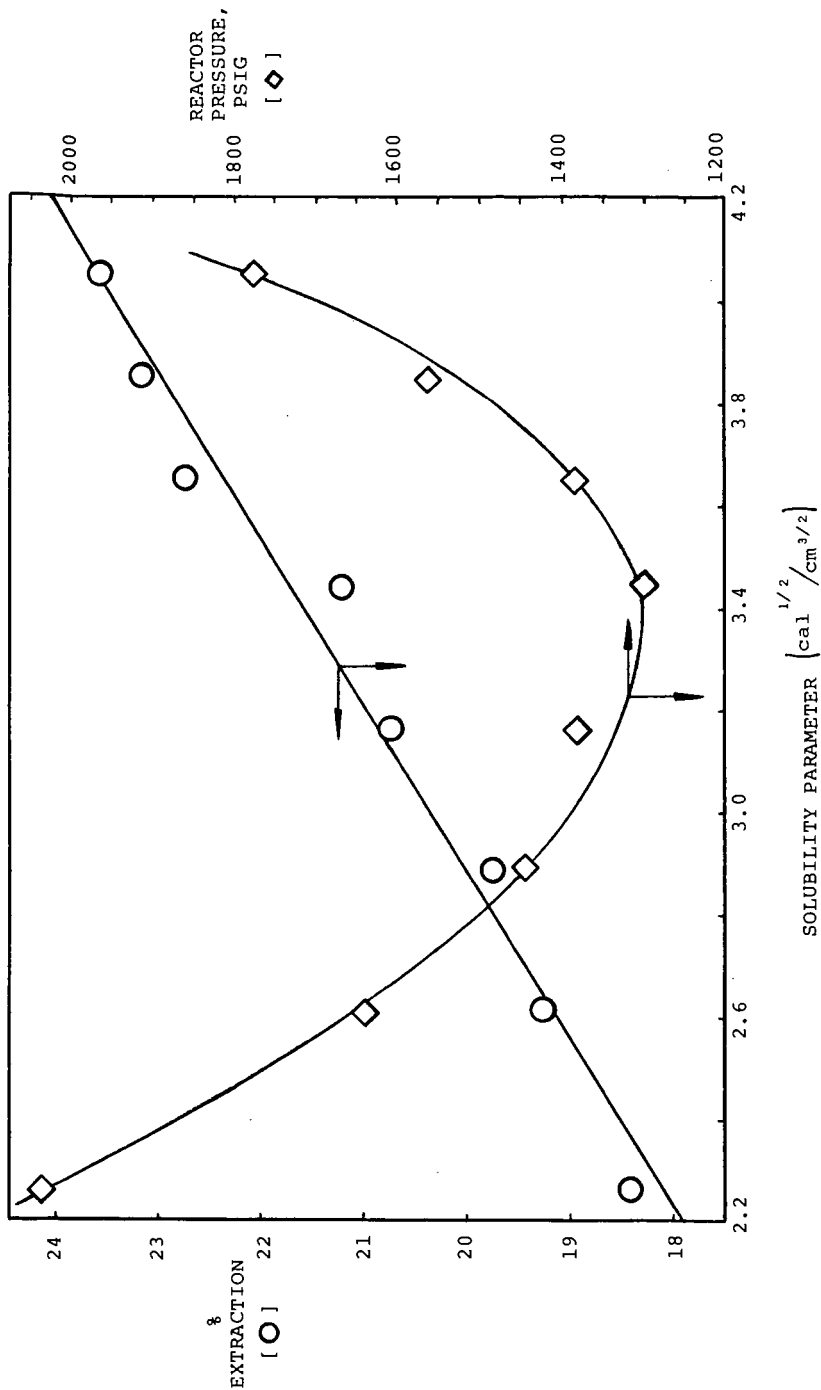
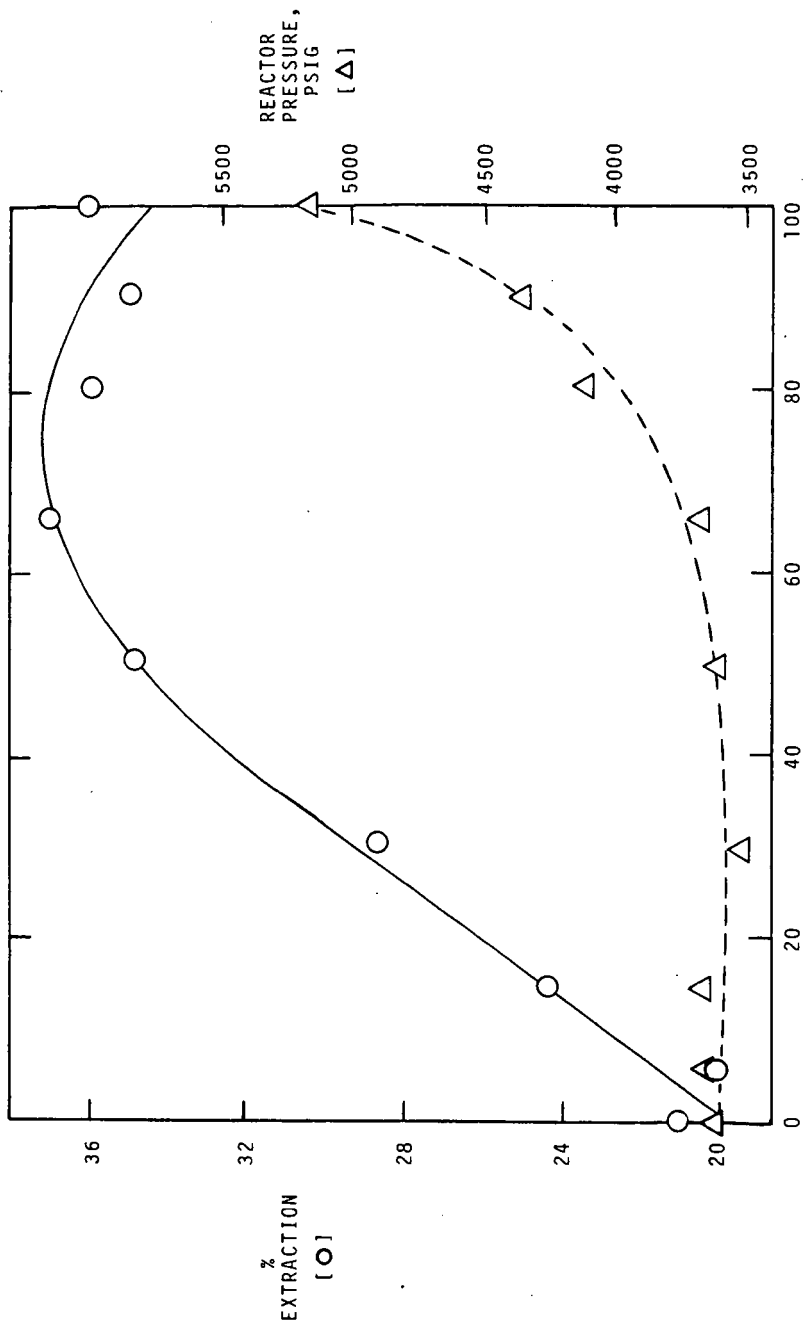


FIG. 1

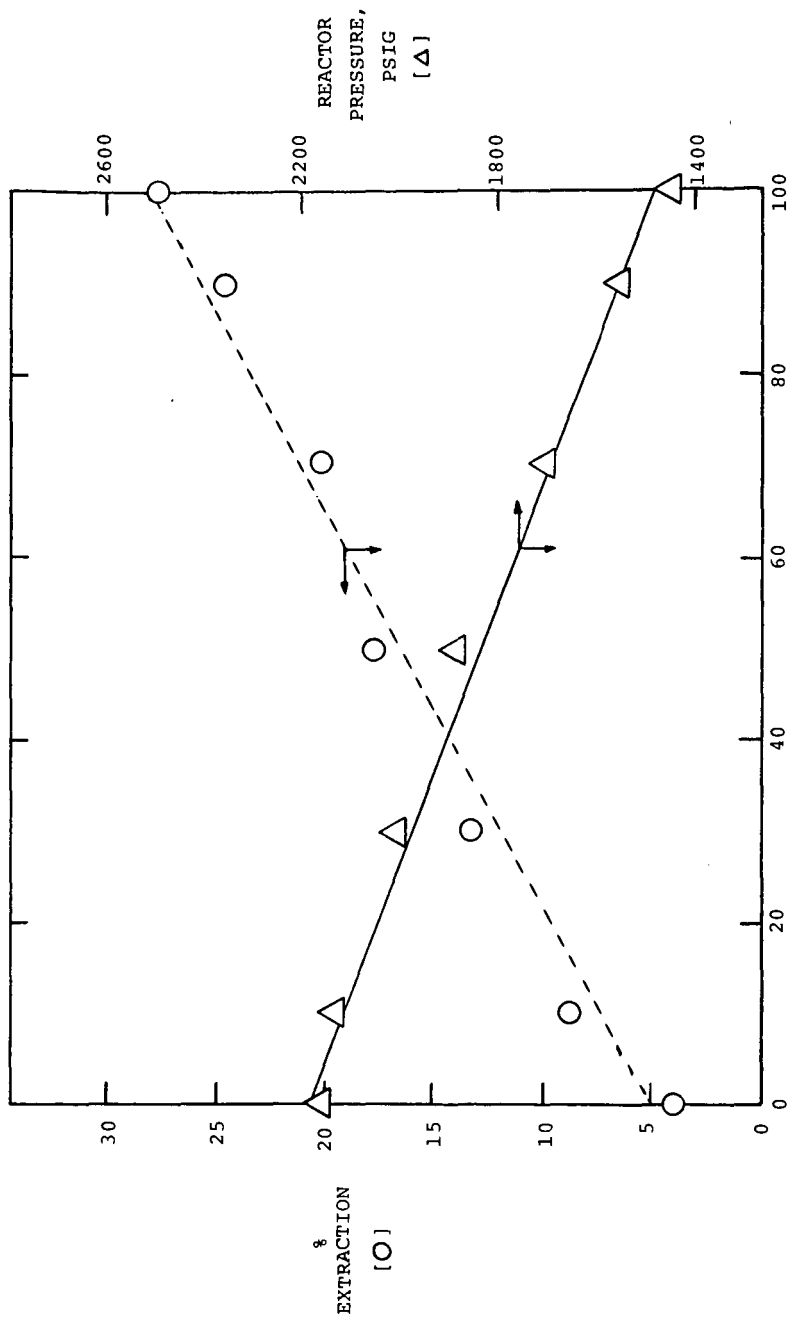
TOLUENE-METHANOL MIXTURES



MOLE % TOLUENE

FIG. 2

TOLUENE-ACETONE MIXTURES



MOLE % TOLUENE

FIG. 3

THE ROLE OF THERMAL CHEMICAL PROCESSES IN SUPERCRITICAL GAS EXTRACTION OF COAL

Thomas G. Squires*, Tetsuo Aida, Yu-Ying Chen, and Barbara F. Smith

Energy & Mineral Resources Research Institute
Iowa State University, Ames, Iowa 50011

INTRODUCTION

Many factors which limit the chemical conversion of insoluble, solid coal to soluble, smaller fragments are due to phenomena which are not routinely encountered in the chemical laboratory or in the chemical processing industry. In the first place, it often appears that the rate and extent of coal conversion is controlled by accessibility to reaction sites rather than by reaction energetics¹. Secondly, the chemical objective, depolymerization, is exactly the reverse of that of a major segment of the present chemical processing industry. While these observations are obvious, the implications for coal conversion are far reaching; and much of our recent research effort has focused on understanding the effects of these phenomena. Problems which limit the efficiency of current coal conversion processes are not necessarily amenable to solution using conventional solvents, standard reactor configurations, or other established chemical conversion concepts.

Currently, we are investigating supercritical fluids (SCF's) as solvents for extracting and chemically converting coal. The advantages of SCF's as solvents for coal extraction have been recognized for some time². Near the critical temperature, the solvent power, viscosity, and diffusion rates can be manipulated over wide ranges by relatively small changes in pressure or temperature³. Thus, SCF's have been touted as solvents which, by suitable manipulation of temperature and pressure, enhance both reagent access to interior reaction sites in coal and product removal from the microporous coal residuum. One of the primary objectives of the present research is to compare the efficacy of subcritical and supercritical solvents in this mass transport function.

In practice, most supercritical gas extractions (SGE's) of coal have been conducted at temperatures above 325°C⁴. While some investigators have acknowledged a thermal chemical contribution to these extractions⁵, others have reasoned that thermal processes are unimportant at 350°C⁶. Still others have sought to elucidate the thermal behavior of coal by investigating model compounds⁷. In any case, the thermal chemical component in SGE of coal has not been experimentally defined, and this is another important objective of our investigations.

Thermal conversion of coal to smaller fragments is best interpreted on the basis of three types of chemical processes. Primary reactions involving thermolysis of weak bonds generate smaller reactive fragments in conjunction with reactive sites within the coal residua. These reactive intermediates can then undergo two kinds of secondary reactions: stabilization to produce tar and light gases; and retrogressive recombination of the fragments and residua to produce refractory char. Obviously maximum liquid yields are obtained under conditions which promote stabilization reactions and inhibit retrogressive char-forming reactions.

In some liquefaction processes, the former objective has been accomplished by introducing a hydrogen donor stabilizing reagent into the conversion mixture^{8,9}. Other processes have sought to achieve the latter objective by heating the reaction mixture rapidly and limiting the reaction time⁹. While this approach has been partially effective, it does not address the root of the problem: intimate contact between reactive fragments and residua at elevated temperature for long periods.

Rapid vacuum pyrolysis of a thin bed of coal effectively minimizes retrogressive char-forming reactions by continuous removal of volatile tar fragments as they are generated¹⁰. Given the effectiveness of this approach to inhibiting char forming reactions, it is surprising that the concept has not been applied to other thermal liquefaction processes. Yet virtually all of these processes operate in the batch mode. Even those processes which purport to operate in a flow mode are not designed to quickly separate reactive coal fragments from reactive coal residua. Moreover, researchers in this area have directed little or no effort to exploring such ideas. Most investigators continue to employ batch mode techniques in which coal fragments and residua are mixed at elevated temperatures for substantial periods. Under such conditions, it is impossible to distinguish between primary and secondary products in a system as complex as coal. Therefore, a third important objective of this research is to develop a flow mode reactor system capable of rapidly separating coal fragments from residua and to investigate primary and secondary reactions in the chemical conversions of coal.

EXPERIMENTAL

General

Illinois #6 coal from the Ames Lab Coal Library was used in these studies. This coal has the following ultimate analysis (dmmf basis): 78.82% C; 5.50% H; 1.59% N; 2.29% S_{org}; and 10.05% ash. Prior to use, this coal was ground, sized to 60 x 100 mesh and dried at 110°C overnight under vacuum. Weight loss, extent of devolatilization, and extraction yields are reported on a raw coal basis.

Vacuum Pyrolysis

Vacuum pyrolysis experiments were conducted with a constant voltage heated grid apparatus¹¹ surrounded by a water jacketed condenser for collecting the tar and equipped with a liquid nitrogen cold finger condenser for collecting the light gases. In a typical experiment, 200 mg of Illinois #6 coal and a Chromel-Alumel microthermocouple were placed in the grid, and the system pressure was adjusted to 0.25 mm by bleeding He into the system. This slow He purge was maintained throughout the run, and the pressure and temperature were continuously monitored. The grid was then heated at an initial rate of approximately 200°C/min. to the programmed final temperature where it was maintained for 60 minutes. The extent of devolatilization was determined by measuring the weight of char remaining in the grid.

Coal Extraction with Methanol

Flow mode extraction of coal with methanol was carried out in the an apparatus described previously¹². A booster heating tape was wrapped around the reactor to provide rapid heat up capability. Coal (ca. 500 mg.) was placed in the tubular reactor, and the ends were sealed with 2 micron stainless steel frits. The free volume in the loaded reactor was found to be 0.70 ml. After connecting the reactor and purging the entire system with nitrogen, the apparatus was filled with methanol and pressurized. In rapid sequence, the reactor was inserted into the preheated furnace; and, as flow through the reactor was initiated, the reactor booster heater

was switched on. The heating profile for this reactor was approximately equivalent to that of the heated grid. A stable final temperature was attained in less than 5 minutes, and the booster heater was switched off. Throughout the extraction constant temperature, pressure, and flow rate (0.8-1.0 ml/min.) were maintained. After extracting for two hours, the system was purged with N_2 and cooled to room temperature. The reactor residuum was removed, dried in a vacuum oven at 110°C overnight, and weighed to determine the extent of extraction.

Solvent Extraction of Coals and Residua

Coal (ca. 500 mg) or residuum (ca. 100 mg) was mixed with 10 ml of pyridine and ultrasonically irradiated under ambient conditions for 30 minutes. The resulting mixture was filtered with suction through a 3 micron Millipore filter, and the solid was washed with an additional 10 ml of solvent. After drying overnight at 110°C under vacuum, the solid was weighed to determine the extent of extraction.

RESULTS AND DISCUSSIONS

The primary objectives of our investigations of the SGE of coal are the following:

- (1) To differentiate the extractive and pyrolytic components of this process;
- (2) To explore flow mode concepts as a mean of inhibiting secondary reactions by rapidly removing products from the reaction zone;
- (3) To compare the effectiveness of subcritical and supercritical solvents in the extraction of coal.

Progress toward the first two objectives has been achieved through two parallel series of experiments.

Extractive and Pyrolytic Phenomena

In the first series of experiments, weight loss of an Illinois #6 coal was determined as a function of the final coal bed temperature using a heated grid vacuum pyrolyzer. The recorded bed temperature was up to 50°C less than the blank grid temperature measured under the same conditions. While the experimental difficulty of measuring the actual bed temperature is recognized¹⁰, we have reported the bed temperature because the grid temperature is assuredly attenuated by heat transfer inefficiencies and because it is the bed temperature that actually effects the coal pyrolysis. The room temperature pyridine solubility of each of the grid residua was also determined. Results from these experiments are reported in Table 1 and plotted in Figure 1.

The occurrence of two types of thermal processes are revealed by Figure 1. The first process, which occurs at a final temperature of approximately 200°C, apparently alters the solid coal structure in a way that reduces its pyridine extractibility. While this may be a physical alteration, one chemical change which would explain this is the formation of crosslinks. Whatever the cause, heating and maintaining the coal at 200°C decreases its ambient solubility in pyridine and, presumably, other solvents as well.

The onset of the second process, devolatilization, is clearly evident at 300 to 350°C. Such behavior has consistently been interpreted as resulting from thermalolysis of weak bonds in coal^{10,13}. An acceleration of these pyrolytic processes, as manifested by more extensive devolatilization, is evident at higher temperatures, e.g. 32% weight loss at 528°C. It is important to note that residua which derive from final temperatures above 350°C are minimally soluble in pyridine.

A parallel series of experiments were conducted using a short residence time flow mode reactor. Flow rates were adjusted so that methanol residence times in

the reactor were less than one minute, and experiments were conducted to determine the effect of extraction time on SGE yields at 320°C and 3000 psi. These results, which are included in Table 2 (Runs 8 and 9), establish that over 90% of the ultimate extraction has been accomplished within 30 minutes under these conditions. On this basis, extraction times of two hours (corresponding to a total extraction volume of 100 to 120 ml) were used for the remainder of the extractions. The two hour extraction yields (at 3000 psi) were then determined as a function of temperature; and these results and the pyridine extractibility of the residua are included in Table 2 and plotted in Figure 2.

The weight loss-temperature profile from these experiments, shown in Figure 2, is remarkably similar to the profile generated by the heated grid experiments. By 200°C a chemical or physical change has occurred which depresses the total extractibility of the coal, and the onset of extensive pyrolysis is again evident above 325°C. The coincidence of these thermal phenomena in the heated grid pyrolyses and the methanol flow mode extraction of Illinois #6 coal is clear evidence that thermal decomposition processes cannot be ignored in SGE experiments conducted above 325°C. These results are in substantial agreement with those of Slomka and Rutkowski in their investigations of toluene ($T_c=320^\circ\text{C}$) flow mode extractibility of an equivalent Polish coal¹⁴. By determining the extraction yield as a function of time and temperature, they found these extractions to be controlled by two distinct energies of activation. Between 200 and 320°C, E_a was about 3kJ/mole which is consistent with the operation of diffusion controlled, physical dissolution process. At higher temperatures (350-410°C), E_a was found to be 101 kJ/mole, and this can be taken as clear evidence for the operation of chemical processes.

In fact when considered in conjunction with the investigations of Slomak and Rutkowski, our experiments provide compelling evidence that, above 350°C, the SGE of coal is controlled by thermal decomposition processes rather than physical extraction processes. In light of this finding, it is surprising to discover a correlation between conversion yields and Hildebrand solubility parameters (δ) for the SGE of coal above 325°C^{4,5}. Yields should be influenced by the chemical nature of the solvent in this temperature range, and any correlation with δ must be coincidental or due to secondary effects.

Flow Mode vs. Batch Mode Extraction

In the flow mode extraction of coal with methanol utilized for these studies, the coal extract, once generated, is in contact with the residua for less than a minute. Although this time is long by molecular standards, it is short compared to contact times (45-100 minutes) in batch extraction of coal. While these considerations are not important below 325°C, they can certainly determine the efficiency and extent of SGE at higher temperatures. At 400°C, one can hardly expect a coal-like fragment to be chemically inert under conditions which cause coal to react or during various encounters with other fragments, residua, and reactive intermediates derived from these species.

The efficacy of flow mode extraction in minimizing secondary, char-forming reactions is demonstrated by the experiments reported here. Previous investigators⁴ have reported maximum methanol extraction yields of 19% at 450°C. In the present investigation a yield of 31% was obtained, indicating that, in the batch mode, at least one-third of the liquid product is lost to char.

Finally, other investigators⁵, using batch mode extraction, have been able to extract up to 12% of the extraction residua with pyridine. Presumably, this is due to extraction inefficiencies and to redeposition of solubilized material. Our results clearly show that this residual pyridine soluble material can be removed using flow mode extraction.

ACKNOWLEDGEMENT

This material was prepared with the support of the U. S. Department of Energy, Grant No. DE-FG22-82PC50786. However, any opinions, findings, conclusions, or recommendations expressed herein are those of the authors and do not necessarily reflect the views of DOE.

REFERENCES

1. Larsen, J. W.; Green, T. K.; Choudhury, P.; Kuemmerle, E. W. In "Coal Structure"; Am. Chem. Soc. Adv. Chem. Ser. 1981, 192, 277.
2. Paul, P. F. M.; Wise, W. S. "The Principles of Gas Extraction;" Mills and Boon: London, 1971.
3. Schneider, G. M. Angew. Chem., Int. Ed. Engl. 1978, 17, 716.
4. Jezko, J.; Gray, D.; Kershaw, J. R. Fuel Processing Tech. 1982, 5, 229 and references cited therein.
5. Blessing, J. E.; Ross, D. S. In "The Organic Chemistry of Coal"; Am. Chem. Soc. Symp. Ser. 1978, 71, 171.
6. Larsen, J. W.; Yurum, Y.; Sams, T. L. Fuel 1983, 62, 476.
7. a. Poutsma, M. L. Fuel 1980, 59, 335.
b. Hung, M.-H.; Stock, L. M. Fuel 1982, 61, 1161.
c. Brucker, R.; Kolling, G. Brennstoff-Chemie 1965, 46, 41.
d. Schlosberg, R. H.; Ashe, T. R.; Pancirov, R. J.; Donaldson, M. Fuel 1981, 60, 155.
8. Gorin, E. In "Chemistry of Coal Utilization. Second Supplementary Volume"; Elliott, M. A., Ed., Wiley-Interscience: New York, 1981; Chapter 27.
9. Whitehurst, D. D. "Coal Liquefaction Fundamentals"; Symp. Ser. No. 139, Am. Chem. Soc.: Washington, DC, 1980.
10. Freihaut, J. D.; Zabielski, M. F.; Seery, D. J. Nineteenth Symposium (International) on Combustion, The Combustion Institute 1982, p. 1159 and references cited therein.
11. Anthony, D. B.; Howard, J. B.; Meissner, H. P.; Hottel, H. C. Rev. Sci. Instrum. 1974, 45, 992.
12. Koll, P.; Metzger, J. Angew. Chem., Int. Ed. Engl. 1978, 17, 754.
13. Solomon, P. R.; et. al. Fuel 1981, 60, 342.
14. Slomka, B.; Rutkowski, A. Fuel Processing Tech. 1982, 5, 247.

TABLE 1. THERMAL CONVERSION OF ILLINOIS #6 COAL BY HEATED GRID VACUUM PYROLYSIS

Run No.	Final Bed Temperature °C	Weight Loss: ^a RVP ^b %	Weight Loss: ^a PyE ^c %	Weight Loss: ^a Total %
Coal	-	-	10.2	-
1	191	0.2	8.6	8.8
2	248	0.8	6.0	6.8
3	326	6.1	-	-
4	337	5.7	2.3	8.0
5	448	19.7	1.0	20.6
6	448	21.1	0.9	22.0
7	528	32.3	0.7	33.0

^aWeight loss based on raw coal.

^bRapid vacuum pyrolysis.

^cPyridine extractibles.

TABLE 2. FLOW MODE EXTRACTION OF ILLINOIS #6 COAL WITH METHANOL

Run No.	Extraction Temperature °C	Extraction Pressure psi	Weight Loss: ^a FME ^b %	Weight Loss: ^a PyE ^c %	Weight Loss: ^a Total %
1	25	3000	2.6	9.7	12.3
2	100	3000	4.0	7.8	11.8
3	220	3000	7.4	0.6	8.0
4	270	1325	5.6	-	-
5	270	2000	8.3	-	-
6	270	3000	12.0	(0.9) ^d	12.0
7	270	4000	12.3	-	-
8	320	3000	12.0 ^e	-	-
9	320	3000	13.0	1.1	14.1
10	370	3000	22.0	-	-
11	420	3000	31.0	0.9	31.9

^aWeight loss based on raw coal.

^bFlow mode extraction.

^cPyridine extractibles.

^dWeight increase due to pyridine retention by the residuum.

^eExtraction time 30 minutes.

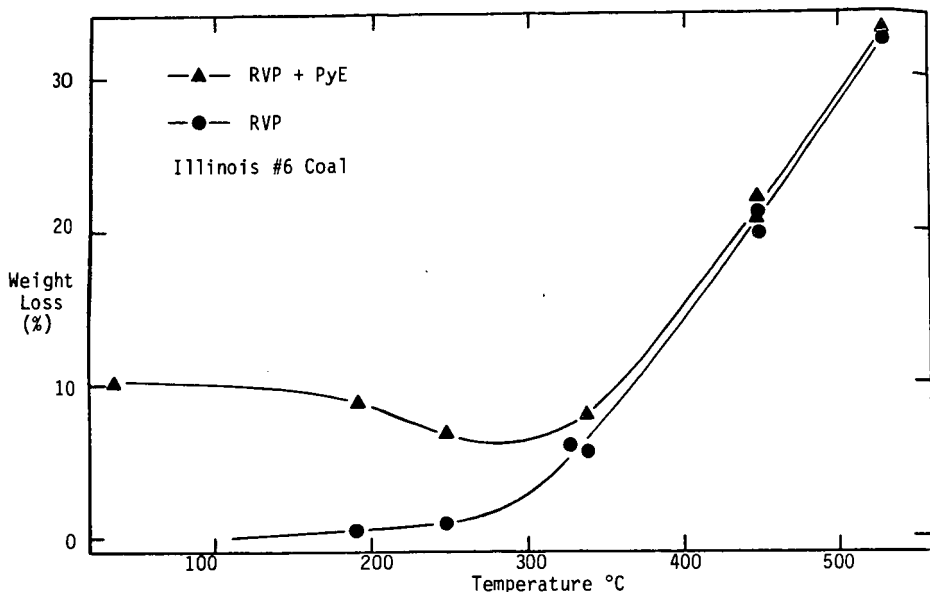


FIGURE 1. Effect of Final Temperature in Rapid Vacuum Pyrolysis

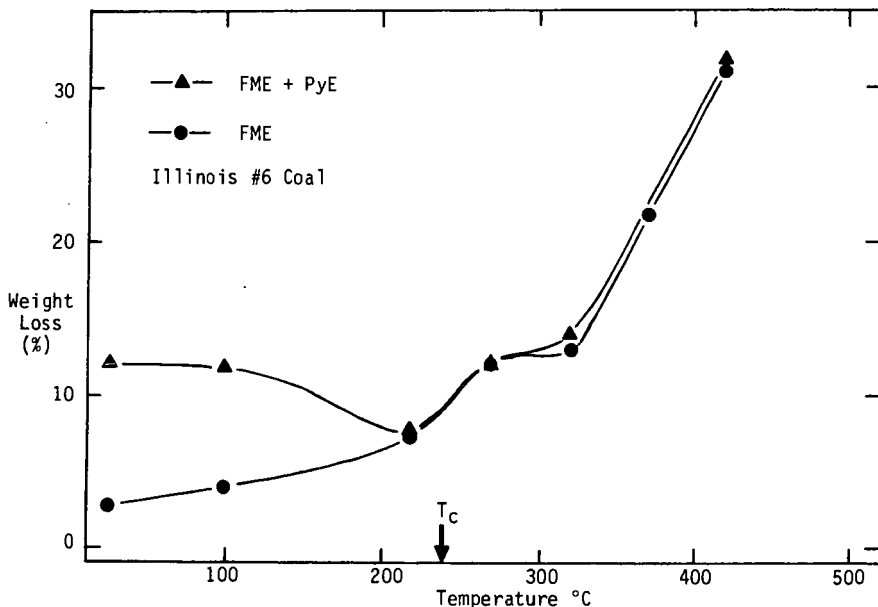


FIGURE 2. Effect of Final Temperature in Methanol Flow Mode Extraction

SUPERCRITICAL FLUID METHODS FOR COAL EXTRACTION, SEPARATION, AND ANALYSIS
R. D. Smith*, B. W. Wright, and H. R. Udseth
Chemical Methods and Kinetics Section
Pacific Northwest Laboratory (Operated by Battelle Memorial Institute)
Richland, WA 99352

INTRODUCTION

Supercritical fluids are attracting increased interest for media for coal liquefaction and gasification, the basis for new separation techniques, and in new analytical techniques for the separation and characterization of coal-derived products. On-going research at Pacific Northwest Laboratory (PNL) is examining a range of supercritical fluid applications, including their use as a reaction media for coal liquefaction and for separation of fuels and coal-derived products. Other programs at PNL are studying the applications for analysis of fuel samples using supercritical fluid chromatography (SFC), the new technique of direct fluid injection-mass spectrometry (DFI-MS), and their combination (SFC-MS). In this report we will present an overview of the range of supercritical fluid applications at PNL related to coal and fuel separation and characterization.

EXPERIMENTAL

Two similar instruments have been utilized in our supercritical fluid studies to date. The first is a micro-scale supercritical fluid extraction/reaction facility designed to allow the rapid study and characterization of the fluid phase under a wide range of conditions. The second instrument is utilized for analytical studies which include direct fluid injection-mass spectrometry⁽²⁾ and capillary column supercritical fluid chromatography-mass spectrometry⁽³⁾. The instrumentation has been described previously⁽¹⁻³⁾. Figure 1 shows a schematic illustration of the DFI-MS instrumentation. Instrumentation for direct supercritical fluid extraction involves replacement of the injector by an extraction cell containing the material to be studied, while SFC-MS involves addition of a suitable open tubular capillary column between the injector and DFI probe⁽³⁾.

RESULTS AND DISCUSSION

The direct fluid injection (DFI) method allows any compound soluble in a supercritical fluid to be transferred to the gas phase for ionization using conventional methods⁽²⁾. Recent work at PNL has led to the design and development of Supercritical Fluid Extraction-Mass Spectrometer (SFE-MS) utilizing the DFI concept. The DFI method has the following advantages: quantitation is straightforward; the process is applicable to essentially any compound; various CI reagents may be selected to vary the degree of spectral complexity (fragmentation); and the technique is inherently sensitive.

The DFI probes have been designed to couple with the direct probe inlet of a modified "simultaneous" chemical ionization-electron impact (CI-EI) ion source⁽¹⁻³⁾. Chemical ionization provides both excellent sensitivity and flexibility due to the potential for the addition of different or mixed CI reagent gases. For cases where additional structural information is necessary for identification one can use either more energetic mixed CI reagents or the collision-induced-dissociation (CID) capability of the tandem quadrupole analyzer. The use of CI analysis for coal extraction is particularly attractive since the gentle ionization mechanism produces primarily protonated molecular ions (MH^+), which allows information on the molecular weight distribution to be obtained directly from the mass spectra. The DFI interface has also allowed the first practical supercritical fluid chromatography (SFC) -mass spectrometer instrumentation to be developed⁽³⁾. The combi-

nation of the selective extraction from substrate materials and detection with more selective collision induced dissociation tandem mass spectrometric methods (e.g., MS/MS) offers a particularly effective rapid analytical method for complex coal extraction and related coal-derived mixtures.

The last few years have seen a dramatic growth in the application of supercritical fluid extraction methods to a variety of extraction, separation, and process areas. The strong and often selective solvating power of supercritical fluids under controlled conditions often allows extraction of specific compounds (e.g., caffeine from coffee, PCB's from transformer oils, etc.) from complex matrices, as well as efficient extraction of a wide range of compounds under more severe conditions. Under more extreme conditions the "extraction" process for materials such as coal is undoubtedly a combination of chemical reactions resulting in breakdown of the complex matrix combined with the extraction-distillation process of the supercritical fluid.

The present methods for direct analysis of coal supercritical fluid extraction (SFE) processes involves the continuous removal of a small sample from an extraction cell for direct mass spectrometric analysis. A high pressure syringe pump, modified for pressure regulation, is used to maintain the desired pressure in the extraction cell. The extract is transported using a 25 cm length of 100 μm I.D. platinum-iridium tubing through the DFI probe which is maintained at the same temperature as the extraction cell. The entire sample line volume is approximately 2 μL and, for our typical flow rates of 10-30 $\mu\text{L}/\text{min}$, the time from extraction to analysis is less than one minute. Fluid from the cell is injected directly into the CI region of a "simultaneous" dual EI-CI source where a constant pressure is maintained. The mass spectrometer, programmable pressure regulated pump, oven temperature controller and data acquisition hardware are all interfaced for complete computer control(3).

The supercritical fluid phase reaction or extraction process can be studied under both nonisothermal and nonisobaric conditions. Small extraction cell volumes allow evaluation of compounds extracted as a function of pressure for the determination of "threshold pressures" for the solubility of individual components. The effects of catalysts can be studied in the extraction cell or a subsequent separate reaction cell. Large reaction volumes allow one to observe the fluid phase processes as a function of either temperature or pressure, where the parameter is varied in some known fashion with time. For large reaction cells (>50 mL) the actual loss due to mass spectrometric sampling (<25 $\mu\text{L}/\text{min}$) can be made insignificant for reasonable reaction times.

An example of preliminary nonisobaric studies is given in Figure 2. A 40 mg sample of a bituminous coal, sized to approximately 80 μm average particle size and previously washed with pentane, was packed into a 75 μL cell for these experiments. The extraction temperature was 280°C and the solvent was a 95% n-pentane-5% 2-propanol mixture; thus the temperature was maintained well above the estimated critical temperature of the solvent mixture. The "gentle" CI conditions result in little molecular fragmentation and a dominant protonated molecular ion, greatly simplifying mass spectral interpretation. The experiment shown in Figure 2 involved an initial 2 hr period at 10 atm after which the pressure was increased at a rate of 0.4 atm/min between 10 atm and 100 atm. Figure 2 gives reconstructed single ion profiles for several typical ions in the mass spectra and the total ion current (TIC) or extraction profile, which serve to illustrate the solubility of extractable components as a function of pressure. Large groups of compounds are clearly extracted in the 10-13 atm and 25-28 atm ranges and similar results showing greater structure are obtained with slower pressure ramps. Between 40 and 80 atm a large amount of complex higher molecular weight material is extracted. Mass spectra for these conditions show that species having molecular weights extending to over 1400

are extracted(1). These results demonstrate the potential for direct mass spectrometric monitoring of supercritical fluid extraction of coal and other related processes. Initial experiments show significant structure in the extraction profiles, suggesting that the potential exists to readily alter the extracted product slate and to obtain significant product fractionation. Approximately 20% of the coal is extracted under these conditions, in reasonable agreement with previous studies.

An example of the application of DFI-MS for fuel characterization is given in Figures 3 and 4. These figures give DFI-mass spectra for four fractions of two diesel fuel marine (DFM) samples, obtained by an alumina column fractionation method, which has been described previously(4). These DFM samples, designated 81-5 and 81-6, represent a typical fuel (81-5) and a fuel which has been determined to exhibit considerable instability and particulate formation (81-6). The first two (less polar) fractions (A-1 and A-2) contain materials which appear to be nearly totally soluble in supercritical carbon dioxide (34°C, 450 atmospheres), and mass spectra representative of the mixtures are obtained (Figure 3). In contrast, however, the more polar A-3 and A-4 fractions exhibit very limited solubility in supercritical CO₂. Good spectra are obtained, however, in supercritical ammonia (134°C, 400 atmospheres). Since these spectra were obtained using relatively "gentle" chemical ionization reagents (isobutane for the A-1 and A-2 fractions and ammonia for the A-3 and A-4 fractions) only limited ionic fragmentation is anticipated in the spectra, with domination by the protonated molecular ion, (M+1)⁺. Thus, the DFI mass spectra provide a good measure of the molecular weight distribution of these materials. Comparison of the two relatively non-polar fractions, A-1 and A-2, indicates these fractions, which account for the bulk of the DFM, are quite similar. In contrast, however, comparison of the polar fractions (the A-3 and more polar A-4 fraction) indicates that fuels having greater instability have significantly greater contributions in the 150 to 300 molecular weight region in the A-3 fraction, and substantial contribution in the 300 to 500 molecular weight region, essentially absent for more stable fuel. These results are consistent with the greater amount of material observed in these fractions for the unstable DFM and with the gas chromatography results for the portions which are chromatographable. Research is presently in progress to apply supercritical fluid chromatography techniques using more polar fluids for separation of these materials, in conjunction with analysis by on-line DFI-MS. The much higher chromatographic efficiencies possible with SFC, in conjunction with DFI-MS analysis, promises significant advances for characterization of fuels and coal-derived materials.

ACKNOWLEDGEMENTS

This work has been supported primarily by the U.S. Department of Energy under Contract DE-AC06-76RLO 1830. Portions of this work have also been supported by the Naval Research Laboratory. We wish to thank Dr. R. N. Hazlett of the Naval Research Laboratory for providing DFM samples and for helpful discussions.

REFERENCES

1. R. D. Smith and H. R. Udseth, Fuel, in press.
2. R. D. Smith and H. R. Udseth, Biomed. Mass Spectrom., in press.
3. R. D. Smith, W. D. Felix, J. Fjeldsted, and M. L. Lee, Anal. Chem., **54**, 1883 (1982).
4. D. W. Later, M. L. Lee, K. D. Bartle, R. C. Kong, and D. L. Vassilaros, Anal. Chem., **53**, 1612 (1981).
5. R. N. Hazlett, personal communication.

DIRECT FLUID INJECTION - MASS SPECTROMETER

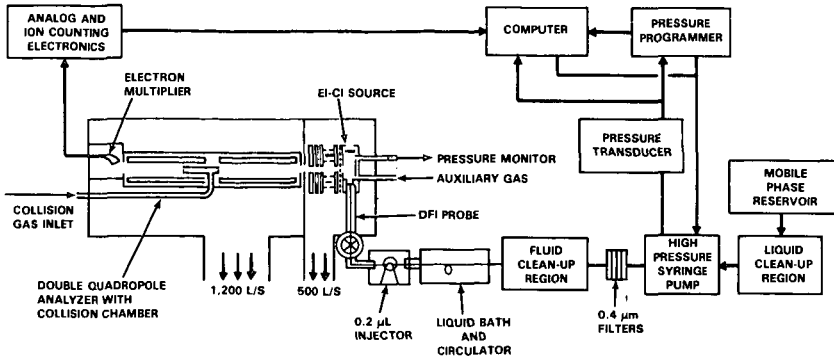


FIGURE 1. Schematic Illustration of the Direct Fluid Injection-Mass Spectrometer. Similar Instrumentation is Used for SFC-MS and Direct Supercritical Fluid Extraction Studies.

SUPERCritical COAL EXTRACTION PROFILES AT 280°C

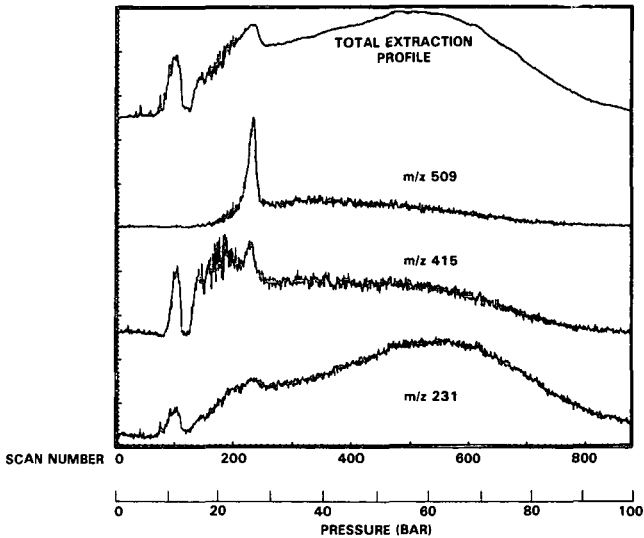


FIGURE 2. Selected Ion Profiles and Total Extraction Profile for a Nonisobaric Supercritical Fluid Coal Extraction Study Using a 95% Pentane-5% 2-Propanol at 280°C.

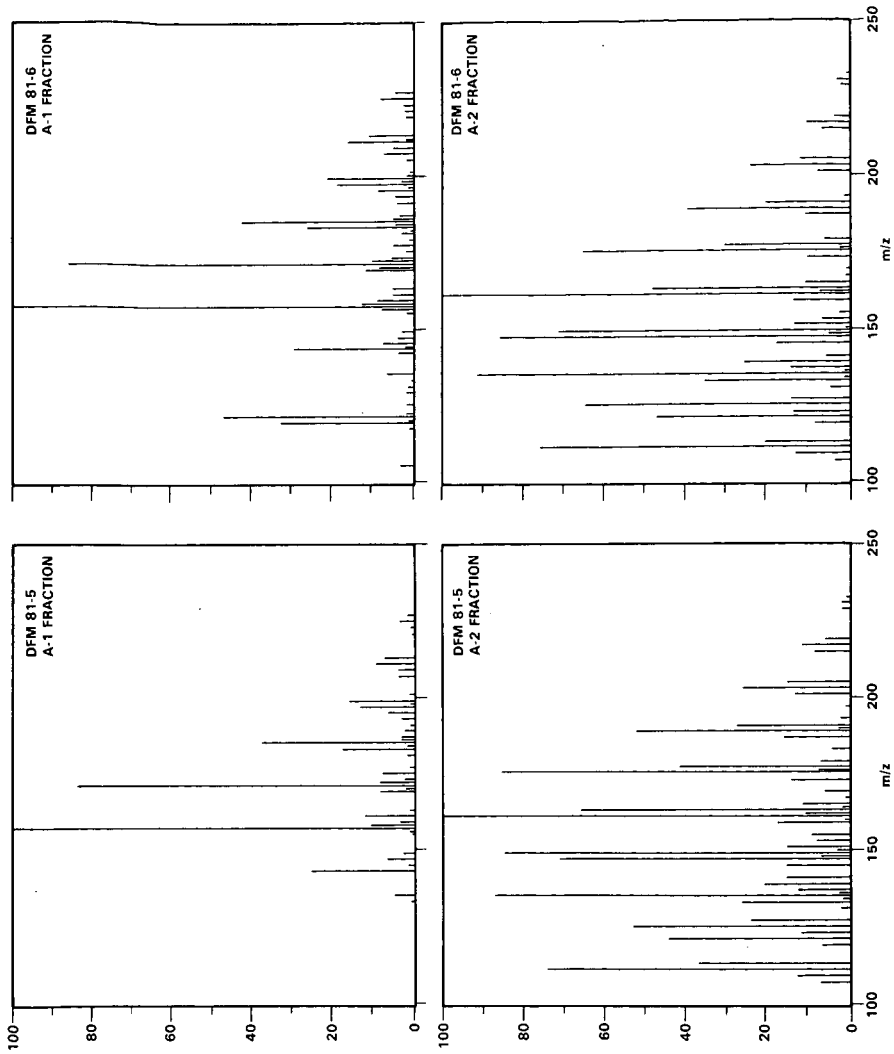


FIGURE 3. DFI-Mass Spectra Using Supercritical CO₂ for the A-1 and A-2 Fractions of Two Diesel Fuel Marine Samples.

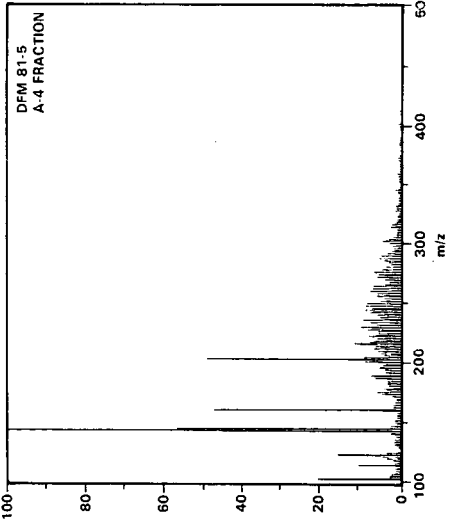
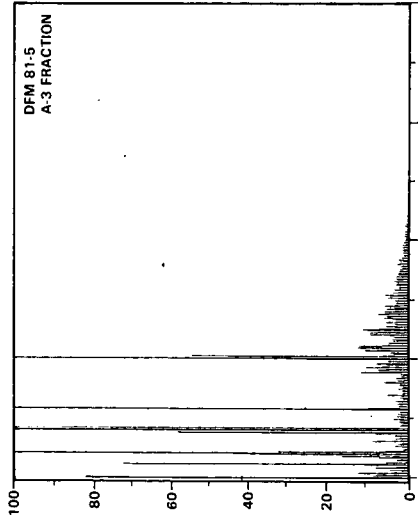
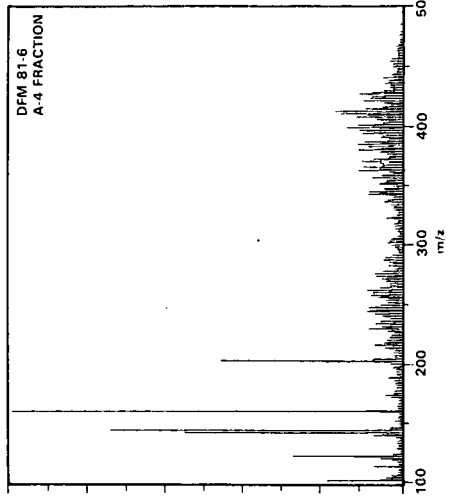
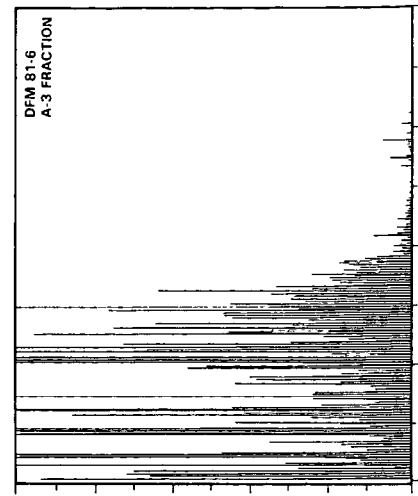


FIGURE 4. DFI-Mass Spectra Using Supercritical NH₃ for the A-3 and A-4 Fraction of Two Diesel Fuel Marine Samples.

FORMATION OF HIGH MOLECULAR WEIGHT AROMATICS IN FUEL-RICH FLAMES

Jack B. Howard

Fuels Research Laboratory, Department of Chemical Engineering
Massachusetts Institute of Technology
Cambridge, Massachusetts 02139

GENERAL OBSERVATIONS

Gas composition measurements as a function of distance or time through the reaction zone of fuel-rich premixed flames reveals the occurrence of high molecular weight aromatics formed by growth reactions that accompany the destruction of the fuel. The lumped concentration profile of all species heavier than molecular weight M exhibits a sharp peak (Fig. 1) indicative of net production of heavy material giving way to net consumption during passage through the reaction zone of the flame (from left to right in the figure). The data in Fig. 1 were obtained by probing along the centerline of a low-pressure, one-dimensional or plug-flow premixed acetylene-oxygen flame using a molecular-beam forming sampling instrument with on-line mass spectrometry. The heavy aromatics at flame temperatures, here about 1800 K, include both ions and neutrals. The heavy ions profile in Fig. 1, obtained (1) with a Faraday cage and electrical deflection of the molecular beam in the sampling instrument (2), includes ions larger than about 300 amu. The profile for $M > 1000$ amu species, obtained (3) with an on-line quadrupole mass spectrometer in the sampling instrument (Fig. 2), includes both ions and neutrals. The reactions involved are rapid, 3 mm of distance in Fig. 2 corresponding to a time interval of about 1 ms. When the fuel equivalence ratio $\phi = (\text{fuel/oxygen})/(\text{fuel/oxygen})_{\text{stoichiometric}}$ is above the critical value for soot formation, it is at the location of the peak concentration of the heavy aromatic compounds that the soot particles begin to form (4). When soot formation is impending, an increase of fuel/oxygen ratio by only a few percent gives a 100-fold increase in the peak concentration of the heavy aromatics.

RESOLUTION OF MOLECULAR WEIGHT GROWTH

In order to gain more understanding of the evolution of heavy hydrocarbons, mass spectrometer intensity profiles such as that for $I_{M>1000}$ in Fig. 1 but with the cutoff mass M varied in 50 amu steps from 200 amu to 750 amu were measured in a near-sooting low-pressure (2.67 kPa) C_6H_6/O_2 flame (4,5). If $I_{M>1000}$ is the signal intensity of all species of molecular weight M greater than the cutoff value m , then a probability distribution function (p.d.f.) $f_{200}(m)$ can be defined as

$$f_{200}(m) = -d[I_{M>m}/I_{M>200}]/dm$$

where $f_{200}(m)$ represents the number fraction of all species greater than 200 amu lying in the range m to $m + dm$.

The p.d.f.'s for five distances from the burner (5) are shown in Fig. 3. The p.d.f. at 7.95 mm is heavily weighted toward the mass range 200-300 amu. As the distance from the burner increases, the p.d.f. increases at the higher masses and decreases at the lower masses. At distances above 10.0 mm, the signal between 200 and 300 amu is a small to negligible fraction of the total, and the distributions are relatively uniform in the range 300-600 amu. At 10.9 and 12.1 mm, the distributions turn upward at the far right indicative of a faster growth of the higher-mass species, but it is not known if this apparent behavior is real or an artifact of the data at this high-mass extreme of the mass range studied.

These observations show that although the number density of high molecular weight species decreases with distance from the burner beyond the location of the

maximum concentration (e.g., Fig. 1), the mean molecular weight continually increases. In order to determine how the total mass of heavy species changes as the number decreases, the p.d.f. has been multiplied by m to convert to a mass basis and by

$$I_{M>200} / (I_{M>200})_{z=7.95\text{mm}}$$

to normalize the mass with the constant number of moles of heavy material existing at an arbitrarily fixed distance ($z = 7.95$ mm) from the burner. The resulting function,

$$mf_{200}^{(m)} I_{M>200} / (I_{M>200})_{z=7.95\text{mm}}$$

is shown in Fig. 4 for different molecular weights as a function of distance from the burner (5). A point on one of the curves represents the mass of species of the indicated molecular weight existing at the indicated distance from the burner, expressed as a ratio to the total number of moles of $M>200$ amu material existing at 7.95 mm.

It can be seen in Fig. 4 that the mass of material at a given molecular weight exhibits a peak at a height above burner which increases with increasing mass number. The shapes of the curves and the location of the peaks are the same as would be seen if number of moles instead of mass were plotted, since the number curves could be produced by vertical displacement of each mass curve in accordance with division by the constant molecular weight indicated thereon. In comparison with mole fraction profiles for individually identified species of m less than or equal to 200 amu, shown later, the curves in Fig. 4 constitute a continuation of the progression seen for the individual hydrocarbon species, namely molar concentration profiles peaking as m increases. Figure 4 shows that the peak concentrations also decrease as m increases. The mean molecular weight and overall mass and number concentrations of the high-mass material (5) are shown in Fig. 5.

INTERPRETED GROWTH BEHAVIOR

The above information shows that the rapid decrease in number concentration of heavy species that occurs immediately downstream of the peak concentration (Fig. 1) is not only accompanied by increasing mean molecular weight but also a net consumption or loss of material. Whether this consumption is due to oxidation, pyrolysis, or a combination of these has been addressed (5) by calculation of fluxes of O_2 and hydrocarbon species at the beginning and end of the zone of the heavy species consumption, both for the above near-sooting flame data and for similar data from a sooting C_6H_6/O_2 flame operated under otherwise identical conditions. The fraction of the initial oxygen remaining as O_2 at the beginning of the zone of rapid consumption of $M>700$ amu material is 37.2% and 18.3% for the near-sooting and sooting flames, respectively, and the O_2 remaining at the end of the zone of rapid consumption of $M>700$ amu material is about 1% of the initial value in both flames. Therefore the amount of oxidation occurring within this zone is indeed substantial, thus allowing the possibility that oxidation plays a role in the destruction of the high-mass material or its pyrolytic decomposition products. It is also found that the amount of $M>700$ amu material increases by a factor of 100 in going from the nearly sooting to the sooting case, even though the benzene fed is only increased by about 10%. In addition, the benzene fuel is almost gone when the $M>700$ material reaches its maximum concentration, indicating that the amount of these heavy species continues to increase as long as benzene is available. This behavior may mean that the concentration of oxidizing radicals that consume heavy species is suppressed by reaction with benzene, and also that benzene serves as a source of growth species for the heavy material. When the heavy species are undergoing rapid consumption, an even larger quantity of the prevalent intermediate, acetylene, is being consumed. Consequently, with regard to the molecular weight growth that accompanies the destruction of heavy compounds, acetylene and related species such as diacetylene (C_4H_2) and vinylacetylene (C_4H_4) may be important reactants.

IDENTIFIED SPECIES

Species and reactions involved in the early stages of the formation of high molecular weight compounds were studied (3,4) in the near-sooting C_6H_6/O_2 flame discussed above using the instrument shown in Fig. 2. Measured mole fraction profiles from which species fluxes and net reaction rates were computed are presented in Figs. 6-10. It will be noted in these figures that numerous intermediates are involved whose formation and subsequent destruction exhibit a general trend to larger molecular weights and smaller peak concentrations. It is this progression or sequential growth that is mentioned above as continuing on to the high molecular weight species. This behavior in both the near-sooting C_6H_6/O_2 flame and the sooting C_2H_2/O_2 flame discussed above is illustrated in Fig. 11 where the mole fractions of selected compounds are plotted with the intensities of heavy species. The growth proceeds on to soot if the fuel/oxygen ratio exceeds the critical soot limit.

MECHANISTIC FEATURES OF AROMATICS GROWTH

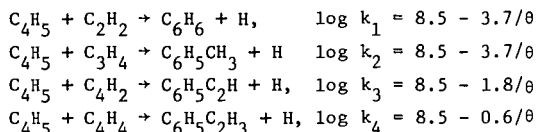
Analysis of these data has provided some insights into possible mechanisms of destruction of the fuel and the formation and destruction of intermediates (3,4,6). There is indication that aromatic hydrocarbons provide a structure capable of stabilizing, by internal aromatic substitution reactions, the radicals formed from addition of aromatic radical species to non-aromatics. Specifically, it appears that the combined presence of aromatic radicals, unsaturated aliphatics such as acetylenic species and H atoms is particularly favorable to growth of PAH and soot. Therefore, the production of phenyl radical (C_6H_5) and the competition between its destruction, especially with O_2 , and addition to unsaturated aliphatics are important factors in the molecular weight growth of aromatics.

With these mechanistic points in mind we return to the earlier discussion of the consumption of species immediately downstream of the peak concentration of the high molecular weight material. While the consumption is mainly by oxidation, it is accompanied by further increase in the mean molecular weight of the heavy species. Since the largest amount of material being consumed is acetylene, diacetylene, and vinylacetylene, and since these unsaturated aliphatics are identified as important species for molecular weight growth by addition reactions with aromatic radicals, one can infer that the acetylenic species do indeed contribute to the growth of the aromatic structures of which the heavy molecules and soot are comprised, presumably by addition reactions with the heavy aromatics. Aromatic species with acetylenic side groups are observed in the mass range (>200 amu) where individual identifications were possible, and the amount of acetylenic species consumed in this region of the flame greatly exceeds the amount of soot eventually formed. However, the peak flux of heavy species also exceeds the amount of soot eventually formed, so the proportions of the final soot mass contributed by the acetylenic species and by the heavy aromatics are not established. Qualitatively similar behavior was observed in a sooting acetylene/oxygen flame. In both the acetylene and benzene flames, the oxidative and possibly pyrolytic destruction of heavy species occurring downstream of their peak concentration would appear to be an important source of polycyclic aromatics emitted from the flame.

FORMATION OF FIRST AROMATIC RINGS

In flames of aliphatic fuels the first aromatic rings must be formed from non-aromatic precursors. Possible mechanisms for this critical step have been assessed (7) by comparing predicted formation rates against experimental values calculated from mole fraction profiles of compounds measured in a low-pressure 1,3-butadiene/oxygen flame using the instrument shown in Fig. 2. Postulated mechanisms involving butadienyl radical (C_4H_5) reacting with an acetylenic species and followed by rapid

cyclization were found to form benzene, toluene, phenylacetylene, and styrene at rates consistent with the data. The rate-controlling steps and predicted rate constants are as follows:



where k 's are in $\ell \text{ mol}^{-1}\text{s}^{-1}$ and $\theta = 2.3 \text{ RT}$ is in kcal mol^{-1} . Aromatics thus formed could subsequently participate in molecular weight growth as discussed above.

CONCLUSIONS

The chemistry of heavy aromatic compounds in fuel-rich flames involves numerous intermediate species whose sequential formation and destruction give a progression to decreasing amounts of increasingly heavy species, leading eventually to soot if the fuel/oxygen ratio is high enough. The combined presence of aromatic radicals, unsaturated aliphatics such as acetylenic species and H atoms is particularly favorable to molecular weight growth. When the initial fuel contains no aromatics, mechanisms controlled by butadienyl radical reacting with acetylenic species can form single-ring aromatics at rates consistent with observed values.

ACKNOWLEDGEMENTS

Support from the following sponsors is gratefully acknowledged: Environmental Protection Agency, Grant No. R803242; National Science Foundation, Particulate and Multiphase Processes Program, Grant No. NSF ENG 75-22679 A01; Exxon Research and Engineering Company, Exxon/MIT Combustion Research Program; and the National Institute of Environmental Health Sciences, Center Grant No. 5 P30 ES02109-02.

REFERENCES

1. Adams, D. E.: Measurement Technique for Charged Soot Particles in Flames, Chemical Engineer's Degree Thesis, Department of Chemical Engineering, M.I.T., Cambridge, Mass. (1976).
2. Wersborg, B. L., Yeung, A. C., and Howard, J. B.: Concentration and Mass Distribution of Charged Species in Sooting Flames, Fifteenth Symposium (International) on Combustion, The Combustion Institute, Pittsburgh, pp. 1439-1447 (1975).
3. Bittner, J. D. and Howard, J. B. (1981): Pre-Particle Chemistry in Soot Formation. In: Particulate Carbon - Formation During Combustion, edited by D. C. Siegla and G. W. Smith, pp. 109-142, Plenum Press, New York.
4. Bittner, J. D. and Howard, J. B.: Composition Profiles and Reaction Mechanisms in a Near-Sooting Premixed Benzene/Oxygen/Argon Flame, Eighteenth Symposium (International) on Combustion, The Combustion Institute, Pittsburgh, pp. 1105-1116 (1981).
5. Howard, J. B. and Bittner, J. D.: Structure of Sooting Flames. In: Soot Formation in Combustion Systems and Its Toxic Properties, edited by J. Lahaye, Plenum Press, New York (1983).
6. Bittner, J. D., Howard, J. B., and Palmer, H. B.: Chemistry of Intermediate

Species in the Rich Combustion of Benzene. In: Soot Formation in Combustion Systems and Its Toxic Properties, edited by J. Lahaye, Plenum Press, New York (1983).

7. Cole, J. A., Bittner, J. D., Longwell, J. P., and Howard, J. B.: Formation Mechanisms of Aromatic Compounds in Aliphatic Flames, presented at ACS National Meeting, Seattle, Washington, March 20-25, 1983 (to be published).

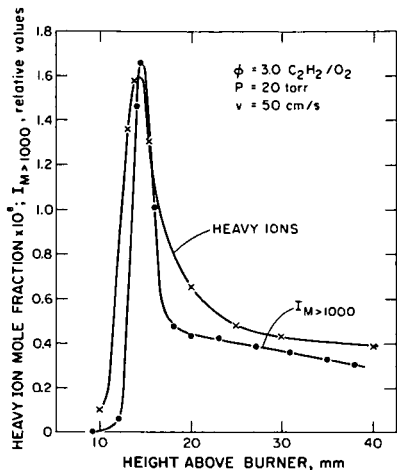


FIGURE 1. Concentration of heavy ions and signal intensity of high-mass ($M > 1000$ amu) species in sooting acetylene-oxygen flame (ϕ = equivalence ratio; P = pressure; v = cold gas velocity).

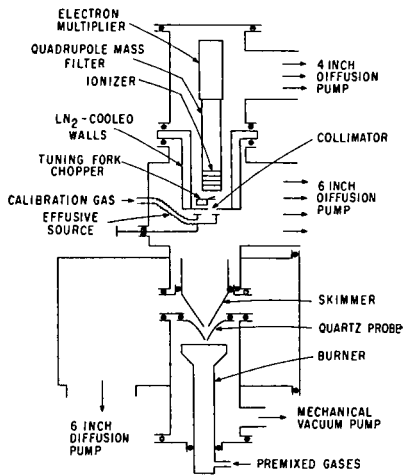


FIGURE 2. Molecular beam mass spectrometer system for the study of one-dimensional low-pressure premixed laminar flames.

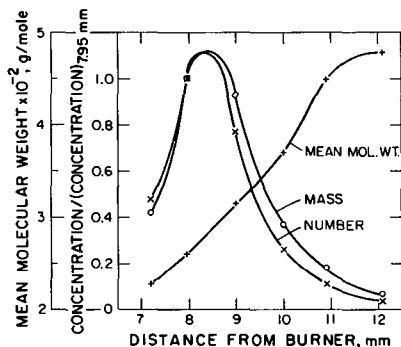
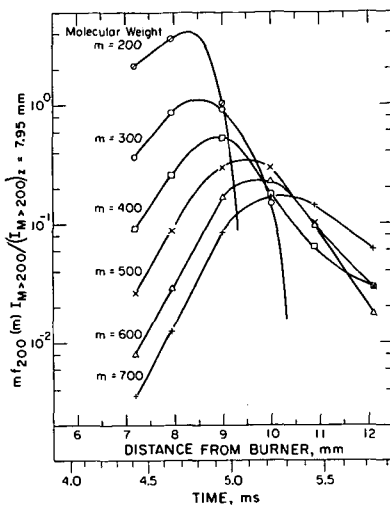
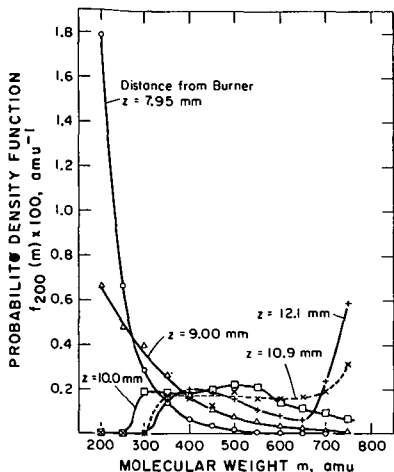


FIGURE 3. (ABOVE, LEFT) Probability density function for high-mass signal at several positions in near-sooting benzene-oxygen flame. (Pressure = 2.67 kPa; cold gas velocity = 50 cm/s; equivalence ratio = 1.8.)

FIGURE 4. (ABOVE, RIGHT) Variation with distance from burner of mass of material in molecular weight range m to $m + dm$ at different molecular weights, normalized with number of moles of $M > 200$ amu material at 7.95 mm above burner. (Same flame as in Fig. 3.)

FIGURE 5. (BELOW) Variation of mean molecular weight and mass and number concentration of $M > 200$ amu material with distance from burner. (Same flame as in Fig. 3.)

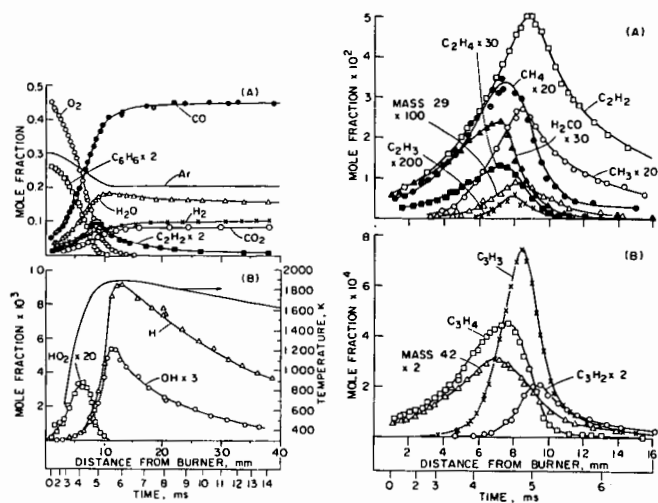


FIGURE 6. (LEFT) Mole fractions and temperature vs. distance from burner in near-sooting benzene-oxygen flame. (Same flame as in Fig. 3.)

FIGURE 7. (RIGHT) Mole fractions of species with masses between 15 and 44 amu vs. distance from burner in near-sooting benzene-oxygen flame. (A) Mass 29 may be C_2H_5 or HCO . (B) Mass 42 may be C_3H_6 or C_2H_2O . (Same flame as in Fig. 3.)

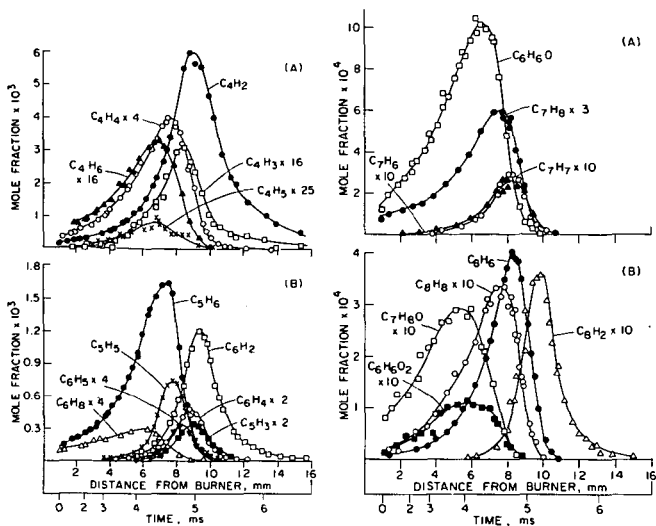


FIGURE 8. (LEFT) Mole fractions of C_4 (A), C_5 and C_6 (B) hydrocarbons vs. distance from burner in near-sooting benzene-oxygen flame. (Same flame as in Fig. 3.)

FIGURE 9. (RIGHT) Mole fractions of species with masses between 90 and 100 amu vs. distance from burner in near-sooting benzene-oxygen flame. (Same flame as in Fig. 3.)

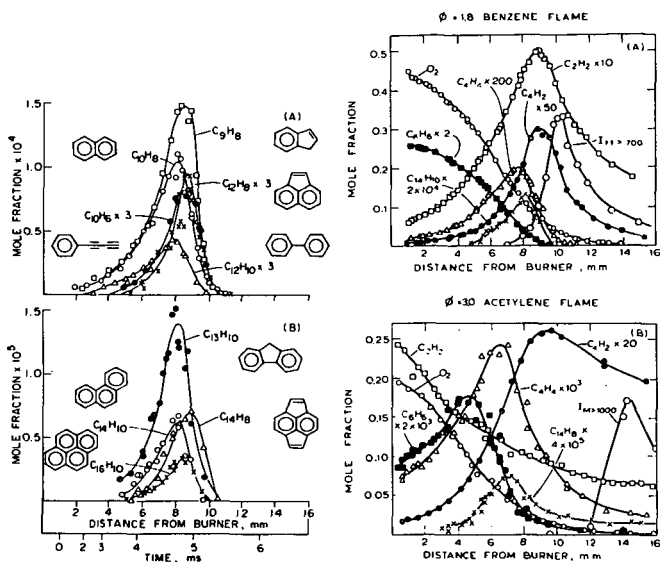


FIGURE 10. (LEFT) Mole fractions of polycyclic aromatic hydrocarbons vs. distance from burner in a near-sooting benzene-oxygen flame. (Same flame as in Fig. 3.)

FIGURE 11. (RIGHT) Mole-fraction profiles of selected compounds and signal intensity profiles of high molecular weight species for benzene-oxygen (above) and acetylene-oxygen (below) flames. [Same flames as in Fig. 3 (above) and Fig. 1 (below).]

POLYCYCLIC AROMATIC COMPOUNDS IN FLUIDIZED BED COMBUSTION OF COAL

P.M. Walsh,^a K.S. Chiu,^b J.M. Beer,^{a,c} and K. Eiemann^b

^aEnergy Laboratory

^bDepartment of Chemistry

^cDepartment of Chemical Engineering

Massachusetts Institute of Technology
Cambridge, Massachusetts 02139

Introduction

Polycyclic aromatic compounds (PAC) have been determined in the gas and particulate effluents from fluidized bed combustion of coal, lignite, and oil shale by a number of investigators. A bibliography of the reports of these investigations is contained in a paper by Chiu, Walsh, Beer, and Eiemann (1983). The concentrations of PAC in the effluents are often quite low, but depend upon the combustor configuration and operating conditions. The goal of the present investigation is to develop a mechanism consistent with measured rates of formation and destruction of PAC in atmospheric pressure fluidized bed combustion (AFBC), so that a rational approach may be taken to adjustment of conditions for minimization of PAC in the effluents. PAC are determined in samples taken from the freeboard (space above the bed), rather than from the exhaust, to observe the evolution of the PAC distribution within the combustor. Mass fractions of the most abundant PAC observed in the freeboard during AFBC of high volatile bituminous coal were reported by Chiu, et al (1983). Some correlation of the rates of disappearance of PAC with particle concentration was noted by Dutta, Chiu, Walsh, Beer, and Eiemann (1983). In the present paper theoretical estimates of the rates at which PAC might be consumed by heterogeneous reactions are compared with experimental rates estimated from PAC profiles determined by Chiu et al (1983).

Experimental

The PAC were determined in samples taken in the MIT AFBC Research Facility. A detailed description of the facility may be found in a report by Beér, Sarofim, Sandhu, Andrei, Bachovchin, Chan, Chaung, and Sprouse (1981). The combustor has a square cross section 0.6 m x 0.6 m and a height, from the combustion air distributor to the outlet, of 4.4 m. Previous publications describe the procedures used for sampling, separation, and identification of PAC (Chiu et al, 1983), permanent gases (Walsh, Chaung, Dutta, Beér, and Sarofim, 1982b), and bed particles (Walsh et al, 1982a; 1982b).

The AFBC was fired with Kentucky No. 9 high volatile bituminous coal crushed to minus 6.35 mm. The apparent ASTM rank of this coal was high volatile B bituminous. Other coal properties are given by Chiu et al (1983). The bed material was Reed limestone (middle ledge) crushed to minus 6.35 mm.

The experimental conditions at which the PAC were measured are listed in Table 1. In the specification of bed heights, sampling points, etc., the height above the distributor is designated by the symbol z . The top of the fluidized bed is at $z = L_f$. Axial profiles of temperature and the mole fractions of O_2 , CO , NO , and CH_4 are shown in Figure 1. The freeboard temperature in this run was relatively low, due to cooling of the combustion products by heat exchanger tubes

Table 1. Experimental Data

Run Number	K10
Fraction of theoretical air:	1.01
Superficial gas velocity based on average bed temperature and pressure at $z = 0$:	1.20 m/s
Minimum fluidization velocity:	0.18 m/s
Fluidized bed height:	0.65 m
Calcium/sulfur feed ratio:	3.7 kmol/kmol
Solid density of bed char particles:	336 kg/m ³
Solid density of bed stone particles:	2163 kg/m ³
Freeboard pressure:	102.6 kPa
Average freeboard temperature from $z = 2.0$ to 3.8 m:	964 K
Average freeboard gas velocity from $z = 2.0$ to 3.8 m:	1.18 m/s
Mass-based geometric mean size of elutriated char particles:	72 μ m
Geometric standard deviation of elutriated char particle size distribution:	1.82
Specific surface area-based geometric mean size of elutriated char particles:	60 μ m
Mass-based geometric mean size of elutriated stone particles:	74 μ m
Geometric standard deviation of elutriated stone particle size distribution:	2.67
Specific surface area-based geometric mean size of elutriated stone particles:	46 μ m
Terminal velocity of mean size elutriated char particles:	0.012 m/s
Terminal velocity of mean size elutriated stone particles:	0.046 m/s
Sherwood numbers of elutriated char and stone particles	~ 2
Total flowrate of elutriate:	0.01167 kg/s
Mass fraction char in elutriate:	0.063
Concentration of entrained char in the freeboard:	0.00169 kg/m ³
Concentration of entrained stone in the freeboard:	0.0260 kg/m ³

located at $z = 0.8, 1.0, \text{ and } 1.2 \text{ m}$. The bed material at the start of the run was fresh calcined limestone, therefore the ratio of CaO to CaSO_4 in the bed is much higher than would be present after sufficient time had elapsed to achieve steady bed composition.

The mole fractions of some of the PAC identified in samples taken from the freeboard at $z = 1.6, 2.1 \text{ and } 3.8 \text{ m}$ are given in Table 2. These mole fractions are based on the volume of dry gas sampled. Table 2 includes all of the compounds which were identified at more than one height. The PAC mole fractions are plotted vs height above the distributor in Figure 2. Most of the profiles indicate only net destruction of PAC in the region of the measurements. There is some evidence that production of PAC is occurring in the freeboard, and a hint that there may be a peak mole fraction resulting from the combined production and consumption processes which tends to shift to longer times (heights) with increasing molecular weight (compare the profiles of naphthalene, phenanthrene, anthracene, and chrysene in Figures 2a and 2g). However, much significance cannot be attached to changes in the slopes of the profiles, because the uncertainty in the reported mole fractions is approximately $\pm 10\%$, -50% . Pseudo-first order rate coefficients, k_{exp} , were derived from the mole fractions at $z = 2.1 \text{ and } 3.8 \text{ m}$:

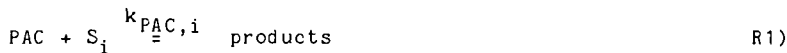
$$u_o \frac{dC_{\text{PAC}}}{dz} = -k_{\text{exp}} C_{\text{PAC}} \quad (1)$$

$$k_{\text{exp}} = - \frac{u_o}{z_2 - z_1} \ln \frac{X_{\text{PAC},2}}{X_{\text{PAC},1}} \quad T, P, \Sigma C_j \approx \text{constant} \quad (2)$$

The definitions of symbols may be found in the Nomenclature. The values of k_{exp} for the PAC identified at $z = 2.1 \text{ and } 3.8 \text{ m}$ are given in Table 2. Lack of a strong dependence of the experimental rate coefficients on oxygen, temperature, or compound, and their tendency to increase with increasing particle concentration (Dutta et al, 1983), suggested that the PAC destruction process might be heterogeneous, with significant resistance from extraparticle diffusion.

Heterogeneous Mechanism for Destruction of PAC

The mechanism of the transformations of PAC in the freeboard gas/particle mixture is undoubtedly extremely complicated. The investigations of Bittner and Howard (1981a; 1981b) and Howard and Bittner (1983) on the reactions of hydrocarbon species in benzene/oxygen flames give an indication of the magnitude of the problems which may be encountered in the freeboard gas/particle mixture. Suppose that we neglect production of a given PAC by char devolatilization, synthesis from lighter species, or formation by degradation of heavier species; and that each PAC is degraded to non-PAC in irreversible, heterogeneous reactions with solid species S_i :



We assume that the freeboard gas/particle mixture is in steady plug flow, and neglect axial dispersion. A rate expression based on this mechanism is:

Table 2. Polycyclic Aromatic Compounds Identified at Two or Three Heights in the Freeboard

Compound	Mole Fractions $\times 10^9$ (dry basis)			k_{exp} (Hz)	$(\epsilon v)_{PAC}^b$ ($m^3/kmol$)	D_{PAC-N_2} $\times 10^{42}$ (m^2/s)
	$z = 1.6m$	2.1m	3.8m			
benzofuran	22.5	5.72 ^a	.093 ^a	2.9	.109	.577
naphthalene	991	324	1.40	3.8	.140	.515
benzo(b)thiophene	112	33.0	.070	4.3	.120	.548
quinoline	17.1	2.11	-	-	-	-
2-methylnaphthalene	25.6	8.81	.244	2.5	.161	.479
3-methylbenzo(b)thiophene	2.80	.10	-	-	-	-
1-methylnaphthalene	25.0	6.23	.04 ^a	3.5	.161	.479
biphenyl	88.1	25.7	.182	3.4	.177	.455
ethylnaphthalene	2.95	.90	-	-	-	-
acenaphthylene	45.4	11.2	-	-	-	-
acenaphthene	2.19	.41	-	-	-	-
1-cyanonaphthalene	6.53	1.15	-	-	-	-
dibenzofuran	44.3	19.8	.108	3.6	.159	.475
methyldibenzofuran	.79	.59	-	-	-	-
9-fluorenone	10.3	2.50	.109	2.2	.195	.431
dibenzothiophene	23.8	9.49	.193	2.7	.170	.458
phenanthrene	125	64.7	.204	4.0	.190	.436
anthracene	9.53	8.43	-	-	-	-
fluoranthene	6.07	14.6	-	-	-	-
benzo(def)dibenzothiophene	2.43	7.34	-	-	-	-
pyrene	4.13	12.0	-	-	-	-
chrysene	1.09	3.42	.101	2.4	.240	.385

a. In the gas chromatographic separation this compound coeluted with another compound. The amount indicated is an estimate based on the relative intensities of peaks characteristic of the two compounds in the mass spectrum.

b. Fuller, Schettler, and Giddings (1966).

$$u_o \frac{dC_{PAC}}{dz} = - \tau k'_{PAC,i} C_{PAC} \quad 3)$$

where $k'_{PAC,i}$, the effective rate coefficient for the heterogeneous reaction of PAC with solid species i , contains the sequential processes of diffusion of PAC to the surfaces of particles, and the heterogeneous reaction at the surfaces:

$$k'_{PAC,i} = \frac{\rho_i}{\frac{6Sh_i D_{PAC}}{\phi_i \rho_i^* d_i^2} + k_{PAC,i} S_i^n} \quad 4)$$

In order to evaluate this rate coefficient we require estimates of the concentration, diameter, solid density, and sphericity of each particle species, and the diffusion coefficients of the PAC .

Freeboard Particle Properties

High particle concentration is an important feature of the freeboard flow, however precise measurements of the particle concentrations are difficult. The problems arise from the facts that large particles ($> 300 \mu m$) are moving both upward and downward with distributed velocities; and that small particles ($\leq 300 \mu m$), which are moving primarily upward, have velocities which depend on particle size and density. Isokinetic sampling of the particles is therefore not possible. Concentrations of particles in the bed are usually determined from measurements of differential pressure. This technique can only be used in the freeboard at low superficial velocity when pressure fluctuations are not large with respect to the changes in pressure due to the presence of particles. This condition is usually not met during combustion measurements. An alternative, approximate method for the determination of particle concentrations has been developed in order to estimate the rates of heterogeneous reactions.

The particles are classified by their terminal velocities into two groups: large particles (terminal velocities greater than the mean gas velocity) and small particles (terminal velocity less than the mean gas velocity). The dependence of the flux of large particles on height in the freeboard is measured by catching descending particles in cups placed at several heights above the bed (Walsh, Mayo, and Beér, 1983). The concentration of large particles is estimated from the flux measurements by a method proposed by Walsh, Yokozeki, and Beér (1982). The basis of this estimate is an assumed initial velocity distribution (Gaussian) of particles leaving the bed surface. For a given particle flux at the bed surface, a given standard deviation of the velocity distribution, and the assumptions of negligible drag and total reflux; both the flux and concentration of particles at a given height are uniquely determined. In this way the large particle concentrations can be estimated from the flux measurements.

The small entrained particles are precipitated by cyclones from the exhaust, so their flux at the freeboard exit is known. By assuming that they move only upward at a constant velocity equal to the mean gas velocity minus the terminal velocity of the mean size particles, their concentration can also be estimated. Errors in this estimate may arise from:

1. Cyclone collection efficiency less than 1.
2. SO_2 and/or CO_2 reactions with stone and combustion of char in the freeboard² and exhaust pipe before the collection point.
3. Refluxing of the small particles down the freeboard wall (Pemberton and Davidson, 1983).

Probably the most important problem, however, is in the initial assumption: that the particles can be divided into two groups having mean sizes independent of height. The particle size and velocity distributions undergo continuous evolution from the top of the bed (and even within the bed itself) to the combustor outlet. A more detailed calculation can be made by machine computation, but the value of such an effort is to some extent negated by the lack of experimental data with which to compare the predictions.

The mass-based particle size distributions of the stone and char particles in a sample of the elutriate precipitated in the cyclones during the present experiment are shown in Figure 3. The mass fractions of stone and char in the elutriate were calculated from the heating value of the material in each size range. The heating value of pure char was estimated using Dulong's formula with a composition derived from the ultimate and proximate analyses of the coal. The specific surface area-based mean particle sizes were calculated from the standard deviation and mass-based mean sizes (Irani and Callis, 1963). The sphericity of the entrained stone and char particles was estimated to be 0.5; their solid densities were assumed to be the same as those of the larger stone and char particles taken from the bed. Terminal velocities of the particles were calculated using the correlation of Pettyjohn and Christiansen (1948). The properties of the entrained particles are summarized in Table 1.

The refluxing particles were assumed to have the same size, sphericity, and solid density as bed particles. Specific surface area-based mean sizes of the bed stone and char particles were 780 and 2900 μm , respectively. The mass fraction of char in the bed and refluxing particles is only 0.43 wt %.

Total particle concentrations estimated in the present experiment by the approximate methods outlined above are shown in Figure 4. The bed particle concentrations were determined from measurements of differential pressure, the refluxing particles from the samples collected in the cups, and the entrained particles from the cyclone catch. An explanation of the second curve on Figure 4 is given in the Discussion section.

Molecular Diffusion Coefficients of Polycyclic Aromatic Compounds

Experimental measurements of the molecular diffusion coefficients of PAC are rare. Diffusion coefficients in air at atmospheric pressure have been reported for naphthalene and biphenyl at 298 K, anthracene at 372 K (Mack, 1925), and biphenyl at 491 K (Gilliland, 1934). Howard and Bittner (1983) determined diffusion coefficients of heavy species ($W = 200$ to 750 kg/kmol) from concentration profiles measured in a near-sooting benzene/oxygen/argon flame (equivalence ratio 1.8), in a region of the flame where the slopes of the species profiles, d^nC/dz , were determined only by diffusion. The pressure in the flame, and the temperature in the region of the measurements were 2.67 kPa and 1800 K, respectively. Assuming that the species observed were polycyclic aromatic hydrocarbons, Howard and Bittner estimated their diffusion coefficients at 300 K from the correlation of Fuller, Schettler, and Giddings (1966), using the temperature dependence

derived from the Lennard-Jones 12-6 potential, as recommended by Sherwood, Pigford, and Wilke (1975). The approximation given by Fristrom and Westenberg (1965) to the temperature dependence of the diffusion collision integral was used. The correlation of Fuller et al, with this modification, becomes (in SI units):

$$D_{AB} = \frac{1.60 \times 10^{-4} T^{1.67} \left(\frac{1}{W_A} + \frac{1}{W_B} \right)^{1/2}}{P \left[(\Sigma v)_A^{1/3} + (\Sigma v)_B^{1/3} \right]^2} \quad \text{m}^2/\text{s} \quad 5)$$

Howard and Bittner (1983) reported good agreement between their experimental diffusion coefficients and those estimated from the modified correlation. The discrepancies between estimated values and the experimental values for PAC reported by Mack (1925), Gilliland (1934), and Howard and Bittner (1983) are ± 10 to 15%.

Estimates of the binary diffusion coefficients of PAC in N_2 using Equation 5 are listed in Table 2. The procedure given by Fuller et al (1966) for the estimation of the molecular diffusion volumes from atomic diffusion volumes was followed. The volume increment $-0.0202 \text{ m}^3/\text{kmol}$ was added for each aromatic and heterocyclic ring, but not for the ring containing the keto group in 9-fluorenone.

Discussion

An upper limit on the rate coefficient for the surface reaction can be estimated from the product of the frequency of collisions of the PAC with unit area of a surface and the particle external surface area per unit volume of gas:

$$k_{PAC,i} S_i n_{PAC,i} \rho_i \leq \left(\frac{RT}{2\pi W_{PAC}} \right)^{1/2} \frac{6}{\phi_i \rho_i^* d_i} \rho_i \quad 6)$$

Using the entrained particle properties in Table 1 the upper limits for naphthalene at 964 K are 310 and 100 Hz for the stone and char particles, respectively.

The rate coefficient for the diffusion process is equal to

$$\frac{6 Sh_i D_{PAC}}{\phi_i \rho_i^* d_i^2} \rho_i \quad 7)$$

Using the elutriated particle properties from Table 1 and the diffusion coefficient for naphthalene in N_2 from Table 2, values of 7 and 2 Hz are obtained for the stone and char, respectively. The rate coefficient for the surface reaction is therefore estimated to be more rapid than that for external diffusion for values of the sticking coefficients greater than about 0.02. If the sticking coefficient were sufficiently large, say ≥ 0.1 , the experimental rate coefficient would be approximately equal to the diffusion limited rate coefficient given by Equation 7.

In general the concentration of particles, ρ_i , is a function of height, as shown in Figure 4. However, the quantity $6 Sh_i \rho_i / \phi_i \rho_i^* d_i^2$ is dominated by the approximately constant concentration of small particles over most of the height of the freeboard under the present conditions, shown by the second curve in Figure 4. We may therefore base estimates of the diffusion limited rate coefficients from Equation 7

on the properties of the small particles alone.

The calculated rate coefficients for destruction of PAC by diffusion limited surface reactions on the small stone and char particles are plotted vs. PAC diffusion coefficient in Figure 5. The rate coefficient for simultaneous diffusion controlled destruction on both types of particles is the sum of the values shown for stone and char. The data points are the experimental rate coefficients determined from the PAC mole fractions at $z = 2.1$ and 3.8 m.

Any values of the experimental rate coefficients which are equal to, or less than the theoretical upper limit (sum of stone and char values) are consistent with the model. Since this condition is not difficult to satisfy the location of the experimental points below the upper limit is little more than a justification for further testing and examination of the model. However, the consistency of the data points (factor of 2) is interesting. If the similarity of the values of the experimental rate coefficients is not due to significant diffusion resistance, then the rate coefficients for the net destruction of PAC by heterogeneous and/or homogeneous reactions are rather insensitive to molecular structure. The location of the experimental points between the rate coefficients for diffusion limited reaction on stone and char is an indication that at least part of the stone is participating in the reaction. Such a conclusion is not justified however, considering the assumptions and approximations used in the model and calculations. The reaction might be occurring only on the char. If the PAC destruction were only via heterogeneous reactions the intercept of a line through the data points would be zero at $D_{PAC} = 0$. The extrapolated value is approximately 0.7 Hz.

Conclusion

A heterogeneous mechanism for destruction of PAC in the AFBC freeboard could not be ruled out by comparison with the rates of disappearance of 2 to 4 ring PAC at one set of operating conditions. If heterogeneous reactions are, in fact, responsible for PAC destruction, a more detailed model accounting for production of PAC and finite rates of the surface reactions may be needed. The relative importance of stone and char particles can only be determined by additional measurements over a range of ratios of the char/stone concentrations. The possibility that only a fraction of the surface area of each type of particle is utilized, due to nonuniform surface composition, will be difficult to assess. Better spatial resolution of the PAC profiles is needed.

Acknowledgements

This work was supported by the National Institute of Environmental Health Sciences, National Institutes of Health (Center Grant No. 5 P30 ES02109). The measurements of PAC were made in conjunction with other AFBC experiments which are supported by the Office of Fossil Energy, U.S. Department of Energy (Grant No. DE-FG22-80PC30215) and by the Tennessee Valley Authority (Contract No. TV-55783).

The authors thank Professor J.B. Howard for helpful discussions of his determination of diffusion coefficients from the flame measurements. We are indebted to Professor J.P. Longwell for his suggestion that interactions of PAC with particles might be a significant determinant of the PAC concentrations in the freeboard. The responsibility for the accuracy of the analysis, however, rests entirely with the authors. We are grateful for the assistance of James R. Byrd of the

Tennessee Valley Authority, Chattanooga, in supplying the coal, limestone, and analyses of the particle samples. We thank Ms. Bonnie Caputo of the MIT Energy Laboratory for patiently and expertly typing the drafts and final manuscript.

Nomenclature

C_j	concentration of gaseous species j , kmol/m ³
d_i	specific surface area-based geometric mean diameter of particles i , m
D_{AB}	binary diffusion coefficient, m ² /s
D_{PAC}	diffusion coefficient of PAC in the freeboard gas, assumed to be equal to D_{PAC-N_2} , m ² /s
k_{exp}	experimental first order rate coefficient, Hz
$k_{j,i}$	rate coefficient for surface reaction of gaseous species j with particles i , m/s
$k'_{j,i}$	effective first order rate coefficient for heterogeneous reaction of gaseous species j with particles i , Hz
L_f	fluidized bed height, m
P	pressure, Pa
R	gas constant = 8314 J/kmol.K
S_i	BET specific surface area of particles i , m ² /kg
Sh_i	Sherwood number for particles i , dimensionless
T	temperature, K
u_o	superficial (empty tube) gas velocity, m/s
W_j	molecular weight of species j , kg/kmol
X_j	mole fraction of gaseous species j , dimensionless
z	height above air distributor, m
$\eta_{j,i}$	effectiveness factor for reaction of gaseous species j with particles i , dimensionless
ρ_i	concentration of particles i , kg/m ³
ρ_i^*	solid density of particles i , kg/m ³
ϕ_i	sphericity of particles i , dimensionless
$(\Sigma v)_j$	sum of atomic diffusion volumes for molecules of gaseous species j , m ³ /kmol

References

- Beér, J.M., Sarofim, A.F. Sandhu, S.S., Andrei, M., Eachovchin, D., Chan L.K., Chaung, T.Z., and Sprouse, A.M., 1981, NO_x Emissions from Fluidized Coal Combustion, Final Report under Grant^xNo. R804978020, U.S. Environmental Protection Agency, Research Triangle Park, NC.
- Bittner, J.D., and Howard, J.B., 1981a, Pre-Particle Chemistry in Soot Formation, In: Particulate Carbon Formation During Combustion, E.C. Siegla and G.W. Smith, eds., Plenum Press, NY, pp. 109-142.

Bittner, J.D., and Howard, J.B., 1981b, Composition Profiles and Reaction Mechanisms in a Near-Sooting Premixed Benzene/Oxygen/Argon Flame, Eighteenth Symposium (International) on Combustion, The Combustion Institute, Pittsburgh, PA, pp. 1105-1116.

Chiu, K.S., Walsh, P.M., Beer, J.M., and Biemann, K., 1983, Polycyclic Aromatic Compounds in Fluidized Bed Combustion of Bituminous Coal, Subbituminous Coal, and Oil Shale. In: Polynuclear Aromatic Hydrocarbons: Combustion Processes, Environmental Effects, and Biochemistry, Battelle Press, Columbus, OH.

Dutta, A., Chiu, K.S., Walsh, P.M., Beer, J.M., and Biemann, K., 1983, The Rates of Methane and Naphthalene Destruction in the Freeboard of a Fluidized Bed Coal Combustor, American Chemical Society, 185th National Meeting, Seattle, WA, March 20-25, Division of Environmental Chemistry, Extended Abstract.

Fristrom, R.M., and Westenberg, A.A., 1965, Flame Structure, McGraw-Hill, NY, p. 276.

Fuller, E.N., Schettler, P.D., and Giddings, J.C., 1966, Industrial and Engineering Chemistry, 58, No. 5, 19.

Gilliland E.R., 1934, Industrial and Engineering Chemistry, 26, 681.

Howard, J.B., and Eittner, J.D., 1983, Structure of Sooting Flames, In: Soot Formation in Combustion Systems and Its Toxic Properties, J. Lahaye, ed., Plenum Press, NY.

Irani, R.R., and Callis, C.F., 1963, Particle Size: Measurement, Interpretation, and Application, Wiley, NY, pp. 43-45.

Mack, E., 1925, J. Am. Chem. Soc. 47, 2468.

Pemberton, S.I., and Davidson, J.F., 1983, Elutriation of Fine Particles from Bubbling Fluidized Beds, Fourth International Conference on Fluidization, Kashikojima, Japan, May 29 - June 3.

Pettyjohn, E.S., and Christiansen, E.B., 1948, Chem. Eng. Prog. 44, 157.

Sherwood, T.K., Pigford, R.C., and Wilke, C.R., 1975, Mass Transfer, McGraw-Hill, NY, p. 18.

Walsh, P.M., Chaung T.Z., Dutta, A., Beer, J.M., and Sarofim, A.F., 1982a, Particle Entrainment and Nitric Oxide Reduction in the Freeboard of a Fluidized Coal Combustor, American Chemical Society, Division of Fuel Chemistry, Preprints, Vol. 27, No. 1, pp. 243-261.

Walsh, P.M., Chaung, T.Z., Dutta, A., Beer, J.M., and Sarofim, A.F., 1982b, Nitric Oxide Reduction in the Freeboard of a Fluidized Bed Coal Combustor, Nineteenth Symposium (International) on Combustion, The Combustion Institute, Pittsburgh, PA, pp. 1281-1289.

Walsh, P.M., Yokozeki, A., and Beer, J.M., 1982, Unpublished work.

Walsh, P.M., Mayo, J.E., and Beer, J.M., 1983, Refluxing Particles in The Freeboard of a Fluidized Bed, American Institute of Chemical Engineers, 1983 Annual Meeting, Washington, DC, October 30 - November 4.

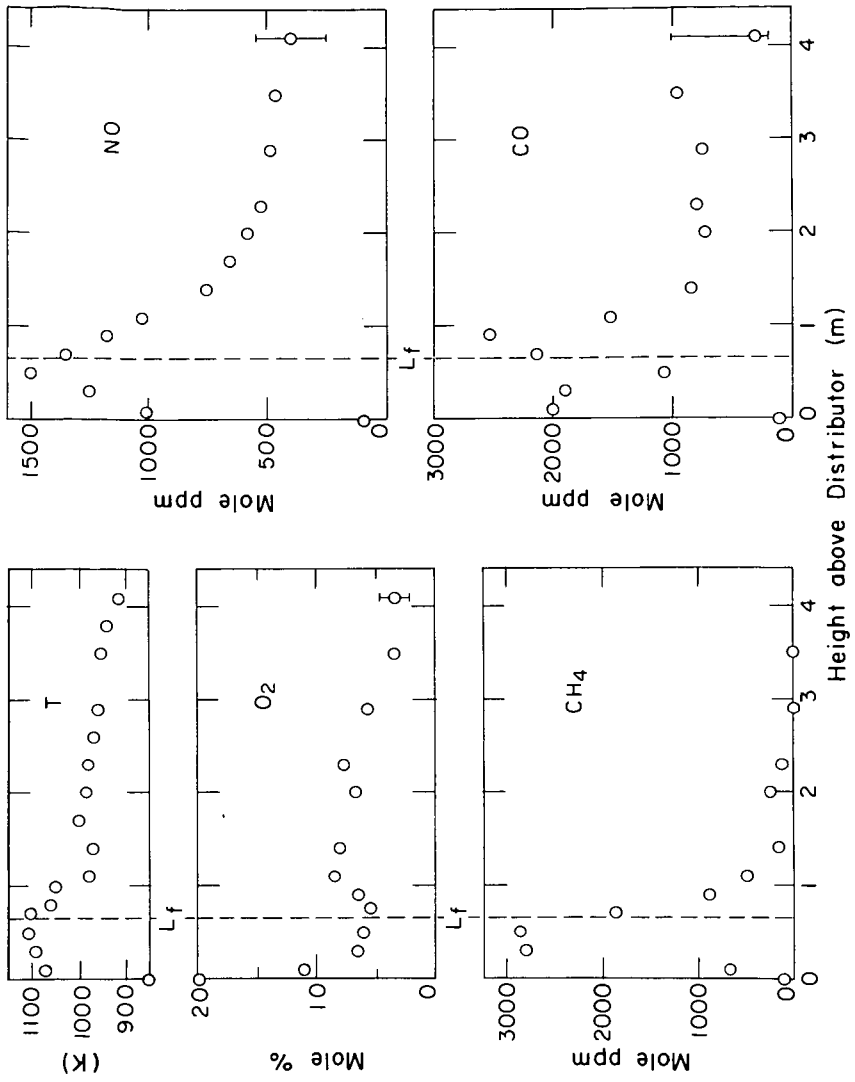


Figure 1. Temperature and mole fractions of light gaseous species (dry basis) vs. height in the bed and freeboard.

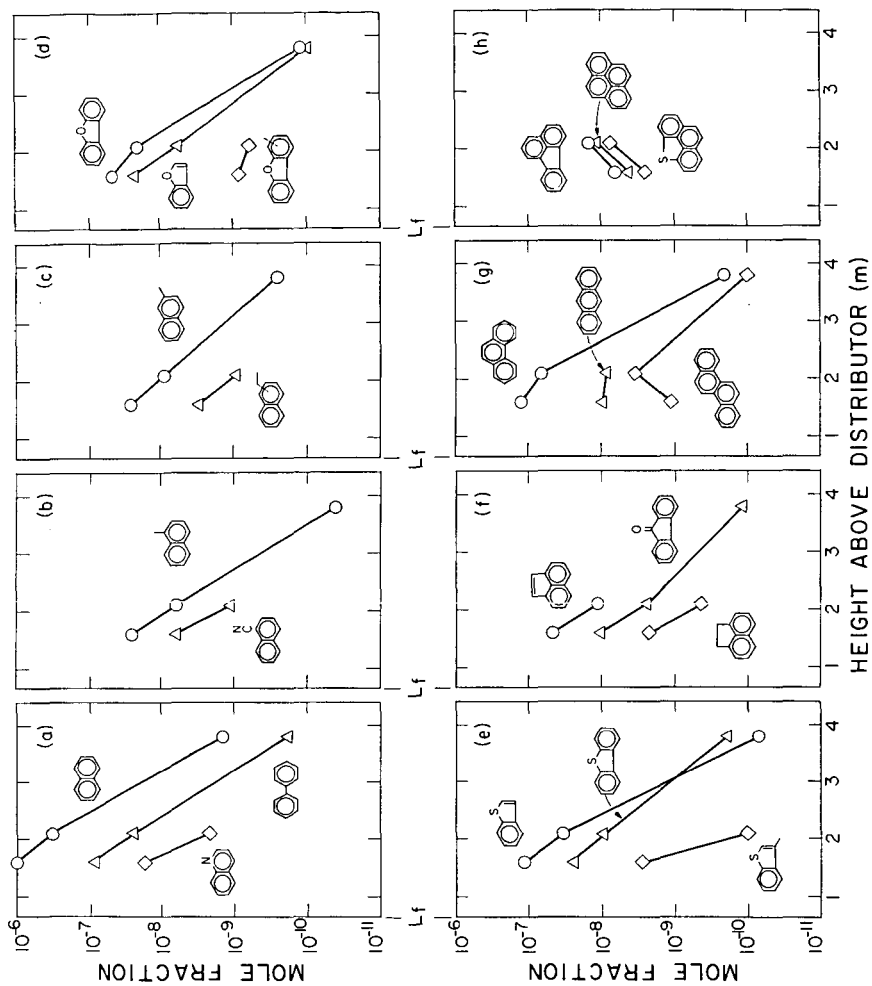


Figure 2. Mole fractions of polycyclic aromatic compounds (dry basis) vs. height in the freeboard.

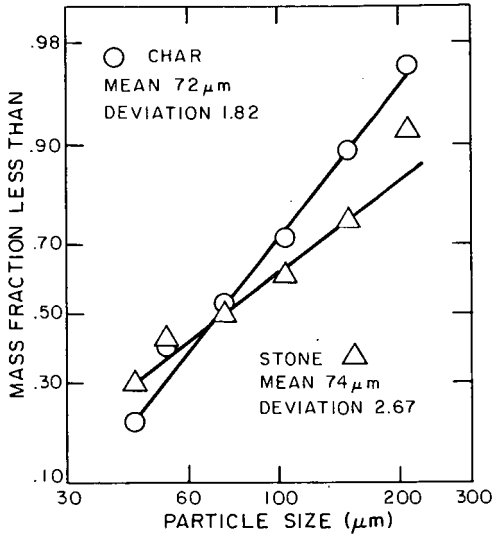


Figure 3. Size distributions of elutriated char and stone.

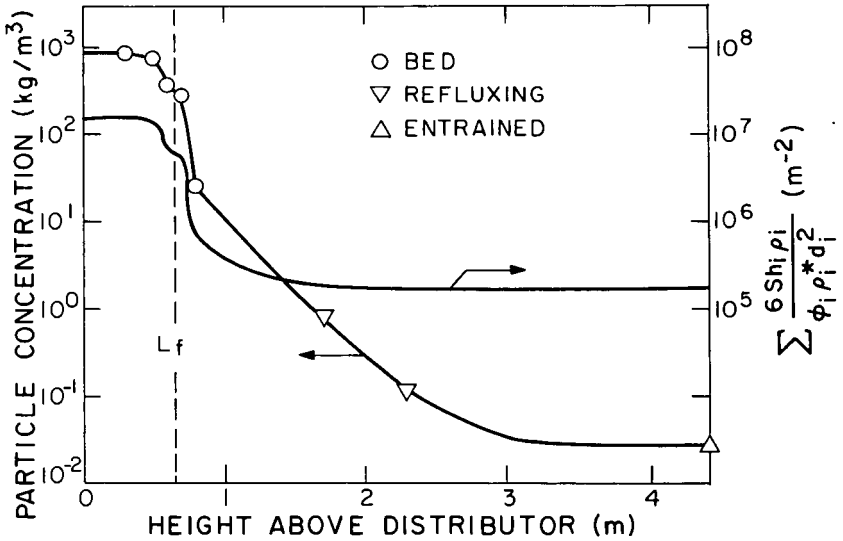


Figure 4. Particle concentration vs. height in the bed and freeboard.

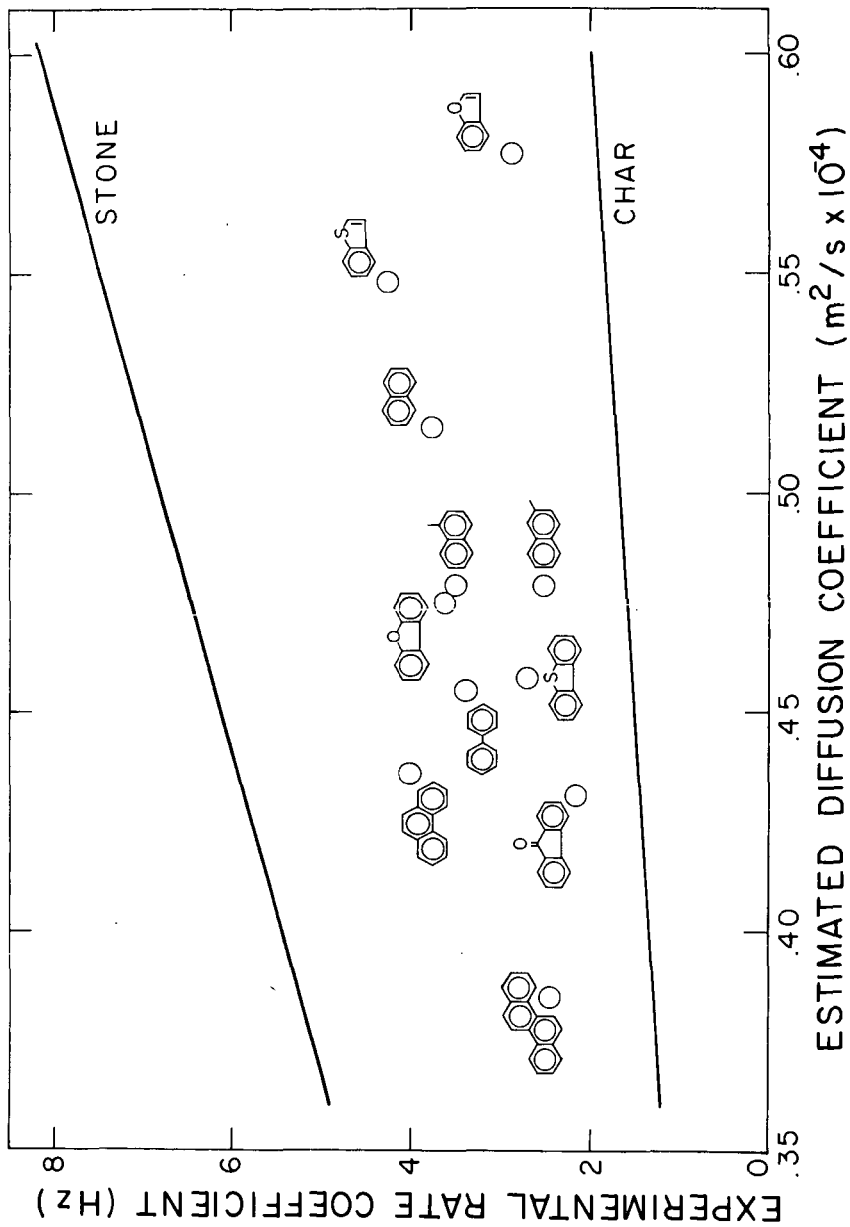


Figure 5. Experimental pseudo-first order rate coefficients vs. estimated molecular diffusion coefficients of the poly-cyclic aromatic compounds.

EFFECTS OF PYROLYSIS CONDITIONS ON COAL DEVOLATILIZATION

J. D. Freihaut and D. J. Seery
United Technologies Research Center
East Hartford, CT 06108

Phenomenological aspects of coal devolatilization are known to vary significantly with coal rank and the experimental conditions (1). Arrhenius rate parameters or volatile yields and product distributions can differ appreciably (2,3,4,5) for coals of similar rank depending on the experimental configuration. Differences in proposed chemical kinetic mechanisms undoubtedly account for part of the differences in reported rate parameters. However, experimentally associated variation of product yields and distributions and temperature sensitivities of global rates for similar coals implies that the observable path of the devolatilization process is the result of coupled chemical and transport processes. The physical characteristics of coal devolatilizing in a given set of conditions are also observed to vary significantly with chemical characteristics of the parent coal (6,7,8). And for a particular coal, the physical characteristics during devolatilization are observed to be a function of the conditions of heating (9,10,11,12). Such associations also imply that observable behavior during coal devolatilization is a result of the coupling between the chemical nature of the parent coal and particular conditions of the experiment.

Polycyclic aromatic hydrocarbon species represent a major fraction of the volatile yields obtained from a wide range of coals. The overwhelming majority of these species are condensible under conditions of normal temperature and pressure and are operationally referred to as coal tars. Tar yields obtained from the devolatilization of coal are sensitive functions of the chemical characteristics of the parent coal and the conditions of devolatilization. As tar yields for a particular coal are changed by variation of either the chemical characteristics of the parent coal or conditions of devolatilization, the yield structure and characteristics of the products are also changed.

The purpose of this communication is to demonstrate that progress in understanding the relative importance of chemical and physical factors in coal devolatilization is linked to progress in understanding the formation, evolution and secondary reactions of PAH species which are apparently formed within the coal particle very early in the devolatilization process. More specifically, the objectives are to demonstrate the significance of the tar formation and evolution phase of coal devolatilization in determining:

1. the yield structure of volatile products from a range of coals;
2. the change in yield structure with conditions of devolatilization;
3. the degree of coupling between chemical and physical phenomena during the main phase of mass release.

Experimental

Two experimental techniques were employed in obtaining the results - a heated grid apparatus and a flash lamp chamber. Figure 1 shows the heated grid and associated control and monitoring connections. Since the power supply driving the grid is programmable, the heating rate of the grid can be controlled by interfacing the power supply to microprocesses or circuitry. Programmed heating rates of $< 10^{\circ}\text{C}/\text{sec}$ to $10^3 \text{ }^{\circ}\text{C}/\text{sec}$ are available by use of this technique. The heated grid cell is interfaced to an infrared gas cell. The cell is coupled to an FT-IR instrument to allow immediate analysis of low molecular weight volatiles. Details of the operation of the heated grid (screen preparation, sample loading, thermocouple measurements) are given elsewhere (13,14).

The grid technique, as employed in this laboratory, cannot be used with particles less than $\sim 70 \mu\text{m}$ and heating rates are practically limited to upper values $\sim 10^3 \text{ }^{\circ}\text{C}/\text{sec}$. A different technique is needed to heat particles in the $1\text{-}70 \mu\text{m}$ range at programmed heating rates of $10^5 \text{ }^{\circ}\text{C}/\text{sec}$. To obtain these conditions of large thermal flux/particle diameter ratios a flash lamp assembly replaces the heated grid chamber of Fig. 1. In this technique the inside of a pyrex or quartz tube is dusted with the coal. The tubes are 2.5 cm in diameter and $\sim 10 \text{ cm}$ long and sealed at one end. The coated reactor tube is placed inside a helical Xenon flash coil. The flash intensity delivered to the reactor tube is varied by the energy stored in the $1125 \mu\text{f}$ capacitor bank attached to the flash lamp. Since the total energy stored in the capacitor system is $\frac{1}{2}CV^2$, an increase in voltage from 1.5 to 2.5 kV represented approximately a 2.8 increase in flash energy output. Since the discharge time and reactor geometry remain constant the increase in programmed voltage represents an increase of 2.8 in radiation flux delivered to the reactor chamber. Pyrex reactor chambers were employed in most tests to avoid UV-induced secondary reactions. Sample sizes range in value from $3\text{-}10 \text{ mg}$.

Coal Characteristics

The location of the samples on a H/C vs. O/C plot are shown in Fig. 2. Figure 3 displays changes in functional group absorption characteristics as a function of rank. In general, an increase in rank is associated with an increase in the resolution of the aromatic -H bending ($680\text{-}920 \text{ cm}^{-1}$ region) and aromatic -H stretching ($3000\text{-}3100 \text{ cm}^{-1}$), a decrease in the hydroxyl -H associated absorption in the $3100\text{-}3600 \text{ cm}^{-1}$ region, and a maximum in aliphatic -H absorption modes $2600\text{-}3000 \text{ cm}^{-1}$ and $\sim 1400 \text{ cm}^{-1}$ regions for hv bituminous coals. It should be noted that these functional group spectra were obtained by artificially establishing a baseline. A chord is drawn through the local spectra absorption minima at $\sim 3600 \text{ cm}^{-1}$ and 2000 cm^{-1} . The so-called "background" absorption beneath this chord line and the raw spectra, zero absorbance line is subtracted, leaving the chord line as the new zero absorbance line. Although this is a convenient method for comparing changes in functional group appearance, it ignores the substantial changes in optical density of coal with rank.

Figure 4 shows the background absorption subtracted in this manner as a function of carbon percentage content of the coal samples. Figure 5 shows the remaining

integrated absorption area ($400-4000\text{ cm}^{-1}$). This is the absorption area assumed to be associated with specific functional group characteristics, the area between the chord drawn baseline and the absorption curve. Inspection of Figs. 4 and 5 indicates that as the functional group absorption characteristics of coal decrease, its amorphous background absorption sharply increases. The underlying cause of the background absorption are not well understood. Some investigators relate such optical attenuation to particle scattering effects in the halide matrix (15,16). Others attribute the bulk of this absorption to photoabsorption by condensed aromatic ring species in the coal sample (17,18,19,20). The greater the aromaticity of the coal the greater the photoabsorption effect, that is, the greater the background absorption. The two phenomena are undoubtedly coupled via the complex refractive index for a particular coal relative to the halide matrix. The strength of coupling remains to be quantified. Overall, the total optical density of a coal is a strong function of rank as measured by $\%C(\text{daf})$.

Within the hv bituminous coals, the Western bituminous coals, although similar in elemental composition to some interior and Appalachian province coals, show absorption characteristics indicating a lower degree of aromaticity. This is indicated by the ill resolved aromatic -H absorption modes ($680-920\text{ cm}^{-1}$ and $3000-3100\text{ cm}^{-1}$) and the lower background absorption than the other bituminous coals.

As noted below, the degree of aromatic ring condensation has a substantial influence on the maximum PAH yields obtainable from a coal as well as the sensitivity of the yield to changes in pyrolysis conditions.

Tar Evolution: Coupling Between Coal Characteristics and Moderate Heating Rates

Figure 6 displays the mass fraction of dry coal evolved as volatiles for the range of coals investigated and at the heating conditions indicated. At these conditions, total yield is essentially independent of rank characteristics through high volatile bituminous coals. However, as Figs. 7 and 8 indicate, the tar yield is a sensitive function of rank characteristics of a coal. Appalachian and Interior province high volatile bituminous coals give highest yields of tars and, with the exception of a medium volatile bituminous coal, display the greatest fraction of volatiles evolved as condensable PAH species. Figure 9 indicates the variation in tar yields with heating conditions for a Western bituminous coal. There is little change in volatile yields with heating conditions for final temperatures beyond 700°C in the time period of this experiment. However, the fraction of volatiles evolved as tar decreases significantly with changes in programmed heating rate from $150^{\circ}\text{C}/\text{sec}$ to $\sim 1000^{\circ}\text{C}/\text{sec}$. Tar yields from Appalachian and Interior province bituminous coals yield tar species which are much less sensitive to changes in programmed heating rates. Such coals show less than 10% change in tar yield with changes in programmed heating rate in the $100-1000^{\circ}\text{C}/\text{sec}$ range, whereas tar yields from sub-bituminous and Western bituminous coals can vary by as much as 50% over this range. The aromaticity, and, consequently the chemical and thermal stability of the mix of molecular components in the parent coal has a great deal of influence on the tar evolution properties of a coal.

The tar evolution potential of a coal is also observed to have a significant influence on the temperature trajectory of the heated grid in immediate contact with the

coal sample. Figure 10 shows the effect which tar evolution properties of a coal can have on a programmed temperature trajectory in low pressure conditions.

Figure 11 shows the time resolved associated between the low pressure evolution of the tar component of the volatiles and the warp in the programmed temperature trajectory. Figures 9 and 11 indicate that in low ambient pressure conditions the formation and evolution of PAH species precedes significant light gas evolution. To verify the relative release times, high speed films of the tar release process were made.

Frame-by-frame inspection of these films were compared to the rapid scan infrared data and real time pressure and temperature data. For the coals examined in this manner.

1. The initial temperature deviations are closely associated with the tar formation and release.
2. The onset of the tar release precedes the onset of the major light gas release.
3. The light gas evolution occurs mainly in the secondary temperature rise.
4. Rocky Mt. province high volatile bituminous coals displayed more overlap in the tar and light gas evolution than the Appalachian province high volatile bituminous coals.
5. Lower rank coals gave increasingly greater degrees of overlap between the light gas and tar evolution phases of devolatilization.

Dependence of Coal Nitrogen Evolution on Tar Evolution Characteristics

For final temperature $< 1000^{\circ}\text{C}$ and heating rates $10^2\text{-}10^3$ $^{\circ}\text{C}/\text{sec}$, the distribution of coal nitrogen in the tar, char or light gases produced by devolatilization is dependent on the chemical characteristics of the coal in a manner analogous to the distribution of coal mass as tar, char or light gas. An increase in the tar fraction of the volatiles with increase in aromaticity of the parent coal results in a proportionate increase in coal nitrogen in the tar. A decrease in tar yield for a particular coal by increases in apparent heating rate results in a proportionate decrease in coal nitrogen evolved as tar. As the tar yield decreases, the tar nitrogen is primarily evolved as HCN. The coupling between the tar and gaseous evolution of the coal nitrogen and the dependence on aromaticity of the parent coal are illustrated by Figs. 12-14. Mass balance details and distributions for other coals are given elsewhere (21).

Effect of Low and High Programmed Heating Rates

Table I displays the sizable variation in solids and tar yields with programmed conditions of heating for two hv bituminous coals. Inspection of Table 1 indicates tar

TABLE 1
 VARIATION OF CHAR AND TAR YIELDS WITH HEATING RATES

Coal	Programmed Heating Rate ($^{\circ}\text{C}/\text{sec}$)	Wt% Char/Soot	Wt% Tar (THF Soluble)	Final Temp. $^{\circ}\text{C}$
Utah Bit.	1	63	10	800
	10^2	53	30	800
	10^3	51	17	900
	$+10^5^*$	76^{\dagger}	14	**
Ken Bit.	1	62	15	800
	10^2	52	39	800
	10^3	50	35	900
	$+10^5^*$	61^{\dagger}	21	**

* Flash lamp operated at 2.5 kV-1125 μf discharge conditions, 2 msec flash pulse
 Particle size range of coal -140+325 mesh in all runs.

** Not known.

† A fraction of non-THF soluble tars has soot-like physical characteristics.

yields and char yields are minimized for hv Bit coals in moderate heating conditions and low pressure conditions. Very low heating rates and very high heating rates have the effect of decreasing tar yields while increasing solids yields, either in the form of char or a combination of char and soot. Light gas yields reflect the thermal flux conditions in the tar formation and evolution stages.

Summary and Discussion of Results

The formation and evolution of PAH species in coal devolatilization is observed to be a sensitive function of the mix of molecular species present in the parent coal. Through high volatile bituminous coals and within moderate heating conditions, PAH yields increase with apparent aromaticity of the coal. Those coals having the greater aromaticity, as indicated by infrared absorption characteristics, give consistently greater tar yields than less aromatic samples. Such coals also show less variation in tar yields with changes in heating rate. For moderate heating rates to final temperatures less than 1000^o C, the coal nitrogen evolution mirrors the parent coal evolution as char, tar or light gas species on a mass fraction basis. Heating rates of 1^o C/sec or less are observed to lower tar yields of bituminous coals while increasing char and light gas yields. On the other hand, programmed heating rates of 10⁵-10⁶ °C/sec also result in a decrease in tar yields with an increase in solid species products. A fraction of these solids appear to be soot particles. Gaseous yields of coals subjected to such high thermal fluxes show C₂H₂, CO, CH₄, HCN, C₂H₄ and polyacetylenes as the predominant gas phase species.

Not only do tar yields vary with heating conditions but evolution times vary significantly as well. Tar formation and evolution times are observed to be of the order of several milliseconds in the highest programmed heating rates employed to fraction of seconds to seconds in moderate heating rate conditions, and hundreds of seconds in the lowest heating rates employed. Formation of polycyclic aromatic species appears to begin at relatively low temperature, that is in the 300-475^o C temperature range. The ultimate tar yield then appears to be a complex function of heat and mass transfer parameters as well as chemical characteristics of these primary tars. For hv Bit coals and lower ranks, the more aromatic the primary tars, the less secondary chemical reactions influence observable behavior. For these coals, the initial mass loss of the coal is likely heat and mass transport limited. For higher rank coals, the primary tars are likely to be of such molecular weights and dimension that secondary char-forming reactions will become competitive with the tar evolution process. In view of such considerations, the wide variation in reported results reflect the coupled effects of intrinsic and extrinsic parameters on primary PAH formation and evolution.

Low heating rates allow secondary char-forming reactions of tars to take place within the coal particle. Very high heating rates introduce secondary cracking and ring condensation reactions of primary tars as they evolve. The susceptibility of primary tars to undergo char-forming or cracking reactions is a fraction of chemical characteristics of the primary tars. As noted in the Introduction the development of a comprehensive model of coal devolatilization/pyrolysis for a single rank of coal in a range of conditions or a range of coals in a single condition is contingent upon fundamental studies of the formation and evolution of primary PAH species.

REFERENCES

1. Howard, J. B., "Fundamentals of Coal Pyrolysis and Hydropyrolysis," Chemistry of Coal Utilization, 2nd Supp. Volume, M. A. Elliott (Editor), Wiley - Interscience, New York, 665 (1981).
2. Solomon, P. R. and Colket, M. B., Seventeenth Symposium (International) on Combustion, The Combustion Institute, Pittsburgh, PA, 131 (1979).
3. Anthony, D. B., Howard, J. B., Hottel, H. C. and Meisner, H. P., Fifteenth Symposium (International) on Combustion, The Combustion Institute, Pittsburgh, PA 1303 (1975).
4. Tyler, R. J., Fuel, 59, 218 (1980).
5. Kobayashi, H, Howard, J. B. and Sarofim, A. F., Sixteenth Symposium (International) on Combustion, The Combustion Institute, Pittsburgh, PA 411 (1977).
6. Brown, H. R., Hesp, W. R., and Waters, P. L., J. Inst. Fuel, 130 (1964).
7. Cameron, A. R. and Botham, J. C., Coal Science, 55, 564 (1966).
8. Habermehl, D., Orywal, F., and Beyer, Hans-Dieter, "Plastic Properties of Coal," Chemistry of Coal Utilization and Supp. Volume, M. A. Elliott (Editor), Wiley-Interscience, New York, 317 (1981).
9. Gryaznov, N. S., Coke Chem. USSR, 1, 5 (1962).
10. Van Kreulen, D. W., Huntjens, F. J., and Dormans, H. N. M., Fuel, 35, 462 (1956).
11. Kreulen, D. J. W., Fuel, 29, 112 (1950).
12. Nadziakiewicz, J., Fuel, 37, 361 (1958).
13. Freihaut, J. D., Zabielski, M. F. and Seery, D. J., Amer. Chem. Soc. Div. of Fuel Chem., 27, No. 2, 89 (1982).
14. Freihaut, J. D., Zabielski, M. F. and Seery, D. J. Nineteenth Symposium (International) on Combustion, The Combustion Institute, Pittsburgh, PA, 1159 (1982).
15. Bergmann, G., Husk, G., Karwell, J. and Luter, H., Brennstoff Chem., 35, 175 (1954).
16. Duyckaerts, G., The Analyst, 84, 201 (1959).
17. Friedel, R. A., Fuel, 38, 541 (1959).

18. Kmetko, E. A. *Phys. Rev.*, 82, 456 (1951).
19. Brown, J. K., Jr. *Chem. Soc.*, 744 (1955).
20. Friedel, R. A., and Queiser, J. A., Jr. *Anal. Chem.*, 28, 22 (1956).
21. Freihaut, J. D., and Seery, D. J., *Am. Chem. Soc. Div. of Fuel. Chem.*, 26, No. 3, 18 (1981).

ACKNOWLEDGMENTS

The authors express their gratitude to G. Wagner and D. Santos for their technical expertise in performing this investigation. Part of this work was sponsored by DOE Contract DE-AC21-81MC16221.

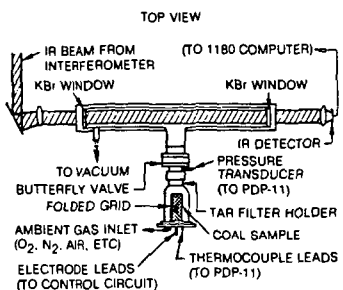


FIG. 1. Schematic of coal/devolatilization apparatus.

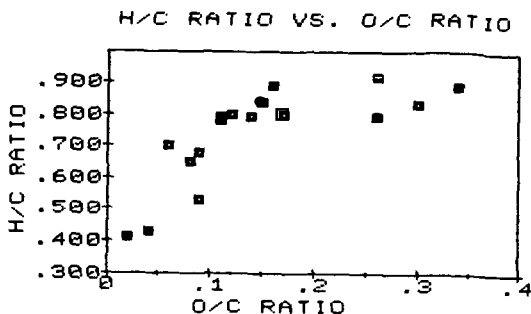


Fig. 2. Sample locations on coalification band.

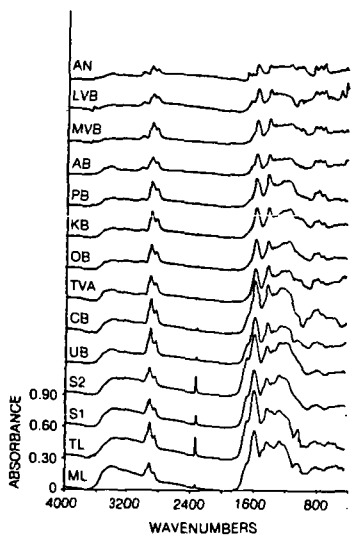


FIG. 3. Infrared absorption spectra of coals. Mineral matter subtracted. Baseline corrected.

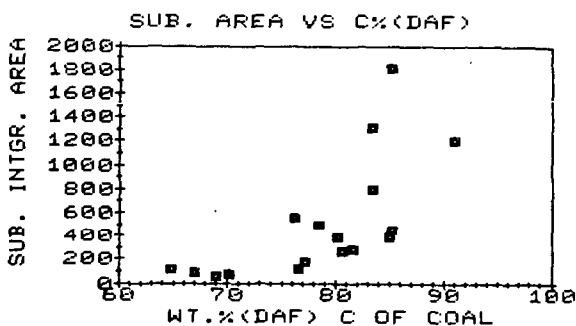


Fig. 4. Integrated area ($400-4000\text{ cm}^{-1}$) beneath chord drawn through tangent points at 3600 cm^{-1} and zero absorbance line: C fraction calculated dry and free (DAF) basis.

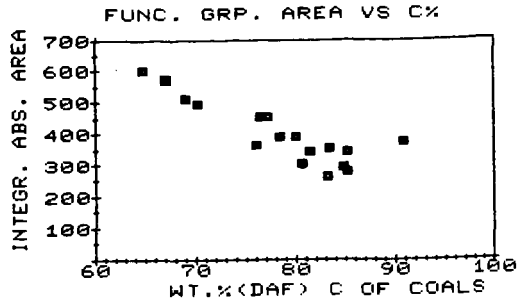


Fig. 5. Integrated area (400-4000 cm^{-1}) between chord baseline and absorption curve.

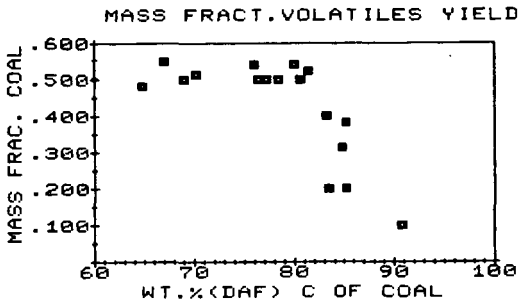


Fig. 6. Programmed heating rate $500^{\circ}\text{C}/\text{sec}$; final temperature 900°C ; see Ref. 13, 14 for sample loading conditions; dry sample used as basis of calculation; ambient pressure $\sim 10^{-2}$ torr; $-140+325$ mesh particles.

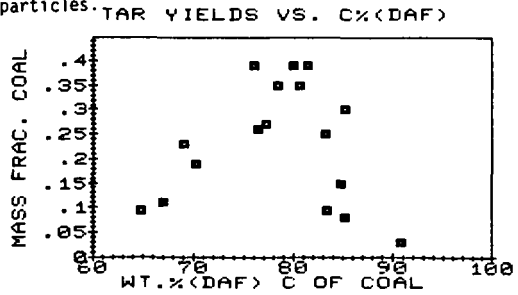


Fig. 7. Conditions as noted in Fig. 6.

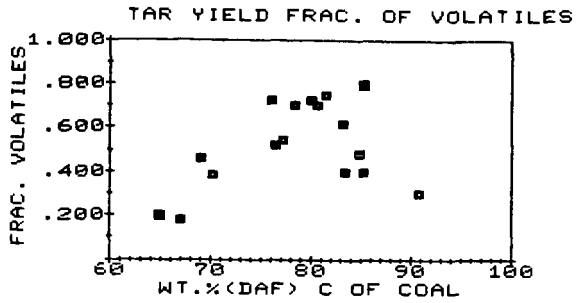


Fig. 8. Fraction of total volatiles evolved as PAH species.

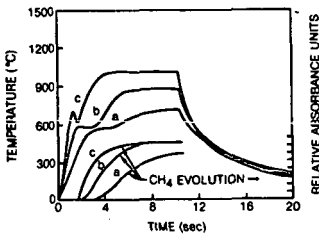


Fig. 9. Time resolved temperature and CH₄ evolution data for Rocky Mt. bituminous coal; a = 55.4% char; 30% tar; b = 52.6% Char, 24.0% tar; C = 51.3% char, 17.0%.

VARIATION OF THERMAL LOADING WITH RANK — CATS SYSTEM

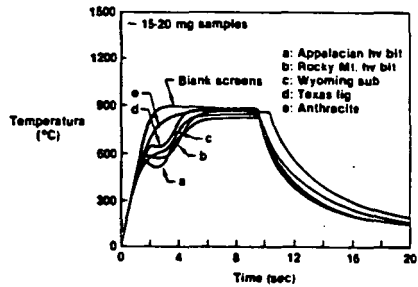


Fig. 10 a = 39% tar; b = 24% tar; c = 20% tar; d = 11% tar; e = 3% tar; see Ref. 13, 14 for loading conditions and thermocouple placement.

TAR AND LIGHT HYDROCARBON YIELDS

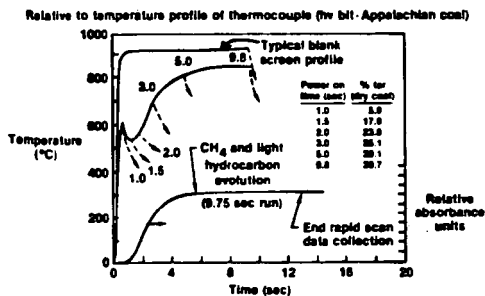


Fig. 11. Effect of tar release on temperature profile; see Ref. 13 and 14 for leading technique and thermocouple placement.

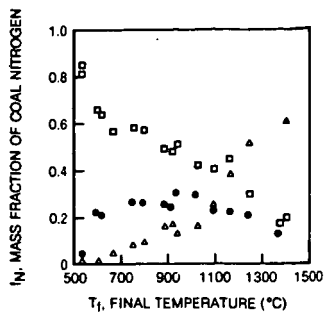


Fig. 12. Nitrogen distribution in devolatilization products; Rocky Mt. bituminous coal; \square = char; \bullet = tar; Δ HCN.

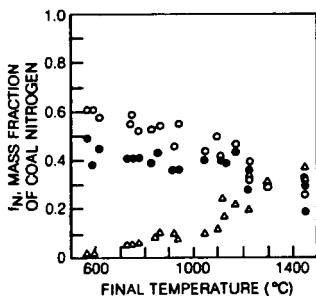


Fig. 13 Nitrogen distribution in devolatilization products; Appalachian Province bituminous coal; \circ = char, \bullet = tar, Δ = HCN.

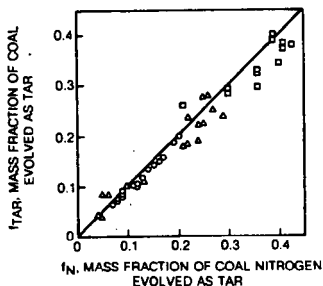


Fig. 14. Mass fraction parity between evolved tar and coal nitrogen as tar; Δ = Rocky Mt. Bit; \square = Appalachian Bit; \circ = Subbituminous.

Internal and External Mass Transfer Limitations in Coal Pyrolysis

Phillip E. Unger*

Dept. of Chem. Eng., Carnegie-Mellon University, Pittsburgh, Pa. 15213

Eric M. Suuberg

Division of Engineering, Brown University, Providence, R.I. 02912

Introduction

The recent work of Professor Howard and colleagues at MIT has helped focus attention upon the significant role that mass transfer limitations can play in shaping the pyrolysis behavior of coals (see, for example, the review by J.B. Howard, 1981). Despite having learned a great deal from these and earlier studies, it is fair to say that much remains to be learned on this topic. The present paper outlines some recent results of relevance. The focus here will be mainly on studies of high heating rate pyrolysis of finely ground coals (less than a millimeter in diameter) in low particle concentration environments. Such conditions of course exist in an enormous variety of coal conversion processes. The present focus is narrowed further by considering only the tar products of pyrolysis. Not only are these species central in discussions of mass transfer limitations, but they are of considerable interest as dominant products of most coal pyrolysis processes. Also, the topic of tar chemistry fits in well with Professor Howard's own discussion in this session, since tars have been suggested as key intermediates in certain soot formation processes during combustion of coal (Seeker et al., 1981; Mclean et al. 1981).

Background

It is customary to explore for internal mass transfer limitations in gas-solid reaction systems by performing experiments at various particle diameters. Unfortunately, data on the variation of pyrolysis product yields with particle diameter are often influenced by unintentional variations in heat transfer conditions (J.B. Howard et al., 1981). In addition, even in situations in which heat transfer to particles is relatively well defined (as in the heated wire mesh technique described below), there are sometimes difficulties in particle size characterization, since particles soften, swell, and/or flow on the surface of solid supports during pyrolysis. Consequently, most reliable information on mass transfer effects during rapid pyrolysis of fine particles has come from experiments in which the primary variable is external gas pressure.

It is well established that pyrolysis of coals under reduced pressures leads to increased volatile matter yields, compared to pyrolysis under atmospheric pressure (H.C. Howard, 1945, 1963; Anthony and J.B. Howard, 1976; J.B. Howard, 1981). There also remains little question that an increase in tar yield is mainly responsible for this increase in volatile matter yields (see above reviews and Suuberg et al., 1979a). Tar

* Present Address: Shell Development Corp., Houston, Texas

is here crudely defined as any room temperature condensable products of pyrolysis; water is excluded, but small amounts of product that is sometimes categorized as "oil" may be included. The increase in tar yields under reduced pressure has been qualitatively explained in the following terms. When heated, the coal "depolymerizes", yielding tar-like species. If these species are quickly transported away from the particle, they are observed as part of the tar products of pyrolysis. If, however, the species are given long times in the hot environment of the particles, they may be "repolymerized" into the mass of the particle, and later be counted in with the char.

While there is little debate over this qualitative picture, the development of quantitative models has revealed a great diversity of opinion concerning the nature of volatiles transport. Some have modeled the controlling transport processes by use of empirical external mass transfer coefficients (Anthony et al., 1974; Reidelbach and Summerfield, 1975), some by postulating internal pore transport to be limiting (Russel et al., 1979; Melia and Bowman, 1982, the latter allowing for bubble formation), one by considering nucleation and motion of bubbles within softened coal particles (Lewellen, 1975) another by considering the motion of volatiles in pseudo-bubbles (not accounting for particle swelling, James and Mills, 1976), and some by employing both a crude model of pore diffusion and an external film coefficient (Chen and Wen, 1979). Other models have more explicitly considered how product compositions may vary during pyrolysis. Of these, several have represented gas film diffusion as controlling, much as in classic droplet evaporation models (Suuberg et al., 1979b; Unger and Suuberg, 1981; and Zacharias, 1979). In other cases, pore transport models have again been developed (Gavalas and Wilks, 1980; Cheong, 1977). Finally, in one case, mass transport limitations have been handled through the use of a pseudo-chemical kinetic model (Solomon and Colket, 1979).

It is apparent that there continues to be considerable disagreement as to the true nature of mass transfer limitations which are responsible for the observed effects of pressure. Part of the disagreement concerns the location of the main transport limitation—whether it is internal or external to the pyrolyzing coal particle. Another source of the apparent disagreement between different workers concerns the nature of the starting coal—whether it is softening or non-softening (in the former case, it makes more sense to model the particle as essentially a droplet). In this paper, some of these issues are readdressed in the context of newly available data on the nature of coal tars.

General Observations Concerning Mass Transfer Limitations During Pyrolysis

There is a paucity of information concerning the effect of pressure on product yields observed during pyrolysis. Figure 1 presents an attempt at summarizing the majority of relevant data concerning pressure effects on tar yields during pyrolysis. It is a plot of reported tar yield vs. pressure, which illustrates the general feature of decreasing tar yield with increasing pressure. In order to compare the results for a wide range of ranks in a single figure, the data for

each coal have been "normalized" by dividing tar yield at a particular pressure by the maximum tar yield which can be obtained with that coal. This maximum tar yield naturally occurs at the lowest pressure examined during the series of experiments on the particular coal. Table 1 summarizes the conditions under which the data in Figure 1 were obtained. Where actual tar yield data were not available, a correlation based on all the available tar yield data was used to estimate normalized tar yields from weight loss data. This correlation was of form:

$$\text{Normalized tar yield} = 1 - 0.55((v_0 - v)/(v_0 - v_H))$$

where v_0 is the weight loss at the lowest pressure employed in the study, v_H is the weight loss at the highest pressure employed in the study, and v is the actual weight loss at the pressure of interest.

A rather consistent trend of decreasing tar yield with increasing pressure is observed in Fig. 1. Note that the data include both softening coals and non-softening coals, ranging in rank from lignite to low volatile bituminous. It is noteworthy that the points which seem to fall above the general trend are mainly those which were normalized with respect to 0.1 atm tar yield data. Both the data of Anthony et al. (1974) and Arendt and van Heek (1981) imply that 0.1 atm is still a high enough pressure such that an additional decrease in pressure might tend to increase tar yields further; thus the normalization factor applied to the data of Arendt and van Heek (1981) and Cavalas and Wilks (1980) might be relatively higher than that applied to the other data. Were lower pressure data available in these latter two cases, it is possible that normalization with respect to such data would pull these groups' results into even better agreement with the general trend.

On the basis of the general agreement between the diverse sets of data shown in Fig. 1, it might be concluded that the effect of external pressure is similar in all ranks of coal. Of course the coals that produce the largest amounts of tar are likewise those whose product yields are most sensitive to variations in pressure. The actual nature of the mass transfer process responsible for such behavior is still unknown, however. Some order of magnitude analyses have been advanced to eliminate a few possibilities.

If a particle is non-softening and ordinary gas phase diffusion were solely responsible for transport of tar, Russel et al. (1979) have pointed out that internal pore diffusion would almost certainly be controlling. It is possible that either pressure driven bulk flow or Knudsen diffusion might play a role in pore transport (though it must be recalled that the latter does not depend upon pressure). Niksa (1981) concludes that bulk flow must control flow out of the pores, so long as the particle retains its identity as a solid; however, the possible role of an external gas film limitation is not considered.

If the coal particle softens, Attar (1978) has proposed that a competition exists between liquid phase diffusion and bubble nucleation within particles. While plausible, it seems equally likely that bubbles are formed by gas pressure swelling pores originally present within the particle. It is not clear how important bubble transport of tar species is. A small bubble breaking the surface of the particle only serves to increase the surface area of the particle slightly, but a large bubble swelling the particle into a cenosphere increases its surface area

enormously. The extent to which bubbles aid in diffusion of species from bulk to surface is also unclear. In addition, it is possible that bubble growth and motion could be a source of internal mixing. It is difficult to make any general statements about the effect of bubbles or their significance, except that it is likely that their presence will enhance transport rates. The remainder of the discussion on transport in the case of softening coals will disregard the role of bubbles.

Softened coal particles have been previously viewed as analogous to multicomponent liquid droplets (Unger and Suuberg, 1981). Consider the ratio of characteristic time for internal liquid phase diffusion of tars from the bulk to the particle surface (t_i) to the characteristic time for external diffusion of the tar through a stagnant vapor film which surrounds the particle (t_e):

$$t_i/t_e = D_v C_v y / D_L C_L x$$

where D_v and D_L are vapor and liquid diffusivities, respectively; C_v and C_L are vapor phase and particle phase molar densities; y is the vapor phase mole fraction of a tar species at the particle surface, and x is the liquid phase mole fraction of a tar species at the particle surface. By use of Raoult's Law, if P^0 is the vapor pressure of the tar species, $y/x = P^0/P_{tot}$. In the case of atmospheric pressure pyrolysis, P_{tot} is 1 atm. and (C_v/C_L) is of order 10^{-2} to 10^{-3} . Neither P^0 nor D_v/D_L is known a priori. In particular, D_L is difficult to estimate, even to an order of magnitude.

It has been suggested that D_L can be estimated by use of the Stokes-Einstein equation to be of the order of 10^{-14} sq. cm/sec (Cavalas, 1982). Unfortunately, such estimates are based on having a knowledge of coal viscosity, which is itself unknown to even an order of magnitude under the high heating rate, high temperature conditions of interest here. In addition, recent measurements of the diffusivity of naphthalene in high viscosity oils have shown the Stokes-Einstein equation to be invalid (Hiss and Cussler, 1973). This is not surprising, since this equation has been derived assuming a large disparity in the size of solvent and solute, a condition which is met in neither coal melts nor the experiments described above. Although it is impossible to make even a crude estimate of D_L , it is reasonably certain that it will be smaller than 10^{-5} sq. cm/sec, implying that (D_v/D_L) is larger than 10^5 or 10^6 . Hence, unless P^0 is of order 10^{-3} or less, internal diffusion will definitely control.

Again, P^0 is difficult to estimate, because there exist no vapor pressure data for the type of coal tars of interest. To make a crude estimate, we have improved a previously used (Suuberg et al., 1979) simple correlation for vapor pressures of high molecular weight hydrocarbons:

$$P^0 \text{ (atm)} = 3756 \cdot \exp(-253 \cdot MW^{0.586}/T)$$

where MW is molecular weight and T is temperature in K. See Table 2 for a comparison of the predictions of the correlation to vapor pressure data. Note that the correlation does not include any structural information, nor has it been tested against data on high molecular weight materials with significant heteroatom contents. Considering "typical" tar molecular weights in the range 500 to 2000 (Unger and Suuberg, 1983a), at temperatures around 1000K, then apparently P^0 is of order 10^{-1} to 10^{-6} atm. On the basis of this range of values, it is impossible to draw a firm conclusion regarding the relative importance of internal and external mass transfer limitations. It is possible that

the escape of light species is limited by internal diffusion rates, but the escape of heavy species is limited by external film diffusion.

In this paper, we explore some new experimental evidence which sheds some light upon the nature of the transport limitations which exist during coal pyrolysis. Other important aspects have been presented elsewhere (Unger and Suuberg, 1983a, 1983b).

Experimental

Data will be presented on the molecular weight distributions of tars produced under a variety of pyrolysis conditions. The experimental technique has been described in detail elsewhere (Unger and Suuberg, 1983a). The widely used heated wire mesh technique was used to pyrolyze small (10-20mg) samples of coal. In these experiments, a thin layer of coal is uniformly spread on a wire mesh which is heated electrically at a predetermined rate to a peak temperature, from which the sample is then immediately recooled without an intervening isothermal period. The mesh is contained inside of a reactor shell which is filled with helium at the desired pressure; the helium remains relatively cold throughout the experiment, as the mesh is the only part of the apparatus which is heated. Since the mesh offers little resistance to escape of volatile products from the thin layer of particles which rest upon it, the volatiles may be assumed to be immediately quenched upon escape from the particle (this point is discussed further below).

Tars are gathered by washing the reactor with tetrahydrofuran (THF) and are analyzed by liquid chromatography for molecular weight distribution. In a few cases, extracts of the chars were obtained by soaking the chars in boiling THF for at least 15 minutes, in an ultrasonic bath. These extracts were analyzed in the same manner as tars for their molecular weights.

In a few cases, tars which had previously escaped the coal particles were reheated in the wire mesh. The sample sizes were roughly 10mg, and the run procedures were identical in every respect to the coal pyrolysis runs.

Finally, a few coal pyrolysis experiments were performed in an atmosphere of pure nitric oxide (NO). Again, the technique was otherwise identical to that used in normal coal pyrolysis experiments.

Table 3 gives elemental compositions of all coals examined in this study.

Results and Discussion

Figure 2 displays molecular weight data for Bruceton standard high volatile bituminous coal tars and extracts. These data will be discussed at length elsewhere (Unger and Suuberg, 1983a) and are shown here only as a framework for subsequent discussion. It should be emphasized that the Bruceton coal is a softening coal. Results for non-softening coals will be given below. Several conclusions have been drawn from these data:

-Tars produced at atmospheric pressure are significantly lighter in molecular weight than tars produced at vacuum. The number average molecular weight for the atmospheric pressure tars is typically

between 330 and 350, whereas for vacuum tar it is 430 to 460.

-Both vacuum and atmospheric pressure tars are significantly lighter than the extractable tars left behind in the particle; there is clearly a selective distillation.

-Neither vacuum nor atmospheric pressure tar molecular weight distributions show much sensitivity to temperature.

Subsequent work has revealed several other points (Unger and Suuberg, 1983b):

-There is a low inventory of extractable material present in the particle over the period of most active tar evolution.

-The large difference in yields of atmospheric pressure and vacuum tars develops mainly at peak temperatures in excess of about 550°C. Above this temperature, vacuum tar continues to be evolved, whereas atmospheric tar evolution is virtually complete at this temperature.

The generality of these conclusions is being tested by examining the behavior of a number of other coals. The temperature dependence of the molecular weight distributions of tars from an Illinois No. 6 high volatile bituminous coal, a Pocahontas low volatile coal and a North Dakota lignite are shown in Figures 3 through 5, respectively. Of these other coals, only the Illinois No. 6 softens during pyrolysis. The behavior of the Illinois No. 6 is very similar to that of the Bruceton coal, including the fact that the molecular weight distribution is relatively independent of temperature. The tar from the North Dakota lignite is likewise very similar in molecular weight range to the tar from the two softening coals. Again, the molecular weight distribution shows little sensitivity to temperature of evolution.

The tar from the Pocahontas coal shows a markedly lower molecular weight range than the tars from the other coals. The number average molecular weight of the Pocahontas tar is 240 at 464°C and 200 at 810°C. As of this writing, no extract molecular weight distribution data are yet available for this coal.

The data which are presently in hand suggest that the evolution of tar during coal pyrolysis is a complex combined transport and reaction process. Clearly, a pure internal liquid phase diffusion limitation cannot explain the trends observed in the softening coals, since it would be impossible to predict a pressure dependence of molecular weight distribution on this basis alone. A simple "batch distillation" transport model is inappropriate, since it would predict increasingly high tar molecular weights with increasing temperature. This has not been observed in any of the coals tested, except over very limited parts of the process (Unger and Suuberg, 1983a). The fact that the tars are apparently a light fraction of the extractable molecules present within the particle nevertheless seems to support an evaporation controlled mechanism. On this basis, a hypothesis that the evaporation process might be essentially analogous to a continuously fed distillation is currently being tested. Other data recently suggested that the pool of evaporating tar is continually being replenished by chemical reactions whose products are basically in a narrow range of molecular weight (Unger and Suuberg, 1983b).

As a further test of the hypothesis that evaporation rate controls tar escape from the particle, additional experiments were performed which involved evaporation of pure tars from the wire mesh.

Several milligrams of tar were collected by ordinary methods from the pyrolysis of the Illinois No. 6 coal. This tar was dried and spread in a pure state over the same type of wire mesh as used for coal pyrolysis. Figures 6 and 7 show the results of reheating the tar samples.

Figure 6 shows the molecular weight distribution of the "raw" tar and the molecular weight distributions of the re-evaporated tar fractions. The "raw" tar in Figure 6 differs from the tar products shown in Fig. 3 because drying of any tar sample promotes condensation of light fractions into heavier fractions (as does exposure of tar solutions to light or peroxides). It is apparent from Fig. 6 that tars up to 2000 in molecular weight can indeed evaporate, since no other transport processes were likely to be important in this experiment. It is interesting that upon repyrolysis, the molecular weight distribution of the re-evaporated tar is similar to the original molecular weight distribution of the Illinois No. 6 tar, prior to drying (see Fig. 7).

The above data imply that some degree of true pyrolysis also occurs in the tar re-evaporation experiments. Note in Fig. 6 that there is more light molecular weight material evaporated than was originally present. It is possible that the destruction of high molecular weight species (>2000 in molecular weight) explains why there is relatively much less of this material in re-evaporated tar than in the original coal tar. Alternatively, the presence of such high molecular weight material in the original tar might imply some role of physical entrainment mechanisms during coal pyrolysis, which do not exist in the tar re-evaporation experiments. The physical entrainment picture receives some support from a crude calculation; from the previously presented vapor pressure correlation, the vapor pressure of a 2000 molecular weight species is less than a microtorr at about 450°C. Yet there is a significant amount of such material present in the low temperature tars of all coals studied at that temperature. Of course, there is a great deal of uncertainty in the use of this correlation (derived for considerably lighter, pure hydrocarbons) for coal tars.

Finally, there was some concern that the observed molecular weight distributions might be influenced by secondary gas phase reactions of tar fragments. It was thought that free radical processes were the most likely pathway for such processes, so a crude attempt was undertaken to trap free radicals that might exist in the gas phase. This involved performing the coal pyrolysis experiments in an atmosphere of nitric oxide (NO, a well-known radical trap) rather than helium. It was postulated that if small free radicals were recombining to give larger tar molecules, there would be evidence of a downward shift in the tar molecular weight in NO. The results in Fig. 8 show no such evidence; in fact the average molecular weight of tar species appears to go up in NO. Unfortunately, the test is not clean by any means, since the NO obviously participated in the solid phase chemistry as well.

Conclusions

It now seems apparent that there is a great deal of similarity in the mechanisms of escape of tar from both softening and non-softening coals. The weight of evidence presently appears to favor an evaporation controlled escape of tar from the particle. A simple "batch distillation" model is obviously inappropriate for describing the process. Instead, it seems that a model which allows for simultaneous

tar precursor formation reactions, evaporation processes, and repolymerization reactions is necessary.

References

- Anthony, D.B. and Howard, J.B., AICHEJ, 22, 625 (1976).
- Anthony, D.B., Howard, J.B., Hottel, H.C., and Meissner, H.P. 15th Symp. (Int.) on Comb., p1303, 1974.
- Arendt, P. and van Heek, K-H., Fuel, 60, 779 (1981).
- Attar, A., AICHEJ, 24, 106 (1978).
- Chen, L.W. and Wen, C.Y., ACS Div. of Fuel Chem. Prepr., 24(3), 141 (1979).
- Cheong, P.H., PhD Thesis, California Institute of Technology, Pasadena, Ca. 1977.
- Gavalas, G.R., Coal Pyrolysis, p 104, Elsevier, 1982.
- Gavalas, G.R. and Wilks, K.A., AICHEJ, 26, 201 (1980).
- Hiss, T.G. and Cussler, E.L., AICHEJ, 19, 698 (1973).
- Howard, H.C. in Chem. of Coal Util., (H.H. Lowry, Ed.), pp761-773, Wiley, 1945.
- Howard, H.C. in Chem. of Coal Util., Suppl. Vol., (H.H. Lowry, Ed.), pp340-394, Wiley, 1963.
- Howard, J.B. in Chem. of Coal Util., Second Suppl. Vol., (M.A. Elliott, Ed.), pp665-784, Wiley, 1981.
- Howard, J.B., Peters, W.A., and Serio, M.A., EPRI Report AP-1803, Electric Power Research Institute, Palo Alto, Ca., April, 1981.
- James, R.K. and Mills, A.F., Letters in Heat and Mass Transfer, 3, 1 (1976).
- Lewellen, P.C., S.M. Thesis, Dept. of Chem. Eng., M.I.T., Cambridge, Ma. 1975.
- McLean, W.J., Hardesty, D.R., and Pohl, J.H., 18th Symp. (Int.) on Comb., p1239, 1981.
- Melia, P.F. and Bowman, C.T., WSS/CI Paper No. 82-7, Paper presented at the Western States Section/Combustion Institute Meeting, Salt Lake City, Ut., April, 1982.
- Niksa, S., PhD Thesis, Dept. of Chem. Eng., Princeton Univ., Princeton, N.J., 1981.
- Reidelbach, H. and Summerfield, M., ACS Div. of Fuel Chem. Prepr. 20(1), 161 (1975).
- Russel, W.B., Saville, D.A., and Greene, M.I., AICHEJ, 25, 65 (1979).
- Seeker, W.P., Samuelson, C.S., Heap, M.P. and Trolinger, J.D., 18th Symp. (Int.) on Comb., p1213, 1981.
- Solomon, P.R. and Colket, M.B., 17th Symp. (Int.) on Comb., p131, 1979.
- Suuberg, E.M., Peters, W.A. and Howard, J.B., I&EC Proc. Des. and Dev., 17, 37 (1978).
- , in Thermal Hydrocarbon Chemistry, (A. Oblad et al., Eds.), ACS Adv. in Chem. Series No. 183, Chap. 14, 1979a.
- , 17th Symp. (Int.) on Comb., p117, 1979b.
- Unger, P.E. and Suuberg, E.M., 18th Symp. (Int.) on Comb., p1203, 1981.
- , Manuscript submitted for publication, 1983a.
- , Manuscript submitted to the International Conference on Coal Science, Pittsburgh, Pa., August, 1983b.
- Zacharias, M.W., S.M. Thesis, Dept. of Chem. Eng., M.I.T., Cambridge, Ma. 1979.

Acknowledgement

We gratefully acknowledge the support of both the U.S. Department of Energy (Grant DE-FG22-81PC40803) and the Department of Chemical Engineering at CMU. We also thank Marilyn Ley and Glenn Swaney for valuable contributions to this work.

Table 1
Conditions for Figure 1

<u>REFERENCE</u>	<u>SYMBOL</u>	<u>COALS⁺</u>	<u>PARTICLE SIZE (μ)</u>	<u>HEATING RATE/MAX. TEMP.</u>	<u>PRESSURE (ATM)</u>	<u>METHOD</u>
ARENDR & VAN HECK (1981)	+	HVB(26), HVB(25), MVB(17), LVB(9)	200-315	200 °C/s 1000 °C	0.1-90	HWM
CAVALAS & WILKS (1980)	⊙	HVB(19), SUBB(6)	110	600 °C/s 500 °C	0.1-2	HWM
SUUBERG ET AL. (1978, 1979)	•	LIGNITE(8) 53-88 HVB(36)		1000 °C/s >900 °C	10 ⁻⁴ -69	HWM
UNGER & SUUBERG (1983b)	⊠	HVB(36)	62-88	1000 °C/s >900 °C	10 ⁻⁴ -1	HWM
H.C. HOWARD (1945)	Δ	HVB(20)	400-800	1 °C/s 525 °C	10 ⁻⁴ -1	RETORT
*ANTHONY ET AL. (1974)	■	HVB	70	>650 °C/s 1000 °C	10 ⁻³ -69	HWM
*NIKSA (1981)	×	HVB	125	1000 °C/s 750 °C	10 ⁻⁴ -100	HWM

* Tar yield data estimated

+ Maximum observed tar yields under vacuum shown in parentheses

HWM= Heated Wire Mesh

Table 2
Comparison of Predicted and Measured Temperatures
for a Vapor Pressure of 0.5mmHg ($^{\circ}$ C)

<u>Compound</u>	<u>MW</u>	<u>Meas. Temp.</u>	<u>Calc. Temp.</u>
1-t-Butyldecahydro-naphthalene	198	59.5	71.2
1,2-Diphenylbenzene	231	124.0	115.3
Perhydroperylene	262	150.5	145.1
3-n hexylperylene	336	198.0	210.8
2-n octylchrysene	339	242.5	213.3
3-n decylpyrene	342	235.5	215.8

MW=Molecular Weight

Vapor pressure data from G. Smith, J. Winnick, D. Abrams, and J. Prausnitz, Can. J. Chem. Eng., 54, 337(1976).

Table 3
Ultimate Analyses of Coals Examined

<u>COAL</u>	<u>C</u>	<u>H</u>	<u>O</u>	<u>N</u>	<u>S</u>	<u>ASH</u>	<u>MOISTURE</u>
BRUCETON PITTS. NO. 8 BITUMINOUS	80.4	5.3	6.7	1.6	1.0	4.6	1.7
HILLSBORO ILL. NO. 6 BITUMINOUS	67.2	4.6	12.3	1.2	3.4	11.7	8.6
W. VA. POCAHONTAS LOW VOLATILE BITUM.	84.4	4.2	3.7	0.3	0.5	6.8	0.2
NORTH DAKOTA LIGNITE	66.7	3.7	19.5	0.9	0.8	9.3	32.4

All results on a dry basis except moisture, which is reported on an as-received basis. North Dakota lignite is dried prior to use.

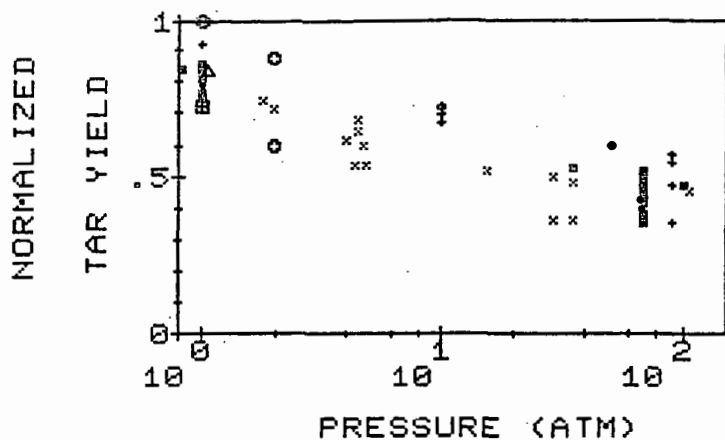


FIGURE 1. VARIATION OF TAR YIELD WITH PRESSURE OF INERT GAS EXTERNAL TO THE PARTICLE DURING PYROLYSIS. SEE TABLE 1 FOR EXPLANATION OF SYMBOLS.

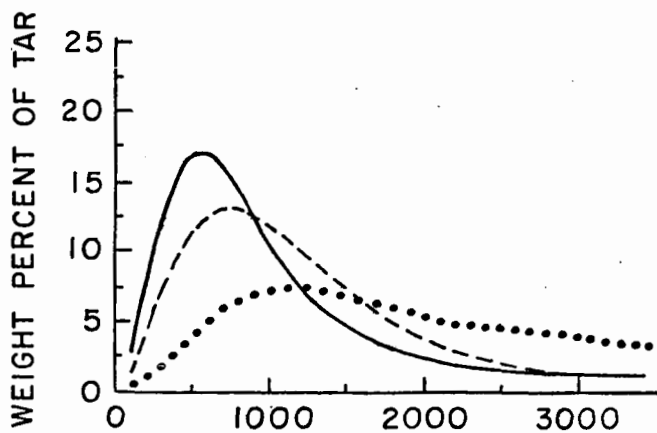


FIGURE 2. MOLECULAR WEIGHT DISTRIBUTIONS OF BRUCETON COAL TARS AND EXTRACTS. SOLID CURVE-ATMOSPHERIC PRESSURE TAR; DASHED CURVE-VACUUM TAR; DOTTED CURVE-COAL EXTRACT. ALL FOR SAMPLES HEATED AT 1000°C/s TO 546°C, FOLLOWED BY COOLING AT 200-400°C/s.

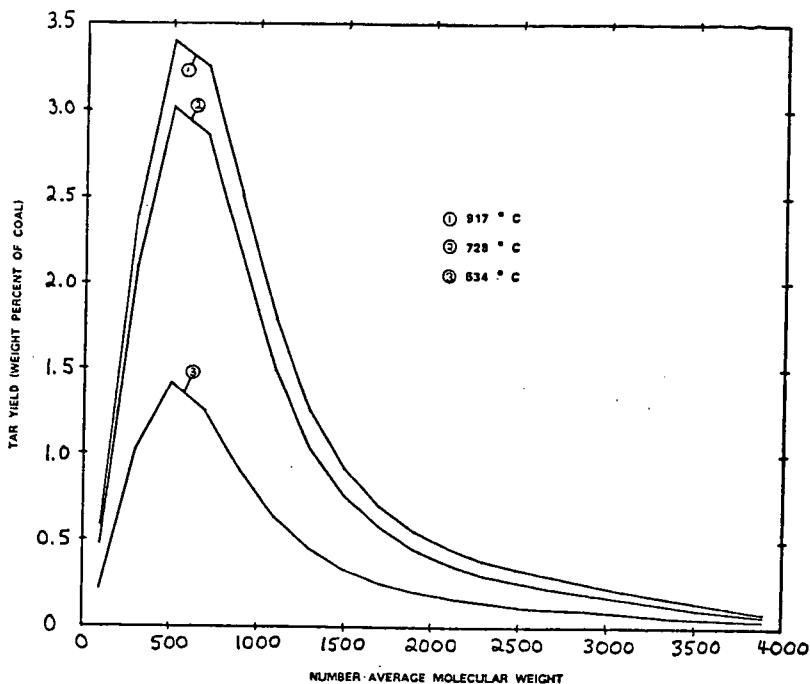


FIGURE 3. MOLECULAR WEIGHT DISTRIBUTIONS OF ILLINOIS NO. 6 ATMOSPHERIC PRESSURE TAR. SAMPLES HEATED AT 1000°C/S TO INDICATED TEMPERATURES.

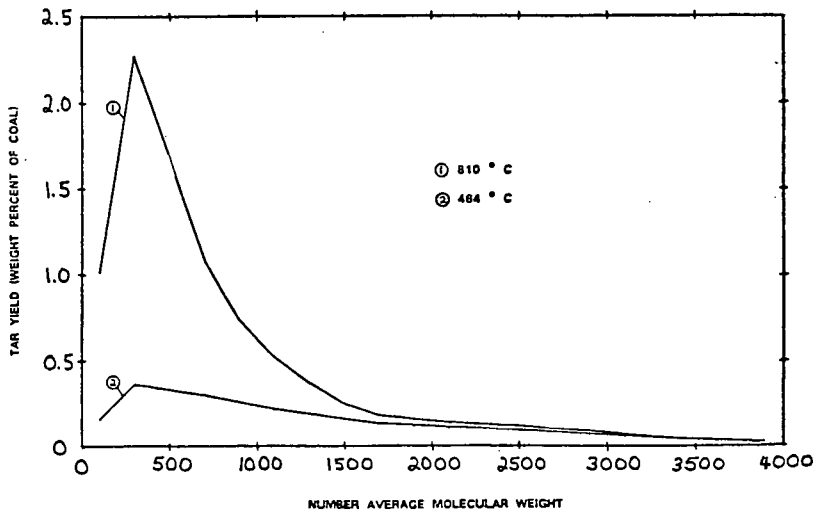


FIGURE 4. MOLECULAR WEIGHT DISTRIBUTIONS OF POCAHONTAS LOW VOLATILE COAL ATMOSPHERIC PRESSURE TAR. SAMPLES HEATED AT 1000°C/S TO INDICATED TEMPERATURES.

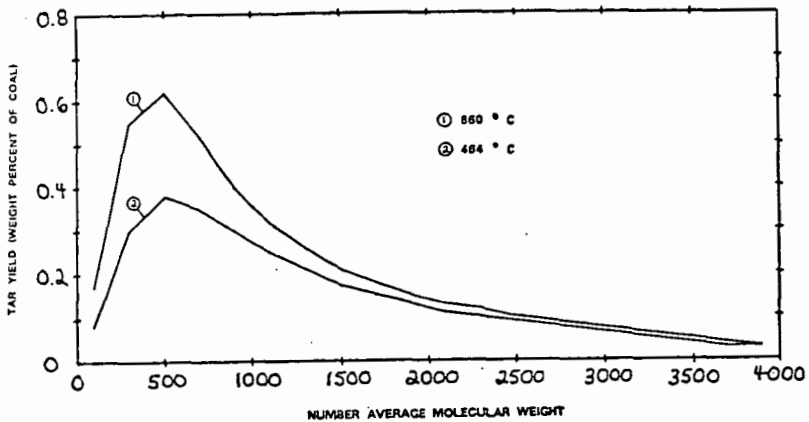


FIGURE 5. MOLECULAR WEIGHT DISTRIBUTIONS OF NORTH DAKOTA LIGNITE ATMOSPHERIC PRESSURE TAR. SAMPLES HEATED AT $1000^{\circ}/s$ TO INDICATED TEMPERATURES.

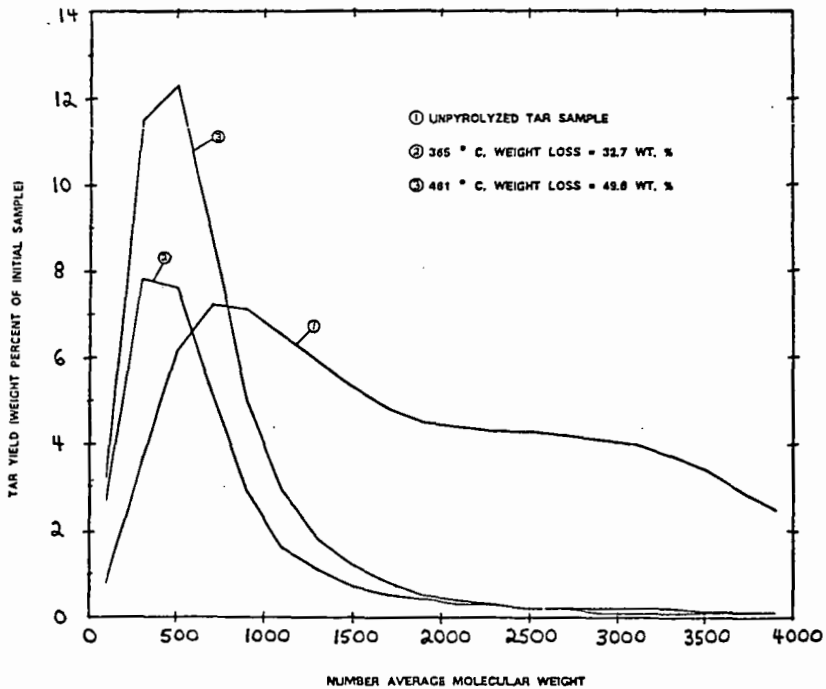


FIGURE 6. MOLECULAR WEIGHT DISTRIBUTIONS OF DRIED "RAW" ILLINOIS NO. 6 TAR, AND RE-PYROLYZED (RE-EVAPORATED) FRACTIONS OF THAT TAR. SAMPLES HEATED AT $1000^{\circ}C/s$ TO THE INDICATED TEMPERATURES.

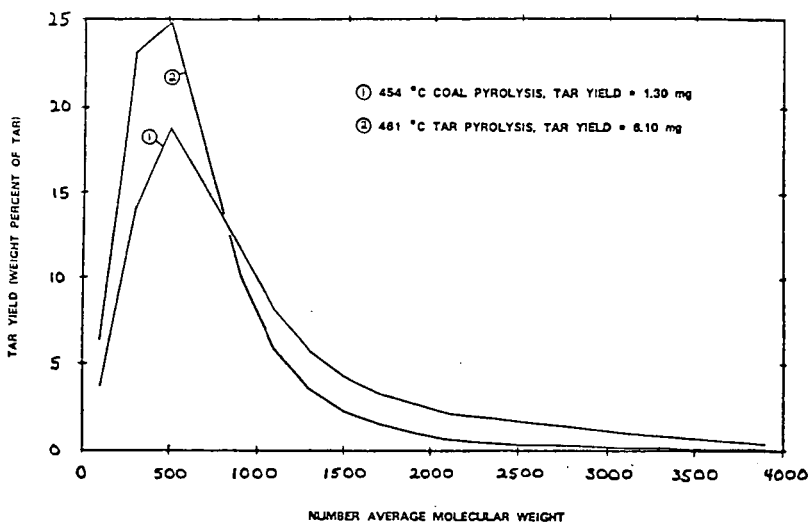


FIGURE 7. A COMPARISON OF THE MOLECULAR WEIGHT DISTRIBUTIONS OF FRESH ILLINOIS NO. 6 TAR (FROM COAL PYROLYSIS) AND RE-PYROLYZED TAR. THESE SAMPLES WERE FORMED UNDER NEARLY IDENTICAL HEATING CONDITIONS (1000°C/S HEATING RATES).

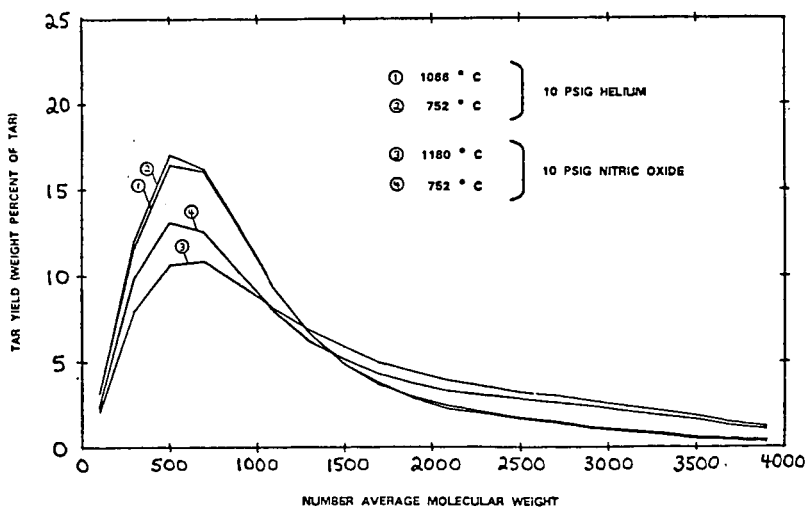


FIGURE 8. A COMPARISON OF MOLECULAR WEIGHT DISTRIBUTIONS OF TARS PRODUCED BY PYROLYSIS OF BRUCETON COAL UNDER HELIUM AND NITRIC OXIDE.

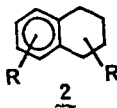
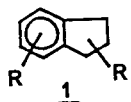
SYNTHESIS OF ALKYLATED INDANES AND TETRALINS
FOR USE IN FOSSIL FUEL ANALYSIS

By

D. S. Watt, M. Adamczyk, and D. A. Netzel
Department of Chemistry, University of Wyoming
and Department of Energy, Laramie Energy Technology Center
Laramie, Wyoming 82070

ABSTRACT

The availability of authentic hydrocarbon samples in the substituted indane and tetralin families would facilitate the analysis of certain fossil fuel mixtures. We have developed general procedures for the efficient preparation of simple alkylated indanes 1 tetralins 2 from common precursors. We have examined the ^{13}C NMR and mass spectral fragmentation data for hydrocarbons 1 and 2 in detail.



A TIME-TEMPERATURE-CONCENTRATION MATRIX FOR INDUCED
SEDIMENT FORMATION IN SHALE DIESEL FUEL

By

J. V. Cooney, E. J. Beal, and R. N. Hazlett
Naval Research Laboratory, Code 6180, Washington, D. C. 20375

INTRODUCTION

Deterioration in fuel quality with time has been a continuing problem in the utilization of middle distillate fuels. These stability problems will intensify as we develop alternative sources of fuel, such as shale oil and coal. Present knowledge has suggested that for some fuels, nitrogen heterocycles may play a causative role in the formation of insoluble sediments and gums under conditions of ambient and accelerated storage (1). In light of the high costs of fuel processing, substantial savings could be realized if it were possible to identify those nitrogen heterocycles which are most actively involved in the formation of insoluble material. Currently, it appears that relatively non-basic nitrogen heterocycles, particularly those which contain alkyl groups in certain positions, may be the most troublesome (2). However, in other fuels and under different test conditions, basic nitrogen compounds may play a significant role (3).

In addressing this subject, we are defining the stability of shale-derived diesel fuel marine (DFM), stressing the sample under accelerated storage conditions, and determining the amount of total insoluble material produced. This report describes results obtained when 2,5-dimethylpyrrole (DMP) was used as a dopant in a time-temperature-concentration matrix. Results of a survey of other nitrogen compounds as fuel additives are also presented.

EXPERIMENTAL

Storage Test Techniques

The experimental procedures used were developed from reported methods (2). In summary, 300 ml samples of filtered fuel were stressed in the dark in 500 ml screw-cap borosilicate Erlenmeyer flasks (Teflon-lined caps). All samples were run in duplicate. Vented tests were accomplished by using modified screw caps which were drilled to hold 6 mm glass tubing (with glass wool plugs). After stress, test flasks were allowed to cool to room temperature before being filtered under slight vacuum through a double layer of Gelman glass fiber filter paper. Flask contents were then rinsed with several ml of *n*-heptane, with additional sediment being collected on the filter paper. The filter cake was rinsed with *n*-heptane to remove adsorbed fuel. The flasks and filter holders were heated (120°C) under vacuum for twelve hours, allowed to equilibrate on a benchtop (several hours), and accurately weighed several times on an analytical balance. Appropriate blank flask/filter holder corrections were applied. Filtrable sediment values were obtained from the corrected net weight change of the filter holder with adherent gum values determined from the weight change of the test flask (4).

Reagents

The base fuel for the present study is DFM refined from Paraho crude shale oil by SOHIO. This fuel, produced in the U. S. Navy's Shale-II demonstration, is well-characterized (4). It was available with (sample "D-1") and without (sample "D-11") antioxidant added. The antioxidant, 2,4-dimethyl-6-*t*-butylphenol (AO-30), was present at the 24 mg/l level in fuel D-11. No other additives were present in either sample. All nitrogen compounds used as dopants were pure by NMR, capillary GC, and/or mp. Fresh DMP was stored frozen under nitrogen so as to prevent autoxidation and it remained colorless under this storage. The concentration matrix was prepared by appropriate dilution of a quantity of stock-doped fuel solution (typically 450 ppm w/v nitrogen).

RESULTS AND DISCUSSION

Accelerated fuel stability tests are important to the producers of fuels and to those performing research on chemical instability phenomena (5). The majority of these tests measure sediment weight in order to estimate fuel instability, and test temperatures have varied between ambient and

150°C. Although higher temperatures enable storage tests to be completed in minimum time periods, the accompanying uncertainty of the significance of the observed conditions may be dominant. Figure 1 summarizes a time-temperature matrix for several accelerated fuel stability tests which have appeared in the literature. It is noteworthy that a majority of the stability tests depicted fall close to the solid line, which represents a doubling of test time for each 10°C drop in temperature. The line extrapolates to approximately one year of ambient storage. The present study has concentrated on the lower temperature range (43, 65, and 80°C) in an effort to examine the reliability of using such accelerated storage tests as measures of ambient stability. As indicated by Figure 1, stress times were selected to bracket the solid line at each of the three temperatures.

The promotion of sediment formation in fuels by DMP has been reported to be a facile process, characterized by an activation energy of 10-15 kcal/mol (1,2). When subjected to storage at 43°C for periods of time ranging from 52 to 179 days DMP-doped Shale-II DFM formed large amounts of insoluble material. The DMP was added to samples D-1 and D-11 at concentrations of 0, 45, 135, 270 and 450 ppm N (w/v), and vented trials were also conducted at 45 and 450 ppm. The deviation between duplicate stress samples was small and indicated very good reproducibility for the test procedure. In general, the adherent gum comprised only 5-10% of the total insolubles. Venting of test flasks did not affect the amount of insoluble material formed. In a similar manner, the presence of the antioxidant (AO-30) in D-11 was of no consequence.

The DMP test matrix at 80°C (stress lengths 4-28 days) provided results which compared exceptionally well with those obtained at 43°C. In general, results at 65°C (11-50 days) also showed good agreement with the other two temperature regimens, although agreement between duplicates was somewhat less satisfactory at this temperature. The results for 80°C stresses of DMP-doped D-1 are shown in Figure 2. The first-order type of behavior which was observed with DMP is illustrated in Figure 3. At all temperatures examined, the amount of total insoluble material formed was directly proportional to the initial concentration of DMP. Furthermore, nitrogen balance calculations are able to account for all of the DMP (after stress) as either unreacted or incorporated into the sediment produced. Nitrogen-specific capillary GC (Hall detector) did not detect any nitrogenous intermediates in the liquid phase.

The sediments produced in all instances have been found to be rich in nitrogen (ca. 12% by weight), and an empirical formula of $C_6, 3H_6, 7NO_{1.4}$ has been determined (oxygen by direct analysis). The energy of activation for the production of total insolubles was calculated to be 11.7 and 11.6 kcal/mol for fuels D-1 and D-11, respectively. No induction periods were observed.

Filtrate hydroperoxide levels were determined in stressed samples by iodometric titration (ASTM D-1583-60). DMP-doped DFM samples exhibited very low peroxide numbers after stress. The DMP either prevents hydroperoxides from forming, or else reacts with any hydroperoxides which have formed. Results obtained in benzene indicated that formation of hydroperoxides from solvent molecules is not a prerequisite for DMP-promoted sedimentation. Mechanistic studies are continuing. Figure 4 shows the peroxide numbers obtained for D-1 and D-11 fuel blanks (un-doped) after 80°C stress. The antioxidant present in D-11 was seen to protect the fuel out to about 21 days, at which point the peroxide numbers increased sharply. Fuel D-11 contained no detectable hydroperoxide prior to stress.

A survey of other nitrogen compounds as fuel dopants has been undertaken in D-1 fuel. The results of 80°C - 14 day trials (unvented) with 450 ppm N (w/v) of a variety of compound classes are shown in Table I. Alkyl substituted pyrroles were found to be the most active species, with pyridines and quinolines less active. Peroxide numbers were low in the case of most pyrrole trials, and the sediments obtained were rich in nitrogen. Curiously, Knorr's pyrrole (2,4-dimethyl-3,5-dicarbethoxy-) was a most inactive species. Thus, electronic factors may be important for pyrroles.

CONCLUSIONS

A common reaction pathway appears to exist for DMP-promoted sedimentation in DFM. Results obtained are consistent with those of other workers (2) A high-precision gravimetric method of fuel storage stability determination has been developed.

ACKNOWLEDGMENT

The authors thank Dr. Dennis W. Brinkman of the Bartlesville Energy Technology Center (DOE) for sponsoring this work under DOE contract DE-AI-81BC10525. References to brand names were made for identification only and do not imply endorsement by DOE or NRL.

FIGURE 2
 Total Deposits for Shale-II DFM
 (D-1) with DMP Added - 80°C

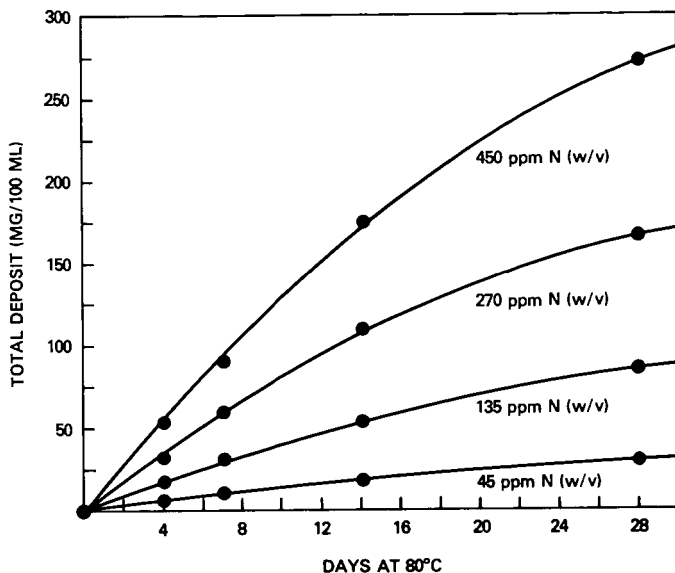


FIGURE 3
 Total Deposit as a Function of Initial DMP
 Concentration Added to DFM (D-11)
 28 Day Stress at 80°C

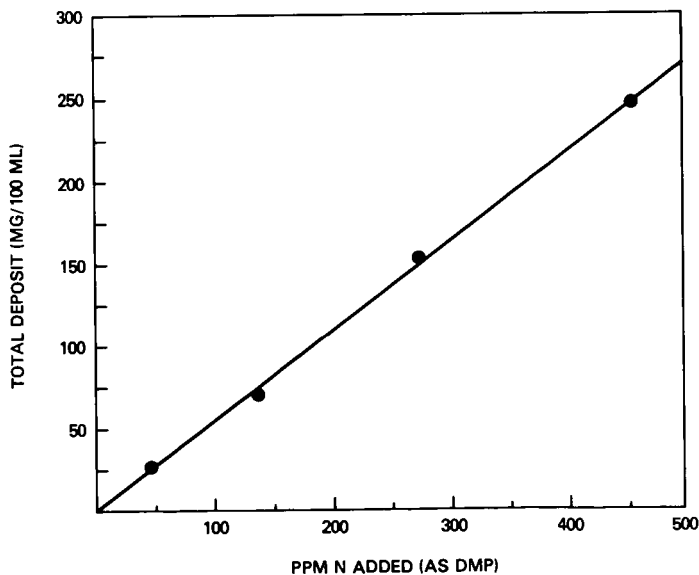


FIGURE 4
Peroxide Numbers for DFM
(D-1 and D-11) at 80°C

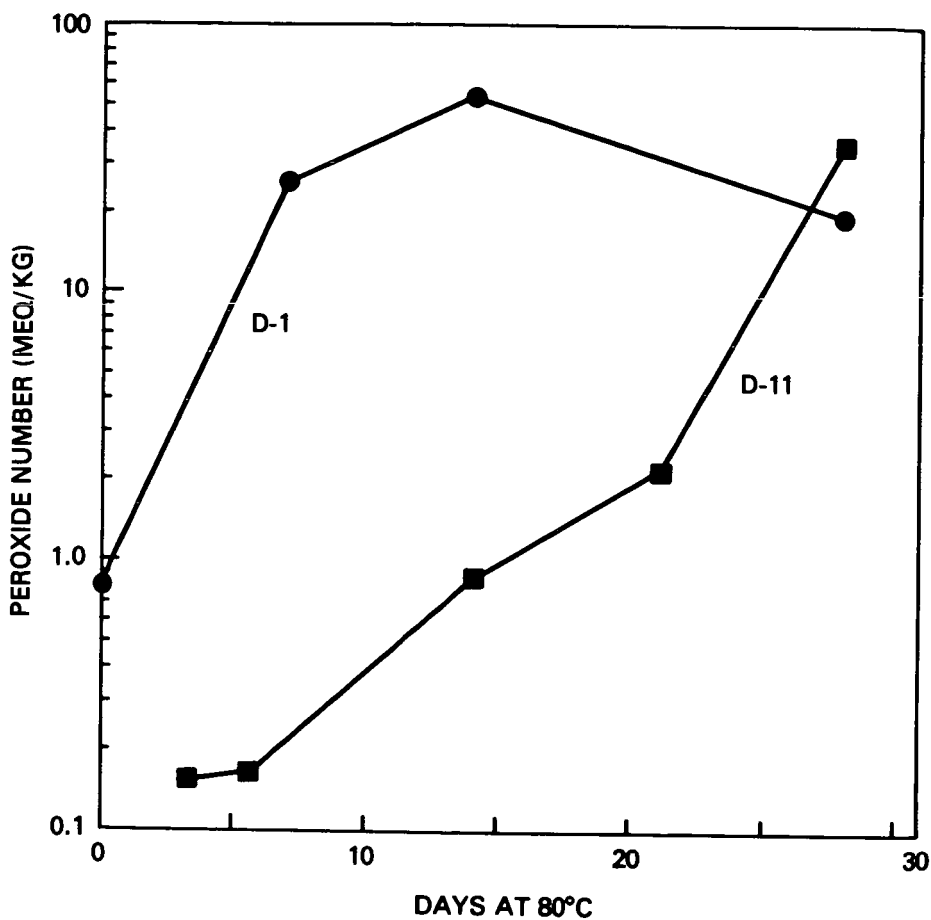


TABLE I
RELATIONSHIP OF NITROGEN COMPOUND STRUCTURE
TO SEDIMENTATION IN DFM (D-1)
(Listed in Approximate Order of Activity)*

<u>Group A (>100 mg/100 ml)</u>	<u>Group C (3-10 mg/100 ml)</u>	<u>Group D (<3 mg/100 ml)</u>
2,3,4,5-Tetramethylpyrrole	2,3-Dimethylindoline	3,5-Dimethylpyridine
Dodecahydrocarbazole	2,6-Dimethylpyridine	3,5-Dimethylpyrazole
2,4-Dimethylpyrrole	2-Methylpyrrole	4-Methylquinoline
2,3-Dimethylpyrrole	4-T-Butylpyridine	2-Methylquinoline
1,2,5-Trimethylpyrrole	3-Methylisoquinoline	3-Methylpiperidine
	Pyrrole-2-Carboxaldehyde	2-Methylpyrazine
	1-Methylpyrrolidine	2,5-Dimethylpyrazine
<u>Group B (10-100 mg/100 ml)</u>	2,6-Dimethylquinoline	Indole-3-Carboxaldehyde
Pentamethylpyrrole	2-Benzylpyridine	5,6,7,8-Tetrahydroquinoline
3-Methylindole	4-Iso-Butylquinoline	5-Ethyl-2-Methylpyridine
	2-Methylpiperidine	Trans-2,5-Dimethylpiperazine
	Pyrrolidine	2-Methylindole
	2-Acetyl-1-Methylpyrrole	2-Methylpyridine
		1,2,3,4-Tetrahydroquinoline
		2,6-Dimethylpiperidine
		2,4-Dimethyl-3,5-Dicarbethoxypyrrrole

LITERATURE CITED

- (1) Frankenfeld, J. W., Taylor, W. F., and Brinkman, D. W., "Fundamental Synthetic Fuel Stability Study", EXXON R and E Co., Rpt. No. DOE/BC/10045-12, February 1981 and references therein.
- (2) Frankenfeld, J. W., Taylor, W. F., and Brinkman, D. W., "Fundamental Synthetic Fuel Stability Study", EXXON R and E Co., Rpt. No. DOE/BC/10045-23, March 1982.
- (3) For example: a) Dahlin, K. E., Daniel, S. R., and Worstell, J. H., Fuel, 60, 477 (1981); b) Worstell, J. H., and Daniel, S. R., Fuel, 60, 481 (1981); c) Worstell, J. H., Daniel, S. R., and Frauenhoff, G., Fuel, 60, 485 (1981).
- (4) For more detail: Hazlett, R. N., Cooney, J. V., and Beal, E., "Mechanisms of Syncrude/Synfuel Degradation - First Annual Report: September 15, 1981 - September 30, 1982", Rpt. No. DOE/BC/ (in press), 1983.
- (5) For a thorough review: Stavinoha, L. L., Westbrook, S. R., and Brinkman, D. W., "Accelerated Stability Test Techniques for Middle Distillate Fuels", Southwest Research Institute, Rpt. No. DOE/BC/10043-12, October 1980.

IGNITION AND COMBUSTION OF COAL PARTICLES

By

C. O. Gomez and F. J. Vastola
Department of Materials Science and Engineering
The Pennsylvania State University, University Park, Pennsylvania 16802

INTRODUCTION

A fundamental understanding of the coal combustion process is important not only in the operation of combustion furnaces but also in the design of equipment for efficient burning, especially now when one of the requirements in the recent emphasis on coal utilization is clean burning. Even when the combustion of coal and char particles has been studied for a long time and extensive literature exists in the subject (1-4), this fundamental understanding has not been established. A clear demonstration is the wide variety of assumptions made in the most recent attempts of modeling the phenomenon (5-10).

The combustion of coal particles is a heterogeneous phenomenon involving a relatively unknown material and occurring in two stages: ignition and burn-out. Ignition depends on a balance between the rates of heat gain and loss to the particle; consequently the particle size, the environmental conditions, and the reactor geometry that defines the fluid dynamics of the system play important roles. The study of this complex phenomenon is difficult, because in addition to its transient character, it involves the simultaneous occurrence of a number of transport processes which apply to a system whose dimensions and characteristics change with time.

Two ignition mechanisms for coal particles are accepted. Their occurrence depends on the relative rates of two phenomena: the heating of the particle surface and the rate of volatile release. When the rate of heating of the particle surface is larger than the rate of volatiles release, the ignition takes place on the particle surface and the mechanism is called heterogeneous. In this case, the particle surface reaches a temperature high enough for reacting and igniting prior to extensive pyrolysis. On the other hand, when the rate of volatile release is larger than the rate of heating of the particle surface, the ignition occurs in the gas phase surrounding the particle and the mechanism is called homogeneous. In this case, the pyrolysis is so rapid that the particle surface is isolated from the external gaseous mixture by a volatile layer. To investigate the conditions which control the mode of ignition we conducted experiments utilizing single particles of coal.

EXPERIMENTAL

A schematic diagram of the apparatus is in Figure 1. The oxygen-nitrogen mixture is heated in the gas preheater and then sweeps the reaction zone where a single coal particle is introduced by gravity, using a specially designed injector. A light beam at location 1 is used to detect the time of the particles entry into the reaction zone. The gaseous products are rapidly cooled and split to be simultaneously measured by two nondispersive infrared analyzers, one for carbon monoxide and one for carbon dioxide. A photo transistor connected to a light pipe placed within the reaction zone is used to detect combustion generated luminosity. A microcomputer-based data acquisition system records the time of injection, the light generated by the particle's ignition and burnout, as well as the carbon monoxide and carbon dioxide concentration in the product gas stream.

In addition to the time of entry of the coal particle into the reaction zone the time of transit of the product gases from the reaction zone to the detector must be determined. This transit time was measured by injecting a short pulse of carbon dioxide into the reaction zone under the same conditions as used in an ignition run and measuring the time to detector response. To characterize any deformation of the product pulse as it flows from the reaction zone to the detector a similar short pulse of carbon dioxide was directly injected into the detector cell. The shape of the pulse after its travel through the system was compared with that resulting from the injection of the pulse directly into the detector cell. No appreciable difference was detected, indicating that the conditions used are very effective in reducing the deformation of the gas release curves.

A subbituminous coal (PSOC 648), whose characteristics are shown in Table I, was used in this study. Particles from the 850-1000 micron sieve fraction were injected into a reaction furnace swept with air at five temperature levels of 928, 980, 1076, 1118 and 1273°K.

TABLE I
CHARACTERISTICS OF COAL PSOC 648

Apparent Rank: Subbituminous B	Proximate Analysis (as received)	
	Moisture	22.10%
Reflectance Rank: HVC	Ash	4.58%
	Volatile Matter	33.78%
	Fixed Carbon	39.59%
Ultimate Analysis	<u>As Received</u>	<u>Dry Basis</u>
Moisture	22.10%	%
Ash	4.58%	5.88%
C	53.01%	68.05%
H	4.00%	5.13%
S (total)	0.33%	0.42%
N	0.80%	1.03%
O (by difference)	15.18%	19.49%

RESULTS AND DISCUSSION

Typical results of the gas evolution during combustion are shown in Figure 2 for selected runs at the different temperatures used in this study. The carbon monoxide and carbon dioxide concentrations are plotted against time with zero time being that time when product gases are first detected. Homogeneous ignition, as evidenced by a peak in the carbon dioxide product curve, is detected at temperatures of 1076°K and higher. The integration of the gas evolution curves will give the total mass of carbon in the original particle, if all the carbon is oxidized to carbon monoxide or carbon dioxide, which means in the case of the combustion of a coal particle, the complete burn-out of the volatiles released in the early stages of the combustion. Experimental results suggest that this was the case, because the most difficult hydrocarbon to be oxidized--methane--detected during the pyrolysis of coal particles, was not found during their combustion.

The occurrence of either of the two mechanisms of ignition previously described can be easily determined from the results of the light intensity measurements presented in Figure 3. When a coal particle ignites homogeneously, the combustion in the gaseous phase of the volatile matter released from the particle produces an initial flash of light, followed by the glowing of the remaining particle as the heterogeneous combustion proceeds. On the other hand, when the ignition mechanism is heterogeneous, the initial flash of light is not observed and only the final glowing is detected.

The ignition mechanisms detected by light intensity and by gas release curves have been summarized in Table II. There is complete agreement between the two techniques, except at the intermediate temperature of 1076°K. This discrepancy however, is consequence of an insufficient amount of volatiles released by the particle for burning with enough intensity to generate a flash of light, when the gas temperature is 1076°K. However, the amount released is enough to be detected before the ignition begins on the surface of the particle. This is a clear advantage of the experimental approach used in this work and shows how both techniques complement each other.

The total combustion time can also be determined from light intensity measurements and from gas evolution curves. A comparison between the results given by the two techniques is presented in Figure 4, where the combustion time measured by carbon dioxide evolution is plotted against the value obtained from light intensity for coal particles. Carbon dioxide was selected over carbon monoxide because of the greater sensitivity of the carbon dioxide detector, which allows the measurement of the combustion time more accurately. The combustion times tend to be larger when they are measured by gas evolution than by light intensity. This tendency is not unexpected because light can be detected only after the particle temperature increases to a point at which it is visible from the background. This high temperature is reached after a period in which gases were already evolving.

An unexpected result is the decrease in the proportion of carbon monoxide in the product gases, as the gas temperature increases. If the measured concentrations of carbon monoxide and carbon dioxide are the results of the chemical reaction on the surface, an increase in the proportion of carbon monoxide is expected as the temperature rises. The opposite trend is a consequence of the gas phase oxidation of carbon monoxide to carbon dioxide, which modifies the relation of the primary products of the reaction. In any case, the occurrence of this gas phase reaction does not affect the results previously discussed, because they are based on the total carbon consumed in the particle, and the gas phase reaction only affects the relative distribution of carbon as carbon monoxide or carbon dioxide, but not the total carbon coming from the particle as the result of the chemical reaction.

TABLE II
MECHANISMS OF IGNITION DETECTED BY DIFFERENT TECHNIQUES
IN THE COMBUSTION OF COAL PARTICLES

Gas Temperature (°K)	Run	Ignition Mechanism Detected by	
		Light Intensity	Gas Evolution
928	150	Het	Het
	151	Het	Het
	152	Het	Het
	153	Het	Het
	154	Het	Het
980	115	Hom	Hom
	116	Het	Het
	117	Het	Het
	118	Het	Het
	119	Het	Het
1076	133	Hom	Hom
	134	Hom	Hom
	135	Het	Hom
	136	Het	Hom
	137	Het	Hom
1118	097	Hom	Hom
	099	Hom	Hom
	100	Hom	Hom
	101	Hom	Hom
	102	Hom	Hom
1283	081	Hom	Hom
	082	Hom	Hom
	083	Hom	Hom
	084	Hom	Hom
	085	Hom	Hom

CONCLUSIONS

A differential approach has been developed for the study of the combustion process of single coal particles. The experimental technique, based in the simultaneous measure of the carbon monoxide, carbon dioxide, and intensity of the light generated during the combustion, gives quantitative information about the ignition and the subsequent burn-off of the residual particle. The apparatus designed provides the special characteristics required in this study and the transition between the two ignition mechanisms is achieved within the range of operation conditions, for the coal used in this study.

The ignition mechanism is determined not only from measurements of light intensity during the combustion, a technique commonly used in the past, but also from the gas evolution curves which allow the quantification of the whole combustion process. The results show the convenience of using both as complementary techniques in the determination of the ignition mechanism.

ACKNOWLEDGMENTS

This study was made possible by financial support from the Coal Cooperative Program at The Pennsylvania State University. The authors thank the Penn State Coal Sample Bank and Data Base for supplying the sample and the analysis of the coal used in this study.

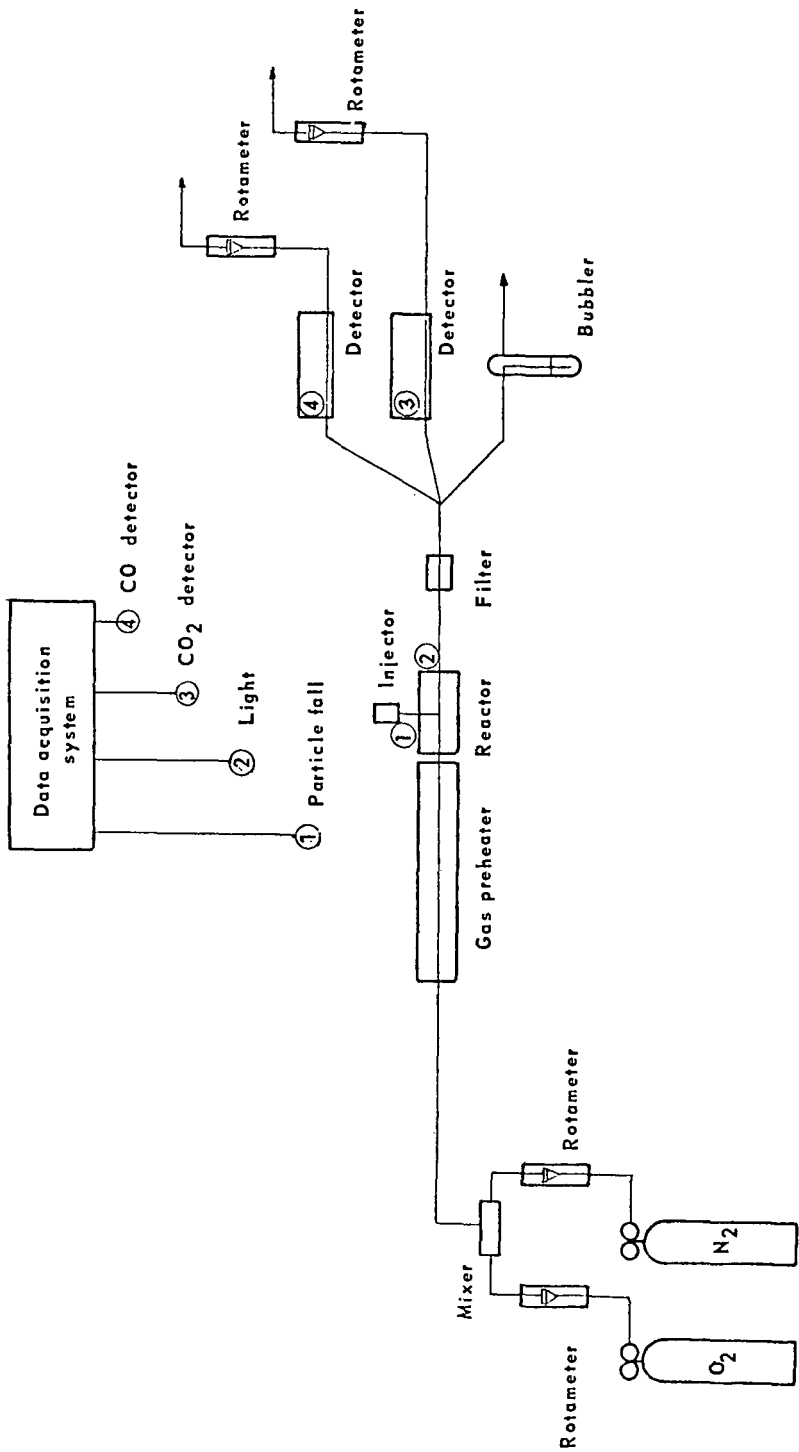


FIGURE 1. SCHEMATIC DIAGRAM OF THE APPARATUS

COAL PARTICLES

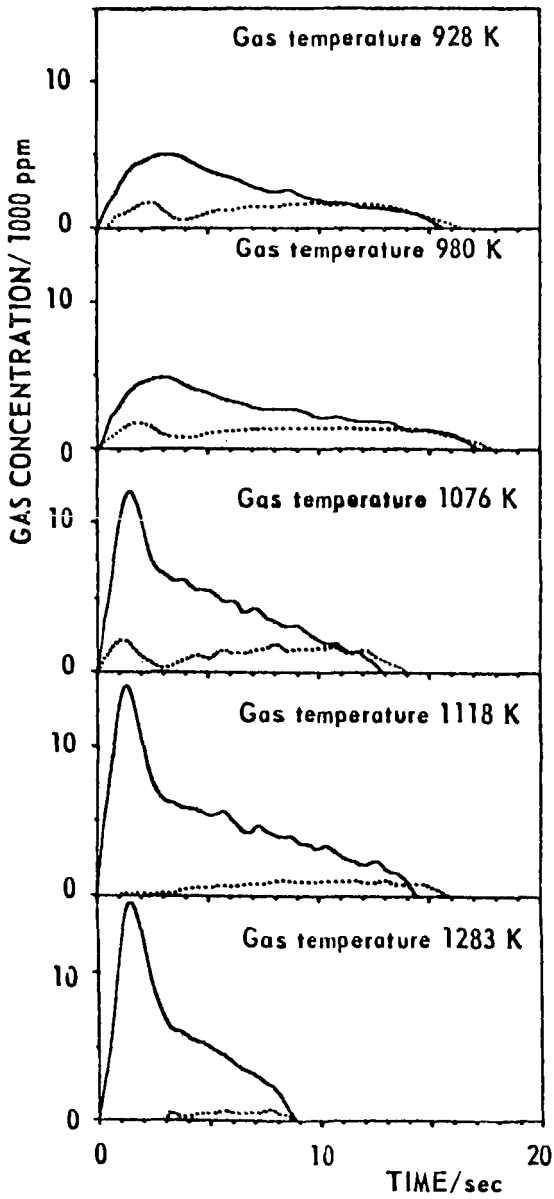


FIGURE 2. TYPICAL GAS EVOLUTION CURVES

(Continuous line CO₂ - Dotted line CO)

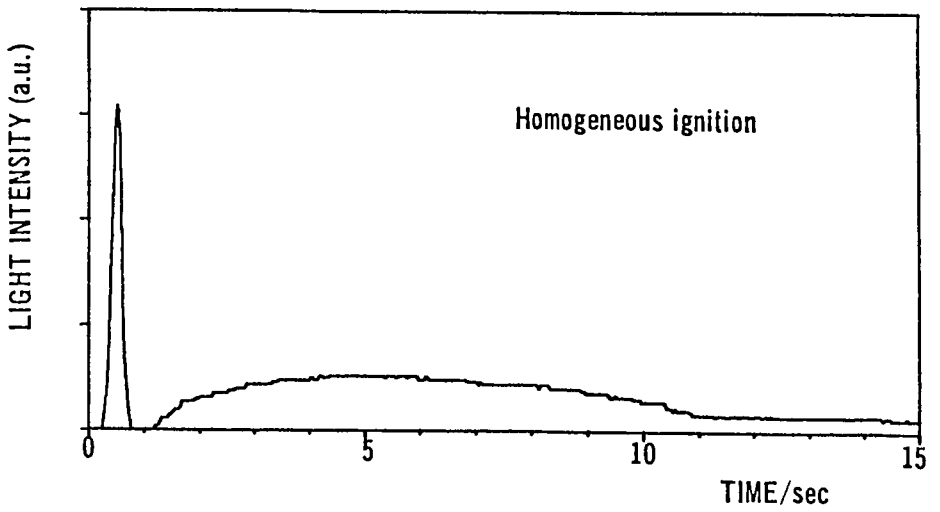
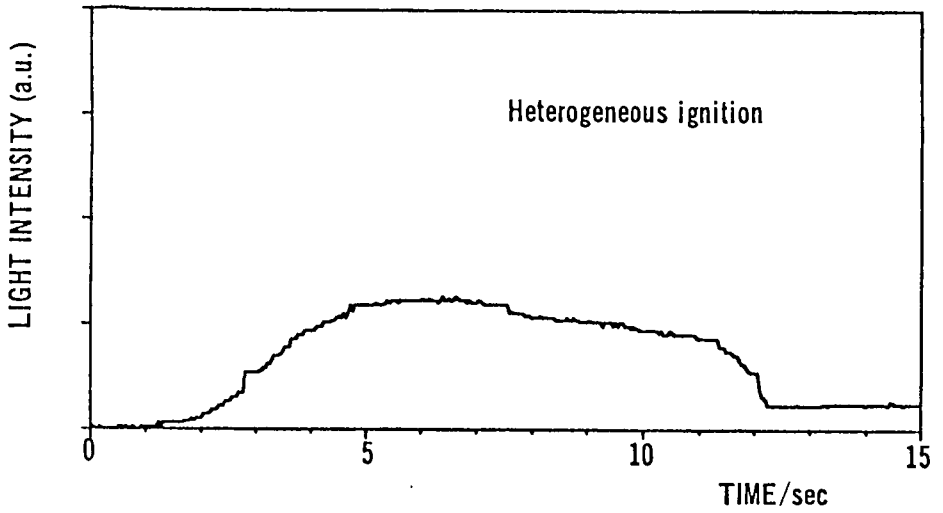


FIGURE 3. TYPICAL RESULTS OF LIGHT EMISSION MEASUREMENTS DURING COMBUSTION OF COAL AND CHAR PARTICLES

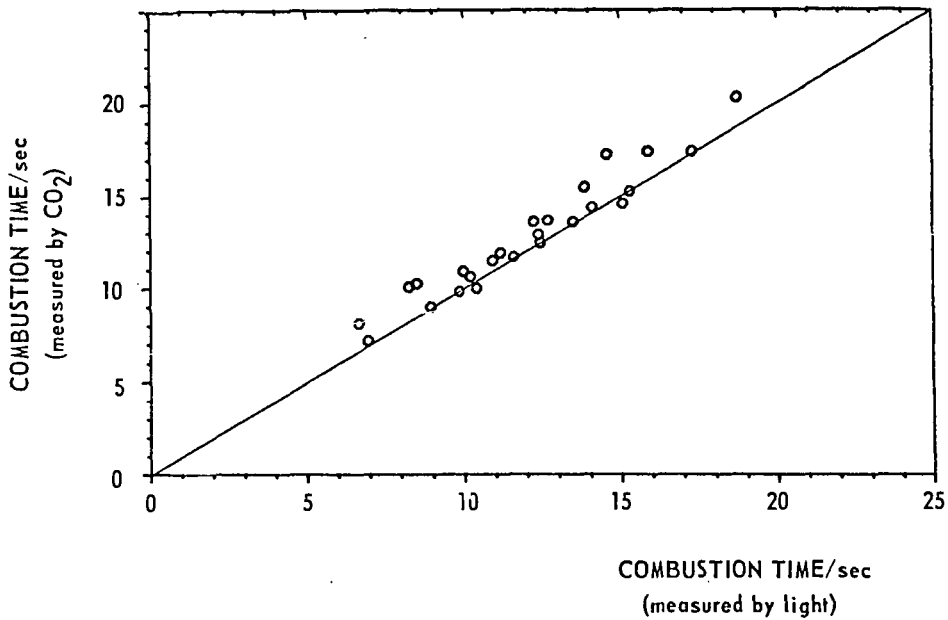


FIGURE 4. COMPARISON BETWEEN THE DIFFERENT TECHNIQUES USED FOR MEASURING COMBUSTION TIMES

LITERATURE CITED

- (1) Essenigh, R. H., *J. Inst. Fuel*, 34, 239 (1961).
- (2) Essenigh, R. H., "Chemistry of Coal Utilization, Second Supplementary Volume" (Ed. M. A. Elliot), John Wiley and Sons, 1981, Ch. 19.
- (3) Field, M. A., Gill, D. W., Morgan, B. B., and Hawksley, P. G. W., "Combustion of Pulverized Fuel", British Coal Utilization Research Association, Leatherhead, Surrey, 1967.
- (4) Mulcahy, M. F. R., and Smith, I. W., *Rev. Pure and Appl. Chem.*, 19, 81 (1962).
- (5) Annamalai, K., and Durbetaki, P., *Combust. Flame*, 29, 193 (1977).
- (6) Bandyopadhyay, S., and Bhaduri, D., *Combust. Flame*, 18, 411 (1972).
- (7) Baum, M. M., and Street, P. J., *Combust. Sci. Technol.*, 3, 231 (1971).
- (8) Juniper, D. A., and Wall, T. F., *Combust. Flame*, 39, 69 (1980).

THE EFFECT OF THE MOLECULAR WEIGHT OF ADDITIVE
ON THE PROPERTIES OF ANTIMISTING FUELS

By

A. F. Hadermann, J. C. Trippe
General Technology Applications, Inc., Arlington, Virginia 22209
and

P. F. Waters
The American University, Washington, D. C. 20016

INTRODUCTION

Antimisting aircraft fuels, when ignited, do not produce the roaring fireball which often accompanies aircraft crashes (1). This result is attributable to the suppression of the aerosolization of the fuel by added macromolecules which alter the structure of the droplets of fuel emanating from rent fuel tanks after the crash.

The first studies of the antimisting effect of macromolecules on aviation fuel were carried out in Great Britain in 1968 (2). In that early work it was established that there was a qualitative relationship between the suppression of the atomization of the fuel and the molecular weight of the additive above a certain critical concentration; the latter being inverse to the molecular weight of the additive. Subsequent investigations have demonstrated a dependence of the antimisting effectiveness of polyisobutylene in diesel fuel on the viscosity average molecular weight to a power exceeding 2 (3), and in jet-A fuel to the $2\alpha + 1$ power (4), where α is the exponent in the Mark-Houwink equation.

In their study Chao et al. were able to demonstrate a strong correlation between the extent of antimisting effectiveness and flammability reduction with the maximum ductless siphon height supported by the solution. They introduced the ductless siphon to the study of antimisting fuels as a measure of the elongational viscosity imparted by the macromolecules to the fuel. The apparatus does not provide a uniform elongational flow field but there is no device, at present, for determining the true elongational viscosity of these solutions and the ductless siphon has the advantage of being easy to assemble and use. The precision of the measurements can be improved by drawing the liquid column in a controlled environment, reading the height optically or with a strain gauge, etc. The principal factor of interest with respect to antimisting fuels, however, is that it has been demonstrated that the ductless siphon is a tool for rapidly screening macromolecules for their effectiveness as antimisting agents.

In this work it is suggested that the ductless siphon might also be used for the rapid estimation of the molecular weight of megadalton macromolecules.

EXPERIMENTAL

Three samples of polyisobutylene (BASF: B-100, B-200, B-200-246) were dissolved in isooctane at room temperature with occasional gentle swirling over several days. The viscosity average molecular weights were determined with an Ostwald viscometer from the Mark-Houwink equation (5):

$$[\eta] = 3.06 \times 10^{-4} \bar{M}_v^{0.65} \quad 1)$$

The values are given in Table I.

The height-at-break of serial dilutions of the stock solutions of the three samples was measured in the apparatus of Figure 1. Six measurements were made on each solution and the measurements were averaged. The averaged heights were plotted against the concentration and the slope of each line, h/c , was determined by linear regression analysis. The slope values, along with the correlation coefficients, r , are entered in Table I.

The effect of the molecular weight on the height-at-break property and, by extension, the antimisting effectiveness and the flammability suppression potential of polyisobutylene in isooctane is dramatic.

In a 1975 paper Williams (6) proposed a theory which explains why high molecular weight macromolecules in dilute solution exhibit quite large extensional viscosities relative to lower molecular

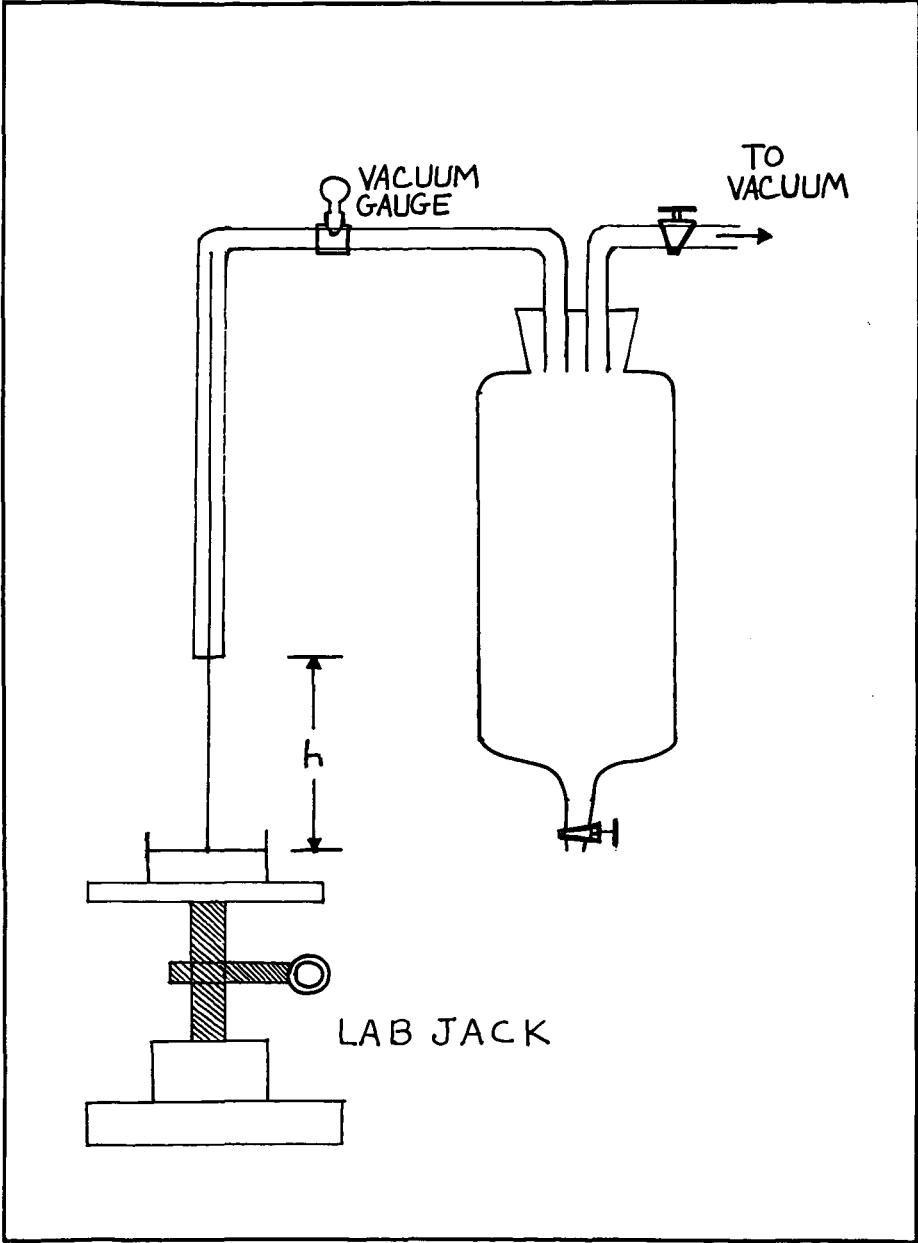


FIG. 1. DUCTLESS SIPHON APPARATUS.

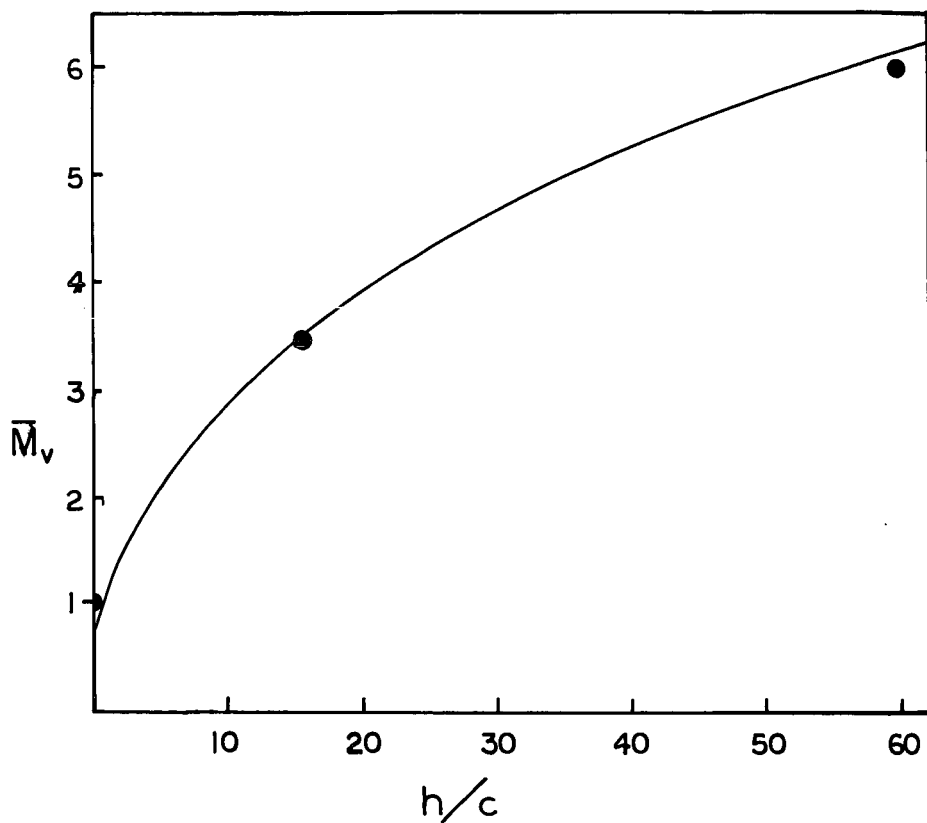


FIG. 2. MOLECULAR WEIGHT VS. SLOPE OF PLOTS OF HEIGHT-AT-BREAK VS. CONCENTRATION OF POLYISOBUTYLENE IN ISO-OCTANE AT 20°C.

weight species. An extension of the theory applied to the use of the ductless siphon for estimating the extensional viscosity of samples of antimisting fuels was completed last year (7). The working equation is:

$$\frac{\bar{n}}{n_0} = 3 (1 + \dot{\epsilon} c n_s K^2 M_V (2\alpha + 1) / RT + \dots) \quad 2)$$

where \bar{n} is the extensional viscosity
 n_0 is the shear viscosity of the solution
 $\dot{\epsilon}$ is the elongation rate in pure extensional flow
 c is the concentration in g/dl
 n_s is the shear viscosity of the solvent
 K and α are the constants of the Mark-Houwink equation.

TABLE I
 VISCOSITY AVERAGE MOLECULAR WEIGHT AND SLOPES OF
 HEIGHT-AT-BREAK VS. CONCENTRATION PLOTS FOR
 SAMPLES OF POLYISOBUTYLENE MEASURED IN
 ISOCTANE AT 20°C

Sample	$M_V \times 10^{-6}$ (g/mol)	$\frac{h}{c}$ (cm/g/dl)	r
B-100	1.00	0	0.951
B-200	3.46	15.7	0.999
B-200-246	5.96	59.7	0.999

For a given polymer/solvent, for megadalton samples with the ductless siphon height-at-break measured at the same temperature at which the exponential term in the Mark-Houwink equation is evaluated, we propose the relation:

$$\frac{h}{c} = k \bar{M}_V (2\alpha + 1) \quad 3)$$

where k is a constant. For the polyisobutylene/isoctane system at 20°C, $\alpha = 0.65$. A plot of \bar{M}_V vs h/c appears in Figure 2, where the theoretical curve, evaluated from the measured height-at-break values, is given by:

$$\bar{M}_V = 1.05 \times 10^6 \left(\frac{h}{c} \right)^{0.44} \quad 4)$$

Inasmuch as interest in antimisting fuels is growing and ultra high molecular weight macromolecules are markedly superior in their performance in antimisting fuels, this method may be used for rapid estimation of molecular weights when the Mark-Houwink exponential term is known.

LITERATURE CITED

- (1) Weatherford, W. D., Jr., and Wright, B. R., AGARD/NATO 45th Meeting, Propulsion and Energetics Panel, London, April, 1975.
- (2) Mossel, J. W., and Waite, F. A., Proc. of the Aircraft Research and Technology for Antimisting Kerosene Conf., Feb. 18-19, 1981, p. 4-1 ff, Report No. FAA-CT-81-181, U.S. Dept. of Trans., June, 1981.
- (3) Investigation of the Application of a Cryogenic Blending Process to Produce Antimisting Diesel Fuels, A. F. Hadermann, P. F. Waters, J. C. Trippe and W. Weitzen, Contract No. DAAK-70-81-C-0134, U.S. Army Mobility Equip. Res. and Dev. Com., Fort Belvoir, Va. Jan. 15, 1982.
- (4) Chao, K. C., Child, C. A., Grens, E. A., and Williams, M. C., Amer. Inst. Chem. Eng. J., in press.
- (5) BASF Tech. Leaflet No. M 2353 E/81538, May, 1978.
- (6) Williams, M. C., Amer. Inst. Chem. Eng. J., 21, 1 (1975).
- (7) Chao, K. K. K., and Williams, M. C., J. Rheology, in press.

GENERAL PAPERS - POSTER SESSION
PRESENTED BEFORE THE DIVISION OF PETROLEUM CHEMISTRY, INC.
AMERICAN CHEMICAL SOCIETY
WASHINGTON, D. C. MEETING, AUGUST 28 - SEPTEMBER 2, 1983

STORAGE STABILITY STUDIES OF U.S. NAVY DIESEL FUEL MARINE

By

L. Jones, D. R. Hardy and R. N. Hazlett
Naval Research Laboratory, Code 6180, Washington, D. C. 20375

INTRODUCTION

An increasing trend in recent years is the utilization of heavier crude sources in producing middle distillate fuels. The U.S. Navy's concern about long-term (up to three years) storage stability of its diesel fuel marine (DFM) from such sources is the driving force for this study. The three major objectives of this work are: 1) to improve empirical predictive storage stability tests; 2) to better understand the chemical mechanism involved in middle distillate storage instability; and 3) to examine various commercial and experimental stabilizer additives as possible storage stability improvers suitable to Navy needs.

In this paper we will deal primarily with the first objective and also include some preliminary work and results on the second objective. Some of the problems and severe time restrictions of utilizing empirical predictive storage stability tests will be specifically addressed.

EXPERIMENTAL

Accelerated Storage Stress Test

An empirical gravimetric test which was shown to be very precise for this type of analysis ($\pm 10\%$ S. E.) of shale-derived diesel fuel marine (DFM) storage stability studies at NRL (1) was adopted for this study. It consists of filtering 300 ml of a fuel through Gelman type A/E glass fiber filters. The filtered fuel is transferred to a clean, dry, borosilicate brown glass 500 ml bottle weighed to the nearest 0.1 mg. The teflon-lined cap is placed on the bottle but not tightened. The bottles are placed in a dark oven held to constant temperatures within $\pm 0.5^\circ\text{C}$ for a specified number of days (± 0.1 days). Temperatures chosen for the accelerated tests were 43, 65, 80 and 100°C . After removal from the oven the bottles are allowed to cool to ambient temperature and relative humidity in the dark for 24 hours (± 2 hours). The fuel is filtered through a Büchner funnel with Gelman type A/E glass fiber filters weighed to the nearest 0.1 mg. The bottles and filter pads are rinsed with 3 x 50 ml of *n*-hexane aliquots to remove fuel and to ensure transfer of all non-adherent material from the bottle. The bottles and filters plus funnels are evacuated in a vacuum oven with a mechanical pump and then heated in vacuo for about 18 hours at 120°C . The vacuum oven is turned off and allowed to return to room temperature before removing the bottles and filter funnels. The bottles and filter funnels are weighed to the nearest 0.1 mg on a Mettler H315 (1000 g capacity) balance. Adherent gum is the weight difference per bottle corrected for a blank, divided by 300 and reported as mg/100 ml of fuel. Filtrable sediment is the weight difference of the filter pads corrected for a blank, divided by 300 and reported as mg/100 ml of fuel. The sum of these two values is reported as total insolubles in mg/100 ml of fuel. The mean and standard deviation of triplicate runs is generally reported. A blank determination is made for each time and temperature run. The filtrable sediment blank is a funnel and filter pad subjected to the same post stress handling a samples. All sample values reported herein have been corrected for a blank determination.

Fuels

In general, fuels used in this work were received in five-gallon metal containers and transferred to five one-gallon epoxy-lined metal containers and stored in a cold room at $+4^\circ\text{C}$ until used. Most fuels were supplied through the Navy Petroleum Office from refineries and storage depots world-wide. All fuels had conformed to military specifications for Navy DFM at time of receipt by the Navy.

Capillary GC-MS was performed on a Hewlett Packard fused silica 0.3 mm I. D. x 50 m cross-linked methyl silicone column directly inserted into the electron impact source of a Hewlett Packard 5982A mass spectrometer through a modified solids probe inlet. Flow was adjusted to one ml/min of helium and the injector split ratio was approximately 50:1.

Elemental analyses were performed on a Perkin Elmer Model 240 Elemental Analyzer for carbon, hydrogen, and nitrogen. Oxygen analysis was performed on a Coulometrics Oxygen Analyzer.

RESULTS AND DISCUSSION

Stress Tests

Four petroleum derived DFM's covering a wide range of storage stability as defined by ASTM D2774 were selected as the test matrix to determine the statistical variations of the accelerated storage stability test described above. Typical data are reported in Table I (at 80°C for 14 days) with standard errors ranging from 1 to 11% of the mean. Data for a series of triplicate tests run at 80°C for these four fuels at 7-21 days are plotted in Figure 1. All four curves are quadratic least squares best fits. Three fuels exhibit a modest acceleration in sediment formation but 82-10 exhibits a deceleration. The data are further broken down and plotted as total and filtrable sediment for two fuels (81-5 and 82-10) in Figures 2 and 3. The filtered sediment line generally follows the shape of the total sediment curve but Figure 3 shows the exception. This type of behavior underscores the importance of fuel dependence on such measurements.

TABLE I
WEIGHT OF TOTAL INSOLUBLES IN Mg/100 ML OF FUEL
STRESSED FOR 14 DAYS AT 80°C

<u>Fuel</u>	<u>Filtered Sediment</u>	<u>Adherent Gum</u>	<u>Total Insolubles</u>	<u>Mean</u>	<u>S. D.</u>
82-8	0.9	2.3	3.2	3.6	0.4
	0.9	3.0	3.9		
	0.9	2.7	3.6		
81-5	5.0	1.3	6.3	6.4	0.4
	4.6	1.6	6.2		
	4.7	2.2	6.9		
81-8	6.5	2.2	8.7	8.5	0.3
	6.4	1.8	8.2		
	6.8	1.7	8.5		
82-10	25.5	3.8	29.3	29.6	0.3
	25.5	4.3	29.8		
	24.4	5.2	29.6		

Five additional current-use Navy DFM's from petroleum were stress-tested in an effort to 1) broaden the total fuel test matrix and 2) screen for a marginal storage stability type of fuel (one which exhibits relatively high weights of total sediment during short stress tests). Table II gives selected results for four fuels which exhibit different trends in the formation of insolubles as stress temperature and time are increased. These results emphasize the fact that simultaneous, not necessarily related, reactions are proceeding, which form varying amounts of two different types of precipitate in the fuel - adherent and filtrable. The total insolubles formed by any particular fuel increase with increase in stress temperature and stress time. Data from Table II indicate that between 80 and 100°C for the five fuels studied the pseudo-Arrhenius plot of Figure 4 may be discontinuous, i. e., the rate of total sediment formation increases about two to four times faster than expected. This needs to be confirmed by running more fuels and by increasing the number of replicate samples. Figure 4 is plotted for one particular fuel, 81-5, and shows the time required at any particular temperature of stressing to form an equivalent weight of total sediment. The expected straight line relationship is not achieved. This may be indicative that accelerated storage stability tests at temperatures above 80°C may not be predicting correctly either the quantitative or the qualitative aspects of the phenomenon. This is an important consideration in future work in this area involving stabilizer additive studies.

Chemical Characterization of Sediments

Since the predominant type of sediment formed (adherent or filtrable insoluble) appears to be fuel dependent it will be necessary to carefully characterize each type in order to be able to postulate possible mechanisms of formation. In general the adherent sediment is more soluble than the filtrable sediment. This means that the adherent gum is more amenable to standard gas chromatographic and GC/MS characterization. Adherent gums formed by stressing DFM fuel samples at 100°C for 21 days were analyzed by GC/MS. Chromatograms of the adherent gum are all quite similar to those of the non-stressed fuel. The most striking feature of the chromatograms is the symmetrical appearance of *n*-alkanes ranging from C-9 to C-20 (in the adherent gum) and C-9 to C-24 (in non-stressed fuel). Preliminary work indicates that oxidized hydrocarbons are co-eluting with the higher *n*-alkanes in adherent gum samples.

TABLE II

ALL WEIGHTS ARE GIVEN IN Mg/100 ML OF FUEL. STRESS TEMPERATURES ARE GIVEN IN °C AND STRESS TIMES ARE GIVEN IN DAYS

<u>Fuel/Temp/Time</u>	<u>Filtered Sediment</u>	<u>Adherent Gum</u>	<u>Total Insolubles</u>	<u>Mean</u>	<u>S. D.</u>
82-8/43/52	0.0	0.5	0.5	0.4	0.4
	0.1	0.6	0.7		
	0.0	0.0	0.0		
82-8/20/21	0.8	4.8	5.6	5.1	1.1
	0.3	5.5	5.8		
	0.5	3.3	3.8		
81-5/43/52	0.2	1.0	1.2	1.4	0.4
	0.2	1.7	1.9		
	0.2	0.9	1.1		
81-5/80/21	5.7	2.7	8.4	9.0	0.6
	6.8	2.7	9.5		
	6.8	2.2	9.0		
82-36/80/21	1.3	1.3	2.6	2.6	0.2
	1.2	1.3	2.5		
	1.7	1.1	2.8		
82-36/100/6	1.1	6.7	7.8	8.0	0.3
	1.4	6.8	8.2		
82-32/80/21	1.5	0.9	2.4	2.3	0.1
	1.0	1.2	2.2		
82-32/100/6	1.0	7.6	8.6	8.4	0.3
	1.0	7.2	8.2		
82-33/80/21	0.5	2.3	2.8	1.3	1.3
	0.0	0.3	0.3		
	0.5	0.2	0.7		
82-33/100/6	1.3	1.6	2.9	2.9	0.0
	1.5	1.4	2.9		
82-35/80/21	1.1	0.5	1.6	1.3	0.5
	0.7	0.8	1.5		
	0.7	0.0	0.7		
82-35/100/6	1.0	2.4	3.4	2.3	1.6
	0.7	0.5	1.2		

TABLE III

ELEMENTAL ANALYSIS OF FILTRABLE SEDIMENT FROM NRL FUEL 82-10 STRESSED FOR 21 DAYS AT 80°C. ALL VALUES IN WEIGHT PERCENT

<u>Element</u>	<u>Weight %</u>
Carbon	62
Hydrogen	5
Nitrogen	3
Oxygen	25
Sulfur	2
Ash	<u>2</u>
Total	99

The filtrable insoluble sediment is much more difficult to solubilize and is not amenable to standard techniques of MS identification. Preliminary VPO measurements indicate that the filtrable

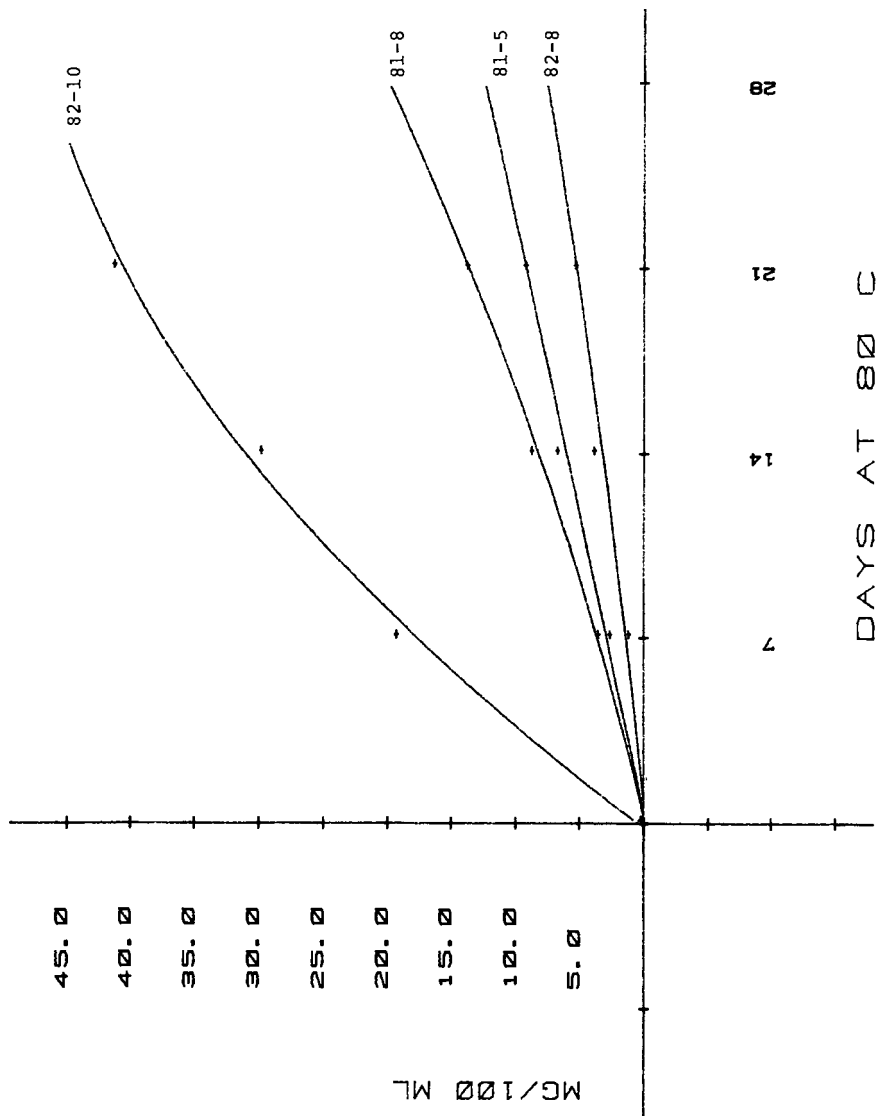


Figure 1. Total insolubles formed for four different DFM fuels stressed at 80°C for 7, 14, and 21 days each. Curves are computer generated quadratic least squares best fits.

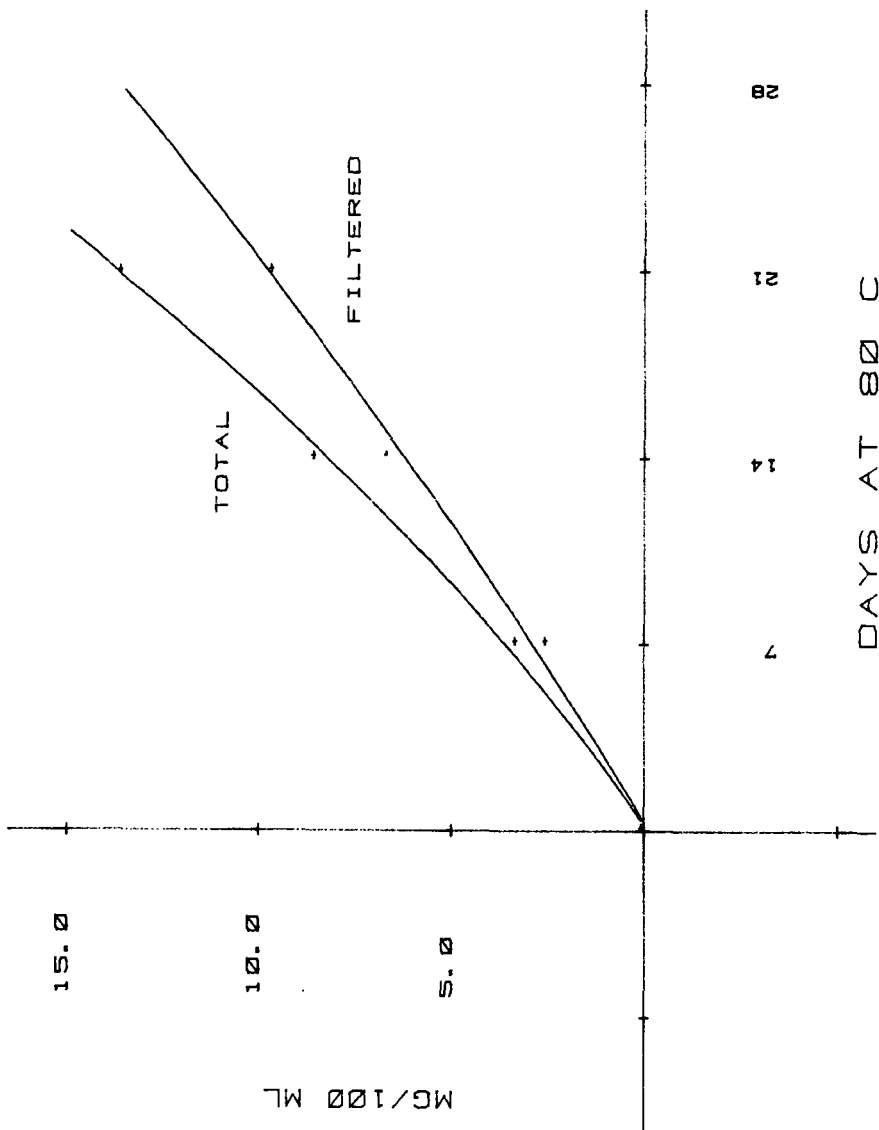


Figure 2. Breakdown of total insolubles into filtered sediment and adherent gum for fuel 81-8 stressed at 80°C for 7, 14 and 21 days. Curves are least squares best fits.

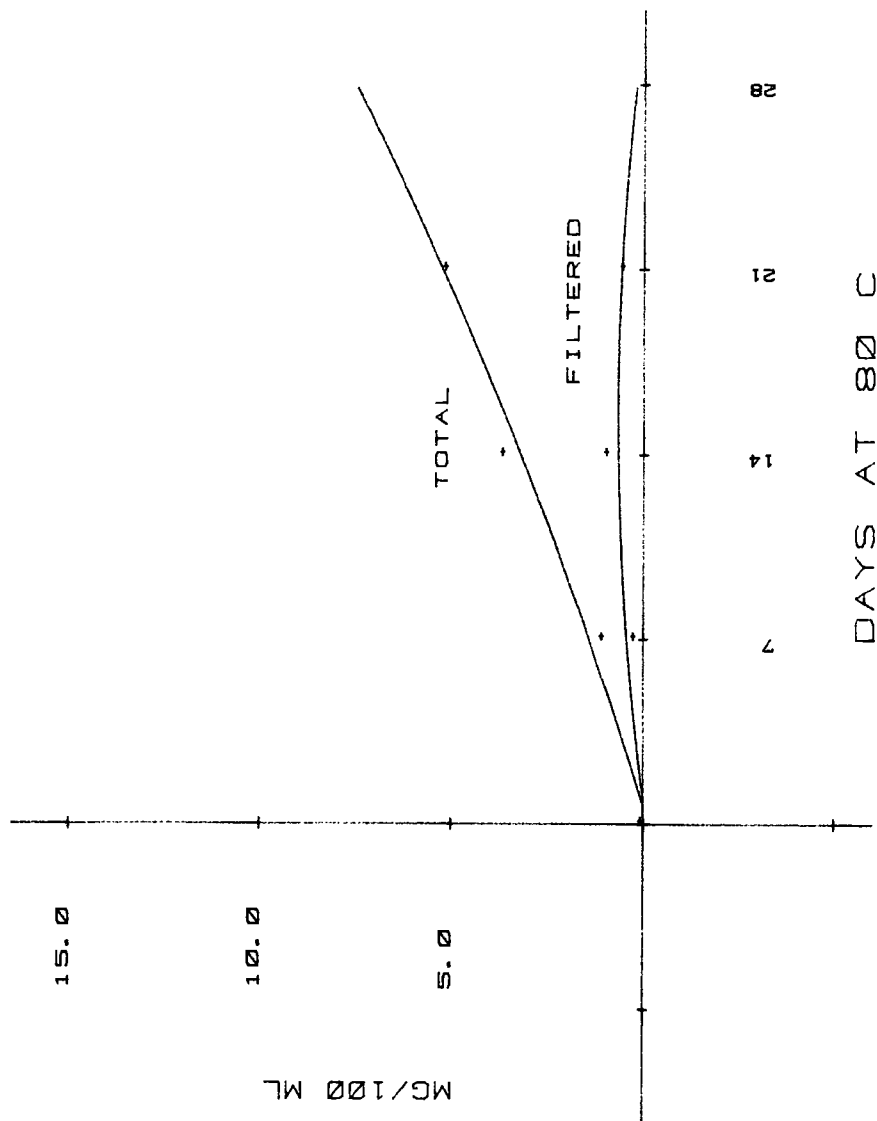


Figure 3. Breakdown of total insolubles into filtered sediment and adherent gum for fuel 82-8 stressed at 80°C for 7, 14, and 21 days. Curves are least squares best fits.

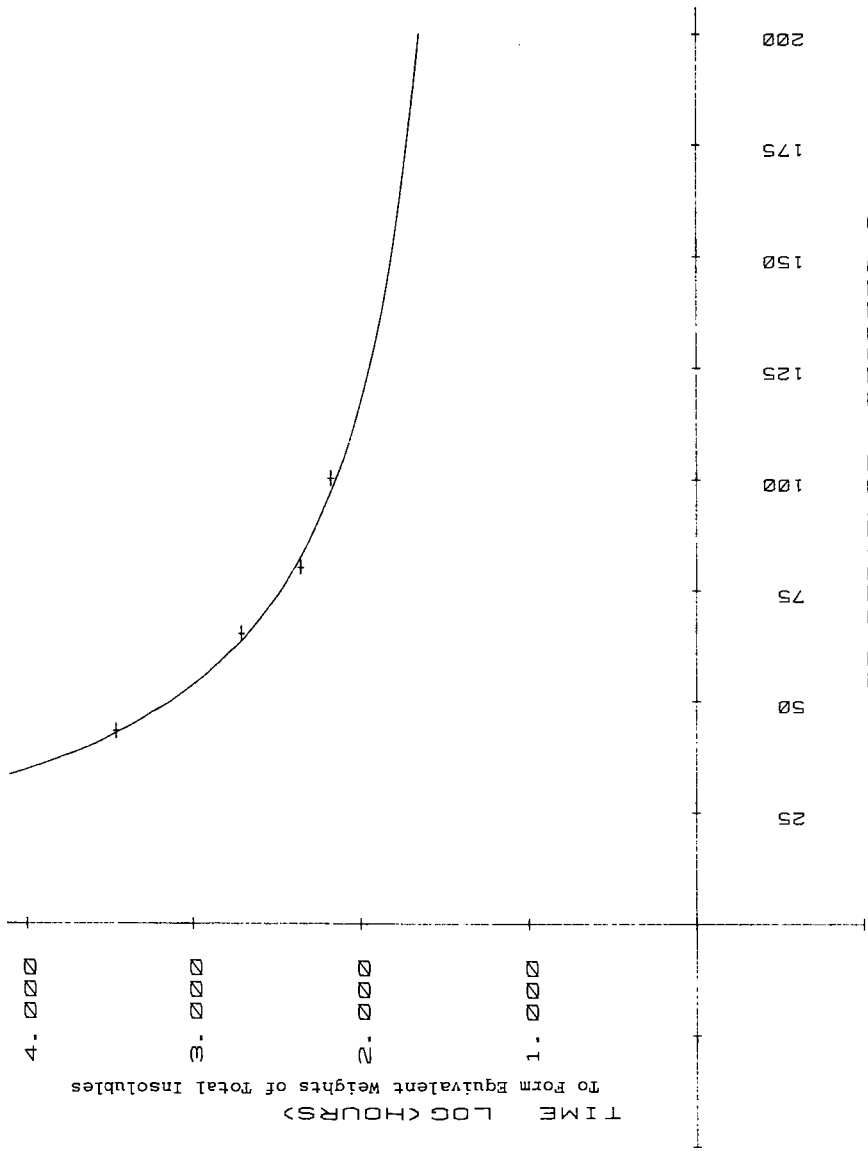


Figure 4. Plot of stress temperature of fuel 81-5 from 48°C to 100°C vs time necessary to form equivalent amount of total insolubles. The curve is a least squares best fit.

insoluble sediment is of higher molecular weight (up to 1500 amu). A typical elemental analysis for filtrable sediment of 82-10 (a particularly unstable DFM) is given in Table III. Oxygen has been directly determined by coulometric measurements. The high heteroatom content is typical for this type of sediment (2). Six major components of a filtered sediment extract in hot THF have been isolated by gas chromatography. Filtered sediments are usually insoluble in most organic solvents. Further analysis of the major fuel degradation components will establish the identity of the reactive species in fuels.

LITERATURE CITED

- (1) Hazlett, R. N., Cooney, J. V., and Beal, E. J., First Annual Report, Sept. 15, 1981-Sept. 30, 1982, NRL, Washington, D. C., to be published by USDOE under contract DE-AI-19-81BC10525.
- (2) Nixon, A. C., "Autoxidation and Antioxidants of Petroleum", Chapter 17 in "Autoxidation and Antioxidants", W. O. Lundberg, Ed., John Wiley, New York, 1962.

GENERAL PAPERS - POSTER SESSION
PRESENTED BEFORE THE DIVISION OF PETROLEUM CHEMISTRY, INC.
AMERICAN CHEMICAL SOCIETY
WASHINGTON, D. C. MEETING, AUGUST 28 - SEPTEMBER 2, 1983

RADIOACTIVE (^{14}C) TRACER STUDIES OF METHANOL CONVERSION
OVER A Ni-ZSM-5 ZEOLITE

By

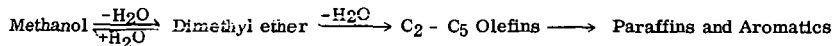
F. S. Hwu* and J. W. Hightower
Department of Chemical Engineering, Rice University, Houston, Texas 77251

INTRODUCTION

Within the last few years, researchers at the Mobil Research and Development Corporation (1) have synthesized a novel zeolite catalyst, ZSM-5, which is capable of converting oxygenates, e.g., methanol, into aliphatics and aromatic hydrocarbons in the gasoline boiling range. Since technology exists for making methanol from coal-derived synthesis gas (2), this new process provides an additional source of chemical feedstocks and transportation fuels.

In the conversion of methanol to hydrocarbons over such catalysts, more than 100 different compounds have been identified (3,4). The major hydrocarbon products can be classified into three categories: olefins, paraffins, and aromatics. There is a strong possibility that some of these products, once formed, react further to produce other products. The objective of this research was to investigate this possibility by labeling some of the products and following the transfer of the label to other products.

The reaction is thought to follow the sequence



The interconversion of methanol and dimethyl ether over such catalysts has been confirmed in several studies (5,6). At very low conversion of methanol, dimethyl ether is the major product, and the transformation of methanol into dimethyl ether is 20 to 30 times faster than hydrocarbon formation (6). On the other hand, when dimethyl ether is the starting material, both methanol and hydrocarbons are formed readily (5,6). The intermediate role of dimethyl ether was also confirmed by using a $^{13}\text{CH}_3\text{-O-}^{13}\text{CH}_3$ tracer technique (6).

The roles played by the lightweight olefins were investigated by Dejaifve et al. (7). They carried out reactions of C_2 , C_3 , and C_4 olefins over ZSM-5 catalysts and observed similar aromatic product distributions from both methanol and all the olefins. Therefore, they concluded that light olefins were intermediates of methanol conversion to gasoline boiling range products.

This research was aimed at identifying some of the major reactions involved in the overall methanol reaction. A ^{14}C -labeled tracer technique was developed to explore the roles played by the various species, including olefins, paraffins, and aromatics. The results are described herein.

EXPERIMENTAL

Catalyst

The original ZSM-5 catalyst was prepared at the Exxon Research and Development Laboratories. This material was in the sodium form and was calcined for 2 hours at 600°C . It was then soaked in a solution of ammonium nitrate (9 wt%) for another 2 hours with constant agitation. After the resulting $\text{NH}_4\text{-ZSM-5}$ had been washed and filtered, it was impregnated with a solution of 0.0439 g nickel acetate/g of dry zeolite and then heated until dry at 120°C . This impregnated Ni-ZSM-5 catalyst was subsequently blended with alumina, which served as a binder, in the proportion 0.3 g alumina/g ZSM-5. All catalysts used for these reaction studies were pelletized, crushed, and screened to 30/40 mesh.

Chemicals

Methanol (99.99% purity) was obtained from Fisher Scientific Company. The radioactive compounds, along with their suppliers, are shown in Table I. Both chemical and radiochemical purities of each were checked by the radio-gas chromatograph described later. Since the methanol,

*Present address: Department of Mechanical Engineering, University of Texas, Arlington, Texas 76019.

propylene, 1-butene, n-hexane, n-heptane, and benzene were satisfactory in both chemical and radiochemical purities, they were used as received. However, radioactive impurities were found in the original ethylene and iso-butane, which necessitated purification with a preparative GLC column (30 ft. long 5/16 in. O. D. Porapak Q at 100-150°C).

Reactor System

Figure 1 shows the experimental set-up. Liquid methanol was admitted into a stream of helium carrier gas by a syringe pump. To facilitate rapid vaporization of the liquid reactant, the glass sections immediately before and after the syringe injection port were packed with glass beads and heated by nichrome wire. A 250 ml mixing volume was installed before the reactor to moderate any pulsations in the reactant concentration.

TABLE I
RADIOACTIVE CHEMICALS

<u>Compound</u>	<u>Specific Activity (mC/mmole)</u>	<u>Chemical Purity</u>	<u>Manufacturer*</u>
Methanol	6.7	98+%	PLI
Ethylene (1,2- ¹⁴ C)	3.5	98%	CBC
Propylene (1- ¹⁴ C)	1.0	98%	CBC
1-Butene (4- ¹⁴ C)	5.0	---	ICN
1-Butane (2- ¹⁴ C)	1.02	98%	CBC
n-Hexane (1- ¹⁴ C)	1.0	---	ARC
n-Heptane (1- ¹⁴ C)	1.0	---	ARC
Benzene	1.0	---	ARC

*PLC - Pathfinder Laboratories, Inc.

CBC - California Bionuclear Corp.

ARC - American Radiochemical Corp.

Pulses of radioactive tracers were introduced into the pre-evacuated doser through the standard taper ST1. The pressure in the doser was monitored with a mercury manometer.

The catalyst bed and a bed of vycor chips, located just upstream from and having the same mesh size as the catalyst, were sandwiched in the reactor between two glass wool plugs. The vycor chips served as a preheater and helped develop plug flow in the catalyst bed.

Radio-Gas Chromatograph System

A radio-gas chromatograph (RGC) system, shown schematically in Figure 1, was integrated with the reaction system to facilitate periodic sampling and on-line analysis of the products from the reactor. This system consisted of a modified Varian model 3700 gas chromatograph, three different types of detectors (TCD, FIC, ICD), a separation column, and a changeable sample loop connected to a 6-port valve V3.

The temperature programmed chromatographic column was a 7-ft. by 1/8-in. O. D. stainless steel tube packed with 15% squalane on 80/100 mesh chromosorb P. Connected to the column exit was a stream splitter which divided the effluent stream into two parts in the approximate ratio 1:10. The smaller stream went to the FID (flame ionization detector) and the larger stream was directed into the ICD (ionization chamber). The argon quench gas was used to sweep the radioactive gases out of the 4.5 ml ionization chamber quickly for improved peak resolution (10).

Experimental Procedure

The reaction was carried out in a finite-tracer but continuous-reactant flow manner. This arrangement was used to minimize the consumption of expensive radioactive chemicals and yet to conduct the experiment in the "steady state" so that meaningful kinetic data could be extracted.

With methanol and helium flowing through the reactor, the reaction was brought to the steady state at a fixed set of conditions with the effluent bypassing the sample loop. A very small amount of tracer was introduced into the large pre-evacuated doser (50 ml). The tracer was then diluted with a portion of the reactant stream to make the pressure in the doser the same as that in the reaction system. This made the composition of material in the doser identical to that in the reactant stream except for the small amount of tracer in the doser.

Each radio-tracer experiment was begun by diverting the reactant stream to flow through the doser, and a liquid nitrogen trap collected all the hydrocarbons (except methane) in the product stream. After all the radioactive materials were trapped in the sample loop (usually about 8 minutes),

the sampling valve was returned to its original position, the liquid nitrogen dewar flask was removed, and the products were flashed into the GLC column. The amount of each product was monitored on the FID, and the radioactivity in each peak was measured by the ICD.

The specific activity A_i in each of the analyzed peaks was calculated by the following equation:

$$A_i = \frac{\frac{\text{(Radioactivity in product } i, \text{ mC)}}{\text{(Total radioactivity in all hydrocarbon products, mC)}}}{\frac{\text{Moles of product } i}{\text{Total moles of hydrocarbon products}}}$$

RESULTS

Different types of ^{14}C -labeled tracers -- olefins (ethylene, propylene, l-butene, paraffins (iso-butane, n -hexane, n -heptane), and aromatics (benzene) -- were used to investigate the roles that these several species play in the overall methanol-to-hydrocarbon reaction.

In all experiments, the reaction was carried out over 100 mg of the Ni-ZSM-5 catalyst at 368°C and 1 atm total pressure. The partial pressure of methanol in the inlet stream was 0.05 atm, and the space time τ was 218 mg cat·sec/cm³-STP. Other reaction conditions for each experiment are given in Table II.

TABLE II
REACTION CONDITIONS FOR TRACERS

	<u>Ethylene</u>	<u>Propylene</u>	<u>l-Butene</u>	<u>i-Butane</u>	<u>n-Hexane</u>	<u>n-Heptane</u>	<u>Benzene</u>
Amount Added (μmole)	0.51	0.76	0.76	1.14	2.53	2.53	1.03
Radioactivity (μC)	1.79	0.76	0.10	1.16	0.10	0.10	0.30
Partial pressure of methanol - 0.05 atm							
τ (Space time) - 218 mg cat·sec/cm ³ -STP							
Reactor temperature - 368°C							

Table III lists the specific activity A_i for all the products (or groups of products) when the olefins, ethylene, propylene, and l-butene, were used as tracers. For propylene and l-butene, the radioactivity was almost uniformly spread among all the products, even including the compound initially labeled. However, for ethylene less than 50% of the radioactivity was incorporated into other products with the majority remaining in the ethylene. For this reason, the radioactivity in the ethylene was excluded from the normalization of the radioactivity in each of the products. In other words, the distribution of radioactivity among the various products was based only on the ethylene that reacted, and not on the total radioactive ethylene admitted.

TABLE III
RADIOACTIVITY DISTRIBUTION AMONG HYDROCARBON PRODUCTS

<u>Tracer</u>	<u>Specific Activity in Products</u>						
	<u>C₂</u>	<u>C₃</u>	<u>C₄</u>	<u>C₅</u>	<u>C₆⁺</u>	<u>Toluene</u>	<u>Xylenes</u>
C ₂ H ₄	----*	1.29	1.03	1.43	1.00	2.18	1.62
C ₃ H ₆	0.39	1.15	1.00	1.38	0.95	2.27	1.81
1-C ₄ H ₈	0.35	0.91	1.35	1.52	1.18	2.06	1.64

*Since more than 50% of the added radioactivity remained in the ethylene, its radioactivity was not included in calculating the specific activity of the other products. Thus, the specific activities given are based only on the ethylene that reacted, not the amount added.

The paraffins were much less reactive than the olefins. For example, in the runs with iso-butane as the tracer, essentially no radioactivity was found in any reaction products other than in the iso-butane. When n -hexane and n -heptane were used as tracers, most (ca. 80%) of the radioactivity

remained in the starting labeled tracer compound. There was a small amount of radioactivity in the C₂ to C₄ aliphatics. Significantly, no radioactivity was detected in the aromatic products.

When labeled benzene was used as a tracer, no radioactivity was found in any of the products except certain aromatics, i. e. there was no measurable radioactivity in the aliphatics. The majority (52%) of the radioactivity remained in the benzene. Considerable radioactivity was in the toluene (26%), followed by (o+m)-xylene (18%), o-xylene (3%), and trimethylbenzene (1%). Since the products contained about 6 times as much (o+p)-xylene as m-xylene, the "specific activity" for these dimethyl aromatics must be the same. Toluene had a higher specific activity (approximately by a factor of 3.4) than the xylenes, while trimethylbenzene had less (about 0.2) relative to the xylenes.

In all cases the conversion of methanol was 100%.

DISCUSSION

Olefin Tracers

The observation of radioactivity in all the hydrocarbons from methanol conversion when labeled ethylene, propylene, or 1-butene were used as tracers clearly indicates that these three light olefins play very important roles in the overall methanol-to-hydrocarbon reaction. Especially, the results have verified that even ethylene is involved in the reactions (as postulated by Dejaifve et al. (7) and suspected by Anderson et al. (8)), although ethylene is much less active than are the larger olefins.

In view of the lower reactivity of gaseous ethylene as evidenced by the retention of much more radioactivity in itself than occurred with the labeled propylene and 1-butene, we suggest that the desorption of ethylene is faster than its reactive chemisorption. Moreover, the appearance of radioactive propylene from the initial ethylene tracer supports the claim that the surface reaction of chemisorbed ethylene with methanol is relatively fast. Such a facile reaction of surface ethylene with methanol and/or dimethyl ether, viewed as an autocatalytic step, has been described by Chen and Reagan (9).

The data in Table III show that specific radioactivities of C₂, C₃, C₄, and C₅ aliphatics are of the same order of magnitude. This strongly suggests that the formation of aliphatics proceeds mainly via a C₁ step addition, or more specifically through alkylation with methanol or dimethyl ether.

The detection of much less specific radioactivity in the C₂ aliphatics from the propylene tracer and in the C₂ - C₃ aliphatics when 1-butene was the tracer implies that these small olefins are not cracked substantially but are rather incorporated into higher molecular weight products. These larger hydrocarbons may then be cracked into lower molecular weight compounds.

Similar specific radioactivities were found in both toluene and in the xylenes, regardless of which olefinic tracer was used. This observation illustrates the common role played by these light olefins in the formation of aromatics during methanol conversion of the Ni-ZSM-5 catalyst. Furthermore, since the specific radioactivities in the aromatics are 1.5 to 2.0 times greater than those in the C₃ and C₄ products, it is reasonable to infer that a major pathway of toluene and xylene formation is the reaction between one C₃ and one C₄ or two C₄ species. This conclusion was also drawn by Derouane and co-workers (7).

Paraffin Tracers

Paraffins are relatively stable final products in the methanol conversion system. The fact that ¹⁴C-tagged iso-butane retains essentially all its radioactivity within itself among the hydrocarbon products shows that neither isomerization of butanes nor alkylation of iso-butane with prevailing olefins is occurring at 368°C.

In methanol conversion over ZSM-5-type zeolites, monomethyl paraffins and olefins predominate over their straight-chain counterparts (5,8). The same was observed with our Ni-ZSM-5 catalyst. In general, this is consistent with thermodynamic equilibrium (the methyl paraffins are more stable than the corresponding straight chain molecules), except for the butanes. At 368°C thermodynamics predicts that n-butane is more stable than iso-butane (57% vs. 43%). Since these two paraffins are not interconverted under reaction conditions, they are probably formed mainly by hydrogen transfer to the respective n-butenes or iso-butene.

Aromatic Tracers

Benzene is a very thermodynamically stable compound. However, its low concentration among the reaction products causes one to question its function in the overall methanol conversion reactions. The radioactivity distribution among the aromatic products when benzene was used as a tracer reveals that alkylation of benzene to form toluene, the xylenes, and trimethylbenzene is a major route for their formation.

Benzene may be alkylated with methanol or with dimethyl ether to produce toluene, which in turn reacts with more methanol or ether molecules to form first the xylenes and then the trimethylbenzenes. This is consistent with the specific activity ratio following the order toluene > xylenes >

FIGURE 1. REACTION, RADIO-GAS CHROMATOGRAPHIC SYSTEMS

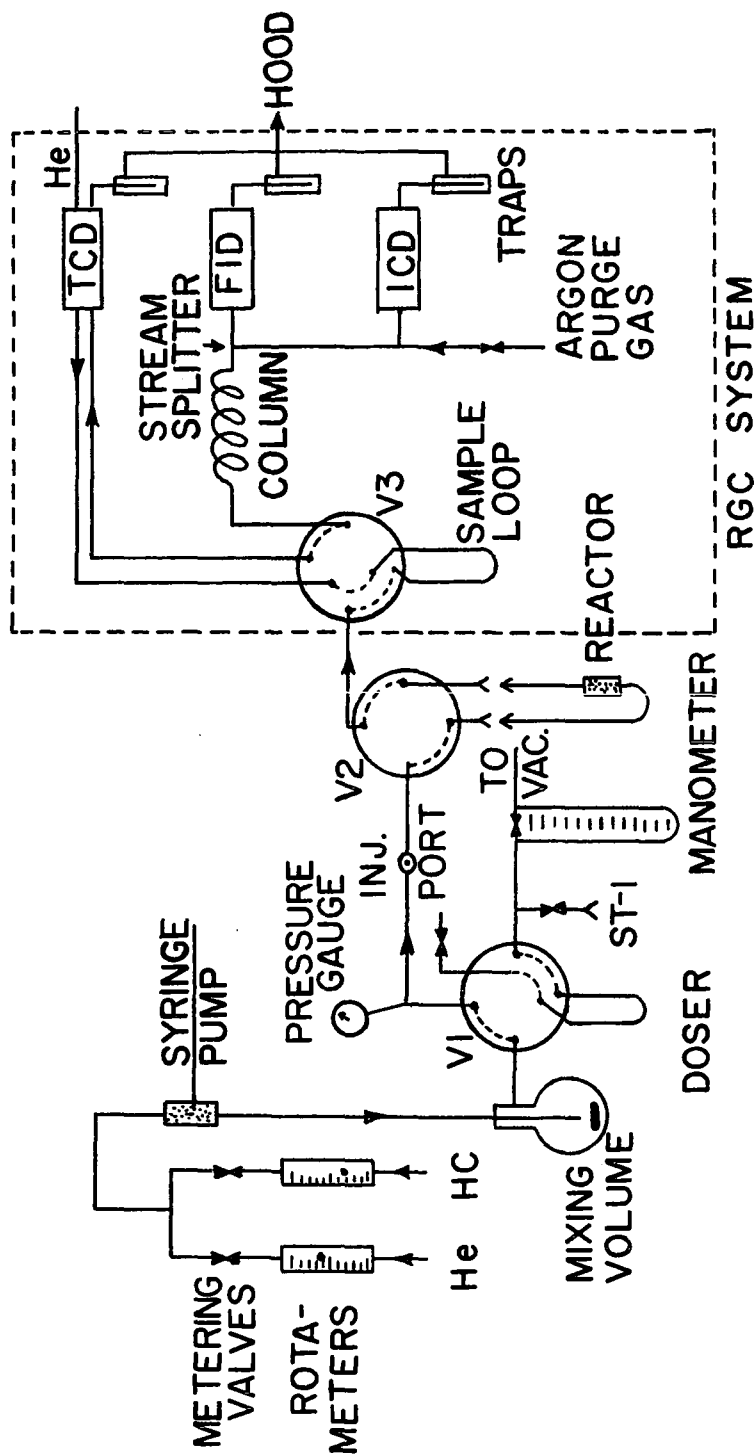
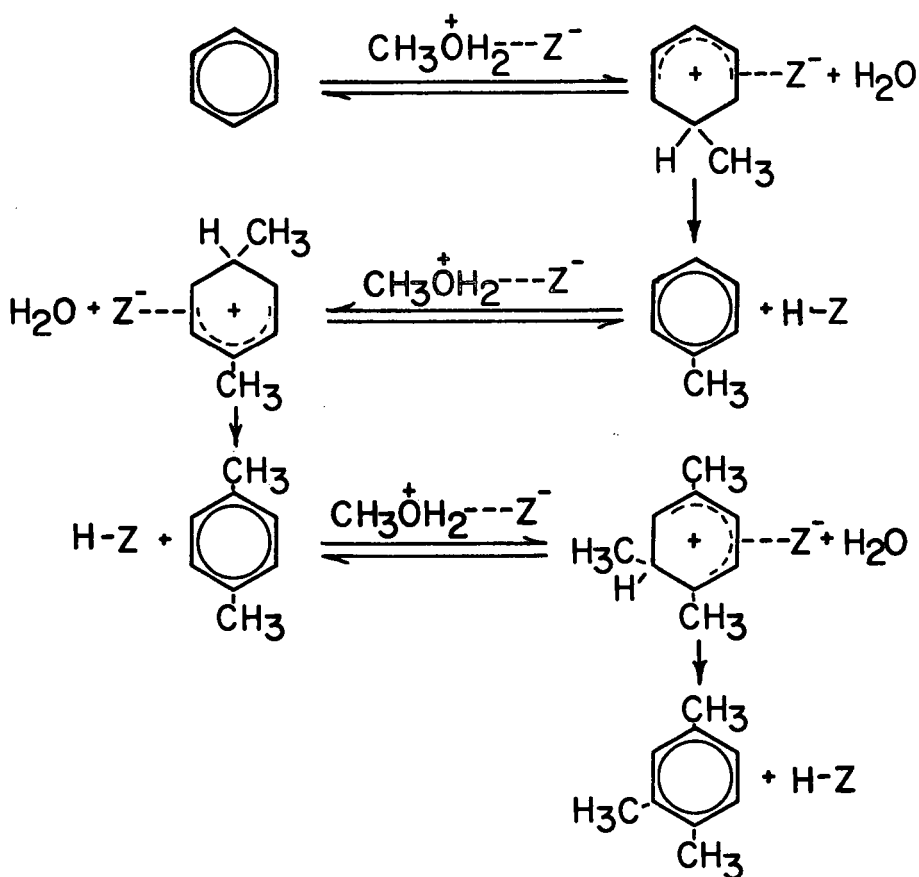


FIGURE 2. ALKYLATION OF AROMATICS



trimethylbenzenes when benzene was used as the tracer.

It is worth noting that the role played by benzene in the formation of alkylated benzenes is quite similar to that of ethylene in the production of higher aliphatics. As observed for the ethylene tracer, ^{14}C -labeled benzene retains most of its radioactivity intact, again indicating that reactive chemisorption is relatively slow. However, the formation of radioactive toluene suggests that the surface reaction of the chemisorbed benzene with methanol or dimethyl ether occurs readily. These results also seem to point out that the nature of this reaction is autocatalytic, as proposed by Chen and Reagan (9) for ethylene reaction with methanol or dimethyl ether to account for the low concentration of ethylene in the product.

In light of the acidic properties of the ZSM-5 catalyst, a carbenium ion mechanism can be proposed for the formation of alkylated benzenes from benzene as indicated in Figure 2.

CONCLUSIONS

Through the use of ^{14}C -labeled tracer compounds, some important secondary reactions have been identified in the overall conversion of methanol to hydrocarbons over a Ni-ZSM-5 catalyst. The major findings are:

1. The alkylation of light olefins with methanol or dimethyl ether is a major pathway for the formation of larger olefins with one more carbon atom.
2. Paraffins are mainly produced by hydrogen transfer reactions to their corresponding olefins, i.e., ones having the same carbon skeleton.
3. Except for minor cracking reactions, paraffins with up to at least 7 C atoms are final stable products; isomerization among paraffin isomers does not take place at 368°C.
4. Light olefins, e.g., ethylene, propylene, and butenes, are reactive intermediates for aromatics formation.
5. Aromatic compounds can also be produced by methanol- or di-methyl ether-alkylation of benzene and subsequent alkylated benzenes.

ACKNOWLEDGMENTS

The authors are grateful to Dr. H. E. Robson at the Exxon Research and Development Labs for providing a sample of the ZSM-5 zeolite and to the Robert A. Welch Foundation and Haldor Topsøe A/S (Denmark) for financial support.

LITERATURE CITED

- (1) Meisel, S. L., McCullough, J. P., Lechthaler, C. H., and Weisz, P. B., *Chem. Technol.*, **6**, 86 (1976).
- (2) Danner, C. A., ed, "Methanol Technology and Economics", *Chem. Eng. Progr. Symp. Ser. No. 98*, 66 (1970).
- (3) Stockinger, J. H., *J. Chromatographic Sci.*, **15**, 198 (1977).
- (4) Bloch, M. G., Callen, R. B., and Stockinger, J. H., *J. Chromatography Sci.*, **15**, 504 (1977).
- (5) Chang, C. D., and Silvestri, A. J., *J. Catal.*, **47**, 249 (1977).
- (6) Perot, G., Cormerais, F., and Guisnet, M., *J. Chem. Res. (S)*, 58 (1982).
- (7) Dejaifve, P., Vadrine, J. C., Bolis, V., and Derouane, E. G., *J. Catal.*, **63**, 331 (1980).
- (8) Anderson, J. R., Foger, K., Mole, T., Rajadhyaksha, R. A., and Sanders, J. V., *J. Catal.*, **58**, 114 (1979).
- (9) Chen, N. Y., and Reagan, W. J., *J. Catal.*, **59**, 123 (1979).
- (10) Hwu, F. S., "Conversion of Methanol and Light Olefins to Gasoline over a Shape Selective Catalyst, ZSM-5", Ph.D. Dissertation, Rice University, 1981.
- (11) Stull, D. R., Westrum, E. F., and Sinke, G. C., "The Chemical Thermodynamics of Organic Compounds", John Wiley and Sons, 1969.

NATURAL GAS BASED TECHNOLOGIES AS REVEALED IN
POSSIBLE NEW ZEALAND ENERGY PROGRAMS

By

P. Jawetz
Independent Consultant on Policy, 415 East 64th Street, New York, New York 10021

INTRODUCTION

New Zealand is an exporter of commodities and thus completely dependent on world market conditions. Its large resources of hydro-electricity, forests, natural gas and fish give it the possibility of industrializing. The off-shore debt on March 31, 1982, stood at US \$ 3,263 million or about US \$ 1,052 per head of population - just about as high as the per capita debt of Argentina - a country mentioned when the world banking system started to worry about possible defaults. In the words of Foreign Minister Warren Cooper before the U.N. General Assembly on October 6, 1982 - "As a small trading nation, New Zealand is acutely sensitive to fluctuations in the health of our major trading partners. New Zealand is classed as a developed country, but we share many of the problems of developing countries".

New Zealand has no oil resources and when the country was hit by the Energy Crisis it decided to develop the gas fields at Kapuni and at Maui in the Taranaki province (in the western part of the North Island) in order to collect associated liquid condensates. The gas was first used to fire electrical plants and later readied for reticulation via pipelines in the Northern Island. Eventually, when the condensate became so much more valuable than the gas - despite its quantity being much smaller - it actually led to flaring the gas to waste in order to obtain the condensate. A "take-or-pay" system was negotiated under which the government is contracted to take a given amount of gas per year from the producing partnership. Assuming that future oil prices will rise only a few percent per year in real terms and performing a standard Discount Cash Flow analysis with a 10% discount rate, the conclusion reached was that there was a higher financial value to be obtained from using the condensate - leading to a zero value for the gas and to a financial justification for flaring it. On the other hand, the gas could be used 1) for reticulation, 2) for promoting a CNG industry (compressed natural gas) or 3) for use in petrochemical industries to produce chemicals or further liquid fuels. Following this logic, and attempting to produce the least change in the transportation system, the New Zealand Ministry of Energy went along with a plan to produce synthetic gasoline from what was then seemingly unwanted gas.

The present paper argues that it would be rather to the long range advantage of New Zealand for the Government to stop at the methanol stage and use methanol as a new liquid fuel in addition to CNG motor fuel rather than go all the way to produce the synthetic gasoline from natural gas.

A MISUSED INNOVATION

Mobil Research and Development Corporation laboratories in Paulsboro, New Jersey, developed spongy, shape-selective catalysts to promote a reaction that transforms alcohol into hydrocarbons by excising water molecules. The catalysts are different pore sized aluminum silicates or clays called zeolites (the Greek word for boiling stones - this because the ancient Greeks observed that certain stones when thrown into fire appeared to boil, thus indicating that the interior structure was hollow enough to contain water and that the pore openings were large enough to allow the water to escape). ZSM-5 is a synthetic zeolite whose uniform pore size and shape is such that when treated in a Mobil-developed process will make possible the chemical reactions involved in the elimination of water molecules from the methanol feedstock. (Z stands for Zeolite; S stands for Socony, and M stands for Mobil as "Socony" or Standard Oil Company of New York was an old name for today's Mobil Oil; 5 is a key for the class of the catalyst.)

When producing the hydrocarbons we define as synthetic gasoline, the catalytic process consumes 10-15% of the energy content in the methanol feedstock (1) but what should be remembered as equally important is that half of the volume of the liquid feedstock is lost when the water molecules are eliminated. Then, depending on how the fuels are used, if the energy content as measured in calorimetric units does not express accurately the work yield of the fuel vehicle engine, or if different fuels show different efficiencies when used in the same engine, the fact that we have lost half

the volume may lead to serious differences in work yield. In other words, reducing the liquid fuel volume of the methanol to approximately one half in order to form the twice higher energy-content synthetic gasoline wastes advantages the alcohol has had per energy unit. This is where the most serious inefficiencies of the Mobil MTG (methanol-to-gasoline) process are incurred - more so than in the energy loss of the process itself (2).

The methanol for the Mobil process can be obtained by passing synthetic gas produced from coal over a copper catalyst or starting with natural gas. Mobil Oil has no proprietary technology for the production of methanol and in New Zealand it will be using an I. C. I. process and 40% of the natural gas feedstock energy content will be lost at this stage. The Mobil ZSM-5 catalyst's competing technology is a $ZnCl_2$ process that was also looked into by the New Zealanders when making their decision (3). To be sure, one does not expect difficulties in upscaling the Mobil MTG process from the four-barrels-a-day pilot unit in Paulsboro, New Jersey to the 13,000-14,000 b. p. d. plant at Motunui, New Zealand, and when completed the plant will most probably deliver as planned but then one could reasonably expect that besides not allowing for a maximum gain to New Zealand from the available natural gas resource, the influx of synthetic gasoline will create an amazing stress on the one and only petroleum refinery in New Zealand that will have to continue to operate on imported crude in order to provide the needed diesel fuel, leading to a future when New Zealand will probably have to import expensive petroleum crude and export cheap gasoline. New Zealand will be left in the process totally dependent on petroleum or "Petroleum-alike" fuels while losing the opportunity it had to move away from petroleum systems by using the natural gas as an entry to a gas and alcohol future to make the two New Zealand islands energy independent indeed. This goal cannot be achieved by providing fuels to existing systems, but rather by adapting its fuel uses to fuels available locally i. e. change its motor vehicle fleets to CNG and methanol cars and opening the future, by establishing now the appropriate end use to biogas, synthetic natural gas from coal, methanol from coal or peat and ethanol from biomass.

New Zealand in answer to its energy needs was destined to experiment with new energy development but it seemingly chose to stay with the old instead of going the way of true innovation. New Zealand, thanks to its geography can go it alone. By not having to worry about cross-border traffic it can isolate itself by going CNG and methanol before the rest of us do so (3).

THE PETROLEUM REFINERY

Petroleum refinery design is dictated by the needs of a relatively small number of products, e. g. , gasoline, jet fuel, diesel fuel, fuel oil. It is generally recognized that the most important part of any refinery is its gasoline manufacturing facility. As the demand for gasoline increased, more and more of the lighter kerosene components were included in gasoline but the maximum suitable portion depended on the kind of crude oil and rarely exceeded 20%. As such, methods more and more complicated were developed to obtain further products that could be blended into the original gasoline fraction. The customary processing in a refinery is thus no more a fractionation process producing relatively pure hydrocarbons, but rather a very complicated system with flows into a general pool of products - the gasoline produced being a mixture of ingredients with different economic costs. Gasoline blending is thus the combining of components to make up the liquid defined by a given set of properties that enable it to be a fuel in a motor vehicle internal-combustion engine. One of the most important properties that must be satisfied is the required octane value. To produce higher octane ingredients that when blended with the first run low octane product, higher temperatures in cracking processes have to be employed. This more severe and energy intensive process, besides being more costly, as it requires higher energy inputs, also creates less valuable by-products - the upshot being that the economics of production at the refinery change. Furthermore, with the requirement to eliminate the octane boosting tetra-ethyl lead from the gasoline formulation because of environmental reasons some refineries, in most cases the smaller refineries, do not even possess some of the needed equipment for these processes.

Both methanol and ethanol when added at about 3% to low octane gasoline will enhance the gasoline's octane number by one point (that is the average over motor octane and research octane). With 10% of the alcohol the average octane value is improved by about 3 points and with 20% of the alcohol 5 points improvement of the average octane value is achieved. Detailed calculation for savings in petroleum crude, when using alcohol octane boosting additives to gasoline, were presented before the First European Communities Conference on Energy from Biomass (4-6). To recapitulate here - it was found that each Btu of ethanol used this way replaces 3.55 Btu of gasoline or one liter of ethanol replaces at least 2.5 liters of gasoline. Following a similar path one can calculate that when using 5% methanol as an additive to gasoline each Btu of methanol used this way replaces 4 Btu of gasoline or one liter of methanol replaces at least 2 liters of gasoline.

In order to calculate the effective energy balance (in the use as well as in the production of the alcohol) the above values have to be multiplied with the energy balance in the manufacture of the alcohol. For the case of biomass ethanol, using a factor calculated by Professor Melvin Calvin - 1.76 each Btu used as energy input in fertilizers, agricultural machinery or distillation equipment

end up displacing 6.6 Btu of petroleum origin when the ethanol is used as an octane boosting additive to gasoline. When the ethanol is used instead as a fuel in an ethanol driven engine (no gasoline involved) in the effective use of the ethanol the potential gain at the refinery is lost. Also, the Btu content of the engine fuel that in the mixture is decreased only by about 3% will be decreased now by rather 30%, while the octane value of the fuel has been increased in the ethanol-alone case to a value higher than required by an unchanged engine. It is expected thus to decrease from the above calculated advantages for the case of the mixed fuels to net gains of only about 20% above the Btu content of the fuel; each liter of ethanol used replaces now only about 0.8 liters of gasoline and each liter of methanol used replaces only 0.6 liters of gasoline - this leading to higher savings in terms of petroleum resources, but also for economics much more difficult. This alternative becomes a possibility when political decision is taken to avoid dependence on petroleum crude. When mentioning alcohol-gasoline mixtures, despite the favorable results of the Brazilian program and many other programs, i. e., in the U.S., West Germany, South Africa, when a New Zealand journalist visited the Mobil Oil Paulsboro facility he was cautioned against such blends "as liable to cause too many technical and distribution problems". Considering that a second plant in New Zealand was built to produce methanol for export - this in a world market that is already saturated with methanol production capacity - Mobil that is already expected to supply one third of New Zealand's need for gasoline in 1985 suggests to use the additional output of methanol in its Motunui plant (7) thus resulting in a production of synthetic gasoline equal to over 50% of what could reasonably be expected to be the New Zealand need for gasoline by a conventional motor-vehicle fleet. Interestingly Shell and B. P., the other corporate partners of the New Zealand refining corporation, did not agree to participate in the Mobil Oil project.

POLICY ISSUES

The Marsden Point refinery used, in 1981, 2,300,000 tonnes of crude oil and 440,000 tonnes of gas condensate and produced 1,236,000 tonnes gasoline and 685,000 tonnes of diesel. After the expenditure of over 1 billion for expansion and for building a hydrocracker, the refinery will use 2,884,000 tonnes of crude and 816,000 tonnes of condensate in order to produce 1,050,000 tonnes of gasoline, 430,000 tonnes of aviation fuel, and 1,125,000 tonnes of diesel. This change at the refinery will also double the refinery fuel loss from 165,000 tonnes/year to 330,000 tonnes/year.

On March 31, 1980, New Zealand Motor Vehicle licenses amounted to 1,283,661 passenger cars, 3,134 taxicabs, 3,397 buses and coaches, 176,692 trucks under 2 tonnes, 76,872 trucks over 2 tonnes. When including all other vehicles such as motorcycles, and motor homes, a grand total of 2,157,516 motor vehicles were licensed. New registrations for the year 1981 amounted to a total of 114,842 cars, the majority of which were assembled in New Zealand from parts imported mainly from Japan (73%). Other important countries of origin were the U.K. with 13.6% and Australia with 11.1%. All other countries of origin, including the U.S., amounted to only 2.3% (nevertheless, when analyzing the manufacturing companies it is clear that Ford and General Motors are well represented, mainly through their Australian and U.K. affiliates, amounting to about 30%).

Two of the motor vehicle assembly corporations were responsible for over 21,000 vehicles each while four other corporations were in the 10,000-18,000 range. Thus it is reasonable to assume that a corporation that may not even produce a CNG or methanol car for its own home market may find it advantageous to send such kits to the New Zealand assembly plant. In effect it would just take the cooperation of two such corporations in order to embark on a slow process of changing the motor vehicle fuels system gradually. The funds for such changes could then easily be found from the \$1.5 billion that could be saved by eliminating some changes at the refinery and by eliminating the methanol-to-gasoline stage at the Motunui plant (8).

It is preferable to go to dedicated vehicles - vehicles that were originally built for non-petroleum fuels use - rather than convert vehicles that were originally built to use gasoline fuels. Such conversions, for the CNG case, leave the vehicle with an undesirable seriously decreased trunk space.

CONCLUSIONS

The Mobil MTG process, to be employed in New Zealand, is being scaled up from the Mobil Oil Paulsboro operation to what could be a commercial size plant. Nevertheless, the economics in the New Zealand case are such that this operation can only prove the technical aspects of the plant but not the economics - the New Zealand economics being figured out on the basis of a practical give-away of the natural gas.

Furthermore, New Zealand being a set of two islands with very little traffic from the outside, could have switched to a transportation system based on CNG and methanol with an intermediary stage that uses the existing Whangarei refinery, without changes, and methanol for an octane enhancer. Such a policy besides having environmental benefits is economically sounder in the long range as 1) it allows for a much larger energy efficiency for the natural gas resource and 2) it prepares

the economy to an eventual switch to other sources of fuel gas and alcohols. New Zealand has large potential for the production of biomass and has as well coal and peat deposits that will eventually form the basis for an industrialization of the South Island. The elimination of the dependence on a petroleum system and the development of an indigenous industry are, reasonably, the real long range interests of New Zealand.

What was said here is in no way an expression of doubt in the technical feasibility of the Mobil MTG process. It is highly possible that for other countries, and in other objective circumstances, this process can be applied in accordance with national interests. Such circumstances could be envisioned for example for the case a country cannot isolate itself when its roads are being used or by cars originating in areas that would not participate in a policy of switching from petroleum fuels.

LITERATURE CITED

- (1) "Energy Research Reports", ER Publications Inc., P.O. Box 157, Watertown, MA 02172, U.S.A. (a) December 11, 1978; (b) October 29, 1979.
- (2) Jawetz, P., "Relative Economics of Alcohol Octane Boosting Additives to Gasoline, Alcohol Fueled Cars, and Synthetic Gasoline from Alcohol". Energy from Biomass, Second European Communities Conference, A. Strub, P. Chartier, G. Schlessler, editors, Applied Science Publishers, London, 1983.
- (3) Jawetz, P., "Natural Gas Based Energy Systems - How New Zealand Decided to Act Not In Its Own Best Interest", Monograph No. 83-Pet-28 (1983). The American Society of Mechanical Engineers, 345 E. 47th St., New York, N. Y. 10017.
- (4) Jawetz, P., "The Economics of Improving Octane Values of Gasoline with Alcohol Additives", Palz, W., Chartier, P., and Hall, D.O., editors, "Energy from Biomass", Applied Science Publications, London 1981.
- (5) Jawetz, P., "Alcohol Additives to Gasoline - An Economic Way for Extending Supplies of Fuels and for Increasing Octane Rations", PREPRINTS, Div. of Petrol. Chem., ACS, 24, 798 (1979).
- (6) Jawetz, P., PREPRINTS, Div. of Petrol. Chem., ACS, 25 (1), 99 (1980).
- (7) New Zealand Press Association correspondent, "The Press", Christchurch, March 18, 1983.
- (8) Peace, D. J., Technical Officer for the Auckland Gas Association, in submission for "The Environmental Impact Audit Synthetic Petrol Plant!", Volume II, April 20, 1981.

APPLICATION OF THERMAL ANALYTICAL TECHNIQUES TO
 ENHANCED OIL RECOVERY

By

K. N. Jha
 Research and Development, Saskatchewan Oil and Gas Corporation
 515 Henderson Drive, Regina, Saskatchewan, Canada S4N 5X1

INTRODUCTION

The world, especially in Canada and Venezuela, has extensive resource of oil sands and heavy oils. These resources are characterized by high viscosity, low API gravity, i. e., high density, and large sulfur contents (Table I). Recovery of Lloydminster heavy oils in Canada under primary and secondary processes are less than 9% of initial oil-in-place, whereas that of bitumen from oil sands is nil.

TABLE I
 PROPERTIES OF HEAVY OILS AND OIL SANDS^{a-c}

Source	Gravity °API	Viscosity cp(°C)	Sulfur Wt%	Asphaltene Wt%	Conradson Carbon Residue Wt%
<u>Canada</u>					
Lloydminster	10-18	2000-20,000(20)	2.6-3.5	8 - 12	8 - 12
S. E. Alberta	12-18	3000 (T _R) ^d	3.5	12	12.2
Athabasca	8-12	1-5x10 ⁶ (T _R)	4.6	17	13.5
Cold Lake	10-12	1 x 10 ⁵ (T _R)	4.7	15	12.6
Peace River	8-9	1 x 10 ⁵ (T _R)	5.6	20	
Wabasca A	8-13	8 x 10 ⁵ (T _R)	5.5	19	
<u>Venezuela</u>					
Boscan	10-12	26 x 10 ³ (38)	5.2	9 - 17	15.0
Tia Juana	12	37 x 10 ² (38)	2.7	6	11.2
Morichal	12	32 x 10 ² (38)	2.1	11	14.0
Jobo	8.4	62 x 10 ³ (38)	3.7-4.1	9	14.1
<u>U.S.A.</u>					
Asphalt Ridge, Utah	8-13	69 x 10 ⁶ (25)	0.2-0.8	12	9.1

- a. Work done in our laboratory on Lloydminster, Saskatchewan crudes.
- b. "The Future of Heavy Crude Oils and Tar Sands", Ed. R. F. Meyer and C. T. Steele, McGraw-Hill, inc., New York (1981), pp. 168, 187, 237.
- c. "The Oil Sands of Canada - Venezuela 1977", Ed. D. A. Redford and A. G. Winestock, CIM Special Volume 17, The Canadian Institute of Mining and Metallurgy, pp. 146, 178, 284.
- d. Reservoir temperature.

For the development and utilization of these resources, enhanced oil recovery (EOR) processes have to be employed (1-3). EOR refers to all techniques used to increase the amount of oil produced after primary recovery. EOR methods encompass pressure maintenance, water-flooding, gas injection, thermal, miscible displacement and chemical processes. The thermal process is most suitable for recovery of heavy oils and oil sand bitumens. In this process oil displacement results from:

- i) viscosity reduction primarily due to heat and secondly due to carbon dioxide dissolution in oil,
- ii) thermal expansion of the oil resulting in increased relative permeability,
- iii) distillation and thermal cracking of oil,
- iv) a solution gas drive from produced gas which facilitates the flow of fluids within the reservoir toward the production wells, and

v) increased pressure gradient imposed by the injected air.

Heat is transferred to the reservoir either by injection of steam/hot water or by *in-situ* combustion. The latter process, of interest to us at present, consists of injecting air/oxygen/water into an oil reservoir to establish a flow path for the movement of fluids, igniting the crude oil and propagating the combustion front by continued air/oxygen injection (Figure 1).

The important factors required to establish the feasibility of initiating an *in-situ* combustion field test are the fuel (coke) content of the oil being burned, the volume of air/oxygen required to sustain combustion and the efficiency of oxygen utilization. These parameters are usually determined by laboratory experiments employing a combustion tube. A sample of the data obtained is presented in Table II. Most of these parameters could be estimated from TGA/DSC data.

TABLE II
TYPE OF DATA GENERATED FROM COMBUSTION TUBE EXPERIMENTS^{a, b}

Fuel Concentration, Kg/m ³	16-48
Air-Fuel Ratio, m ³ /Kg	10
Oxygen Utilization, %	90+
Combustion Front Velocity, m/h ^c	0.1
Steam Front Velocity, m/h	0.1
Vaporization Front Velocity, m/h	0.1
Fuel Required to Sustain Combustion, Kg/m ³	20
Maximum Peak Temperature, °C	450-700
Hydrogen to Carbon Ratio of Fuel	0.6-2.0
Oil Recovery, %	90
Produced Gas Analysis, Vol. %	CO ₂ , CO, O ₂ , N ₂ , C ₁ -C ₄ , SO ₂ , H ₂

- a. D. W. Bennion et al., "Proceeding II International Conference on Heavy Crude and Tar Sands", Caracas, February 7-17, 1982.
 b. "The Future of Heavy Crude and Tar Sands", Ed. R. F. Meyer and C. T. Steele, McGraw-Hill, Inc., New York, pp. 413-25, 1981.
 c. Meters per hour.

Although combustion tube experiments generate data useful for the design and operation of the field-pilot, it is imperative that the numerical simulation of the *in-situ* combustion process be carried out in making meaningful predictions of the parameters for planning, construction and optimum operation of field pilots.

Numerical *in-situ* combustion simulation usually requires reservoir description, reservoir fluid properties, thermodynamic, chemical kinetics and well data (4). Experimental data for thermodynamic properties and chemical kinetics required in the area of low temperature oxidation, cracking, combustion and coking reactions are lacking in order to make meaningful predictions of an *in-situ* combustion project (5-7). To this end, we have employed thermal analytical techniques, thermal gravimetric analysis (TGA) and differential scanning calorimeter (DSC) to generate the required data such as energy of activation, pre-exponential factor, rate constant, and heat of reaction for chemical reactions. Thermal techniques can also provide data on minimum ignition temperature of crude oil to sustain combustion, fuel content of the core, fluid-rock interaction, decomposition of the mineral matter present in the core and residue left after heating.

This paper presents TGA and DSC results obtained for two Lloydminster heavy oil core samples under flow of helium, nitrogen and air.

EXPERIMENTAL

Tests were performed using a DuPont 951 Thermogravimetric Analyzer and a 910 Differential Scanning Calorimeter attached to the 1090 Data Analysis System. A sample size of 25-60 mg and a temperature range of 40° to 900°C for TGA, and 1-3 mg and 40° to 580°C for DSC studies were used. Samples were heated at a rate of 5° or 10°C/min. in air, nitrogen or ultra pure helium flowing at 60 cm³/min. for TGA and 20 cm³/min. for DSC experiments. Thermograms recorded the percentage weight loss as a function of temperature and its derivative for TGA and heat flow in mW versus temperature for DSC runs. The DSC cell constant was determined to be 1.081 using an indium standard. DSC experiments were performed using hermetic pans.

Samples A and B used for this study had an initial oil saturation of 63 and 85%, a porosity of 29 and 33%, and a permeability of 1.9 and 2.3 Darcies, respectively. Gravity and viscosity of crude oils were 16°API and 236 cp at 38°C for sample A and 11°API and 46,000 cp at 38°C for sample B.

RESULTS

Thermograms of weight loss versus temperature for Lloydminster core A are shown in Figure 2. The total weight losses were 6.92% in He, 7.57% in N₂, and 7.79% in air. The higher weight loss under air than under He indicates that the coke produced in the process is oxidized by oxygen, resulting in additional weight loss. The results under N₂ atmosphere imply that N₂ contains oxygen as an impurity.

Figures 3, 4 and 5 show weight loss curves and their derivatives (DTG) against rising temperature for sample A in He, N₂ and air. The derivative curves suggest that there are at least four groups of reactions which can be convoluted in four temperature zones. Kinetics for loss in weight in each temperature zone is described later.

TGA and DTG thermograms are presented in Figures 6 and 7 for core sample B. The total weight loss was 14.8% in He and 15.6% in air in the temperature range 40° to 880°C. The characteristics of the TGA and DTG curves are similar to those obtained for sample A. It should be noted, however, that the oil content of sample B is twice as much as that of A.

For further understanding of reaction kinetics, differential scanning calorimeter experiments were conducted for samples A and B in He and air at a heating rate of 10°C/min. (Figures 8-11). The thermograms produced with He have three peaks, the last one representing the cracking reactions. The large exothermic peak produced under air is attributed to combustion reactions. The peak temperatures for these tests range between 453° and 484°C. Arrhenius and thermal parameters obtained by using the Borchardt and Daniels kinetics data analysis program supplied by DuPont are discussed later (8-10).

DISCUSSION

Derivatives of TGA thermograms for core samples A and B have demonstrated that there are four temperature regimes for weight loss. The temperature ranges and percentage weight loss for the total material and organic components within each range are listed in Table III. The percentage weight loss in the first region (50°-380°C) was approximately the same under He and air for sample A or B. This weight representing 40 to 55% of the total loss is attributed largely to volatilization and to some extent to low temperature oxidation. The weight loss in the second temperature regime (340°-540°C) was 19% in He and 43% in air for sample A and 27% in He and 54% in air for sample B. This indicates that volatilization and thermolysis of heavy oil present in the core is taking place under He whereas more efficient reactions, such as oxidation and subsequent decomposition and volatilization, are involved in the presence of air. The third regime (450°-630°C) is characterized by cracking, volatilization and combustion reactions whereas the last fraction of the weight loss between 550° and 900°C is assigned to coking, decomposition of mineral matter and oxidation. Oxidation and combustion reactions take place when sample is in contact with oxygen.

Weight loss kinetics for pyrolysis and combustion processes is extremely complex for such systems because of the numerous components present and their simultaneous and competing reactions. Kinetic treatment of the data is described below.

Solid phase thermal decomposition is described by the rate expression (11-12):

$$\frac{d\alpha}{dt} = k(1-\alpha)^n \quad 1)$$

$$\alpha = (\omega_0 - \omega_t) / (\omega_0 - \omega_\infty) \quad 2)$$

$$k = A e^{-E/RT} \quad 3)$$

where k is rate constant; n, order of reaction; ω_0 initial sample weight; ω_t sample weight at time t; ω_∞ final weight; A, pre-exponential factor; E, activation energy; R, gas constant; and T, absolute temperature in K. For a linear heating rate, β , °C/min:

$$\beta = dT/dt \quad 4)$$

By combining Equations 1, 3 and 4, rearranging, integrating and taking the natural logarithm and assuming n = 1, we obtain:

$$\ln \left[\frac{-\ln(1-\alpha)}{T^2} \right] = \ln \frac{AR}{\beta E} \left[1 - \frac{2RT}{E} \right] - \left(\frac{E}{R} \right) \frac{1}{T} \quad 5)$$

A plot of $-\ln \left[\frac{-\ln(1-\alpha)}{T^2} \right]$ versus $1/T$ should result in a straight line of slope E/R. The value of E obtained graphically is substituted in Equation 5 to calculate the pre-exponential factor, A. Typical plots to obtain apparent activation energies are shown in Figures 12-15 for reactions

occurring in the four temperature zones for sample A under He flow.

Equation 3 is used to estimate rate constant at any temperature. Values of E, A, and rate constant at mean temperature for each reaction zone are presented in Table III.

TABLE III
THERMAL DECOMPOSITION PARAMETERS FOR LLOYDMINSTER
HEAVY OIL CORES

Sample (Purge Gas)	Reaction Zone	Temp. Range, °C	Wt. Loss %		E kcal/mol	A s ⁻¹	10 ³ k _{mean} ^b s ⁻¹	Fuel (Coke) Kg/m ³	
			Total	Organic ^a					
A. (He)	1	50-340	3.01	2.94	4.6	1.3 x 10 ⁻¹	0.92)39.2 29.3)	
	2	340-475	1.25	1.08	20.2	3.3 x 10 ³	1.1		
	3	475-550	0.69	0.45	49.9	2.5 x 10 ¹¹	3.3		
	4	550-800	1.62	1.33	18.3	1.5 x 10 ¹	0.91		
	(N ₂)	1	50-360	3.09	3.01	4.9	1.3 x 10 ⁻¹	0.75	
		2	360-450	0.89	0.79	29.3	5.0 x 10 ⁶	1.8	
		3	450-550	1.18	0.88	36.3	3.3 x 10 ⁷	1.8	
		4	550-900	2.32	1.98	14.8	1.8	1.0	
	(Air)	1	50-340	3.17	3.10	4.9	1.2 x 10 ⁻¹	0.62	
		2	340-480	3.26	3.00	23.5	6.7 x 10 ⁴	2.0	
		3	480-550	0.62	0.45	45.5	1.7 x 10 ¹⁰	4.1	
		4	550-800	0.48	0.08	14.2	2.5	1.3	
B. (He)	1	50-380	8.10	8.01	6.2	6.4 x 10 ⁻¹	1.1)49.1 28.8)	
	2	380-500	3.90	3.66	35.3	3.8 x 10 ⁸	5.8		
	3	500-600	1.15	0.92	46.4	1.0 x 10 ¹⁰	4.8		
	4	600-800	1.52	1.31	21.5	1.2 x 10 ²	1.8		
	(Air)	1	50-380	6.85	6.74	6.6	8.8 x 10 ⁻¹	1.0	
		2,3	380-540	8.32	7.95	39.4	1.8 x 10 ⁹	3.2	
		3,4	540-630	0.22	0.10	29.2	2.0 x 10 ⁵	7.3	

a. Contribution from decomposition of mineral matter was subtracted from % total weight loss to get organic weight loss.

b. Mean temperature.

The apparent activation energy obtained for reaction zone 1, E₁, varies between 4.6 and 6.6 kcal/mol for samples A and B under He, N₂ and air. E₁ values being very close to the latent heat of vaporization for hydrocarbons confirms our suggestion that weight loss in this reaction zone is mostly due to volatilization (13). E₂ values for sample A range from 20.2 to 29.3 kcal/mol and for sample B 35.3 to 39.4 kcal/mol. These values are similar to those reported for thermolysis and oxidation of hydrocarbons and crude oils (14-16). E₃ values of 49.9 and 46.4 kcal/mol for samples A and B in He are larger than 45.5 and 29.2 kcal/mol for A and B, respectively, in air. Cracking reactions under inert environment are known to have higher E values than under oxidizing atmosphere (5-6). Hayashitani et al. have postulated a series of cracking reactions in helium involving light oil, heavy oil and asphaltene components in the pyrolysis of bitumen extracted from the Athabasca oil sand (17). Activation energies for cracking reactions reported by them range between 57.4 and 65.2 kcal/mol. Bennion et al. have reported that these values of activation energies were divided by 1.37 to be used in numerical simulation in order to obtain reasonable values of temperature and fuel lay-down (5). These activation energies divided by 1.37 produce an average value of 44.1 kcal/mol which agrees with 49.9 and 45.5 kcal/mol obtained by us for reactions in zone 3 under He atmosphere. This indicates that the results obtained from TGA are more meaningful for use in the numerical simulation than those obtained from pyrolysis experiments in a closed system. Activation energies for reactions in zone 4 ranging between 14.2 and 21.5 kcal/mol are typical of reactions involving either coke formation or its oxidation (6).

The fuel (coke) contents of samples A and B have been determined to check if the minimum amount of fuel required to sustain combustion front is available. Calculation of fuel lay-down was based upon percentage organic loss in He in reaction zone 4 because coke is formed in this region. Since the maximum combustion temperature of the fire front listed in Table II ranges between 450° and 700°C, it is expected that for some fireflood tests, weight loss in zone 3 in He will also contribute to fuel lay-down. The fuel content under both scenarios calculated by assuming the density of the sample 2.2 g/cm³ is included in Table III. Estimated fuel content values under either assumption are greater than the value required (20 kg/m³) to sustain combustion.

Activation energies, pre-exponential factors, rate constants at peak temperatures, and heats of reactions obtained from treating DSC data for the last peak using the Borchardt and Daniels kinetics program are listed in Table IV. Order of reaction was assumed to be 1.0. Activation energies for cracking under He of sample A was 55.9 and of sample B was 61.7 kcal/mol and for combustion under air of sample A was 20.5 and of sample B was 28.9 kcal/mol. These values are higher for cracking and lower for combustion reactions than those obtained from kinetic treatment of TGA data in temperature zone 3 (Table III). Although inhomogeneity of core samples is always a problem in generating reproducible data, it is believed that more experimental data is needed before such discrepancy can be resolved. Heats of reaction for tests under air are much larger, 147 for A and 240 cal/g for B, than in He, 38 for A and 91 cal/g for B. It is evident that heat of reaction for sample A is lower than that of B. This is because oxidation reactions are much more exothermic than cracking reactions and oil content of sample A is one-half of B. Table IV includes peak and ignition temperatures derived from DSC thermograms. Ignition temperature is defined here as the temperature to which the product must be heated in the presence of air to sustain combustion. Temperature at the onset point of the combustion peak on DSC thermograms has been assigned to this value. Ignition temperature for sample A is 325°C and for sample B is 345°C.

TABLE IV
REACTION PARAMETERS FROM DSC EXPERIMENTS^a

Sample (Purge Gas)	Peak Temp. °C	Activation Energy kcal/mol	A s ⁻¹	10 ³ k s ⁻¹ peak	Heat of Reaction cal/g	Ignition Temp. °C
A. (He)	462	55.9	2.6 x 10 ¹⁴	5.7	38	
	(Air) 453	20.5	6.2 x 10 ³	3.9	147	325
B. (He)	484	61.7	4.2 x 10 ¹⁵	5.2	91	
	(Air) 480	28.9	9.2 x 10 ⁵	3.3	240	345

- a. Order of reaction was assumed to be 1.0 for estimation of activation energy and pre-exponential factor.

SUMMARY

Thermal degradation of Lloydminster heavy oil core samples has been investigated in He, N₂ and air using TGA and DSC techniques. TGA and DTG thermograms demonstrated four distinct types of chemical reactions occurring in four different temperature zones. Reactions in zone 1 are attributed to volatilization and low temperature oxidation; in zone 2 to thermolysis of heavy oil fractions, volatilization and oxidation; in zone 3 to cracking and combustion; and in zone 4 to coking, decomposition of mineral matter and oxidation of the coke produced. Oxidation reactions take place when the sample is in contact with air. Fuel (coke) contents of sample A ranged between 29.3 and 39.2 Kg/m³ and that of B, 28.8 and 49.1 Kg/m³. Arrhenius and thermal parameters obtained for reactions in TGA/DSC studies are listed in Tables III and IV.

Data generated from TGA/DSC experiments are essential for running numerical simulation of the *in-situ* combustion process and verifying their match to the laboratory results. In addition, TGA/DSC data can be manipulated to yield air-fuel ratio, oxygen utilization, combustion front velocity, produced gas composition and hydrogen-to-carbon ratio of the fuel. It is evident that thermal analytical techniques have the potential to produce data which can be used for planning, design and construction of the field *in-situ* combustion tests and for numerical simulation to predict process variables and economics.

ACKNOWLEDGMENTS

I wish to thank G. Perron for technical assistance and A. Leu for calculation of some of the data. Partial financial support from Saskatchewan Energy and Mines is acknowledged for this work.

Figure 1. Schematic diagram of in-situ combustion process.

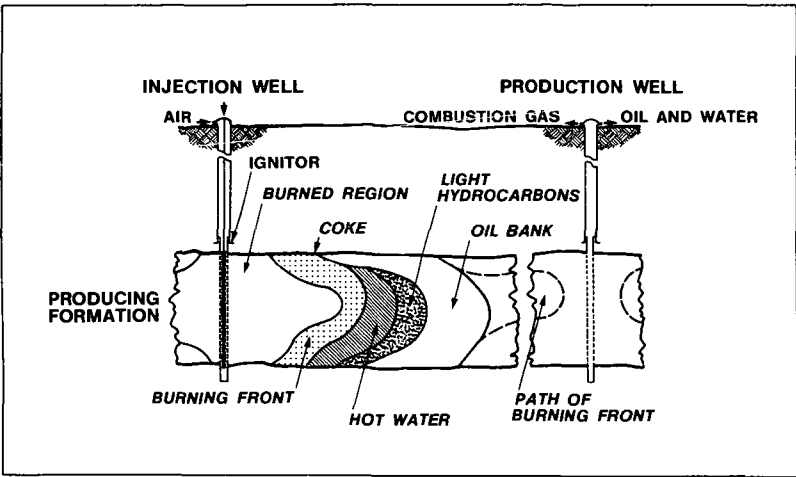


Figure 2. TGA thermograms of core sample A under the flow of He, N₂ and air.

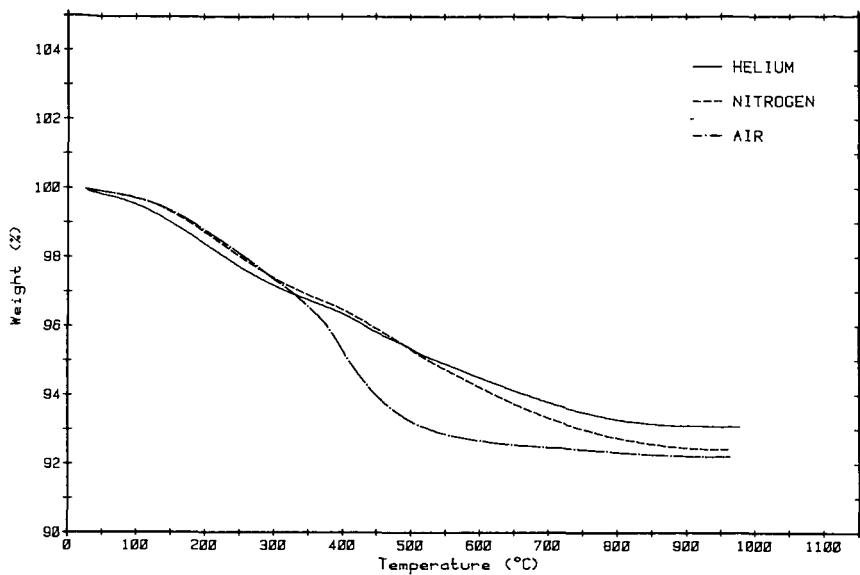


Figure 3. TGA and DTG thermograms of core sample A under He.

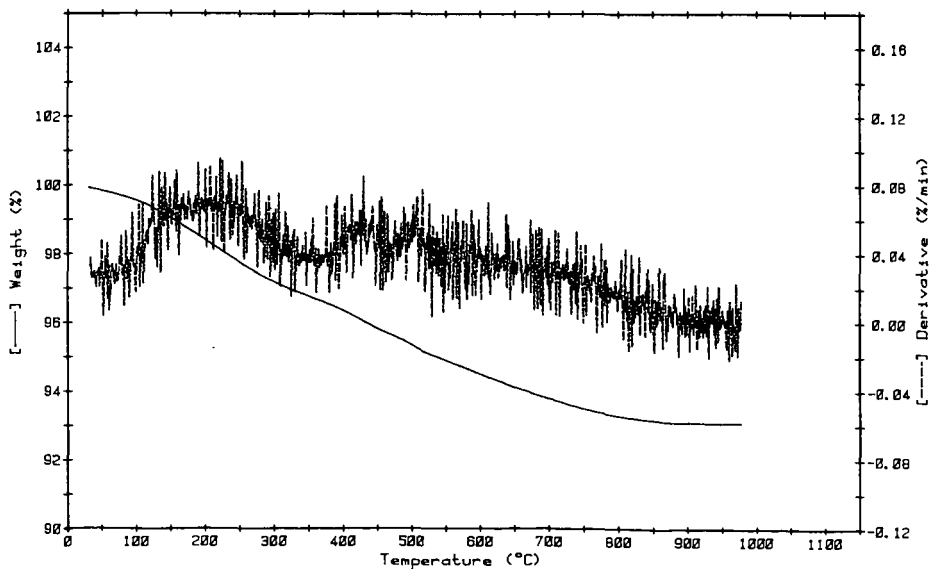


Figure 4. TGA and DTG thermograms of core sample A under N₂.

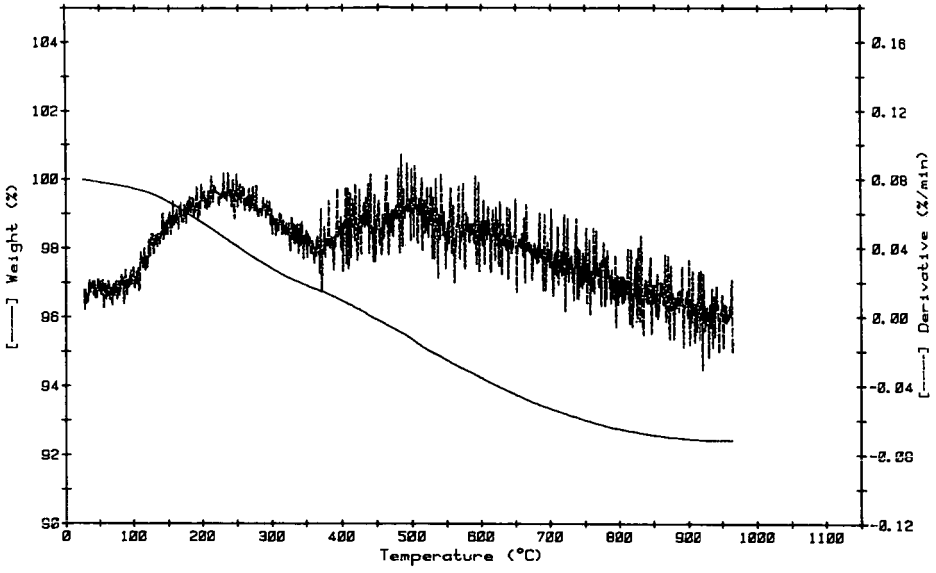


Figure 5. TGA and DTG thermograms of core sample A under air.

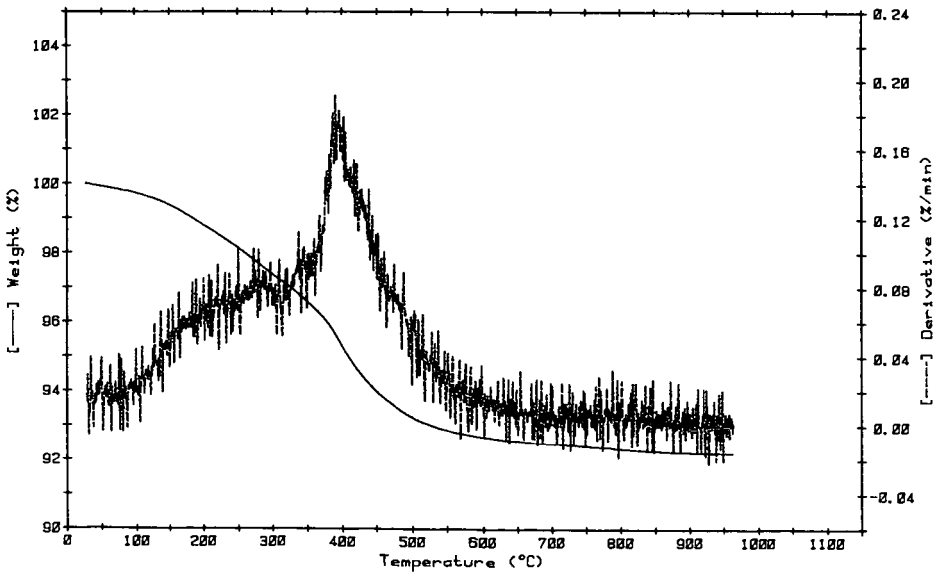


Figure 6. TGA and DTG thermograms of core sample B under He.

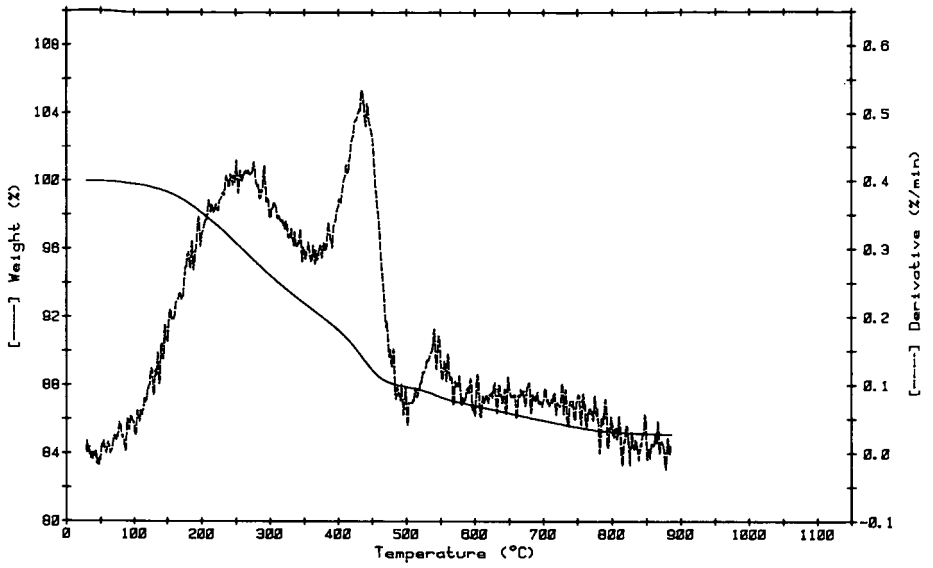


Figure 7. TGA and DTG thermograms of core sample B under air.

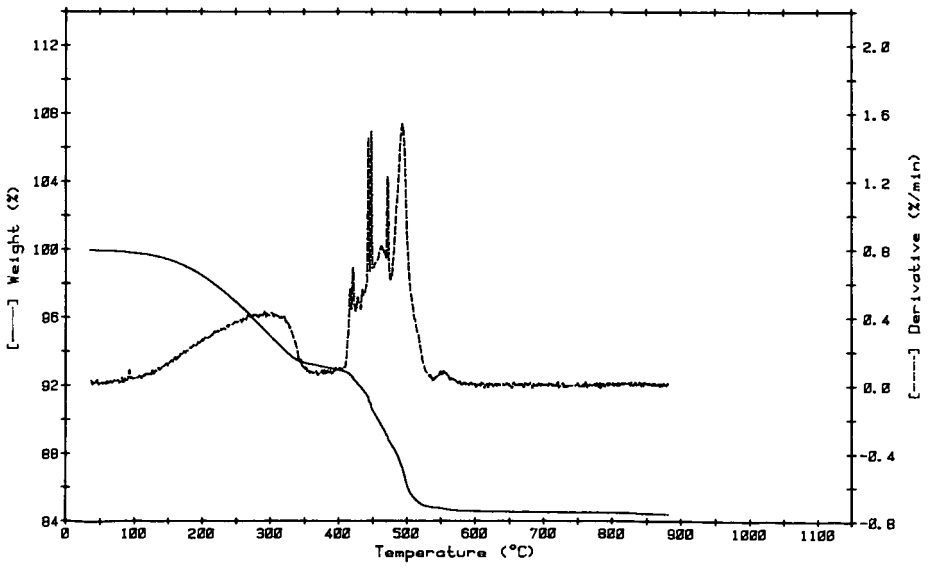


Figure 8. DSC thermograms of sample A under He.

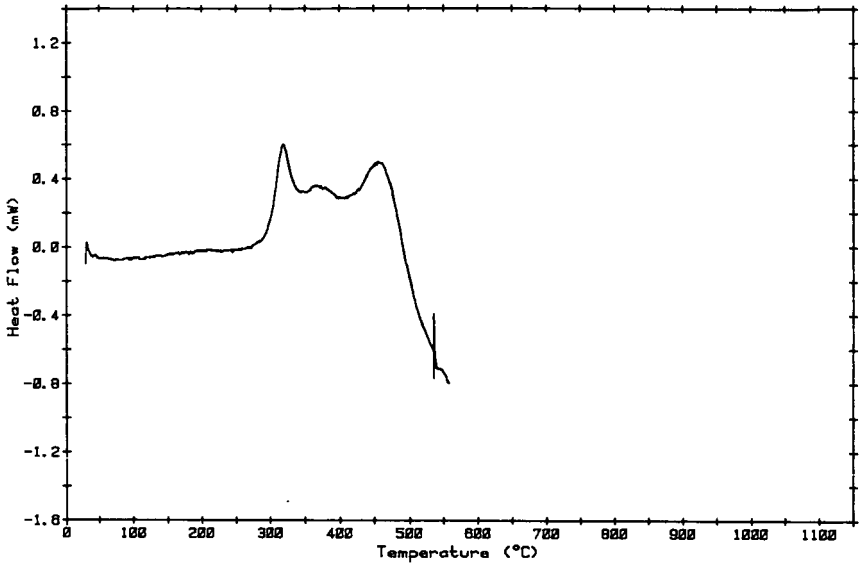


Figure 9. DSC thermograms of sample A under air.

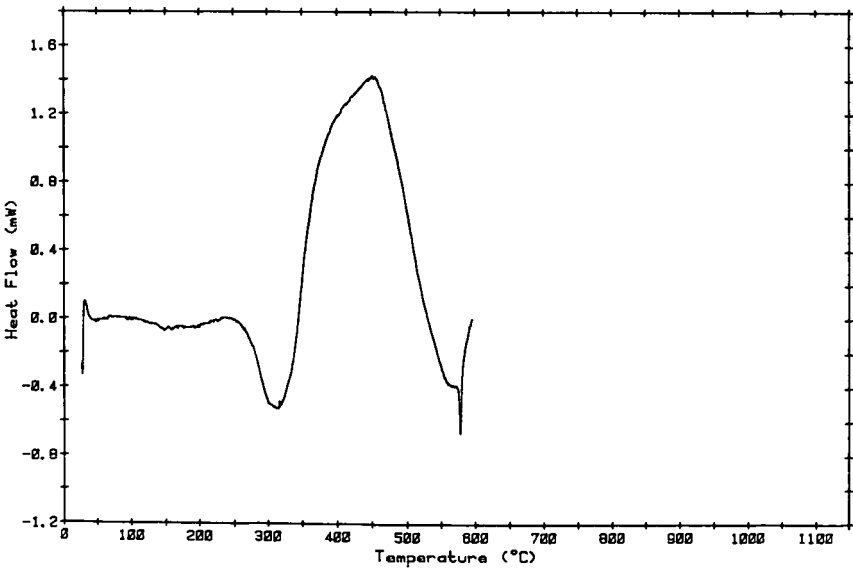


Figure 10. DSC thermograms of sample B under He.

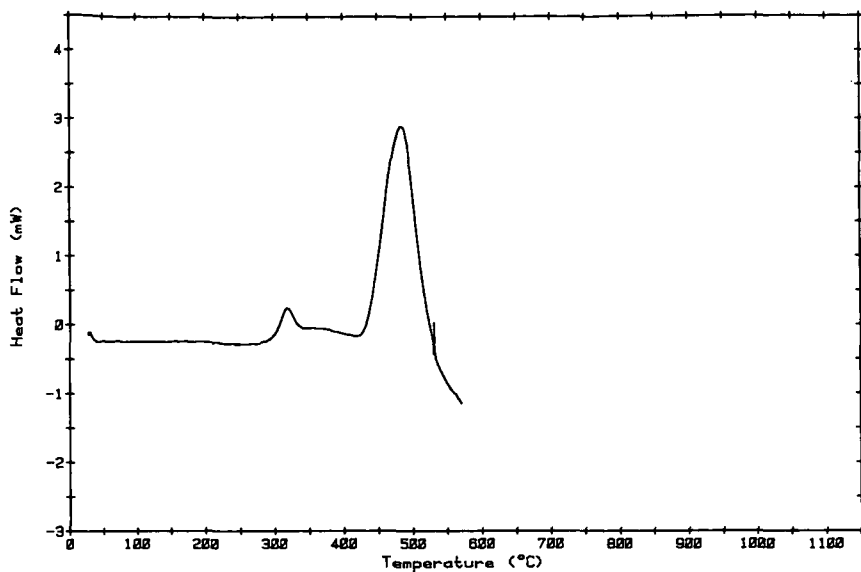


Figure 11. DSC thermograms of sample B under air.

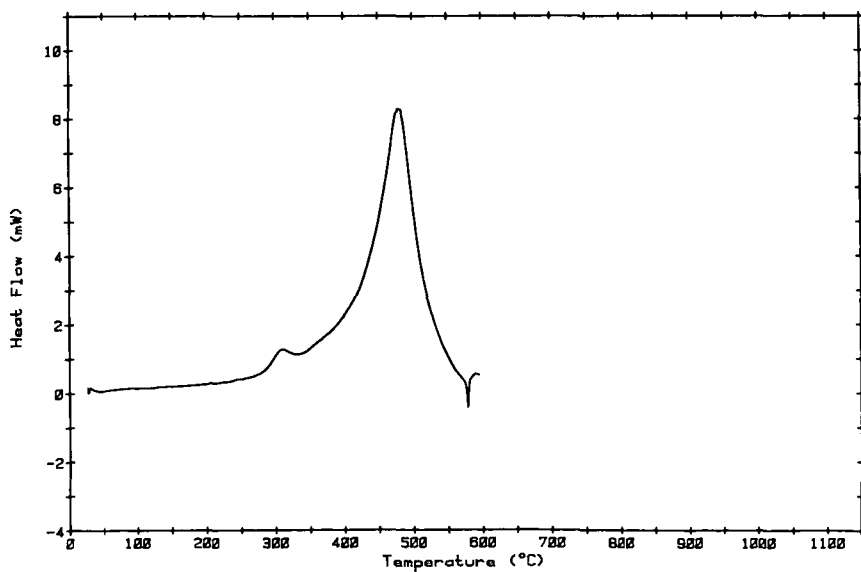


Figure 12. Arrhenius plot for sample A under helium between 50° and 340°C.

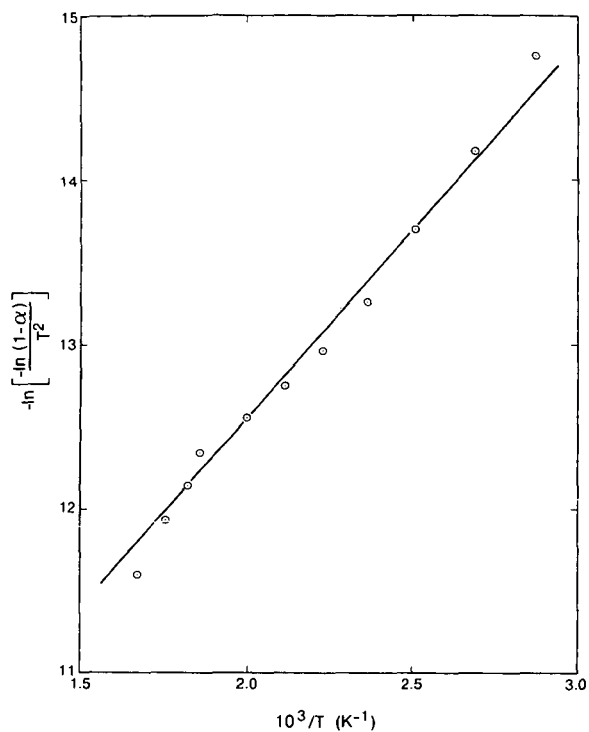


Figure 13. Arrhenius plot for sample A under helium between 340° and 475°C.

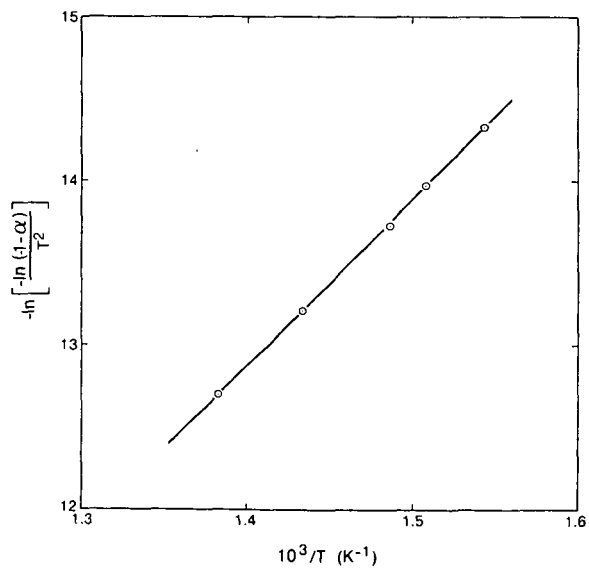


Figure 14. Arrhenius plot for sample A under helium between 475° and 550°C.

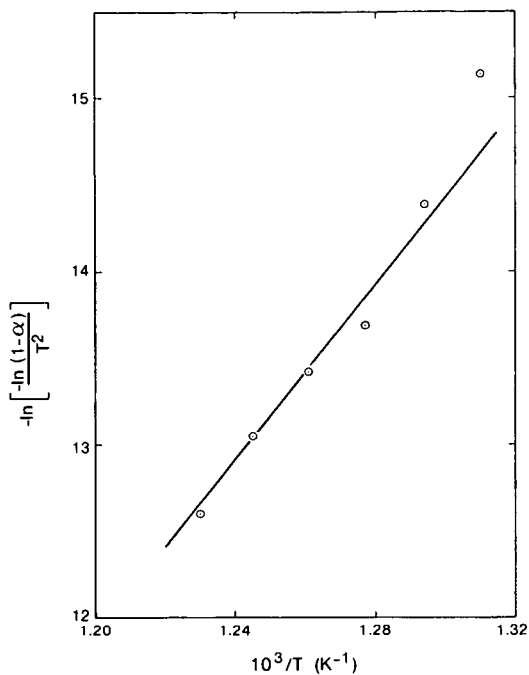
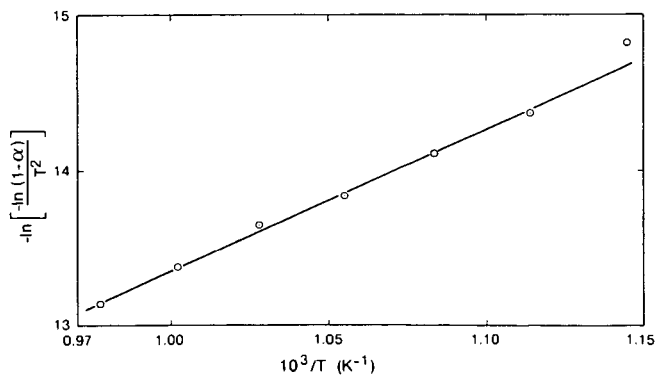


Figure 15. Arrhenius plot for sample A under helium between 550° and 800°C.



LITERATURE CITED

- (1) Jha, K. N., *Chemistry in Canada*, pp. 19-26, September 1982.
- (2) Jha, K. N., and Verma, A., *Proc. II International Conf. on Heavy Crudes and Tar Sands in Caracas, Venezuela*, Vol. IV, Feb. 7-17, 1982.
- (3) "Fundamentals of Enhanced Oil Recovery", K. H. van Poolen and Assoc. Inc., PennWell Books, Tulsa, Oklahoma, U.S.A., 1980.
- (4) "Fully Implicit *In Situ* Combustion and Steam Model", ISCOM User Manual, Version 2.2, April, 1981, Computer Modelling Group, Calgary, Alberta, Canada.
- (5) Bennion, D. W., Moore, R. G., Donnelly, J. K., and Erian, A., *Proc. II International Conf. on Heavy Crudes and Tar Sands in Caracas, Venezuela*, Vol. II, February 7-17, 1982.
- (6) Lin, C. Y., Chen, W. H., Lee, S. T., and Culham, W. E., 57th Ann. Fall Tech. Conf., Soc. Pet. Engg. SPE 11074, New Orleans, U.S.A., September 26-29, 1982.
- (7) Vossoughi, S., Barlett, G. W., and Willhite, G. P., 57th Ann. Fall Tech. Conf., Soc. Pet. Engg. SPE 11073, New Orleans, U.S.A., September 26-29, 1982.
- (8) Borchardt, H. J., and Daniels, F., *J. Am. Chem. Soc.*, 79, 41-46 (1957).
- (9) Grentzer, T. H., Holsworth, R. M., and Provder, T., *National ACS*, 3/81, ORPL.
- (10) "Borchardt and Daniels Kinetics Data Analysis Program", PN994377-912, DuPont, Wilmington, Delaware, U.S.A., August 1982.
- (11) Coats, A. W., and Refdern, J. P., *Nature*, 201, 68-69 (1964).
- (12) Thakur, D. S., Nuttal, H. E., and Cha, C. Y., Preprint, Div. Fuel Chem., 27 (2), 131 (1982).
- (13) Yaws, C. L., "Physical Properties", *Chem. Engg.*, McGraw-Hill Co., New York, p. 205 (1977).
- (14) Baldwin, R. R., Bennett, J. P., and Walker, R. W., 16th International Symp. on Combustion, MIT, Cambridge, Mass., U.S.A., August 15-20, 1976.
- (15) Jha, K. N., Rao, P. M., and Stausz, O. P., Preprint, Div. Fuel Chem., 23 (4), 91 (1978).
- (16) Campbell, J. H., Koskinas, G. H., and Stout, N. D., *Fuel*, 57, 372 (1978).
- (17) Hayashitani, M., Bennion, D. W., Donnelly, J. K., and Moore, R. G., "The Oil Sands of Canada-Venezuela 1977", Ed. Redford, D. A., and Winestock, A. G., *Can. Ins. Mining and Met.*, pp. 233-247 (1977).

GENERAL PAPERS - POSTER SESSION
PRESENTED BEFORE THE DIVISION OF PETROLEUM CHEMISTRY, INC.
AMERICAN CHEMICAL SOCIETY
WASHINGTON, D. C. MEETING, AUGUST 28-SEPTEMBER 2, 1983

DEVELOPMENT OF AN ALTERNATIVE S.A.R.A. METHOD FOR THE
CHARACTERIZATION OF COAL-DERIVED LIQUIDS

By

F. M. Lancas, H. S. Karam and H. M. McNair
Department of Chemistry, Virginia Polytechnic Institute and State University
Blacksburg, Virginia 24061

INTRODUCTION

Coal-derived liquids have been studied extensively, because of their potential applications in many fields such as fuel and feedstocks generation (1). One of the most popular methods by which to characterize fossil fuels is by fractionation of the sample into saturates, aromatics, resins and asphaltenes (S.A.R.A.). Two different approaches are widely used for this purpose: solvent extraction and liquid chromatography. Although much work has been done using these two approaches, characterization of fossil fuels is still unsatisfactory and exhaustive research is still required. Solvent extraction methods currently used, though simple and inexpensive, present problems with reproducibility, time consumption, solvent evaporation, co-extraction and loss of volatiles (2, 3). In most of the liquid chromatographic methods used, the fossil fuel extract is first treated with a non-polar hydrocarbon (such as n-pentane) to precipitate the asphaltenes and the remaining solution is applied to an Attapulugus clay column to separate resins from oils. Finally, the oils are fractionated to saturates and aromatics on alumina and/or silica columns (4). All these steps, in addition to being unnecessary and inconvenient, do not provide the actual group-type distribution in the extract since part of the resins could be co-precipitated with asphaltenes (5). With these problems in mind, we have developed and applied an alternative S.A.R.A. method for the characterization of Brazilian coal-derived liquids.

RESULTS AND DISCUSSION

Fractionation by Solvent Extraction

Coal was finely ground, sieved through a 60 mesh (U. S. Standard) sieve, extracted with different solvents for 30 minutes using a magnetic stirrer (100 ml of solvent to 10 g of coal). Results showed that stirring time is not critical. After one hour of stirring with hexane, the unextracted coal was 96.6% of the original sample, while after 12 hours it was 95.6%. Following extraction, the solvent was evaporated and the extract redissolved in 2 ml of solvent. Asphaltenes were precipitated by adding 80 ml of n-pentane to the concentrated extract solution (volume ratio of 40 to 1). In all experiments solvents were evaporated by a combination of rotary evaporation for sample concentration and controlled heating under nitrogen flow until dryness of the extract. Figure 1 shows the results of a study comparing the relative amounts of asphaltenes and maltenes present in the "Mina do Leao" (high-ash Brazilian coal). The relative amounts extracted by the different solvents are displayed in Figure 2. Although pyridine is the best solvent examined, we decided to use tetrahydrofuran (THF) since it has a similar performance and it is less toxic and less polar.

In a different set of experiments, the fractionation of the THF coal extract into asphaltols, asphaltenes and oils was carried out utilizing the schematic shown in Figure 3. The results of this study appear in Table I.

Fractionation by Column Chromatography

A 50 cm (L) x 11 mm (I.D.) glass column fitted with a teflon stopcock was dry or slurry packed for comparison purposes. Dry packing was done by constantly tapping the column while adding 2 g of the packing material in small portions. A plug of glass wool and a layer of white sand (ca. 0.5 cm) on the top were used to support the solid adsorbent and to prevent it from washing through the stopcock. Slurry packing was performed by first adding the solid adsorbent a little at a time to hexane in a beaker, swirling the beaker and pouring the slurry into a draining column (previously filled about 1/3 full with the first eluent, hexane). The results of a comparative study using different packing techniques and materials are displayed in Table II. A set of five identical columns was employed, to determine the reproducibility of each system as applied to a hexane coal extract. For this study, the hexane soluble materials were filtered following extraction into a 100 ml

volumetric flask. 10 ml of this stock solution was loaded into the chromatographic column. The eluents used to generate the fractions were hexane (50 ml), toluene (75 ml) and methanol (50 ml) for saturates, aromatics and resins, respectively, following precipitation of asphaltenes, in accordance with the Phillips method (6). The results show that slurry packing with silica is the most reproducible system investigated. (It is well-established in the literature that asphaltols are highly adsorbed on alumina, while fewer substances are adsorbed on silica gel because of its mildly acidic properties (7, 8).)

TABLE I

SOLUBILITY CHARACTERISTICS OF HIGH-ASH BRAZILIAN COAL THF EXTRACT

Sample	Wt % Asphaltols	Wt % Asphaltenes	Wt % Oils	
1	38.5	35.2	26.3	
2	38.5	32.4	29.1	
3	37.8	36.9	25.4	
4	36.4	37.6	26.0	
5	42.1	34.8	23.1	
	\bar{x}	38.7	35.4	26.0
	σ	2.1	2.0	2.1
	R. S. D.	5.4	5.7	8.3

TABLE II

COMPARISON OF DIFFERENT PACKING SYSTEMS AS APPLIED TO HEXANE COAL EXTRACT

Group Type	Column Type ^a :	1	2	3
		Wt %	40.4	35.3
Saturates	σ	8.8	3.4	2.3
	R. S. D.	22	9.8	9.5
	Wt %	30.1	22.4	30.1
Aromatics	σ	5.9	3.1	2.2
	R. S. D.	20	14	7.1
	Wt %	29.4	42.3	45.6
Resins	σ	10	2.5	1.8
	R. S. D.	35	5.8	4.0

a. 1=dry-packed alumina; 2=slurry-packed alumina; 3=slurry-packed silica.

Since the best performance was shown with THF as extracting agent and silica gel as an adsorbent for slurry packing technique, we have applied the whole coal extract (a maximum of 200 mg) to the column to avoid problems associated with the asphaltenes precipitating in non-polar solvents. The characteristics of the chromatographic elution utilizing this new system as well as the relative group type distribution of the THF coal extract appear in Table III.

TABLE III

CHROMATOGRAPHIC ELUTION CHARACTERISTICS AND RELATIVE GROUP TYPE DISTRIBUTION OF THF COAL EXTRACT

Eluent	Volume of Eluent	Color of Eluent	Identity	Wt %
Hexane	50 ml	Colorless	Saturates	3.3
Toluene	75 ml	Orange	Aromatics	20.2
Methanol	50 ml	Red-Wine	Resins	51.8
THF	50 ml	Dark Brown	Asphaltenes	24.7

- : Hexane Extract
- ▨ : Asphaltene
- : Maltene
- (1): Hexane
- (2): Methyl-t-Butyl Ether
- (3): Toluene
- (4): Methanol
- (5): THF
- (6): Pyridine

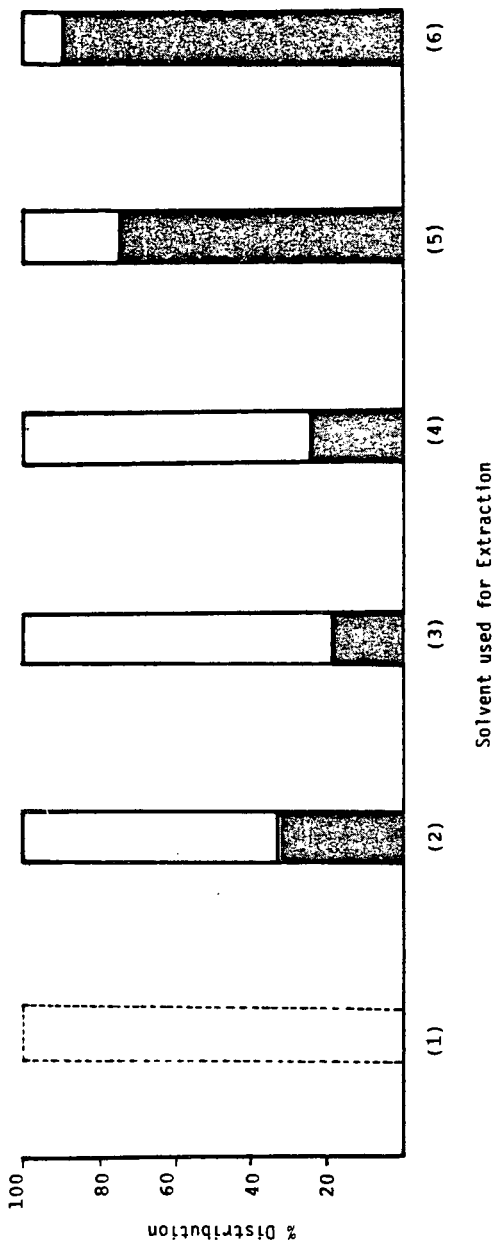


Figure 1. Relative amounts of asphaltene and maltene in the high-ash Brazilian coal.

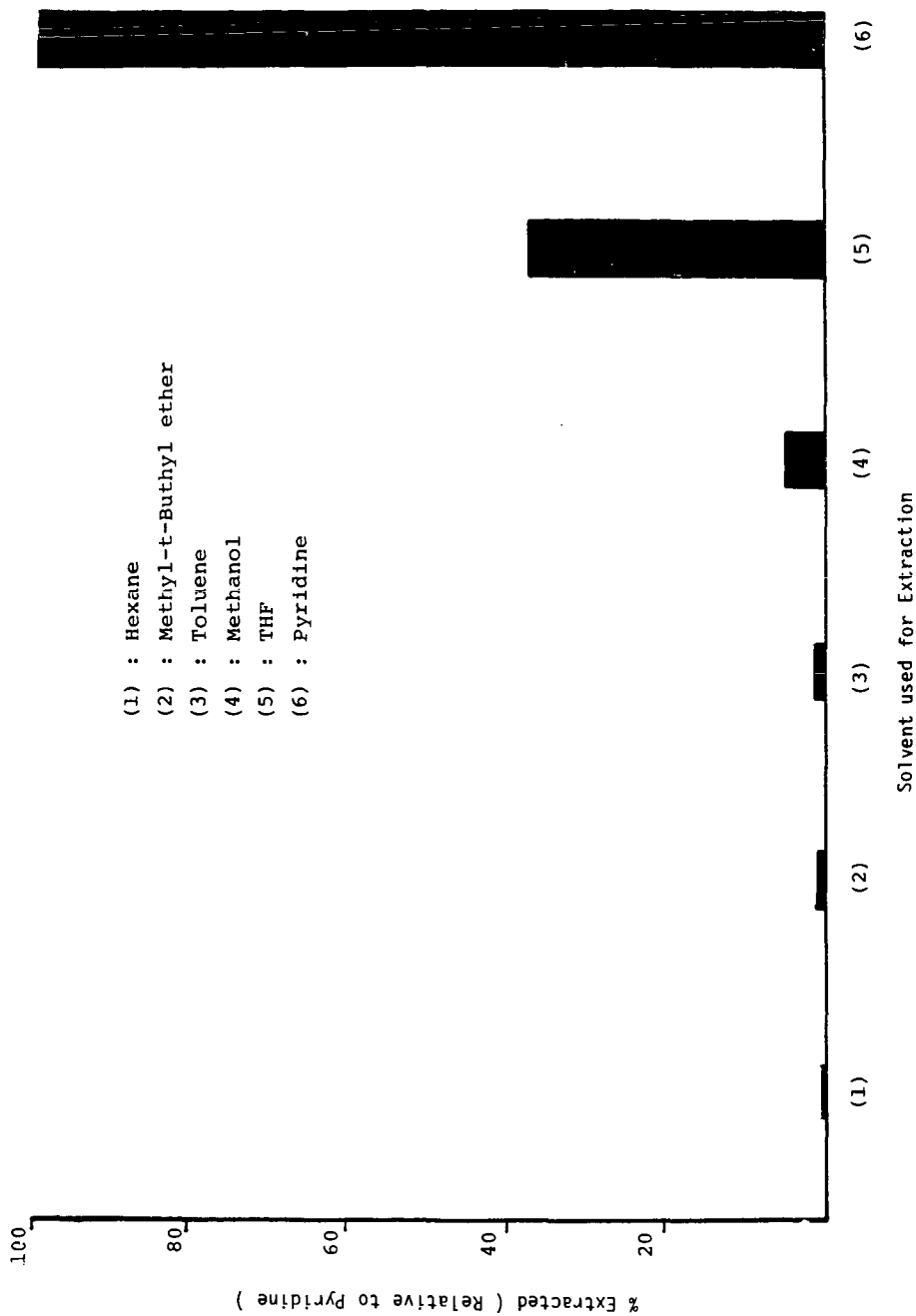
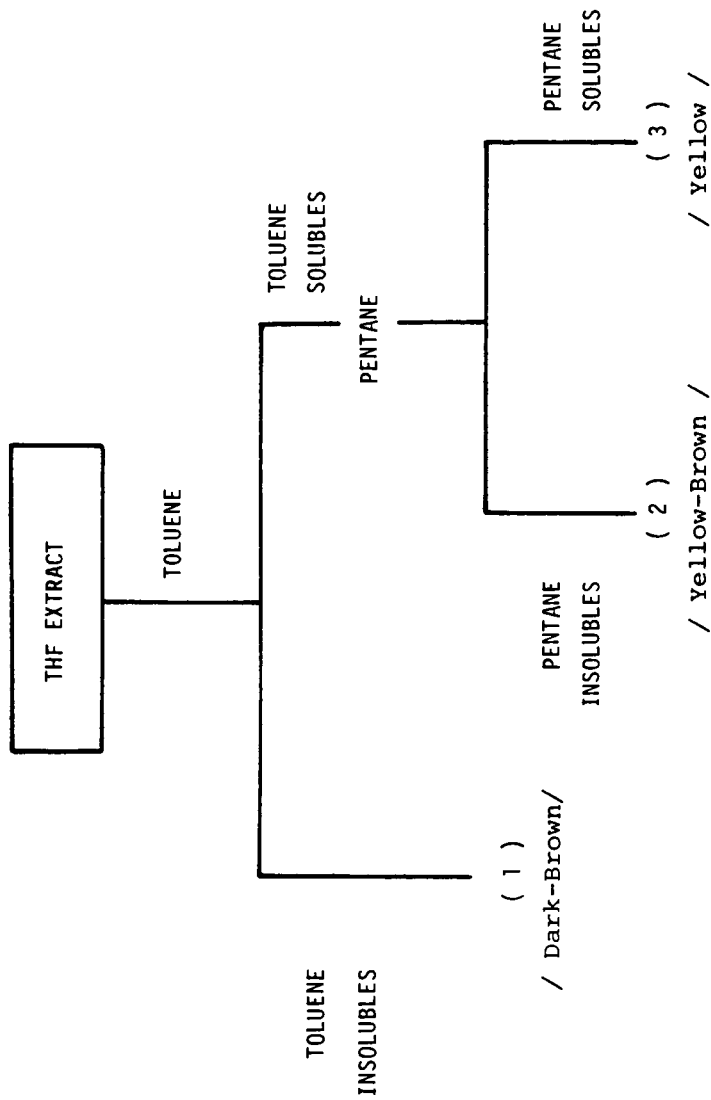


Figure 2. Percentage extracted (relative to Pyridine) using different solvents.



- (1): Asphaltols
- (2): Asphaltenes
- (3): Oils

Figure 3. Fractionation schematic of the THF extract

CONCLUSION

Compared with methods of characterization of coal extract described in the literature, the method we have developed has the following advantages:

1. Extraction Step: Using THF instead of hexane, pyridine, toluene, etc., gives more reproducible results and avoids extracting very polar compounds and loss of volatiles during the evaporation step. Magnetic stirring instead of manual stirring or Soxhlet extraction is an easier, faster and more reproducible extraction procedure.

2. Column Chromatography: Slurry packing with silica permits a better stationary bed and, at the same time, avoids irreversible adsorption. By fractionating the whole THF coal extract, one avoids the precipitation of asphaltenes prior to column chromatography. In addition, fractionating the whole extract permits collection of the four S.A.R.A. (saturates, aromatics, resins and asphaltenes) fractions for further characterization.

ACKNOWLEDGMENTS

F. M. Lancas would like to thank Fundacao de Amparo a Pesquisa do Estado de Sao Paulo (FAPESP) for the fellowship (Processo 16-Quimica 81/0557-2) and Universidade de Sao Paulo for the free absence.

LITERATURE CITED

- (1) Whitehurst, D. D., Mitchell, T. O. and Farcasiu, M., "Coal Liquefaction. The Chemistry and Technology of Thermal Processes", Academic Press, NY (1980).
- (2) Boduszynski, M. M., Hurtubise, R. J. and Silver, H., Anal. Chem., 54, 372 (1982).
- (3) Bockrath, B., Schroeder, K. T. and Steffgen, F. W., Anal. Chem., 51, 1168.
- (4) Galya, L. G. and Suatoni, J. C., J. of Liquid Chromatogr., 3, 229 (1980).
- (5) Bunger, J. W. and Li, N. C., eds., "Chemistry of Asphaltenes", Advances in Chem. Series, No. 195, AMS (1981).
- (6) Phillips Petroleum Company, Research and Development, Method 8045-AS (1980).
- (7) Whitehurst, D. D., Farcasiu, M. and Mitchell, O., "The Nature and Origin of Asphaltenes in Processed Coals", EPRI Annual Report (1976).
- (8) Given, P. H., Cronauer, D. C., Spakman, K., Lovell, H. L., Davis, A. and Biswas, B., Fuel, 54, 34 (1975); 54, 40 (1975).

A CORRELATIVE INVESTIGATION OF THE EFFECTS OF OXIDATION ON THE MINERALS,
MACERALS AND TECHNOLOGICAL PROPERTIES OF COAL

By

M. C. Lin, F. E. Huggins, G. P. Huffman and D. E. Lowenhaupt
U. S. Steel Corporation, Research Laboratory, 125 Jamison Lane
Monroeville, Pennsylvania 15146

INTRODUCTION

The oxidation of coal by natural weathering processes is well known to degrade those properties important for cokemaking (1, 2). Conversely, the loss of fluidity and enhancement of char reactivity resulting from low-temperature coal oxidation are desirable properties for coal gasification (3). Thus, better understanding of the oxidation mechanisms of coal components and of the effect of such oxidation on technological processes is highly desirable.

⁵⁷Fe Mossbauer spectroscopy and diffuse reflectance infrared Fourier transform (DRIFT) spectroscopy were used to investigate the oxidation of minerals and macerals, respectively, and measurements of the Gieseler plasticity were made as representative of an important technological property, coal fluidity, that is affected by oxidation. The relative sensitivity of these techniques to coal oxidation were compared by correlating measurements made on a variety of bituminous coals.

SAMPLES AND EXPERIMENTAL TECHNIQUES

The naturally oxidized coal discussed in this paper is a low-volatile bituminous coal obtained from a strip mine on the Pocahontas No. 4 seam in West Virginia. Samples were collected from an outcrop (most oxidized) and the mine highwall (least oxidized), and at an intermediate location to obtain an oxidation profile across the strip pit.

Two high-volatile bituminous coals (Pittsburgh and Harlan seams) were used in long-term, room-temperature oxidation treatments. The -60 mesh coals were put into several 100-ml beakers and stored separately in dry, ambient and humid air atmospheres at room temperature in the laboratory for 950 days. The dry environment was simulated by placing the coals in a desiccator containing Drierite, whereas the humid environment was simulated by placing the coal in a similar desiccator vessel, but with water present. The ambient samples were stored in beakers open to the laboratory atmosphere.

Channel samples of two additional bituminous coals, one collected from the Pittsburgh seam in Pennsylvania and the other from the Pocahontas No. 3 seam in West Virginia, were used in two simulated weathering treatments. In one treatment, -40 mesh coal was placed in a gas-tight oven at 50°C. The moisture level of the air in the oven was maintained at approximately 65% RH (6.9 ± 0.2% H₂O). In the other treatment, stockpiled samples of -1/8-inch coal were exposed to the atmosphere in 20-pound aliquots in plywood boxes.

The iron-bearing minerals in the various coals were investigated by ⁵⁷Fe Mossbauer spectroscopy. Details of sample preparation and data reduction procedures can be found in previous papers (4, 5, 6). The diffuse reflectance infrared Fourier transform (DRIFT) spectra were measured on a Nicolet 7000 series FTIR spectrometer with data reduction capability. Samples for FTIR were either -60 mesh or -200 mesh coals without KBr dilution. Typical measurement times were 285 seconds and the resolution of the spectra was typically 4 cm⁻¹.

Standard ASTM methods were used for Gieseler plastometer measurements. The extent of coal oxidation was also monitored by an alkali extraction test (7).

RESULTS AND DISCUSSION

Gieseler Plastometer Measurements

Results of Gieseler plastometer measurements on the strip-mined coal samples are summarized in Table I. The thermal plasticity of the coal samples decreases markedly as a result of oxidation. The softening temperature increases and solidification temperature decreases by approximately 30°C, narrowing the plastic range from 90°C to 30°C. The maximum rate of rotation,

which corresponds to the maximum fluidity of coal samples, decreased by several orders of magnitude to the level of essentially no fluidity at all for the outcrop coal.

TABLE I

RESULTS OF LIGHT TRANSMISSION VALUES AND GIESELER PLASTOMETER MEASUREMENTS FOR POCAHONTAS NO. 4 SEAM

Coal	Percent Transmission	Max. ddpm	°C			
			Soft Temp.	Max. Fluid Temp.	Solid. Temp.	Plastic Range
Highwall	97	3.5	401	461	491	90
Middle	58	2.3	412	457	481	71
Outcrop	28	0.2	413	448	463	30

The results of the alkali extraction test, also summarized in Table I, correlate fairly well with results of Gieseler plastometer measurements. This test is used in the metallurgical coal industry to detect coal oxidation prior to the coking operation. Usually, a coal with a light transmission value less than 80% is regarded as too oxidized for metallurgical usage (7). It is noted that the badly oxidized coal taken from the outcrop of the pit has a transmission value of only 30%, while the least oxidized highwall coal has a value of 97%.

Similar plasticity behavior as a result of oxidation was also found for the Pittsburgh and Harlan seam coals stored in dry, ambient and wet atmospheres for over 950 days at room temperature, as summarized in Table II. These results indicate that the extent of oxidation depends greatly on the humidity of the coal environment, with high humidity accelerating coal oxidation.

TABLE II

GIESELER PLASTOMETER RESULTS OF COALS "WEATHERED" FOR 950 DAYS AT ROOM TEMPERATURE

Sample	Max. ddpm	Soft Temp.	Max. Fluid Temp.	Solid. Temp.	Plastic Range
Pittsburgh (dry)	22400.0	347	410	464	117
Pittsburgh (ambient)	1600.0	365	422	467	102
Pittsburgh (wet)	580.0	366	420	459	93
Harlan (dry)	18.0	365	410	440	75
Harlan (ambient)	9.0	387	432	459	72
Harlan (wet)	5.0	391	427	454	63

An extremely rapid decrease of Gieseler plasticity due to oxidation is shown in Figure 1, where the maximum fluidity is plotted versus time of oxidation treatment for coals treated at 65% RH and 50°C. Accompanying this rapid reduction of fluidity, there is also a significant decrease of the plastic range. The -1/8-inch stockpiled samples of the same coals show similar but less rapid changes.

57

Fe Mossbauer Spectroscopy

The distribution of iron among minerals obtained by low-temperature Mossbauer spectroscopy is summarized in Table III for the strip-mined Pocahontas No. 4 samples. The data indicate that the pyrite has been completely converted to iron oxyhydroxide in both the middle and outcrop coals. Additionally, with increasing oxidation, a decrease in the percentage of iron contained in clay minerals and an increase in the percentage of iron present as an unidentified ferric phase (Fe^{3+}) are observed. This Fe^{3+} phase is most probably either a ferric sulfate or Fe^{3+} in clays.

TABLE III

MOSSBAUER DATA ON DISTRIBUTION OF IRON AMONG MINERALS FOR
POCAHONTAS NO. 4 COAL SAMPLES

Sample	Percentage of the Total Sample Iron Contained in:					
	Clay	Siderite	Pyrite	Jarosite	Iron Oxyhydroxide	Fe ⁺³
Highwall	76	13	6	1	-	4
Middle	64	14	-	1	10	12
Outcrop	51	11	-	-	21	17

Results of Mossbauer spectroscopy investigations on the room-temperature oxidation of Pittsburgh and Harlan coals are summarized in Tables IV and V. The data indicate that in Harlan coal, the clay and siderite are apparently little affected by oxidation, whereas the pyrite is extensively oxidized and transformed to jarosite, iron oxyhydroxide and a ferric iron phase. For the Pittsburgh coal, the pyrite was transformed to ferrous sulfate initially and then to ferric sulfates and iron oxyhydroxide. As discussed elsewhere (8), this and other differences in mineral oxidation reflect the significantly different sulfur content and mineralogies of the two coals.

TABLE IV

MOSSBAUER DATA ON THE DISTRIBUTION OF IRON AMONG MINERALS FOR
PITTSBURGH COAL SAMPLES

Sample	Phases	% Fe ^a
Fresh	Pyrite	100
Dry	Pyrite	96
	Szomolnokite	4
Ambient	Pyrite	76
	Szomolnokite	20
	Rozenite	4
Wet	Pyrite	26
	α -FeOOH	23
	Jarosite	4
	Fe ³⁺	25
	Unidentified Fe ⁺²	22

a. Percentage of the total iron in the sample contained in the indicated phase.

The low-temperature Mossbauer spectra of Pittsburgh coal, treated in the experimental oven (50°C, 65% RH) and coal stockpiled out of doors, are shown in Figure 2. For both Pittsburgh and Pocahontas No. 3 coals treated in the oven, the iron sulfate, szomolnokite, was detected after 40 and 124 days of treatment, respectively. As the oxidation proceeds, the iron sulfate content continues to increase at the expense of pyrite. However, for the coals stockpiled out of doors, iron oxyhydroxide is the oxidation product of pyrite and no iron sulfate has yet been detected. This indicates that different oxidation processes or different rate-determining steps are involved in the oxidation of pyrite in the two environments.

Diffuse Reflectance Infrared Fourier Transform (DRIFT) Spectroscopy

The infrared spectra of the strip-mined coal samples are shown in Figure 3. The most obvious trend with increasing oxidation is increases in intensity of various carbonyl bands between 1600 cm⁻¹ and 1800 cm⁻¹. These increases in intensity were also accompanied by an increase in intensity of the region between 1100 cm⁻¹ and 1300 cm⁻¹, which is associated with the C-O stretching vibration and O-H bending modes of phenols, ethers and esters (9, 10). Similar increases in intensity can also be found in the absorption bands of hydroxyl groups ranging from 3200 cm⁻¹ to

3600 cm^{-1} . However, the intensity of absorption bands at 2860, 2920 and 2950 cm^{-1} , which correspond to the aliphatic C-H stretching modes, show systematic decreases from the least oxidized to the most oxidized coal samples. Similar decreases in intensity also occur for the aromatic C-H stretching mode at 3040 cm^{-1} , and the absorption bands between 700 and 900 cm^{-1} , which correspond to the aromatic C-H out-of-plane bending modes.

TABLE V

MOSSBAUER DATA ON THE DISTRIBUTION OF IRON AMONG MINERALS FOR HARLAN COAL SAMPLES

Sample	Phases	% Fe ^a
Fresh	Pyrite	53
	Clays	43
	Siderite	4
Dry	Pyrite	46
	Clays	43
	Siderite	5
	Jarosite	6
Ambient	Pyrite	42
	Clays	43
	Siderite	6
	Jarosite	9
Wet	Pyrite	12
	Clays	42
	Siderite	6
	Jarosite	20
	Iron Oxyhydroxide	7
	Fe ⁺³	13

a. Percentage of the total iron in the sample contained in the indicated phase.

For the laboratory-oxidized Pittsburgh and Harlan coal samples, the carbonyl and carboxylic-acid absorption bands between 1600 cm^{-1} and 1800 cm^{-1} , which are found in naturally oxidized coals from strip-mines and are closely associated with effects of coal oxidation, were not detected. This suggests that the oxidation of these coal samples is still at a relatively early stage, although both Mossbauer spectroscopy and Gieseler plastometer measurements clearly show changes due to oxidation. This observation is further supported by the DRIFT results obtained after severely oxidizing the dry and wet Pittsburgh coal samples in air at 110°C for seven days. Figure 4 shows that, in addition to the 1650 cm^{-1} and 1735 cm^{-1} bands observed before, carbonyl and carboxyl bands near 1585, 1680, 1690, 1710 and 1765 cm^{-1} also appear after this rather severe oxidation treatment.

DRIFT spectra were also obtained from all oven-oxidized and stockpiled coal samples. No significant difference between the treated and fresh coals was found. This indicates that DRIFT spectroscopy is not sufficiently sensitive to detect the early stages of oxidation that cause the large decreases observed in plasticity.

CONCLUSIONS

Mossbauer spectroscopy shows that pyrite in coal is readily altered by low-temperature coal oxidation. The oxidation of pyrite in coals subjected to simulated weathering treatments at constant temperature and humidity in the laboratory gives rise to a variety of iron sulfates. This is in contrast to coal samples stockpiled out-of-doors and strip-mined coals, in which the principal pyrite oxidation product is iron oxyhydroxide.

A reduction in intensity of aliphatic and aromatic bands with increasing oxidation of a strip-mined coal is detected in DRIFT spectra. These changes accompany the enhancement in intensity of certain carbonyl and carboxyl bands. However, these carbonyl bands are not detected in spectra of laboratory oxidized coals until oxidation is quite extensive.

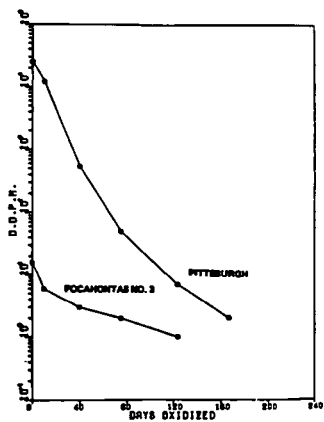


Fig. 1 Variations of maximum fluidity as measured by Gieseler plastometer with days of oxidation at 50°C, 65% RH.

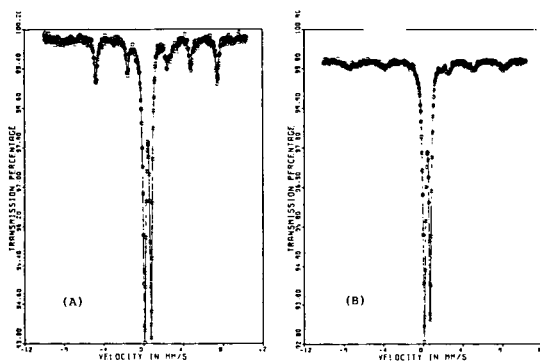


Fig. 2 Low-temperature Mossbauer spectra of Pittsburgh coals: (A) treated in 50°C, 65% RH for 167 days; (C) stockpiled out of doors for 139 days.

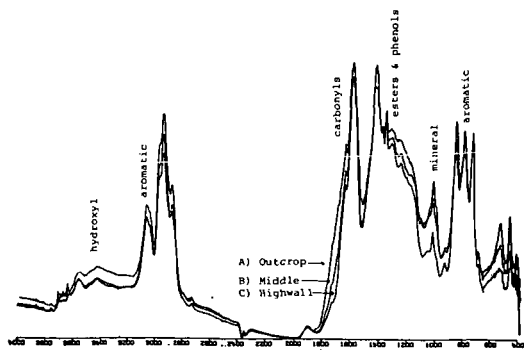


Fig. 3 FTIR spectra of Pocahontas No. 4 seam coals: (A) outcrop, (B) middle, (C) highwall.

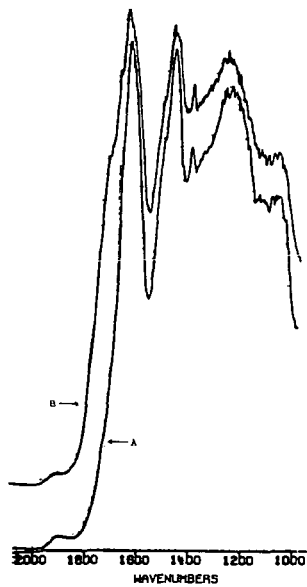


Fig. 4 FTIR spectra of (A) Pittsburgh coals oxidized for over 30 months in wet air atmosphere at room temperature; (B) wet Pittsburgh coal oxidized in air at 110°C for seven days.

The plastic properties of coal, as determined by Gieseler plastometer measurements, are extremely sensitive to oxidation. The maximum fluidity shows a very rapid reduction with oxidation. There is also a significant narrowing of the plastic range. Of the three techniques, the Gieseler plasticity measurement is the most sensitive and DRIFT spectroscopy the least sensitive to the initial stages of coal oxidation. This order of sensitivity is inverse to their applicability to coals as the Gieseler measurements are restricted to coking bituminous coals and Mossbauer techniques are best applied to high pyrite coals, whereas DRIFT spectroscopy can be applied to all coals with little or no modification.

The extreme sensitivity of the thermoplastic behavior of coal to initial oxidation as determined by the Gieseler measurements is in contrast to the insensitivity of DRIFT spectroscopy and the relative minor oxidation of pyrite detected by Mossbauer spectroscopy, both of which are bulk-oriented techniques. The explanation must be attributed to the fact that the first stages of coal oxidation are surface controlled, as are most oxidation processes. Even though plasticity is determined by a macroscopic measurement, it is dependent upon the fusing together of separate coal particles. Consequently, it is likely to be highly sensitive to very thin surface layers on the coal particles. Further investigations involving the characterization of oxidized coal surfaces are currently underway.

LITERATURE CITED

- (1) Gray, R. J., Rhoades, A. H. and King, D. L., *Trans. AIME, Soc. Min. Engineers*, 260, 334 (1976).
- (2) Crelling, J. C., Schrader, R. H. and Benedict, L. G., *Fuel*, 58, 542 (1979).
- (3) Mahajan, O. P., Komatsu, M. and Walker, P. L., Jr., *Fuel*, 59, 3 (1980).
- (4) Huffman, G. P. and Huggins, F. E., *Fuel*, 57, 592 (1978).
- (5) Huggins, F. E. and Huffman, G. P., *Analytical Methods for Coal and Coal Products*, Clarence Karr, Jr., ed., Academic, New York, Vol. 3, Chapter 50 (1979).
- (6) Huggins, F. E., Huffman, G. P. and Lee, R. J., *Coal and Coal Products: Analytical Characterization Techniques*, E. L. Fuller, Jr., ed., ACS Symp. Series No. 205, p. 239 (1982).
- (7) Lowenhaupt, D. E. and Gray, F. J., *Internatl. Journal of Coal Geology*, 1, 63 (1980).
- (8) Huggins, F. E., Huffman, G. P. and Lin, M. C., to be published in *Internatl. Journal of Coal Geology* (1983).
- (9) Painter, P. C., Snyder, R. W., Starsinic, M., Coleman, M. M., Keuhn, D. W. and Davis, A. H., *Applied Spectroscopy*, 35, 475 (1981).
- (10) Painter, P. C., Snyder, R. W., Pearson, D. E. and Kwong, J., *Fuel*, 59, 282 (1980).

GENERAL PAPERS - POSTER SESSION
PRESENTED BEFORE THE DIVISION OF PETROLEUM CHEMISTRY, INC.
AMERICAN CHEMICAL SOCIETY
WASHINGTON, D. C. MEETING, AUGUST 28-SEPTEMBER 2, 1983

EFFECT OF FRACTURE MODES ON SHAPE AND SIZE OF COAL PARTICLES
AND SEPARATION OF PHASES*

By

J. M. Lytle and L. R. Bunnell
Battelle, Pacific Northwest Laboratory, Richland, Washington 99352
and
K. A. Prisbrey
University of Idaho, Moscow, Idaho 83843

INTRODUCTION

Studies of coal grinding are becoming one of the most important and interesting areas of coal research. Consequently, the Department of Energy sponsored "Study Group on Research Planning for Coal Utilization and Synthetic Fuel Production" emphasized size-dependent phenomena during coal grinding as one of the seven most important areas of research needed for development of an advanced coal and synfuels industry (1, 2). Nearly every use of coal involves grinding to some extent and modern processes are requiring finer and finer coal powders. Knowledge of the properties of these coal powders is essential in developing these processes. For example, knowledge of shapes and sizes of particles is important in defining the viscosity and transport behavior of coal-liquid slurries for combustion or pipeline transport. Knowledge of separation of phases is important in developing beneficiation processes to remove impurities.

The study reported in this paper used microscopy, shape, size and sulfur analyses to show the influence of fracture modes and mechanisms on shape and size of coal particles and separation of phases. The preferential lines of fracture during coal grinding were identified microstructurally and related to the size and shape of particles produced and the separation of mineral and organic phases. For example, weaker phases that were lean in organic sulfur were observed to concentrate into finer particle size ranges and stronger phases that were rich in organic sulfur concentrated into coarser particle size ranges.

EXPERIMENTAL

Two coals of widely differing rank were selected for this study: a lignite from the Fort Union Bed near Savage, Montana and a medium volatile bituminous (MVB) from the Beckley seam near Duo, West Virginia. These two coals (PSOC-837 and PSOC-985) were obtained from the Pennsylvania State University's coal sample bank.

Prior to ball milling, the coals were preground in nitrogen to minus 20 mesh (U. S. standard screen, 840 μm opening size) in a wheel-type pulverizer. The coal (350 g) was transferred in the N_2 atmosphere to a 1.8 L steel ball mill, which was then evacuated and backfilled with helium. During rotation of the mill, coal powders were withdrawn in a long, cylindrical scoop inserted along the axis of rotation through a hole plumbed with a rotary union and ball valves to maintain the atmosphere.

RESULTS AND DISCUSSION

During coal grinding, particle microstructure affected the fracture modes which in turn affected shape and size of particles and separation of phases. Optical micrographs of polished particle cross-sections (Figure 1) illustrate the tendency for separation of organic phases in the early stages of grinding. With both lignite and MVB, fracture tended to proceed preferentially along organic-to-organic interfaces, as shown by the separate and microstructurally more uniform particles already present after the pregrind step and the incomplete but progressing fractures along interfaces in the particles, indicated by arrows.

Fracture also tended to preferentially proceed along mineral-to-organic interfaces and

* The Pacific Northwest Laboratory is operated by Battelle Memorial Institute for the Department of Energy. The research was sponsored by the Basic Energy Science, Division of Material Science, under Contract DE-AC06-76RLO 1830.

cracks and pores. This tendency is illustrated by the scanning electron micrographs of particle cross sections shown in Figure 2. In the lignite particles, cracks and pores--highlighted in the photographs by electron microscope edge effects-- were apparent in the pregrind particles but were depleted after 7 h of grinding. In the MVB particles, mineral inclusions were separated from the organic phases during grinding as shown by the presence of separate mineral particles after 7 h.

Distinct organic phases that were separated during the pregrind step tended to grind at their own individual rates during subsequent grinding (3). The particles that were microstructurally more heterogeneous and contained more cracks and pores were rapidly ground according to the larger set of particle size-dependent rate constants shown in Table I. The stronger particles were ground more slowly according to the set of smaller rate constants.

TABLE I

Breakage rate constants, S_i^a , (10^{-3} min^{-1}) for lignite grinding where the weaker particles were rate controlling for the first 30 min of grinding. After weaker particles were reduced to fines, the stronger particles controlled the grinding rate.

Particles	Particle size, μm								
	210	149	105	74	53	83	30	20	15
Weaker	10.1	8.2	5.6	4.0	2.8	2.0	1.6	1.0	0.77
Stronger	4.2	2.5	1.4	0.79	0.46	0.26	0.18	0.090	0.046

$$a. \text{ rate} = \frac{dm_i}{dt} = -S_i m_i + \sum_{j=1}^{i-1} S_j b_{ij} m_j$$

m_i = mass fraction of size i

S_i = breakage rate constant for size i

b_{ij} = primary breakage fragment distribution

During lignite grinding, the stronger particles contained more organic sulfur than the weaker particles, as can be seen from the particle-by-particle compositional analysis done previously (4). The weaker, more porous, particles averaged 0.26% organic sulfur whereas the stronger, less porous, particles averaged 0.46% (4). During grinding, the sulfur content of a given particle size range steadily increased as the weaker particles passed through that size range and the stronger particles lingered (see Table II). Thus, during grinding, sulfur-rich and sulfur-lean particle size ranges developed, depending on the grinding time.

TABLE II

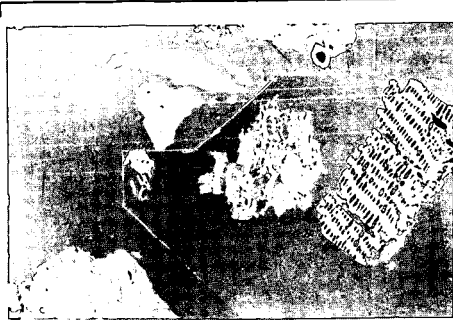
Average organic sulfur content (percent) of lignite particles as determined by particle-by-particle analysis of particle cross sections using X-ray fluorescence in a scanning electron microscope.

Particle Size, μm	Grinding Time, Minutes		
	15	60	420
20 - 30	0.37	0.38	0.45
5 - 10	0.11	0.19	0.23

The microstructure of coal is a major factor in the sizes and shapes of particles produced during grinding. One of the best examples of the effect of microstructure on shape is the needle-like and plate-shaped particles produced from the fracture of the weaker particles during the initial stages of grinding (Figure 3). As seen in Figure 3, in the 10 to 15 μm particle size range, many needle-like or plate-shaped particles were present after 15 min of grinding, but these particles were no longer present in this size range after 60 and 420 min. The microstructure of the stronger particles did not lead to needle-like or plate-shaped particles but instead blocky and rounded particles were produced throughout grinding. The stronger particles of the 20 to 30 μm size range did, however, become increasingly spherical during grinding, as shown by an increasing shape factor (4 x cross sectional area/perimeter squared) which would be one if the projected shape was a circle.

LIGNITE

MEDIUM VOLATILE BITUMINOUS



100 μm

FIGURE 1. OPTICAL MICROGRAPHS OF POLISHED, PREGRIND PARTICLE CROSS SECTIONS SHOWING SEPARATION OF ORGANIC PHASES DURING THE EARLY STAGES OF GRINDING. ARROWS INDICATE FRACTURE PROGRESSING ALONG INTERFACES.

LIGNITE

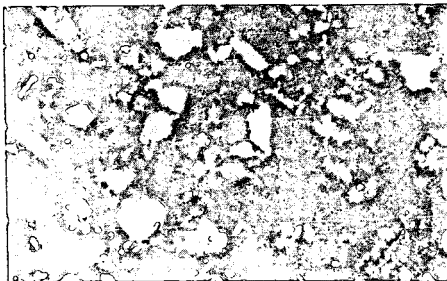
MEDIUM VOLATILE BITUMINOUS



PREGRIND

100 μm

100 μm



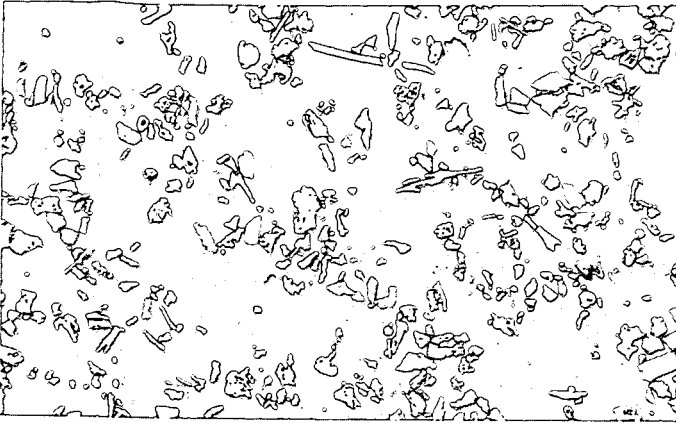
AFTER 7 hrs
GRINDING

100 μm

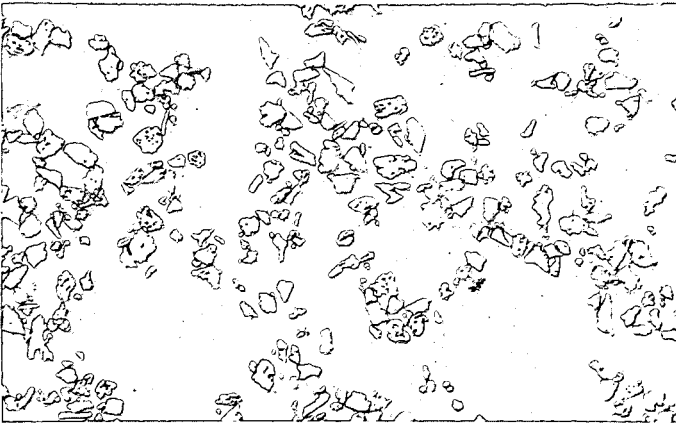
100 μm

FIGURE 2. SCANNING ELECTRON MICROGRAPHS OF PARTICLE CROSS SECTIONS SHOWING THE DEPLETION OF PORES AND CRACKS AND THE SEPARATION OF MINERAL INCLUSIONS.

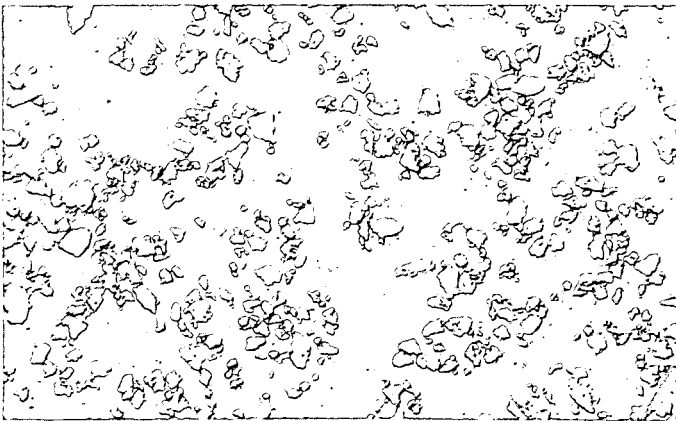
GRINDING TIME



15 min



60 min



420 min

FIGURE 3. OPTICAL MICROGRAPHS OF 10 TO 15 μm LIGNITE PARTICLES AFTER VARIOUS GRINDING TIMES.

The shape factor was 0.47, 0.47 and 0.62 after 15, 60 and 420 min of grinding, respectively.

CONCLUSIONS

During coal grinding, the modes and mechanisms of fracture change with time and particle size. Fracture tends to proceed preferentially first along organic-to-organic interfaces, then along mineral-to-organic interfaces and cracks and pores: first, through the largest cracks and pores, then through gradually smaller cracks and pores as encountered by the stress field. Thus, particles with limited porosity and mineral inclusions are the stronger particles that tend to grind at lower rates.

Modeling studies indicate that two sets of comminution rate constants are required to model the grinding of lignite because weaker components control the rates initially and stronger components control the rates later in grinding.

These modes and mechanisms of fracture cause changes in the shape and size of particles and the separation of phases. The shapes and sizes of particles are first changed by fracture through organic-to-organic interfaces, then by the microstructure of the weaker phases and finally by the microstructure of the stronger phases. During lignite grinding, the weaker phases produce needle-like or plate-shaped particles that are changed to more blocky and rounded shaped particles as particle size is decreased. The stronger phases produce blocky and rounded shaped particles that become more rounded with longer grinding times.

In both coals the organic phases are separated initially by the tendency for fracturing preferentially through organic-to-organic interfaces. Then the stronger phases are ground more slowly than the weaker phases. The stronger phases of lignite have greater organic sulfur content than the weaker phases. Thus, there is a stage in grinding where low-sulfur particles are concentrated in the fines and high-sulfur particles are concentrated in the larger size ranges.

Mineral phases are separated from the organic phases during grinding. The extent of separation depends on the size distribution of the mineral phases and the extent of grinding.

The size and shape of particles and the separation of phases are important factors in modern coal processes. For example, in producing and using coal-liquid slurries important factors include coal-to-liquid ratio, rheological properties of slurry, particle size distribution and mineral content. The results of this study impact all of those factors. The shapes of particles can have a marked effect on slurry viscosity as well as the packing density of slurries, thus, it may be advantageous to grind a coal more extensively in some cases to produce more rounded particles. The potential for removal of mineral impurities increases with grinding time. However, the potential for removal of organic sulfur may be greater at an intermediate stage of grinding. Thus, detailed knowledge of the coal grinding process can greatly increase the potential for more efficient and environmentally safe ways of using coal.

LITERATURE CITED

- (1) Robinson, A. L., "Can Physicists Clean Up Coal's Act?", *Science*, 213, 1484 (1981).
- (2) Study Group on Research Planning for Coal Utilization and Synthetic Fuel Production, B. R. Cooper, Chairman, *Rev. Mod. Phys.* 53 (4, Part 2) (1981).
- (3) Lytle, J. M., Daniel, J. L. and Prisbrey, K. A., "The Effect of Microstructure on the Size and Shape of Coal Particles During Comminution", submitted to *Fuel* (1983).
- (4) Lytle, J. M., Daniel, J. L. and Tingey, G. L., "Concentration of Sulfur and Mineral-Rich Components in Particle Classes During Coal Comminution", submitted to *Fuel* (1982).

GENERAL PAPERS - POSTER SESSION
PRESENTED BEFORE THE DIVISION OF PETROLEUM CHEMISTRY, INC.
AMERICAN CHEMICAL SOCIETY
WASHINGTON, D. C. MEETING, AUGUST 28 - SEPTEMBER 2, 1983

RAPID DISSOLUTION OF COAL FOR ANALYSIS FOR
SULFUR, IRON, AND OTHER ELEMENTS

By

R. Markuszewski, B. C. Wheeler, and R. S. Johnson
Iowa State Mining and Mineral Resources Research Institute
Iowa State University, Ames, Iowa 50011

and

C. C. Hach
Hach Chemical Company, P.O. Box 389, Loveland, Colorado 80537

ABSTRACT

Most dissolution methods necessary for the determination of major, minor, and trace constituents in coal are tedious and require unusual procedures. A rapid dissolution method is based on heating 250 mg coal with 10 ml of a 4:3:3 mixture of HNO_3 , HClO_4 (72%), and H_3PO_4 (85%). In numerous analyses of 8 subbituminous and bituminous coals using a simple digestion apparatus, the entire sample was dissolved in 20-45 min., leaving silica in a pure form suitable for determination by filtration, ignition, and weighing as SiO_2 . In the clear filtrate, total sulfur was determined by a turbidimetric measurement of BaSO_4 . For the 8 coals, containing 0.41-4.20% S, the results agreed well with those obtained by using a combustion method followed by automatic iodometric titration of the SO_2 . In other aliquots of the same filtrate, total iron was determined spectrophotometrically using FerroZine. For an iron range of 0.113-1.762%, the standard deviations were 0.001-0.050. The clear digest can be also used to determine other elements by spectrophotometric, atomic absorption, or other procedures.

GENERAL PAPERS - POSTER SESSION
PRESENTED BEFORE THE DIVISION OF PETROLEUM CHEMISTRY, INC.
AMERICAN CHEMICAL SOCIETY
WASHINGTON, D. C. MEETING, AUGUST 28-SEPTEMBER 2, 1983

GUM AND DEPOSIT FORMATION FROM JET TURBINE AND DIESEL FUELS

By

F. R. Mayo and B. Y. Lan
SRI International, Menlo Park, California 94025

INTRODUCTION

The objective of this work is to determine the chemistry of deposit formation in hot parts of jet turbine and diesel engines and, thus, to predict and prevent deposit formation.

Previous work in the field has been extensive (1, 2), but a real understanding of deposit formation has been elusive. Work at SRI started on the basis that deposit formation from fuels must take place stepwise and is associated with autoxidation and the hydroperoxide produced (3). More recent work (4) showed that in the absence of dissolved oxygen, higher temperatures are required for deposit formation. Our recent report (5) indicated that gum and deposit formation proceed mainly through oxidation products of the parent hydrocarbon, coupling of these products to dimeric, trimeric and higher condensation products (partly or wholly by radicals from hydroperoxides) and precipitation of insoluble products. We know of no information on how these first precipitates are converted to the ultimate, very insoluble, carbonaceous materials that cause engine problems.

The present paper describes measurements of rates of oxidation and soluble gum formation in both pure hydrocarbons and mixed hydrocarbon fuels. Some patterns appear that can be largely explained on the basis of what is known about co-oxidations of hydrocarbon mixtures.

EXPERIMENTAL PROCEDURES

All of our hydrocarbons and fuels were distilled at about 10 torr before use. This step eliminated the highest boiling 2-5% of the fuels, but was essential to eliminate whatever gum had accumulated before the fuel was distilled. The fuels were then stored under nitrogen at -8°C until used. Some of the purchased "pure" hydrocarbons exhibited marked induction periods on oxidation, but in all such cases, chromatography through acidic alumina resulted in faster oxidations at fairly steady rates.

All of our oxidations were carried out in an oil bath at 130°C , with shaking under air. At intervals, 70- μL samples of gas were withdrawn and analyzed for oxygen/nitrogen ratio by gas chromatography on a 6' x 1/8" O. D. stainless steel column packed with 13X molecular sieve and attached to a thermal conductivity detector. Soluble gum was determined by evaporating a weighed 5-mL sample of fuel in a gentle stream of nitrogen at 160°C (without spattering). The residue (~0.1 mL) was then transferred with 1-2 mL of acetone to a tared aluminum dish weighing about 50 mg. This sample was then brought to constant weight (3-10 h) in a gentle stream of nitrogen in a furnace at 200°C . Weighings were made on a Perkin Elmer AD-22 electromicrobalance. This method gave results reproducible within 20% at low levels of gum, usually within 5% at higher levels.

Fuels A and C are very stable and very unstable jet turbine fuels supplied by NASA-Lewis Research Center. Fuels 1, 10, 13, 14 and 15 are diesel fuels supplied by the U. S. Army Fuels and Lubricants Research Laboratory.

RESULTS

Table I summarizes our work on pure hydrocarbons and several fuels; it shows that gum formation is closely associated with oxidation. Indene and N-methylpyrrole (NMP) are listed separately at the bottom of the table because they are special cases. The other materials are listed in the first column of figures according to decreasing rates of oxygen absorption under air at 130°C . There is a clear distinction between the pure compounds, which oxidize faster and the fuels, which oxidize slower. The second column of figures lists the same materials in order of decreasing rate of gum formation, which is nearly the same as the order for oxidation. The figures in the last column are the quotients of the rates for the indicated fuels in the previous columns. This column shows that the pure, fastest oxidizing compounds usually require the most oxygen to produce a milligram of gum, or that the fuels at the bottom of this column produce the most gum for the oxygen absorbed. The quotient is constant with time for Fuel A; similar information is lacking for other fuels.

TABLE I
RATES OF OXIDATION, GUM FORMATION AND RATIOS OF
OXYGEN ABSORBED TO GUM FORMED

	umole O ₂	Mg gum		100 umole O ₂	
	g fuel/hr	100 g fuel/hr		mg gum	
1-Phenylhexane	27.5	EtN	6.4	1-PH	40
Phenylcyclohexane	27.2	PCH	5.7	DOD	15
n-Dodecane	24.0	C	5.1	BCH	4.8
Bicyclohexyl	18.5	BCH	3.9	PCH	4.7
2-Ethyl-naphthalene	4.7	DOD	1.6		
		1-PH	.71	14	1.3
Fuel C	3.8			A	.80
Fuel 14	.78	14	.58	C	.75
Fuel 13	.20	13	.48	EtN	.73
Fuel 15	.17	15	.28	10	.65
Fuel 10	.09	1	.19	15	.59
Fuel 1	.06	10	.14	13	.42
Fuel A	.05	A	.05	1	.34
N-Methylpyrrole	97	IND	1282	NMP	.14
Indene	91	NMP	684	IND	.07

Table I shows that the rate of gum formation increases with the rate of oxygen absorption. Although the unstable Fuel C oxidizes and produces gum 80-100 times as fast as stable Fuel A, the oxygen required to make a milligram of gum is the same for the two fuels.

The special cases of indene and NMP are now considered. The other compounds and fuels in Table I apparently give mostly hydroperoxides as primary oxidation products. Other products are peroxide decomposition products and small yields of condensation products (gum). However, indene (6) and probably NMP copolymerize with oxygen to give alternating polyperoxides that are nonvolatile until they decompose thermally. The rates of oxygen absorption and gum formation are very high and more gum is left after decomposition of the polyperoxide and, therefore, less oxygen is required to produce this gum than for any other pure compound or fuel in Table I.

Study of the data in Table I gives rise to the question: Why do all the fuels oxidize slower than all the pure compounds, even though the fuels contain mostly compounds like the models? How does Fuel A differ from Fuel C? What are the important minor components in the fuels?

The classic work of Russell (7) on the co-oxidation of cumene and tetralin and the expansions by Mayo and coworkers (8) and Sajus (9) provide examples of rates of oxidation of hydrocarbon mixtures. Figure 1 is a plot of Russell's data on the rate of oxidation of cumene-tetralin mixtures at 90°C at a constant rate of chain initiation. Although tetralin alone oxidizes faster than cumene alone under these conditions, 4% of tetralin significantly retards the rate of oxidation of cumene. The high reactivity of pure tetralin with tetralylperoxy radicals can offset the high reactivity of tetralylperoxy radicals with each other (chain termination), but in dilute tetralin, which reacts with peroxy radicals much faster than cumene, the effect of fast chain termination predominates. Figure 1 shows that increasing proportions of tetralin may either decrease (at <4% tetralin) or increase (at >4% tetralin) the rate of oxidation of a mixture that is mostly cumene.

Figure 2 shows how these principles apply in mixtures of indene (which oxidizes much faster) and dodecane. At the lowest concentrations of indene, rates of oxidation are lower than for either pure hydrocarbon, at least until the indene is depleted, but with 1 M indene in dodecane, the rate of oxidation is faster than for dodecane alone and approaches the rate for indene in an inert solvent. NMP has a similar effect. The curves in Figure 3 show that the oxidation of Fuel A is so slow that it is not clear whether the initial oxidation is retarded by a little NMP. But the rate of oxidation increases as more NMP is added. These results are qualitatively satisfying, but they cannot be treated quantitatively. The Russell treatment (6) requires a constant rate of chain initiation, which is uncontrolled in our experiments. Our results do not suggest any catalytic effects of impurities or additives; as far as we can tell, these accelerators and retarders are consumed when they produce effects.

Several of our distilled fuels have been passed through acidic alumina to remove minor polar components, which have sometimes been returned to chromatographed fuel to reconstitute the original fuel. Figure 4 shows triplicate experiments with Fuel 10. The chromatographed fuel oxidizes faster initially than the distilled fuel (the usual situation) and the reconstituted fuel behaves

like the distilled fuel. Figure 4 shows the reproducibility of both the oxygen absorption and gum measurements (numbers at final points on curves). There is a close parallel in Figure 4 between the oxygen absorbed and the gum found.

The data in Tables II and III provide a comparison of Fuel A with Fuel C. By H/C ratio, Fuel C contains more aromatic material than Fuel A. Both fuels were examined by field ionization mass spectroscopy by Dr. S. E. Buttrill, Jr. and Mr. G. A. St. John, with the results shown in Table III. The instrument used could not distinguish between paraffins and alkylnaphthalenes, but to be consistent with the differences in H/C ratios in Table II, Fuel C must be higher in alkylnaphthalenes.

TABLE II
ANALYSES OF FUELS

	%C	%H	%N	%S	% (diff.)	H/C
Fuel A	86.4	13.3	<0.02	<0.02	<0.36	1.83
Gum from A + NMP	68.0	5.9	6.2	19.9	O + S	1.03
NMP, calc	74.3	7.1	17.3	0	0	1.40
Fuel C	87.6	11.9	<0.02	0.03	<0.19	1.63

TABLE III
CLASSES OF HYDROCARBONS BY MOLE % IN FUELS A AND C

Hydrocarbon Class →	Alkanes +C ₁₀ H ₇ R	Ring or C=C			PhR	Indanes, Tetralins	\bar{M}_n
		1	2	3			
Fuel A	20.0	16.9	15.7	5.0	28.3	14.1	151
Fuel C	45.4	10.3	6.9	2.9	19.3	15.2	159

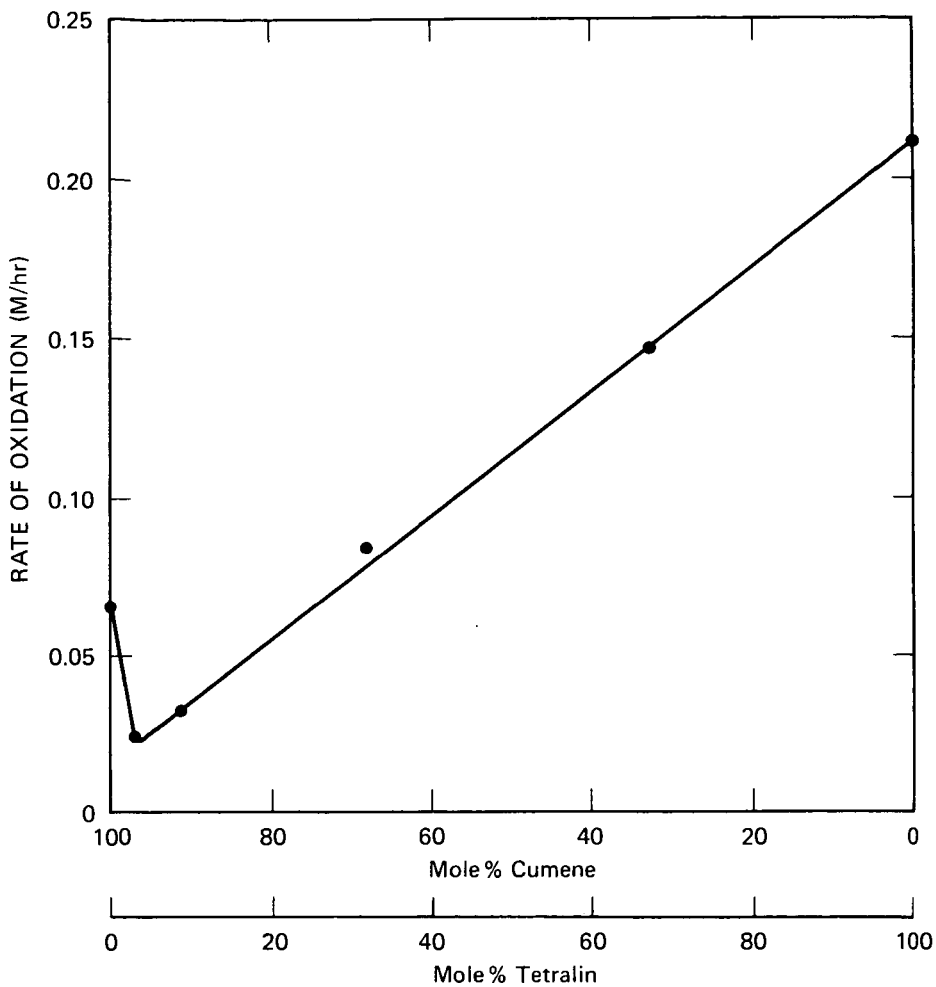
Table IV lists analyses of polar concentrates from three fuels. The polar concentrates contain more oxygen, nitrogen and sulfur than Fuels A and C and two of them are especially high in oxygen, suggesting that the fuels had undergone some oxidation before they reached us. The polar components of Fuels 10 and 13 were also analyzed by gas chromatography/mass spectroscopy. The Fuel 10 residues were rich in fluorene and phenanthracene/anthracene and their alkyl derivatives. Fuel 13 contained a wider range of products, in which carbazole and alkylcarbazoles were identified.

TABLE IV
ANALYSES OF POLAR CONCENTRATES

	%C	%H	%N	%S	% (diff.)	H/C
Fuel C	74.9	6.0	0.20	18.9	O + S	0.98
Fuel 10	85.8	8.5	0.94	1.87	2.85	1.18
Fuel 13	80.0	9.1	1.14	0.85	9.0	1.35

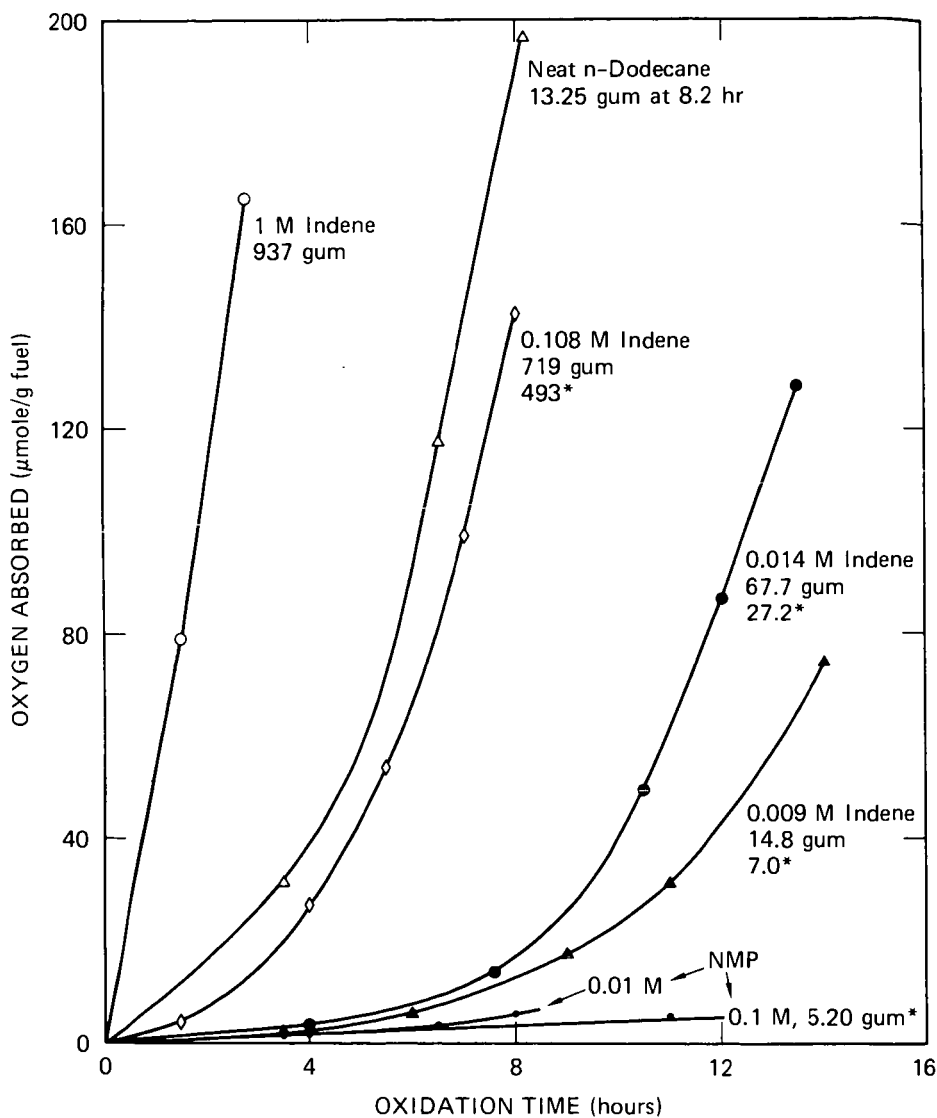
CONCLUSIONS

Our present working hypothesis is that deposits on hot engine parts come mostly from soluble gum formed on storage but maybe partly during heating of the fuel in the engine. The compounds that copolymerize with oxygen to give polyperoxides require the least oxygen to give a milligram of gum, but among other pure hydrocarbons and fuels, the rates of gum formation and oxygen absorption decrease together. It appears that the coupling of fuels and their primary oxidation products to form products of higher molecular weight, soluble gum and deposits is a small part of the chain termination reaction in which some of the free radicals that are involved in oxidation couple (terminate) instead of propagating. The faster the oxidation, the more coupling occurs. The dependence of rate of oxidation on rate constants for initiation, propagation and termination is expressed by the well known equation,



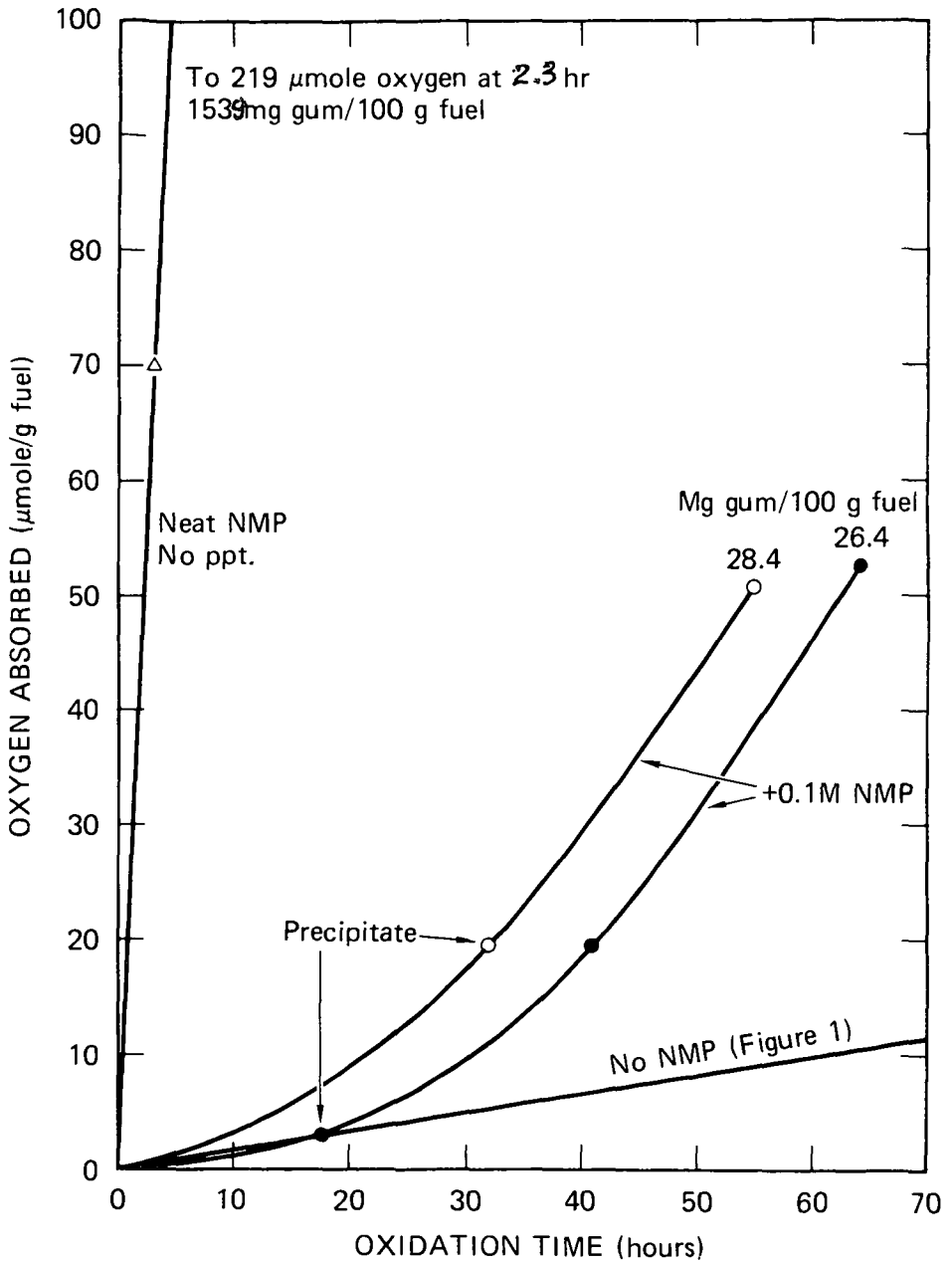
JA-2115-18

FIGURE 1 COOXIDATION OF CUMENE AND TETRALIN WITH 0.02 M $t\text{-BuO}_2\text{Bz}$ AT 90°C
 Data of G. A. Russell (ref. 6)



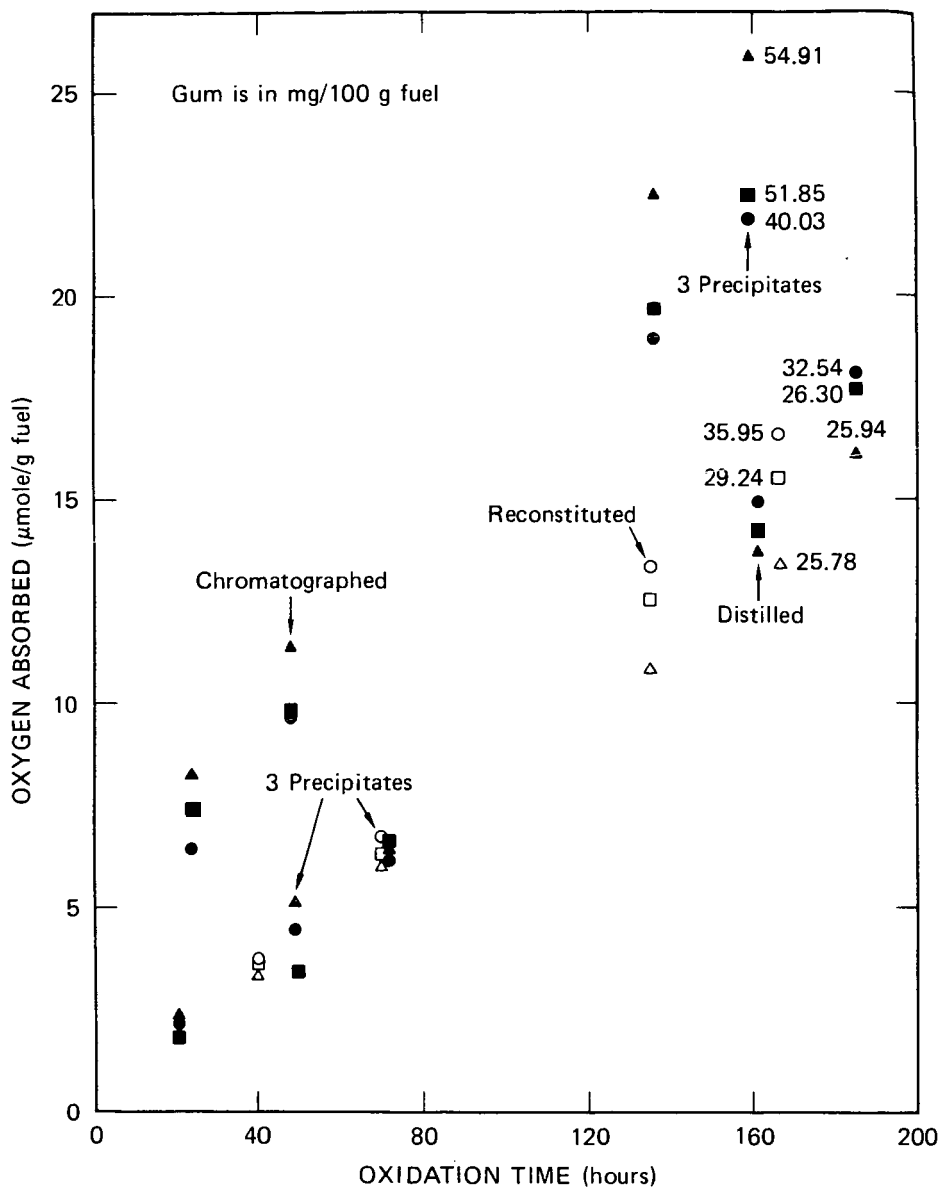
JA-2115-16A

FIGURE 2 OXIDATIONS OF n-DODECANE WITH INDENE AND NMP AT 130°C
Gum is in mg/100 g fuel, determined at 100°C except when marked * for 200°C.



JA-2115-22

FIGURE 3 OXIDATION OF FUEL A AND NMP AT 130°C



JA-1924-16

FIGURE 4 OXIDATION OF FUEL 10 IN AIR AT 130°C

$$R_O = (k_i/k_t)^{1/2} k_p [RH]$$

For fuels that contain mostly paraffins, naphthenes and alkylbenzenes, the k_p s should be quite similar. We think that k_t is the most susceptible of the three constants to the effect of other fuel components, which may explain why nearly all the fuels oxidize and produce gum slower than the pure hydrocarbons. Although k_i can be affected moderately by minor components, any effect on increasing the rate of peroxide decomposition will be offset by a decrease in the steady state concentration of peroxides. It is known that polynuclear aromatic hydrocarbons and their alkyl derivatives are very reactive toward peroxy radicals and that their chain termination constants in oxidation vary over a wide range (10).

Although a non-radical condensation mechanism has not been excluded and although details of a radical condensation mechanism are lacking, it appears to us now that the most fruitful approach to understanding and reducing gum and deposit formation in fuels is through the effects of condensed aromatic and heterocyclic compounds on the rates of oxidation of fuels.

Other factors that appear to be critical in gum and deposit formation are the effects of oxygen concentration and metals and the mechanism by which soluble gum evolves into insoluble deposits. Our conclusions based on oxidation at 130°C should eventually be confirmed by tests at storage temperatures, although the relative stabilities of fuels appear not to change much between 40 and 150°C (11).

ACKNOWLEDGMENT

This research was supported by the U. S. Army Research Office and NASA-Lewis Research Center.

LITERATURE CITED

- (1) Nixon, A. C., Chapter 17 in *Autoxidation and Antioxidants*, W. O. Lundberg, ed., Wiley Interscience, NY (1962).
- (2) CRC Literature Survey on the Thermal Oxidation Stability of Jet Fuel, Report No. 509 of Coordinating Research Council, Inc., Atlanta (1979).
- (3) Mayo, F. R., Richardson, H. and Mayorga, G. D., PREPRINTS, Div. of Petrol. Chem., ACS, 20 (1), 33 (1975).
- (4) (2), pg. 71.
- (5) Mayo, F. R., Buttrill, S. E., Jr., Lan, B., St. John, G. A. and Dulin, D., Preprints, Div. of Fuel Chem., 27 (2), 76 (1982).
- (6) Russell, G. A., J. Amer. Chem. Soc., 78, 1035, 1041 (1956).
- (7) Ibid., 77, 4583 (1955).
- (8) Mayo, F. R., Syz, M. G., Mill, T. and Castleman, J. K., Adv. Chem. Series, 75, 38 (1968).
- (9) Sajus, L., Adv. Chem. Series, 75, 59 (1968).
- (10) Huntington, J. G., Mayo, F. R. and Kirschen, N. A., Fuel, 58, 31 (1979).
- (11) Stavinocha, L. L., Westbrook, S. R. and Brinkman, D. W., DOE/BC/10043-12 (1980).

GENERAL PAPERS - POSTER SESSION
PRESENTED BEFORE THE DIVISION OF PETROLEUM CHEMISTRY, INC.,
AMERICAN CHEMICAL SOCIETY
WASHINGTON, D. C. MEETING, AUGUST 28 - SEPTEMBER 2, 1983

FT-IR MEASUREMENTS OF ALIPHATIC AND AROMATIC
C-H GROUPS IN COAL

By

B. Riesser, M. Starsinic, A. Davis, and P. C. Painter
College of Earth and Mineral Sciences
The Pennsylvania State University, University Park, Pennsylvania 16802

ABSTRACT

The experimental difficulties involved in the study of coal structure are both notorious and well-documented. Nevertheless, recent improvements in spectroscopic instrumentation have allowed the determination of what are thought to be reasonably accurate parameters describing an average coal structure. For example, Fourier transform infrared spectroscopy (FT-IR) has been applied to the determination of aromatic and aliphatic hydrogen. Unlike measurements of aromaticity by NMR, however, infrared methods rely on calibrating the intensities of specific bands to the concentration of the appropriate functional groups, using model compounds or other procedures. We have recently found that the values obtained depend heavily on the choice of bands and the methodology employed. In addition, the calibration coefficients vary considerably with rank. We will discuss the various approaches we have employed and the errors involved in each. Our results indicate that the best that can be achieved is the definition of a band of values of aromatic and aliphatic hydrogen.

SULFUR COMPONENTS ANALYSIS IN HYDROCARBON MATRIX BY GAS CHROMATOGRAPHY

By

O. Puzic
Esso Chemical Canada, P. O. Box 3004, Sarnia, Ontario, Canada N7T 7M5

INTRODUCTION

Determination of low concentrations of sulfur-containing gases has received considerable attention in recent years (1-6). The need is particularly acute in the petroleum industry, since the trace amounts of sulfur compounds cause corrosion and poison catalysts. Because of their reactivity and labile nature, as well as diversity of stream composition, determination of sulfur components in hydrocarbon matrix is a complex and intricate task. This paper presents a method for GC analysis of trace levels (0-200 ppm) of sulfur compounds in gaseous hydrocarbon streams.

EXPERIMENTAL

Chromatography

Varian Model 3700 Gas Chromatograph equipped with a Dual Flame Photometric and a Flame Ionization Detector (FPD and FID, respectively) and Vista 401 Dual Channel Data System was employed. Material used for sample transfer lines, 1 cc gas sample loop and the column was high grade, acetone-washed nickel. The gas sample was introduced onto the column via a six port teflon Valco valve. Two certified standard gas blends, compressed in an aluminum gas cylinder from Scott Specialty Gases, were used as calibration gases. Standard 1 contained: hydrogen sulfide, methyl mercaptan, ethyl mercaptan, dimethyl sulfide and dimethyl disulfide in nitrogen matrix. Standard 2 contained: dimethyl sulfide, methyl ethyl sulfide, diethyl sulfide and diethyl disulfide in nitrogen matrix. The concentration of each component was certified within $\pm 2\%$. Ultra high purity He was used for the carrier gas and high purity hydrogen and air for the flame gases in the two detectors. The optimal flow rates for the flame photometric detector fuel gases were found to be: H_2 , 142 ml/min; air #1, 80 ml/min; air #2, 170 ml/min. In the first flame, decomposition of the sample takes place. Combustion products from sulfur-containing compounds will produce optical emission in the second flame from the S_2 radicals formed. The Varian flame photometric detector employs a filter with maximum optical transmission at 365 nm for sulfur detection. For the flame ionization detector, the fuel gas flow rates were: H_2 , 30 ml/min; and air, 300 ml/min. The carrier gas flow rate was 26 ml/min.

The type of column packing material used for trace sulfur analysis depends on the stream composition and the hydrocarbon concentration. For most applications, a complete separation of various sulfur species as well as resolution between hydrocarbons and sulfur compounds such as H_2S , C_1 and C_2 mercaptans, sulfides and disulfides was achieved using a 6' x 1/8" acetone-washed nickel column packed with oxo-propionitrile/Porasil C - Durapak 80-100 mesh. However, when analyzing H_2S in propylene rich streams (propylene concentration greater than 10%), there is no longer a baseline separation between H_2S and propylene with this column. A phenomenon referred to as "quenching effect" takes place in the detector, whereby the decrease in sulfur response is apparently due to inactivation of the excited S_2 species by its combination or collision with a hydrocarbon and its degradation products (5, 7). Silicone, QF-1 (5%) on Porapak QS column packing material will provide the necessary separation in the H_2S region when high propylene concentration is expected (6).

An effluent splitter (ratio 50:50) is placed on the outlet of the column to send identical gas streams to the FPD and the FID, thereby allowing detection of components on both detectors simultaneously. The temperature programming profile suitable for most applications was: initial temperature, 70°C; final temperature, 100°C; hold, 45 min.; rate 10°C/min. Retention times for various sulfur compounds obtained using the chromatographic conditions described above are presented in Table I.

Calibration and Analysis

For quantitative analysis of sulfur species, an external standard method was used for calibration. After the sample loop had been purged with the calibration gas for several minutes, the sample of calibration gas was injected, at atmospheric pressure, by means of a six-port injection

valve. The temperature program and data acquisition were then activated simultaneously. After the calibration run was completed the response factors were generated or updated (8).

TABLE I

<u>Compound</u>	<u>Mol. Wt</u>	<u>B. P. (°C)</u>	<u>Retention Time, min.</u>
Hydrogen sulfide	34.08	-60.7	0.71
Methyl mercaptan	48.11	6.2	1.99
Ethyl mercaptan	62.13	35.0	3.38
Dimethyl sulfide	62.13	37.3	4.98
Methyl ethyl sulfide	76.16	66.6	9.05
Dimethyl disulfide	94.20	109.7	9.63
Methyl propyl sulfide	90.19	95.5	14.79
Diethyl sulfide	90.19	92.1	16.90
Methyl isobutyl sulfide	104.22	112.5	21.88
Diethyl disulfide	122.25	154.0	30.89
Dipropyl sulfide	118.24	142.4	46.62

Providing that the flow rates of the fuel gases to the flame photometric detector have not changed, there should be no need for frequent recalibration. However, the calibration blend is analyzed daily to assure optimal performance of the system. Following calibration, a hydrocarbon sample from a high pressure gas cylinder is purged through the sample loop and injected in the same manner. Figure 1 presents a typical chromatogram for sulfur analysis in a hydrocarbon matrix.

Precision data for 10 replicate runs of the two calibration blends is presented in Table II.

TABLE II

<u>Compound</u>	<u>Level (ppm)</u>	<u>Std. Dev.</u>	<u>Retention Time (min.)</u>	<u>Std. Dev.</u>
Hydrogen sulfide	15.4	0.2	0.71	0.03
Methyl mercaptan	16.2	0.1	2.00	0.04
Ethyl mercaptan	15.9	0.1	3.38	0.03
Dimethyl sulfide	15.7	0.1	4.99	0.03
Dimethyl disulfide	15.9	0.3	9.63	0.04
TOTAL	79.1	0.7		
Dimethyl sulfide	16.3	0.1	4.99	0.03
Methyl ethyl sulfide	16.1	0.1	9.05	0.04
Diethyl sulfide	15.9	0.1	16.90	0.04
Diethyl disulfide	15.3	0.4	30.89	0.04
TOTAL	63.6	0.7		

Sampling

During the course of the quantitative GC analysis of sulfur compounds in gaseous hydrocarbon streams it was observed that the light sulfur compounds (namely hydrogen sulfide and methyl mercaptan) were being depleted in the standard high pressure sampling cylinders.

Figure 2 presents the rate of H₂S depletion in standard 2250-ml stainless steel sampling cylinders (Cyls. No. 1 to 3). The cylinders were filled with Matheson certified standard containing 230 ppm H₂S in nitrogen. Within four minutes, 70% of the sulfur content was lost (cylinder No. 1). After 20 minutes no H₂S could be detected in the sample cylinder. Cylinder No. 1A is actually cylinder No. 1 that was steam cleaned, dried under house vacuum and refilled with the Matheson standard. A similar sulfur loss was confirmed by the Dohrman Sulfur Analyzer.

In another experiment, a clean sampling cylinder was filled with 290 ppm of H₂S in ethylene to determine if the hydrocarbon matrix affects the rate of sulfur loss. As illustrated in Figure 3 (curve I), the concentration of H₂S decreased 50% in less than 10 minutes. The same cylinder was flushed with helium, evacuated on a high vacuum line and refilled with the same amount of H₂S in ethylene. Although the number of active sites on the inner walls had been reduced, the passivation in this manner did not eliminate the problem entirely (curve II). After the initial drop in sulfur concentration, the rate of loss had reduced. Eventually, sulfur was lost completely overnight.

The same cylinder used in the above experiment was emptied but not cleaned and again refilled with 290 ppm H₂S in ethylene (Figure 4).

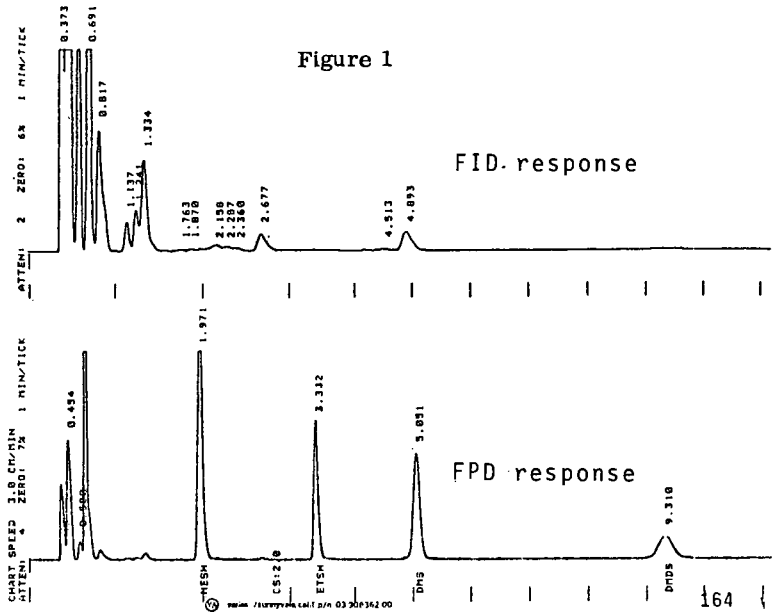


Figure 2.

HYDROGEN SULFIDE IN NITROGEN MATRIX

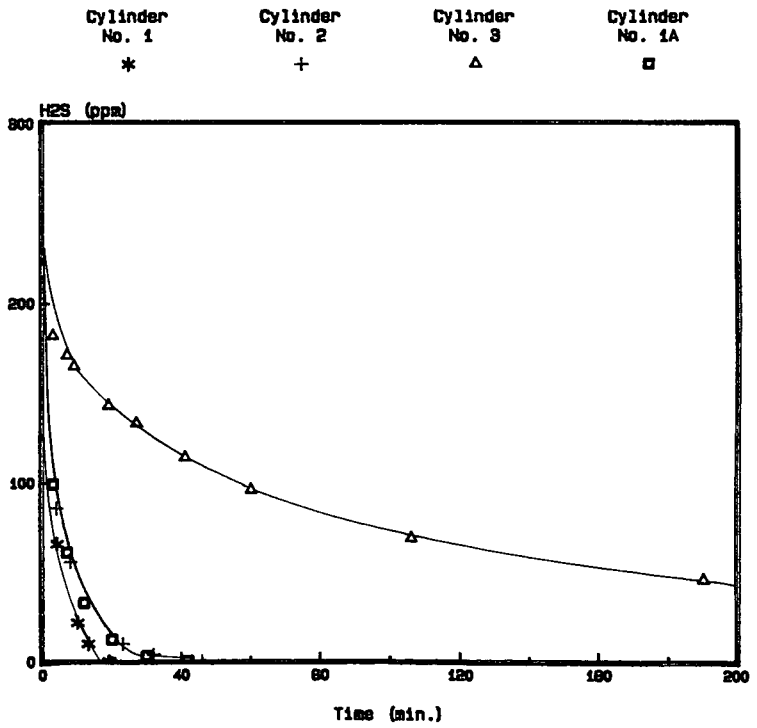


Figure 3. HYDROGEN SULFIDE IN HYDROCARBON MATRIX

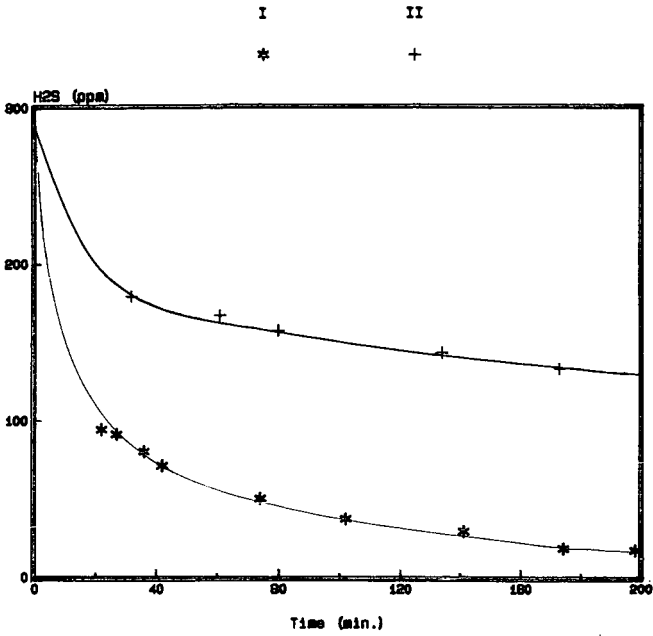


Figure 4. EFFECT OF MOISTURE

CYLINDER A

Δ

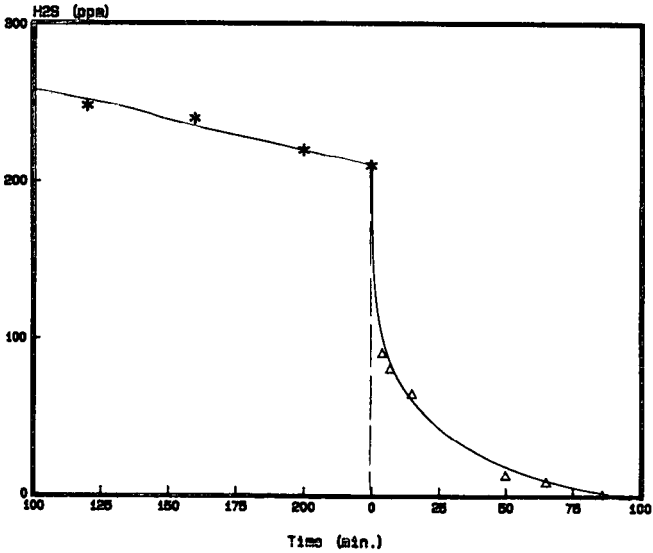


Figure 5. TEFLON-GRAPHITE COATING

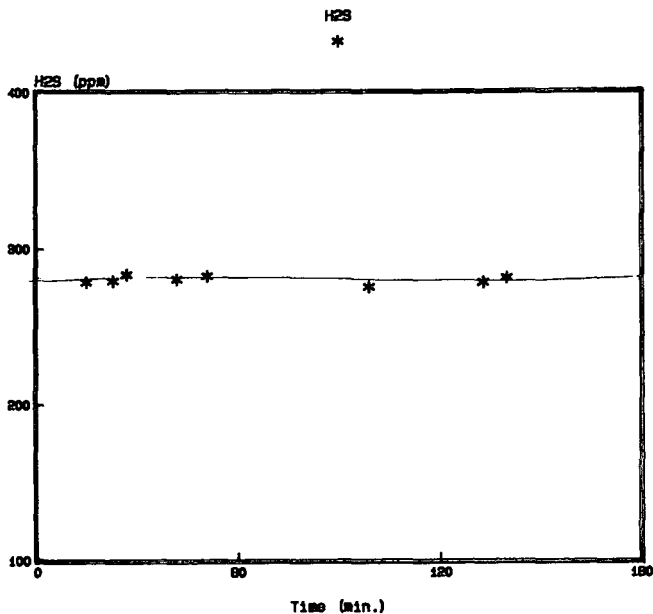
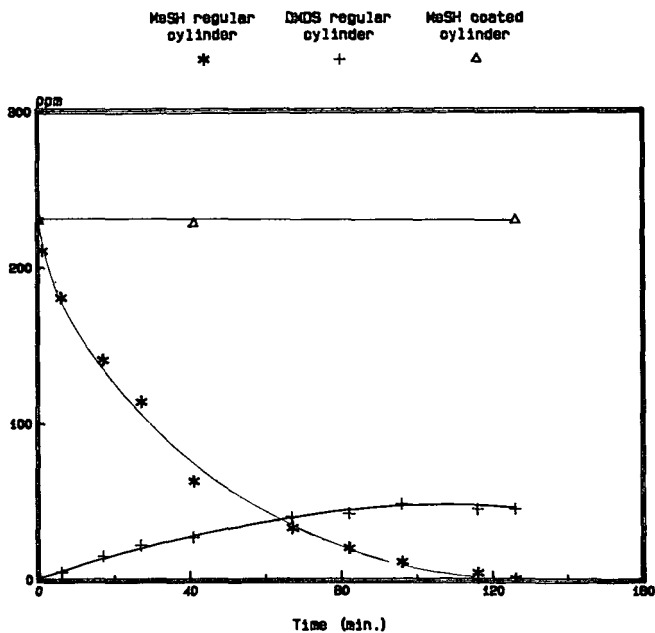


Figure 6. METHYL MERCAPTAN IN HYDROCARBON MATRIX



Presumably, the walls of the sample cylinder were further passivated, and the sulfur depletion rate was very low. After about 4 hours at a sulfur concentration of 210 ppm, the sample was transferred to a cylinder (passivated in the same manner) that contained 0.2 ml of water. A sudden drop in sulfur content (curve A) illustrates the high solubility of H₂S in water according to the reaction:



Provided a moisture-free environment is assured, adsorption on the metal walls appears to be the predominant cause for the decrease in sulfur concentration.

In an attempt to contain light sulfur compounds, a 2250 ml gas sample cylinder was lined with 0.0005 inch of teflon-graphite where the coating was baked onto the metal surface. The cylinder was tested with the same H₂S in ethylene mixture as in previous experiments (Figure 5). There was no apparent decrease in H₂S concentration over a period of 48 hours.

Figure 6 presents the comparative study of the two types of sample cylinders, i. e., teflon-graphite coated and regular (stainless steel) when methyl mercaptan is present in the hydrocarbon environment (ethylene matrix). Rapid oxidation of methyl mercaptan to dimethyl disulfide, reaction probably being catalyzed by the metal surface, as well as depletion on the walls is evident in the "regular" cylinder. However, in the teflon-graphite coated cylinder, the reaction did not take place and mercaptan content was unchanged over the time period indicated.

DISCUSSION

The unique and reactive properties associated with sulfur gases have presented difficult obstacles in attempts to contain low levels of these gases in high pressure cylinders (9, 10). Many factors are responsible for the apparent loss of sulfur content in the standard sample cylinders, such as, among others:

- Chemical reaction with, or promoted by, water molecules.
- Adsorption and/or reaction on the walls of the sampling cylinders.
- Oxidation of mercaptans to disulfides.

The results of this study indicate that gas mixtures containing low concentrations of sulfur compounds can exhibit stability if proper cylinder material and cylinder treatment techniques are used. Further evaluation of the teflon-graphite coated cylinders for their suitability in sampling of sulfur containing gases in various plant streams is under way. In addition, long term experience is being gathered.

LITERATURE CITED

- (1) Ferguson, D. A. and Luke, L. A., *Chromatographia*, 12, 197 (1979).
- (2) Patterson, P. L., *Anal. Chem.*, 50, 345 (1978).
- (3) Feeney, M., DeGood, J. and Warren, E., *Pittsburgh Conf., Abstracts*, No. 350 (1982).
- (4) McGaughey, J. F. and Gangwal, S. K., *Anal. Chem.*, 52, 2079 (1980).
- (5) Farwell, S. O. and Gluck, S. J., *Anal. Chem.*, 51, 609 (1979).
- (6) Pearson, C. D. and Hines, W. J., *Anal. Chem.*, 49, 123 (1977).
- (7) Fredriksson, S. A. and Cedergren, A., *Anal. Chem.*, 53, 614 (1981).
- (8) *Vista 401 Chromatography Data System Operators Manual*, Varian (1980).
- (9) Kramer, F. J. and Wechter, S. G., *J. Chrom. Sci.*, 18, 674 (1980).
- (10) Shultz, J. F., Karn, F. S. and Anderson, R. B., *Ind. Eng. Chem.*, 54, 44 (1972).

AN ANALYTICAL MODEL OF COMBUSTION OF SPENT OIL SHALE BLOCKS:
THE MODEL AND EXPERIMENTS

By

M-D. Ho, E. M. Suuberg^a and H. L. Toor
Department of Chemical Engineering, Carnegie-Mellon University, Pittsburgh, Pennsylvania 15213

INTRODUCTION

Oil shale, a potential source of liquid fuel, is a fine-grained, sedimentary rock composed of both organic and inorganic solid compounds. The production of liquid fuel from oil shale requires the retorting of the shale, in which oil and gas are destructively distilled from the shale rock, leaving behind a highly carbonaceous char within the spent shale matrix. The amount of char left depends on the richness of the raw shale. Typically, 23% by weight of the organic material originally present in the shale is left as char (1).

Combustion of this char could potentially provide all or part of the heat requirement for retorting of the shale (2). There have recently been several studies dealing with the combustion behavior of spent shale (2-8). Although char in shale is not pure carbon, most studies have treated it as carbon with reasonable success.

In the combustion of spent oil shale in an environment of air with other inert gases, there are three active components to be considered, O₂, CO₂ and CO and four major chemical reactions (9, 10), namely:

• Direct oxidation of the residual char, a process which is limited by the diffusion of oxygen and which creates an "unburned core".



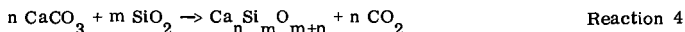
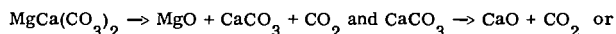
• Oxidation of CO



• CO₂-C gasification reaction



• Carbonate decomposition reactions^b



Therefore, the combustion of spent shale consists of two competing schemes: one is the direct oxidation of char; the other is the gasification of the char by CO₂ released from the carbonate decomposition reactions.

There have been several modeling studies of the combustion of spent shale in the presence of oxygen and nitrogen (2-7) which used the classical shrinking core model. This model assumes that the reaction rate is limited only by the internal diffusion of oxygen; hence, it neglects the other reactions (2, 3 and 4) which may play a major role at elevated temperature (above 875°K).

Mallon and Braun (7, 11) have included the decomposition and gasification reactions (3 and 4) in their model, but they treated the gasification reaction and the direct oxidation reaction independently and then superposed the two results. This approximation was inaccurate. Braun et al.

a. Present address: Division of Engineering, Brown University, Providence, Rhode Island 02912.
b. For the detail and kinetics of this reaction, see Manor et al (8).

(2) modeled gasification of spent oil shale blocks by steam and CO₂ but did not consider oxidation reactions. Their solution scheme involved solving differential equations numerically.

Our previous publication (Manor et al. (8)) offered a model which successfully predicted the combustion behavior of shale in nitrogen diluted air, but that model also required the numerical solution of differential equations.

The model that we present here is an improvement over the model of Manor et al. The major advantage of the new model lies in the simplicity of the closed form result which eliminates the necessity of cumbersome numerical solution of the differential equations. Our new model thus allows more convenient use of the single particle (or block) combustion model in the modeling of packed bed retorts. Experiments similar to those carried out earlier were used to extend the data.

DEVELOPMENT OF THE MODEL

Consider the burning sample shown schematically in Figure 1. We will use the assumptions that were employed by Manor et al. (8).

1. Mass transfer processes may be treated as pseudo-steady.
2. Only radial transport in a cylinder is considered.
3. Temperature is spatially uniform.
4. No significant pressure gradient exists within the shale.
5. The reaction of char with oxygen is fast enough to be lumped at the surface of the unburned core.
6. The gasification Reaction 3 occurs uniformly within the unburned core.
7. Carbonates decompose uniformly throughout the shale.
8. The bulk flow of all species out of the shale is dominated by the release of carbon dioxide from the decomposition of carbonates.
9. Fick's law holds for each component and all effective diffusivities are equal.

An additional assumption that allows the model to be treated analytically is that the oxidation reaction of carbon monoxide is instantaneous^a.

Transport Model

The formal statement of assumption 8 is:

$$N_t = R_4 (7r^2/2\pi r) = R_4 r/2 = G L y \quad 1)$$

where

$$L = C D_e / r_s$$

$$G = R_4 r_s^2 / (2 D_e C)$$

$$y = r/r_s$$

and where r_s is the radius of the cylinder. Other symbols are defined in the table of nomenclature.

The formal statement of assumption 9 is:

$$N_i = -C D_e dX_i/dr + X_i N_t \text{ or } N_i = -L dX_i/dy + X_i G L y, \quad i = \text{CO}, \text{CO}_2, \text{O}_2 \quad 2)$$

The species conservation equation for each component can be written as:

$$1/r d/dr (r N_i) = \sum_j \nu_{ij} R_j \quad 3)$$

where ν_{ij} is the stoichiometric coefficient of component i with respect to R_j . At the surface of the cylindrical sample ($r=r_s$ or $y=1$), external mass transfer resistance is taken into account by specifying:

$$N_{i,s} = (K_x + N_t) [2 Q / (K_x + 2Q)] X_{i,s} - K_x [2 Q / (K_x + 2Q)] S_{i,f} \quad 4)$$

- a. The measured CO/CO₂ ratio at the surface of the shale never exceeded 20% in the ignition stage and then declined very rapidly to a negligible value, therefore, we assume all CO is burned to CO₂ very quickly in the presence of oxygen. See also Manor et al. (8) for more detail.

where Q is the molar flow rate of sweeping gas per unit surface area of the sample. The new correction term, $[2Q/(K_x + 2Q)]$, is used to take into account the change in sweeping gas compositions due to the mass transfer to and from the sample. When the gas flow rate is very large, the correction term reduces to unity and is not required.

Define a pseudo-component concentration:

$$X_1 \equiv 1/2X_{CO} + X_{CO_2} + X_{O_2}, \quad N_{x_1} \equiv 1/2N_{CO} + N_{CO_2} + N_{O_2}$$

It follows from Equation 3 and the stoichiometry of the reactions that

$$1/r \, d/dr (r N_{x_1}) = R_4 \quad 5)$$

The substitution of Equation 2 into Equation 5 yields:

$$1/y \, d/dy (-y (dX_1/dy) + X_1 G y^2) = G \quad 6)$$

subject to the boundary conditions that, at the center of the sample, the flux is zero and at the surface of the sample, Equation 4 holds for pseudo-component 1.

Thus, Equation 6 can be solved to give:

$$X_1 = 1 + Kx/(Kx + G L) (X_{1,f} - 1) \exp((y^2 - 1) G/2) \quad 7)$$

which eliminates one unknown.

For the sake of convenience, we shall first consider the two regions of shale separately: the unburned core region and the product of shell layer.

Core Reaction Model

The core reaction model is similar to the one in Manor et al. (8), it is rederived here for the convenience of the reader. Within the unburned core section, the conservation equation for CO can be written as:

$$1/r \, d/dr (r N_{CO}) = 2 R_3 \quad 8)$$

with boundary conditions:

$$r = 0, \quad dX_{CO}/dr = 0; \quad r = r_c, \quad X_{CO} = X_{CO,c}$$

where r_c is the radius of the edge of the unburned core. Assumption 6 allows R_3 to be treated as position independent. Its value is evaluated at the average concentrations of reactants within the core. Therefore, Equation 8 can be integrated to give:

$$X_{CO} = (X_{CO,c} - B) \exp[(y^2 - y_c^2) G/2] + B$$

where

$$B = 2 R_3 / R_4 = R_3 (4GL/r_s)$$

Note that $X_{CO_2} = X_1 - 1/2X_{CO}$ in the core region, since $X_{O_2} = 0$ and the average mole fractions are:

$$\langle X_{CO} \rangle = (X_{CO,c} - B) \left[\frac{1 - \exp(-G y_c^2/2)}{G y_c^2/2} \right] + B \quad 9)$$

$$\langle X_{CO_2} \rangle = (X_{CO_2,c} - 1 + B/2) \left[\frac{1 - \exp(-G y_c^2/2)}{G y_c^2/2} \right] + 1 - B/2 \quad 10)$$

where

$$X_{CO_2,c} = X_{1,c} - 1/2 X_{CO,c}$$

It is assumed that C₂O-C gasification proceeds at a rate given by the equation suggested by Ergun (13)

$$R_3 = \frac{K_a G_c}{1 + \langle X_{CO} \rangle / K_{ex} \langle X_{CO_2} \rangle} \quad (\text{gmole/cm}^3 \text{sec}) \quad 11)$$

where $K_a = 4.5 \times 10^7 \exp(-24,500/T) + 3.75 \times 10^2 \exp(-16,000/T) \text{ sec}^{-1}$ (as suggested by Campbell and Burnham (9)). C_c is the molar concentration of char (gmole/cm³) and $K_{ex} = 138 \exp(-7,500/T)$ (from Ergun and Menster (14)).

Shell Transport and Reaction Model

In order to eliminate reaction terms in the conservation equation, let us again create a pseudo-component X₂, where

$$X_2 \equiv X_{O_2} - 1/2 X_{CO}, \quad N_{x_2} \equiv N_{O_2} - 1/2 N_{CO}$$

It follows that in the shell region,

$$1/r \, d/dr (r N_{x_2}) = 0 \quad 12)$$

and with Equation 2 and dimensionless variables,

$$1/y \, d/dy [-y (dX_2/dy) + X_2 G y^2] = 0 \quad 13)$$

Equations 12 and 13 can be integrated to give

$$y N_{x_2} = M \quad 14)$$

and

$$X_2 = M/L F(y, y_c) \exp(G y^2/2) + X_{2,c} \exp[G/2(y_c^2 - y^2)] \quad 15)$$

where:

$$X_{2,c} = X_{O_2,c} - 1/2 X_{CO,c}, \quad F(y, y_c) = \int_{y_c}^y \frac{\exp(-G\tau^2/2)}{\tau} \, d\tau$$

and M is an integration constant. At y=1, Equation 4 is used as the other boundary condition.

Since we have assumed that the oxidation reaction of carbon monoxide is instantaneous, it follows that the coexistence of carbon monoxide and oxygen is not allowed and the flame front at which all the oxidation reactions occur is assumed to be infinitely thin.

The flame front occurs either at the core surface, case 1, or out of the core surface (i.e., at $r > r_c$), i.e., case 2.

Case 1: Flame Front at the Core Surface

In this case, oxygen flux to the core surface will be consumed both by the reaction with carbon monoxide produced in the core and by the direct oxidation of char, i.e.,

$$-N_{O_2,c} = (R_1 + R_3) r_c / 2$$

where

$$R_1 = K_1 C_c X_{O_2,c}$$

and the value of K_1 is provided by Sohn and Kim (10) as $1.503 \times 10^7 \exp(-11102/T) \text{ sec}^{-1}$. (In Manor et al. (8), K_1 was assumed to be infinitely large.)

Since oxygen is present at the core surface in this case, we can assume $X_{CO,c}$ and $N_{CO,c}$ to be zero, which requires

$$X_{2,c} = X_{O_2,c} \text{ and } M = y_c N_{O_2,c}.$$

Therefore, we can calculate the oxygen flux by solving Equation 15 to get:

$$N_{O_2,s} = N_{x_2,s} = \frac{K_x X_{O_2,f}^{-1} X_{O_2,c} \exp((1-y_c^2)G/2)}{(K_x + 2Q)/2Q + (G + K_x/L) F(1, y_c) \exp(G/2)} \quad (16)$$

where

$$X_{O_2,c} = \frac{K_x X_{O_2,f} - R_3 r_s y_c^2 / 2 [(K_x + 2Q)/2Q + (G + K_x/L) F(1, y_c) \exp(G/2)]}{K_1 C_c r_s y_c^2 [(K_x + 2Q)/2Q + (G + K_x/L) F(1, y_c) \exp(G/2)] + (K_x + GL) \exp((1-y_c^2)G/2)}$$

Case 2: Flame Front Out of Core Surface

In case 2, the flame front is being pushed outward by carbon monoxide, so oxygen cannot reach the core surface and $X_{2,c}$ must be less than zero, since $X_{2,c} = 1/2 S_{CO,c}$

Note that since

$$N_{O_2,c} = 0, N_{x_2,c} = -1/2 N_{CO,c},$$

a mass balance around the core surface gives:

$$N_{CO,c} = R_3 r_c \quad (17)$$

Using Equations 14 and 17, we can get

$$M = -R_3 r_s y_c^2 / 2 \quad (18)$$

Equations 15 and 18 allow us to compute the value of $X_{2,c}$ as:

$$X_{CO,c} = -2X_{2,c} = \frac{-2K_x X_{O_2,f} + r_s y_c^2 R_3 ((K_x + 2Q)/2Q + (G + K_x/L) F(1, y_c) \exp(G/2))}{(G L + K_x) \exp(G/2 (1-y_c^2))} \quad (19)$$

Model Solution

Note that in the core region, if we substitute Equations 9 and 10 into Equation 11, R_3 can be solved as a function of $X_{CO,c}$, while in the reacted shell region $X_{CO,c}$ is either zero in case 1, or can be obtained from Equation 19 as a function of R_3 in case 2. Simultaneous solution of these two regions gives the following equation:

$$R_3 = \sqrt{\frac{(K_3 K_5 K_{ex}^2 - 2K_3 K_4 K_5 K_{ex}^2 + (K_4 K_{ex})^2 - 2K_2 K_{ex} (K_3 K_5 + K_4) + 4K_1 K_4 K_5 K_{ex} + K_2^2)}{+ K_2 - K_3 K_5 K_{ex} - K_4 K_{ex}} / (4K_1 - 4K_3 K_{ex})} \quad (20)$$

where

$$K_1 = C_4 - 2 C_4 C_5 + 2 C_1 C_5$$

$$K_2 = 2 C_2 C_5$$

$$K_3 = C_1 C_5 + 1/2 C_4 - C_4 C_5$$

$$K_4 = 1 + 2 C_3 C_5 - 2 C_5$$

$$K_5 = 2 K_{ab} \rho_c / MW_c$$

and

$$C_1 = 0 \quad (\text{Case 1})$$

or

$$r_s y_c^2 \exp(G y_c^2) [F(1, y_c) / L + \exp(-G/2)(kx + 2Q) / 2Q / (k_x + GL)] \quad (\text{Case 2})$$

$$C_2 = 0 \quad (\text{Case 1})$$

or

$$2X_{O_2, f} \exp(G/2(y_c^2 - 1)) [k_x / (GL + k_x)] \quad (\text{Case 2})$$

$$C_3 = 1 + \exp(G/2(y_c^2 - 1)) [k_x / (GL + k_x)] (X_{O_2, f} + X_{CO_2, f} - 1) \quad (\text{Case 1})$$

or

$$1 + \exp(G/2(y_c^2 - 1)) [k_x / (GL + k_x)] (2X_{O_2, f} + S_{CO_2, f} - 1) \quad (\text{Case 2})$$

$$C_4 = r_s / 2GL$$

$$C_5 = \left[\frac{1 - \exp(-G y_c^2 / 2)}{G y_c} \right]$$

Thus, R_3 can be obtained from Equation 20 and all the other quantities desired, such as

$$N_{O_2, s}$$

(the oxygen consumption rate) and dy/dt (the rate of shrinkage of the core) can be calculated in a straightforward fashion. A trial and error calculation procedure is used to determine whether case 1 or case 2 is true. This model is then integrated numerically only over time, with the reaction rates and temperature recalculated at each time step.

PHYSICAL PROPERTIES

In the model calculation, the temperature is calculated from

$$\rho_s C_p (dT_s/dt) = h S \Delta T + \sum R_i \Delta H_i$$

where the heat capacity is:

$$C_p = 0.72 + 7.7 \times 10^{-4} T_s^2 / (T_s + 300) \text{ J/gm-K}$$

and the heat transfer coefficient^a is:

$$h = 9.76 \times 10^{-4} + 2.48 \times 10^{-6} (T_s - 755) \text{ W/cm}^2\text{K}$$

The temperature difference ΔT in the heat loss term is actually measured in our experiments, it usually maintains a constant value throughout an experiment due to the configuration of the reactor.

A general correlation based on a random pore model (15) allows us to estimate the effective diffusivity of spent oil shale as:

$$D_e = \epsilon^2 D_{O_2, \text{air}}$$

where ϵ is the porosity and

$$D_{O_2, \text{air}}$$

is the bulk binary diffusivity of oxygen in air. Note that there are no adjustable parameters in the above equation. This approach is a modification of that used by Manor et al.

For the purpose of prediction, porosity, char concentration and shale grade can be conveniently estimated from shale density using correlations in the literature (16, 17).

Smith provided a theoretical relationship between density and oil yield for oil shale (17) and he supported his prediction with experimental results. The correlation was found to be very good in our experiments.

The data on the carbonaceous char contents of spent shales was gathered by Stanfield et al. (1) and his result can be correlated as follows:

$$W_c = 1.903 \times 10^{-3} + 2.283 \times 10^{-4} A$$

where W_c is the char density as percentage of the raw shale density (not weight fraction of the spent shale, as Dockter and Turner stated) and A is the shale grade in liters of oil per ton. The initial porosity of the spent shale returned to 750°K can also be estimated with Tisot's data which is correlated by Dockter and Turner (5):

$$\epsilon = 0.111 + 1.55 \times 10^{-3} A + 1.23 \times 10^{-5} A^2$$

EXPERIMENTAL VERIFICATION

The analytical model gives results very close to the numerical model of Manor et al., which agreed reasonably well with the experimental data reported earlier. In addition, a number of new experiments were carried out to further test the validity and applicable range of the model. The experimental conditions used were similar to the earlier one (8). Colorado oil shales were machined into cylinders and retorted in a furnace in nitrogen to a maximum temperature of 750°K. The combustion was then initiated by switching the sweep gas from nitrogen to air or nitrogen diluted air. Heat transfer to and from the furnace wall was minimized by controlling the furnace wall to within two °K of the shale surface temperature.

The effects of shale grades (from 40 to 229 liter/ton), cylinder sizes (from 1 cm to 10 cm

a. The heat transfer coefficient sometimes has been adjusted to account for non-ideal temperature distribution in the furnace during rapid temperature rise.

in diameter) and feed gas oxygen concentration (from 5% to 21%) were examined. It was found that this model adequately accounts for these effects in the testing range. Shown in Figure 2 is the comparison of experimental and model prediction of average temperatures and dimensionless reaction rates of rich shale cylinders (208 liter/ton) of two different sizes (3.5 cm, and 9.3 cm in diameter) in 13.5% oxygen plotted against dimensionless time. A 5 cm sample from the same piece of rock was also tested against the model with similar success but the result was excluded from the figure to avoid crowding. It can be seen from Figure 2 that the two different size samples give very similar curves on a dimensionless time scale (the 5 cm sample gave similar curves), but other grades of shale do not scale this way.

Various sizes (1 cm, 3.4 cm, 5.1 cm and 9.7 cm diameters) of 104 liter/ton shale have also been used and the model also predicted the combustion behavior successfully. In Table I, we compare measured and predicted total burn out times for these samples.

TABLE I

BURN OUT TIME FOR MEDIUM GRADE SHALE^a (104 LITER/TON) OF FOUR DIFFERENT SIZES: EXPERIMENTS AND MODEL PREDICTION

Expt. No.	Shale Diameter	O ₂ %	Burn Out Time	
			Expt.	Model
55	9.7 cm	21%	660 min.	670 min.
65	5.1 cm	15%	340 min.	330 min.
67	3.4 cm	15%	160 min.	163 min.
69	1.0 cm	15%	20 min.	22 min.

- a. Important parameters used are: Initial porosity = 30%, carbon density = 0.06 gm/cm³, spent shale density = 1.87 gm/cm³.

CONCLUSION

An analytical model satisfactorily predicts the combustion behavior of spent oil shale blocks. The only additional assumption besides those employed by Manor et al. (8) is that the oxidation reaction of carbon monoxide is instantaneous.

ACKNOWLEDGMENTS

We wish to thank Occidental Petroleum Corporation and Rio Blanco Oil Shale Company for supplying the oil shale used in this work.

NOMENCLATURE

A	shale grade, liter/ton
B	constant defined as $2R_3/R_4$, dimensionless
C	molar concentration in gas phase, gmole/cm ³
C _c	molar concentration of char in shale, gmole/cm ³
C _i	constants, defined below Equation 20
C _p	heat capacity of the shale, J/gm-K
D _e	effective diffusivity of gases in the shale, cm ² /sec
G	constant = $R_4 r_s^2 / 2CD_e$, dimensionless
h	heat transfer coefficient, W/cm ² K
K _i	constants, defined below Equation 20
K _x	mass transfer coefficient, gmole/sec-cm ²
L	constant = CD_e / r_s , gmole/sec-cm ²
N _t	net molar flux anywhere within the sample, gmole/sec-cm ²

N_i	molar flux of any species i , gmole/sec-cm ²
Q	the molar feed rate of gas per unit surface area of the sample
R_1	molar rate of the direct oxidation of char, gmole/sec-cm ³
R_2	molar rate of the oxidation reaction of CO, gmole/sec-cm ³
R_3	molar rate of CO ₂ -C gasification reaction, gmole/sec-cm ³
R_4	molar rate of release of CO ₂ from carbonate decomposition reactions, gmole/sec-cm ³
r	radial position within shale sample, cm
r_s	the radius of the shale sample, cm
S	surface area of sample per unit volume, cm ⁻¹
T_s	shale temperature, K
ΔT	temperature difference between the shale and the sweeping gas
ΔH_j	heat of reaction j , J/gm-K
W_c	weight fraction of carbonaceous char in raw shale, dimensionless
x_i	mole fraction of any species i , i =CO, O ₂ , CO ₂ , dimensionless
$\langle x_i \rangle$	average mole fraction of species i in the core region, i =CO ₂ , CO, dimensionless
y	$=r/r_s$, normalized radial position within sample, dimensionless
ϵ	porosity, dimensionless

SUBSCRIPTS

c	value at the core edge
f	value in the feed stream
i	CO, O ₂ or CO ₂
s	value at the shale surface

Figure 1: Reaction scheme. This diagram indicates the locations at which the four main reactions occur, and indicates the sources and sinks of the three key reactant species.

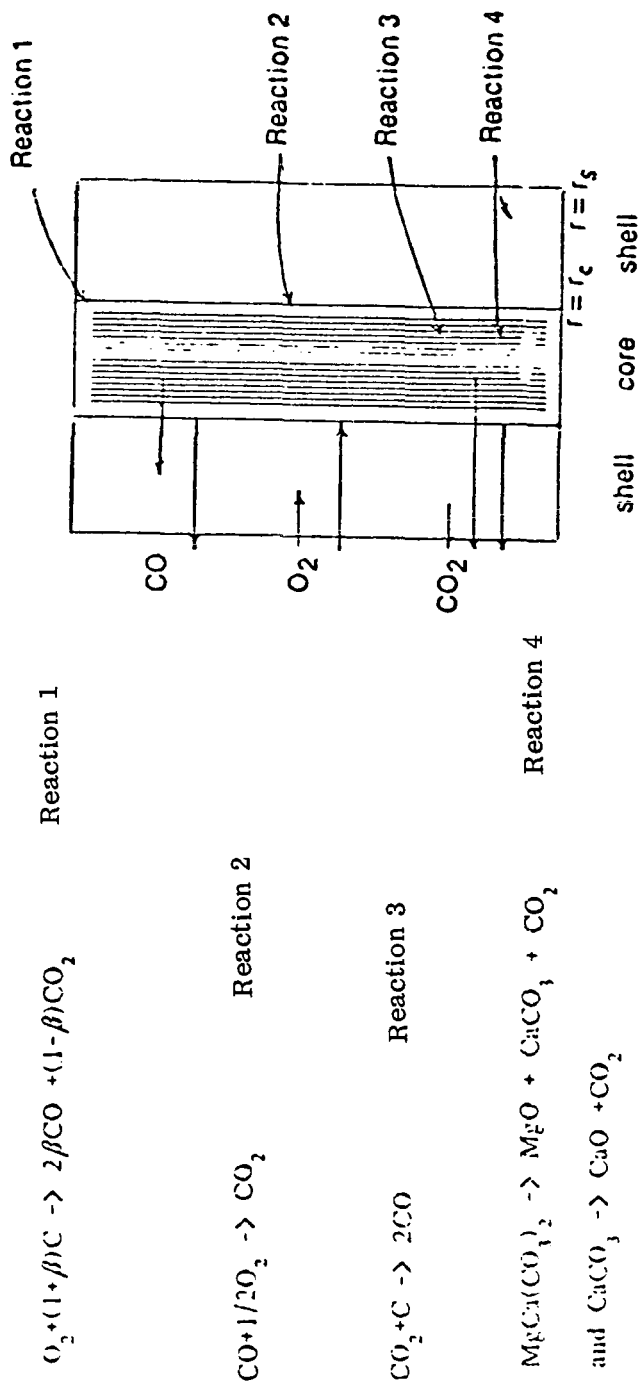
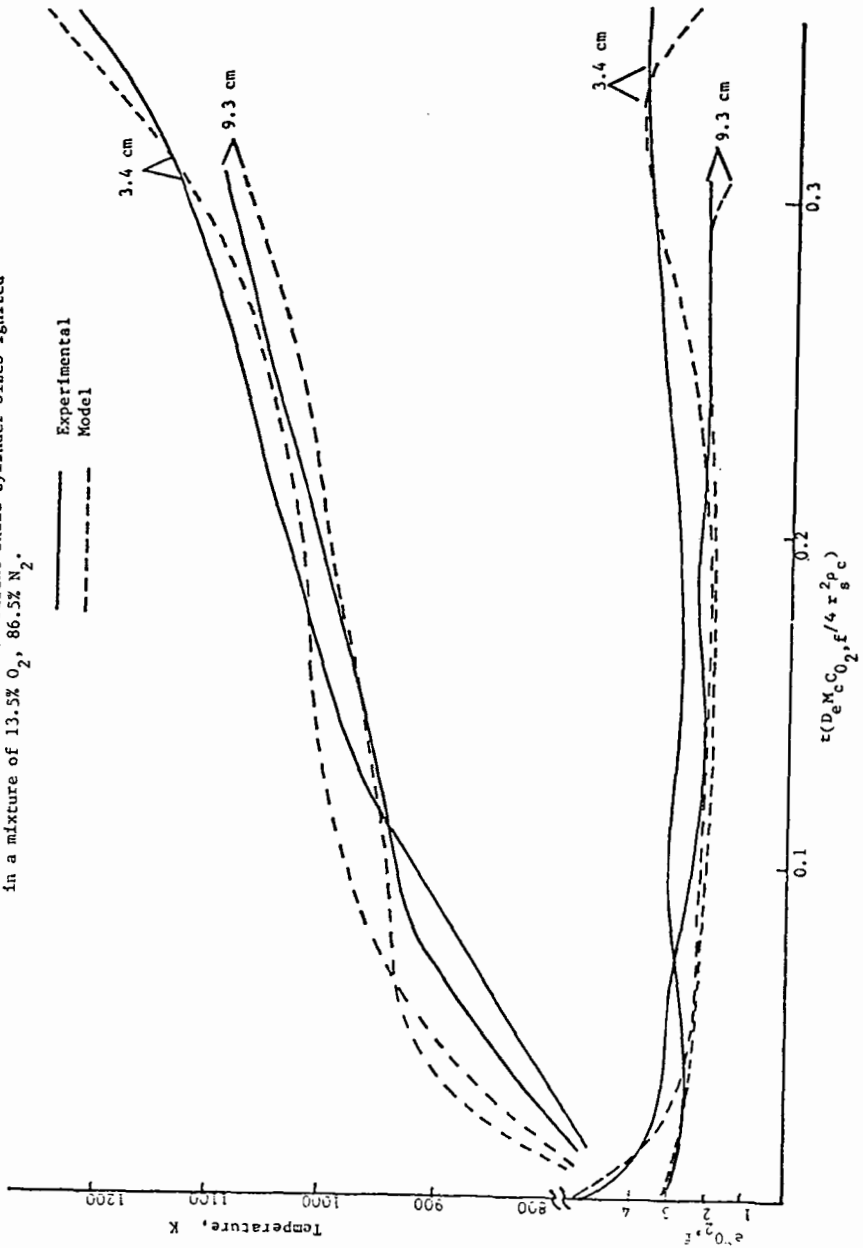


Figure 2: Comparisons of experimental results and model predictions. Average temperatures and dimensionless reaction rates vs. dimensionless time. Two different shale cylinder sizes ignited in a mixture of 13.5% O₂, 86.5% N₂.



LITERATURE CITED

- (1) Stanfield, K. E. , Frost, I. E. , Mcauley, W. S. and Smith, W. S. , "Properties of Colorado Oil Shale", U. S. Bureau of Mines, RI 4825 (1951).
- (2) Dockter, L. , "Combustion of Oil-Shale Carbon Residue", AICHE Symp. Series, Vol. 72, No. 155 , p. 24 (1975).
- (3) Huang, E. T. S. , "Retorting of Single Oil-Shale Blocks with Nitrogen and Air", SPE Journal, p. 331 (October 1977).
- (4) Thomson, W. J. and Soni, Y. , "Oxidation of Oil Shale Char", In Situ, Vol. 4, No. 1, p. 61 (1980).
- (5) Dockter, L. and Turner, T. F. , "Combustion Rates for Oil Shale Carbonaceous Residue", In Situ, Vol. 2, No. 3, p. 197 (1978).
- (6) Duvall, J. J. and Tyner, C. E. , "Laboratory and Modeling Studies of the Combustion Retorting of Large Clocks of Oil Shale", Tech. report, Sandia Laboratories (1979).
- (7) Mallon, R. and Braun, R. , "Reactivity of Oil Shale Carbonaceous Residue with Oxygen and Carbon Dioxide", Quarterly of the Colorado School of Mines, Vol. 71, No. 4, Proceedings of the 9th Oil Shale Symp. (1976).
- (8) Manor, Y. , Suuberg, E. M. , Ho, M. and Toor, H. L. , "The Ignition and Combustion Behavior of Spent Shale Particles", in 19th Interntl. Symp. on Combustion, The Combustion Institute, Pittsburgh, PA, p. 1093 (1982).
- (9) Campbell, J. H. and Brunham, A. K. , "Reaction Kinetics for Modeling Oil Shale Retorting", In Situ, Vol. 4, No. 1 (1980).
- (10) Sohn, H. Y. and Kim, S. K. , "Intrinsic Kinetics of the Reaction between Oxygen and Carbonaceous Residue in Retorted Oil Shale", Ind. Eng. Chem. , Process Design and Development, Vol. 19, No. 4, p. 550 (1980).
- (11) Braun, R. L. , "Mathematical Modeling of Modified In-Situ and Aboveground Oil Shale Retorting", Tech. report UCRL-53119, Lawrence Livermore Laboratory (1981).
- (12) Braun, R. L. , Mallon, R. G. and Sohn, H. Y. , "Analysis of Multiple Gas-Solid Reactions during the Gasification of Char in Oil Shale Blocks", Tech. report UCRL-85279, Lawrence Livermore Laboratory (April 1981).
- (13) Ergun, S. , "Kinetics of Reaction of Carbon Oxidide with Carbon", Journal of Physical Chem. , Vol. 60, p. 480 (1956).
- (14) Ergun, S. and Menster, M. , "Reaction of Carbon with CO₂ and Steam", in Chem. and Physics of Carbon, P. L. Walker, ed. , p. 203 (1965).
- (15) Smith, J. M. , Chem. Engineering Kinetics, McGraw-Hill Co. , p. 466 , 3rd ed. (1981).
- (16) Tisot, R. , "Alterations in Structure and Physical Properties of Green River Oil Shale by Thermal Treatment", J. Chem. Eng. Ref. Data, Vol. 12, p. 405 (1967).
- (17) Smith, J. W. , "Theoretical Relationship Between Density and Oil Yield for Oil Shales", Tech. report R17248, Bureau of Mines (April 1969).

THE EFFECT OF CRYOGRINDING ON THE MOLECULAR WEIGHT OF
SAMPLES OF POLYISOBUTYLENE

By

P. F. Waters

The American University, Washington, D. C. 20016
and

A. F. Hadermann and J. C. Trippe

General Technology Applications, Inc., Arlington, Virginia 22209

INTRODUCTION

A significant recent development in polymer technology is the discovery that megadalton-molecular-weight macromolecules can be dissolved instantaneously in liquids which are normally solvents for the materials. This finding portends increasing development and use of ultra high molecular weight macromolecules deriving from the superior effects they exhibit in a variety of applications. Past studies have demonstrated that macromolecules, added in small quantities, (1) enhance the flow of liquids through pipelines; (2) impart high extensional viscosities to and (3) impede the aerosolization of liquids in which they are dissolved. The latter is a property of antimisting fuels.

In the event that antimisting fuels gain wide use, a not inconsiderable facilitation of the feasibility might well be the on-site dissolution of the macromolecules in the fuels. This requirement is occasioned by the high susceptibility of some dissolved macromolecules to shear degradation; a concomitant of fuel transportation and transfer by pumping. The cryogenic comminution and subsequent blending of macromolecules with the fuels offers a direct route to instantaneous dissolution. The process is described elsewhere (3-5).

The antimisting effect is a strong function of the molecular weight of the additive (2, 6, 7). Consequently, an understanding of the effect of cryogrinding on the molecular weight of a potential antimisting fuel additive is required. In this study, samples of polyisobutylene of three different molecular weights were cryofractured and dissolved. Measurements of the viscosity and height-at-break in a ductless siphon (8) of the solutions were compared with those of solutions of unground samples and the comparative values were used as indicators of the extent of degradation.

EXPERIMENTAL

Samples of BASF polyisobutylene of three different molecular weights (B-100, B-200, B-200-246) were fractured in a mill, under nitrogen, at 77°K. However, they were not added immediately to the solvent as was the procedure followed in the work reported earlier. Instead, the samples were allowed to warm to room temperature under nitrogen and each was dissolved in isooctane in the usual manner, i. e., with occasional swirling in a flask over a period of several days. Simultaneously, unground samples of the same materials were similarly dissolved.

The viscosity and ductless siphon measurements were made on relatively low concentrations of the samples, because the reduced viscosities become nonlinear at concentrations near 0.1 wt % in good solvents for the molecular weights used in this study.

The data are displayed in Table I.

CONCLUSIONS

The viscosity data show that there was apparently no detectable degradation on cryogrinding the sample with the lowest molecular weight. The sample with the intermediate molecular weight suffered a molecular weight decrease of a bit above 5%. It was reported earlier that cryogrinding reduced the molecular weight of a sample of B-200 by about 6% (5). In that instance, \bar{M}_v was determined in cyclohexane at 30°C, with the material cryoground directly into the solvent and the concentration measured by weight after precipitation of the macromolecules from solution with acetone. The molecular weight of the sample with the highest molecular weight decreased by about 9%. The relative decrease in the molecular weight on cryogrinding,

$$\frac{\overline{\Delta M}_v\%}{\overline{M}_v}$$

approaches a limiting value of 1.5.

TABLE I
VISCOSITY AVERAGE MOLECULAR WEIGHT^a AND REDUCED HEIGHT-AT-BREAK OF
SOLUTIONS OF POLYISOBUTYLENE IN ISOCTANE AT 20°C

Sample	$\overline{M}_v \times 10^{-6}$ (g/mol)	$C \times 10^{-2}$ (g/dl)	h/C cm (g/dl)
B-100 (unground)	1.00	1.91	0
		3.76	0
		7.74	0
B-100 (cryoground)	1.00	3.83	0
		5.94	0
		7.72	0
B-200 (unground)	3.59	3.84	11.9
		5.70	12.9
		7.69	13.8
B-200 (cryoground)	3.40	4.03	14.2
		5.15	14.6
		8.07	16.3
B-200-246 (unground)	5.96	3.89	53.8
		5.91	54.7
		7.85	56.8
B-200-246 (cryoground)	5.42	3.85	43.7
		5.82	48.0
		7.76	49.3

a. $[\eta] = 3.06 \times 10^{-4} \overline{M}^{0.65}$ (9)

The reduced height-at-break data reveal a strong molecular weight dependency. Whereas the cryogrinding appears to have improved the viscoelastic properties of the sample with intermediate molecular weight, it causes a decided decrease in the effect in the sample with the highest molecular weight. The latter change is in the expected direction, commensurate with the degradation revealed by the viscosity measurements. In the cryogrinding process free radicals are generated (5) and while the viscosity average molecular weight decreases by about 5% for the B-200 sample, the alteration of the molecular weight distribution due to post-grinding free radical coupling might conceivably lead to an increase in the reduced ductless siphon height-at-break because in the polyisobutylene/isooctane system, the intrinsic viscosity is related to

$$\overline{M}_v^{0.65}$$

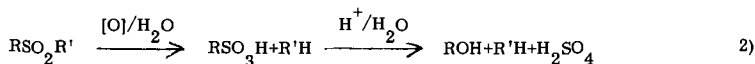
whereas the height-at-break is proportional to

$$\overline{M}_v^{2.3}$$

A relatively few such coupled molecules would contribute far less to the shear viscosity than to the extensional viscosity. Indeed, it may well be that only the very largest molecules in a sample contribute to the antimisting effect.

LITERATURE CITED

- (1) Proceedings of the IUTAM Symp. on Structure of Turbulance and Drag Reduction, F. Frenkel, M. Landahl and J. Tumley, eds., Phys. Fluids 20, No. 10, Part II (1977).
- (2) Chao, K. C., Child, C. A., Grens, E. A. and Williams, M. S., Am. Inst. Ch. Eng. J., in press.
- (3) Waters, P. F., Trippe, J. C. and Hadermann, A. F., Proceeding of the Aircraft Research and Technology for Antimisting Kerosene Conf., p. 5-1 ff, Atlantic City, NJ, February 18-19, 1981. Report No. FAA-CT-81-181, U. S. Dept. of Trans., June, 1981.
- (4) Trippe, J. C., Waters, P. F. and Hadermann, A. F., Application of GTA Blending Process to Antimisting Fuel Additives, Report No. FAA-CT-81-51, U. S. Dept. of Trans., May, 1981.
- (5) Waters, P. F., Hadermann, A. F., Weitzen, W. and Trippe, J. C., IUPAC 28th Macromolecular Symp. Proceedings, p. 679, July 12-16, 1982.
- (6) Hadermann, A. F., Waters, P. F., Trippe, J. C. and Weitzen, W., Contract No. DAAK-70-81-C-0134, U. S. Army Mobility Equip. Res. and Dev. Com., Fort Belvoir, VA, January 15, 1982.
- (7) Waters, P. F., Hadermann, A. F. and Trippe, J. C., Proceedings of the 2nd Internl. Conf. on Reactive Processing of Polymers, pp. 11-22, J. T. Lindt, ed., University of Pittsburgh, November 2-4, 1982.
- (8) Chao, K. K. K. and Williams, M. C., J. Rheology, in press.
- (9) BASF Tech. Leaflet No. M 2353 E/81538; May, 1978.



The first step in the sequence, i. e. the oxidation of sulfur compounds to sulfones, is extensively documented in the literature. Numerous oxidants have been reported which can effect the conversion of even the most stable organosulfur compounds (thiophenes) to the corresponding sulfones, including NO_2 (4), $\text{Cl}_2/\text{H}_2\text{O}$ (5), H_2O_2 /acetic acid and hydroperoxides (6).

The oxidation of sulfur beyond the sulfone stage (Reaction 2) has not been studied to any significant extent and there are very few references in the literature on the desulfurizing effects of extended oxidation of organosulfur compounds. Vasilakos (7) has reported the complete desulfurization of aliphatic sulfides by oxidative chlorination in aqueous systems at low temperatures (60°C) and atmospheric pressure.

The key to an economically feasible desulfurization process based on oxidation is, of course, selectivity. Concurrent oxidation of the remainder of the coal matrix by the sulfur-oxidizing agent should be minimized to prevent excessive loss of the heat content of the coal. A comparison of half-wave potentials for oxidation of organic substrates of the type found in coal (8) shows that organosulfur compounds as well as alcohols and amines are vastly more susceptible to oxidation than are ether and benzene derivatives. Thus, given a mild oxidizing agent, it may be possible to oxidize the organic sulfur compounds, amines and alcohols without destroying the hydrocarbon portion of the coal molecule.

One of the most promising oxidants in this direction is hydrogen peroxide, particularly in acid solutions, where it has a standard oxidation potential approximately 1.4 V more positive than that of pyrite and about 1.6 V more positive than the SO_2/S couple (9). Thus, H_2O_2 is an oxidizing agent capable of oxidizing effectively the pyritic sulfur to the sulfate form.

Mukai et al. (10) studied the treatment of several Japanese bituminous coals with 3 wt % aqueous hydrogen peroxide. This treatment was claimed to give nearly quantitative removal of pyritic sulfur without changing the caking properties of the coal. No data on organic-sulfur reduction were given. Nalwalk and coworkers (11) also reported that decomposition of coal with 30 wt % H_2O_2 slowly oxidized pyrite to sulfate.

Smith (12) investigated the desulfurization of U. S. coals with 10-15 wt % H_2O_2 , 0.1-0.3 N H_2SO_4 , aqueous solutions. Treatment of several coals at ambient temperature with H_2O_2 alone had a noticeable effect in removing pyritic sulfur, but the reaction was significantly enhanced when a small amount of sulfuric acid was added to the peroxide solutions. Although pyritic sulfur and ash were effectively removed in this way, organic sulfur remained unaffected. Minimal attack on the organic constituents of the coal matrix was observed. The reaction mechanism was postulated to involve the intermediate formation of peroxysulfuric acid, H_2SO_5 (catalyzed by metal ions and sulfates present in coal), followed by oxidation of the pyrite, with competing peroxide decomposition by metal ions.

The apparent resistance of the organic sulfur in coal to oxidative desulfurization in this case does not necessarily imply that organic sulfur functionalities are not affected by the $\text{H}_2\text{O}_2/\text{H}_2\text{SO}_4$ treatment. As we will show in the section on model compounds, all the basic organosulfur structures present in coal can be readily converted to the sulfone form under the conditions of the $\text{H}_2\text{O}_2/\text{H}_2\text{SO}_4$ attack. In most cases, however, the oxidation does not proceed beyond the sulfone stage, and the additional desulfurization steps necessary to free the organic sulfur from the coal matrix (Equation 2) do not take place.

In a recent study (13), Kralik has reported that a hot aq. Na_2CO_3 wash of coal pretreated with a mild oxidizing agent results in significant organic-sulfur reduction, mainly by splitting off relatively low-molecular-weight, oxidized sulfur compounds from the hydrocarbon matrix. It is feasible that the high selectivity of the peroxide treatment of coal towards sulfur oxidation could be combined with a subsequent alkaline hydrolysis step to leach out a significant portion of the oxidized organosulfur compounds, thus affecting not only pyritic, but also organic-sulfur removal from coal.

EXPERIMENTAL

Chemical beneficiation experiments were carried out in batch mode at ambient temperature and pressure with a Redstone high-volatile A, bituminous coal. The ultimate analysis and sulfur forms for this coal, designated as PSOC-715, are included in Table I. In each run, approximately 20 grams of the dried and sized (200x325 mesh) coal was slurred in a 500-ml Pyrex Erlenmeyer flask with 300 ml of a 15 wt % H_2O_2 solution of the desired H_2SO_4 concentration. At the end of the reaction period the slurry was vacuum-filtered through a fine-porosity fritted glass funnel and the coal was washed several times with water for analytical purposes. Treated coal samples were dried for 24 hours under vacuum at 110°C and then analyzed for proximate and ultimate composition and heating value. A portion of the $\text{H}_2\text{O}_2/\text{H}_2\text{SO}_4$ treated coal was further subjected to an extended

leaching cycle with a hot (80°C) 0.1 molar Na_2CO_3 solution, then washed with water and dried as before. Both the Eschka and the Fisher methods for total-sulfur content and the ASTM-D-2492 wet method for forms of sulfur were employed in the analysis of the raw and treated coals. The wet method was modified to eliminate any ash interference in the determination of the pyritic and, thus, the organic sulfur (14). In this modified method, the pyritic-sulfur content of the coal is determined by oxidation of the pyrite to ferric sulfate and subsequent gravimetric analysis of barium sulfate precipitate, rather than by atomic absorption determination of the iron as described in the ASTM method.

TABLE I

ULTIMATE ANALYSES AND SULFUR FORMS OF COAL SAMPLES TREATED WITH A 15 WT % H_2O_2 , 1N H_2SO_4 AQUEOUS SOLUTION AT 25°C FOR VARIOUS LENGTHS OF TIME^a

Reaction Time ^b (min)	Carbon	Hydrogen	Oxygen	Nitrogen	Ash	Total Sulfur	
						Eschka	Fisher
0 (Raw Coal PSOC 715)	73.6	4.73	11.2	1.08	7.02	2.46	-
15	78.0	5.50	8.24	1.16	5.14	2.04	-
	77.7	5.45	8.78	1.18	5.00	1.85	1.94
30	78.6	5.20	7.99	1.15	5.07	2.01	-
	78.3	5.47	8.47	1.18	4.76	1.80	1.83
60	74.4	4.98	13.3	1.17	4.41	1.71	-
	74.5	4.84	13.5	1.19	4.44	1.55	1.37
90	74.6	4.90	13.6	1.10	4.18	1.58	-
	74.9	4.91	13.3	1.18	4.26	1.47	1.29
120	78.2	5.27	9.46	1.15	4.38	1.57	-
	78.2	5.35	8.75	1.24	5.08	1.38	1.48
180	77.4	5.21	10.8	1.06	4.16	1.35	-
	77.5	5.22	10.8	1.24	3.96	1.26	1.23
240	77.5	4.99	11.4	1.14	3.76	1.23	-
	77.2	5.21	11.7	1.03	3.72	1.12	1.17

Reaction Time ^b (min)	Sulfate Sulfur	Pyritic Sulfur	Organic Sulfur ^c	Heating Value (Btu/lb)
0 (Raw Coal PSOC 715)	0.39	1.31	0.76	12869
15	<0.05	1.11	0.93	13805
	<0.05	0.96	0.89	13811
30	<0.05	1.04	0.97	13877
	<0.05	0.91	0.89	13693
60	<0.05	0.89	0.82	12915
	<0.05	0.80	0.75	12969
90	<0.05	0.70	0.88	12921
	<0.05	0.60	0.87	12885
120	0.07	0.65	0.86	13743
	<0.05	0.47	0.91	13895
180	<0.05	0.50	0.85	13587
	<0.05	0.37	0.89	13592
240	0.09	0.35	0.79	13530
	<0.05	0.20	0.92	13526

- All reported values are wt % (on a dry basis), unless otherwise noted.
- For each reaction time, the first row of data corresponds to a single-step, $\text{H}_2\text{O}_2/\text{H}_2\text{SO}_4$ treatment. The second row of data corresponds to the same $\text{H}_2\text{O}_2/\text{H}_2\text{SO}_4$ treatment followed by an aqueous wash of the treated coal with a hot (80°C) 0.1M Na_2CO_3 solution.
- Determined by difference using the Eschka total-sulfur value.

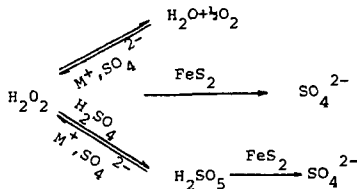
RESULTS AND DISCUSSION

Tables I and II summarize our data on the treatment of the PSOC-715 coal with a 15 wt % aqueous H_2O_2 solution of various H_2SO_4 concentrations, at 25°C and for various lengths of time. Total sulfur and pyrite and ash removal from coal are depicted in Figures 1 and 2, respectively, as functions of the reaction time. Figure 3 shows the effect of the H_2SO_4 concentration of the peroxide solution on pyritic sulfur removal.

The results indicate that there is a very significant reduction in total sulfur content for the $\text{H}_2\text{O}_2/\text{H}_2\text{SO}_4$ treated coal under the given experimental conditions. This reduction ($\sim 55\%$ in 4 hours) comes entirely from the almost complete elimination of pyrite and sulfates from coal. While sulfate sulfur (and ash) is leached out at the very early stages of the peroxide treatment, pyritic sulfur removal continues at a reasonable rate even after 4 hours of reaction. The results confirm earlier observations about the high selectivity of the peroxide reactions towards sulfur, the rest of the organic coal matrix being affected to a minimal extent. Carbon, hydrogen, nitrogen and oxygen contents of the treated coal remain at approximately the raw coal levels. No organic sulfur is removed in these room temperature experiments. On the other hand, pyritic sulfur reduction is accompanied by a significant reduction in the ash content of the coal ($\sim 47\%$ in 4 hours), and by a slight but noticeable increase in its heating value. This increase of about 5% is most probably due to the removal of low-heat-content inorganic matter from coal.

Subsequent wash of the $\text{H}_2\text{O}_2/\text{H}_2\text{SO}_4$ treated coal with a sodium carbonate solution does not result in additional ash reduction, or, as was expected, in any organic sulfur removal. However, a small but consistent decrease in the total sulfur content is observed in all cases, due to further removal of pyritic sulfur from the coal. The exact mechanism of this alkaline pyrite desulfurization is not clear at this point.

Pyritic sulfur removal also displays an interesting dependence on the H_2SO_4 concentration of the peroxide solution. The data in Table II show that aqueous hydrogen peroxide alone is quite efficient in removing a substantial portion of the pyrite and the ash from coal. At the other extreme, treatment of the coal with a 1N sulfuric acid solution has absolutely no effect on pyritic sulfur, although some ash is actually removed. The combination of H_2O_2 and H_2SO_4 in aqueous solution results in a synergistic effect, where pyrite and ash reduction in coal significantly exceed the corresponding reduction brought about by each reagent alone. The effect is pronounced at low acid concentrations, but above a concentration of approximately 0.2N H_2SO_4 the trend is reversed. Concentrated sulfuric acid seems to have an adverse effect on the oxidation of pyrite by hydrogen peroxide, so that, for example, the level of pyritic sulfur removal for a 2N H_2SO_4 peroxide solution falls below even that for pure hydrogen peroxide. As Smith (12) has pointed out, the H_2SO_4 -assisted oxidation of iron pyrite by hydrogen peroxide involves a complex system of parallel and consecutive reactions that may be strongly catalyzed by metal ions and sulfates present in coal. A simplified reaction mechanism can be schematically represented as follows:



The concentration of sulfuric acid in the peroxide solution may affect the kinetics and/or the equilibrium of any of these reactions (14), but the extent of the specific contribution of each step to the overall concentration effect that was observed experimentally is very difficult to estimate.

Model Compound Studies

To investigate the effect of the $\text{H}_2\text{O}_2/\text{H}_2\text{SO}_4$ treatment on organic sulfur under more controlled conditions, a series of kinetic experiments was carried out with three organosulfur compounds modeling possible sulfur functionalities in coal, namely dibenzothiophene, phenyl sulfide and *t*-butyl sulfide.

In each run with phenyl sulfide or dibenzothiophene, an aqueous phase consisting of 5ml 30 wt % H_2O_2 and 3.3 ml 36N H_2SO_4 was emulsified under intense stirring with 100 ml of a hexane phase containing 0.006 moles of the sulfide. The sulfide/peroxide-acid proportion corresponds to a 2.5 fold excess of the oxidant (assumed to be the intermediate peroxy-sulfuric acid) over the stoichiometric requirement for complete conversion (oxidation) of the sulfidic sulfur to sulfate

(Equations 1 and 2). All the reactions were carried out at 25°C. Samples of the hexane phase were withdrawn every 15 minutes and analyzed quantitatively on a Tracor 565 capillary-column gas chromatograph equipped with a Hall Electrolytic Conductivity Detector set at the sulfur detection mode. The corresponding sulfone was found to be the only final product of oxidation of phenyl sulfide and dibenzothiophene, with small amounts of the sulfoxide formed intermediately. Due to the very low solubility of the sulfoxides and the sulfones in hexane, these products were obtained mostly as solid crystals separating from the reaction mixture. The crystals were filtered, dissolved in tetrahydrofuran and analyzed on the gas chromatograph. Under the given reaction conditions, a 25% conversion of phenyl sulfide to the sulfone was obtained in 8 hours and 75% in 24 hours. For dibenzothiophene, the 24-hour conversion level was 42%. The oxidation rate was strongly dependent on the concentration of the sulfuric acid and complete conversion of the sulfide to sulfone could be achieved in a few minutes of reaction with a much higher excess of the H_2O_2/H_2SO_4 oxidant.

In the t-butyl sulfide runs, 14 ml of the (liquid) sulfide was directly dispersed under intense stirring in an aqueous phase consisting of 140 ml 30 wt % H_2O_2 and 96 ml 36N H_2SO_4 (= 5 fold excess of oxidant). The oxidation reaction was carried out at 25°C for various lengths of time. At the end of each run, the reaction mixture was exhaustively extracted with hexane. The aqueous phase was separated and analyzed for total SO_4^{2-} content by the $BaCl_2 \rightarrow BaSO_4$ precipitation method. The difference in sulfate contents between this phase and the initial aqueous phase (before reaction) was used to determine the SO_4^{2-} yield of the sulfide oxidation reaction. The hexane phase was analyzed for sulfur species on the gas chromatograph. After 8 hours of reaction, the t-butyl sulfide had been completely converted, t-butyl sulfone and SO_4^{2-} being the only reaction products that were detected. The sulfone yield (based on the sulfide) was approximately 20%, the remaining 80% appeared as sulfate.

The results with t-butyl sulfide are very encouraging, because they demonstrate the ability of the H_2O_2/H_2SO_4 system to promote complete oxidative desulfurization of aliphatic sulfide structures under ambient reaction conditions. The fact that no organic sulfur removal was observed under similar conditions with the PSOC-715 coal may simply be an indication that most of the organic sulfur in this coal is in stable phenyl and thiophenic forms that can survive the oxidative peroxide attack. Vasilakos (7) has reported a similar case in his studies of the selective desulfurization of two bituminous coals with aqueous chlorine solutions. The coals displayed completely different organic-sulfur-reduction characteristics despite the almost identical extent and pattern of the chlorinolysis reactions.

The effect was attributed to the different distribution of the organic sulfur in the two coals in aliphatic and aromatic structures. We are currently conducting a series of H_2O_2/H_2SO_4 experiments with two high organic-sulfur coals, a Texas Darco lignite and an Illinois #5 bituminous coal, to test this hypothesis and to study further the removal of sulfur functionalities from the coal matrix.

SUMMARY

The removal of sulfur and ash from coal treated with aqueous hydrogen peroxide/sulfuric acid solutions at ambient temperature was studied under a variety of experimental conditions. Almost complete elimination of the sulfate and the pyritic sulfur was observed in most cases, as well as substantial reduction in the ash content. The rest of the organic coal matrix was not affected to any significant extent, indicating a high selectivity of the H_2O_2/H_2SO_4 system towards sulfur oxidation. An optimal H_2SO_4 concentration level was established, beyond which sulfuric acid was found to have an adverse effect on the oxidation of pyrite by hydrogen peroxide. The oxidative desulfurization of model organosulfur compounds, such as t-butyl sulfide, phenyl sulfide and dibenzothiophene, by the H_2O_2/H_2SO_4 system was also investigated.

ACKNOWLEDGMENTS

This work was supported by the Texas Energy and Natural Resources Advisory Council under Grant No. 82-UCRC-2. The support is gratefully acknowledged.

TABLE II

ULTIMATE ANALYSES AND SULFUR FORMS OF COAL SAMPLES TREATED WITH A 15 WT % H_2O_2 SOLUTION (OF VARYING H_2SO_4 CONCENTRATION) AT 25°C FOR TWO HOURS^a

H_2SO_4 Concentration ^b , (N)	Carbon	Hydrogen	Oxygen	Nitrogen	Ash	Total Sulfur	
						Eschka	Fisher ^a
Raw Coal (PSOC 715)	73.6	4.73	11.2	1.08	7.02	2.46	-
0	77.7	5.29	9.53	1.19	4.73	1.50	-
(H ₂ O ₂ only)							
0.1	80.3	5.63	7.93	1.22	3.88	1.08	-
	79.1	5.38	9.47	1.24	3.71	1.05	1.06
0.3	78.2	5.40	10.2	1.15	3.80	1.27	-
	78.3	5.36	9.98	1.25	3.92	1.18	1.16
0.5	78.0	5.31	10.1	1.21	4.04	1.33	-
	77.8	5.29	10.4	1.20	4.05	1.23	1.21
2.0	77.3	5.15	10.8	1.11	4.15	1.47	-
	77.5	5.09	10.8	1.24	4.02	1.31	1.35
5.0	78.1	5.26	9.78	1.10	4.23	1.48	-
	77.6	5.16	10.6	1.24	4.13	1.30	1.40
10.0	77.9	5.19	10.4	1.12	4.04	1.33	-
	77.6	5.19	10.9	1.15	3.93	1.25	1.32
1N H_2SO_4	76.6	5.17	9.43	1.04	5.46	2.24	-
(No H_2O_2)	76.0	4.95	10.6	1.22	5.13	2.10	2.19
H_2SO_4 Concentration ^b , (N)	Sulfate Sulfur	Pyritic Sulfur	Organic Sulfur ^c	Heating Value (Btu/lb)			
Raw Coal (PSOC 715)	0.39	1.31	0.76	12869			
0	<0.05	0.54	0.96	13282			
(H ₂ O ₂ only)							
0.1	<0.05	0.13	0.95	14064			
	<0.05	0.13	0.92	14014			
0.3	<0.05	0.32	0.95	13800			
	<0.05	0.26	0.92	13762			
0.5	<0.05	0.47	0.86	13735			
	<0.05	0.34	0.89	13648			
2.0	<0.05	0.55	0.92	13600			
	<0.05	0.42	0.89	13595			
5.0	<0.05	0.54	0.94	13568			
	<0.05	0.40	0.90	13599			
10.0	0.11	0.37	0.85	13552			
	<0.05	0.37	0.88	13559			
1N H_2SO_4	<0.05	1.30	0.94	13563			
(No H_2O_2)	<0.05	1.22	0.88	13368			

a. All reported values are wt % (on a dry basis), unless otherwise noted.

b. For each concentration, the first row of data corresponds to a single-step, $\text{H}_2\text{O}_2/\text{H}_2\text{SO}_4$ treatment. The second row of data corresponds to the same $\text{H}_2\text{O}_2/\text{H}_2\text{SO}_4$ treatment followed by an aqueous wash of the treated coal with a hot (80°C) 0.1M Na_2CO_3 solution.

c. Determined by difference using the Eschka total-sulfur value.

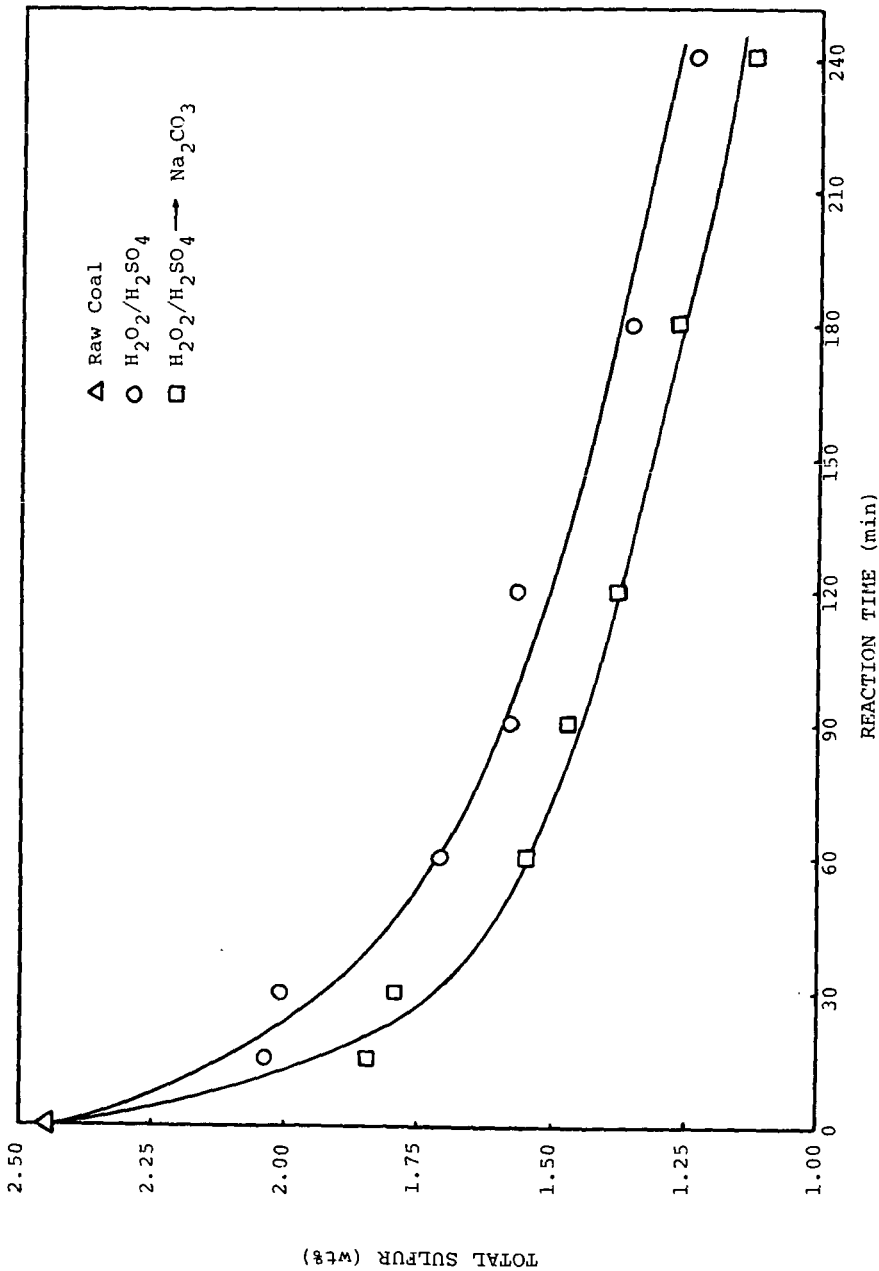


Figure 1: Total-sulfur dependence on reaction time (coal treated with a 15 wt% H_2O_2 , 1N H_2SO_4 aqueous solution at 25°C)

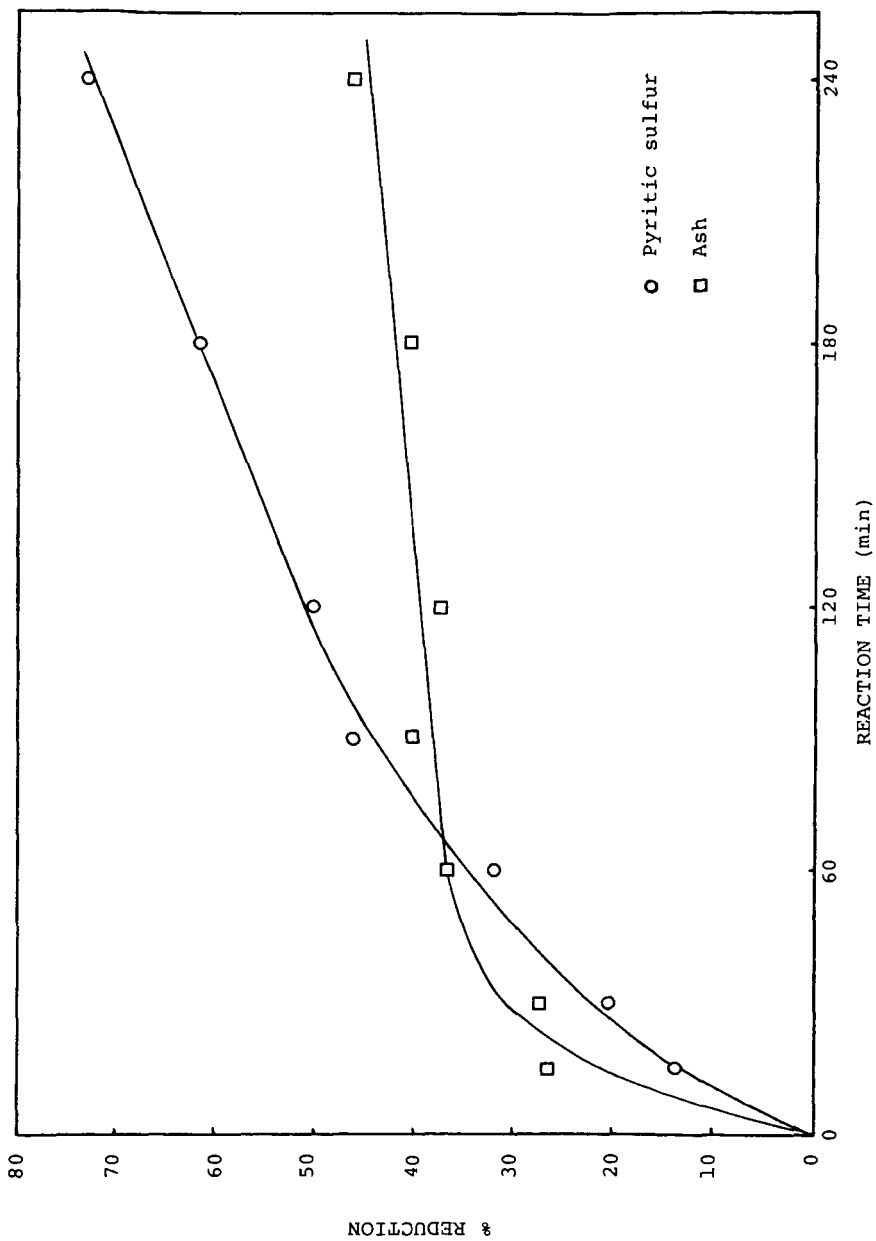


Figure 2: Pyritic-sulfur and ash reduction versus reaction time (coal treated with a 15 wt% H_2O_2 , 1N H_2SO_4 aqueous solution at 25°C)

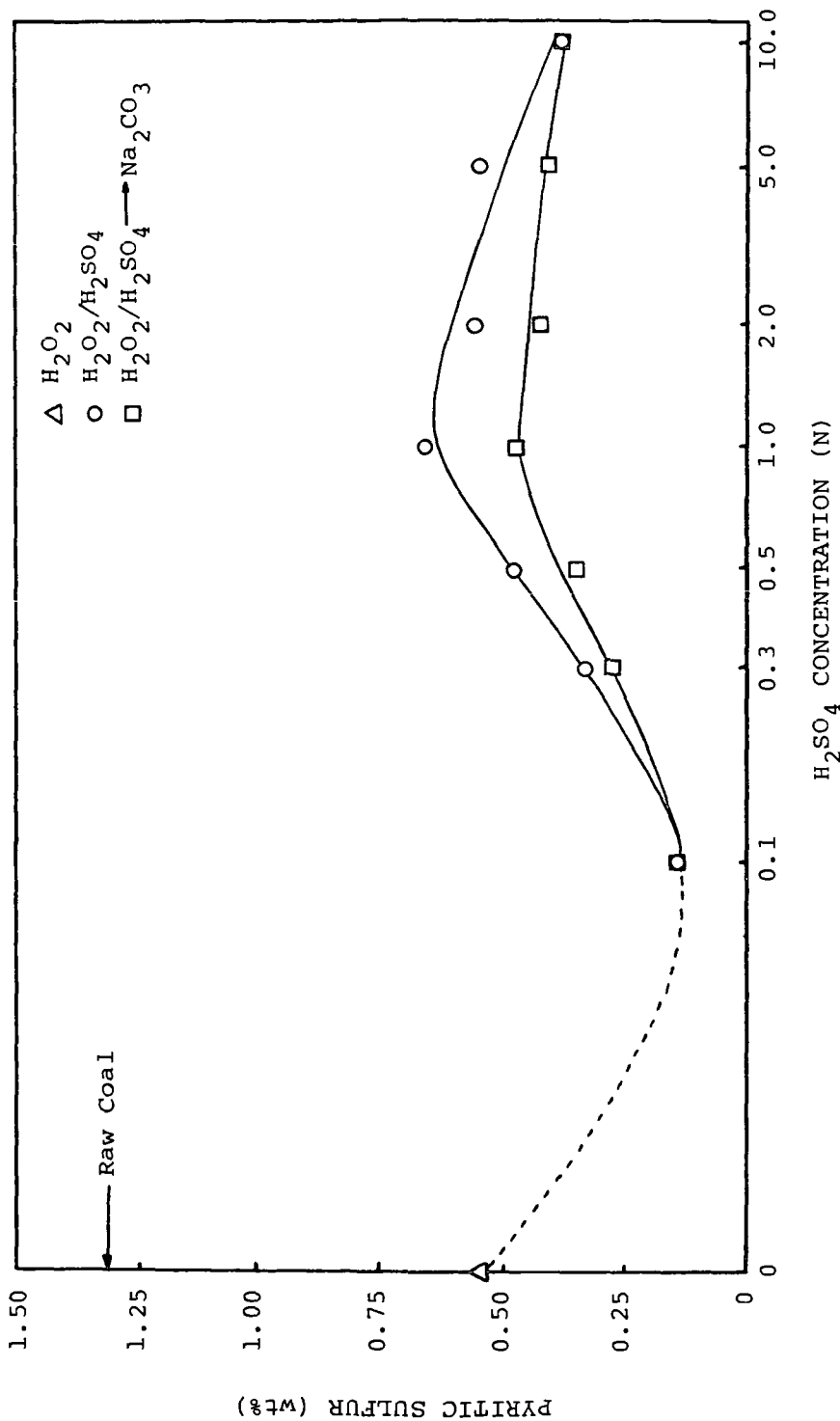


Figure 3: Effect of the acid concentration of the peroxide solution on pyritic sulfur (coal treated for 2 hours at 25°C)

LITERATURE CITED

- (1) Du Fresne, E. R. , "Coal Cleaning Versus Flue-Gas Desulfurization in Meeting New Proposed Air Pollution Standards", Assessment Report, Jet Propulsion Lab. , Pasadena, CA (1979).
- (2) Attar, A. and Corcoran, W. H. , *Ind. Eng. Chem. Prod. Res. Dev.* , 17, 102 (1978).
- (3) Kalvinskis, J. J. , et al. , "Final Report for Phase II - Coal Desulfurization by Low Temperature Chlorinolysis", Jet Propulsion Lab. Publication 80/15, Pasadena, CA (1980).
- (4) Friedman, S. , Lacount, R. B. and Warzinski, R. P. , "Oxidative Desulfurization of Coal", in "Coal Desulfurization", ACS Symp. Series No. 64, Washington, DC (1977).
- (5) Vasilakos, N. P. , Bone, R. L. and Corcoran, W. H. , *Ind. Eng. Chem. Prod. Res. Dev.* , 20, 376 (1981).
- (6) Reid, E. E. , "Organic Chemistry of Bivalent Sulfur", Chemical Publishing Co. , Inc. , NY (1960).
- (7) Vasilakos, N. P. , "Coal Desulfurization by Selective Chlorinolysis", Ph. D. Thesis, California Inst. of Tech. , Pasadena, CA (1980).
- (8) Ross, S. D. , Finkelstein, M. and Rudd, E. J. , "Anodic Oxidation", Academic Press, Inc. , NY (1975).
- (9) Meyers, R. A. , "Coal Desulfurization", Marcel Dekker, Inc. , NY (1977).
- (10) Mukai, S. , Araki, Y. , Konish, M. and Otomura, K. , *Nenryo Kyoka-shi* 48, 905 (1969); *Chem. Abstr.* 72, 123720d (1970).
- (11) Nalwalk, A. J. , Friedel, R. A. and Queiser, J. A. , *Energy Sources* 1, 179 (1974).
- (12) Smith, E. B. , "Lowering the Sulfur and Ash Contents of High-Sulfur Coals by Peroxide-Acid Treatment", ACS, Div. of Fuel Chem. , Preprints, 20, 140 (1975).
- (13) Kralik, J. G. , "An Investigation of the Applied Chemistry of the Reactions of Coal and Nitrogen Dioxide with Particular Emphasis on Oxidative Desulfurization", Ph. D. Thesis, California Inst. of Tech. , Pasadena, CA (1982).
- (14) Monger, J. M. and Redlick, O. , *J. Phys. Chem.* , 60, 797 (1956).